

***Novel in vitro and in silico tools for the development of mesoporous silica formulations with optimal precipitation inhibitors***

Dissertation zur Erlangung des Doktorgrades der Naturwissenschaften

vorgelegt beim Fachbereich Biochemie, Chemie und Pharmazie der  
Johann Wolfgang Goethe -Universität in Frankfurt am Main

von

**Daniel Joseph Price**

aus Liverpool

*Frankfurt 2020*

## **i. Dedication**

**Molly:** my best friend, wife and partner. Without you, none of this is possible.

**Rosella, Daisy and Atlas:** my three wonderful children, you keep me motivated, positive and joyful- **this is for you.**

**My Parents:** You got me to where I needed to be, I will be forever grateful for your sacrifice and support.

**My Family:** All of you. Thank you for everything you have given me, your support, your faith and encouragement.

## **ii. Acknowledgements**

First and foremost, my thanks and gratitude are extended to Prof. Dr. Jennifer Dressman, Prof. Dr. Christoph Saal, Prof. Dr. Martin Kuentz and Dr. Anita Nair for their support, guidance and supervision throughout the duration of my PhD studies. It has been a pleasure to work together and I hope to continue doing so in the future.

I feel fortunate to have been part of a multi-cultural, multi-disciplinarian PhD consortium. Special thanks are extended to all of my PEARRL colleagues. It was a pleasure to progress through this journey together and I hope our paths continue to cross in the future. In the same light, thanks are extended to all of the beneficiaries, partners, supervisors and funding bodies that made PEARRL a reality.

Finally, I would like to thank all of my colleagues at Merck KGaA, Frankfurt Goethe University and BfArM for enabling me to achieve everything I have in the duration of my studies. Access to cutting edge technologies, equipment and expertise has been a big contributor to my progress these past four years.



## TABLE OF CONTENTS

|     |  |    |
|-----|--|----|
| i.  | <b>Dedication</b> .....  | 2  |
| ii. | <b>Acknowledgments</b> .....   | 2  |
| I.  | <b><u>Introduction</u></b> .....   | 5  |
| 1.  | <b><u>Overview</u></b> .....   | 5  |
| 2.  | <b><u>Theoretical Background</u></b> .....   | 8  |
|     | 2.1 <i>Factors Impacting Oral Drug Absorption</i> .....  | 8  |
|     | 2.1.1 Solubility .....   | 8  |
|     | 2.1.2 Supersaturation .....  | 9  |
|     | 2.1.3 Impact of Solubility and Supersaturation on Oral Absorption .....                              | 10 |
|     | 2.1.4 Dissolution and Impact on Oral Absorption .....  | 12 |
|     | 2.2 <i>Approaches to Improve Drug Solubility, Dissolution and Oral Absorption</i> .....              | 14 |
|     | 2.2.1 Formulation Technologies to Tackle Poor Drug Solubility.....                                   | 14 |
|     | 2.2.2 Preventing Precipitation from the Supersaturated State.....                                    | 18 |
| 3.  | <b><u>Recent Advances in Supersaturating Formulations</u></b> .....                                  | 26 |
|     | 3.1 <i>Mesoporous Silica: An Emerging Formulation Technology</i> .....                               | 26 |
|     | 3.2 <i>Mesoporous Silica and Precipitation Inhibitors</i> .....                                      | 38 |
|     | 3.3. <i>Investigating the Importance Drug-Polymer Interactions in Precipitation Inhibition</i> ..... | 39 |
|     | 3.3.1 UV-vis Spectroscopy .....  | 39 |
|     | 3.3.2 FTIR .....   | 40 |
|     | 3.3.3 Raman Spectroscopy .....   | 42 |
|     | 3.3.4 Nuclear Magnetic Resonance (NMR) Spectroscopy .....  | 44 |
|     | 3.3.5 Differential Scanning Calorimetry (DSC) .....  | 50 |
|     | 3.3.6 Modelling Precipitation Inhibition.....  | 51 |
|     | 3.4. <i>Bridging the Gap to Systematic and Facile Precipitation Inhibitor Screening</i> .....        | 57 |
| 4.  | <b><u>Aims of the Thesis</u></b> .....   | 59 |

|              |   |            |
|--------------|---|------------|
| <b>II.</b>   | <b><u>Results and Discussion</u></b> .....  | <b>60</b>  |
| 1.           | <u>Approach</u> .....   | <b>60</b>  |
| 2.           | <u>Selected Compounds</u> .....   | <b>62</b>  |
| 3.           | <u>Selected Polymers</u> .....  | <b>63</b>  |
| 4.           | <u>Co-Incorporation: A New Method to Combine Precipitation Inhibitors with Mesoporous Silica</u> ..     | <b>65</b>  |
|              | 4.1 <i>Approach</i> .....   | <b>65</b>  |
|              | 4.2 <i>Solid State of Formulations</i> .....  | <b>66</b>  |
|              | 4.3 <i>Experimental Considerations for Dissolution Selection</i> .....                                  | <b>68</b>  |
|              | 4.4 <i>Dissolution of Simple Blends: The Importance of Precipitation Inhibitors</i> .....               | <b>69</b>  |
|              | 4.5 <i>Co-Incorporating HPMCAS in the Loading Method: Precipitation and Dissolution</i> .....           | <b>70</b>  |
|              | 4.6 <i>Co-Incorporated Formulations: Just a Solid Dispersion?</i> .....                                 | <b>74</b>  |
|              | 4.7 <i>Mechanistic Rationale</i> .....  | <b>75</b>  |
| 5.           | <u>In Silico Pharmaceutics: A New Method to Select Precipitation Inhibitors for Mesoporous Silica</u> . | <b>77</b>  |
|              | 5.1 <i>The Role of Molecular Interactions: Quality by Selection</i> .....                               | <b>77</b>  |
|              | 5.2 <i>COSMO-RS: Combining Quantum Chemistry and Thermodynamics</i> .....                               | <b>78</b>  |
|              | 5.3 <i>COSMO-RS for Precipitation Inhibitor Screening: Theory</i> .....                                 | <b>82</b>  |
|              | 5.4 <i>Incorporation of Precipitation Inhibitors with Mesoporous Silica Formulations</i> .....          | <b>84</b>  |
|              | 5.5 <i>COSMO-RS for Precipitation Inhibitor Screening: Output</i> .....                                 | <b>84</b>  |
|              | 5.6 <i>Correlation between COSMO-Rank and Formulation Performance</i> .....                             | <b>87</b>  |
|              | 5.7 <i>Limitations of the Approach</i> .....  | <b>90</b>  |
|              | 5.8 <i>Implications of the COSMO-RS Approach</i> .....  | <b>91</b>  |
| <b>III.</b>  | <b><u>Conclusion and Outlook</u></b> .....  | <b>92</b>  |
| 1.           | <u>Summary</u> .....  | <b>92</b>  |
| 2.           | <u>Co-incorporation: A New Method to Combine Precipitation Inhibitors with Mesoporous Silica</u> ..     | <b>93</b>  |
| 3.           | <u>In Silico Pharmaceutics: A New Method to Select Precipitation Inhibitors for Mesoporous Silica</u> . | <b>93</b>  |
| 4.           | <u>Future Work</u> .....  | <b>94</b>  |
| <b>IV.</b>   | <b><u>Deutsche Zusammenfassung</u></b> .....  | <b>95</b>  |
| <b>V.</b>    | <b><u>References</u></b> .....  | <b>101</b> |
| <b>VI.</b>   | <b><u>Publications and Posters</u></b> .....  | <b>114</b> |
| <b>VII.</b>  | <b><u>Curriculum Vitae</u></b> .....  | <b>116</b> |
| <b>VIII.</b> | <b><u>Declaration</u></b> .....   | <b>118</b> |
| <b>IX.</b>   | <b><u>Thesis Papers</u></b> .....   | <b>119</b> |

## **I. Introduction**

### **1. Overview**

Due to benefits around convenience, patient compliance and cost-effectiveness, the oral drug delivery route is by far the most favored for administration of medications (Krishnaiah, *et al.* 2010). For an orally delivered drug to exert its biological effect, it must first pass through the gastrointestinal tract (GI-tract) and into the systemic circulation. Therefore, the pharmacological effect of an orally delivered drug is related to its bioavailability, the percentage of the administered amount of drug reaching systemic circulation. The bioavailability of a drug is related to its ability to cross the barriers from the GI-tract, particularly passage from the GI milieu via the intestinal membrane (Zheng, *et al.* 2010). To achieve this, a drug must be sufficiently soluble in the fluids of the GI-tract and permeable to the cell membrane of the intestine. It is on these two parameters that the Biopharmaceutics Classification System (BCS) is based, which groups drugs into classes based on solubility and permeability (Amidon, *et al.* 1995).

In order to develop a framework for understanding the molecular properties that demonstrate a bioavailability risk, Lipinski proposed his 'rules of five' (Lipinski, *et al.* 2000). These rules propose that, for good oral bioavailability, a drug must have no more than five hydrogen bond donors and not more than 10 hydrogen bond acceptors, a molecular weight less than 500 Da and a log P of less than 5. Over the years, there has been an exponential increase in compounds not passing the rule of 5, with poor physicochemical properties becoming more common (Gardner, *et al.* 2004). As a result, there is a higher incidence of drugs with low solubility in compound development pipelines, resulting in reduced bioavailability. Such low bioavailability significantly increases the risk of drug attrition, representing a loss in both therapeutic and economic potential. For example, although it is reported that 60 % of approved drugs are poorly soluble, it is hypothesized that up to 90 % of candidates in the development pipeline will fall under this category (Taylor, *et al.* 2016). This highlights the big challenge of poor drug solubility to the pharmaceutical industry and demonstrates the importance of avoiding the low bioavailability risks

associated with poor aqueous solubility. In response, chemists and formulation scientists have developed a toolkit of strategies that can improve the solubility and subsequent bioavailability of these poorly soluble candidates. These approaches include chemical modifications that can be incorporated into synthesis such as salt formation and prodrugs; or formulation modification approaches such as micelle systems, co-solvents, particle size reduction, complexation and amorphous technologies (Timpe, *et al.* 2007).

Amorphous formulations are especially appealing due to the significant improvement in solubility the amorphous form can provide (Timpe, *et al.* 2007). By definition, an amorphous solid does not have a long-range order. This is in contrast to a crystalline solid. The absence of long-range order leads to a less dense packing of molecules in an amorphous, solid-state form and decreased intermolecular interaction (Leuner, *et al.* 2000). Due to this, amorphous solids tend to have substantially higher solubilities than their crystalline counterparts. However, amorphous solids are usually physically unstable or metastable due to the high energy associated with this solid-state form. Re-crystallization can drive an amorphous solid-state form to decrease its energy. Due to this tendency, it is unusual for a drug candidate to be used as a pure amorphous solid (Timpe, *et al.* 2007). Instead, formulation scientists can modify and stabilize the solid-state form of the poorly soluble drug molecule using various approaches. Most common amongst these approaches involve immobilizing the drug in the amorphous form in a polymeric matrix (Chokshi, *et al.* 2007). The two main methods to produce such polymeric amorphous solid dispersions are hot melt extrusion and spray drying.

One under-utilized route to amorphous solids is the use of mesoporous materials as drug carriers. A mesoporous material is defined by the International Union of Applied and Pure Chemists (IUPAC) as “any material containing pores of dimensions between 2 and 50nm” (McCarthy, *et al.* 2016). In recent years, mesoporous silica has emerged as a novel formulation option for stabilization and deliver of amorphous molecules. Mesoporous silica is a silicon dioxide excipient that possesses a highly porous network. Upon impregnation of the silica with a concentrated drug solution, the drug can be molecularly adsorbed onto

the surface of the silica. Due to the size of the pores, which have an approximate mean diameter of 6 nm, the molecularly adsorbed molecule is locally and sterically confined, preventing recrystallization (Ditzinger, 2018). Upon administration of mesoporous silica formulations to the body, there is a displacement of individual drug molecules from the surface of the silica into solution, which generates supersaturation with regards to the crystalline drug. Mesoporous silica is therefore an example of a supersaturating formulation. As the supersaturated solution in GI-fluids usually is not stable, it requires incorporation of a precipitation inhibitor to sustain the supersaturated concentrations for physiologically relevant timescales (Guzman, *et al.* 2007).

The combination of supersaturating formulation technology with a precipitation inhibitor is commonly referred to as “The Spring and Parachute” model. Here, the spring is the technology that generates a high concentration of the drug in solution and supersaturation. The precipitation inhibitor is the “parachute” that sustains supersaturated drug concentrations and slows the inevitable return towards thermodynamic concentrations (Guzmann, *et al.* 2007).

Given that mesoporous silica is a relatively novel formulation technology, little work has been done to understand how to most effectively select and formulate precipitation inhibitors for silica formulations. Therefore, the aim of this thesis is to update the state of the art of precipitation inhibitor theory, selection and design and to propose new experimental and *in silico* methods for the screening, selection and incorporation of precipitation inhibitors with mesoporous silica formulation technology.

## 2. Theoretical Background

### 2.1. Factors impacting oral drug absorption

#### 2.1.1 Solubility

Solubility is the ability of a substance, or solute, to dissolve in a solvent to form a homogenous mixture of the two (Grant, *et al.* 1990). The thermodynamic solubility is the equilibrium state where dissolution rate is equal to precipitation rate, i.e. the point at which no change is observed in the concentration in the system (Yalkowsky, *et al.* 1999).

Solubility of a solute in a solvent is governed by a number of factors, which, when simplified, can be broken down into three main components. First, the individual solute molecule must be separated from the solid material. This requires the breaking of solute-solute intermolecular interactions, or the crystal lattice in case of crystalline solids. Next, a cavity must be created within the solvent, this is referred to as cavitation. Finally, the solute molecule must be inserted into the newly created cavity. Therefore, the process of solvation is dictated by the energy costs or gains associated with each individual step in the process (**Eq. 1**) (Yalkowsky, *et al.* 1999).

$$S = f(\text{crystal lattice energy} + \text{cavitation energy} + \text{solvation energy}) \quad \text{(Equation 1)}$$

It is generally accepted that the cavitation energy is negligible. Therefore, the solvation energy can be seen as a function of the affinity of the drug for the solvent and the crystal lattice energy of the drug. In the case of oral drug delivery, the solvents in question are the media of the GI tract. The affinity of the drug for the solvent is usually a molecular property relating to the hydrophilicity, lipophilicity and hydrogen-bonding capability of the molecule. The crystal lattice energy is related to the strength of the intermolecular interactions in the crystal lattice (Yalkowsky, *et al.* 1999).

### 2.1.2 Supersaturation

Supersaturation can be defined from a physicochemical perspective as a system in which the free energy of the solute in solution is higher than the free energy of a crystalline or amorphous solid phase at equilibrium (**Figure 1**) (Taylor, *et al.* 2016). Essentially, this refers to a solution in which the concentration of drug is higher than the thermodynamic solubility, representing an excess energy system.

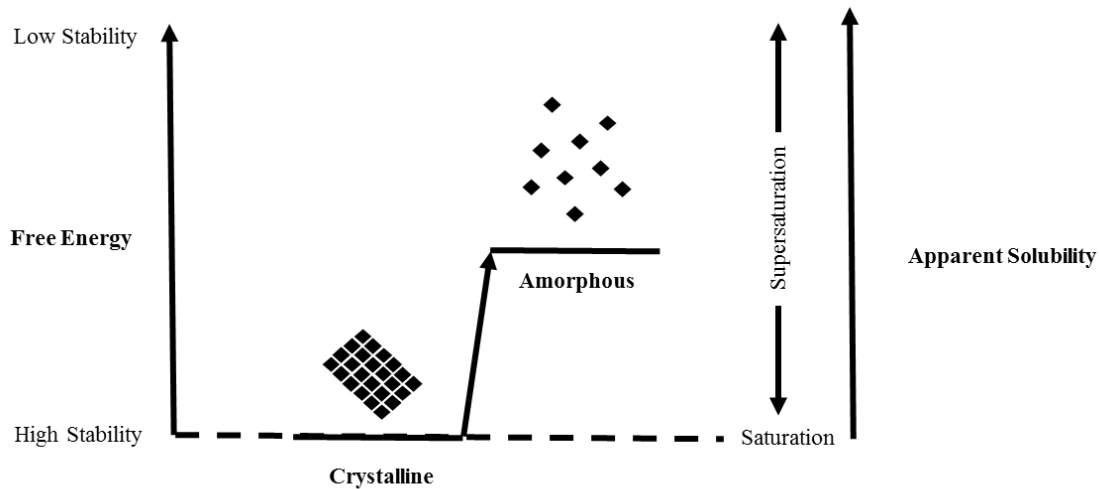


**Figure 1.** Energy diagram showing the advantages and disadvantages of crystalline and amorphous solid-state form from a stability and solubility perspective. Reproduced with permission from the publisher (Price, *et al.* 2018)

During a dissolution process yielding a supersaturated solution of a drug, the concentration of the drug in solution increases until its thermodynamic solubility is exceeded (Taylor, *et al.* 2016) (Yalkowsky, *et al.* 1999). Starting from this point supersaturation is established. Given the excess energy of the supersaturated state, this system exists in a metastable state. Ultimately, this metastability acts as a driving force for precipitation of the solute in either an amorphous or a crystalline form. This precipitation behavior must be considered if the goal of the generation of supersaturation is to increase absorption across the intestinal membrane (Price, *et al.* 2018).

Supersaturation can be triggered either by delivering the drug in a pre-solubilized form (e.g. SEDDS or lipid-based formulations) or in a rapidly dissolving, metastable solid-state form (e.g. amorphous solid solution, amorphous dispersion, metastable polymorphs, nanosized particles, or even pharmaceutical salts or co-crystals and prodrugs) (Timpe, *et al.* 2007).

### 2.1.3 Impact of Solubility and Supersaturation on Oral Absorption

For an orally delivered drug to reach its physiological target, it must first pass through the stomach, into the intestine and through the intestinal membrane to the systemic circulation. Therefore, absorption of the drug from the intestine is a critical stage in the action of a drug (Zheng, *et al.* 2012).

This adsorption through the cell membrane is referred to as flux (F) and is related to the concentration gradient through the membrane and the innate permeability of the molecule. **(Equation 2)**.

$$F = \frac{DKA}{h} (C_{lumen} - C_{basolateral}) \quad \text{(Equation 2)}$$

$C_{lumen}$  is the drug concentration adjacent to the membrane, while  $C_{basolateral}$  is the concentration of drug absorbed through the membrane, resulting in the concentration gradient. K is the partition coefficient of drug between the aqueous intestinal fluid and membrane, h is the width of the membrane, D is the diffusion coefficient of the drug and A is the surface area of the intestinal membrane, which collectively represent the permeability of the drug through the membrane (Zheng, *et al.* 2012).

One can assume, based on the circulation of blood away from the point of absorption, that the concentration of drug in the intestinal lumen is significantly higher than the concentration of drug at the basolateral membrane, so  $C_{lumen}$  can be neglected. Furthermore, D, K, A and h are fixed values that are related to the drug's permeability through the cell membrane, and can be collectively referred to as a permeability constant, **P**. Therefore, the maximum flux of the drug through the intestinal membrane is usually considered to be a product of the intestinal constant, **P**, and the thermodynamic solubility of the



drug in the intestine,  $C_{lumen}$ . As a result, **Eq 1.** can be re-written (**Equation 3**). However, in the case of a supersaturating formulation, this would be the apparent solubility upon generation of supersaturation.

$$F = P \cdot C_{lumen} \quad \text{(Equation 3)}$$

In other words, absorption of the drug through the intestinal membrane into systemic circulation is a function of permeability and solubility or *apparent* solubility. A low thermodynamic solubility is expected to result in reduced absorption from the GI tract. However, if the intestinal concentration can be enhanced *via* the generation of supersaturation, oral absorption of the drug can be substantially improved (Ditzinger, *et al.* 2018).

The importance of solubility and permeability in oral drug absorption is underpinned in the Biopharmaceutics Classification System (BCS), which groups compounds into various classes related to these two properties (Amidon, *et al.* 1995).

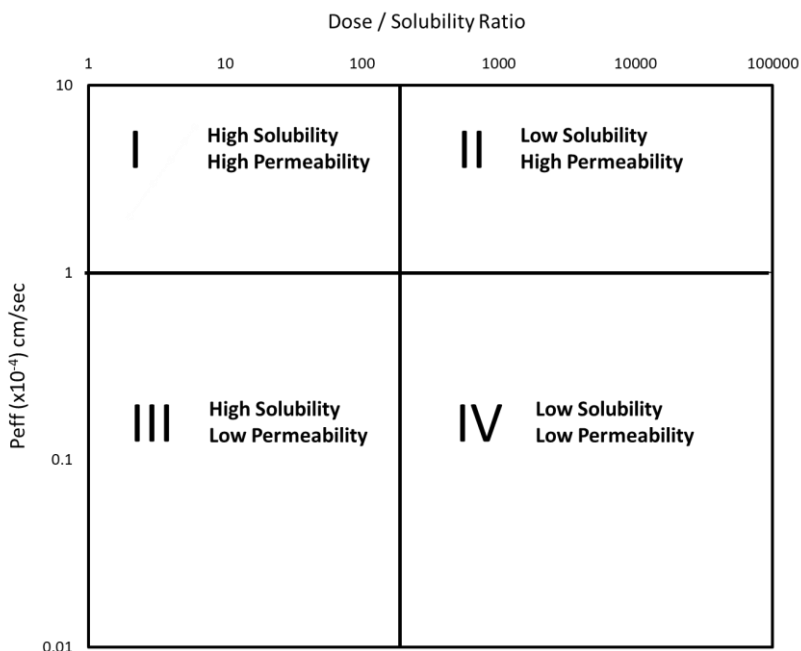


**Figure 2.** The Biopharmaceutical Classification System. Reproduced with permission from the publisher (Price, *et al.* 2018)

As per the BCS, a drug is counted as “highly soluble” if the highest dose strength is soluble in 250 mL of aqueous media across physiological pH range (pH 1.2 – 7.5). A drug is considered to be highly permeable if the extent of absorption through a cell-membrane is 90% or more based on mass-balance determination (Amidon, *et al.* 1995). This can be assessed in *in vitro* permeability assays or in *in vivo* studies relative to an intravenous dose.

#### 2.1.4 Dissolution and Impact on Oral Absorption

Although solubility and permeability are important components of drug absorption in the GI tract, another important consideration is dissolution (Dokoumetzidis, *et al.* 2006). Thermodynamic solubility, by definition, is an equilibrium value and contains no information about the *rate* at which the system reaches this equilibrium. Therefore, it is also crucial to consider the dissolution rate of the compound, to ensure that the equilibrium concentrations will be realized before the compound is cleared from the body *via* waste, with typical small intestinal transit times of between 2 and 5 hours being reported (Dokoumetzidis, 2006).

According to the film theory of dissolution, in order for a drug particle to dissolve, a concentration gradient must exist between the drug in solution ( $C$ ) and the drug concentration at equilibrium ( $C_s$ ), the two of which are separated by a layer of unstirred aqueous phase ( $h$ ). This gradient is the driving force for dissolution, and the rate of dissolution is therefore related to the rate of diffusion through the unstirred boundary layer (Noyes and Whitney, 1897).

This rate of diffusion across the unstirred boundary layer can be considered by simple diffusion kinetics

**(Equation 4):**

$$\frac{dcx}{dt} = \frac{DA}{h} (C_s - C) \quad \text{(Equation 4)}$$

where  $D$  is the diffusion rate of the drug and  $A$  is the surface area of the dissolving solid.

Practically speaking, the dissolution rate of a drug is related to its surface area, or particle size, and its equilibrium solubility.

Given the importance of *both* solubility and dissolution, it is clear that the BCS class of a molecule may be misleading, if the rate of dissolution is not known. Recently, the BCS has been refined and expanded in a framework referred to as the “developability classification system” (DCS). This system, developed by Butler and Dressman, was designed to facilitate the appropriate formulation of BCS II compounds (**Figure 3**) (Butler, *et al.* 2010). Key changes in the DCS include the measurement of solubility in biorelevant media, rather than compendial buffers. Furthermore, the volume of solvent which is used for the assessment is changed from 250 mL to 500 mL. Perhaps the most impactful change is in the separation of BCS II into two subcategories: DCS IIa and IIb, depending on whether the absorption of the compound is dissolution limited (IIa) or solubility limited (IIb). This is a significant distinction that can aid pharmaceutical scientists in developing formulations for DCS II compounds, as dissolution limited solubility can be overcome with simple techniques such as particle size reduction which accelerates dissolution, in accordance with the Noyes Whitney equation based on offering a higher specific surface (Dokoumetzidis, *et al.* 2006). However, using the same approach for DCS IIb drugs would be ineffective, as here it would be key to increase concentration of the dissolved drug, e.g. by realizing a supersaturated system in the GI tract.

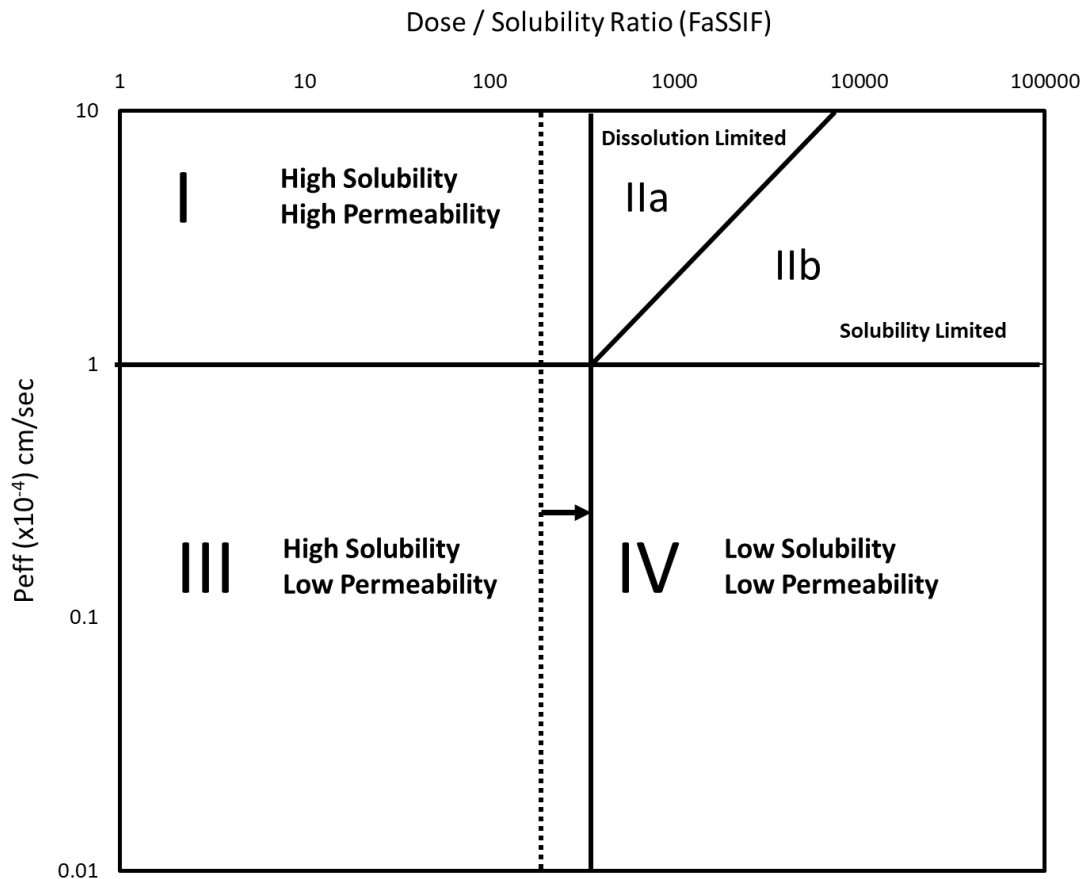


**Figure 3.** The Developability Classification System (Butler, *et al.* 2010). Reproduced with permission from the publisher (Price, *et al.* 2018).

## **2.2 Approaches to Improve Drug Solubility, Dissolution and Oral Absorption**

### **2.2.1 Formulation Technologies to Tackle Poor Drug Solubility**

60 % of approved drugs meet the BCS criteria for low solubility. However, it has been reported that 90% of drug candidates in pharmaceutical R&D pipelines meet this definition (Zheng, *et al.* 2008). Therefore, approaches to overcome the biopharmaceutical barriers for poorly soluble compounds are an increasingly important component of a successful drug development campaign. For this purpose, several formulation options exist.

### ***Lipid-Based Formulations***

Lipid-based formulations (LBFs) are a relatively common approach to overcome solubility limited (DCS IIb) oral absorption (Ditzinger, 2018). They are defined as delivery systems, in which the drug is dissolved or suspended in a lipidic system. LBFs can consist of triglyceride oils, partial glycerides, surfactants or co-surfactants and co-solvents (Pouton, *et al.* 2000). Generally, solubilized LBFs are more common, and the bioavailability enhancement is related to generation of solubilized and/or supersaturated drug upon the dispersion and digestion of the lipid in the GI tract. As previously discussed, in the case of supersaturation being generated in LBFs, there is a risk of precipitation due to the metastable nature of the supersaturated state, which may require a precipitation inhibitor to sustain concentrations and thus improve oral drug absorption. A wide variety of drugs have been formulated in LBF (Ditzinger, *et al.* 2018). Drugs that are especially suited to LBF are the so-called “grease-ball” molecules, those with a high lipophilicity represented by a high log P. Furthermore, such compounds may also have relatively weak crystal lattices, improving the likelihood of complete solubilization into the lipid phase. For “brick-dust” molecules, those with a relatively high crystal lattice energy, solubilization generally will be limited in the lipid phase and LBFs are not as useful for formulation of these drugs. However, recent work has been carried out to demonstrate the possibility of supersaturating such “brick-dust” molecules in lipid formulations using heat-cool cycles (Koehl, *et al.* 2019). Of course, such formulations may encounter long-term stability issues, which could limit practical application as commercially viable formulations, but they are an attractive option for pre-clinical studies where dose-escalation requires high concentrations in easily deliverable formulations, e.g. for toxicological studies (Koehl, *et al.* 2019).

### ***Complexation***

Complexation in the context of drug solubilization generally refers to formulation with a class of excipients known as cyclodextrins and is a common strategy for improving performance of drugs with solubility

limitations (DCS IIb) (Brewster, *et al.* 2007). Cyclodextrins are cyclic oligosaccharides that are derived from starch and are composed of  $\alpha$ -(1,4)-linked  $\alpha$ -D-glucopyranose units. The classification of CDs is related to the number of glucose units, with  $\alpha$ ,  $\beta$ ,  $\gamma$  CDs consisting of six, seven or eight units, respectively. CDs have a distribution of polarity throughout the molecule, with polar hydroxyl groups on the outer rim of the characteristic “torus” shape and less polar oxygen and hydrogen groups on the inside (Brewster, *et al.* 2007). As a result, hydrophobic drugs can complex with the hydrophobic inner core whilst the outer hydrophilic groups facilitate the aqueous solubility of the entire complex, thus potentially enhancing oral drug absorption. A critical factor for enhanced bioavailability with CDs is the drug’s off rate from the complex. If a drug is bound too strongly to the hydrophobic inner core, the solubilized drug substance will pass through the GI tract staying bound to the CD (Brewster, *et al.* 2008). As the molecular weight of the CD-drug complex is much higher than that of the drug substance, it cannot be absorbed through the gut wall and the drug would be excreted as the complex with the feces (Ditzinger, *et al.* 2019).

### ***Particle Size Reduction***

In accordance with the Noyes-Whitney equation, reduction of particle size can increase dissolution rate of a drug (Noyes and Whitney, *et al.* 1897) Therefore, especially for DCS IIa drugs, reduction of particle size is a viable and often used technique to overcome limited oral absorption. Historically, particle size reduction has referred to micronization of drugs, in which drug particles are deconstructed into smaller particles *via* mechanical activation with milling approaches including, but not limited to ball milling, wet milling and cryo-milling. Recent technologies enable the production of particles on the nanoscale (Khadka, *et al.* 2014). Such nanosizing approaches can be described as either “top-down” or “bottom-up” depending on the method employed. The top down approach is analogous to the micronization approaches, in which specialized milling approaches such as pearl milling or high-pressure homogenization are applied to deconstruct micron-sized particles into nanoparticles that enhance dissolution and thus improve absorption (Khadka, *et al.* 2014). The “top-down” approach, by contrast, engineers the particle

properties during the precipitation process, such that nanoprecipitates are generated (Khadka, *et al.* 2014). For compounds whose high crystal lattice energy is limiting to solvation (e.g. brick-dust molecules) nano-suspensions are attractive alternatives to solubilization techniques (Koehl, *et al. et al.* 2019). This is especially the case for those compounds whose solubility is limited in both polar and apolar solvents.

A key difference between micronization and nano-sizing is the necessity to stabilize nanoparticles to prevent agglomeration and a return to micron-sized particles. Typically, surfactants or polymers can be incorporated to ensure particles remain on the nanoscale (Ditzinger, *et al.* 2019). Long-term stability can be an issue with nano-suspensions, which limit their application. However, they are especially useful in pre-clinical trials where large doses of drug candidates are required but have also found application in approved formulations.

### ***Formulation Technologies for Amorphous Systems***

Solubility and dissolution of a poorly soluble drug can be enhanced by altering the solid-state form of a drug substance to the amorphous form. The amorphous state is defined by a lack of long-range order, in contrast to a crystal structure (Williams, *et al.* 2013). Without the need to disturb a crystal lattice, the energy required to break the intermolecular interactions in the amorphous phase is significantly reduced. Therefore, creating a solution of an amorphous solid is inherently energetically more favorable than for the corresponding crystalline solid.

Energetically speaking, the amorphous form is in a state of higher energy (**Figure 4**) and is therefore unstable or metastable and unlikely to remain amorphous over the duration of the shelf-life of the product (Taylor, *et al.* 2016). Amorphous drugs are therefore generally not used directly in drug products without an additional stabilizing component (Williams, *et al.* 2013).

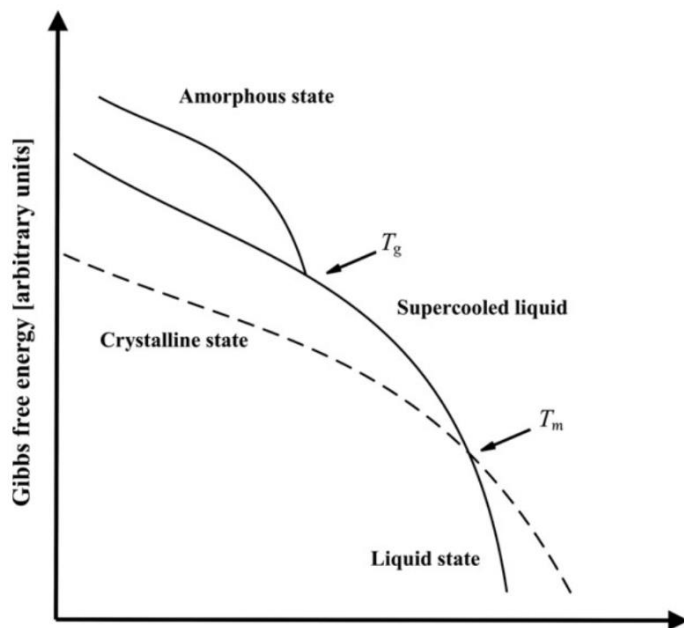


**Figure 4.** Gibbs Free Energy curve demonstrating the excess energy present in the amorphous state. Reproduced with permission from the publisher (Price, *et al.* 2018).

Therefore, the critical issue for successful amorphous formulation is stabilization of the amorphous form. Historically, this has been achieved through formulation in amorphous solid dispersions (ASD) (Ditzinger, *et al.* 2018). According to definition, an ASD is any formulation in which amorphous drug substance is distributed throughout a carrier, typically a polymer. For optimal stability, it is desirable that the drug is distributed homogeneously throughout the carrier, allowing stabilization of the amorphous form in the polymer matrix (Williams, *et al.* 2013).

### 2.2.2 Preventing Precipitation from the Supersaturated State

Collectively, the combination of a supersaturating formulation technology with a precipitation inhibitor is known as the “Spring and Parachute” model. The formulation generates the “spring” of supersaturation leading to a fast and high increase of drug concentration in solution, while the precipitation inhibitor acts



as a “parachute” by slowing the system’s inevitable return to thermodynamic concentrations (Guzman, *et al.* 2004) (Figure 5).

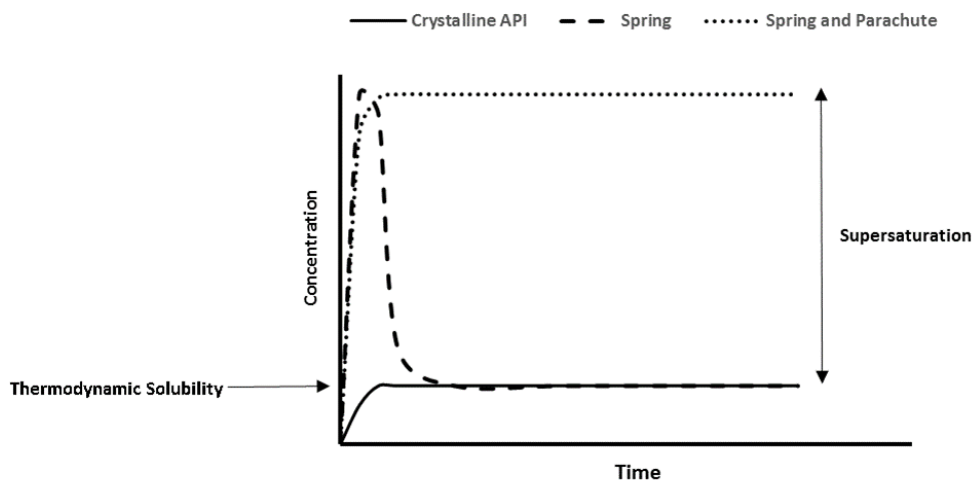


**Figure 5.** The Spring and Parachute model. A common formulation approach where a ‘spring’ generates supersaturation and a ‘parachute’ prevents precipitation. Reproduced with permission from the publisher (Price, *et al.* 2018).

Ultimately, the success of supersaturating formulations is related to the appropriate selection and combination of precipitation inhibitors, i.e. the “parachute”, with the selected “spring” formulation technology. To ensure this, a thorough understanding of the underpinnings of precipitation and precipitation inhibition is essential.

### **Precipitation**

Precipitation or crystallisation of supersaturated drug from solution is an energy driven process related to the excess energy of a supersaturated solution that has reached a critical labile point where phase separation of solute molecules occurs instantaneously and without external influence (Mullin, *et al.* 2000). This process is a function of concentration, temperature and composition of the solution. A higher

concentration of solute increases the lability of the system, whereas an increase in temperature decreases the lability of the system (**Figure 6**).

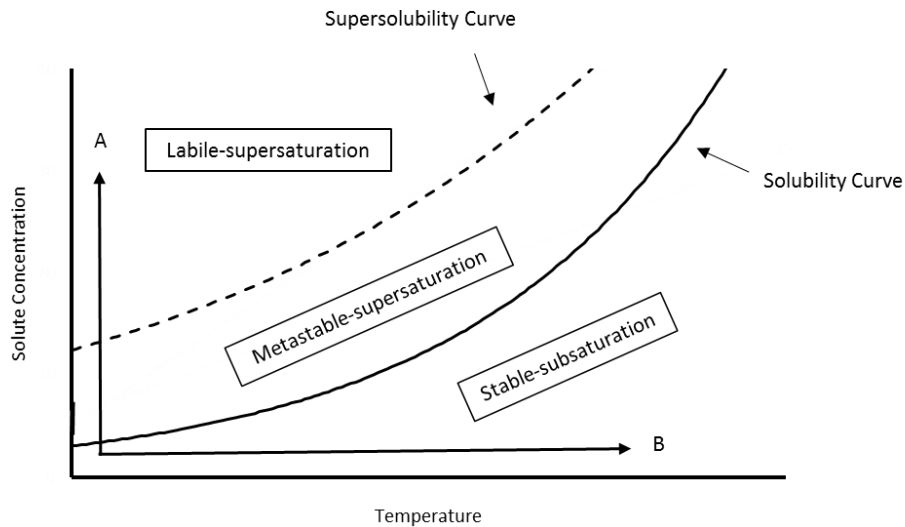


**Figure 6.** Solubility–supersolubility diagram (Mullin, 2007). A more labile solution is obtained with a higher drug concentration (arrow A). A more stable solution is obtained by the increase in temperature (arrow B). Reproduced with permission from the publisher (Price, *et al.* 2018).

The process of crystallization or precipitation occurs in two key stages: a) nucleation and b) crystal or particle growth (Mullin, *et al.* 2000). For crystal and particle growth, a critical nucleus consisting of solute molecules must first be attained. Nucleation and particle growth can occur at the same time and at different rates, depending on the system and stage of precipitation (Warren, *et al.* 2010). The exact mechanism of nucleation remains unclear but can occur spontaneously or can be induced. It can be induced with or without seed crystals and in the presence or absence of a cluster surface, e.g. foreign particles or surface defects. In any case, nucleation can be described mathematically by classical nucleation theory (CNT) (Mullin, *et al.* 2000) (**Equation 5**).

$$J = A \exp\left(-\frac{B}{\ln^2 S}\right) \quad \text{(Equation 5)}$$

Where  $J$  is the rate of nucleation,  $S$  is the supersaturation,  $A$  is a nucleation constant,  $B$  is a thermodynamic value related to the energy cost of nucleation. Both  $A$  and  $B$  are considered fixed for practical purposes, which underscores the importance extent of supersaturation play in the precipitation processes.

Crystal growth can occur once critical nuclei are formed. Various mechanistic hypotheses have been proposed for crystal growth, but the predominant model is the Adsorption Layer Theory (Mullin, *et al.* 2000). In this model, it is assumed that a layer of adsorbed molecules exists on the growing crystal or precipitate. This layer exists in equilibrium with the bulk solution. The model states that the solid precipitate will only grow if the solute molecules in solution can adsorb to a site on the growing nucleus or particle which represents an energy minimum (Warren, *et al.* 2010). These contacts are typically found at imperfections or kinks on the growing crystal or particle surface. This process results in the formation of the thermodynamically favourable polymorph over time, but kinetic forms may arise first. This phenomenon is known as Ostwald's rule of stages, which indicates that the fastest forming polymorph does not represent the thermodynamic stable polymorph but rather that polymorphs are obtained in the order of decreasing energy (Nyvlt, *et al.* 1995).

For supersaturating formulations, it is critical to prevent both nucleation and crystal growth to allow for increased absorption.

### ***Precipitation Inhibition***

Typically, inhibition of precipitation from the supersaturated state is achieved by incorporating polymers into the formulation (Warren, *et al.* 2010). These polymeric "precipitation inhibitors" have seen widespread usage in the literature, with the most common polymers used including cellulose derivatives, methacrylates and polyvinylpyrrolidones (Warren, *et al.* 2010). This kinetic effect is related to polymeric interference with nucleation and crystal growth through interaction with *both* the supersaturated drug and the aqueous environment (Xu, *et al.* 2013). These interactions generally prevent the adsorption of

drug molecules onto the growing crystal face and therefore precipitation is arrested. As previously alluded to, this is a kinetic effect and usually has no impact on the thermodynamic saturation concentrations of the system. In some systems, the polymer may also have a co-solvent effect, thus contributing to both a thermodynamic and kinetic stabilization of the drug in solution (Warren, *et al.* 2010).

For kinetic inhibition, interaction between the drug and polymer is key. Specifically, polymers can interact with the drug *via* hydrogen bonds, polar, or dispersion forces, to varying degrees (Price, *et al.* 2018; Price, *et al.* 2019; Warren, *et al.* 2010; Brouwers *et al.* 2009; Gao, 2 *et al.* 2012) Although extensive work has been carried out on the application and screening of precipitation inhibition, the exact mechanism of interaction remains unclear. In any case, it is likely to vary from system to system. More broadly, PI effectiveness has been related to properties such as temperature, molecular weight, polarity and hydrogen bonding capabilities of both the drug and polymer (Warren, *et al.* 2010). In addition to the more general discussion about potential properties relating to effective inhibition, some modes of action have also been proposed. For example, the extent of polymer adsorption onto the surface of the growing crystal is often discussed as one of the critical factors for successful precipitation inhibition. This adsorption introduces steric hindrance, which disrupts the diffusion of supersaturated drug through the solid-liquid boundary layer to the surface of the growing crystal (Brouwers, *et al.* 2009). In addition, the crystal conformation can be disrupted by polymers in solution. Also discussed, is the effect of polymers on the surface tension and viscosity of the solution, which can reduce the diffusion of the drug to the crystal growth sites (Warren, *et al.* 2010). Thus, an important factor to consider is the effect of the polymer on solution viscosity. The effect of the viscosity is two-fold: first, an increased viscosity results in a slower solute diffusion coefficient and second, an increased viscosity is often related to an increased number of potential binding sites for polymer-drug interaction. However, even considering the potential PI mechanism, there are still differing conclusions in the literature. Some studies show polymer hydrophobicity to be a critical property in precipitation inhibition (Prasad, *et al.* 2016), some suggest that

hydrogen bond interactions play a pivotal role (Warren, *et al.* 2010), while yet others propose that polymer surface coverage is an important factor (Schram, *et al.* 2015). Ultimately, although many precipitation inhibition mechanisms have been proposed, it remains unclear to what extent these factors effect precipitation inhibition. In all likelihood, multiple precipitation inhibition mechanisms contribute to the observed effect, with the balance depending on the specific properties of both the drug substance and the precipitation inhibitor.

### ***Selection of Precipitation Inhibitors***

Given the large number of substances that can act as PIs reported in the literature, various screening methods to select drug-PI combinations have been developed. Invariably, these screening methods involve the generation of supersaturation in combination with a variety of analytical techniques that can determine the rate and extent of precipitation of a drug over time in many samples. A wide variety of methods to generate supersaturation are reported in the literature, including use of amorphous solids, shifts in temperature or pH, use of pharmaceutical salts or solvent shifts. (Warren, *et al.* 2010) Of these techniques, the most common is the solvent shift method. This involves dissolving the drug in high concentrations in a favourable organic solvent which is miscible with water (e.g. DMSO). A small volume of this solution is added to an aqueous phase to generate a supersaturated state. Analytical techniques such as UV spectroscopy, HPLC or nephelometry can be used to assess drug concentration or amount of precipitate over time, which in turn gives information about the efficiency of the inhibitor being studied. (Warren, *et al.* 2010)

For example, during a drug development campaign, two Johnson and Johnson drugs, A and B, required addition of PIs to a surfactant-based bioenabling formulation that generated supersaturation but did not itself prevent precipitation (Creasey, *et al.* 2011). In order to select an appropriate PI candidate, supersaturation was generated in the presence of a range of potential PIs for both compounds, and then

HPLC was employed to determine residual drug concentration in solution after 24 hours. This screening platform identified Pluronic F127 as the most efficient PI (Creasey, *et al.* 2010; Li, *et al.* 2012). This type of experimental set-up is particularly attractive when pursuing surfactant-based formulations, as the methodology can simultaneously screen surfactant systems as well as PIs. In this respect, one can simultaneously assess the extent of the supersaturation generated by the surfactant and how sustained the profile is in the presence of PIs (Li, *et al.* 2012). The main drawback of the given experimental design is that barely any information is obtained about the kinetics of drug precipitation in the presence of polymer when using a single time point.

An alternative screening platform which utilises off-line chromatography was reported by Petrusevska and co-workers (Petrusevska, *et al.* 2013). In this study, supersaturation was generated for fenofibrate and carbamazepine, in the presence of various potential PIs, using a solvent shift from DMSO into aqueous buffer. Experiments were carried out in 96 well plates. The plates were sealed and incubated, with samples being taken at 30, 90, 180 and 360 minutes, filtered and analysed with UPLC for drug content. This method provides more information about which PI is the most efficient over physiologically relevant time scales. In this study, it was found that surfactants such as Tween® and Cremophor® were most efficient for fenofibrate, whereas for carbamazepine cellulose derivatives such as HPMC and HPMCAS were the optimal systems (Petrusevska, *et al.* 2013).

Despite the limited time-resolution that such 'off-line' methods can provide, they can be very reliable when it comes to predicting performance of the final formulation. Yamashita and colleagues performed a similar high-throughput screen for a range of surfactants, oils and polymers in combination with itraconazole. The screen demonstrated that HPMCAS was the most efficient PI. When itraconazole-HPMCAS spray-dried dispersions were manufactured and compared to the commercially available Sporanox® HPMC-based dispersions, the HPMCAS-based formulations significantly outperformed the commercial product in dissolution tests (Yamashita, *et al.* 2011).

Analytical techniques that offer *in situ* analysis are very appealing as they can provide a real-time picture of supersaturation-precipitation behaviour. It was demonstrated by Warren and colleagues that utilising *in situ* nephelometry, a technique that uses light-scattering to measure particle concentration, can provide an indirect measure of drug concentration in a high-throughput screen (Warren, 2010). In this instance, the nephelometer measures light scattering of the samples, which directly relates to the total concentration of particular matter in suspension and drug in solution. A large number of species was screened for precipitation inhibition using a plate reader, according to which the researchers were able to sort the PIs into three distinct groups. (Warren, *et al.* 2010)

Chauhan and co-workers expanded upon this technique by utilising an *in-situ* UV probe that provided time-resolved information about the concentration of drug in solution (Chauhan, *et al.* 2014). This method was used to assess the interactions between indomethacin and a wide range of polymers. After a solvent-shift to generate supersaturation, the turbidity and drug concentration were measured using an *in-situ* UV-probe. The time-resolved data so obtained enable further calculation and processing. Chauhan and colleagues subsequently used these data to calculate the precipitation induction time (time delay between supersaturation and precipitation) as well as the rate of precipitation, which indicated that PVP, HPMC and Eudragit E100 increased induction time and decreased the precipitation rate. Subsequently, successful solid dispersions of indomethacin-PVP, indomethacin-HPMC and indomethacin-Eudragit® E100 were developed (Chauhan, 2014). A similar study with dipyridamole was also carried out (Chauhan, *et al.* 2013). The downside of using nephelometry as a screening tool is the difficulty of screening systems that are insoluble. For example, some supersaturating formulations, e.g. mesoporous silica, contain insoluble excipients that would interfere with the light scattering and make analysis difficult.

Recent advances in PI screening have seen the introduction of smaller scale dissolution techniques, such as the  $\mu$ DISS profiler™ apparatus, produced by Pion. The  $\mu$ DISS™ utilises *in situ* UV in combination with liquid handling and can be used to efficiently study supersaturation and precipitation in real-time.

Palmelund and co-workers studied six different poorly soluble drugs in combination with HPMC or PVP at different degrees of supersaturation using this technique (Palmelund, *et al.* 2016). They were able to successfully discriminate between innate solubility enhancements of the polymers vs. precipitation inhibition. For the BCS IV drug, aprepitant, for example, both polymers increased solubility by approximately 150 %, with the solubility being the same in both polymer systems. There were distinct differences in the curves observed in the real-time data display, with HPMC showing a more pronounced effect on the dissolution profile than PVP. Therefore, for this system, HPMC acted as a more effective PI than PVP (Palmelund, *et al.* 2016). According to the authors, the  $\mu$ DISS profiler™ is particularly appealing as the experimental protocols can be easily standardised to reduced inter- and intra-lab variability. (Palmelund, 2016). The  $\mu$ DISS profiler™ has also been applied to investigate the effect of prandial state and PIs on the precipitation of supersaturated zafirlukast (Madsen, *et al.* 2016).

### **3. Recent Advances in Supersaturating Formulations**

#### **3.1 Mesoporous Silica: An Emerging Formulation Technology**

Mesoporous silica is a relatively novel formulation option for poorly soluble drugs, with no examples of approved drug products and only one proof of concept study in man (Bukara, 2016). However, there has been a dramatic increase in interest around mesoporous silica-based formulations in the past decade. A summary of all mesoporous silica formulations reported to date is shown in **Table 1**.

Mesoporous silica refers to a variety of materials synthesized to produce a SiO<sub>2</sub> mesoporous structures. (Limnell *et al.*, 2011) Mesoporous silica can be ordered or non-ordered (Barbe *et al.* 2008; Kresse *et al.* 1992). The former include classic structures such as SBA-15 and MCM-41, (Mellaerts *et al.* 2010) whilst the latter include novel, proprietary excipients manufactured by drug delivery specialists, such as Parteck SLC® (Merck Milipore) (Laine *et al.*, 2016; O'Shea *et al.* 2017) and Neusilin™ (Fuji Chemical) (Khanfar and Al-Nimry, 2017). Such materials have a wide range of applications, including tissue engineering



(Vallet-Regi *et al.*, 2010), catalysis (Saad, *et al.* 2017), chromatography (Majors, *et al.* 1972), adsorbents in environmental sciences (Bhatnagar *et al.*, 2010) and drug delivery for poorly soluble drugs (Wang, *et al.* 2009). With respect to drug delivery applications, it has been widely reported that mesoporous silica can act as a dissolution enhancer by 'trapping' drug in the amorphous form within the mesoporous network (O'Shea, *et al.* 2017; Laine, *et al.* 2016; Van Speybroeck, *et al.* 2010; Vialpando, *et al.* 2011; Dressman, *et al.* 2010; Xu, *et al.* 2013).

For ordered mesoporous silica, a template synthesis process is carried out, in which pores are constructed with consistent pore size and geometry. For unordered mesoporous silica, pore size and geometry are not controlled. An exhaustive comparison of the advantages and disadvantages of ordered vs. unordered mesoporous silica is lacking in the literature. However, the costs of producing ordered mesoporous silica limits their applicability from an economic perspective. Mesoporous silica, by definition, are porous in nature with pores from between 2-50 nm in diameter (McCarthy, *et al.* 2016). However, in line with their usual intended application, pore sizes on the lower end of this range are more common. This porosity results in a high surface area, up to 1000 m<sup>2</sup>/g, which is important for loading drugs inside the porous network.

There are various methods of loading crystalline drugs onto mesoporous silica. The methods can be grouped into three categories: solvent-based (e.g. Laine *et al.* 2016), mechanical activation (e.g. Qian and Bogner, 2011) and vapour-mediated (e.g. Gignone, *et al.* 2014). A thorough overview of the loading methods of poorly soluble drug onto mesoporous silica is beyond the scope of this thesis, but the interested reader is referred to a number of publications that provide a good overview of the different routes to drug-loaded silica (McCarthy, *et al.* 2016; Wantanabe, *et al.* 2000; Qian and Bogner, 2011; Hillerstrom, *et al.* 2014; Limnell, *et al.* 2011).

Of the methods described in the literature, the solvent-based approach is most commonly employed. This can be attributed to the poor loading efficiencies and time-consuming processes involved in the solvent-free loading methods (Qian and Bogner, 2011). The solvent approaches can be grouped into two main categories: solvent impregnation and incipient wetness. During the solvent impregnation loading approach, the drug is dissolved in an organic solvent and the solution is added to mesoporous silica. Adsorption of the drug onto the silica is initiated through mechanical agitation or sonication of the slurry. Finally, the solvent is removed, which can be achieved using a number of methods including vacuum drying, spray drying, lyophilization or rotary evaporation. (Laine, *et al.* 2016; Wei, *et al.* 2017; Limnell, *et al.* 2011; Meer, *et al.* 2013). Incipient wetness involves the steady addition of small volumes of a concentrated solution of the drug in an organic solvent onto the heated silica, such that the full amount of solvent is adsorbed into the network and then rapidly evaporated, leaving the drug within the pores (O'Shea 2017; Dressman, *et al.* 2015). Both methods result in a drug-loaded silica, in which the previously crystalline drug substance is now amorphous or molecularly dispersed on the surface of the silica. This can be confirmed with analytical methods such as DSC or PXRD.

The theoretical maximum drug content that can be loaded onto mesoporous silica is dependent on the surface area (Vallet-Regi, *et al.* 2007), pore volume (Wang *et al.* 2012) and pore geometry of the silica (Heikkila, *et al.* 2007) with potential values as high as 75% (w/w drug/silica) reported in the literature (Wei, *et al.* 2017). Experimentally, however, such high drug loadings are not achievable, with residual crystallinity often observed in drug-loads exceeding 50% (wt/wt) (Wei, *et al.* 2017). Indeed, most cases of drug-loaded silica in the literature do not exceed 40% loading, in line with other amorphous formulation technologies (**Table 1**).

**Table 1.**

Drugs for which formulations based on mesoporous silica have been elaborated and characterized

| Compound      | Ref.                            | Mwt     | BCS Class | Log P | Tg (K)  | Ref.                        | Tm (K) | Tm/Tg | pKa (acid) | pKa (base) | Loading (%) |
|---------------|---------------------------------|---------|-----------|-------|---------|-----------------------------|--------|-------|------------|------------|-------------|
| Atorvastatin  | Maleki<br>et al. (2016)         | 558.64  | II        | 5.39  | 685.325 | Shete<br>et al. (2010)      | 433.5  | 0.63  | 4.33       | -          | 20          |
| Valsartan     | Biswas<br>(2017)                | 435.519 | III       | 5.27  | 349.5   | Skotnicki<br>et al. (2013)  | 390    | 1.12  | 4.37       | -          | 43.25       |
| Carvedilol    | Hu<br>et al. (2012)             | 406.482 | II        | 3.42  | 312.53  | Wyttenbach<br>et al. (2016) | 388    | 1.24  | -          | 8.74       | 41.6        |
| Furosemide    | Ambrogi<br>et al. (2012)        | 330.745 | IV        | 1.75  | 374.7   | Nielsen<br>et al. (2015)    | 479.5  | 1.28  | 4.25       | -          | 30          |
| Glibenclamide | Van Speybroeck<br>et al. (2011) | 494.004 | II        | 3.79  | 345.4   | Bartsch et al. (2005)       | 442.5  | 1.28  | 4.32       | -          | 30          |
| Ezetimibe     | Kiekens et al.<br>(2012)        | 409.4   | II        | 4.56  | 336.35  | Knapik et al. (2014)        | 436.5  | 1.30  | -          | -          | 20          |

**Table 1. (contd.)**

Drugs for which formulations based on mesoporous silica have been elaborated and characterized

| Compound     | Ref.                       | Mwt     | BCS Class | Log P | Tg (K) | Ref.                         | Tm (K) | Tm/Tg | pKa (acid) | pKa (base) | Loading (%) |
|--------------|----------------------------|---------|-----------|-------|--------|------------------------------|--------|-------|------------|------------|-------------|
| Celecoxib    | Laine<br>et al. (2016)     | 381.373 | II        | 4.01  | 331.1  | Wytttenbach<br>et al. (2016) | 431.5  | 1.30  | -          | -          | 33          |
| Felodipine   | Hu<br>et al. (2015)        | 384.259 | II        | 3.44  | 317.9  | Wytttenbach<br>et al. (2016) | 418.5  | 1.32  | -          | 5.39       | 25          |
| Itraconazole | Mellaerts<br>et al. (2008) | 705.64  | II        | 7.31  | 332.7  | Wytttenbach<br>et al. (2016) | 439.7  | 1.32  | -          | 3.7        | 25          |
| Indomethacin | Wang<br>et al. (2010)      | 357.79  | II        | 3.53  | 319.6  | Wytttenbach<br>et al. (2016) | 424.5  | 1.33  | 3.8        | -          | 20          |
| Curcumin     | Hartono<br>et al. (2016)   | 368.38  | II        | 3.28  | 343    | Pawar<br>et al. (2012)       | 456.5  | 1.33  | -          | -          | 25          |

**Table 1. (contd.)**

Drugs for which formulations based on mesoporous silica have been elaborated and characterized

| Compound     | Ref.                            | Mwt     | BCS Class | Log P | Tg (K) | Ref.                        | Tm (K) | Tm/Tg | pKa (acid) | pKa (base) | Loading (%) |
|--------------|---------------------------------|---------|-----------|-------|--------|-----------------------------|--------|-------|------------|------------|-------------|
| Telmisartan  | Aftab Alam<br>et al. (2013)     | 514.617 | II        | 6.04  | 401.4  | Lepek<br>et al. (2013)      | 535.5  | 1.33  | 3.65       | 6.13       | 37.5        |
| Ketoprofen   | Abd-Elrahman<br>et al. (2016)   | 254.281 | II        | 3.61  | 270.58 | Wyttenbach<br>et al. (2016) | 367.5  | 1.36  | 3.88       | -          | 20          |
| Griseofulvin | Salonen<br>et al. (2005)        | 352.766 | II        | 2.17  | 361.5  | Zhu<br>et al. (2010)        | 493.5  | 1.37  | -          | -          | 16.5        |
| Fenofibrate  | Bukara<br>et al. (2016)         | 360.831 | II        | 5.28  | 254.8  | Wyttenbach<br>et al. (2016) | 354    | 1.39  | -          | -          | 30          |
| Nifedipine   | Xu<br>et al. (2013)             | 346.335 | II        | 1.82  | 320.3  | Wyttenbach<br>et al. (2016) | 446.5  | 1.39  | -          | 5.33       | 20          |
| Cinnarizine  | Van Speybroeck<br>et al. (2009) | 368.514 | II        | 5.88  | 281.1  | Wyttenbach<br>et al. (2016) | 392.5  | 1.40  | -          | 8.4        | 20          |

**Table 1. (contd.)**

Drugs for which formulations based on mesoporous silica have been elaborated and characterized

| Compound       | Ref.                                  | Mwt     | BCS Class | Log P | Tg (K) | Ref.                               | Tm (K) | Tm/Tg | pKa (acid) | pKa (base) | Loading (%) |
|----------------|---------------------------------------|---------|-----------|-------|--------|------------------------------------|--------|-------|------------|------------|-------------|
| Phenylbutazone | Van Speybroeck<br><i>et al</i> (2009) | 308.374 | II        | 4.14  | 270.75 | Wyttenbach<br><i>et al.</i> (2016) | 378.5  | 1.40  | 5.13       | -          | 20          |
|                | Danazol                               | 337.5   | II        | 3.46  | 352    | Alhalaweh<br><i>et al.</i> (2015)  | 498.5  | 1.42  | -          | -          | 20          |
| Flurbiprofen   | Tozuka<br><i>et al.</i> (2005)        | 244.261 | II        | 3.94  | 268.7  | Wyttenbach<br><i>et al.</i> (2016) | 384    | 1.43  | 4.42       | -          | 30          |
|                | Hesperidin                            | 610.565 | II        | 2.68  | 346.9  | Shete<br><i>et al.</i> (2014)      | 501    | 1.44  | -          | -          | 28.6        |
| Etravirine     | Mellaerts<br><i>et al.</i> (2013)     | 435.28  | IV        | 5.54  | 372.5  | Weuts<br><i>et al.</i> (2010)      | 538.5  | 1.45  | -          | 4.13       | 20          |

**Table 1. (contd.)**

Drugs for which formulations based on mesoporous silica have been elaborated and characterized

| Compound      | Ref.                    | Mwt      | BCS Class | Log P | Tg (K) | Ref.                        | Tm (K) | Tm/Tg | pKa (acid) | pKa (base) | Loading (%) |
|---------------|-------------------------|----------|-----------|-------|--------|-----------------------------|--------|-------|------------|------------|-------------|
| Carbamazepine | Wang<br>et al. (2012)   | 236.269  | II        | 2.77  | 329.5  | Li<br>et al. (2000)         | 478.5  | 1.45  | -          | -          | 20          |
| Lovastatin    | Khafar<br>et al. (2017) | 404.54   | II        | 3.9   | 301.5  | Elder<br>et al. (1990)      | 448    | 1.49  | -          | -          | 36.26       |
| Acetaminophen | Hacene<br>et al. (2016) | 151.163  | III       | 0.91  | 298.1  | Wyttenbach<br>et al. (2016) | 443.5  | 1.49  | -          | -          | 18.8        |
| Aceclofenac   | Kumar<br>et al. (2014)  | 353.0216 | II        | 3.88  | 284.8  | Wyttenbach<br>et al. (2016) | 424.5  | 1.49  | 3.44       | -          | 50          |
| Ibuprofen     | Zhang<br>et al. (2011)  | 206.29   | II        | 3.84  | 230.7  | Wyttenbach<br>et al. (2016) | 349.5  | 1.51  | 4.85       | -          | 32.6        |

**Table 1. (contd.)**

Drugs for which formulations based on mesoporous silica have been elaborated and characterized

| Compound    | Ref.                        | Mwt     | BCS Class | Log P | Tg (K) | Ref. | Tm (K) | Tm/Tg | pKa (acid) | pKa (base) | Loading (%) |
|-------------|-----------------------------|---------|-----------|-------|--------|------|--------|-------|------------|------------|-------------|
| Pretomanid  | Xia<br>et al. (2014)        | 359.258 | -         | 3.11  | -      | -    | 140    | N/A   | -          | -          | 40.4        |
| Cilostazol  | Wang<br><i>et al</i> (2014) | 369.46  | II        | 3.31  | -      | -    | 160    | N/A   | -          | -          | 25          |
| Resveratrol | Summerlin<br>et al. (2016)  | 228.247 | II        | 3.4   | -      | -    | 254    | N/A   | -          | -          | 20          |
| Mefloquine  | Letchmanan<br>et al. (2017) | 378.312 | II        | 4.11  | -      | -    | 243    | N/A   | -          | 9.46       | 33          |
| Atazanivir  | Xia<br>et al. (2012)        | 704.856 | II        | 4.54  | -      | -    | 195    | N/A   | -          | 4.42       | 32.8        |



The loading process can be considered from an energetic perspective: the surface of the silica has high energy and a large area. Therefore, the loading and uptake of drug onto the surface allows the system to lose excess energy, thus decreasing the Gibbs energy of the system. At the moment, there is insufficient information in the literature to state definitively how the drug is taken up within the porous network, and the mechanism is likely to vary with the chemical structure of the drug substance. Some hypotheses include: hydrogen bond interactions (Wang, *et al.* 2010; Kinnari, *et al.* 2011) , hydrophobic interactions (Xu, *et al.* 2013), capillary action (Yanagihara, 2013) and ionic interactions (Atkin, *et al.* 2003; Turku, *et al.* 2007), although the latter depends on the silol groups on the surface of the silica to be in the anionic state, which may not be the case under physiological or ambient conditions.

One of the key differentiators of mesoporous silica from alternative amorphous formulation approaches is the superior stability that can be introduced *via* nanoconfinement within the mesoporous structure. High stability of the amorphous or molecularly dispersed drug is generally obtained once it is adsorbed into the porous network of the silica. The work of Muller and co-workers demonstrated amorphous stability at ambient and accelerated conditions for 30 different mesoporous silica formulations (Muller, *et al.* 2013).

This enhanced stability is especially attractive for so-called “GFA-1” or glass-forming ability 1 drugs. The glass forming ability of a drug is based on the overall propensity of a molecule to re-crystallize. First described by Avramov in 2003 as “the propensity of a liquid to vitrify upon cooling” (Avramov, *et al.* 2003), the GFA of a molecule can be determined experimentally based on a DSC method developed by Baird *et al.* (Baird, *et al.* 2010). In this approach, drug is placed in a DSC pan and subjected to a melt-cool-melt cycle. In this cycle, the DSC curves are examined for any crystallization behaviour. For GFA-3 compounds, no crystallization is observed at any point, indicating good stability in the amorphous form. For GFA-2 compounds, no crystallization is observed in the first melt-cool cycle, but when additional energy is supplied to the system in the second melt cycle, crystallization is observed, indicating a moderate stability

in the amorphous form. For GFA-1 compounds, crystallization is observed in the first melt-cool cycle, indicating that even when the system is decreasing in energy, crystallization is favoured. This so-called “cold crystallization” is indicative of poor stability in the amorphous form. GFA-1 compounds are therefore very challenging to formulate in the amorphous form. A recent study by Wytttenbach and Kuentz confirmed the level of challenge, as only 6.25% of commercially available amorphous formulations fall into this class (Wytttenbach *et al.* 2017).

Recent work has demonstrated that mesoporous silica can successfully stabilize such compounds whereas traditional polymer-based technologies are unsuccessful (Ditzinger and Price, 2019). Furthermore, it has been shown that molecular mobility is significantly reduced, regardless of moisture or temperature, which is a critical consideration when carrying out the required ICH Q1 stability studies during drug development. Brás and colleagues demonstrated how adsorption and nanoconfinement of ibuprofen onto mesoporous silica resulted in a significant reduction of all known types of molecular mobility (Brás *et al.*, 2014). Most interestingly, the Johari-Goldstein relaxation, a type of molecular flexibility which has been related to physical instability of the amorphous form, was reduced (Brás *et al.*, 2014; Mehta *et al.*, 2016). Similar to the work by Mehta and colleagues, this work focused on a good glass forming drugs (GFA-3). However, follow-on work also demonstrated reduction in molecular mobility for the successful stabilization of the very poor glass former Menthol (GFA-1), which has a glass transition temperature of -54.3 °C (Cordeiro *et al.*, 2017). In the study, Cordeiro and colleagues successfully stabilized amorphous menthol due to nanoconfinement within mesoporous silica. This stabilization was related to a decrease in molecular mobility associated with  $\alpha$  and  $\beta$  relaxation, which correspond to free-range mobility and molecular flexibility, respectively, and are critical for crystallization. Furthermore, a new type of molecular mobility, S-type, was observed, which was related to hindered mobility and nanoconfinement in the pore and was significantly slower than standard molecular mobility events (Cordeiro *et al.*, 2017). As a result, drug-loaded silica can often be stored in open containers and at elevated temperature and/or humidity.

Upon delivery to an aqueous medium, such as the GI tract, the drug is displaced from the mesoporous network and has the potential to generate a supersaturated solution. Although yet to be extensively studied in the literature, the release mechanism can likely be described using diffusion kinetics. Simplified, upon administration to an aqueous environment, there is a diffusion of water into the porous network *via* capillary action. This in turn solubilizes the loaded drug, which generates a concentration gradient between the inside of the silica and the external medium. This in turn drives release of drug *via* diffusion along said concentration gradient, generating supersaturation and potentially increased absorption (Xu, *et al.* 2012).

Broadly speaking, this kind of release behavior can be described by the classical Higuchi Equation (**Equation 6**), which was proposed by Higuchi in 1961 to explain the release behavior of drug from thin ointment films (Higuchi, *et al.* 1961). Further work and modifications allowed this equation to be expanded to describe the release of any drug adsorbed or entrapped within an inorganic and insoluble matrix into an external medium *via* diffusion (Siepmann and Peppas, 2011) as follows:

$$M_t = A\sqrt{2c_{ini}Dc_s t} \quad \text{(Equation 6)}$$

where  $M_t$  is the amount of drug released from the inorganic carrier,  $A$  is the surface area available for release,  $c_{ini}$  is initial drug concentration in the carrier,  $D$  the diffusion coefficient of drug in the insoluble carrier and  $c_s$  is the maximum (saturation) concentration of the drug in the carrier.

Based on the Higuchi equation, the release of drug from mesoporous carriers can be described as a diffusion-driven process that, similarly to the loading process, is dependent on pore surface area, pore volume and pore morphology. Indeed, there have been a number of examples in the literature where Higuchi diffusion kinetics successfully predicted and modelled release of ibuprofen from mesoporous materials (Andersson, *et al.* 2004; Horcajada, *et al.* 2004; Zhao, *et al.* 2008).

Although the Higuchi diffusion model is a good starting point to understand the release behavior of a drug from mesoporous materials, it is not the whole picture. Indeed, in most studies that have attempted to

model release, it has been over-predicted using Higuchi diffusion kinetics (Bathfield, *et al.* 2016; Bouchoucha, *et al.* 2016; Kinnari, *et al.* 2011). The Higuchi equation treats the diffusion process of a drug from the inorganic carrier as a one-step diffusion limited process. In reality, the release of most drugs from mesoporous silica likely follows a two-step dissociation-diffusion process: (1) Dissociation of the drug from the silica surface, which involves breaking interactions between the drug and the silica surface, and creating interactions between the diffused water and the silica surface (hydrogen bond and dipolar interactions), and (2) Diffusion out of the pore. For example, Kinnari and co-workers demonstrated that release of itraconazole from porous silica can be described with the Higuchi equation for about 80 % of drug release, with a significant deviation for the remaining 20 %. In this instance, the first 80 % accounted for physically entrapped drug within the pores, which diffused out of the carrier as previously described. The remaining 20% accounted for itraconazole that was interacting with the carrier *via* H-bonding. Therefore, the release of the final 20 % proceeded *via* the two-step dissociation-diffusion process and did not align with the Higuchi equation (Kinnari, *et al.* 2011).

### **3.2. Mesoporous Silica and Precipitation Inhibitors**

Like other formulations that generate supersaturation, it is essential to prevent precipitation from the supersaturated state for physiological time frames in order to increase oral absorption (Price, *et al.* 2018). The key difference between mesoporous silica and other bio-enabling formulations such as polymeric ASDs is that the silica – unlike excipients used in ASDs - itself does not inhibit precipitation from the supersaturated state (Laine, 2016). Therefore, it is essential to incorporate an additional polymeric excipient to function as a precipitation inhibitor (PI) in mesoporous silica formulations. One crucial difference between precipitation inhibition in mesoporous silica formulations and polymer ASDs is that one is less confined by the formulation process in the selection of the precipitation inhibitor for mesoporous silica formulations. For example, for an HME formulation, the polymer must be able to act as a precipitation inhibitor and

meet the restrictive requirements for successful processing with HME including heat resistance and accessible melting point (Timpe, *et al.* 2007). The same is true for spray-dried dispersions, which require the polymer to be soluble in organic solvents and resistant to the friction and heat generated in the spray-dry process (Timpe, *et al.* 2007). For mesoporous silica, however, the process of loading is simple and requires basic lab equipment, and the available polymer space for PI selection is broader, increasing the likelihood of good performance (Laine, *et al.* 2016). This characteristic of mesoporous silica formulations could be especially beneficial when considering recent advances in understanding precipitation inhibition, where optimal precipitation inhibitors could be combined with mesoporous silica formulations that would be unsuitable for formulation with either spray dry dispersion or hot melt extrusion.

### **3.3. Investigating the Importance of Drug-Polymer Interactions in Precipitation Inhibition**

Recently, there has been an increased interest in understanding the process of precipitation inhibition from a fundamental mechanistic perspective (Warren, *et al.* 2011; Price, *et al.* 2018). Specifically, advanced analytical tools have been used to study the interaction between dissolved, supersaturated drug and precipitation inhibitor on a molecular level. Interactions between drug and polymer has been shown to be the most critical success factor for a precipitation inhibitor system (Price, *et al.* 2018). The following techniques have been used to gain insight into such interactions:

#### **3.3.1 UV-vis Spectroscopy**

UV-vis-spectroscopy has been used more recently to investigate in detail kinetics of precipitation and drug-polymer interactions during precipitation inhibition.

Patel and co-workers applied second-derivative UV-spectroscopy to model the supersaturation and precipitation of indomethacin from supersaturated conditions in a solvent-shift experiment [Include reference]. This approach was able to extract a large amount of information from the system, especially relating to mechanism of precipitation. They found that precipitation of indomethacin was related to diffusion towards the growing crystal face, and that incorporation of a precipitation inhibitor

could interfere with the crystal binding domains of the growing crystal, due to favourable hydrogen bond interactions between the polymers and indomethacin (Patel, *et al.* 2014).

Nie and colleagues used UV-vis spectroscopy as an orthogonal technique to support their mechanistic hypothesis for clofazimine-HPMCP interaction (Nie, *et al.* 2014). This was especially useful as clofazimine is red in both the crystalline and amorphous forms, but a colour shift to purple occurred in the presence of HPMCP in solid dispersions. Qualitatively, this was also observed for mixtures of drug and carboxylic acid analogues (e.g. glacial acetic acid), but not for polymers without carboxylic acids, such as HPMC. It was concluded that the bathochromic shift was associated with a proton-transfer from the carboxylic acid functional group of HPMCP (Nie, *et al.* 2014). In combination with principal component analysis, the drug: PI (w: w) ratio below which no interaction was observed was calculated to be 1:0.5. Using the same approach, it was concluded that the drug: PI ratio at which full protonation of the imine occurs, i.e. the strongest interaction, was at 1:1.5 (Nie, *et al.* 2014). Such information can be valuable in the design and development of PI-based formulations. A similar study was conducted by Misic and co-workers in the investigation of acid-base interactions between the poorly soluble drugs, loratadine and carvedilol, and oleic acid (Misic, *et al.* 2014).

Patel and co-workers also utilized UV-vis spectroscopy in combination with mathematical modelling. This study involved the combination of online second-derivative UV-spectroscopy and modelling using the diffusion reaction model in order to give real-time concentration values and mechanistic insight for indomethacin in supersaturated solutions. This methodology was able to provide a large amount of information about the precipitation behavior, including that at high degrees of supersaturation the precipitation is diffusion limited, which fits in well with the diffusion-reaction model (Patel, *et al.* 2011).

### 3.3.2. FTIR Spectroscopy

Fourier-Transform Infrared (FTIR) spectroscopy is one of the most commonly employed spectroscopic techniques and can provide functional group information based on a molecule's vibrational response to IR light absorption. FTIR spectroscopy is highly attractive from a drug development setting as it can

be employed to study interactions between compounds in complex mixtures. Due to this, FTIR spectroscopy is a good prospect for the investigation of drug-polymer interactions (Gaffney, *et al.* 2012)

For example, Nie and co-workers performed an experiment to determine interactions between clofazimine and HPMCP, which has been previously reported to have very high drug loading capacity in solid dispersions (Nie, *et al.* 2015). IR spectra were analysed in order to identify changes in the vibrational modes of clofazimine and HPMCP in a solid dispersion (Nie, *et al.* 2016). A new peak, at  $3310\text{ cm}^{-1}$  was observed in the IR spectrum of the solid dispersion, which corresponded to the stretching mode of the ionised imine in the clofazimine, protonated by the carboxylic acid groups in the phthalate substituent of the HPMCP due to *in situ* formation of a polymeric, amorphous salt with the drug. Furthermore, a sensitivity analysis showed that at ratios less than 1:0.5 w/w (drug: polymer), this effect was not observed. Additionally, the intensity of the peak increased with increasing HPMCP concentration. This acid-base interaction between HPMCP and clofazimine was further supported by the appearance of peaks at  $1540\text{ cm}^{-1}$  and  $1395\text{ cm}^{-1}$ , which both correspond with the formation of a carboxylate group (Nie, *et al.* 2016). Knowledge about solid-state interactions such of these can be directly correlated to solid-state stability and loading capacity as well as to enhanced precipitation inhibition and supersaturation. Indeed, the combination of HPMCP and clofazimine in a solid dispersion resulted in a 10-fold increase in apparent clofazimine solubility (Nie, *et al.* 2015).

Petrusevska and colleagues also employed FITR spectroscopy to investigate the mechanism of interactions between a successful drug-PI formulation, sirolimus and HPMC, which was developed during a commercial screening platform. Solid dispersions of HPMC and sirolimus demonstrated significant variation from the neat samples of amorphous sirolimus as well as a physical blend. Specifically, the sirolimus peaks at  $1680\text{-}1640\text{ cm}^{-1}$  (C=C) and  $1760\text{-}1670\text{ cm}^{-1}$  (C=O) in the solid dispersion were significantly broader than the pure drug, which the authors concluded was a result of interaction between the two species (Petrusevska, *et al.* 2013b). This interaction was suggested to be

partly responsible for the 2-fold increase in supersaturation and dissolution in the sirolimus-HPMC solid dispersion versus the commercially available Rapamune nanoparticles. Finally, this formulation was used in a clinical pharmacokinetics trial, in which the novel formulation significantly outperformed the commercial formulation, Rapamune. This effect was attributed to the enhanced precipitation inhibition properties of HPMC in the novel formulation (Petrusevska, *et al.* 2013b). This study is a good demonstration of how FTIR can be employed to aid in the development of a precipitation inhibitor formulation from screening to clinical testing.

Another application of FTIR spectroscopy is the characterization of precipitates, which can provide information about the effect of precipitation inhibitors. This was carried out in a recent study by Chavan, in which IR spectroscopy was used to ensure that a range of polymers being studied for precipitation inhibitors did not affect the solid-state phase behaviour (polymorphism) of the drug, nifedipine (Chavan, *et al.* 2016). In this instance, the FTIR spectra of the precipitates for all three polymers (HPMC, PVP and HPC) aligned well with crystalline nifedipine, indicating no polymorphic change was induced by the polymers. This is an important consideration as when the drug does precipitate from the supersaturated condition (precipitation being just a kinetic effect) a change in polymorphism could have unintended pharmacokinetic effects.

### 3.3.3. Raman Spectroscopy

Raman spectroscopy is a technique that uses inelastic (Raman) scattering from laser light sources to study vibrational transitions. This information can be used to ascertain structural information about a sample. Raman spectra are obtained by recording the light scattered by a sample, which can be difficult as a majority of this light will be of similar frequency as the excitation source, so-called Rayleigh scattering. Only a small proportion of light scattered will be shifted based on vibrational transitions in the sample. This is called Stokes- and anti-Stokes-scattering. It is the intensity of the Stokes-shifted light that is plotted against Stokes-shift to create Raman spectra (Rostron, *et al.* 2016). Raman spectroscopy is a technique that is complementary to IR spectroscopy, and has certain advantages.



Similar to IR spectroscopy, Raman spectra can be interpreted to ascertain information about interactions between two species. Unlike IR, this can be carried out in aqueous solution, which has particular advantages when considering drug polymer interactions, where water often plays an essential role (Paudel, *et al.* 2015).

Raut and co-workers utilized an *in-situ* Raman probe, placed inside a dissolution set-up, in order to investigate the precipitation inhibition effect of Vitamin E TPGS on two model drugs, probucol and indomethacin, in self-emulsifying drug delivery systems compared to labrasol formulations. In order to achieve this, the formulations were added to a solution at pH 1.2, followed by a pH shift to pH 6.8. Insertion of a Raman probe into these solutions allowed the collection of time-resolved Raman spectra for both the solid precipitate and the species in solution, which were analyzed for molecular interactions between the drug and excipients. For probucol, Raman peaks were observed at 540 and 1164  $\text{cm}^{-1}$ , corresponding to the hydroxyl groups in the molecules. However, in the presence of Vitamin E TPGS, this peak dropped significantly in intensity, with the peak at 1164  $\text{cm}^{-1}$  disappearing completely. This was due to the interaction of the probucol hydroxyl groups with carbonyl groups of the precipitation inhibitor. These interactions had a profound effect on precipitation, with no precipitation being observable in the presence of Vitamin E TPGS, in spite of the system being supersaturated to 100-fold of the thermodynamic solubility of ProbucoL (Raut, *et al.* 2015).

Similar observations were made for indomethacin, in which a shift was observed from the typical 1689  $\text{cm}^{-1}$  carbonyl peak to a peak at 1680  $\text{cm}^{-1}$  in the presence of Vitamin E TPGS, indicating a hydrogen bonded carbonyl group of indomethacin is present. Indeed, this moiety was essential for the precipitation inhibition effect of Vitamin E TPGS as this peak was not observed in the formulations where precipitation occurred. In addition, this effect was enhanced due to the presence of further interactions between the hydroxyl groups of indomethacin with the carbonyl groups of Vitamin E TPGS, indicated by diminished hydroxyl intensities in the presence of the inhibitor. Interestingly, in the case of indomethacin, it was observed that interactions were only evident whenever a certain

“supersaturation threshold” was obtained, below which interactions were not observable, and precipitation occurred. This is an important factor to bear in mind: although a drug and polymer may theoretically interact strongly, the formulation in question must generate a particular concentration before interactions will be present. For Labrasol formulations of both compounds, however, there were no discernible interaction motifs in the Raman spectra, and the subsequent formulations performed poorly, with all samples precipitating (Raut, *et al.* 2015). Although not all drugs and formulations would be suitable for this methodology, model drugs, such as the ones mentioned, can be used in combination with a range of polymeric PIs to gain fundamental information about the important binding sites of polymers. Such information could be used to fine-tune the selection process.

In addition to probing interactions in solution, Raman spectroscopy is a useful tool for investigating short-range interactions in the solid state. This can be particularly beneficial in the development of solid dispersion formulations, such as hot melt extrusion (HME) and spray-dried dispersions (SDD), where both drug-polymer miscibility and the precipitation inhibition performance of the polymer is based on these interactions. Chauhan and co-workers utilized this technique, among a wide range of spectroscopic tools, to develop solid dispersions of dipyridamole (Chauhan, *et al.* 2013). The team found that the most successful formulations consisted of drug-HPMC and drug-Eudragit E100®, which performed significantly better than all other polymers screened. Further investigation, utilizing solid-state Raman spectroscopy, revealed that interactions were present between the drug and HPMC and Eudragit E100® (Chauhan, *et al.* 2013).

#### 3.3.4 Nuclear Magnetic Resonance (NMR) Spectroscopy

Nuclear magnetic resonance (NMR) spectroscopy is a spectroscopic technique that exploits the electromagnetic emission of nuclei in a magnetic field to gain structural information about the sample (Gunter, *et al.* 2013). Proton NMR is the most commonly utilised, but other nuclei can be studied, e.g. carbon, fluorine, silicon and lithium (Gunter, *et al.* 2013). NMR spectroscopy has wide application in

drug development and can be a particularly useful in formulation design (Garido and Beckman, *et al.* 2014).

### ***One-dimensional (1D) NMR Spectroscopy***

Ueda and colleagues utilised 1D NMR spectroscopy as a tool to assess the impact of HPMCAS substitution patterns on the precipitation behaviour of carbamazepine (Ueda, *et al.* 2014). In the study, it was observed that HPMCAS successfully inhibited the precipitation of carbamazepine, depending on the ratio of succinyl and acetate groups in the polymer. Highest degrees of carbamazepine supersaturation were sustained in the presence of HPMCAS grades with low succinyl and high acetyl substitutions. This observation was explained by the hypothesis that the more hydrophobic the polymer, the higher the affinity for the growing crystal surface (see section 4.6. Polymer Surface Coverage). In order to expand upon this theory, the group utilised 1H NMR spectroscopy to provide information about the molecular mobility of carbamazepine in solution, with a range of HPMCAS variants. A good correlation was observed between precipitation inhibition and the molecular mobility. A lower molecular mobility, associated with an increased interaction between the drug and the polymer, corresponded to a more successful precipitation inhibition. It was hypothesized that this interaction was the insertion of HPMCAS into growing aggregates that have not yet reached the critical nuclei size for crystal growth to occur, which prevents the formation of the crystal lattice (Ueda, *et al.* 2014). Thus, 1D NMR spectroscopy can be a useful tool to assess the effect of polymers on drug mobility, which can provide information about potential precipitation inhibition effects.

In a recent study by Prasad and co-workers, 1D 1H NMR spectroscopy was utilised to probe the inhibitory effect of a range of polymers on indomethacin precipitation after the generation of supersaturation. It was hypothesized that interactions between the polymers and the carboxylic acid functionality of indomethacin was essential for precipitation inhibition. Therefore, focus was placed on studying this interaction. The chemical shift of the carboxylic acid group, at 3.70 ppm, was closely monitored for changes in chemical shift, which could indicate a change in the chemical environment

surrounding the protons and therefore may indicate an interaction mechanism between the drug and the polymer. Eudragit® E100 and PVP, when combined with the drug in solution, shifted the carboxylic acid peak to a lower value, due to shielding effects (Prasad, *et al.* 2016). The investigators utilised this shift to quantify the strength of drug-polymer interaction and subsequent precipitation inhibition effect. Eudragit E100 resulted in a larger down shift than PVP. For both polymers this shift was directly proportional to the concentration of the polymer. Additionally, it was observed that when the formulation was changed from a binary system, with drug and one polymer, to a ternary system, with both polymers, this shift was even more pronounced. This provided evidence for a synergistic contribution of the two polymers to the precipitation inhibition. This NMR data supported the dissolution performance of the drug in the presence of polymers, where a larger and more sustained supersaturation was generated with Eudragit E100 in a binary system.

#### ***Two-dimensional (2D) NMR Spectroscopy: NOESY and DOSY***

There are a range of 2D NMR spectroscopic techniques that can give information about correlations of different atoms through space such as Nuclear Overhauser effect spectroscopy (NOESY) and diffusion ordered spectroscopy (DOSY).

NOEs occur when there is an enhancement of an NMR signal following cross relaxation and magnetic transfer in systems where there are dipolar spin interactions (Kwan and Huang, *et al.* 2008). NOEs are observable when two nuclei are close in space. This can be exploited to determine if two different molecules (for example a drug and a polymer) are close enough to each other for an interaction to take place which will have an influence on precipitation behaviour. Furthermore, the resultant NOESY spectra can be interpreted to determine which part of the drug molecule is interacting with which part of the precipitation inhibitor, based on the standard 1D structural NMR spectra.

Prior to their work surrounding the importance of substituent ratios for HPMCAS precipitation inhibition, which utilised 1D NMR for the calculation of molecular mobility, Ueda and colleagues first established the mechanism of interaction between HPMCAS and carbamazepine in solution utilising

NOESY (Ueda, 2013). During this experiment, it was observed that HPMCAS-HF (a grade of HPMCAS, relating to the ratio of acetyl to succinyl substituents) had cross-peak interactions with the aromatic protons and amide protons of carbamazepine, suggesting the possibility of both hydrogen bond interactions and hydrophobic interactions. After further inspection of the intensities of the cross-peaks, it was concluded that the more predominant effect was a hydrophobic interaction between the HPMCAS acetyl substituents and the aromatic region of carbamazepine (Ueda, *et al.* 2013). This interaction appeared to be essential for successful precipitation inhibition.

NOESY has also been used in combination with High Resolution Magic-Angle Spinning (HR-MAS) NMR spectroscopy to understand the interactions between the poorly soluble drug mefenamic acid with Eudragit® EPO in supersaturated solutions (Higashi, *et al.* 2014). Although MAS was originally developed to study solids in NMR, HR-MAS NMR spectroscopy can also offer improved resolution for the study of highly viscous solutions and has been used in the pharmaceutical industry to detect and quantify drug in formulations such as gels and creams (Marzarati, *et al.* 2013). Higashi and co-workers were able to significantly improve the recorded NMR spectra for mefenamic acid-Eudragit EPO solution under MAS conditions. This allowed cross-peaks to be observed during the NOESY experiments. These cross-peaks showed evidence of multiple points of interaction between the drug and the polymer, indicating two different motifs. Firstly, a hydrophobic interaction between the aromatic portion of the drug and the EPO backbone and, secondly, a hydrophilic hydrogen-bond interaction between the amino alkyl part of EPO and the carbonyl groups of mefenamic acid. Furthermore, it was observed that the intensities of the two sets of cross-peaks were similar, leading the authors to conclude that both interactions play an important role in precipitation inhibition (Higashi, *et al.* 2014).

DOSY is a tool that allows the calculation of diffusion coefficients based on how quickly a species moves in a given time. In order to obtain this information, DOSY excites the species with multiple pulses and then measures the distance travelled between pulses, from which diffusion coefficients can be obtained. These diffusion coefficients are directly related to the size and molar mass of the species.

Therefore, based on the presence of signals specific for the drug and the polymer, DOSY spectra can be used to distinguish whether one is observing the drug on its own or in a complex with a polymer, which would have a different diffusion coefficient based on the increased size (Johnson, *et al.* 1998). For the study of drug-polymer interactions, DOSY can be used alongside NOESY to offer an orthogonal confirmation of drug-polymer interactions.

DOSY was an essential part of a study to assess a novel spray dried dispersion matrix, HPMCAS and dodecyl (C12) poly(N-isopropylacrylamide) (PNIPAm), for suitability to enhance the delivery of the poorly soluble drug, phenytoin (Li, *et al.* 2017). After dissolution of the solid dispersion, the C12-PNIPAm polymers formed micelles with the dodecyl groups at their core, which successfully sustained the supersaturated state of phenytoin generated by the SDD. Furthermore, a novel observation was recorded in that the C12-PNIPAm inhibited precipitation of the supersaturated phenytoin by inclusion of the drug within the corona of the micelles, as opposed to the core. It was also concluded that the HPMCAS in the formulation had little effect on sustaining the supersaturation compared to C12-PNIPAm, and instead, was responsible for the enhanced dissolution of the drug from the SDD (Li, *et al.* 2017). These conclusions were backed by both NOESY and DOSY data. The NOESY spectra of the novel formulation showed cross-peak interactions between the phenyl groups of the phenytoin and the isopropyl groups of the PNIPAm polymer. Conversely, NOESY spectra revealed no cross-peaks for phenytoin combined with HPMCAS. On application of DOSY as an orthogonal approach, no reduction in diffusion coefficient for phenytoin was observed in HPMCAS. Conversely, the diffusion coefficient decreased dramatically, in a concentration-dependent manner, in the presence of C12-PNIPAm. This provided the researchers with strong evidence that the C12-PNIPAm was responsible for the remarkable sustained supersaturation that was observed upon dissolution of this novel SDD, and that this mechanism was taking place within the corona of the micelles (Li, *et al.* 2017).

### ***Solid State NMR Spectroscopy***

Solid state (SS) NMR spectroscopy can be utilised to gain structural information about solids. One key distinguishing property of solids from an NMR perspective is the presence of anisotropy, that is, directionally dependent interactions. These anisotropic effects have a significant impact on the magnetic interactions of nuclei, and so are of critical importance for the structural elucidation of solids via this technique. Furthermore, these effects result in very broad NMR signals if no magic angle spinning (MAS) conditions are applied. Therefore, SS NMR spectroscopy is generally carried out in combination with MAS, which reduces these effects and results in narrower peak width and better resolved spectra. SS NMR spectroscopy has been utilised in the literature for determining interactions between drugs and precipitation inhibitors in the solid state, such as in solid dispersions or hot melt extrudates. Chauhan and colleagues utilised <sup>13</sup>C cross-polarization magic angle spinning SS NMR spectroscopy to investigate the interactions between indomethacin and polymers in solid dispersions (Chauhan, *et al.* 2014). Three different polymers, Eudragit® S100, PVP and HPMCAS, were screened for indomethacin interactions using this method. Chemical shift changes of the indomethacin signals were recorded in the presence of the polymers, with a larger chemical shift change indicating a stronger interaction. For the aromatic region, a slight chemical shift change was observed for all three polymers, with the biggest shift occurring in the PVP solid dispersions. This correlated well with the observed performance of the SDD during biorelevant dissolution, which outperformed all other polymers due to enhanced precipitation inhibition (Chauhan, *et al.* 2014).

NMR spectroscopy can provide definitive details about the molecular interactions between drug and precipitation inhibitors. Such mechanistic detail can be valuable when considering the selection of precipitation inhibitors. Therefore, NMR spectroscopy is a valuable tool to be applied by the pharmaceutical scientist in the development of supersaturating formulations. The use of NMR spectroscopy for this purpose remains 'exotic' in the literature, with key examples coming from just a few research groups. This may be due to the difficulties associated with obtaining meaningful spectra

from drug-polymer systems, which make up most examples in the literature. Firstly, the drugs used in supersaturating formulations are innately poorly soluble, which can make preparing NMR samples with high enough concentrations for analysis difficult. Secondly, polymers themselves often have very broad and poorly resolved spectral peaks, which can be difficult to interpret. Thirdly, a 'catch-22' exists between resolved spectral data and strong interactions: the stronger the interactions between drug and polymer, the broader and less resolved the peaks become, which also leads to difficulties. For these reasons, the MAS design described by Higashi and co-workers (Higashi, *et al.* 2014) is a very attractive prospect, due to the increased resolution that can be provided.

### 3.3.5. Differential Scanning Calorimetry (DSC)

Differential scanning calorimetry (DSC) is a thermal analysis technique that sees wide application in the pharmaceutical sciences (Sheng, *et al.* 2016). DSC records the amount of heat required to increase the temperature of a sample compared to a reference material (e.g. indium). This produces a DSC curve, from which a wide range of information can be obtained about key thermal events such as melting, crystallization, glass formation and decomposition. One particularly useful application of DSC is in the identification of amorphous materials, which will exhibit a glass-transition instead of a melting thermal event in a DSC curve (Sheng, *et al.* 2016). Although not as common, DSC can also be used to investigate interactions between two different species. Traditional DSC cannot achieve this and instead, modulated DSC (MDSC) is utilised. MDSC differs from traditional DSC in that it operates using two simultaneous heating rates, in contrast to the single linear heating rate used in DSC. MDSC utilises both a linear heating rate and a modulated heating rate that allows simultaneous measurement of the heat capacity of the sample. Such an approach allows the analysis of more complex mixtures due to its higher sensitivity and resolution.

Chauhan and co-workers used MDSC to learn about the mechanism of interaction between dipyrindamole and a range of precipitation inhibitors. Previously, MDSC has been used to assess miscibility between a drug and polymer, based on a change in melting event. Expanding on this idea,



in this study, the melting temperatures of dipyrindamol and dipyrindamol precipitates in the presence of polymers were essential to determining whether any drug-polymer interaction was taking place. For Eudragit® E100, Eudragit® S100 and HPMC, additional melting and glass endotherms were observed in the MDSC curves. The authors of the study reasoned that this shift occurred due to interaction of the drug with the polymers in solution, which corresponded with an increased precipitation inhibition. Indeed, of the six polymers studied, only those polymers where a change in melting temperature of the precipitates was observed were successful precipitation inhibitors (Chauhan, *et al.* 2013). But the authors also offered a word of caution, saying that, although melting point changes were present, this is not definitive proof of interaction. Certain polymers, e.g. PEG, can dissolve a drug and therefore alter the melting temperature. Rather, the authors suggest that MDSC is a useful tool to determine if there are no interactions present, as was the case with the unsuccessful precipitation inhibitors, Eudragit S100, Eudragit L100 and PEG 8000 (Chauhan, *et al.* 2013). To state that an interaction is definitely present, MDSC should be used with complementary analytical techniques.

### 3.3.6 Modelling Precipitation Inhibition

#### **Adsorption Modelling**

Initial work on adsorption modelling for precipitation inhibition used the well-established adsorption isotherms, including the Langmuir (Langmuir, *et al.* 1918), and Freundlich models (Skopp, *et al.* 2009), often combined with crystallization models such as the Kubota-Mullin model (Kubota, *et al.* 1995; Kubota, *et al.* 1997; Kubota, *et al.* 2000) to predict the adsorption of additives on crystal surfaces and the effect on crystal growth. The Kubota-Mullin model proposes a monolayer by monolayer crystal growth, in which precipitation inhibition depends on the surface coverage,  $\theta$ , and space between polymers absorbed onto the growing crystal surface,  $L$ , where  $l$  is the free energy of the unit length (**Equation 7**). (Kubota, *et al.* 1995; Kubota, *et al.* 1997; Kubota, *et al.* 2000)

$$\theta = \frac{L}{l}$$

**(Equation 7)**

Schram and colleagues adapted the model in order to predict polymer performance from the experimentally obtained surface coverage values (Schram, *et al.* 2015b). In this case, polymer effectiveness,  $R_p/R_0$ , is the ratio of crystal growth in the presence ( $R_p$ ) and absence of polymer ( $R_0$ ) and depends on the fractional surface coverage,  $\vartheta$ ; the relative supersaturation,  $\sigma$ ; the edge free energy per unit length,  $\gamma$ ; the size of a growth unit,  $a$ ; the temperature,  $T$ , the Boltzman constant,  $k$ , and the average distance between absorbed polymers,  $l$  (**Equation 8**)

$$\frac{R_p}{R_0} = 1 - \frac{\gamma a}{kT\sigma(\theta l)} \theta \quad \text{(Equation 8)}$$

The average distance between polymers is specific for each system and depends on the amount of polymer adsorbed to the surface. Thus,  $l$  was proportional to the experimental polymer surface coverage determined by AFM. Consequently, a correlation was established, with which  $l$  could be determined from the polymer surface coverage. This correlation enables the calculation of the fractional surface coverage in the Kubota-Mullin model and subsequently the theoretical effectiveness of crystal growth inhibitors. In this study, the theoretical effectiveness calculations were in good agreement with the experimental values (Schram, *et al.* 2015b).

This approach was also adopted by Alonzo and co-workers to determine the effect of polymers on crystal growth and nucleation of felodipine (Alonzo, *et al.* 2012). The team observed experimentally that the efficiency of HPMC inhibiting precipitation of felodipine from supersaturated solution was dependent on the extent of supersaturation generated. This was supported using a Langmuir adsorption model that indicated at high degrees of supersaturation the fractional surface coverage of the growing crystals was decreased, due to the higher propensity to re-crystallize at such high supersaturation (Alonzo, *et al.* 2012).

The use of adsorption models to study precipitation inhibition of indomethacin was extensively studied by Patel and co-workers (Patel, *et al.* 2015; Patel, *et al.* 2014; Patel, *et al.* 2011). Using second-

derivative UV spectroscopy in combination with a first-order crystal growth model, Patel and Anderson investigated growth rates of indomethacin in the presence of various PIs. For HP- $\beta$ -CD, precipitation inhibition was modelled using diffusion layer theory (Patel, *et al.* 2011). This model successfully predicted that, at high degrees of supersaturation, HP- $\beta$ -CD inhibition could be related to the reversible complexation between the two species at the diffusion layer (Patel, *et al.* 2011).

Furthermore, it was observed experimentally that HPMC and PVP significantly outperformed HP- $\beta$ -CD, in agreement with the inhibition models (Patel, *et al.* 2011).

In a further study by Patel and co-workers, molecular weight of PVP and its effect on precipitation inhibition was studied using Langmuir isotherms generated with the solution depletion method. In this method, PVP with varying molecule weight was mixed with solution of the model drug, indomethacin. These systems were then allowed to equilibrate before being passed through a size exclusion column. The sample weight was then determined through the column to determine the concentration of the adsorbed polymer on the surface of the growing crystal. Adsorption isotherms based on surface coverage were then constructed, which showed that adsorption potential for PVP was directly proportional to PVP molecular weight. This was also validated experimentally, with higher molecular weight PVP inhibiting the precipitation of indomethacin most effectively, due to an increased surface coverage (Patel, *et al.* 2014).

### ***Molecular Modelling***

Many different types of molecular models have been applied to mechanistically study crystallization and precipitation, ranging in complexity from Monte Carlo methods to molecular dynamics simulations and quantum mechanics (Myerson, *et al.* 1999).

Mandal and co-workers developed a coarse-grained (CG) model for crystal growth based on force fields obtained from simulators (Mandal *et al.* 2016). Coarse graining allows the simulation of complex systems without the need for extensive computation time, due to the use of simplified atomistic representations. Such an approach is often used to model the interaction of proteins and small

molecules (Levitt, *et al.* 1975). There are many software packages that can carry out the CG process, such as MARTINI (Levitt, *et al.* 1975), however, such software packages often oversimplify the molecules, leading to the danger that information important to understand crystallisation behaviour may be lost. In order to improve upon these established CG processes, Mandal and colleagues utilised a CG model based on the radial distribution functions of the molecules, which were obtained from atomic simulations carried out in the crystalline state (Mandal *et al.* 2016). As a result, the CG model developed was able to simulate crystal growth of the organic molecule, phenytoin, in the absence and presence of the polymer HPMCAS (Mandal *et al.* 2017). Furthermore, the simulation was able to correctly predict that inhibition of phenytoin by HPMCAS is highly dependent on the substitution of the polymer, with an increased acetate substitution slowing crystal growth most effectively. The results of this simulation robustly predicted the experimental data (Mandal *et al.* 2017).

### ***Thermodynamic and Kinetic Modelling***

The interplay between drug, polymer and the aqueous environment is complex from a thermodynamic perspective. In order to consider such a system in its entirety, a thermodynamic model would need to assess the polymer, drug and water in a ternary system. In this system, both liquid-liquid phase separation and solid-liquid equilibrium would need to be considered (Taylor, *et al.* 2016; Paus, *et al.* 2016). Although such an approach is attractive due to the high level of detail of information that could be obtained, it remains a difficult task. Emerging statistic thermodynamic models such as the perturbed-chain statistical associating fluid theory (PC-SAFT) (Paus, *et al.* 2016) could handle the required complexity of such a system. However, as yet, there have been no examples of such an approach in the literature and it remains unlikely due to the difficulties associated with establishing such a model. Therefore, currently, application of thermodynamic models is limited, and instead kinetic approaches have been adopted to describe the interaction between polymers and drugs in precipitation inhibition. Specifically, the interaction parameter  $\chi$  of the Flory-Huggins (FH) theory has often been employed (Flory, *et al.* 1953; Flory, *et al.* 1942; Chen, *et al.* 2014; Baghel, *et al.* 2016).

The Flory-Huggins solution equation (**Equation 9**) is used to describe the behavior of polymers in solution. It is an adaption of the standard Gibbs energy equation incorporating an extra term to modify entropy to consider molecules of different sizes. In the Flory-Huggins equation the enthalpic portion of the Gibbs equation is represented by the Chi parameter,  $\chi$ :

$$\Delta G = RT[n_1 \ln\phi_1 + n_2 \ln\phi_2 + n_1 \phi_2 \chi_{1,2}] \quad \text{(Equation 9)}$$

where  $R$  is the ideal gas constant and  $T$  is the absolute temperature.  $n_1$ ,  $n_2$  and  $\phi_1$  and  $\phi_2$  are the number of moles and volume fraction, respectively, for component 1 and 2 of the system, and  $\chi$  is the interaction enthalpy upon association of component 1 and 2.

Using the Flory-Huggins equations one can consider mixtures of drug and polymers, whereby the enthalpic contribution becomes  $\chi$ . Specifically, it is hypothesized that the interaction related to the  $\chi$  parameter in the equation can be related to the interaction between drug and polymer in solution, which is essential for inhibition of precipitation. Specifically, this is related to the hydrophobic, polar or hydrogen bond interactions between the drug (D) and polymer (P) (Warren, *et al.* 2011). The  $\chi$  parameter can be determined experimentally by combining the Flory-Huggins equation with experimental DSC measurements (Marsac, *et al.* 2009).

In addition, it is possible to utilize *in silico* predictions of the  $\chi$  parameter, which reduces the number of experiments required, thus allowing experimental work to focus on the most promising formulations. This can be achieved in several ways. One common method is to calculate the drug,  $\delta_D$ , and polymer,  $\delta_P$ , in relation to the molar volume of the drug,  $V_m$ , the temperature,  $T$ , and the ideal gas constant,  $R$  (Rubenstein, *et al.* 2003) (**Equation 10**):

$$\chi_{DP} = \frac{V_m(\delta_D - \delta_P)^2}{RT} \quad \text{(Equation 10)}$$

The extended Hansen solubility parameters,  $\delta_D$ , and  $\delta_P$ , can be predicted based on chemical structure alone, using group contribution methods, quantitative structure property relationships (QSRP), molecular dynamics or quantum approaches such as the Continuum Order Solvation model for Real Solvents (COSMO-RS) (Van Krevelen, *et al.* 2009; Tian, *et al.* 2015; Gharagheizi, *et al.* 2011; Gharagheizi, *et al.* 2015; Tantishaiyakul, *et al.* 2006; Niederquell, *et al.* 2018). In addition to group contribution methods, it has been shown that solubility parameters can be predicted from quantitative structure property relationships (QSPR) (Gharagheizi, *et al.* 2011; Gharagheizi, *et al.* 2015; Tantishaiyakul, *et al.* 2006). A first calculation option is to simulate the internal energy change due to vaporization,  $\Delta E_v$  (Gupta, 2011), which can then be incorporated into the cohesive energy density equation along with  $V_m$ , the molar volume (Hilderbrand, *et al.* 1950) (**Equation 11**):

$$\delta = (CED)^{1/2} = \left[ \frac{\Delta E_v}{V_m} \right]^{1/2} \quad \text{(Equation 11)}$$

In this instance, the total energy difference for isolated molecules and for the bulk system with periodic boundary conditions provides an estimate of  $\Delta E_v$  (Hilderbrand, *et al.* 1950).

Although there has been a lot of work in determining experimental and *in silico* methods to determine the  $\chi$  parameter, there are only a few examples of this parameter being used to understand inhibition of precipitation. Baghel and co-workers studied solid dispersions of dipyrindamole and cinnarizine with PVP and polyacrylic acid (PAA) (Baghel *et al.* 2016). It was found that the combinations capable of forming hydrogen bonds (dipyridamol-PVP; dipyrindamol-PAA and cinnarizine-PAA) in the solution state were more effective at keeping the drug in a supersaturated state than those not able to hydrogen bond (cinnarizine-PVP). In this instance, cinnarizine-PVP had the highest predicted  $\chi_{DP}$  parameter, suggesting weakest interactions, in line with the observed precipitation inhibition results. However, it was noted that, despite their significantly different supersaturation performance, the difference

between the  $\chi_{DP}$  parameters of cinnarizine-PVP and cinnarizine-PAA was not great, and that other aspects such as the hydrophilicity of the polymer should also be considered.

Similar findings were also reported by Chen and co-workers who compared solid dispersions of griseofulvin, felodipine, and ketoconazole with PVP vinyl acetate (PVP-VA) and HPMC-AS (Chen *et al.*, 2014). Although felodipine interacted much more effectively with PVP-VA in the solid-state ( $\chi_{DP} = -1.9$ ) than with HPMC-AS ( $\chi_{DP} = -0.21$ ), this behavior was not replicated in aqueous dispersions, where the HPMCAS solid-dispersion generated higher and more sustained supersaturation profiles upon dissolution. This was likely due to the hydrophilic interactions of PVP-VA with water upon exposure to an aqueous environment, which may have reduced or negated the favorable interactions with felodipine.

#### **3.4. Bridging the Gap to Systematic and Facile Precipitation Inhibitor Screening**

There has been an exponential increase in the number of research papers addressing precipitation inhibition from a mechanistic perspective. This effort, combined with the use of advanced analytical tools, has led to a deeper understanding of drug-polymer interactions. Techniques to investigate experimental drug-polymer interactions are time-consuming and not ideally suited to early stage pharmaceutical development, where such decisions must be made. Furthermore, although the *de novo* design of PIs to maximize interaction with the drug and water in a balanced way is an exciting prospect, there are some key hurdles to this technology becoming widely applicable. For example, from a regulatory perspective such an approach could be very costly and restrictive, since additional safety studies would be required to demonstrate an absence of polymer-related toxicity, if new PIs are used. Therefore, a rather more interesting and applicable approach would be “*de novo* selection” of PIs based on an understanding of interaction between the drug and polymer. Such an approach would retain some of the advantages of a bespoke PI selection process whilst avoiding the additional regulatory burden associated with creating a novel excipient, designed based solely on optimal

interactions. For excipient selection, *in silico* tools are an attractive prospect, as they can limit the time required by reduce the experimental screening requirements.

However, the *in-silico* tools that have recently been employed in the design and selection of precipitation inhibitors are currently costly and time-consuming, making them less attractive for “de novo selection” of a precipitation inhibitor from a large database. Therefore, there exists a gap between the current understanding of drug-polymer interactions and a quick and efficient screening tool for the selection of precipitation inhibitors that are already approved for pharmaceutical use. A simplified computational approach that can predict interactions between drugs and pharmaceutically relevant polymers would therefore be of great value to the development of supersaturating formulations in the pharmaceutical industry.



#### **4. Aims of the Thesis**

The aim of the thesis studies was to develop and optimize a new workflow to formulate mesoporous silica with precipitation inhibitors, leading to the design of robust supersaturating formulations for the oral delivery of poorly soluble drugs. This involved five key activities:

- 1) Review of the current state of the art of mesoporous silica formulations with respect to the importance of drug loading and interactions to the release profile. In addition, subsequent supersaturation and precipitation on release were examined and reviewed.
- 2) Identification of the critical parameters involved in precipitation inhibition, including recent advances in the use of advanced analytical tools for understanding and selecting precipitation inhibitors.
- 3) Optimization of the formulation method for combining precipitation inhibitors with mesoporous silica. This approach shifted away from the standard approach of physically combining precipitation inhibitors post-loading. The number of formulation steps required was reduced and the efficiency of precipitation inhibition upon dissolution was improved.
- 4) Resolution and rationalization of a mechanistic physical analysis of co-incorporated drug/PI mesoporous silica formulations, closely examining the importance of drug-polymer interaction.
- 5) Application of new-found knowledge regarding the importance of drug-polymer interactions to develop a quantum-chemical based *in silico* screening tool for the selection of optimal precipitation inhibitors for mesoporous silica formulations.

These goals were achieved by combining advanced and novel analytical tools and *in silico* models identified from an extensive literature review.

## II. Results and Discussion

### 1. Approach

Precipitation inhibitors, and understanding of how they function, are essential components of modern enabling formulations, which is reflected in the large body of work on this topic that has been published in the past decade. To form a basis for the thesis studies, a review article covering fundamental considerations of supersaturation and precipitation as well as recent innovative efforts combining modelling and analytical tools to understand the importance of drug-polymer interaction in effectively maintaining supersaturated drug concentrations was prepared (Price *et al.* 2018). The review revealed that formulation scientists can now incorporate top-level analytical tools such as advanced NMR spectroscopy techniques to determine the optimal precipitation inhibitor for a given drug.

While advances in PI selection were identified in the literature review, experimental incorporation precipitation inhibitors into supersaturating formulations remains at a basic level, with simple physical mixtures being the most common approach. To rectify this situation, a new processing method for combining precipitation inhibitors with mesoporous silica was developed: the co-incorporation approach. This development avoids having to add the PI as a physical mixture post-loading by instead incorporating the precipitation inhibitor at the very first step i.e. in the solvent-mediated loading of drugs onto mesoporous silica (Price *et al.* 2020). This approach significantly improved the precipitation inhibition effect of HPMCAS when combined with mesoporous silica for formulations of celecoxib and glibenclamide. One of the key reasons for this enhancement was the generation of drug-polymer interactions in the formulation itself, rather than first being generated when the formulation is dissolved (which is the case when the drug-loaded silica is physically blended with the PI) (Laine, 2016; Price, 2018). The importance of drug-polymer interactions was highlighted in both the review article and the co-incorporation studies. Despite this success, there remains a gap between our knowledge around the importance of drug-polymer interactions and the practicalities of incorporating this consideration in standard formulation development. Although the use of 2D NMR spectroscopy to

determine drug-polymer interaction is described in the literature, its routine use is not realistic during the early stage of pharmaceutical development where efficiency and time are key. Instead, precipitation inhibitors are still routinely selected using trial-and-error based approaches, noting that these are also inefficient from a time and resource perspective. Therefore, the next stage of this work was to bridge this efficiency-knowledge gap by developing a quick and easy *in silico* protocol to calculate drug-polymer enthalpy using minimal resources (Price *et al.* 2019). This was achieved using the COSMO-RS model, which combines quantum mechanics and thermodynamics to calculate the drug-polymer excess enthalpy of interaction. Combining the new approaches described in this body of work will enable development of optimal mesoporous silica formulations in the pharmaceutical industry (Figure 7).

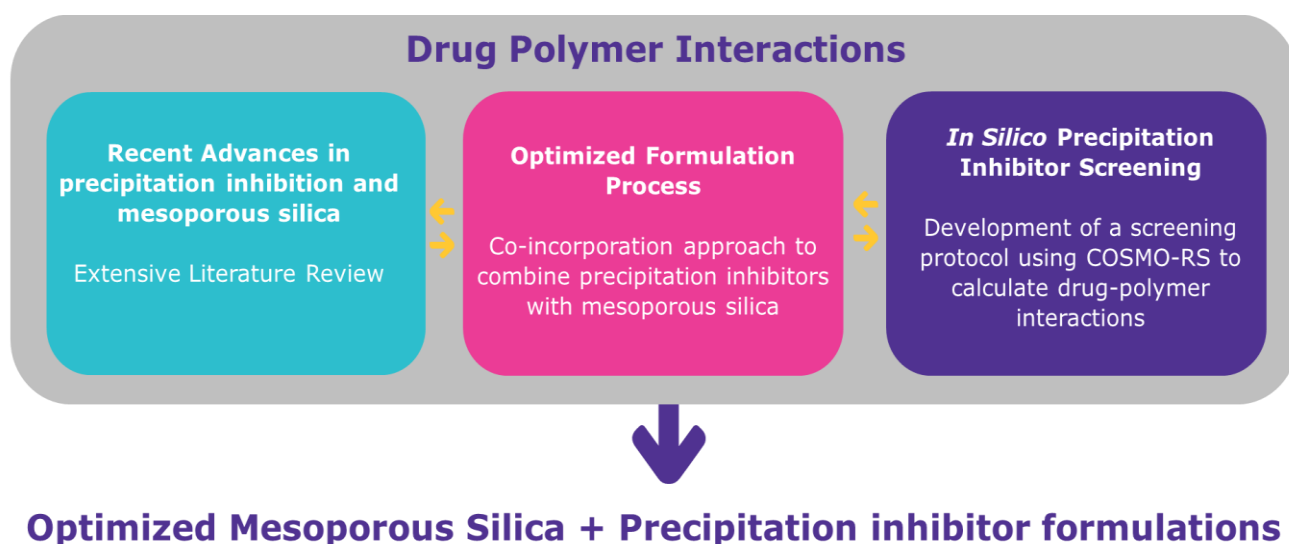
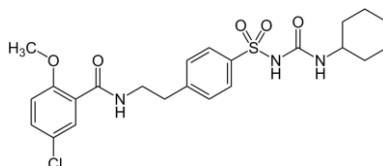


Figure 7. Overview of the thesis

## 2. Selected Compounds

Three model BCS II compounds, with a broad range of physicochemical properties were selected.

### Glibenclamide



**Figure 8.** Glibenclamide

Glibenclamide is an orally administered hypoglycemic drug used for treatment of diabetes, via stimulation of pancreatic beta cells to secrete insulin (Furman, *et al.* 1977). Glibenclamide is a BCS II compound, indicating that the highest dose of the drug is not soluble in 250 mL of water across physiological pH range (Amidon, *et al.* 1995). Glibenclamide has been utilized in a range of supersaturating drug formulations, including mesoporous silica (Van Speybroeck, *et al.* 2011).

### Dipyridamole

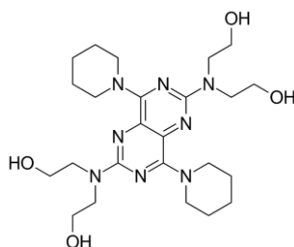


**Figure 9.** Dipyridamole

Dipyridamole is an anticoagulant that inhibits clot formation *via* blood vessel dilation and interaction and inhibition of phosphodiesterase (Brown, *et al.* 2015). Dipyridamole is also a BCS II compound. Dipyridamole has previously been formulated with amorphous technologies such as spray-dried dispersions and hot melt extrusion (Peng, *et al.* 2018).

## Fenofibrate

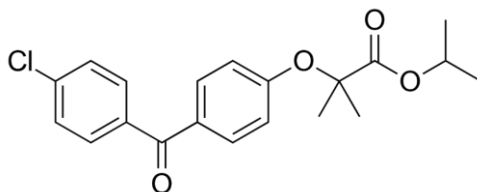


**Figure 10.** Fenofibrate

Fenofibrate is the pro-drug form of fibric acid. Fibric acid is used in the treatment of elevated blood lipid levels (Staels, *et al.* 1998). Like glibenclamide and dipyridamole, fenofibrate is a BCS II compound. Fenofibrate has been utilized in a wide range of supersaturating drug formulations, including mesoporous silica (Dressman *et al.* 2015).

**Table 2.** Physicochemical Property Comparison of the Model Drugs

| Compound      | Log P | pKa (acid) | pKa (basic) | Molecular Weight | FaSSIF Solubility (µg/mL) |
|---------------|-------|------------|-------------|------------------|---------------------------|
| Glibenclamide | 5.3   | 4.3        | -           | 494.0            | 14.0                      |
| Dipyridamole  | 4.7   | -          | 6.4         | 504.6            | 8.1                       |
| Fenofibrate   | 1.5   | -          | -           | 360.8            | 20.0                      |

### 3. Selected Polymers

A wide range of polymers was selected for the polymer database. Initially, polymers were identified from the pool of polymers which have been proposed as PIs in the literature. This included those typically used in precipitation inhibition and amorphous solid dispersion applications. Expanding upon these typical polymers, further polymers approved for pharmaceutical use were chosen from the literature and from online databases.

For input into COSMO-RS, it was necessary to convert polymer structures into smiles notation. Due to the restrictions associated with quantum chemistry, it is not possible to consider structures larger than

50000 Da. Therefore, polymer structures were represented as trimers in the *in-silico* screening. This was not deemed counterproductive to the study, as the hypothesis was related to local molecular interactions, which are assumed to be sufficiently captured by trimer sequences of the polymer.

The following polymers were included in the database, along with lactose and sorbitol:

|  |  |
|--|--|
| <i>Alginate gum</i>  | <i>Polyethylene oxide (PEO)</i>                                    |
| <i>Cellulose acetate phthalate (CAP)</i>                         | <i>Poly(lactic acid) (PLA)</i>                                     |
| <i>Chitosan</i>  | <i>Poly(lactide-co-polyglycolide) (PLGA)</i>                       |
| <i>Eudragit EPO</i>  | <i>Poly (methyl methacrylate) (PMMA)</i>                           |
| <i>Eudragit L100</i>   | <i>Polyvinyl acetate (PVAc)</i>                                    |
| <i>Eudragit RL100</i>  | <i>Polyacetylene</i>   |
| <i>Hydroxyethyl methyl cellulose (HEMC)</i>                      | <i>Polyether polyol</i>  |
| <i>Hydroxypropyl methyl cellulose (HPMC)</i>                     | <i>Polyethylene Imine</i>  |
| <i>Hydroxypropyl methyl cellulose acetate succinate (HPMCAS)</i> | <i>Polyvinyl acetate-co-poly (methyl methacrylate) (PVAc-PMMA)</i> |
| <i>Hydroxyethyl cellulose (HEC)</i>                              | <i>Polypropylene glycol (PPG)</i>                                  |
| <i>Lactose</i>   | <i>Poly (vinyl alcohol) (PVA)</i>                                  |
| <i>Locust bean gum</i>   | <i>Poly (vinyl alcohol)-co-polyvinylpyrrolidone (PVA-PVP)</i>      |
| <i>Methyl cellulose</i>  | <i>Polyvinylpyrrolidone (PVP)</i>                                  |
| <i>Polyethylene glycol (PEG)</i>                                 | <i>Sodium carboxymethyl cellulose (SCMC)</i>                       |
| <i>Polyglycolide (PGA)</i>                                       | <i>Sorbitol</i>  |

## **4. Co-incorporation: A New Method to Combined Precipitation Inhibitors with Mesoporous Silica**

### **4.1 Approach**

To date no systematic study of how best to incorporate precipitation inhibitors into mesoporous silica formulations has appeared in the scientific literature. The current standard practice involves combining inhibitors in a physical mixture with the drug-loaded silica, either with a mortar and pestle or by overhead stirring. Due to the lack of a standard protocol, there is uncertainty about how reliably the precipitation inhibitor is combined with the drug-loaded silica on a batch to batch basis. In addition to the practical limitations of the approach, the incorporation of inhibitor post-loading represents a potentially unnecessary and not insignificant step in the formulation procedure. By contrast, co-incorporating the PI alongside the drug not only abbreviates the formulation manufacturing procedure but can also improve the dissolution performance of the formulation. Previous work by the author demonstrated how incorporation of HPMCAS alongside celecoxib onto mesoporous silica substantially improved both *in vitro* and *in vivo* performance of the poorly soluble drug (Laine *et al.* 2016). Still, to gain more traction in the field, further evidence was needed a) to demonstrate that a co-incorporation approach can significantly improve the performance of drug-loaded silica formulations, and b) to resolve the mechanisms behind this formulation performance enhancement via robust and extensive analytical characterization of the co-incorporated formulation.

Glibenclamide was the drug selected for these studies. One of the key concerns of the co-incorporation approach is whether the accessibility of larger molecules to the porous network is hindered by the presence of a polymer. This was addressed with glibenclamide, which is a relatively large molecule with a molecular weight of 494 Da. Glibenclamide is also optimal from an analytical perspective due to the presence of fluorine in the molecule, which enables it to be tracked using energy dispersive x-ray scanning electron microscopy (EDX SEM). This tool could then be leveraged to track the location of the drug within the co-incorporated formulations, to help build a mechanistic rationale for the co-incorporated formulation performance.

HPMCAS was the polymer selected for the mechanistic study. HPMCAS is a well-established PI and has a track record in the literature of successfully sustaining supersaturated solutions for a range of drugs (Warren *et al.* 2010; Price *et al.* 2018; Laine *et al.* 2016). For example, Laine and co-workers demonstrated the successful precipitation inhibition of supersaturated celecoxib with HPMCAS in both single-medium FaSSIF dissolution and transfer dissolution (Laine *et al.* 2016). HPMCAS has been regularly combined with mesoporous silica formulations to successfully sustain supersaturated drug concentrations. For glibenclamide, HPMCAS has the capacity to interact with the drug *via* hydrogen bond interactions, which have been shown to be crucial for successful precipitation inhibition. (Price *et al.* 2018; Price *et al.* 2019) Additionally, it has been demonstrated that HPMCAS successfully sustained supersaturated concentrations of glibenclamide in a solvent-shift-based precipitation inhibitor experimental screen (Ueda *et al.* 2015).

#### **4.2. Solid State of Formulations**

Loading of glibenclamide onto mesoporous silica, both with and without HPMCAS, resulted in successful shift from a crystalline to an amorphous solid-state form. Encouragingly, the inclusion of HPMCAS in this process did not have an impact on the ability of the drug to enter the pores, in line with earlier findings in which HPMCAS was successfully co-incorporated during the loading of celecoxib onto mesoporous silica without any impact on the final solid-state form of the formulation (Laine *et al.* 2016). This work paralleled attempts at incorporating mesoporous silica in HME platforms, in which Hanada and co-workers demonstrated that silica could be successfully utilized alongside HPMC to yield a high drug-load, ternary drug-silica-polymer system (Hanada *et al.* 2018).



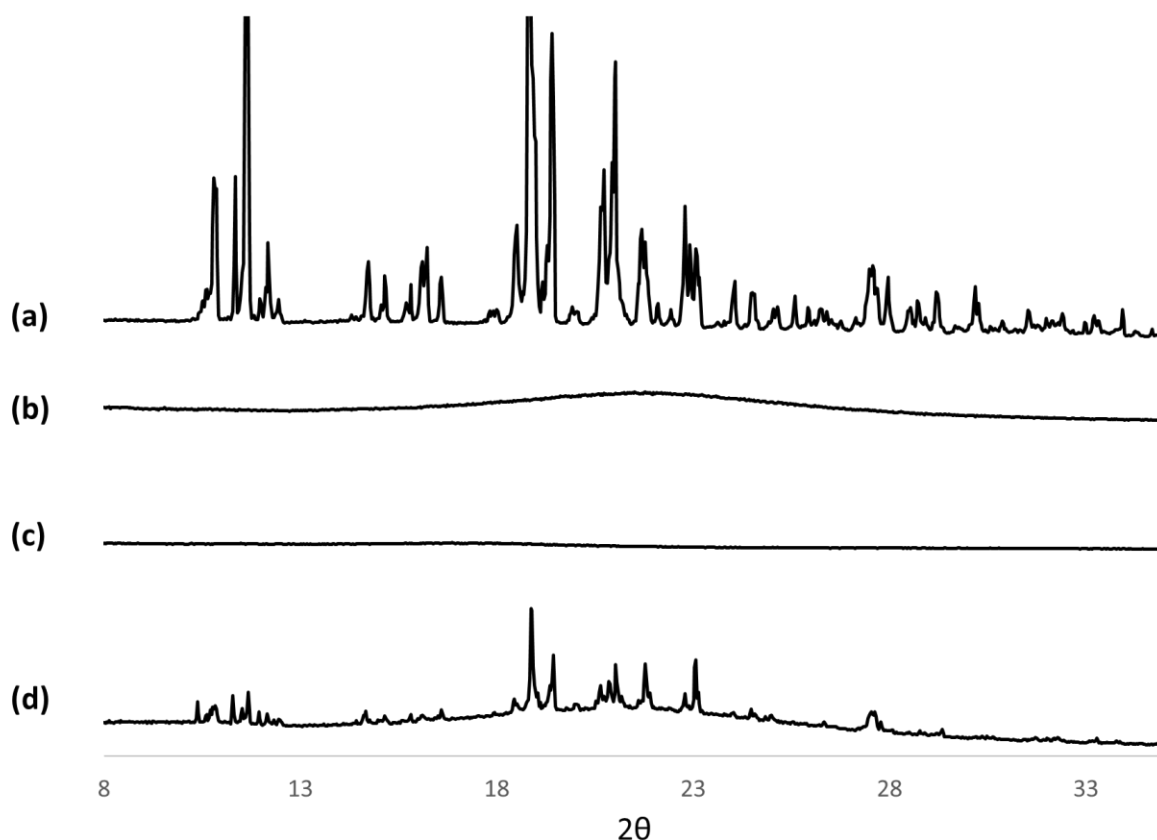


**Figure 11.** XRPD pattern for crystalline glibenclamide (GB) (a), glibenclamide loaded silica (b), co-incorporated GB/HPMCAS loaded silica (c) and GB and HPMCAS prepared by rotary evaporation (d).

One significant difference, however, was the appearance of the particles when HPMCAS was incorporated during the loading process. The particles in the co-incorporated sample looked significantly bigger and different in shape than the simple drug-loaded silica samples (**Figure 12**). Upon further investigation, it was observed that these large particles consisted of polymer plates upon which drug-loaded silica was dispersed. This is analogous to a standard polymeric amorphous solid dispersion and is believed to be the first example of a solid dispersion of loaded silica to be described in the literature.

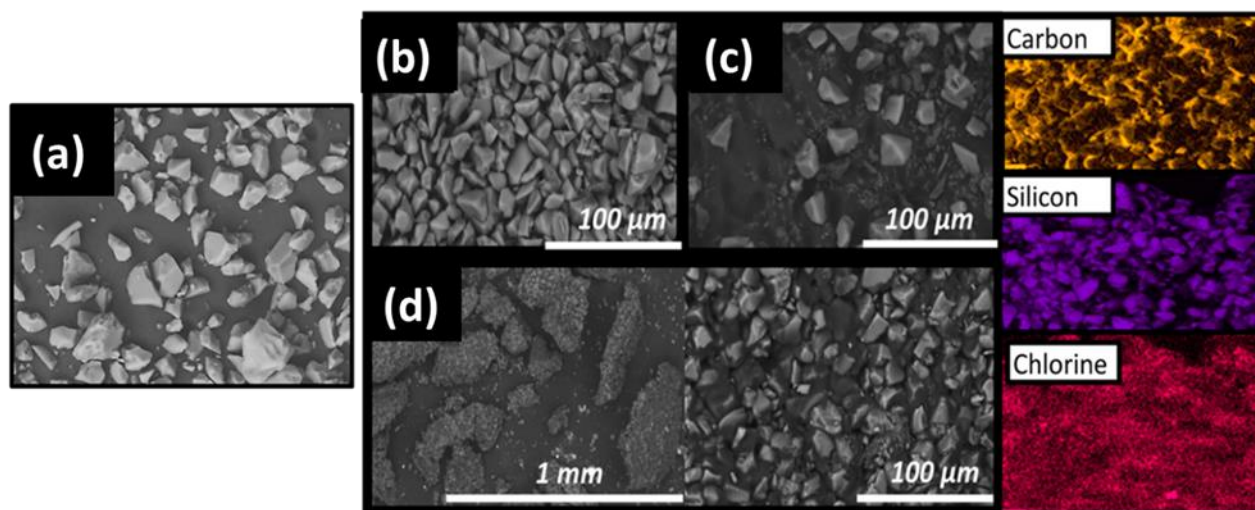


**Figure 12.** *Left:* SEM of unloaded mesoporous silica (a), glibenclamide loaded silica (b), glibenclamide loaded silica + HPMCAS blend (c) and co-incorporated glibenclamide/HPMCAS loaded silica (d). *Right:* SEM EDS of co-incorporated glibenclamide/HPMCAS loaded silica showing carbon (yellow), silicon (purple) and chlorine (pink) atoms are highlighted. Chlorine is a marker for glibenclamide.

#### **4.3 Experimental Considerations for Dissolution Selection**

Recently, there has been a shift away from traditional sink dissolution tests towards non-sink dissolution for supersaturating formulations (Augustijns *et al.* 2012; Sun *et al.* 2015). The reason for this shift is that supersaturation and precipitation are unlikely to be detected under sink conditions. Most supersaturating formulations are now routinely characterized in non-sink dissolution tests. However, unless the effect of transfer of the formulation out of the stomach into the small intestine can be considered, a robust *in vitro-in vivo* correlation can be hard to obtain. Although supersaturation results in single-medium (e.g. FaSSIF) dissolution tests may seem promising, the full extent of precipitation can often only be realized by generating transfer dissolution data. Supersaturation or a higher thermodynamic solubility of the drug in gastric fluid may trigger the generation of seeds when the solution is transferred to the intestine. In some cases, this results in significantly poorer dissolution performance of the formulation in the FaSSIF portion of the experiment, with no enhancement versus the crystalline drug substance (Kambayashi, *et al.* 2019). During investigation into the co-incorporation

approach, biorelevant transfer dissolution experiments were utilized to capture the full precipitation inhibition picture, and to help elucidate a mechanistic rationale.

#### **4.4. Dissolution of Simple Blends: The Importance of Precipitation Inhibitors**

Based on the dissolution of silica loaded with pure glibenclamide (Figure 13), it is clear that a PI is required to sustain the supersaturation over a physiologically relevant timescale. Although a simple blend with HPMCAS did have a marked effect on the dissolution compared to pure glibenclamide-loaded silica, it did not successfully sustain supersaturation, with concentrations falling towards that of the crystalline drug substance by the end of the experiment.

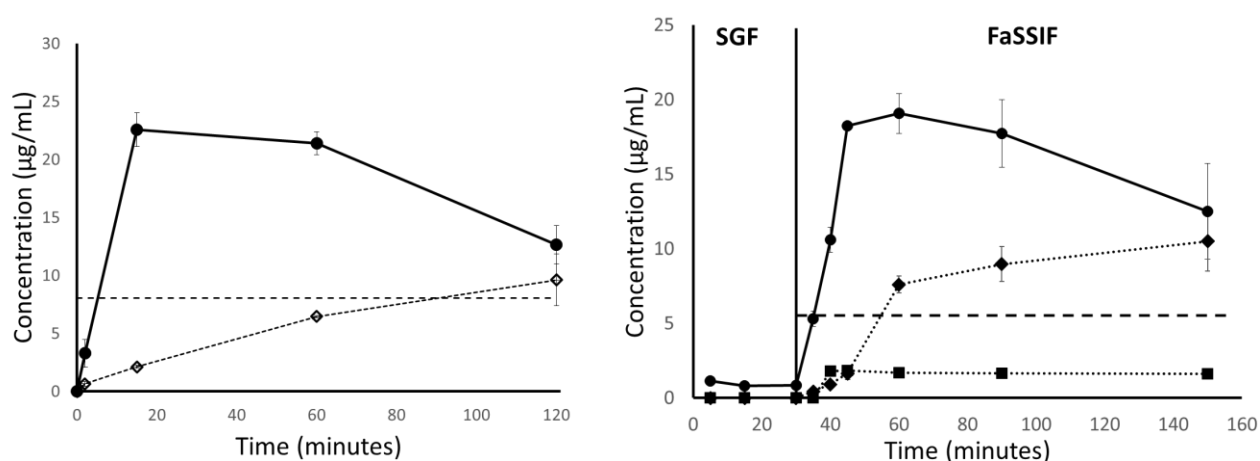


**Figure 13.** (left) FaSSIF mini-dissolution (37c, pH 6.5) and (right) transfer dissolution of glibenclamide (diamonds), glibenclamide loaded silica (crosses) and glibenclamide loaded silica + HPMCAS blend (circles). Equilibrium solubility is shown by the dashed lines. Equilibrium solubility in SGF is below limit of detection.

XRPD on the solid residues from both experiments revealed drug crystallinity (**Figure 14**), suggesting the precipitation inhibition effect of the polymer in the simple blend was only temporary. For the transfer dissolution, the crystallinity observed in the post-SGF residue was especially important, as the formation of seed crystals early in the experiment has the potential to increase the precipitation rate in the intestinal portion of the experiment, suggesting that the full formulation potential had not been realized.

The effect of seed crystals on the precipitation of supersaturated drugs is well-known. Patel and colleagues demonstrated the increased precipitation rate of supersaturated indomethacin in the presence of seed crystals, compared to in their absence (Patel *et al.* 2013). This effect is related to first principles of nucleation and crystallization, in which a solid precipitate can act as a trigger for heterogeneous nucleation, reducing the critical nuclei induction time (Price *et al.* 2018). Therefore, although blending glibenclamide loaded silica with HPMCAS improved the formulation performance relative to the loaded silica alone, the precipitation inhibition is not optimal, and significant precipitation still occurs during dissolution.

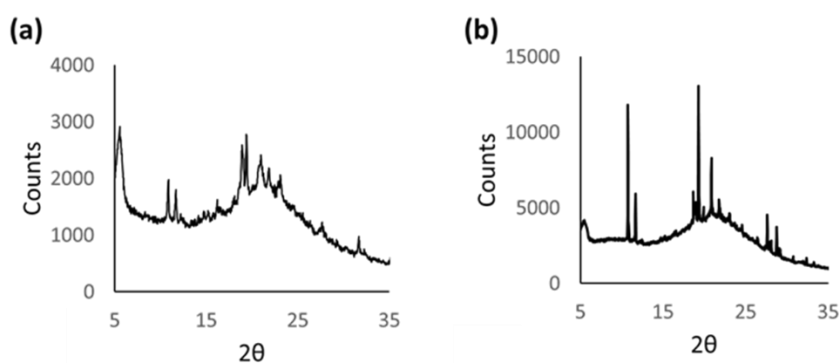


**Figure 14.** XRPD patterns for post-FaSSIF dissolution residues for (a) glibenclamide loaded silica and (b) glibenclamide loaded silica + HPMCAS blend

#### **4.5. Co-Incorporating HPMCAS in the Loading Method: Precipitation and Dissolution**

In contrast to the simple HPMCAS blend, incorporating HPMCAS during the loading step resulted in a substantial and sustained supersaturation in the single medium-FaSSIF dissolution assay (**Figure 15**). Furthermore, the post-dissolution residue for the co-incorporated formulation was amorphous, suggesting the co-incorporated HPMCAS was able to more effectively inhibit precipitation than when simply blended with the formulation (Figure 15).

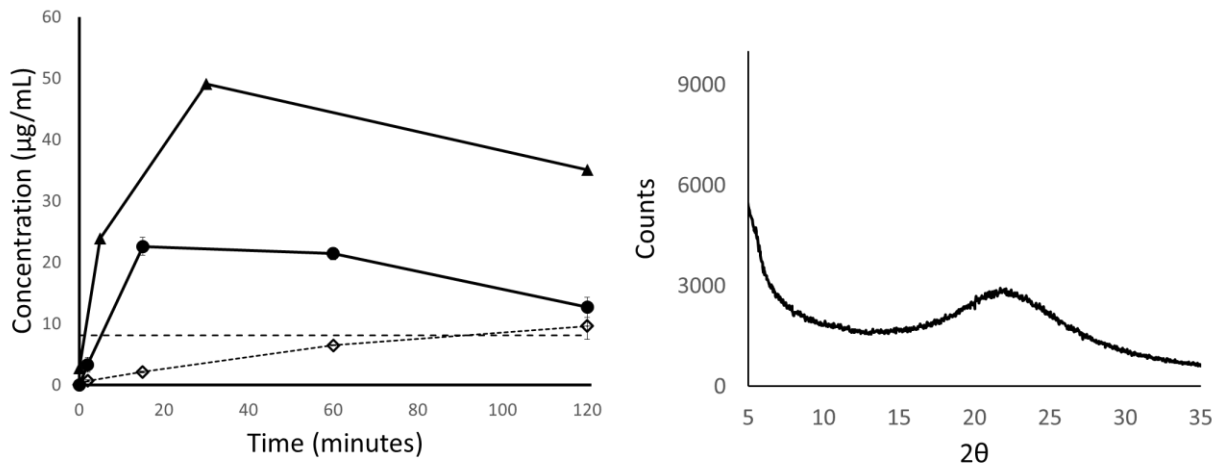


**Figure 15. Left:** FaSSIF mini-dissolution (37°C, pH 6.5) of glibenclamide (diamonds), glibenclamide loaded silica + HPMCAS blend (circles) and co-incorporated HPMCAS/GB loaded silica (triangles). Thermodynamic solubility is shown by the dashed line. **Right:** XRPD residue of co-incorporated HPMCAS/GB loaded silica post-FaSSIF dissolution. **Bottom:** Appearance of glibenclamide loaded silica (a), glibenclamide loaded silica + HPMCAS blend (b) and co-incorporated GB/HPMCAS loaded silica (c) dispersed in simulated gastric fluid.

In line with the previous discussion on the importance of transfer dissolution tests for supersaturating formulations, it is in this experiment that the true potential of the co-incorporation approach can be observed. In contrast to both the simple, drug-loaded silica and its physical blend with the PI, no drug was released from the co-incorporated sample in the SGF portion of the assay, and the residue remained amorphous.

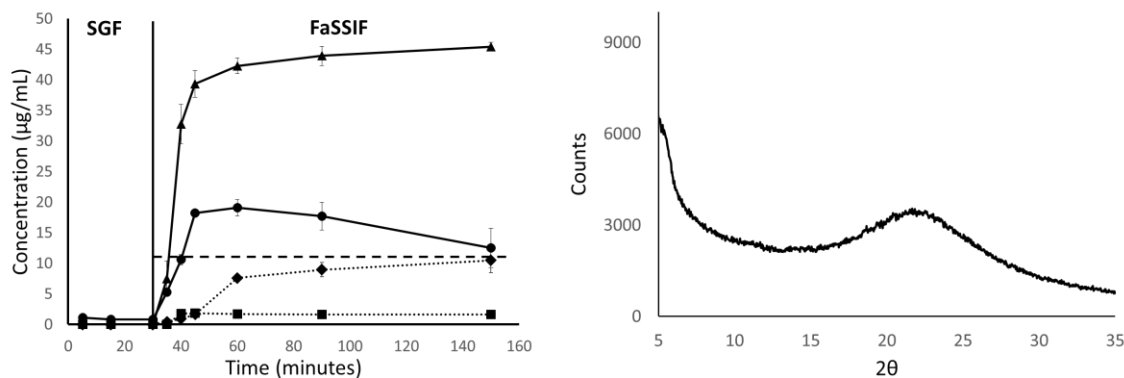


**Figure 16. Left:** Biorelevant transfer dissolution of glibenclamide loaded silica (squares), crystalline glibenclamide (diamonds), glibenclamide loaded silica + HPMCAS blend (circles) and co-incorporated glibenclamide/HPMCAS loaded silica (triangles). Thermodynamic solubility is shown by the dashed line. Thermodynamic solubility in SGF was less than the limit of detection. **Right:** XRPD pattern of co-incorporated GB/HPMCAS loaded silica post-transfer dissolution.

The mechanism for this significant benefit is that the HPMCAS plates remain intact and thus the drug-loaded silica remains immobilized under gastric conditions, preventing drug release from the silica and the formation of seed crystals. These results demonstrate clearly that changing the manufacturing process, without changing the qualitative and quantitative composition of the formulation, can introduce new properties to the formulation. By incorporating the HPMCAS alongside the drug in the loading process instead of merely physically blending it in, enteric properties were easily introduced without the addition of extra excipients, coating processes or special capsules, which are typically required to prevent drug release in the stomach (Qiu, 2017). The enteric property should be especially advantageous in the delivery of poorly soluble weakly basic compounds, for which premature release in the stomach and subsequent supersaturation followed by precipitation in the small intestine could be avoided by this approach.

Combination of weak bases with mesoporous silica has been investigated as a potential formulation approach. For example, Van Speybroeck and colleagues described the improved oral absorption of itraconazole loaded silica in rats. However, the authors found that HPMCAS-based silica formulations

were unsuccessful in preventing the release and precipitation of the drug in the stomach and therefore absorption was not optimized (Van Speybroeck *et al.* 2010). It is reasonable to assume from the glibenclamide studies described above that a HPMCAS-based co-incorporated formulations would be a suitable way forward to improving the *in vivo* absorption of poorly soluble weak bases by avoiding release in the stomach. However, further work is needed to verify the advantages of the co-incorporation approach in a range of poorly soluble weak bases.

A critical factor for effective precipitation inhibition is the presence of drug-polymer interactions (Price *et al.*, 2018). Specifically, hydrogen bond interaction, hydrophobic interactions and Van de Waals interactions have all been shown to play a critical role in the inhibition of precipitation (Prasad, *et al.* 2016; Schram, *et al.* 2015; Warren *et al.* 2015; Price *et al.* 2018). Therefore, one hypothesis for the improved precipitation inhibition of the co-incorporated formulation was the 'pre-formation' of drug-polymer interactions in the solid state. This was confirmed by solid-state NMR data, which showed a peak-shift indicative of interaction in the co-incorporated sample, but not in the simple blend (Figure 17).

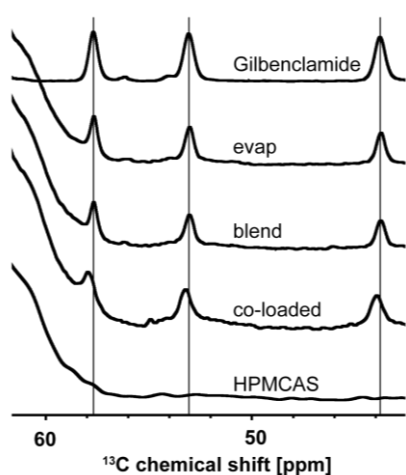


**Figure 17.**  $^{13}\text{C}$  NMR spectra for different formulations studied in the co-incorporation study, showing a distinct spectral shift for the co-incorporated samples, indicative of a molecular interaction.

SS-NMR spectroscopy was carried out on all samples (Figure 17). The  $^{13}\text{C}$  peaks for the drug were identical in all samples except the co-incorporated formulation. In the co-incorporated formulation, a low field shift of 0.2 – 0.5 ppm for all drug peaks was observed. For example, the characteristic drug peak at 53 ppm was observable in all samples except the co-incorporated formulation, in which the peak shifted to 53.5 ppm. This is indicative of an interaction taking place between the drug and the polymer in the solid state, which can take place once the drug is immobilized in the silica and subsequently in the HPMCS plate. The results suggest that solid-state drug-polymer interactions and hence dissolution performance can be altered by changing the method used to manufacture the formulation. Demonstration of a solid-state interaction between the HPMCAS and the drug in the co-incorporated formulations provided further rationale for the importance of such interactions on the effective performance of a precipitation inhibitor.

#### **4.6. Co-incorporated Formulations: Just a Solid Dispersion?**

Polymeric amorphous solid dispersions are the most common amorphous formulation technology applied. In particular, ASDs produced by spray-drying from organic solution are regularly used in commercial formulations (Timpe, *et al.* 2007). Therefore, it was important to rule out the possibility of a polymeric ASD being formed during the removal of solvent in the rotary evaporator step, with the silica having no impact on the overall performance. To assess this, a control sample consisting of HPMCAS-glibenclamide, i.e. without mesoporous silica, was prepared by evaporation from an organic solvent. Visually, the control sample appeared similar to the co-incorporated formulation, with plate-like particles observed in SEM (**Figure 18**). However, EDS data showed that the drug substance was no longer only confined within the polymer platelets, and instead was distributed throughout the entire sample (**Figure 18**).



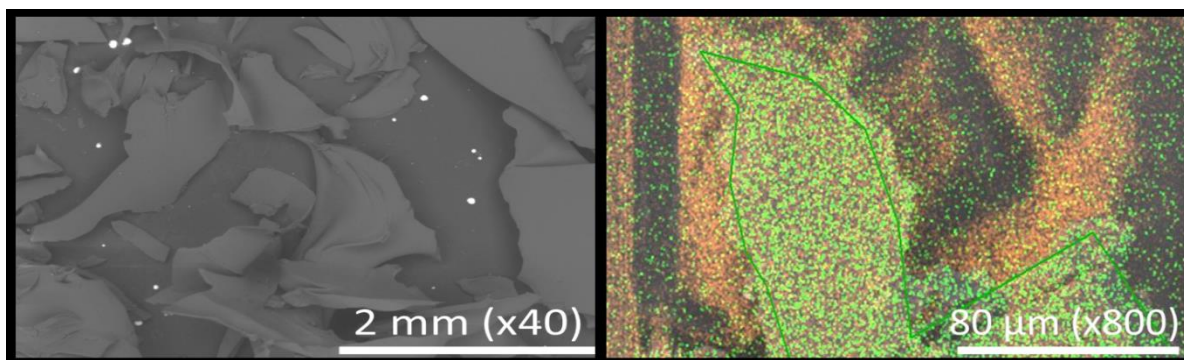


**Figure 18.** SEM (left) and EDS (right) images of glibenclamide and HPMCAS prepared by solvent evaporation shows the same particle size and morphology as the co-incorporated samples. However, in this sample the drug (indicated by green) is no longer confined within the polymer plate and is freely distributed throughout the sample.

Without the nano-confinement effects of the silica (Ditzinger, *et al.* 2018; Ditzinger/Price, *et al.* 2019), the drug was able to re-crystallize, which was observed in the XRPD (**Figure 11**). Ultimately, this resulted in the control sample showing no improvement in FaSSIF dissolution versus crystalline drug (**Figure 19**). These results are in stark contrast to the co-incorporation formulation, where the drug was confined within the mesoporous silica particles, which in turn were immobilized in the polymer platelets and released only when the formulation was subjected to intestinal conditions.

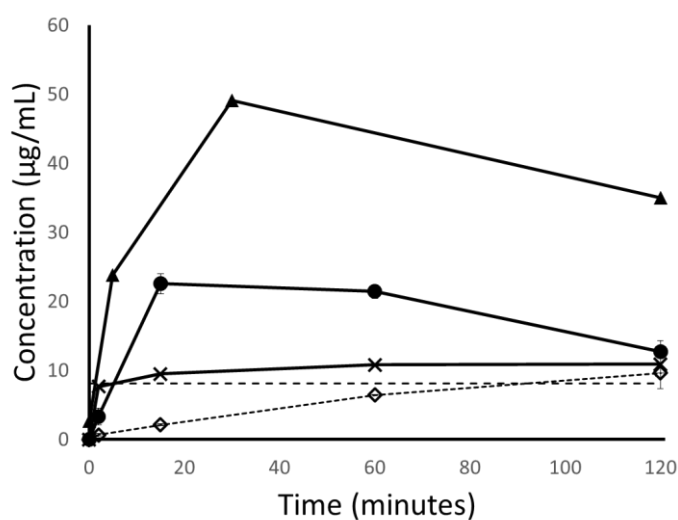


**Figure 19.** FaSSIF Mini dissolution (37c, pH 6.5) of the control sample, GB/HPMCAS prepared via rotary evaporator (X) compared to co-incorporated GB/HPMCAS loaded silica (triangles), GB loaded silica + HPMCAS blend (circles), and crystalline glibenclamide (X).

Finally, even if a portion of the sample was able to remain amorphous in the polymer platelets, the lack of drug-polymer interaction (as indicated by the solid-state NMR spectra from the control sample) would lead to a reduction in the precipitation inhibition effect of the polymer (**Figure 17**). Thus, it can be concluded that the silica and the polymer played a synergistic role in the co-incorporated formulation, which out-performed both the physical blend and the control.

#### **4.7 Mechanistic Rationale**

Incorporating the precipitation inhibitor alongside the drug when loading onto mesoporous silica substantially improves formulation performance compared to a simple physical blend. Both dissolution and supersaturation were improved in both single-medium FaSSIF dissolution and biorelevant transfer dissolution. Furthermore, the co-incorporation approach allowed the removal of a time-consuming and inefficient blending step. To provide a physical mechanistic basis for the improved performance, a range of spectroscopic tools was utilized. It was concluded that the improved dissolution performance is a synergistic effect related to two key factors: formation of drug-polymer interactions in the solid state, and lack of release and premature precipitation under gastric conditions due to the immobilization of drug-loaded silica particles within the enteric HPMCAS plates (**Figure 20**). Crucially, both properties are absent in a simple blend of HPMCAS with the drug-loaded silica. The incorporation of precipitation inhibitors with the drug during loading onto mesoporous silica formulations has the potential to improve both the process and formulation efficiency in the development of poorly soluble drugs and underlines the importance of effective drug-polymer interactions in inhibiting precipitation from mesoporous silica formulations.

#### API/PI Co-loaded Silica Formulations: The Optimal Method for PI Incorporation

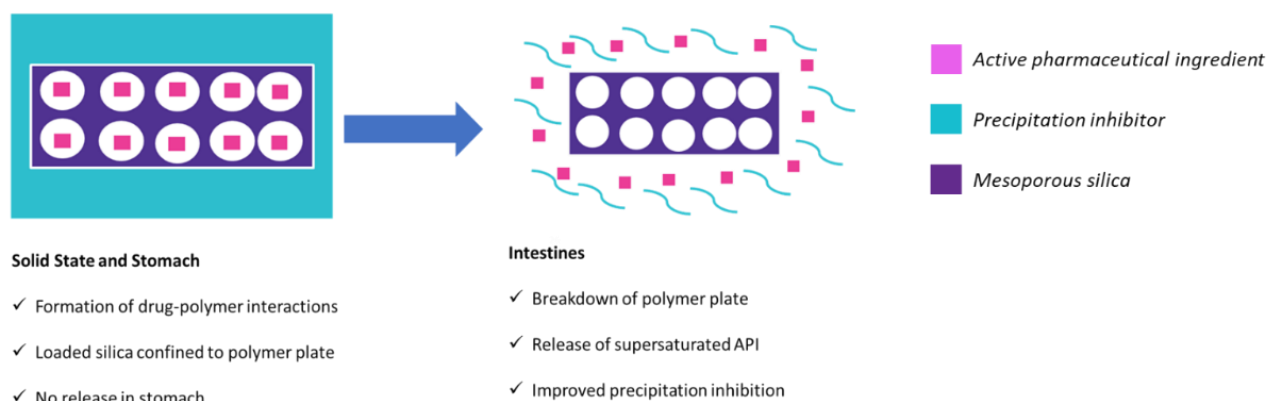


**Figure 20.** Mechanistic rationale for enhanced performance of co-incorporated PI/drug loaded silica formulations.

### 5. *In Silico* Pharmaceuticals: A New Method to Select Precipitation Inhibitors for Mesoporous Silica

#### 5.1 The Role of Molecular Interaction: Quality by selection

The mechanistic rationale for improved formulation performance with the co-incorporation approach reaffirms the importance of drug-polymer interactions in successful precipitation inhibition. However, the polymer selected, HPMCAS, demonstrated solid-state interactions only when it was co-incorporated rather than simply blended into the formulation. Although this was a positive outcome, it suggests that there is still further room for improvement by selecting a precipitation inhibitor that interacts optimally with the drug, i.e. able to generate an effective and strong precipitation inhibition effect while avoiding an overly strong interaction with a slow off-rate. Such an approach, “quality by selection”, could enable optimization of the formulation process for supersaturating systems. There have been previous attempts at rationalizing drug-polymer interactions in precipitation inhibition, but those approaches are mostly complicated and therefore not practicable for screening in early pharmaceutical development (Price *et al.* 2018). On the other hand, current empirical experimental screening approaches can be intensive both from a time and labor perspective, as well as a resource perspective in terms of the amount of drug required, which may be difficult due to paucity of available compound in the early stages of development (Price *et al.* 2018). Therefore, an approach that can

incorporate understanding of the drug-polymer interactions with a quick and efficient screening process would be very useful. For this purpose, the Conductor like Screening Model for Real Solvent (COSMO-RS), which was developed by Klamt (Klamt, *et al.* 1993; 1995; 2003), is a highly interesting prospect.

## **5.2 COSMO-RS: Combining Quantum Chemistry and Thermodynamics**

The conductor like screening model (COSMO) is a quantum mechanical solvent-based theory that is used to generate sigma surface profiles for molecules of interest (Klamt, *et al.* 1993; 1995; 2003). This is achieved *via* conventional quantum chemistry, which treats molecules in isolation at  $T = 0$  K within a cavity inside a dielectric continuum (**Figure 21**) (Klamt, *et al.* 1993; 1995; 2015). The polar surface distribution, or  $\sigma$  profile, of this cavity is solved using the Schrodinger equation. The  $\sigma$  profile describes the distribution of charge throughout the cavity surrounding a molecule and, as such, the charges counteract that of the molecule. For example, the electron withdrawing ability of oxygen results in a small  $\delta^-$  charge on the oxygen atom, this is counteracted with a positive  $\sigma$  charge in the molecular cavity (Klamt, *et al.* 1993).

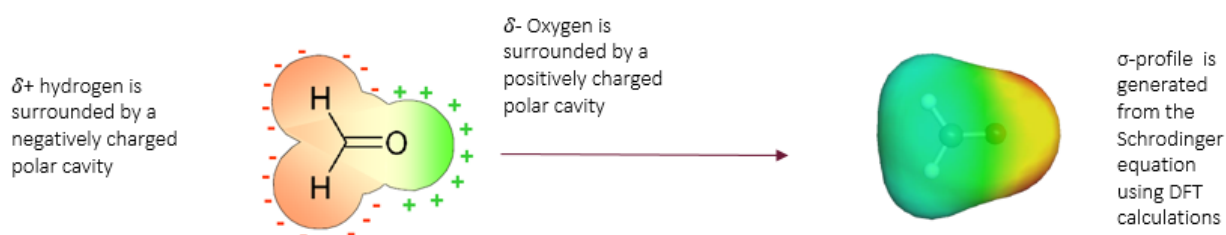


**Figure 21.** COSMO applies quantum mechanical methods to calculate the polar surface cavity of a molecule in isolation at 0 K. The charge distribution in the polar cavity counteracts the charge distribution of the molecule. *Taken from the COSMOlogic website, with permission.*

The chemical potential,  $\mu$ , can be derived from sigma profiles. This is very useful as chemical potential can be used to calculate thermodynamic parameters of interest. However, due to the assumptions

applied by COSMO, this process is unreliable for all but the most neutral compounds (Klamt, *et al.* 1995)

Thus, COSMO-RS (Conductor like Screening Model for Real Solvents), was developed in order to extend applicability of this theory to real-world problems. COSMO-RS implements COSMO as highlighted above to generate  $\sigma$  profiles, however, it then assumes that the sigma profile segments are in close contact and can interact with one another in a pair-wise fashion (Klamt, *et al.* 1995) (**Figure 22**).

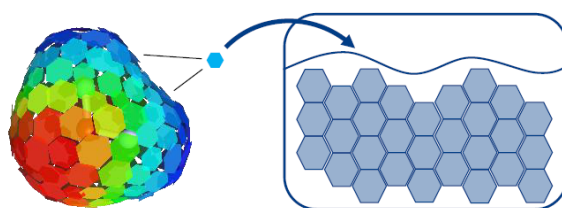


**Figure 22.** COSMO-RS is a statistical thermodynamic theory that assumes sigma profile surface segments can come in contact and interact in a pairwise fashion

Application of COSMO-RS allows the calculation of the sigma potential of a mixture of two systems (Klamt, *et al.* 1995). The sigma potential is calculated by considering the energy requirements of combining sigma segments of one system within the sigma surface of the other (Klamt, *et al.* 1998). Assuming a system consisting of Compound A and Compound B: First, a segment must be removed from A to create a cavity for the incorporation of segment B; this requires energy associated with removing pre-existing contacts between A-segments,  $-\mu_s(\mathbf{A})$ . Second, the new B-segment must be added to the cavity in sigma surface A; this involves forming new interactions between A and B, with related energy costs and gains associated with the two segments interacting,  $E(\mathbf{B}, \mathbf{A})$ , referred to as the COSMO-RS energy. Taken together, these two energy terms describe the thermodynamic cost of combining one B sigma-segment with a one cavity in the sigma-surface of A. To solve the energy cost for the whole system, this calculation is carried out iteratively for all possible combinations of A and B sigma-segments (**Equation 12**). This value is referred to as the Sigma Potential of A and B.

$$\mu_s(A, B) = -kT \ln \int p_s(\sigma A) \exp\left\{\frac{E(\sigma A, \sigma B) - \mu_s(\sigma B)}{RT}\right\} dA\sigma \quad \text{(Equation 12)}$$

This equation has high real-world applicability as the COSMO-RS energy term,  $E(B, A)$ , is calculated such that all binding modes (electrostatic, hydrogen bonding, van der Waals and combinatorial) are considered in the equation **(Equations 13-15)**.

**Electrostatic interaction:**

$$E_{coloumb}(\sigma) = \frac{\alpha}{2}(\sigma + \sigma')^2 \quad \text{(Equation 13)}$$

where  $\alpha$  is an adjustable parameter that is calculated *in situ* via parameterization, and  $\sigma$  and  $\sigma'$  are the solute and solvent segment, respectively.

**Hydrogen bond interactions:**

$$E_{hb}(\sigma) = c_{hb} T \max[0, \sigma_{acc} - \sigma_{hb}] \min[0, \sigma_{don} + \sigma_{hb}] \quad \text{(Equation 14)}$$

where  $\sigma_{acc}$  and  $\sigma_{don}$  are the sigma profile densities of the hydrogen bond acceptor and donor, respectively.  $c_{hb}$  and  $\sigma_{hb}$  are the adjustable parameters corresponding to the hydrogen bond prefactor and the hydrogen bond threshold, respectively. This equation is constructed with minimum and maximum thresholds to ensure that the screening charges exceed the required values for hydrogen bonding to occur.

**Van der Waals interactions:**

$$E_{vdw} = \sum_k \gamma_k A_k \quad \text{(Equation 15)}$$

where the dispersion energy,  $E_{vdw}$ , is related to the surface area of the contact point, A, on the specific element, k, and on an adjustable pre-factor,  $\gamma$ .

From the sigma potential of A, B the chemical potential can be derived, from which a wide range of thermodynamic parameters can be calculated.

**Chemical Potential A, B:**

The full implementation of COSMO and COSMO-RS can be carried out using the software *COSMOtherm* with both quantum mechanics and thermodynamics being carried out by the software. The rate determining step in this process is, by far, the quantum mechanical calculations. Depending on the complexity of the molecules in question, these calculations can take days or weeks and require a large amount of computing power. This is especially problematic for screening purposes, which should be as quick and efficient as possible. Of course, there is the option of bypassing the need for quantum mechanics calculations if the  $\sigma$  profile of the molecule of interest is already in the master database. This, is, however, especially unlikely for complicated organic molecules, especially drug candidates in development.

To avoid this time intensive step, one can create additive sigma surfaces based on pre-calculated fragments stored in a database. This database is available in the software package *COSMOquick* (Loschen, *et al.* 2012). In short, when a molecule is entered into *COSMOquick* the database is searched for molecules with similar chemical structures. The relevant parts of these sigma profiles are then either 'switched on' or 'switched off' and combined to form a new sigma profile for the molecule in question (**Figure 23**). This additive sigma profile can then be used in combination with COSMO-RS in the same way described above. (Loschen, *et al.* 2012)

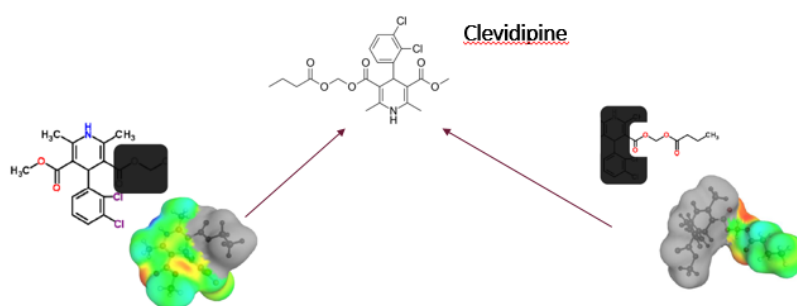


**Figure 23.** COSMOquick applies a fragmentation-based approach to predict the sigma profile of unknown molecules. This avoids the use of time-consuming quantum mechanical calculations. *Taken from the COSMOlogic website, with permission.*

This equation is constructed with minimum and maximum thresholds to ensure that the screening charges exceed the required values for hydrogen bonding to occur.

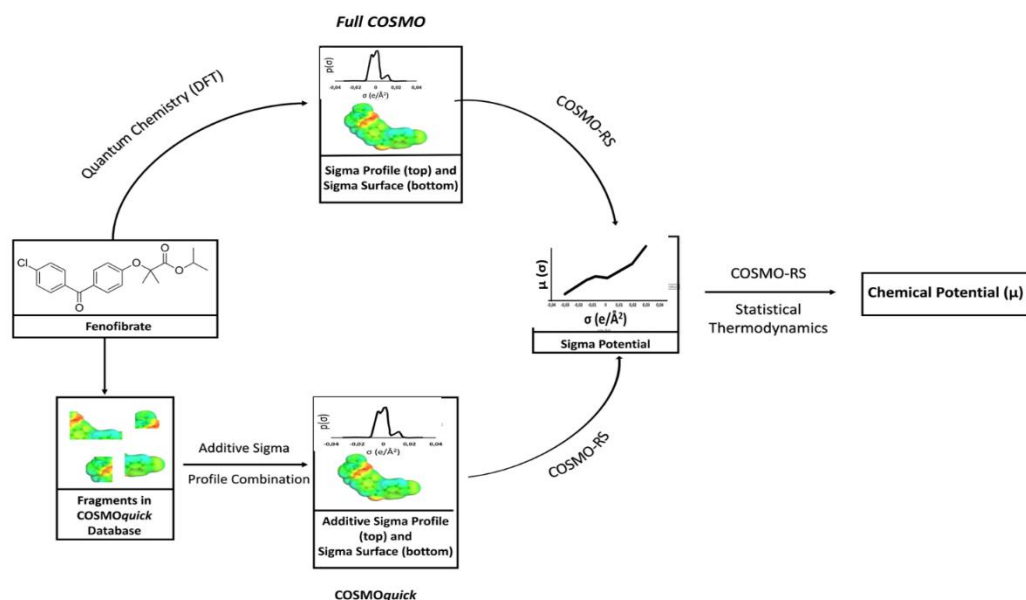


**Figure 24.** Chemical potential, and in turn a wide-range of thermodynamic properties, can be derived from sigma profiles using COSMO-RS theory. Sigma profiles can be obtained by two ways, either through de novo quantum chemical calculations or through an additive combination of previously calculated molecular fragments stored in a large database. The former approach is applied in the full COSMO calculation, whilst the latter is applied in the software package COSMOquick (bottom).

### **5.3 COSMO-RS for Precipitation Inhibitor Screening: Theory**

As previously discussed, the interaction between drug and polymer is essential for effective precipitation inhibition (Price *et al.* 2018; Price *et al.* 2020). The interaction is complex, essentially involving a ternary system where drug, polymer and water all interact to various degrees. Current methods, such as PC-SAFT, would be able to capture such a system but would involve a large amount of time and computing intensity (Paus, *et al.* 2015). We propose a simplified approach, in which the mixing (or excess) enthalpies of drug and excipient are calculated using COSMOquick. This estimated enthalpy is then used to rank potential precipitation inhibitors based on the strength of their molecular





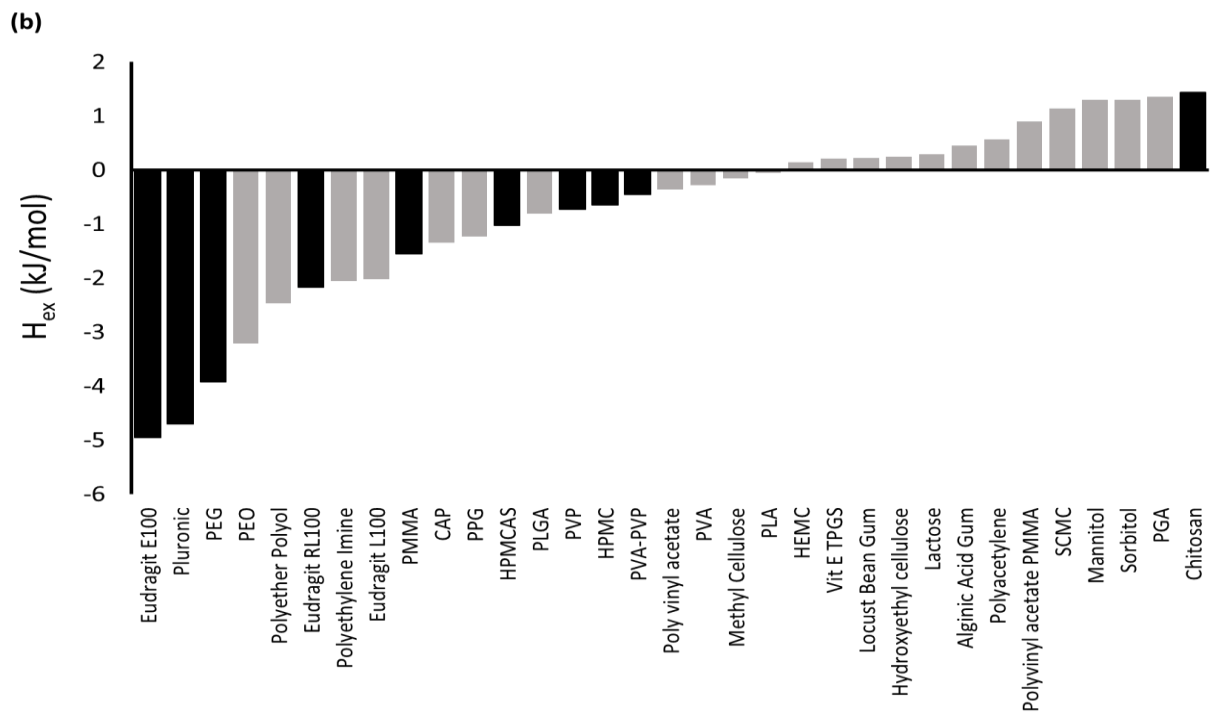
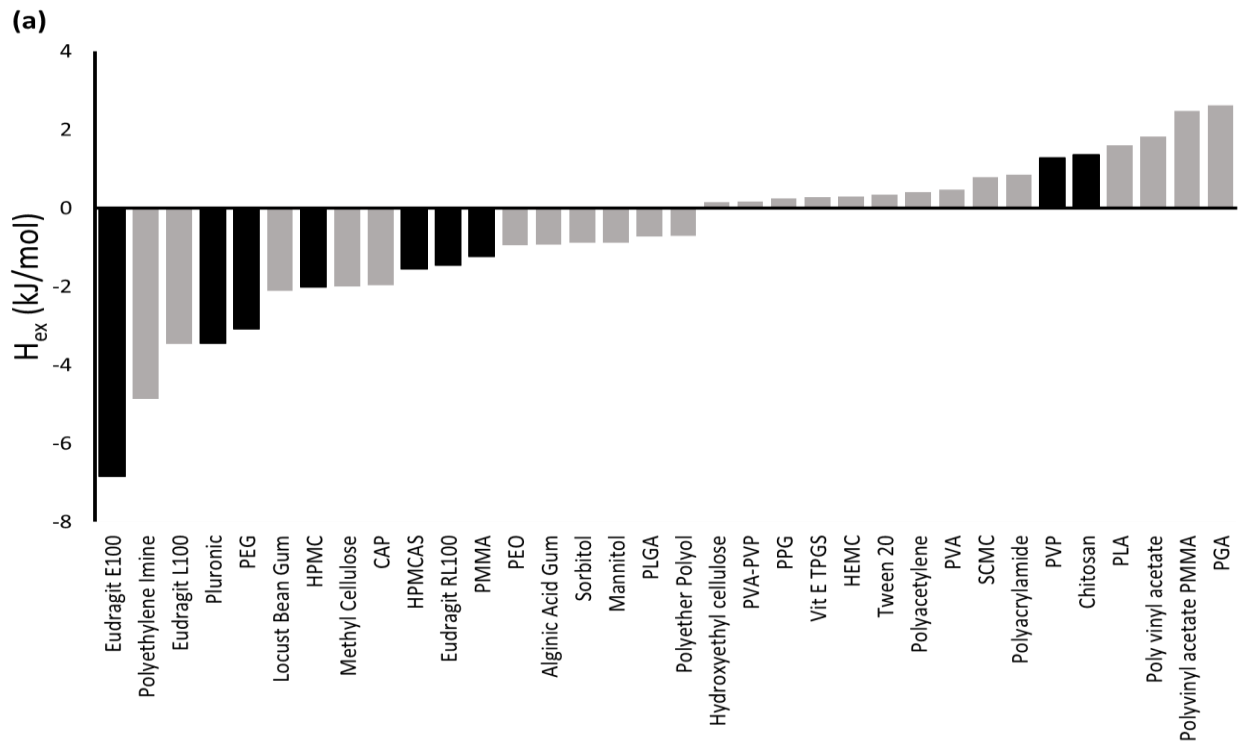
#### **5.4 Incorporation of Precipitation Inhibitors with Mesoporous Silica Formulations**

Although incorporating precipitation inhibitors alongside the drug in mesoporous silica formulations was a main theme of the doctoral studies, this formulation approach was not included in the development of the *in-silico* screening approach. This was to ensure that any relationship between the calculated drug-polymer interactions and the overall formulation performance was related only to the innate precipitation inhibition potential of the polymer, and not to processing techniques.

#### **5.5 COSMO-RS for Precipitation Inhibitor Screening: Output**

Using the COSMO-RS screening protocol, excess enthalpy of interaction upon mixing drug and polymer can be calculated for a given drug in combination with ~50 potential precipitation inhibitors in as little as five minutes. This represents a significant time saving versus traditional experimental screening. All potential inhibitors can be assessed using enthalpy of interaction as a rank-order parameter, which is designated the “COSMO Rank” (**Figure 5 a-c**). This is related to the hypothesis that the more negative the enthalpy, the higher the chance of successful precipitation inhibition based on interactions between drug and PI.

The output from all three polymer screenings is shown in **Figure 26**. Without consideration of the dissolution data, the initial observations point towards a correlation between predicted performance and experimental performance. For example, Chauhan and co-workers reported that Eudragit EPO and HPMC were the most successful polymers to inhibit precipitation of dipyridamole vs. a selection of alternative polymers (Eudragit S100, Eudragit RL100, PEG and PVP) (Chauhan *et al.* 2014). Importantly, the initial COSMO-RS calculations were able to predict the poor ability of PVP to inhibit dipyridamole precipitation experimentally, since a positive enthalpy of interaction was predicted. This was observed experimentally in the same study by Chauhan and co-workers.



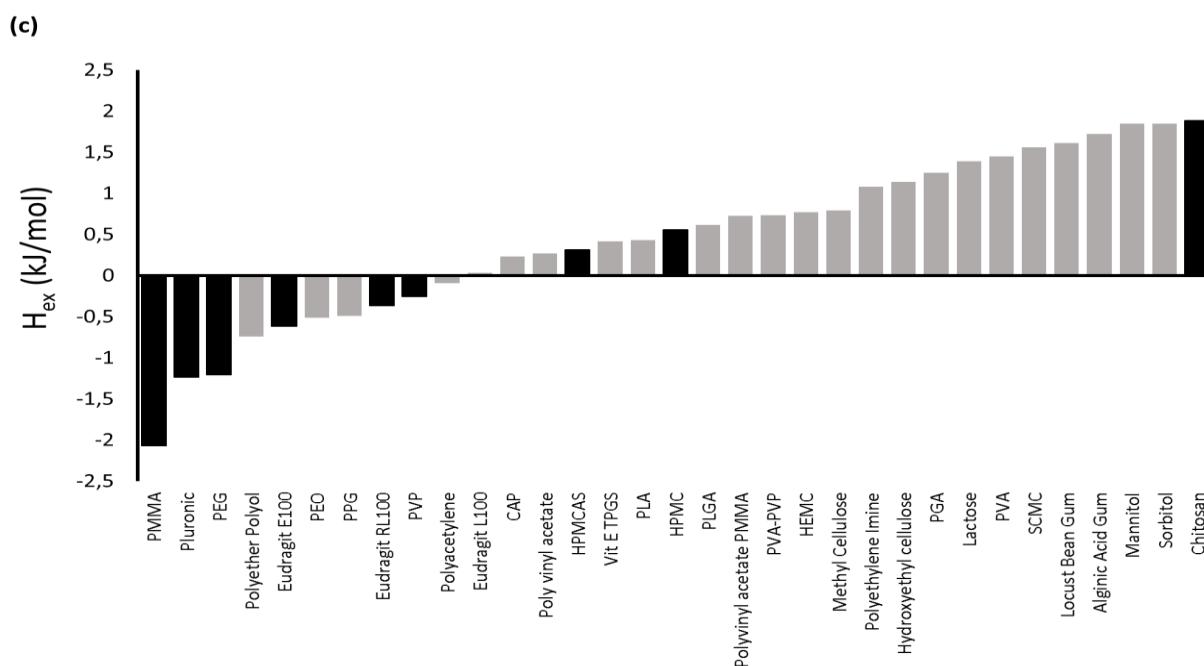


**Figure 26.** COSMO-RS Screen: calculated excess enthalpy of interaction between dipyrnidamole (a), glibenclamide (b) and fenofibrate (c) with a range of potential precipitation inhibitors. Polymers studied experimentally to test the correlation are highlighted as dark bars: Eudragit EPO, Pluronic (PLR), PEG, HPMCAS, PVP, HPMC, Eudragit RLPO, PMMA and Chitosan.

The advantages of the COSMO-RS screening method can be readily seen by comparing it to traditional screening approaches. For example, Petrusavska *et al.* employed an experimental high-throughput screening to arrive at the conclusion that cellulose-based polymers were most effective in inhibiting precipitation of carbamazepine, in contrast to fenofibrate, which performed best in the presence of surfactant. (Petrusavska *et al.* 2013). This was achieved using a combination of solvent-shift method and off-line chromatography. There are two main limitations to this experimental approach. First, inclusion of organic solvents in order to generate supersaturated concentrations provides some uncertainty due to the potential impact of the solvent on the dissolution, interaction and supersaturation of the drug-polymer mixtures. Second, although there have been significant advances in throughput, there is still a practical limit to the number of polymers that can be reasonably screened using these experimental platforms. Illustratively, the top-performing polymers indicated by

the *in-silico* screening protocol were not included in the Petrusevska studies. This shows that experimental screening limits the polymer selection space and reduces the likelihood that the best polymer will be found. Instead, from a selection of standard polymeric precipitation inhibitors such as PVP, HPMCAS and HPMC a “good enough” polymer will be identified. This approach introduces a large amount of uncertainty as to whether the most efficient formulation has been realized and, as observed in our theoretical calculations, these polymers are often mediocre compared to the extended polymer toolbox (He, *et al.* 2010; O’Shea, *et al.* 2017; Laine, *et al.* 2016; Vora, *et al.* 2016)

### **5.6. Correlation between COSMO-Rank and Formulation Performance**

The correlation between the rank order predicted by COSMO and the rank order observed in the dissolution experiments was determined to be 0.91 (0.001,  $p < 0.05$ ), 0.81 (0.01,  $p < 0.05$ ) and 0.61 (0.076,  $p < 0.5$ ) for dipyrindamole, glibenclamide and fenofibrate, respectively (**Table 3-5**). For dipyrindamole and glibenclamide, this indicated a very strong positive correlation between COSMO prediction and formulation performance. This demonstrates that the COSMO-RS screening protocol can be used to select the most optimal precipitation inhibitors whilst avoiding the costly and time-consuming experimental screening. For fenofibrate, a positive correlation was observed between the prediction and results, but to a lesser extent, and was especially impacted by the poor performance of PEG (see section 6.5).

**Table 3.** Spearman's rank correlation coefficient analysis: dipyridamole results

| Polymer              | Calculated Enthalpy (kJ/mol) | AUC ( $\mu\text{g}\cdot\text{mg mL}^{-1}$ ) | COSMO Rank | Dissolution Rank |
|----------------------|------------------------------|---|------------|------------------|
| <i>Eudragit EPO</i>  | -6.84                        | 29000                                       | 1          | 1                |
| <i>PLR</i>           | -3.45                        | 14000                                       | 2          | 3                |
| <i>PEG</i>           | -3.08                        | 8600  | 3          | 5                |
| <i>HPMC</i>          | -2.12                        | 19000                                       | 4          | 2                |
| <i>HPMCAS</i>        | -2.01                        | 13000                                       | 5          | 4                |
| <i>Eudragit RLPO</i> | -1.55                        | 6600  | 6          | 6                |
| <i>PMMA</i>          | -1.46                        | 5800  | 7          | 7                |
| <i>PVP</i>           | -1.23                        | 5300  | 8          | 8                |
| <i>Chitosan</i>      | 1.28                         | 5100  | 9          | 9                |

|   |             |              |                          |
|---|-------------|--------------|--------------------------|
| Spearman's Rank Correlation Coefficient | <b>0.91</b> | Significance | <b>0.001</b><br>P < 0.05 |
|---|-------------|--------------|--------------------------|

**Table 4.** Spearman's rank correlation coefficient analysis: glibenclamide results

| Polymer              | Calculated Enthalpy (kJ/mol) | AUC ( $\mu\text{g}\cdot\text{mg mL}^{-1}$ ) | COSMO Rank | Dissolution Rank |
|----------------------|------------------------------|---|------------|------------------|
| <i>Eudragit EPO</i>  | -4.96                        | 11000                                       | 1          | 1                |
| <i>PLR</i>           | -4.70                        | 7200  | 2          | 2                |
| <i>PEG</i>           | -3.92                        | 960   | 3          | 7                |
| <i>HPMC</i>          | -2.17                        | 6000  | 4          | 4                |
| <i>HPMCAS</i>        | -1.55                        | 6100  | 5          | 3                |
| <i>Eudragit RLPO</i> | -1.03                        | 2100  | 6          | 5                |
| <i>PMMA</i>          | -0.72                        | 2000  | 7          | 6                |
| <i>PVP</i>           | -0.64                        | 600   | 8          | 8                |
| <i>Chitosan</i>      | 1.44                         | 100   | 9          | 9                |

|   |             |              |                         |
|---|-------------|--------------|-------------------------|
| Spearman's Rank Correlation Coefficient | <b>0.81</b> | Significance | <b>0.01</b><br>P < 0.05 |
|---|-------------|--------------|-------------------------|

**Table 5.** Spearman’s rank correlation coefficient analysis: fenofibrate results

| Polymer       | Calculated Enthalpy (kJ/mol) | AUC ( $\mu\text{g}\cdot\text{mg mL}^{-1}$ ) | COSMO Rank | Dissolution Rank |
|---------------|------------------------------|---|------------|------------------|
| PMMA          | -2.07                        | 10000                                       | 1          | 3                |
| PLR           | -1.24                        | 9000  | 2          | 4                |
| PEG           | -1.21                        | 5200  | 3          | 7                |
| Eudragit EPO  | -0.62                        | 19000                                       | 4          | 1                |
| Eudragit RLPO | -0.37                        | 13000                                       | 5          | 2                |
| PVP           | -0.26                        | 5400  | 6          | 5                |
| HPMCAS        | 0.31                         | 5300  | 7          | 6                |
| HPMC          | 0.55                         | 4200  | 8          | 8                |
| Chitosan      | 1.88                         | 1700  | 9          | 9                |

|   |             |              |                         |
|---|-------------|--------------|-------------------------|
| Spearman’s Rank Correlation Coefficient | <b>0.63</b> | Significance | <b>0.08</b><br>P < 0.05 |
|---|-------------|--------------|-------------------------|

From a mechanistic perspective, the COSMO approach is highly attractive as all potential modes of interaction are considered in the calculation. Specifically, when considering the total energy required to combine sigma contacts of the drug and polymer molecules, the sigma potential is calculated ( $\rho\sigma'$ ). One key component of this energy term is the COSMO-RS energy co-efficient  $E(\sigma, \sigma')$ , which considers all major modes of molecular interaction including hydrogen bond, coulombic and Van der Waals interactions. All these modes of interaction have been shown to have a pivotal impact on the overall precipitation inhibition performance of a polymer (Price, *et al.* 2018). The most common interactions are hydrogen bond and Van de Waals interactions (Warren, *et al.* 2010). Eudragit EPO is a good example, being the best performing polymer in both the calculation screening and experimental dissolution. There are several publications reporting that the superior inhibitory potential of Eudragit EPO is related to strong hydrogen bonding and hydrophobic interactions (Price, *et al.* 2018; Higashi, *et al.* 2014). These authors recorded hydrophobic interactions between the aromatic portion of the drug and the EPO polymer backbone as well as a hydrophilic hydrogen bond interaction between

the amino alkyl groups of EPO and the carbonyl groups of the drug in solid state NMR spectroscopy. Such strong interactions between Eudragit EPO and all the drugs studied are possible, hence the good performance of this polymer in both the *in silico* and experimental screenings.

Furthermore, considering the precipitation inhibitors that did not perform well, one can relate the calculation, dissolution performance and potential points of interaction from a mechanistic perspective. One of the interesting cases here is the lack of successful inhibition of dipyridamole precipitation by PVP. As previously mentioned, PVP is one of the polymers most commonly used as a precipitation inhibitor. However, PVP has been shown to be ineffective in sustaining dipyridamole in solution. Chauhan and colleagues demonstrated that no interaction takes place between PVP and dipyridamole in the solid state or in solution (Chauhan *et al.* 2013). This was successfully identified by the COSMO screen and is reflected in the dissolution performance of the formulation in this study.

Ultimately, these robust mechanistic calculations increase the successful prediction of drug-PI interaction and thus precipitation inhibition, as reflected in the strong positive correlations achieved between the COSMO-rank and the final formulation performance.

### **5.7. Limitations of the Approach**

COSMO-RS does not take into consideration the impact of water on the interaction between the drug and PI. It has been widely reported that for a precipitation inhibitor to successfully sustain drug into solution, it must interact with both the drug and the water in the medium or GI tract (Ting, *et al.* 2016; Schram, *et al.* 2015; Price, *et al.* 2018). This simplification becomes especially problematic when considering polymers that have very high hydrophobicity or hydrophilicity, as demonstrated by Schram and co-workers (Schram, *et al.* 2015; Schram, *et al.* 2016). From the data presented in this study, the COSMO prediction for PEG does not correlate to the overall dissolution performance, with PEG being the major deviation in the correlation for all three drugs. This is likely related to the hydrophilicity issue. PEG is very hydrophilic and will bind and interact preferentially with water, this reduces the interaction with the drug and therefore in failure to realize the desired precipitation inhibitor performance. When



the Spearman's rank correlation coefficient analysis was repeated without PEG, the correlation between COSMO-rank and dissolution-rank significantly improved to 0.98 (0.0004,  $p < 0.05$ ) for dipyridamole and glibenclamide. Furthermore, the fenofibrate correlation, which was previously weaker and did not pass significance improves to 0.8 (0.022,  $p < 0.05$ ) and passes the significance test.

These results show that the COSMO-RS protocol should be applied with the foresight that outliers and exceptions may be possible for very hydrophobic and hydrophilic inhibitors. To improve the model, logP could be calculated for all of the trimers within the inhibitor database, and with further work, an upper and lower logP threshold could be incorporated to remove any false positives related to this assumption.

Another limitation is the lack of information regarding molecular weight and viscosity of the inhibitors for incorporation into the calculations. Although conflicting values for these parameters can be found in the literature, both play an important role in precipitation inhibition (Price, *et al.* 2018). Two main hypotheses have been put forward to explain why these parameters should play an important role. The first, and lesser reported, states that molecular weight and viscosity affect precipitation inhibition *via* changes in the diffusion kinetics of both the drug and polymer in solution (Price, *et al.* 2018; Warren, *et al.* 2010). This is something that is not and cannot be considered in the COSMO-RS protocol. The second, and more widely reported, hypothesis relates to an increasing number of binding sites when molecular weight and viscosity are increased (Price, *et al.* 2018; Warren, *et al.* 2010). Given that the COSMO-RS protocol considers in its calculations the interaction between a PI trimer and a drug, this parameter is already considered and therefore, any effect of viscosity between different PIs should be minimized. When considering different viscosities of the same inhibitor, however, the COSMO-RS protocol cannot guide selection of a particular viscosity grade.

### **5.8. Implications of the COSMO-RS Approach**

*In silico* tools are an attractive option for bridging the gap between our current understanding of precipitation inhibitors and practical selection of inhibitors to be used in supersaturating formulations

in pharmaceutical development. In this work, the COSMO-RS model was applied as a novel *in silico* screening tool to successfully predict the formulation performance of a wide range of precipitation inhibitors in formulations of glibenclamide, fenofibrate and dipyridamole. Specifically, it was hypothesized that free enthalpy of mixing (drug-polymer) could be used as a parameter for ranking inhibitors, from highest potential for successful precipitation inhibition to lowest, based on the theoretical interaction between the inhibitor and the drug. For all three compounds a strong positive correlation was observed between the rank assigned based on the calculated free enthalpy of mixing and the overall dissolution performance of the formulation. Conceptually, such an approach can be applied for any formulation that requires precipitation inhibitors. Given the high-throughput and high-speed nature of the *in-silico* calculations, the screening protocol can be carried out for a large number of drug-PI combinations in very short timeframes. Ultimately, this study highlights how *in silico* tools can be used to improve efficiency of PI selection as well as the likelihood that the most optimal formulation can be realized.

### **III. Conclusion and Outlook**

#### **1. Summary**

This body of work aimed to improve the processes underpinning the design and development of mesoporous silica with precipitation inhibitors. First, this involved two extensive literature reviews in the areas of solubility enhancement formulation technologies and precipitation inhibition. Second, a mechanistically rational experimental approach was developed to improve the formulation of precipitation inhibitors with mesoporous silica. The “co-incorporation” approach significantly improved process efficiency and formulation performance. Finally, combining insights from the aforementioned reviews with learnings from the mechanistic analysis of the “co-incorporation” approach, an *in silico* screening protocol was developed to calculate the enthalpy of interaction between drug and polymer, and thus identify the most optimal precipitation inhibitor for a given formulation. Ultimately, these activities have resulted in a substantially optimized workflow for

selecting and combining precipitation inhibitors in mesoporous silica formulations, resulting in more efficient and effective results.

## **2. Co-incorporation: A New Method to Combine Precipitation Inhibitors with Mesoporous Silica**

A novel co-incorporated formulation of glibenclamide and the precipitation inhibitor, HPMCAS, onto mesoporous silica was described. By co-incorporating the precipitation inhibitor, the formulation significantly outperformed the commonly applied simple physical blend, regarding improved supersaturation and dissolution in both single-medium FaSSIF and transfer dissolution assays. Furthermore, the co-incorporation approach allows the removal of a time-consuming and inefficient blending step. To provide a physical mechanistic basis for the improved performance the co-incorporated formulation, a range of spectroscopic tools were utilized. It was concluded that the improved dissolution performance is a synergistic effect related to two key factors: formation of drug-polymer interactions in the solid state, and lack of release and premature precipitation under gastric conditions due to the immobilization of API-loaded silica particles within the enteric HPMCAS plates. Crucially, both of these properties are absent in a simple HPMCAS blend. Ultimately, the co-incorporation of precipitation inhibitors with the API on mesoporous silica formulations has the potential to improve both the process and formulation efficiency in the development of poorly soluble drugs. Furthermore, the mechanistic analysis of the formulation performance underlines the importance of drug-polymer interactions for successful precipitation inhibition and performance of mesoporous silica formulations.

## **3. *In Silico* Pharmaceuticals: A New Method to Select Precipitation Inhibitors for Mesoporous Silica**

Building on the extensive review article and the critical parameters identified during the co-incorporation study, drug-polymer interactions were identified as a critical factor in determining formulation success in supersaturating formulations. Building on this, and the general absence of any technique or screening approach that is suitable for pharmaceutical screening, a novel *in silico* screening protocol for the selection of precipitation inhibitors for supersaturating formulations was developed. The protocol used the COSMO-RS model to calculate excess enthalpy of interaction between API and precipitation inhibitors, which was then applied as a rank-order parameter to select potential precipitation inhibitors. Conceptually, such an approach may be applied for any enabling formulation that requires precipitation inhibitors, for example HME or SDD, but further work is required to validate this cross-formulation applicability. Despite the simplifications and assumptions in the COSMO-RS protocol, strong positive correlations were obtained between the rank-order prediction and formulation performance for the APIs studied. Furthermore, given the high-

throughput and high-speed nature of the *in-silico* calculations, the screening protocol is very attractive as a score-card approach for the design of enabling formulations for poorly soluble APIs in the pharmaceutical industry. Ultimately, this study highlights how *in silico* tools can be used to improve efficiency of precipitation inhibitor selection as well as the likelihood that the most optimal formulation will be realized.

#### **4. Future Work**

Looking forward, further work will be carried out to combine the co-loading approach with the COSMO-RS screening protocol to assess if the correlations observed using the blending method also apply to the co-loading approach. Furthermore, there are potentially further applications of the COSMO-RS model in pharmaceutical screening, including, but not limited to screening of polymers for spray dried dispersion or hot melt extrusion formulations, assessment of co-crystal or co-amorphous excipients and assessment of excipients for effective lipid formulation. Further down the line, it is expected that computation approaches will have a transformative impact on the efficiency and outcome of pharmaceutical development, with tools such as artificial intelligence and machine learning already on the horizon to assist in the design and development of oral solid dosage form formulations.

## **V. Deutsche Zusammenfassung**

### **1. Einführung**

Damit ein oral verabreichtes Arzneimittel seine biologische Wirkung entfalten kann, muss es zunächst durch den Magen-Darm-Trakt (GI-Trakt) in den systemischen Kreislauf gelangen. Um dies zu erreichen, muss ein Medikament in den Flüssigkeiten des GI-Trakts ausreichend löslich sein. In den letzten Jahren gab es in den Entwicklungspipelines vermehrt Arzneimittel mit geringer Löslichkeit, was zu einer verringerten Bioverfügbarkeit und einem erhöhten Risiko des Scheiterns während des Entwicklungsprozesses führte. Als Reaktion darauf haben Chemiker und Formulierer Strategien entwickelt, die die Löslichkeit und die daraus resultierende Bioverfügbarkeit dieser schwer löslichen Kandidaten verbessern können. Zu diesen Ansätzen gehören chemische Modifikationen in der Synthese, wie Salzbildung und Prodrugs oder Formulierungsmodifizierungsansätze wie mizellare Systeme, Co-Solventie, Partikelgrößenreduzierung, Komplexbildung und Technologien mit amorphen Phasen (Timpe, *et al.* 2007). Amorphe Formulierungen sind besonders attraktiv aufgrund der deutlichen Verbesserung der Löslichkeit, die die amorphe Form bieten kann (Timpe, *et al.* 2007). Amorphe Feststoffe haben wesentlich höhere Löslichkeiten im Vergleich zu Formulierungen, die die entsprechenden kristallinen Phasen verwenden. Allerdings sind amorphe Feststoffe aufgrund der hohen Energie, die mit dieser Festkörperform verbunden ist, in der Regel instabil oder metastabil. Daher müssen spezielle Formulierungstechnologien eingesetzt werden, um die amorphe Form des schwer löslichen Arzneimittels zu stabilisieren. Die häufigste dieser Methoden besteht darin, den Wirkstoff in der amorphen Form in einer polymeren Matrix zu immobilisieren (Chokshi, *et al.* 2007). Amorphe Formulierungen erzeugen in Lösung Konzentrationen, die höher sind als die thermodynamische Löslichkeit. Dies wird als Übersättigung bezeichnet. Übersättigung ist ein energetisch ungünstiger Zustand. Deshalb müssen solche Formulierungen auch sicherstellen, dass eine Ausfällung aus diesem Zustand verhindert wird. Typischerweise können polymere Hilfsstoffe als Fällungsinhibitoren eingesetzt werden.

## **2. Die Bedeutung von Arzneistoff-Polymer-Wechselwirkungen bei der Fällungsinhibierung**

Polymere Präzipitationsinhibitoren haben in der Literatur eine weite Verbreitung gefunden, wobei die am häufigsten verwendeten Polymere Cellulosederivate, Methacrylate und Polyvinylpyrrolidone beinhalten (Warren, *et al.* 2010). Die Wirkung von Polymeren zur Verhinderung von Ausfällungen beruht auf der Interferenz mit der Keimbildung und dem Kristallwachstum durch Wechselwirkung sowohl mit dem in übersättigter Lösung vorliegenden Molekülen des Arzneimittels als auch mit der wässrigen Umgebung (Xu, *et al.* 2013). Diese Wechselwirkungen verhindern die Adsorption von Wirkstoffmolekülen an der wachsenden Kristallfläche, so dass die Präzipitation gestoppt wird. Für die kinetische Hemmung ist die Wechselwirkung zwischen dem Arzneimittel und dem Polymer von entscheidender Bedeutung. Polymere können insbesondere über Wasserstoffbrückenbindungen, polare oder Dispersionskräfte in unterschiedlichem Ausmaß mit dem Arzneimittel wechselwirken (Price, *et al.* 2018; Price, *et al.* 2019; Warren, *et al.* 2010; Brouwers *et al.* 2009; Gao, *et al.* 2012). In der Literatur wurde über viele Techniken berichtet, bei denen Technologien wie die NMR-Spektroskopie zum Einsatz kommen. Der derzeitige Stand der Technik zur Untersuchung der Wechselwirkungen zwischen Wirkstoff und als Präzipitationsinhibitor eingesetztem Polymer ist jedoch für das Screening nicht geeignet, da hohe API-Mengen und ein hoher zeitlicher Aufwand benötigt werden, die für die pharmazeutische Entwicklung in einem frühen Stadium nicht verfügbar sind.

## **3. Mesoporöse Kieselsäure: Eine neue Formulierungstechnologie**

Eine neue Technologie zur Formulierung amorpher Feststoffe ist die Verwendung mesoporöser Materialien als Träger für den Wirkstoff. Mesoporöses Siliziumdioxid ist ein Siliziumdioxid-Hilfsstoff, der ein hochporöses Netzwerk besitzt. Mit Beladung des Siliziumdioxids mit einer konzentrierten Lösung des Wirkstoffs wird dieser molekular an der Oberfläche des Siliziumdioxids adsorbiert. Aufgrund der Größe der Poren, die einen mittleren Durchmesser von etwa 6 nm haben, ist das molekular adsorbierte Molekül des Wirkstoffs lokal und sterisch fixiert, wodurch eine Rekristallisation verhindert wird (Ditzinger, *et al.* 2018). Bei der Verabreichung mesoporöser

Siliziumdioxidformulierungen kommt es zu einer Verdrängung einzelner Wirkstoffmoleküle von der Oberfläche des Siliziumdioxids in Lösung, wodurch eine Übersättigung gegenüber dem kristallinen Wirkstoff entsteht, die mit Präzipitationsinhibitoren stabilisiert werden muss (Guzman, *et al.* 2007). Da es sich bei mesoporösem Siliziumdioxid um eine neue Formulierungstechnologie handelt, ist bisher wenig darüber bekannt wie Fällungsinhibitoren am effektivsten ausgewählt und mit mesoporösen Siliziumdioxidformulierungen kombiniert werden können.

#### **4. Ziele der Dissertation**

Das Ziel der Arbeit war die Entwicklung und Optimierung eines neuen Arbeitsablaufs zur Auswahl von Präzipitationsinhibitoren in mesoporösen Siliziumdioxidformulierungen. Hierzu wurde zunächst der aktuelle Stand der Technik von mesoporösen Siliziumdioxidformulierungen und Präzipitationsinhibitoren betrachtet. Danach wurde die Methode zur Kombination von Präzipitationsinhibitoren mit mesoporösem Siliziumdioxid analysiert und verbessert, indem ein Co-Inkorporationsansatz entwickelt wurde. Drittens wurde eine physikalisch-mechanistische Rationale des neu entwickelten Ansatzes entwickelt. Schließlich wurden die Erkenntnisse hieraus in Kombination mit dem oben erwähnten Stand der Technik, zur Entwicklung eines neuen computergestützten Arbeitsablaufs zur Auswahl der optimalen Präzipitationsinhibitoren für ein gegebenes Wirkstoff verwendet. Dieser basierte auf der Kombination von Quantenmechanik und Thermodynamik zur Berechnung der Mischungsenthalpie von Arzneistoff und Polymeren als Prädiktor für eine wirksame Inhibition der Präzipitation.

#### **5. Eine neue Methode zur Kombination von Präzipitationsinhibitoren mit mesoporösem Siliziumdioxid**

Es gibt keine systematische Studie darüber, wie Präzipitationsinhibitoren am besten in mesoporösen Siliziumdioxidformulierungen verwendet werden können. Die derzeitige Praxis beinhaltet die Verwendung von Präzipitationsinhibitoren in einer physikalischen Mischung mit dem mit dem Wirkstoff beladenen Siliciumdioxid. Der Mischvorgang erfolgt entweder durch Pistill und Mörser oder

durch einfaches Rühren. Da es keine fest definierte Methode hierfür gibt, besteht Unsicherheit darüber, wie zuverlässig der Präzipitationsinhibitor mit dem mit dem Wirkstoff beladenen Siliziumdioxid kombiniert wird, so dass eine konstante Qualität der Chargen erhalten wird. Zusätzlich zu den praktischen Einschränkungen des Ansatzes stellt die Einarbeitung des Präzipitationsinhibitors nach der Beladung des Siliziumdioxids einen unnötigen und nicht unbedeutenden Schritt im Formulierungsprozess dar. Das Auflösen des Präzipitationsinhibitors zusätzlich zum Wirkstoff in die zur Beladung des Siliziumdioxid verwendeten Lösung kann das Auflösungsverhalten und die Verhinderung der Präzipitation verbessern. In dieser Arbeit wurde eine neuartige Formulierung von Glibenclamid und dem Präzipitationsinhibitor HPMCAS auf mesoporösem Siliciumdioxid beschrieben. Durch die gemeinsame Einarbeitung des Präzipitationsinhibitors übertraf die Formulierung die physikalische Mischung deutlich. Darüber hinaus ermöglicht der Co-Inkorporationsansatz das Weglassen eines zeitaufwändigen und ineffizienten Mischungsschritts. Um ein physikalisch-mechanistisches Verständnis für die verbesserte Leistung der Formulierung zu schaffen, wurde eine Reihe von spektroskopischen Werkzeugen eingesetzt. Daraus resultiert, dass das verbesserte Auflösungsverhalten und die bessere Inhibition der Präzipitation ein synergistischer Effekt ist, der mit zwei Faktoren zusammenhängt: Wirkstoff-Polymer-Wechselwirkungen in der festen Phase und Verhinderung der Freisetzung unter den Bedingungen des Magens aufgrund der Immobilisierung von API-beladenen Siliziumdioxidpartikeln im enterischen HPMCAS. Entscheidend ist, dass diese beiden Eigenschaften bei einer einfachen HPMCAS-Mischung fehlen. Letztlich hat die Co-Inkorporation von Präzipitationsinhibitoren mit dem Wirkstoff auf mesoporösen Siliziumdioxidformulierungen das Potenzial, sowohl die Prozess- als auch die Formulierungseffizienz bei der Entwicklung schwerlöslicher Arzneimittel zu verbessern.



## **6. Eine neue Methode zur Auswahl von Präzipitationsinhibitoren für mesoporöse Siliziumdioxidformulierungen mittels in-silico Verfahren**

Das mechanistische Verständnis für eine verbesserte Formulierungsleistung mit dem Co-Inkorporationsansatz bestätigt die Bedeutung von Wirkstoff-Polymer-Interaktionen für eine erfolgreiche Präzipitationsinhibition. Die Bedeutung dieser wurde schon in der Literaturrecherche identifiziert. Daher wäre ein Ansatz, der das Verständnis der Wirkstoff-Polymer-Wechselwirkungen mit einem schnellen und effizienten Screening-Verfahren verbinden kann, sehr nützlich. Zu diesem Zweck wurde das „Conductor like Screening Model for Real Solvent“ (COSMO-RS), das von Klamt (Klamt, *et al.* 1993; 1995; 2003) entwickelt wurde, identifiziert. COSMO-RS ist ein quantenmechanisches Modell, mit dessen Hilfe thermodynamische Eigenschaften abgeleitet werden können (Klamt, *et al.* 1993; 1995; 2003). Aufbauend auf diesem theoretischen Ansatz schlugen wir vor, die Mischungsenthalpien von Wirkstoff und Polymer mit Hilfe der COSMO-RS-Theorie zu berechnen. Nach der Entwicklung des in-silico Ansatzes zur Berechnung dieser Eigenschaft wurde die Wirkstoff-Polymer-Mischungsenthalpie verwendet, um potenzielle Präzipitationsinhibitoren auf der Grundlage der Stärke der molekularen Wechselwirkung mit dem Wirkstoff zu klassifizieren. Es wurde die Hypothese aufgestellt, dass dieses neuartige in-silico Protokoll für das Screening potenzieller Fällungsinhibitoren verwendet werden kann. Dies ermöglicht eine gezieltere Auswahl und reduziert somit den experimentellen Aufwand für das Screening vieler potenzieller Präzipitationsinhibitoren erheblich. Dieser neue Ansatz wurde beim Screening von Präzipitationsinhibitoren für drei Modellverbindungen angewandt: Glibenclamid, Dipyridamol und Fenofibrat, die mit mesoporösem Siliziumdioxid formuliert wurden. Für alle drei Wirkstoffe wurde eine starke positive Korrelation zwischen dem Rang, der aufgrund der berechneten freien Mischungsenthalpie vergeben wurde, und der gesamten Formulierungsleistung beobachtet. Letztendlich zeigt diese Studie auf, wie in-silico Werkzeuge eingesetzt werden können, um die Effizienz der Auswahl des Präzipitationsinhibitors zu verbessern.

## 7. Schlussfolgerung und Ausblick

Diese Arbeit zielte darauf ab, die Prozesse zu verbessern, die dem Design und der Entwicklung von mesoporösem Siliziumdioxidformulierungen mit Präzipitationsinhibitoren zugrunde liegen. Dazu gehören zunächst zwei umfangreiche Literaturrecherchen auf dem Gebiet der Löslichkeitsverbessernden Formulierungstechnologien und der Präzipitationsinhibition. Zweitens wurde ein mechanistisch-rationaler experimenteller Ansatz zur Verbesserung der Formulierung von Präzipitationsinhibitoren mit mesoporösem Siliziumdioxid entwickelt, wobei der "Co-Inkorporations Ansatz" die Formulierungsleistung deutlich verbesserte. Schließlich wurde ein in-silico Screening-Protokoll zur Berechnung der Wechselwirkung zwischen Wirkstoff und Polymer entwickelt, um den optimalen Präzipitationsinhibitor für eine Formulierung zu identifizieren. Dazu wurden die Erkenntnisse aus der Literaturrecherche und die Erkenntnisse aus der mechanistischen Analyse des "Co-Inkorporations Ansatzes" kombiniert. Diese Aktivitäten haben zu einem optimierten Arbeitsablauf für die Auswahl und Kombination von Präzipitationsinhibitoren in mesoporösen Siliziumdioxidformulierungen geführt. In Zukunft werden weitere Arbeiten durchgeführt, um den „Co-Loading-Ansatz“ mit dem COSMO-RS-Screening-Protokoll zu kombinieren. Ziel ist zu beurteilen, ob die mit der Mischmethode beobachteten Korrelationen auch auf den „Co-Loading-Ansatz“ zutreffen. Darüber hinaus gibt es mögliche weitere Anwendungen des COSMO-RS-Modells beim Screening, einschließlich, aber nicht beschränkt auf: Screening von Polymeren für sprühgetrocknete Dispersion von hot-melt Extrudaten, Bewertung von co-kristallinen oder co-amorphen Formulierungen und Bewertung von Lipidformulierung. Für die Zukunft wird erwartet, dass in-silico Ansätze einen Einfluss auf die Effizienz und Leistung in der pharmazeutischen Entwicklung haben werden, wobei Werkzeuge wie künstliche Intelligenz und maschinelles Lernen bereits in Sichtweite sind, um Design und Entwicklung von oralen festen Dosierungsformulierungen zu unterstützen.

## VI. References

**Abd-Elrahman, AA.** *et al.* Ketoprofen mesoporous silica nanoparticles SBA-15 hard gelatin capsules: preparation and in vitro/in vivo characterization. *Drug Delivery*. 2016; **23**(9): 3387-3398

**Alhalaweh, A.** *et al.* Physical stability of drugs after storage above and below the glass transition temperature: Relationship to glass-forming ability. *International Journal of Pharmacy*. 2015; **495**(1): 312-317

**Alonzo, DE.** *et al.* Characterizing the impact of hydroxypropylmethyl cellulose on the growth and nucleation kinetics of felodipine from supersaturated solutions. *Crystal Growth & Design*. 2012; **12**(3): 1538-1547

**Ambrogi, V.** *et al.* Use of SBA-15 for furosemide oral delivery enhancement. *European Journal of Pharmaceutical Science*. 2012; **46**(1-2): 43-48

**Amidon, GL.** *et al.* A theoretical basis for a biopharmaceutic drug classification: the correlation of in vitro drug product dissolution and in vivo bioavailability. *Pharmaceutical Research*. 1995; **12**(3)

**Andersson, J.** *et al.* Influences of material characteristics on ibuprofen drug loading and release profiles from ordered micro- and mesoporous silica matrices. *Chemistry of Materials*. 2004; **16**: 4160-4167

**Atkin, R.** *et al.* Mechanism of cationic surfactant adsorption at the solid–aqueous interface. *Advanced Colloid and Interface Sciences*. 2003; **103**(3): 219-304

**Augustijns, P.** and Brewster, ME. Supersaturating drug delivery systems: fast is not necessarily good enough. *Journal of Pharmaceutical Sciences*. 2012; **101**(1): 7-9

**Avramov, I.** *et al.* Glass-forming ability versus stability of silicate glasses. II. Theoretical demonstration. *Journal of Non-Crystalline Solids*. 2003; **320**: 9-20

**Baghel, S.** *et al.* Theoretical and experimental investigation of drug-polymer interaction and miscibility and its impact on drug supersaturation in aqueous medium. *European Journal of Pharmaceutics and Biopharmaceutics*. 2016; **107**, 16-31.

**Baghel, S.** *et al.* Theoretical and experimental investigation of drug-polymer interaction and miscibility and its impact on drug supersaturation in aqueous medium. *European Journal of Pharmaceutics and Biopharmaceutics*. 2016; **107**, 16-31.

**Baird, JA.** *et al.* Classification System to Assess the Crystallization Tendency of Organic Molecules from Undercooled Melts. *Journal of Pharmaceutical Sciences*. 2010; **99**: 3787–3806.

**Barbe, C.** *et al.* Silica particles: A Novel Drug Delivery System. *Advanced Materials*. 2004; **16**: 1959-1966.

**Bartsch, S.** *et al.* Physicochemical properties of the binary system glibenclamide and polyethylene glycol 4000. *Journal of Thermal Analysis and Calorimetry*. 2005; **77**(2): 1321-1337

**Bathfield, M.** *et al.* Thermosensitive and Drug-Loaded Ordered Mesoporous Silica: A Direct and Effective Synthesis Using PEO-b-PNIPAM Block Copolymers. *Chemistry of Materials*. 2016; **28**(10): 3374-3384

**Bhatnagar, A** and Sillanpaa, M. Utilization of Agro-industrial and Municipal Waste Materials as Potential Adsorbents for Water Treatment- a Review. *Chemical Engineering Journal*. 2010; **157**: 277-296.

**Biswas N.** Modified mesoporous silica nanoparticles for enhancing oral bioavailability and antihypertensive activity of poorly water soluble valsartan. *European Journal of Pharmaceutical Science*. 2017; **99**: 152-160

**Bouchoucha, M. et al.** Size-Controlled Functionalized Mesoporous Silica Nanoparticles for Tunable Drug Release and Enhanced Anti-Tumoral Activity. *Chemistry of Materials*. 2016; **28**(12): 4243-4258

**Brás, AR. et al.** 2014. Influence of Nanoscale Confinement on the Molecular Mobility of Ibuprofen. *Journal of Physical Chemistry C*. 2014; **118**: 13857–13868

**Brewster, ME. et al.** Supersaturating Drug Delivery Systems: Effect of Hydrophilic Cyclodextrins and other Excipients on the Formation and Stabilisation of Supersaturated Drug Solutions. *Archiv der Pharmazie*. 2008, **63**(3), 217-220

**Brewster, ME. et al.** The Utility of Cyclodextrins for Enhancing Oral Bioavailability. *Journal of Controlled Release*. 2007, **123**, 78-99.

**Brouwers, J. et al.** Supersaturating drug delivery systems: The answer to solubility-limited oral bioavailability? *Journal of pharmaceutical science*. 2009; **98**(8): 2549-2572.

**Brown, DG. et al.** A review of traditional and novel oral anticoagulant and antiplatelet therapy for dermatologists and dermatologic surgeons. *Journal of the American Academy of Dermatology*. 2015; **72** (3): 524-534.

**Bukara, K. et al.** Ordered mesoporous silica to enhance the bioavailability of poorly water-soluble drugs: Proof of concept in man. *European Journal of Pharmaceutics and Biopharmaceutics*. 2016; **108**: 220-225.

**Butler, JM.** And Dressman, JB. The developability classification system: application of biopharmaceutics concepts to formulation development. *Journal of Pharmaceutical Sciences*. 2010; **99**(12).

**Chauhan, H. et al.** Correlating the behaviour of polymers in solution as PI to its amorphous stabilization ability in solid dispersions. *Journal of Pharmaceutical Sciences*. 2013; **102**(6): 1924-1935

**Chauhan, H. et al.** Correlation of inhibitory effects of polymers on indomethacin precipitation in solution and amorphous solid crystallization based on molecular interaction. *Pharmaceutical Research*. 2014; **31**(2): 500-515.

**Chavan, B. et al.** Evaluation of the inhibitory potential of HPMC, PVP and PC polymers on nucleation and crystal growth. *RSC Advances*. 2016; **6**: 77569-77567

**Chen, Y. et al.** Drug-polymer-water interaction and its implication for the dissolution performance of amorphous solid dispersions. *Molecular Pharmaceutics*. 2014; **12**: 576-589.

**Chen, Y. et al.** Drug-polymer-water interaction and its implication for the dissolution performance of amorphous solid dispersions. *Molecular Pharmaceutics*. 2014; **12**: 576-589.

**Chokshi, RJ.** et al. Improving the Dissolution Rate of Poorly Soluble Drugs by Solid Dispersion and Solid Solution: Pros and Cons. *Drug Delivery*. 2007; **14**(1): 33-45

**Cordeiro, T.** et al. Stabilizing Unstable Amorphous Menthol through Inclusion in Mesoporous Silica Hosts. *Molecular Pharmaceutics*. 2017; **14**: 3164–3177.

**Creasey, AA.** et al. Inhibiting the Precipitation of Poorly Water-Soluble Drugs from Labrasol Formulations. *Pharmaceutical Technology*. 2011; **35**(6)

**Ditzinger, F.** and Price, DJ. et al. Opportunities for Successful Stabilization of Poor Glass-Forming Drugs: A Stability-Based Comparison of Mesoporous Silica Versus Hot Melt Extrusion Technologies. *Pharmaceutics*. 2019; **11**(577).

**Ditzinger, F.** et al. Lipophilicity and hydrophobicity considerations in bio-enabling oral formulations approaches—a PEARRL review. *Journal of Pharmacy and Pharmacology*. Epub ahead of print

**Dokoumetzidis, A.** and Macheras, P. A Century of Dissolution Research: From Noyes and Whitney to the Biopharmaceutics Classification System. *International Journal of Pharmaceutics*. 2006, **321**(1-2): 1-11.

**Dressman, B.** et al. Mesoporous silica-based dosage forms improve release characteristics of poorly soluble drugs: case example fenofibrate. *Journal of Pharmacy and Pharmacology*. 2015; **68**(5): 634-645

**Elder, JP.** A new accelerated oxidative stability test for glass-forming organic compounds. *Thermochimica Acta*. 1990; **166**: 199-206

**Flory, PJ.** Principles of Polymer Chemistry. Cornell University Press. 1953

**Flory, PJ.** Thermodynamics of high-polymer solutions. *Journal of Chemical Physics*. 1942; **10**: 51–61.

**Furman, BL.** et al. Studies on the hypoglycaemic action of gliclazide, a sulphonyl-urea drug. *Journal of Pharmacy and Pharmacology*. 1977; **55**.

**Gaffney, JS.** et al. Fourier Transform Infrared (FTIR) Spectroscopy. In: *Characterization of Materials*. 2<sup>nd</sup> edn. Hoboken, NJ, USA, Wiley, 2012

**Gao, P.** and Shi, Y. Characterization of supersaturating formulations for improved absorption of poorly soluble drugs. *The AAPS journal*. 2012; **5**: 1-11.

**Gardner, CR.** et al. Drugs as Materials: Valuing Physical Form in Drug Discovery. *Nature Reviews: Drug Discovery*. 2004; **3**: 926-943.

**Garido, L.** and Beckmann, N. *New Applications of NMR in Drug Discovery and Development*. 1<sup>st</sup> edn. London, UK, Royal Society of Chemistry, 2014

**Gharagheizi, F.** et al. Group contribution-based method for determination of solubility parameter of nonelectrolyte organic compounds. *Journal of Industrial Engineering and Chemistry Research*. 2011; **50**: 10344-10349.

**Gharagheizi, F.** QSPR studies of solubility parameter by means of genetic algorithm-based multivariate linear regression and generalized regression neural network. *QSAR and Combinatorial Sciences*. 2008; **27**(2): 165-170.

**Gignone, A. et al.** Incorporation of clotrimazole in Ordered Mesoporous Silica by supercritical CO<sub>2</sub>. *Microporous and Mesoporous Materials*. 2014; **200**: 291-296

**Grant, D.** and Higuchi, T. Solubility Behaviour of Organic Compounds. *John Wiley and Sons*. 1990

**Gunther, H.** NMR Spectroscopy: Basic Principles, Concepts and Applications in Chemistry. 3<sup>rd</sup> edn. Hoboken, NJ, USA, Wiley, 2013

**Gupta, J. et al.** Prediction of solubility parameters and miscibility of pharmaceutical compounds by molecular dynamics simulations. *Journal of Physical Chemistry B*. 2011; **115**, 2014–2023

**Guzmán, HR. et al.** A “spring and parachute” approach to designing solid celecoxib formulations having enhanced oral absorption. *The AAPS Journal*. 2004; **6**(1): T2189

**Hacene, YC. et al.** Drug loaded and ethylcellulose coated mesoporous silica for controlled drug release prepared using a pilot scale fluid bed system. *International Journal of Pharmacy*. 2016; **506**: 132-147

**Hanada, M. et al.** Enhanced Dissolution of a Porous Carrier-Containing Ternary Amorphous Solid Dispersion System Prepared by a Hot Melt Method. *J Pharm Sci*. 107(1), (2018), 362-371

**Hartono, SB. et al.** Amine functionalized cubic mesoporous silica nanoparticles as an oral delivery system for curcumin bioavailability enhancement. *Nanotechnology*. 2016; **27**(50)

**He, H. et al.** In vitro and in vivo evaluation of fenofibrate solid dispersion prepared by hot-melt extrusion. *Drug Dev Ind Pharm*. 2010; **36**(6): 681-687.

**Heikkila, T. et al.** Evaluation of mesoporous TCPSi, MCM-41, SBA-15, and TUD-1 materials as API carriers for oral drug delivery. *Drug Delivery*. 2007; **14**(6): 337-347

**Higashi, K. et al.** Insights into Atomic-level Interaction between Mefenamic Acid and Eudragit® EPO in a Supersaturated Solution by High Resolution Magic-Angle Spinning NMR Spectroscopy. *Molecular Pharmaceutics*. 2014; **11**(1): 351-357.

**Higuchi, T.** Rate of Release of Medicaments from Ointment Bases Containing Drugs in Suspension. *Journal of Pharmaceutical Sciences*. 1961; **50**(10): 874-875

**Hildebrand, J.** and Scott, R. 1950. *Solubility of Nonelectrolytes*. Reinhold Pub Co., New York

**Hillerstrom, A. et al.** Solvent strategies for loading and release in mesoporous silica. *Colloid and Interface Science Communications*. 2014; **3**: 5-8

**Horcajada, P. et al.** Influence of pore size of MCM-41 matrices on drug delivery rate. *Microporous and Mesoporous Materials*. 2004; **68**: 105-109

**Hu, L. et al.** Multilayer encapsulated mesoporous silica nanospheres as an oral sustained drug delivery system for the poorly water-soluble drug felodipine. *Materials Science and Engineering C*. 2015; **47**: 313-324

**Hu, Y. et al.** 3D cubic mesoporous silica microsphere as a carrier for poorly soluble drug carvedilol. *Microporous and Mesoporous Materials*. 2012; **147**(1): 94-101.

**Johnson, CS.** Diffusion ordered nuclear magnetic resonance. *Progress in Nuclear Magnetic Resonance Spectroscopy*. 1999, **34**, 203-256

**Kambayashi, A. et al.** Predicting the Changes in Oral Absorption of Weak Base Drugs Under Elevated Gastric pH Using an In Vitro-In Silico-In Vivo Approach: Case Examples- Dipyridamole, Prasugrel, and Nelfinavir. *Journal of Pharmaceutical Sciences*. 2019; **108**: 584-591

**Khadka, P. et al.** Pharmaceutical particle technologies: An approach to improve drug solubility, dissolution and bioavailability. *Asian Journal of Pharmaceutical Sciences*. 2014; **9**(6): 304-316.

**Khanfar, M.** and Al-Nimry, S. Stabilization and Amorphization of Lovastatin Using Different Types of Silica. *AAPS PharmSciTech*. 2017; **6**: 3321-3343

**Khanfar, M.** and Al-Nimry, S. Stabilization and Amorphization of Lovastatin Using Different Types of Silica. *AAPS PharmSciTech*. 2017; **18**: 2358-2367

**Kiekens, F. et al.** Use of ordered mesoporous silica to enhance the oral bioavailability of ezetimibe in dogs. *Journal of Pharmaceutical Science*. 2012; **101**: 1136-1144

**Kinnari, P. et al.** Comparison of mesoporous silicon and non-ordered mesoporous silica materials as drug carriers for itraconazole. *International Journal of Pharmaceutics*. 2011; **414**: 148-156

**Kinnari, P. et al.** Comparison of mesoporous silicon and non-ordered mesoporous silica materials as drug carriers for itraconazole. *International Journal of Pharmaceutics*. 2011; **414**: 148-156

**Klamt, A.** and Schuurmann, G. COSMO: a new approach to dielectric screening in solvents with explicit expressions for the screening energy and its gradient. *Journal of the Chemical Society*. 1993 ; **2**(5) : 799–805

**Klamt, A.** Conductor-like Screening Model for Real Solvents: A New Approach to the Quantitative Calculation of Solvation Phenomena. *Journal of Physical Chemistry*. 1995; **99**(7): 2224-2235.

**Klamt, A. et al.** A Comprehensive Comparison of the IEFPCM and SS(V)PE Continuum Solvation Methods with the COSMO Approach". *Journal of Chemical Theory and Computation*. 2015; **11**(9): 4220–4225.

**Klamt, A.** Refinement and Parametrization of COSMO-RS. *Journal of Physical Chemistry*. 1998; **102**(26): 5074-5085.

**Knapik, J. et al.** Physical stability of the amorphous anticholesterol agent (ezetimibe): the role of molecular mobility. *Molecular Pharmaceutics*. 2014; **11**(11): 4280-4290

**Koehl, NK. Et al.** New Insights into Using Lipid Based Suspensions for ‘Brick Dust’ Molecules: Case Study of Nilotinib. *Pharmaceutical Research*. 2019; **36**(56)



**Kresse, CT.** et al. Ordered Mesoporous Molecular Sieves Synthesized by a Liquid-crystal Template Mechanism. *Nature*. 1992; **359**: 710-712.

**Krishnaiah, YSR.** Pharmaceutical Technologies for Enhancing Oral Bioavailability of Poorly Soluble Drugs. *Journal of Bioequivalence and Bioavailability*. 2010; **2**: 28-36.

**Kubota, N** and Mullin, JW. A kinetic model for crystal growth from aqueous solution in the presence of impurity. *Journal of Crystal Growth*. 1995; **152**(3): 203-208

**Kubota, N.** et al. Supersaturation dependence of crystal growth in solutions in the presence of impurity. *Journal of Crystal Growth*. 1997; **182** (1-2): 86-94.

**Kubota, N.** et al. The combined influence of supersaturation and impurity concentration on crystal growth. *Journal of Crystal Growth*. 2000; **212** (3-4): 480-488.

**Kumar, D.** et al. Impact of surface area of silica particles on dissolution rate and oral bioavailability of poorly water soluble drugs: a case study with aceclofenac. *International Journal of Pharmacy*. 2014; **461**(1-2): 459-468

**Kwan, EE.** and SG. Huang. Structural Elucidation with NMR Spectroscopy: Practical Strategies for Organic Chemists. *European Journal of Organic Chemistry*. 2008; **4**: 671-2688

**Laine, AL.** et al. Enhanced oral delivery of celecoxib via the development of a supersaturable amorphous formulation utilising mesoporous silica and co-loaded HPMCAS. *International Journal of Pharmaceutical Sciences*. 2016; **8**(1):118-25

**Langmuir, I.** The Adsorption of Gases on Plane Surfaces of Glass, Mica and Platinum. *Journal of the American Chemical Society*. 1918; **40**(9): 1361-1403

**Letchmanan, K.** et al. Dissolution and physicochemical stability enhancement of artemisinin and mefloquine co-formulation via nano-confinement with mesoporous SBA-15. *Colloids and Surfaces B Biointerfaces*. 2017; **1**(155): 560-568.

**Leuner, C** and Dressman, J. Improving Drug Solubility for Oral Delivery Using Solid Dispersions. *European Journal of Pharmaceutical Science*. 2000; **351**: 209-218.

**Levitt, M.** and Warshel, A. Computer simulation of protein folding. *Nature*. 1975; **253**: 694-698

**Li, S.** et al. Enhanced bioavailability of a poorly water-soluble weakly basic compound using a combination approach of solubilization agents and PIs: a case study. *Molecular Pharmaceutics*. 2012; **9**(5): 1100-1108

**Li, Y.** et al. In situ dehydration of carbamazepine dihydrate: a novel technique to prepare amorphous anhydrous carbamazepine. *Pharmaceutical Development Technology*. 2000; **5**(2): 257-266

**Li, Z.** et al. Enhanced Performance of Blended Polymer Excipients in Delivering a Hydrophobic Drug through the Synergistic Action of Micelles and HPMCAS. *Langmuir*. 2017; **33**(11): 2837-2848



**Linnell, T.** et al. Drug Delivery Formulations of Ordered and Nonordered Mesoporous Silica: Comparisons of Three Drug Loading Methods. *Journal of Pharmaceutical Sciences*. 2011; **100**(8): 3294-3306.

**Lipinski, CA.** Drug-like Properties and the Causes of Poor Solubility and Permeability. *Journal of Pharmacological and Toxicological Methods*. 2000; **44**: 235-249.

**Loschen, C.** and Klamt, A. COSMOquick: A Novel Interface for Fast  $\sigma$ -Profile Composition and Its Application to COSMO-RS Solvent Screening Using Multiple Reference Solvents. *Industrial Engineering and Chemical Research*. 2012; **51**(43): 14303-14308.

**Vialpando, JA.** et al. Use of ordered mesoporous silica for oral delivery of poorly soluble drugs. *Therapeutic Delivery*. 2011; **2**(8): 1079-1091.

**Madsen, CM.** et al. Supersaturation of zafirlukast in fasted and fed state intestinal media with and without precipitation inhibitor. *European Journal of Pharmaceutical Sciences*. 2016; **91**: 31-39

**Majors, RE.** High Performance Liquid Chromatography on Small Particle Silica Gel. *Analytical Chemistry*. 1972; **44**: 1722-1726.

**Maleki, A.** et al. Dissolution enhancement of a model poorly water-soluble drug, atorvastatin, with ordered mesoporous silica: comparison of MSF with SBA-15 as drug carriers. *Expert Opinion Drug Delivery*. 2016; **13**(2): 171-181

**Mandal, T.** et al. A framework for multi-scale simulation of crystal growth in the presence of polymers. *Soft Matter*. 2017; **13**: 1904-1914

**Mandal, T.** et al. Coarse-grained modeling of crystal growth and polymorphism of a model pharmaceutical molecule. *Soft Matter*. 2016; **12**(39): 8246-8255

**Marsac, PJ.** et al. Estimation of drug-Polymer miscibility and solubility in amorphous solid dispersions using experimentally determined interaction parameters. *Pharmaceutical Research*. 2009; **26**: 139–151.

**Marzarati, M.** et al. Feasibility of 1H-high resolution-magic angle spinning NMR spectroscopy in the analysis of viscous cosmetic and pharmaceutical formulations. *Analytical Chemistry*. 2013; **85**(8): 3822-3827

**McCarthy, CA.** Mesoporous silica formulations strategies for drug dissolution enhancement. *Expert Opinion Drug Delivery*. 2016; **13**(1): 93-108

**Meer, T.** et al. Solubility modulation of bicalutamide using porous silica. *Journal of Pharmaceutical Investigation*. 2013; **43**

**Mehta, M.** et al. Effect of Water on Molecular Mobility and Physical Stability of Amorphous Pharmaceuticals. *Molecular Pharmaceutics*. 2016; **13**, 1339–1346.

**Mellaerts, R.** et al. Aging Behaviour of Pharmaceutical Formulations of Itraconazole on SBA-15 Ordered Mesoporous Silica Carrier Material. *Microporous and Mesoporous Materials*. 2010; **180**(1-3): 154-161.

**Misic, Z.** et al. Understanding the interactions of oleic acid with basic drugs in solid lipids on different biopharmaceutical levels. *Journal of Excipients and Food Chemistry*. 2014; **5**(2): 113-134.

**Mohd AA. et al.** Commercially bioavailable proprietary technologies and their marketed products. *Drug Discovery Today*. 2013; **18**.

**Müller, RH. et al.** CapsMorph: >4 Years long-term stability of industrially feasible amorphous drug formulations. *International Controlled Release Symposium 40*. 2013; Honolulu/Hawai.

**Mullin, JW.** Crystallisation. Butterworth-Heinemann, 2001.

**Myerson, EAS.** Molecular Modeling Applications in Crystallisation. *Cambridge University Press*. 1999

**Nie, H. et al.** Investigating the interaftion pattern and structural elements of a drug.polymer complex at the molecular level. *Molecular Pharmaceutics*. 2015; **12**(7): 2459-2468

**Nie, H. et al.** Solid-State Spectroscopic Investigation of Molecular Interactions between Clofazimine and Hypromellose Phthalate in Amorphous Solid Dispersions. *Molecular Pharmaceutics*. 2016; **13**(11): 3964-3975

**Niederquell, A. et al.** New prediction methods for solubility parameters based on molecular sigma profiles using pharmaceutical materials. *International Journal of Pharmaceutics*. 2018; **546**(1-2): 137-144.

**Nielsen, LH. et al.** Stabilisation of amorphous furosemide increases the oral drug bioavailability in rats. *International Journal of Pharmacy*. 2015; **490**(1-2): 334-340

**Noyes, AA.** And **Whitney, WR.** 1897. The rate of solution of solid substances in their own solutions. *Journal of the American Chemical Society*. 1897; **19**: 930–934.

**Nyvt, J.** The Ostwald Rule of Stages. *Crystal Research and Technology*. 1995; **30**(4): 443-449

**O'Shea, JP et al.** Mesoporous silica-based dosage forms improve bioavailability of poorly soluble drugs in pigs: case example fenofibrate. *Journal of Pharmacy and Pharmacology*. 2017 (epub ahead of print)

**Palmelund, H. et al.** Studying the propensity of compounds to supersaturate: A practical and broadly applicable approach. *Journal of Pharmaceutical Sciences*. 2016; **105**: 3021-3029

**Patel, DD** and Anderson BD. Adsorption of Polyvinylpyrrolidone and its Impact on Maintenance of Aqueous Supersaturation of Indomethacin via Crystal Growth Inhibition. *Journal of Pharmaceutical Sciences*. 2015; **104**(9): 2923-2933

**Patel, DD.** and Anderson, BD. Effect of precipitation inhibitors on indomethacin supersaturation maintenance: mechanisms and modeling. *Molecular Pharmaceutics*. 2014; **11**(5): 1489-1499.

**Patel, DD. et al.** Maintenance of Supersaturation I: Indomethacin Crystal Growth Kinetic Modeling Using an Online Second-derivative Ultraviolet Spectroscopic Method. *Journal of Pharmaceutical Sciences*. 2011; **100**(7): 2623-2641

**Paudel, A. et al.** Raman spectroscopy in pharmaceutical product design. *Advanced Drug Delivery Reviews*. 2015; 89, 3-20

- Paus, R. et al.** Predicting the solubility advantage of amorphous pharmaceuticals: A novel thermodynamic approach. *Molecular Pharmaceutics*. 2015; **12**: 2823–2833.
- Pawar, Y B. et al.** Phase behavior and oral bioavailability of amorphous Curcumin. *European Journal of Pharmaceutics and Biopharmaceutics*. 2012; **47**(1): 56-64
- Peng, T. et al.** Influence of Polymers on the Physical and Chemical Stability of Spray-dried Amorphous Solid Dispersion: Dipyridamole Degradation Induced by Enteric Polymers. *AAPS PharmSciTech*. 2018; **19**: 2620-2628.
- Petrusevska, M. et al.** Evaluation of a high-throughput screening method for the detection of the excipient-mediated precipitation inhibition of poorly soluble drugs. *Assay Drug Development Technology*. 2013a; **11**(2): 117-129
- Petrusevska, M. et al.** Hydroxypropyl methylcellulose mediated precipitation inhibition of sirolimus: from a screening campaign to a proof-of-concept human study. *Molecular Pharmaceutics*. 2013b; **10**: 2299-2310.
- Pouton, CW.** Lipid Formulations for Oral Administration of Drugs: Non-emulsifying, Self-emulsifying and “Self-Microemulsifying” Drug Delivery Systems. *European Journal of Pharmaceutical Sciences*. 2000, **11**: S93-S98.
- Prasad, D. et al.** Role of molecular interactions for synergistic precipitation inhibition of poorly soluble drug in supersaturated drug-polymer-polymer ternary solution. *Molecular Pharmaceutics*. 2016; **13**: 756-765
- Prasad, D. et al.** Role of molecular interactions for synergistic precipitation inhibition of poorly soluble drug in supersaturated drug-polymer-polymer ternary solution. *Molecular Pharmaceutics*. 2016; **13**: 756-765
- Price, DJ. et al.** Approaches to increase mechanistic understanding and aid in the selection of precipitation inhibitors for supersaturating formulations - a PEARL review. *Journal of Pharmacy and Pharmacology*. 2018; **71**, 483–509.
- Price, DJ. et al.** Calculation of drug-polymer mixing enthalpy as a new screening method of precipitation inhibitors for supersaturating pharmaceutical formulations. *European Journal of Pharmaceutical Sciences*. 2019; **132**: 132-142
- Price, DJ. et al.** Incorporation of HPMCAS during loading of glibenclamide onto mesoporous silica improves dissolution and inhibits precipitation. *European Journal of pharmaceutical Sciences*. 2020; **141**: 105-113.
- Qian KK, and Bogner RH.** Spontaneous crystalline-to-amorphous phase transformation of organic or medicinal compounds in the presence of porous media, part 1: Thermodynamics of spontaneous amorphization. *Journal of Pharmaceutical Science*. 2011; **100**(7): 2801-2815.
- Qiu, Y. and Lee, PI.** Rational Design of Oral Modified-release Drug delivery systems. In: Developing Solid Oral Dosage Forms. *Pharmaceutical Theory and Practice*. 2017, 519-554
- Raut Desai, S.** Investigating the mechanism of supersaturation and precipitation inhibition of poorly soluble drugs from self-emulsifying drug delivery systems (SEDDS). 2013 *Ph.D. Thesis, Massachusetts College of Pharmacy and Health Sciences*.

**Rostron, P. et al.** Raman Spectroscopy, Review. *International Journal of Engineering and Technical Research*. 2016; **6(1)**

**Rubenstein, M.** and Colby, R. 2003. Polymer Physics. Oxford University Press, Oxford, UK.  
Saad, A. Triazole/Triazine-Functionalized Mesoporous Silica As a Hybrid Material Support for Palladium Nanocatalyst. *Langmuir*. 2017 (epub ahead of print)

**Salonen, J. et al.** Mesoporous silicon in drug delivery applications. *Journal of Pharmaceutical Sciences*. 2008; **97(2)**

**Schram, CJ. et al.** Influence of Polymers on the Crystal Growth Rate of Felodipine: Correlating Adsorbed Polymer Surface Coverage to Solution Crystal Growth Inhibition. *Langmuir*. 2015b; **31(41)**: 11279-11287

**Schram, CJ. et al.** Influence of Polymers on the Crystal Growth Rate of Felodipine: Correlating Adsorbed Polymer Surface Coverage to Solution Crystal Growth Inhibition. *Langmuir*. 2015b; **31(41)**: 11279-11287

**Sheng, Q.** *Thermal Analysis of Pharmaceuticals*. In: *Analytical Techniques in the Pharmaceutical Sciences*. Ed: Mullertz, A. et al. Springer, New York City, USA; 2016

**Shete, G. et al.** Solid State Characterization of Commercial Crystalline and Amorphous Atorvastatin Calcium Samples. *AAPS PharmSciTech*. 2010; **11(2)**: 598-609

**Shete, G.** Molecular Relaxation Behavior and Isothermal Crystallization above Glass Transition Temperature of Amorphous Hesperetin. *Journal of Pharmaceutical Sciences*. 2014; **103(1)**: 167-178

**Siepmann, J. et al.** Higuchi equation: Derivation, applications, use and misuse. *International Journal of Pharmaceutics*. 2011; **418(1)**: 6-12

**Skopp, J.** Derivation of the Freundlich Adsorption Isotherm from Kinetics. *Journal of Chemical Education*. 2009; **86(11)**: 1341

**Skotnicki, M. et al.** Thermal behavior and phase identification of Valsartan by standard and temperature-modulated differential scanning calorimetry. *Drug Development and Industrial Pharmacy*. 2013; **39(10)**: 1508-1514

**Staels, B. et al.** Mechanism of action of fibrates on lipid and lipoprotein metabolism. *Cardiovascular Drugs*. 1998; **98**: 2088-2093.

**Summerlin, N. et al.** Colloidal mesoporous silica nanoparticles enhance the biological activity of resveratrol. *Colloids and Surfaces B: Biointerfaces*. 2016; **144**: 1-7

**Sun, DD.** and Lee, PI. Haste Makes Waste: The Interplay Between Dissolution and Precipitation of Supersaturating Formulations. *AAPS Journal*. 2015; **17(6)**: 1317-1326

**Tantishaiyakul, V. et al.** Prediction of solubility parameters using partial least square regression. *International Journal of Pharmaceutics*. 2006; **325**: 8-14.

**Taylor, L.** and Zhang, GGZ. Physical chemistry of supersaturated solutions and implications for oral absorption. *Advanced Drug Delivery Review*. 2016; **101**: 122-142

**Tian, B. et al.** Theoretical prediction of phase diagram for solid dispersion. *Pharmaceutical Research*. 2015; **32**, 840–851.

**Timpe, C.** Strategies for Formulation Development of Poorly Water Soluble Candidates- A Recent Perspective. *American Pharmaceutical Reviews*. 2007; **10(3)**: 104-109.

**Ting, M. et al.** High-Throughput Excipient Discovery Enables Oral Delivery of Poorly Soluble Pharmaceuticals. *ACS Central Science*. 2016; **2(10)**: 748-755

**Tozuka, Y. et al.** Effect of pore size of FSM-16 on the entrapment of flurbiprofen in mesoporous structures. *Chemical and Pharmaceutical Bulletin*. 2005; **53**: 974-977

**Turku, et al.** Thermodynamics of tetracycline adsorption on silica. *Environmental Chemistry Letters*. 2007; **5(4)**: 225-228

**Ueda, K. et al.** Inhibitory effect of hydroxypropyl methylcellulose acetate succinate on drug recrystallization from a supersaturated solution assessed using nuclear magnetic resonance measurements. *Molecular Pharmaceutics*. 2013; **10(10)**: 3801-3811

**Ueda, K. et al.** The effect of HPMCAS functional groups on drug crystallisation from the supersaturated state and dissolution improvement. *International Journal of Pharmaceutics*. 2014; **464**: 205-213

**Vallet-Regi M.** Ordered Mesoporous Materials in the Context of Drug Delivery and Tissue Engineering. *Chemistry: A European Journal*. 2010; **27**: 5593-5604.

**Van Krevelen, DW.** and Te Nijenhuis, K. Properties of Polymers: Their Correlation with Chemical Structure; Their Numerical Estimation and Prediction from Additive Group Contributions. Elsevier. New York, 2009.

**Van Speybroeck, M. et al.** Enhanced absorption of the poorly soluble drug fenofibrate by tuning its release rate from ordered mesoporous silica. *European Journal of Pharmaceutical Sciences*. 2010; **41(5)**: 623-630

**Van Speybroeck, M. et al.** Ordered mesoporous silica material SBA-15: a broad-spectrum formulation platform for poorly soluble drugs. *Journal of Pharmaceutical Science*. 2009; **98**: 2648-2658

**Van Speybroeck, M. et al.** Preventing release in the acidic environment of the stomach via occlusion in ordered mesoporous silica enhances the absorption of poorly soluble weakly acidic drugs. *Journal of Pharmaceutical Sciences*. 2011; **100(11)**: 4864-4876

**Vora, C. et al.** Preparation and characterization of dipyridamole solid dispersions for stabilization of supersaturation: effect of precipitation inhibitors type and molecular weight. *Pharmaceutical Development Technologies*. 2016; **21(7)**: 847-855

**Wang, S.** Ordered Mesoporous Materials for Drug Delivery. *Microporous Materials*, 2009; **117**: 1-9.

**Wang, Y. et al.** The investigation of MCM-48-type and MCM-41-type mesoporous silica as oral solid dispersion carriers for water insoluble cilostazol. *Drug Development and Industrial Pharmacy*. 2014; **40**(6): 819-828

**Warren, DB et al.** Using polymeric precipitation inhibitors to improve the absorption of poorly water-soluble drugs: A mechanistic basis for utility. *Journal of Drug Targeting*. 2010; **18**(10): 704-731.

**Watanabe T, et al.** Solid state radical recombination and charge transfer across the boundary between indomethacin and silica under mechanical stress. *Journal of Solid State Chemistry*. 2000; **164**(1): 27-33.

**Wei, Q. et al.** Oral hesperidin-Amorphization and improved dissolution properties by controlled loading onto porous silica. *International Journal of Pharmacy*. 2017; **518**(1-2): 253-263

**Weuts, I. et al.** Physicochemical Properties of the Amorphous Drug, Cast Films, and Spray Dried Powders to Predict Formulation Probability of Success for Solid Dispersions: Etravirine. *Pharmaceutical Technology*. 2010; **100**(1)

**Wie, Q. et al.** Oral hesperidin-Amorphization and improved dissolution properties by controlled loading onto porous silica. *International Journal of Pharmaceutics*. 2017; **518** (1-2): 253-263.

**Williams, H.D. et al.** Strategies to Address Low Drug Solubility in Discovery and Development. *Pharmacological Reviews*. 2013, **65**, 3

**Wytenbach, N. et al.** Theoretical Considerations of the Prigogine–Defay Ratio with Regard to the Glass-Forming Ability of Drugs from Undercooled Melts. *Molecular Pharmaceutics*. 2016; **13**: 241-250

**Wytenbach, N. and Kuentz, M.** Glass-forming ability of compounds in marketed amorphous drug products. *European Journal of Pharmaceutics and Biopharmaceutics*. 2017; **112**: 204–208.

**Xia, X. et al.** Encapsulation of Anti-Tuberculosis Drugs within Mesoporous Silica and Intracellular Antibacterial Activities. *Nanomaterials*. 2014; **4**(3): 813-826

**Xia, X. et al.** In vivo enhancement in bioavailability of atazanavir in the presence of proton-pump inhibitors using mesoporous materials. *ChemMedChem*. 2012; **7**: 43-48

**Xu, S. and Dai, W. G.** Drug PIs in supersaturating formulations. *International journal of Pharmaceutics*. 2013; **453**(1): 36-43.

**Xu, W. et al.** Mesoporous systems for poorly soluble drugs. *International Journal of Pharmaceutics*. 2013; **453**(1): 181-197

**Yalkowsky, SH.** Solubility and Solubilization in Aqueous Media. *Oxford University Press*. 1999.

**Yamashita, T. et al.** Solvent shift method for anti-precipitant screening of poorly soluble drugs using biorelevant medium and dimethyl sulfoxide. *International Journal of Pharmaceutics*. 2011; **419**(1-2): 170-174

**Yanagihara, H. et al.** Adsorption–Desorption and Transport of Water in Two-Dimensional Hexagonal Mesoporous Silica. *The Journal of Physical Chemistry C*. 2013; **117**(42): 21795-21802.

**Zhang, H.** *et al.* Synthesis of novel mesoporous silica nanoparticles for loading and release of ibuprofen. *Journal of Controlled Release*. 2011; **152**; 38-39.

**Zhao, et al.** Uniform mesoporous carbon as a carrier for poorly water soluble drug and its cytotoxicity study. *European Journal of Pharmaceutics and Biopharmaceutics*. 2012; **80**: 535-543

**Zheng, W.** *et al.* Selection of Oral Bioavailability Enhancing Formulations during Drug Discovery. *Drug Development and Industrial Pharmacy*. 2012; **38**(2): 235-247

**Zhu, L.** *et al.* Fast surface crystallization of amorphous griseofulvin below T<sub>g</sub>. *Pharmaceutical Research*. 2010; **27**(8): 1558-1567



## **VII. Publications**

- 1) **Price, DJ.** *et al.* Approaches to increase mechanistic understanding and aid in the selection of precipitation inhibitors for supersaturating formulations – a PEARRL review. *Journal of Pharmacy and Pharmacology*. 2019. **71**(4); 483-509. doi: [10.1111/jphp.12927](https://doi.org/10.1111/jphp.12927)

**Personal Contribution:** lead author, project management, editing of chapters, collation of final manuscript.

- 2) **Price, DJ.** *et al.* Calculation of drug-polymer mixing enthalpy as a new screening method of precipitation inhibitors for supersaturating pharmaceutical formulations. *European Journal of Pharmaceutical Sciences*. 2019. **132**; 142-156. doi: [10.1016/j.ejps.2019.03.006](https://doi.org/10.1016/j.ejps.2019.03.006)

**Personal Contribution:** lead author, concept development, experimental design, data collection

- 3) **Price, DJ.** *et al.* Incorporation of HPMCAS during loading of glibenclamide onto mesoporous silica improves dissolution and inhibits precipitation. *European Journal of Pharmaceutical Sciences*. 2020. **141**; 105-113. doi:[10.1016/j.ejps.2019.105113](https://doi.org/10.1016/j.ejps.2019.105113).

**Personal Contribution:** lead author, concept development, experimental design, data collection

- 4) **Price, DJ.** *et al.* Opportunities for Successful Stabilization of Poor Glass-Forming Drugs: A Stability-Based Comparison of Mesoporous Silica Versus Hot Melt Extrusion Technologies. *Pharmaceutics*. 2019. **11**(11); 577. doi: [10.3390/pharmaceutics11110577](https://doi.org/10.3390/pharmaceutics11110577)

**Personal Contribution:** co-lead author, concept development, experimental design, data collection

- 5) Ditzinger, FS. and **Price, DJ.** *et al.* Lipophilicity and hydrophobicity considerations in bio-enabling oral formulations approaches – a PEARRL review. *Journal of Pharmacy and Pharmacology*. 2019. **71**(4); 464-482. doi: [10.1111/jphp.12984](https://doi.org/10.1111/jphp.12984)

**Personal Contribution:** co-author and editing the final manuscript

- 6) Jancovic, S. and **Price, DJ.** *et al.* Application of the solubility parameter concept to assist with oral delivery of poorly water-soluble drugs – a PEARRL review. *Journal of Pharmacy and Pharmacology*. 2019. **71**(4); 441-463. doi: [10.1111/jphp.12948](https://doi.org/10.1111/jphp.12948)

**Personal Contribution:** co-author and editing the final manuscript

- 7) Laine, AL. and **Price, DJ.** *et al.* Enhanced oral delivery of celecoxib via the development of a supersaturable amorphous formulation utilising mesoporous silica and co-loaded HPMCAS. *International Journal of Pharmaceutics*. 2016. **512**(1); 118-125. doi: [10.1016/j.ijpharm.2016.08.034](https://doi.org/10.1016/j.ijpharm.2016.08.034)

**Personal Contribution:** concept development, experimental design, data collection, co-lead author

- 8) Koehl, N. and **Price, DJ.** *et al.* *In silico*, *in vitro* and *in vivo* evaluation of precipitation inhibitors in supersaturated lipid based formulations of venetoclax. *Molecular Pharmaceutics*. **Under Review**

**Personal Contribution:** concept development, computation pharmaceutics calculations, data analysis, co-author



## Posters

1. **Price, DJ.** *et al.* A Novel In Silico Screening Protocol For The Selection Of Optimized Precipitation Inhibitor Systems For Supersaturable Formulations. Poster presented at: AAPS Annual Meeting; 2017 November 12-15; San Diego, CA. USA.
2. **Price, DJ.** *et al.* API and Precipitation Inhibitor Co-Loaded Mesoporous Silica: A Novel Synergistic Formulation Type with Advantageous Dissolution Performance. Poster presented at: PharmSci 360; 2018 October 26<sup>th</sup>- November 5<sup>th</sup>; Washington DC, USA.
3. **Price, DJ.** *et al.* Molecular-level insight into mesoporous silica formulations: Effect of surface interaction on formulation performance. Poster presented at: PBP European Meeting; 2019 March 23-25; Bologna, Italy.



E-mail: [danjosephprice@gmail.com](mailto:danjosephprice@gmail.com)/[daniel-joseph.price@merckgroup.com](mailto:daniel-joseph.price@merckgroup.com) Mobile: +4917645623482 Born: 31/01/94, U.K.

## EDUCATION AND QUALIFICATIONS

---

### PhD in Pharmaceutical Technology:

**October 2016- Current** Goethe University Frankfurt in collaboration with Merck KGaA

- Thesis title: *Novel in vitro and in silico tools for the development of mesoporous silica formulations with optimal precipitation inhibitors*

### Master and Bachelor of Science in Industrial Medicinal Chemistry: 1<sup>st</sup> Class Honours

**September 2012- May 2016**, University of Leeds

- Master's thesis title: "Controlled release of doxorubicin with novel polymer architects"
- Bachelor thesis title: "Improving the bioavailability of poorly soluble drugs with mesoporous silica"
- Industrial Research Prize for highest graded bachelor thesis carried out in industry.
- Craig Jordan Prize for top graduating student (Masters and Bachelors).
- Master's research prize for top graded thesis.
- Salters' Graduate Prize, nationwide prize for the top 5 chemistry graduates in the UK, based on academic achievement, leadership and potential for impacting the global chemical industry.

### International Baccalaureate Diploma: Top 5% in China

**August 2010-May 2012**, Dulwich College Shanghai, Shanghai, China

## RELEVANT EXPERIENCE

---

April 2019-Present

**Technical Product Manager, Merck Group: Darmstadt, Germany**

- Responsible for marketing strategy and execution for a portfolio of solubility enhancing functional excipients within Merck Life Science.
- Project management and long-term strategy planning for innovation projects.
- Co-ordinating and leading marketing activities on product development and launch.
- Influencing strategic business decisions within solid formulation.
- Interface between commercial and R&D organizations.

October 2016-April 2019

**PhD Researcher, Merck Group: Darmstadt, Germany**

- Marie Cure Fellow investigating supersaturating drug formulations for poorly soluble drugs, specifically mesoporous silica. This was part of the Horizon 2020 project PEARRL ([www.pearrl.eu](http://www.pearrl.eu)).
- Increased understanding of the fundamental mechanistic details of mesoporous silica technology.
- Development of an *in silico* protocol that calculated API-polymer mixing enthalpy.
- Led a team of 10 authors to publish an extensive review article on the selection of precipitation inhibitors in early development. This article was designed and executed to act as a formulation guide for industrial pharmaceutical scientists developing poorly soluble drug formulations.
- Delivered training courses on the use of Parateck SLC<sup>®</sup> mesoporous silica.



February 2018-May 2018

*Visiting Scientist, BfArM: Bonn, Germany*

- Observed the EMA Quality Working Party and contributed to training on „mathematical modelling in regulatory submissions“.
- Attended scientific advice meetings with companies visiting BfArM gave me an understanding of the interactions that take place between industry and the regulatory bodies.
- Completed a mock assessment of a marketing authorization application (MAA), which gave me an insight into the key requirements for submission of new APIs and excipients to the EMA.

September 2015-May 2016

*Research Student, University of Leeds School of Chemistry: Leeds, UK*

- Investigated the synthesis of novel biodegradable polymers for controlled-release drug delivery.
- Demonstrated how O-carboxyanhydride and N-carboxyanhydride ring-opened co-polymers could successfully deliver doxorubicin directly to tumour cells *via* acid-based hydrolysis.

September 2014-September 2015

*Formulation Scientist, Pfizer: Cambridge, UK*

- Investigated Parateck SLC® mesoporous silica for increasing the bioavailability of poorly soluble drugs.
- Regularly presented data within the company and in collaboration with Merck Millipore to a high standard of presentation and professionalism, which spurred an increased interest in Parateck SLC®.
- Instilled a legacy for the use of Parateck SLC® mesoporous silica in Pfizer for pre-clinical candidates.

July 2012-August 2012

*Research Intern, Shanghai Institute of Materia Medica: Shanghai, China*

- Gained first-hand exposure to a Chinese research environment during a molecular biology-based lab project, during which I contributed to elucidation efforts for GPCR LGR-4.

## SKILLS AND HOBBIES

---

- Living and studying in China for my high school education instilled in me a passion for Chinese culture, people and language.
- Prior to moving to China, I was enrolled in theatre school full-time. This has resulted in a strong confidence in communication, public speaking and effective presentation.
- My hobbies include rugby, acting, singing and playing piano.

## PERSONAL DETAILS

---

D.O.B: 31/01/1994

**Nationality:** British

**Marital Status:** Married

**Current Address:** Franklinstrasse 25, 64285, Darmstadt, Hessen, Germany

**Current Employer:** Merck KGaA, Darmstadt, Germany

## IX. Declaration

I hereby declare that this thesis has not been and will not be submitted in whole or in part to another University for the award of any other degree. Except where stated otherwise by reference or acknowledgment, the work presented was generated by myself under the supervision of my advisors during my doctoral studies.

Darmstadt, 2010

Daniel Joseph Price

## Approaches to increase mechanistic understanding and aid in the selection of precipitation inhibitors for supersaturating formulations – a PEARL review

Daniel J. Price<sup>a,b</sup>, Felix Ditzinger<sup>c,d</sup>, Niklas J. Koehl<sup>e</sup>, Sandra Jankovic<sup>c,d</sup>, Georgia Tsakiridou<sup>f,g</sup>, Anita Nair<sup>a</sup>, René Holm<sup>h</sup>, Martin Kuentz<sup>d</sup>, Jennifer B. Dressman<sup>b</sup> and Christoph Saal<sup>a</sup>

<sup>a</sup>Merck KGaA, Darmstadt, <sup>b</sup>Frankfurt Goethe University, Frankfurt, Germany, <sup>c</sup>Department of Pharmaceutical Sciences, University of Basel, Basel, <sup>d</sup>Institute of Pharma Technology, University of Applied Sciences and Arts Northwestern Switzerland, Muttens, Switzerland, <sup>e</sup>School of Pharmacy, University College Cork, Cork, Ireland, <sup>f</sup>Pharmathen SA, Product Design & Evaluation, <sup>g</sup>Department of Pharmacy, University of Athens, Athens, Greece and <sup>h</sup>Drug Product Development, Janssen Research and Development, Johnson and Johnson, Beerse, Belgium

### Keywords

controlled and sustained release systems; development of novel analytical techniques; dosage form design and characterisation; pharmaceutical analysis; pharmaceuticals and drug delivery

### Correspondence

Christoph Saal, Merck KGaA, 250 Frankfurter Strasse, 64293 Darmstadt, Hessen, Germany.  
E-mail: christoph.saal@merckgroup.com

Received January 3, 2018  
Accepted April 16, 2018

doi: 10.1111/jpp.12927

### Abstract

**Objectives** Supersaturating formulations hold great promise for delivery of poorly soluble active pharmaceutical ingredients (APIs). To profit from supersaturating formulations, precipitation is hindered with precipitation inhibitors (PIs), maintaining drug concentrations for as long as possible. This review provides a brief overview of supersaturation and precipitation, focusing on precipitation inhibition. Trial-and-error PI selection will be examined alongside established PI screening techniques. Primarily, however, this review will focus on recent advances that utilise advanced analytical techniques to increase mechanistic understanding of PI action and systematic PI selection.

**Key findings** Advances in mechanistic understanding have been made possible by the use of analytical tools such as spectroscopy, microscopy and mathematical and molecular modelling, which have been reviewed herein. Using these techniques, PI selection can be guided by molecular rationale. However, more work is required to see widespread application of such an approach for PI selection.

**Summary** Precipitation inhibitors are becoming increasingly important in enabling formulations. Trial-and-error approaches have seen success thus far. However, it is essential to learn more about the mode of action of PIs if the most optimal formulations are to be realised. Robust analytical tools, and the knowledge of where and how they can be applied, will be essential in this endeavour.

### Introduction

Among the various routes of administration for drugs, oral administration is the most commonly employed. It is cost-effective and convenient for the patient, leading to a very high patient compliance.<sup>[1]</sup> Various dosage forms are available for oral delivery including solid formulations such as capsules and tablets, as well as liquid formulations such as solutions, suspensions and syrups. For the active pharmaceutical ingredient (API) to exert its pharmacological effect, it must be released from the dosage form and absorbed from the gastrointestinal (GI) tract into the systemic circulation, where it can be transported to its physiological

target. Thus, the bioavailability of a drug relies, among other parameters, on its capability to dissolve in the GI milieu and pass through the intestinal membrane.<sup>[2]</sup> It is from these two parameters (solubility and permeability) that the Biopharmaceutics Classification System arose, a system which groups drugs into four classes, based on solubility and permeability.<sup>[3]</sup>

Due to recent scientific advances such as high-throughput screening in combination with combinatorial chemistry; X-ray diffraction of target proteins and computational chemistry, we now have an increased understanding of how small molecules bind to targets. Therefore, it has become easier to identify 'hits' that have therapeutic

potential. In parallel, there has been a large increase in the number of druggable targets which have been discovered and validated using a broad spectrum of novel methods, such as proteomics, genomics and even gene editing.<sup>[2,4-7]</sup> On the other hand, it is recognised that use of such discovery tools often results in the identification of a higher proportion of lipophilic, high molecular weight and poorly soluble molecules, which do not adhere to Lipinski's rules of 5.<sup>[5]</sup> Albeit positive for the industry, these shifts have also increased the number of drug candidates with poor physicochemical profiles (low solubility, high log *P*, high molecular weight, poor solubility) appearing in research and development pipelines. As a result, there is a higher risk of attrition during pharmaceutical research and development due to insufficient oral bioavailability, which represents a loss in therapeutic and economic potential. It has been reported that approximately 40% of all commercial drugs are classified as poorly soluble.<sup>[8]</sup> Extending this trend to those compounds still in the development pipeline, it has been reported that anywhere between 80% and 90% are 'not highly soluble'.<sup>[8]</sup> Therefore, the need for effective formulation approaches for these compounds, to avoid low bioavailability due to poor aqueous solubility, has never been greater.

Faced with these challenges, pharmaceutical scientists have developed a toolkit of strategies, which use physicochemical knowledge of solvation and dissolution to enhance solubilisation and to overcome poor oral bioavailability.<sup>[7]</sup> These approaches can involve modifying the chemical form of an API for example with (1) salt formation,<sup>[9]</sup> (2) co-crystals<sup>[10]</sup> or (3) prodrugs.<sup>[11]</sup> Or, alternatively, formulation approaches such as (4) solvents, co-solvents and lipids<sup>[12-15]</sup>; (5) micelle systems<sup>[16-18]</sup>; (6) particle size reduction<sup>[19]</sup>; (7) complexation<sup>[20]</sup>; and (8) solid amorphous dispersions, produced by techniques such as hot melt extrusions (HMEs), spray-dried dispersions (SDDs), co-precipitates or mesoporous silica.<sup>[21-26]</sup>

In recent years, formulations that generate and stabilise a supersaturated state *in vivo* have come to the forefront when considering the delivery of poorly soluble drugs.<sup>[8,27,28]</sup> Supersaturation is a state in which the concentration of a solute exceeds the thermodynamic (equilibrium) solubility of the molecule. Such a state is highly attractive for compounds with low aqueous solubility as artificially high API concentrations can be generated in the GI tract. This increases the absorptive flux, which can subsequently increase absorption and bioavailability.<sup>[27,29]</sup> Such an approach must, however, be considered from an energetic perspective as well.<sup>[30]</sup> The free energy of the supersaturated state is significantly higher than that of the saturated solution, and there is a strong driving force for the system to return to its thermodynamically stable state *via* crystallisation and precipitation processes.<sup>[8]</sup> Therefore,

successful supersaturating formulations should not only generate increased API concentrations in solution, but should also be able to stabilise the supersaturated state. Often, this stabilising factor takes the form of a precipitation inhibitor (PI), which prevents the recrystallisation and precipitation process. Therefore, PIs are an integral part of supersaturating formulations, and a robust understanding of the mechanisms behind precipitation inhibition is essential for effective formulation design.<sup>[8]</sup> This review offers a brief overview of the physical chemistry underpinning supersaturation and precipitation before examining recent work utilising cutting-edge analytical techniques and methods that have led to an increased understanding of precipitation inhibition mechanisms, and how such understanding can be used in the selection of optimal PI systems for supersaturating formulations. To the best of our knowledge, this review is the first to consider precipitation inhibition and precipitation inhibitor selection from this perspective.

## Supersaturating formulations

In order to understand the process of precipitation inhibition, it is important to have an overview of the physical-chemical underpinnings of drug supersaturation. As a complete treatment of supersaturated solutions is beyond the scope of this review, the interested reader is referred to an excellent review recently published by Taylor and Zhang.<sup>[8]</sup>

Supersaturation, from a physicochemical perspective, is generally defined as a system in which the free energy of the solute in solution is higher than that of the crystal form or amorphous solid phase of the drug at equilibrium (Figure 1).<sup>[8,31]</sup> Practically speaking, this is any system in which the concentration of drug in solution exceeds the thermodynamic solubility of the pure API. Increasing the concentration in the GI tract *via* supersaturation can increase the overall absorption of the drug. As a result, supersaturating formulations are highly appealing for drugs with low thermodynamic solubility, which often exhibit poor bioavailability.<sup>[3]</sup>

The gap between the free energy of the supersaturated state and the equilibrium state can lead to stability issues.<sup>[8,30]</sup> Therefore, the absorption advantages previously mentioned are not always realised, as this instability can lead to precipitation of amorphous or crystalline material from the supersaturated solution.<sup>[27,32]</sup> Any precipitated drug would have to redissolve in the GI tract in order to become available for absorption and, therefore, the potential absorption advantage is typically diminished.<sup>[33]</sup> Consequently, an effective supersaturating formulation needs not only to generate high supersaturation, but also to maintain this for a physiologically relevant time. With typical upper GI transit time, this would be 2–4 h, the time during which



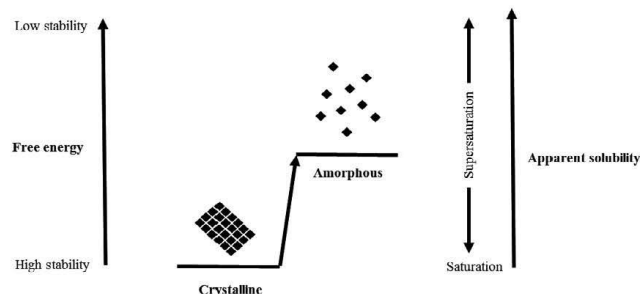


**Figure 1** Energy diagram showing crystalline and amorphous solid states of drug substance from a stability and solubility perspective.

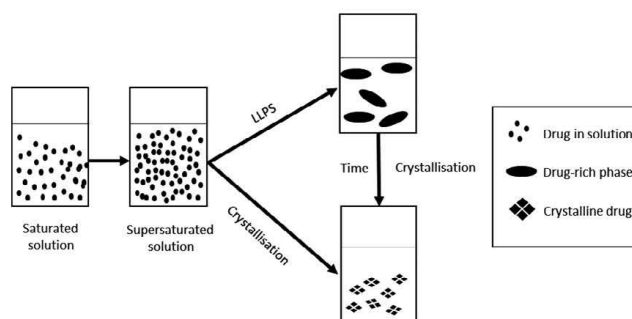


**Figure 2** Liquid-liquid phase separation (LLPS) generates drug-rich phases in solution, which eventually crystallise. Effective use of precipitation inhibition can prolong the supersaturation lifetime post-LLPS.

most drug absorption takes place after gastric emptying when the drug is taken in the fasted state.<sup>[34]</sup> In order to successfully develop such a formulation, it is important to have a good understanding of the physical basis of supersaturation, and how this knowledge can be exploited to maximal effect.

During the dissolution of supersaturating formulations, drug concentration increases until the crystalline saturation solubility is exceeded. After this point, supersaturation is achieved, which exists in a metastable state.<sup>[35]</sup> This metastability is the driving force of nucleation and thus precipitation of either amorphous or crystalline solids.<sup>[36,37]</sup> The rates of nucleation and precipitation, in relation to the dissolution rate of the formulation, are the key parameters when considering whether the supersaturated state will be maintained.

Successful supersaturating formulations may also exceed the so-called amorphous solubility, a metastable state in which amorphous drug exists in a pseudo-equilibrium with the dissolution medium, eventually returning to the crystalline form.<sup>[31,38-41]</sup> 'Amorphous solubility' has been

calculated theoretically based on the crystalline saturation solubility and by considering the amorphous material as a supercooled liquid.<sup>[42,43]</sup> High drug concentrations of slowly crystallising drugs are typically limited by a kinetically favoured liquid-liquid phase separation (LLPS), (Figures 2 and 3) in which separation of drug molecules into drug-rich 'droplets' (100–500 nm) from the aqueous phase occurs *via* spinodal decomposition.<sup>[8,44-48]</sup>

At, or approaching, the theoretical amorphous solubility, the LLPS state is at a lower energy than the supersaturated solution, and so is thermodynamically favoured. LLPS proceeds *via* quick spinodal decomposition and so can only occur when fast crystallisation does not occur. Drug molecules in the drug-rich regions exist in the amorphous state and usually tend to fall back to the more stable crystalline state over time.<sup>[49,50]</sup> Thus, the process of LLPS extends the lifetime of the molecule in solution, such that high concentrations can be achieved over longer periods of time, compared to the unstable supersaturated state. Typically, precipitation inhibition would aim to avoid any precipitation from the supersaturated state. However, given that

precipitation inhibition is concerned with the biopharmaceutical performance of a drug, the effect of a PI on sustaining LLPS is also relevant to the current body of work. In this instance, LLPS can be considered a 'reservoir' of supersaturation such that the initially unstable supersaturation results in a plateau of supersaturation at the LLPS due to the separation of API in droplets.<sup>[8]</sup> This is a direct analogy to the 'Spring and Parachute' model proposed by Guzman *et al.*<sup>[51]</sup> (Figure 4) and has also been referred to as a 'Spring and Plateau' approach.<sup>[8]</sup> Generally, the spring effect is generated either by delivering the drug in a presolubilised form (e.g. SEDDS or lipid-based formulations) or in a rapidly dissolving form (e.g. amorphous, less stable polymorphs, particle size engineering, amorphous dispersion, solid solutions and prodrugs).<sup>[27]</sup> To complete the model, PIs act as 'parachutes' by hindering nucleation and arresting precipitation<sup>[33,52]</sup> or, maintaining the lifetime of the droplet state after LLPS. Both of these processes increase the concentration and lifetime of the supersaturated drug in solution.

The success of supersaturating formulations is dependent on appropriate selection of 'Spring-Parachute' combinations. Consequently, mechanistic understanding of the role of the PI in supersaturating formulations is imperative for the educated choice of successful PI-drug combinations.

### Precipitation inhibition: theory and practice

From a pharmaceutical perspective, precipitation is a process whereby a solid phase separates from a liquid phase. This can yield either amorphous or crystalline materials, or mixtures of both. Although precipitation in the amorphous form is possible from supersaturated solutions, the vast majority of work has focussed on crystallisation theory. Fortunately, when considering inhibition, classical crystallisation theory can be applied to the precipitation of both crystalline and amorphous solids.<sup>[27,28,54]</sup> In the following section, a short overview of the current theories of crystallisation is presented. For more details, the reader is referred

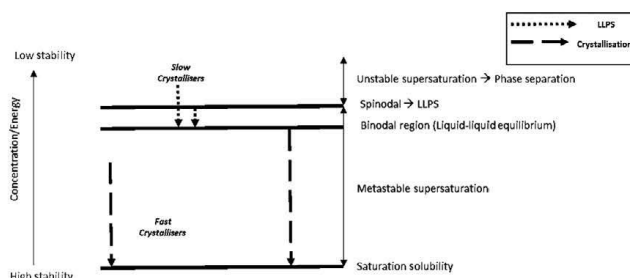


**Figure 3** The fate of a drug molecule in a highly supersaturated solution depends on the kinetics of crystallisation, with slow crystallizers (dotted arrows) often undergoing liquid liquid phase separation. Fast crystallizers (dashed arrow) do not undergo liquid liquid phase separation. Adapted from Taylor and Zhang.<sup>[8]</sup>

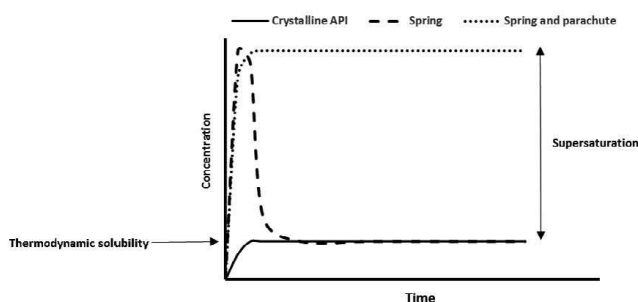


**Figure 4** The Spring and Parachute model. A common formulation approach where a 'spring' generates supersaturation and a 'parachute' prevents precipitation. Collectively, this can improve the absorption of a poorly soluble API.<sup>[51,53]</sup>



to the book by Mullin on 'Crystallisation'<sup>[30]</sup> and to an excellent review by Warren *et al.*<sup>[54]</sup>

### Crystallisation and precipitation

Crystallisation is an energy-driven process whereby a molecule in solution at supersaturated concentrations precipitates to a solid, crystalline material.<sup>[55]</sup> As supersaturation concentrations approach a critical level, the system becomes labile and 'precipitation is self-influenced instantaneously without any external influence'.<sup>[30]</sup> Before this critical point, the supersaturation is said to be metastable and precipitation may not occur instantaneously and/or spontaneously, but can be easily induced *via* mechanical activation or the addition of seed crystals.<sup>[30,56]</sup> Crystallisation from a supersaturated solution is a function of the concentration, temperature and pressure of the solution. Practically speaking, however, it is generally only temperature and concentration that are considered (Figure 5). A higher concentration of solute increases the lability of the system, whereas an increased temperature decreases lability. For concentration, the higher the concentration of a solute in solution, the higher the degree of supersaturation, which increases excess energy of the system. Conversely, as temperature increases, the saturation concentration usually also increases, and the degree of supersaturation is decreased (Figure 5).

Crystallisation occurs in two key stages: nucleation and crystal growth. Simply put, solute molecules must come together (nucleate) until a critical size of a nucleus is reached, after which crystal growth can occur. During crystallisation, both nucleation and crystal growth are occurring simultaneously at different rates, depending on the stage of the crystallisation process and the conditions of the system (*vis à vis* solute concentration and solvent temperature).<sup>[54]</sup> Nucleation can occur spontaneously or

artificially,<sup>[30]</sup> for example *via* agitation, mechanical shock, pH change or dilution. The exact process of nucleation is still unclear, although several mechanisms have been proposed in the literature, none have been fully validated.<sup>[57]</sup> Nevertheless, nucleation can occur in a number of ways, either with or without seed crystals (secondary and primary nucleation, respectively) or in the presence or absence of a cluster surface, for example foreign particles or container defects (heterogenous/2D and homogenous/3D crystallisation, respectively).<sup>[30]</sup> The nucleation rate ( $J$ ) can be described by the classical nucleation theory (CNT) (Equation 1).<sup>[58]</sup>

$$J = A \exp\left(-\frac{B}{\ln^2 S}\right) \quad (1)$$

$S$  is the supersaturation of the system. The pre-exponential factor  $A$  is a kinetic measure that describes how the molecules come together to form nuclei. Given the random nature of this process, with a wide range of accessible clusters, which can grow or decay in multiple directions, the pre-exponential factor is often calculated using Monte Carlo simulations. The thermodynamic factor,  $B$ , describes the free energy barrier for the formation of a nucleus, which is also referred to as 'nucleation work'. For practical purposes,  $A$  and  $B$  are considered to be constant in systems with fixed temperatures. This equation underscores the importance and significance that supersaturation,  $S$ , plays in the nucleation process.<sup>[58,59]</sup>

After stable nuclei have been formed, they increase in size and form visible crystals *via* crystal growth.<sup>[30]</sup> The process of crystal growth has been extensively described in the literature.<sup>[30,37,60,61]</sup> Various models have been put forward to provide a theoretical mechanism for the process of crystal growth including (1) surface energy theory, (2) diffusion theory and (3) adsorption layer theory.<sup>[30]</sup> All three models have significant failings; however, the most widely accepted and quoted model is the adsorption layer theory.<sup>[30]</sup>

Adsorption layer theory is based on the thermodynamic assumption that there is a layer of adsorbed molecules on the surface of a growing crystal, which is in an equilibrium state with the bulk solution surrounding the layer. The crystal will grow if the adsorbed molecules on the surface find a position that is thermodynamically favourable and exhibits high attraction forces between the adsorbed molecule and the crystal, enabling extension of the lattice.<sup>[30]</sup> This occurs at imperfections and kinks on the surface of the growing crystal face.<sup>[30,54]</sup> Despite this process, the resultant crystal may not be the thermodynamically most favourable. It is common for metastable polymorphs to form,<sup>[62]</sup> based on the quick access of surface adsorbed solutes to energetically stable, but not *the most* energetically stable sites. This phenomenon, whereby the first crystal formed is simply kinetically favoured and leads via different stages to a more

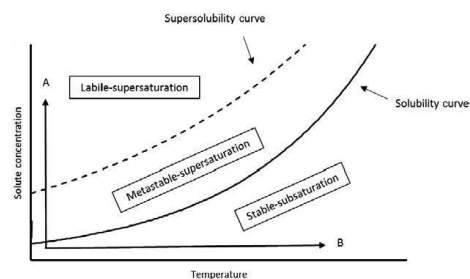


**Figure 5** Solubility supersolubility diagram amended from Mullin.<sup>[30]</sup> A more labile solution is obtained with a higher drug concentration (arrow A). A more stable solution is obtained by the increase in temperature (arrow B).

stable solid, was first suggested by Wilhelm Ostwald and is now referred to as ‘Ostwald’s rule’.<sup>[63]</sup> That being said, if left for a sufficient time period, the thermodynamically most stable polymorph should form in most cases.<sup>[61]</sup>

For supersaturating formulations, nucleation of the generated supersaturated solution would be highly probable if the formulation was not stabilised by addition of PIs.<sup>[33]</sup> If the process of precipitation is arrested for physiologically relevant time scales, the supersaturated state can be maintained for long enough to allow for increased absorption.<sup>[54]</sup> Polymers, surfactants and cyclodextrins have been investigated as excipients that can maintain the supersaturated state.<sup>[33]</sup> Another consideration is the effect that endogenous molecules (e.g. bile salts) in the body can have on precipitation inhibition.<sup>[64, 65]</sup>

### Polymers as precipitation inhibitors

The most common PIs employed in the pharmaceutical industry are polymers. Table 1 lists a large range of polymers, including cellulose derivatives, polyvinylpyrrolidones and methacrylates, which have been evaluated as precipitation inhibitors in oral drug products.

Polymers function by slowing down the process of nucleation and crystal growth through interaction with the dissolved API molecules and interaction with and adsorption onto growing crystals.<sup>[33,54]</sup> Given the kinetic nature of this effect, the thermodynamic equilibrium solubility is usually not affected by the polymer, except in a number of limited cases, where polymers can have a co-solvent effect as well.<sup>[54,66-68]</sup> Kinetic inhibition of nucleation relies on molecular interactions between the polymer and the drug, that is hydrogen bonds, polar, or dispersion forces.<sup>[27,28,54]</sup> Each of these interactions may contribute to varying degrees, especially when considering the impact of water. This is an area that has seen increasing interest in the literature lately,<sup>[65,68-70]</sup> but more work is required to resolve the exact contributions and nature of the PI-API interaction. More generally, such interactions can be influenced by temperature, molecular weight, polarity and hydrogen bonding capabilities of both the drug and the polymer. One potential mode of action is the adsorption of the polymer onto the growing crystal surface, blocking the access of the solute to the surface. Furthermore, polymers can disrupt the growth rate on crystal surfaces by binding onto imperfection sites, thus flattening the surface and removing the interaction point. This is highly dependent on the balance of interactions between the solid and the polymer and the interaction between the liquid and the polymer.<sup>[71]</sup> The adsorption of the polymer onto the surface of the particle also introduces steric hindrance, which disrupts the diffusion of the molecules at the solid-liquid interface.<sup>[72-74]</sup> It has previously been reported that the hydrophobicity of the polymer

**Table 1** Examples of PIs studied in the literature

| Inhibitor name  | Reference(s)        |
|---|---------------------|
| Eudragit® S100  | [91]                |
| Eudragit® E100  | [91,92]             |
| Poly(ethylene oxide)- <i>b</i> -poly(propylene)- <i>b</i> -poly(ethylene oxide) (Poloxamer) (Pluronic®) | [93,94]             |
| Poly(ethylene glycol) (PEG)   | [91,95]             |
| Poly(ethylene imine) (PEI)  | [54,72]             |
| Eudragit RL100  | [54,96]             |
| Poly(ether)- <i>co</i> -poly(ol) (PEPO)   | [72]                |
| Poly(propylene glycol) (PPG)  | [54,97,98]          |
| Poly(styrene) sulfonic acid (PSS)   | [99,100]            |
| Poly(vinylpyrrolidone) (PVP) (Povidone) (Copolydione)   | [69,101-106]        |
| Poly(vinyl acetate)- <i>co</i> -poly(vinylpyrrolidone) (PVA-PVP)  | [106,107]           |
| Hydroxyethyl cellulose (HEC)  | [93,94]             |
| Poly(methyl methacrylate) (PMMA)  | [54,98]             |
| Poly(lactic acid) (PLA)   | [91]                |
| Poly(vinyl acetate) phthalate (PVAP)  | [54]                |
| Hydroxypropyl methyl cellulose acetate succinate (HPMCAS)   | [23,24,68,108-113]  |
| Cellulose acetate phthalate (CAP)   | [113]               |
| Hydroxypropyl methyl cellulose (HPMC)   | [74,114-117]        |
| Poly(vinyl alcohol) (PVOH)  | [28,54]             |
| Poly(acrylic acid) (PAA)  | [28,54,118]         |
| Poly(acetylene)   | [28,54,116]         |
| Methyl cellulose  | [28,54]             |
| Poly(lactid- <i>co</i> -glycolid) (PLGA)  | [54]                |
| Sodium carboxymethyl cellulose (SCMC)   | [54]                |
| Chitosan  | [54]                |
| Poly(urethane) (PUR)  | [119]               |
| Mannitol  | [54]                |
| Poly(glycolide) (PGA)   | [54]                |
| Locust bean gum   | [54,119-129]        |
| Alginate acid gum   | [54]                |
| Hydroxy propyl- $\beta$ -cyclodextrin (HP $\beta$ CD)   | [20,54,115,121-123] |
| Sulfobutyl ether- $\beta$ -cyclodextrin (SBE $\beta$ CD) (Captisol®)                                    | [54]                |
| Sodium dodecyl sulphate (SDS)   | [54]                |
| PEG-40 hydrogenated castor oil (Cremophor®)   | [54]                |
| Poly(ethylene glycol) sorbitan monolaurate (Tween® 20)  | [54]                |
| Sorbitol  | [54]                |
| Sodium cholate  | [65]                |
| Sodium deoxycholate   | [65]                |
| Sodium chenodeoxycholate  | [65]                |
| Sodium lithocholate   | [65]                |
| Sodium ursodeoxycholate   | [65]                |
| Sodium hyodeoxycholate  | [65]                |
| Sodium taurocholate   | [65]                |
| Sodium glycocholate   | [65]                |
| Sodium glycodeoxycholate  | [65]                |
| Sodium glycochenodeoxycholate   | [65]                |
| Sodium glycooursodeoxycholate   | [65]                |
| Sodium taurodeoxycholate  | [65]                |
| Sodium taurochenodeoxycholate   | [65]                |

influences this balance.<sup>[71,75]</sup> Additionally, the pH of the solvent affects ionisable polymers and ionisable APIs.<sup>[58,76]</sup> Another potential mode of action for polymeric PIs is *via* alteration of the solid-liquid interface, which can cause a change in surface energy and hinders the diffusion of new molecules to the crystal surface. Furthermore, the solubility and surface tension in the bulk solution can undergo changes and therefore may contribute to the precipitation inhibition.<sup>[72,77]</sup> However, for this purpose, it is not currently understood to what extent the polymer needs to be in a colloidal state vs solubilised as random coils.<sup>[54]</sup> Another important factor to consider is viscosity; as the viscosity of the solution increases, the molecular mobility of the drug in solution decreases. This increases the energy required for the diffusion of drug through the solution and can have a profound effect on both nucleation and crystal growth, both of which depend on diffusion of drug to another solute molecule or to the growing crystal, respectively.

For a given polymer, a high molecular weight is associated with an increase in viscosity as well as an increase in the number of binding sites. For this reason, it is often unclear which factor is responsible for any increased inhibition when considering a range of molecular weight polymers. For example, Chavan *et al.*<sup>[78]</sup> concluded that viscosity was an important polymer characteristic in the precipitation inhibition of nifedipine from supersaturated solution by HPMC, with higher viscosity samples of HPMC delaying the induction time of crystallisation for the longest periods of time. However, viscosity is not the only determinant of precipitation inhibition by polymers, other reports in the literature were unable to show a significant impact of polymer viscosity.<sup>[69]</sup> In any case, it is likely that the mechanism(s) of interaction and the biggest contributor to the inhibitory effect will vary with the individual system.

### Surfactants and cyclodextrins as precipitation inhibitors

Similar to polymers, surfactants and cyclodextrins have also been reported to sustain drugs in solution kinetically through molecular interactions.<sup>[79,80]</sup> However, they also have the potential to inhibit precipitation by increasing the solubility of the API, thereby reducing supersaturation. For surfactants and cyclodextrins, this can occur *via* micellar solubilisation and complexation, respectively.<sup>[79-82]</sup> Thus, surfactants and cyclodextrins have often been called thermodynamic precipitation inhibitors.<sup>[20,54,79-88]</sup> This distinction relates to the mechanism of action of the inhibitory affect. For conventional polymer PIs, the drug is sustained in solution only temporarily, and precipitation will eventually occur. Therefore, polymers have a kinetic effect on drug precipitation. For surfactants and cyclodextrins, however, increasing the solubility (i.e. reduction in

supersaturation) is a more sustained effect. The classification of cyclodextrins and surfactants as precipitation inhibitors is therefore somewhat tentative, and the distinction of kinetic inhibition vs solubilisation effects has typically not been addressed in the literature. Therefore, further mechanistic work surrounding the mode of action of surfactants and cyclodextrins on precipitation inhibition will be required to better understand the relevance of these compounds as PIs. For a list of all surfactants and cyclodextrins reported in the literature to act as PIs, please refer to Table 1.

### Endogenous precipitation inhibitors

Endogenous surfactants in the GI tract can also inhibit the precipitation of supersaturating formulations during dissolution *in vivo*. In theory, surfactants such as bile salts and lecithin have the potential to inhibit crystallisation *via* the mechanisms mentioned in the previous sections. For example, Chen *et al.*<sup>[89]</sup> showed that sodium taurocholate was able to extend nucleation time significantly (up to 11-fold) for a group of 11 structurally diverse compounds. This may partly explain why many *in vitro* dissolution tests overestimate the precipitation of supersaturated API.<sup>[90]</sup> Further work by Li *et al.*<sup>[65]</sup> expanded the precipitation screen to 13 different bile salts. It was observed that most of the 13 bile salts investigated inhibited precipitation of celecoxib, nevirapine and flibanserin, with varying degrees. Further, it was concluded that van de Waal and hydrogen bond interactions between the inhibitor and the molecule in solution were the key factors determining PI effects.<sup>[65]</sup> In this respect, there are clear similarities with formulation-based PIs. Although more work is required, it is clear already that it is important to understand and take into account the effect of endogenous molecules on supersaturating formulation, especially in the design of *in vitro* dissolution tests.

### Precipitation inhibitor screening methods

Given the large number of PIs reported in the literature, (Table 1) various screening methods to select API-PI combinations have been developed. Invariably, these screening methods involve the generation of supersaturation in combination with a variety of analytical techniques that can determine the rate and extent of precipitation of a drug over time in a large number of samples. A wide variety of methods to generate supersaturation are reported in the literature, including use of amorphous solids, shifts in temperature or pH, use of salts or solvent shifts.<sup>[54]</sup> Of these techniques, the most common is solvent shift, which involves dissolving the API in high concentrations in a favourable solvent (e.g. DMSO), a small volume of which is then added an aqueous phase to generate a supersaturated



state. Analytical techniques such as UV spectroscopy, HPLC or nephelometry can then be used to assess API concentration or concentration of precipitate over time, which in turn gives information about the efficiency of the inhibitor being studied.<sup>[54]</sup>

For example, during a drug development regime, two Johnson and Johnson drugs, A and B, required addition of PIs to a surfactant based bioenabling formulation that generated supersaturation but did not itself prevent precipitation.<sup>[124]</sup> To select an appropriate PI candidate, supersaturation was generated in the presence of a range of potential PIs for both compounds, and then, HPLC was employed to determine residual drug concentration after 24 h. This screening platform identified Pluronic F127 as the most efficient PI.<sup>[93,124]</sup> As a side note, this type of experimental set up is particularly attractive when pursuing surfactant based formulations, as the methodology can simultaneously screen surfactant systems as well as PIs. In this respect, one can simultaneously assess the extent of the supersaturation generated by the surfactant and how sustained the profile is in the presence of PIs.<sup>[93]</sup> The main drawback of the given experimental design is that barely any information is obtained about the kinetics of drug precipitation in the presence of polymer as only a single time point is used.

An alternative screening platform, which utilised off line chromatography, was reported by Petrusewska *et al.*<sup>[125]</sup> In this study, supersaturation was generated for fenofibrate and carbamazepine, in the presence of PIs, using a solvent shift from DMSO into aqueous buffer. The plates were sealed and incubated, with samples being taken at 30, 90, 180 and 360 min, filtered and analysed with UPLC for API content. This method provides more information about which PI is the most efficient over physiologically relevant

timescales. In this study, it was found that surfactants such as Tween<sup>®</sup> and Cremophor<sup>®</sup> were most efficient for fenofibrate, whereas for carbamazepine, cellulose derivatives such as HPMC and HPMCAS were the optimal systems.<sup>[125]</sup>

In spite of the limited time resolution that such 'off line' methods can provide, they can often be very reliable when it comes to predicting performance of the final formulation. Yamashita and colleagues performed a similar high throughput screen for a range of surfactants, oils and polymers in combination with itraconazole.<sup>[126]</sup> The screen demonstrated that HPMCAS was the most efficient 'anti precipitator'. When itraconazole HPMCAS spray dried dispersions were manufactured and compared to the commercially available Sopranox<sup>®</sup> HPMC based dispersions, the HPMCAS based formulations significantly outperformed the commercial product in dissolution tests.<sup>[126]</sup>

Analytical techniques that offer *in situ* analysis are very appealing as they can provide a real time picture of supersaturation precipitation behaviour. It was demonstrated by Warren and colleagues that utilising *in situ* nephelometry, a technique that uses light scattering to measure particle concentration, can provide an indirect measure of API concentration in a high throughput screen.<sup>[54]</sup> In this instance, the nephelometer measures light scattering of the samples, which directly relates to the total concentration of particulate matter in suspension and API in solution. A large number of species were screened for precipitation inhibition using a plate reader, after which the researchers were able to sort the PIs into three distinct groups based on the nephelometry data (Figure 6).<sup>[54]</sup>

Chauhan *et al.*<sup>[70]</sup> expanded upon this technique by utilising an *in situ* UV probe that provided time resolved information about the concentration of API in solution. This

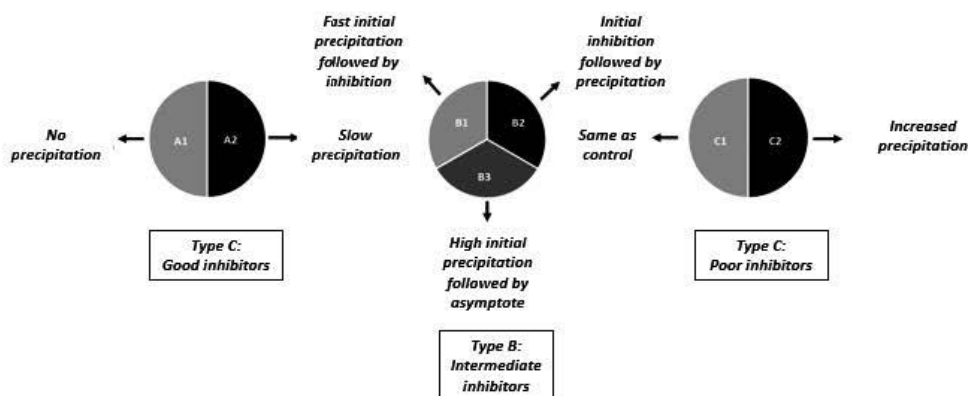


Figure 6 An empirical classification scheme devised by Warren *et al.*<sup>[54]</sup> group inhibitors into three classes depending on their performance, developed using high-throughput PI screening.

method was used to assess the interactions between indomethacin and a wide range of polymers. After a solvent shift to generate supersaturation, the turbidity and API concentration were measured using an *in situ* UV probe. The time-resolution of the data is highly useful and allows further calculation and processing to be carried out. Chauhan and colleagues subsequently used their data to calculate precipitation induction time (time delay between supersaturation and precipitation) as well as rate of precipitation, in which they showed that PVP, HPMC and Eudragit E100 increased induction time and decreased the rate. Subsequently, successful solid dispersions of indomethacin-PVP, indomethacin-HPMC and indomethacin-Eudragit® E100 were developed.<sup>[70]</sup> A similar study, with dipyridamole, was also carried out.<sup>[91]</sup> The downside of using nephelometry as a screening tool is the difficulty of screening any systems that are insoluble. For example, some supersaturating formulations, for example mesoporous silica, contain insoluble excipients that would interfere with the light scattering and make analysis difficult.

Recent advances in PI screening have seen the introduction of smaller scale dissolution techniques, such as the  $\mu$ DISS profiler™ apparatus, produced by Pion. The  $\mu$ DISS utilises *in situ* UV in combination with liquid handling and can be used to efficiently study supersaturation and precipitation in real-time. Palmelund *et al.*<sup>[127]</sup> were able to study six different poorly soluble drugs in combination with HPMC or PVP at different degrees of supersaturation. This method was successful in discriminating between innate solubility enhancements of the polymers vs precipitation inhibition. For the BCS IV drug, aprepitant, for example, both polymers increased solubility by approximately 150%, with the solubility being the same in both polymer systems. That being said, there were distinct differences in the curves observed in the real-time data display, with HPMC showing a more pronounced effect on the dissolution profile than PVP. Therefore, for this system, HPMC acted as a more effective PI than PVP.<sup>[70]</sup> The  $\mu$ DISS profiler™ is particularly appealing as the experimental protocols can be easily standardised to reduce inter- and intralaboratory variability.<sup>[127]</sup> The  $\mu$ DISS profiler™ has also been applied to investigate the effect of prandial state and PIs on the precipitation of supersaturated zafirlukast.<sup>[129]</sup> Further methods have also been employed in small-scale precipitation testing.<sup>[128 130]</sup>

### Approaches for precipitation inhibitor selection and increased mechanistic understanding

Although screening, and especially small-scale screening, of PIs is attractive from a throughput perspective, it adds little to the mechanistic understanding of precipitation inhibition. Detailed mechanistic investigations usually require a

comparatively larger testing scale that employs advanced analytical methods. In recent years, such studies have come to the forefront as the need for precipitation inhibitors has become greater. This section offers an overview of these recent advances as well as a more general overview of the analytical tools that are important, and will continue to be of importance, in the design and selection of PI systems for supersaturating formulations. Also important to the development of PI formulations is their *in vivo* performance. Although this has been covered extensively in the literature, it is beyond the scope of this review. The interested reader is referred to a number of recent papers that study the effect of PI selection on *in vivo* performance of supersaturating formulation.<sup>[24,115,131]</sup>

### Experimental approaches

Recently, there have been a wide range of novel experimental approaches applied to precipitation inhibitor selection. In addition, these approaches often offer a wealth of mechanistic detail. For a summary of the experimental approaches described in this section, please see Table 2.

#### NMR spectroscopy

Nuclear magnetic resonance (NMR) spectroscopy is a spectroscopic technique that exploits the electromagnetic emission of a nuclei in a magnetic field to gain structural information about the sample.<sup>[132]</sup>

Ueda and colleagues utilised 1D NMR spectroscopy as a tool to assess the impact of HPMCAS substitution patterns on the precipitation behaviour of carbamazepine.<sup>[133]</sup> In their study, it was observed that HPMCAS successfully inhibited the precipitation of carbamazepine, depending on the ratio of succinyl and acetate groups in the polymer. Specifically, it was observed that the highest degrees of carbamazepine supersaturation were sustained in the presence of HPMCAS grades with low succinyl and high acetyl substitutions. The increased acetyl substitution was concluded to be essential for precipitation inhibition, in line with the idea that the more hydrophobic the polymer, the higher the affinity for the growing crystal surface as discussed above. In order to expand upon this assumption, the group utilised <sup>1</sup>H NMR spectroscopy to provide information about the molecular mobility of carbamazepine in solution, with a range of HPMCAS variants. A good correlation was observed between precipitation inhibition and the molecular mobility. A lower molecular mobility corresponded to a more successful precipitation inhibition, due to increased interaction between the drug and the polymer. It was hypothesised that this interaction consisted of insertion of HPMCAS into growing aggregates before nucleation, which prevents the formation of the crystal lattice.<sup>[133]</sup>

**Table 2** Summary of experimental techniques recently applied for selection and increased understanding of precipitation inhibition

| Method   | Type          | Theory  | Application   | Limitations   | Ref.      |
|--|---------------|---|---|---|-----------|
| 1D nuclear magnetic resonance (NMR) spectroscopy | Spectroscopic | <ul style="list-style-type: none"> <li>Individual nuclei have unique response to magnetic fields</li> <li>Molecules have a distinct NMR spectrum based on their response</li> <li>Changes to the environment of the nuclei can affect the response</li> </ul> | <ul style="list-style-type: none"> <li>Structural information</li> <li>Interaction between two species</li> <li>Mobility</li> </ul>   | <ul style="list-style-type: none"> <li>Molecule must be sufficiently soluble</li> <li>Weaker interactions cannot be studied</li> <li>No information about intermolecular bonding</li> </ul> | [131-133] |
| Nuclear Overhauser Effect Spectroscopy (NOESY)   | Spectroscopic | <ul style="list-style-type: none"> <li>Cross-relaxation and magnetic transfer during spin interactions lead to NOE effects</li> <li>For NOEs to occur, the two nuclei must be close in space</li> </ul>   | <ul style="list-style-type: none"> <li>Determination of intermolecular interactions</li> </ul>  | <ul style="list-style-type: none"> <li>Molecule must be sufficiently soluble</li> <li>Atoms of interest must not have overlapping spectra</li> <li>Resolution can be poor</li> </ul>        | [134]     |
| Diffusion-ordered spectroscopy (DOSY)            | Spectroscopic | <ul style="list-style-type: none"> <li>Uses pulses to measure the speed of travelling complexes</li> <li>Diffusion coefficients can be calculated</li> </ul>  | <ul style="list-style-type: none"> <li>DOESY diffusion coefficients can be correlated to size of interacting species</li> <li>Can differentiate between API in solution and an API-PI complex</li> <li>Orthogonal confirmation of NOE interactions</li> </ul> | <ul style="list-style-type: none"> <li>Molecule must be sufficiently soluble</li> <li>Atoms of interest must not have overlapping spectra</li> <li>Resolution can be poor</li> </ul>        | [135]     |
| Solid-state (SS) NMR spectroscopy                | Spectroscopic | <ul style="list-style-type: none"> <li>NMR spectroscopy applied to solids</li> <li>Magic angle spinning (MAS) is used to limit the effects of directionally dependent interactions, also known as anisotropy</li> </ul>                                       | <ul style="list-style-type: none"> <li>MAS conditions can be applied to liquids</li> <li>This can be used to improve resolution of interactions</li> </ul>  | <ul style="list-style-type: none"> <li>Not common</li> <li>Equipment can be hard to access</li> </ul>   | [136]     |
| FTIR spectroscopy                                | Spectroscopic | <ul style="list-style-type: none"> <li>Infrared light absorption produces a different vibrational response depending on chemical environment</li> </ul>   | <ul style="list-style-type: none"> <li>Structural elucidation</li> <li>Determination of intermolecular interactions</li> </ul>  | <ul style="list-style-type: none"> <li>Difficult to carry out in solution due to water's individual response to IR light</li> <li>Weak molecular interactions cannot be resolved</li> </ul> | [137]     |
| UV Vis spectroscopy                              | Spectroscopic | <ul style="list-style-type: none"> <li>Absorption of light in the UV-visible range produces a different vibrational response depending on chemical environment</li> </ul>   | <ul style="list-style-type: none"> <li>Concentration quantification by Beer-Lambert law</li> <li>Determination of intermolecular interactions</li> <li>Dissolution kinetics</li> <li>Precipitation kinetics</li> </ul>  | <ul style="list-style-type: none"> <li>Weak molecular interactions cannot be resolved</li> <li>Molecule must absorb in the UV/vis range</li> </ul>  | [138]     |
| Raman Spectroscopy                               | Spectroscopic | <ul style="list-style-type: none"> <li>Absorption of inelastic Raman light from lasers produces a different vibrational response depending on chemical environment</li> </ul>   | <ul style="list-style-type: none"> <li>Structural elucidation</li> <li>Determination of intermolecular interactions</li> <li>Analysis in solution</li> </ul>  | <ul style="list-style-type: none"> <li>Only a small proportion of light will be in the Raman range (ca. 10-8%)</li> <li>Weak interactions cannot be resolved</li> </ul>                     | [144-145] |



**Table 2** (Continued)

| Method                                  | Type           | Theory  | Application   | Limitations   | Ref.      |
|---|----------------|---|---|---|-----------|
| Fluorescence Spectroscopy               | Spectroscopic  | <ul style="list-style-type: none"> <li>Measured fluorescence after adsorption of light</li> </ul>   | <ul style="list-style-type: none"> <li>Determination of intermolecular interactions</li> <li>Highlight changes in hydrophobicity and hydrophilicity</li> <li>Demonstration of phase change behaviour</li> </ul> | <ul style="list-style-type: none"> <li>Required a fluorescent probe</li> </ul>  | [49]      |
| Differential Scanning Calorimetry (DSC) | Thermal        | <ul style="list-style-type: none"> <li>Measures the heat input required to raise the temperature of a sample</li> </ul>   | <ul style="list-style-type: none"> <li>Determination of the glass transition temperature</li> <li>Solid state characterization</li> <li>Determination of intermolecular interaction</li> </ul>                  | <ul style="list-style-type: none"> <li>Does not consider the effect of water</li> <li>Cannot measure weak interactions</li> </ul> | [150]     |
| Synchrotron                             | Diffractometry | <ul style="list-style-type: none"> <li>Electromagnetic radiation emitted from charged particles accelerated in a curved path</li> <li>Synchrotrons can be used as an x-ray source</li> <li>Enhances the flux of x-rays, which improves the resolution</li> </ul>  | <ul style="list-style-type: none"> <li>Detection of early stage crystals</li> </ul>   | <ul style="list-style-type: none"> <li>Expensive</li> <li>Equipment is not widely available</li> </ul>                            | [147-149] |
| Video Microscopy                        | Microscopy     | <ul style="list-style-type: none"> <li>Video microscopes can be combined with image analysis to record precipitation in progress</li> </ul>   | <ul style="list-style-type: none"> <li>Image analysis can calculate precipitation initiation time</li> <li>Detection of early crystallization events</li> </ul>   | <ul style="list-style-type: none"> <li>Complicated set up</li> <li>Not well-established</li> </ul>                                | [118]     |
| Atomic Force Microscopy (AFM)           | Microscopy     | <ul style="list-style-type: none"> <li>High-resolution microscopy</li> <li>Cantilever, or tip, interacts with the surface of the sample</li> <li>This interaction deflects an electron beam</li> <li>The pattern of the electron beam can provide information about the sample down to the nanometer scale</li> </ul> | <ul style="list-style-type: none"> <li>Image of crystal surfaces</li> <li>Can be used to study polymer surface coverage</li> </ul>  | <ul style="list-style-type: none"> <li>Expensive</li> <li>Equipment is not common place</li> </ul>                                | [49]      |

In a recent study by Prasad *et al.*,<sup>[92]</sup>  $^1\text{H}$  NMR spectroscopy was utilised to probe the interactions behind the inhibitory effect of a range of polymers on indomethacin precipitation after the generation of supersaturation. It was hypothesised that interactions between the polymers and the carboxylic acid functionality of indomethacin were essential for precipitation inhibition. Thus, the chemical shift of the carboxylic acid functional group, at 3.70 ppm, was closely monitored for changes that could indicate that the chemical environment surrounding the protons had been altered. Eudragit<sup>®</sup> E100 and PVP, when combined with drug in solution, shifted the carboxylic acid peak to a

lower value, due to shielding effects.<sup>[92]</sup> The investigators utilised this shift to quantify the strength of drug-polymer interaction and subsequent precipitation inhibition effect. Eudragit E100 resulted in a larger downward shift than PVP, and for both polymers, this shift was directly proportional to the concentration of the polymer. Additionally, it was observed that when the formulation was changed from a binary system (drug/polymer), to a ternary system (drug/polymer 1/polymer 2), the shift was even more pronounced. This provided evidence for a synergistic contribution of both polymers to the precipitation inhibition. Dissolution performance of the drug in the presence of

polymers revealed that a larger and more sustained supersaturation was generated with Eudragit E100 than with PVP, while the ternary system gave the best results.<sup>[92]</sup> Therefore, the change in chemical shift was shown to be a useful parameter when assessing the effect of polymers on indomethacin precipitation.

Although use of 1D NMR spectroscopy to gain information about molecular mobility and chemical shift variations can be a useful tool when assessing the impact of PIs, it is somewhat limited in its ability to detect weaker intermolecular interactions, which are likely to play a highly important role in precipitation inhibition. Furthermore, typical 1D NMR spectroscopy gives information about atoms that are chemically bonded and can only provide limited information about intermolecular or supramolecular effects. However, there is a range of 2D NMR spectroscopic techniques that can yield information about correlations of different atoms through space such as nuclear Overhauser effect spectroscopy (NOESY) and diffusion-ordered spectroscopy (DOSY).<sup>[134,135]</sup>

Prior to their work surrounding the importance of substituent ratios for HPMCAS precipitation inhibition, which utilised 1D NMR spectroscopy for the calculation of molecular mobility, Ueda and colleagues first established the mechanism of interaction between HPMCAS and carbamazepine in solution by utilising NOESY.<sup>[145]</sup> During this experiment, it was observed that HPMCAS-HF (a particular grade of HPMCAS, relating to the ratio of acetyl to succinyl substituents) had cross-peak interactions with the aromatic protons and amide protons of carbamazepine, suggesting the possibility of both hydrogen bond interactions and hydrophobic interactions. After further inspection of the intensities of the cross-peaks, it was concluded that the more predominant effect was a hydrophobic interaction between the HPMCAS acetyl substituents and the aromatic region of carbamazepine.<sup>[145]</sup> This interaction was concluded to be essential for successful precipitation inhibition.

Nuclear Overhauser effect spectroscopy has also been used in combination with high-resolution magic angle spinning (HR-MAS) NMR spectroscopy, to understand the interactions between the poorly soluble drug mefenamic acid and Eudragit® EPO in supersaturated solutions.<sup>[136]</sup> HR-MAS NMR spectroscopy is an enhanced spectroscopic technique that can offer improved resolution for the study of complex solutions and has been used in the pharmaceutical industry to detect and quantify API in complex formulations such as gels and creams.<sup>[137]</sup> Higashi *et al.* were able to significantly improve the NMR spectra for mefenamic acid-EPO solutions under MAS conditions. This allowed cross-peaks to be observed during the NOESY experiments. These cross-peaks showed evidence of multiple points of interaction between the API and the polymer, indicating two different interactions: first, a hydrophobic interaction

between the aromatic part of the API and the EPO backbone, and, second, a hydrophilic hydrogen bond interaction between the aminoalkyl groups of EPO and the carbonyl groups of mefenamic acid was described. Furthermore, it was observed that the intensities of the two sets of cross-peaks were similar, leading the authors to conclude that both interactions played an important role in precipitation inhibition.<sup>[136]</sup>

Diffusion-ordered spectroscopy was an essential part of a study assessing the suitability of a novel spray-dried dispersion matrix, HPMCAS and dodecyl (C<sub>12</sub>) poly(N-isopropylacrylamide) (PNIPAm), for the system's suitability to enhance the delivery of a poorly soluble drug, phenytoin.<sup>[146]</sup> After dissolution of the solid dispersion, the C<sub>12</sub>-PNIPAm polymers formed micelles with the dodecyl groups, which successfully sustained the supersaturated state of phenytoin generated by the spray-dried dispersion (SDD). Furthermore, it was observed that the C<sub>12</sub>-PNIPAm inhibited precipitation of the supersaturated phenytoin by inclusion of the drug within the corona of the micelles, rather than the core. It was also concluded that the HPMCAS in the formulation had little effect on sustaining the supersaturation compared to C<sub>12</sub>-PNIPAm, which instead, was responsible for the enhanced dissolution of the drug from the SDD.<sup>[146]</sup> These conclusions were reached using both NOESY and DOSY data. The NOESY spectra of the novel formulation showed cross-peak interactions between the phenyl groups of the phenytoin and the isopropyl functionality on the PNIPAm polymer. Conversely, NOESY spectra revealed no cross-peaks for phenytoin combined with HPMCAS. On application of DOSY as an orthogonal approach, no reduction in diffusion coefficient for phenytoin was observed in HPMCAS or C<sub>2</sub>-PNIPAm. Conversely, the diffusion coefficient decreased dramatically in the presence of C<sub>12</sub>-PNIPAm, in a concentration-dependent manner. This provided the researchers with strong evidence that the C<sub>12</sub>-PNIPAm was responsible for the remarkable sustained supersaturation that was observed upon dissolution of this novel SDD, as well as the mechanism taking place within the corona of the micelles, which was not present in the C<sub>2</sub> variant.<sup>[146]</sup>

#### Solid-state NMR spectroscopy

Chauhan *et al.*<sup>[70]</sup> utilised carbon cross-polarisation magic angle spinning SS-NMR spectroscopy to investigate the interactions between indomethacin and polymers in solid dispersions. Three different polymers: Eudragit® S100, PVP and HPMCAS were screened for indomethacin interactions using this method. Chemical shift changes in the indomethacin signal were recorded in the presence of the polymers, with a larger chemical shift change indicating a stronger interaction. For the aromatic region, a slight



chemical shift change was observed for all three polymers, with the biggest shift occurring in the PVP SDD: this correlated well with the observed performance of the SDD during biorelevant dissolution, which outperformed all other polymers due to enhanced precipitation inhibition.<sup>[70]</sup>

### IR/FTIR spectroscopy

FTIR spectroscopy is highly attractive in a drug development setting as it can be employed to study interactions between compounds, even in complex mixtures.<sup>[137]</sup> Nie *et al.*<sup>[147,148]</sup> performed an experiment to determine interactions between clofazimine and hypromellose phthalate (HPMCP), which has been previously reported to have very high drug loading capacity in solid dispersions. IR spectra were analysed to identify changes in the vibrational modes of clofazimine and HPMCP in a solid dispersion.<sup>[147]</sup> A new peak, at 3310  $\text{cm}^{-1}$ , was observed in the IR spectrum of the solid dispersion, which corresponded to the stretching mode of the ionised imine in the clofazimine. This was present due to protonation by the carboxylic acid groups in the phthalate substituent of the HPMCP. A sensitivity analysis showed that the effect was no longer observed at ratios less than 1 : 0.5 w/w (API/polymer). Additionally, the intensity of the peak increased with increasing HPMCP concentration. This acid–base interaction between HPMCP and clofazimine was further supported by the appearance of peaks at 1540 and 1395  $\text{cm}^{-1}$ , which both correspond to the formation of a carboxylate group.<sup>[147]</sup> Knowledge about solid-state interactions can be directly correlated to solid-state stability and loading capacity, that is drug to polymer ratio, as well as to enhanced precipitation inhibition and supersaturation. Indeed, the combination of HPMCP and clofazimine in a solid dispersion resulted in a 10-fold increase in apparent clofazimine solubility.<sup>[147]</sup>

Petrusevska and colleagues also employed FTIR spectroscopy to investigate the mechanism of interactions between a successful API-PI formulation: sirolimus and HPMC.<sup>[149]</sup> Solid dispersions of HPMC and sirolimus demonstrated significant variation from the neat samples as well as a physical blend. Specifically, the sirolimus peaks at 1680–1640  $\text{cm}^{-1}$  (C=C) and 1760–1670  $\text{cm}^{-1}$  (C=O) in the solid dispersion were far broader than those from the pure drug, which the authors concluded was a result of interaction between the two species.<sup>[149]</sup> This interaction was suggested to be partly responsible for the two-fold increase in supersaturation and dissolution in the sirolimus-HPMC solid dispersion vs the commercially available Rapamune<sup>®</sup> nanoparticles. In a subsequent human pharmacokinetic study, the novel formulation significantly outperformed the commercial formulation. This effect was attributed to the enhanced precipitation inhibition properties of HPMC in the novel formulation.<sup>[149]</sup>

Another application of FTIR spectroscopy is the characterisation of precipitates. In a recent study by Chavan, IR spectroscopy was used to verify that potential polymeric PIs did not affect the solid-state phase behaviour (polymorphism) of the drug, nifedipine.<sup>[143]</sup> In this instance, the FTIR spectra of the precipitates for all three polymers (HPMC, PVP and HPC) aligned well with crystalline nifedipine, indicating that no polymorphic change was induced by the polymers.

### UV-Vis spectroscopy

UV-Vis spectroscopy enables quantitative analysis of any molecule that absorbs light in the UV-Vis range, which make it a very useful spectroscopic technique, arguably, one of the most widely used in pharmaceutical sciences.<sup>[138]</sup> This section will focus on instances where UV-Vis spectroscopy has been applied for more advanced studies, such as in the determination of interactions between drug and polymer or in-depth studies looking at precipitation kinetics during dissolution of supersaturating formulations.

Nie and colleagues used UV-Vis spectroscopy as an orthogonal technique to support their mechanistic hypothesis for clofazimine-HPMCP interaction.<sup>[147]</sup> This was especially useful as clofazimine is red in both crystalline and amorphous forms, but a colour shift to purple occurred in the presence of HPMCP in solid dispersions. Qualitatively, this was also observed for mixtures of drug and carboxylic acid analogues (e.g. glacial acetic acid), but not for polymers without carboxylic acids, such as HPMC. It was concluded that the bathochromic shift was associated with a proton transfer from the carboxylic acid functional group of HPMCP.<sup>[147]</sup> In combination with principal component analysis, the API : PI ratio at which no interaction was observed was calculated to be at ratios below 1 : 0.5. Using the same approach, it was concluded that the API : PI ratio at which full deprotonation of the imine occurs, that is the strongest interaction, was at 1 : 1.5.<sup>[147,148]</sup> Such information can be valuable in the design and development of PI-based formulations. A similar study was conducted by Mistic *et al.*<sup>[150]</sup> in the investigation of acid–base interactions between the poorly soluble drugs, loratadine and carvedilol, and oleic acid.

Patel *et al.*<sup>[151]</sup> also utilised UV-Vis spectroscopy in combination with mathematical modelling. This study involved the combination of online second-derivative UV spectroscopy and modelling using the diffusion-reaction model to give real-time concentration values and mechanistic insight for indomethacin in supersaturated solutions. This methodology was able to provide a large amount of information about the precipitation behaviour, including that at high degrees of supersaturation, the precipitation

was bulk diffusion limited, which fits in well with the diffusion–reaction model.<sup>[151]</sup>

UV–Vis spectroscopy can also be employed to increase the understanding of phase behaviour of supersaturated solutions, which can aid in the selection of PIs. Jackson *et al.*<sup>[48]</sup> utilised two techniques, UV–Vis spectroscopy and fluorescence spectroscopy to determine the phase change behaviour of danazol during LLPS into drug-rich amorphous or drug-rich crystalline phases in the presence and absence of PIs. During phase separation (e.g. LLPS), danazol scatters light, which increases UV extinction. Therefore, it is possible to use UV–Vis spectroscopy to determine the concentration at which LLPS occurs in supersaturated solution.<sup>[47]</sup> It was reported that LLPS onset occurred at 13 µg/ml, a value which could be decreased to varying degrees in the presence of polymers. Furthermore, it was determined that apparent decrease in the LLPS induction time in the presence of polymers correlated well with the ultimate performance of the polymer, with HPMCAS and HPMC showing both the biggest decrease on LLPS induction time (both to 8 s) and the biggest increase in precipitation induction time (277 and 163 s, respectively).<sup>[48]</sup> Therefore, *in-line* UV spectroscopy could be a valuable tool in the assessment of precipitation inhibition efficiency *via* the study of LLPS induction times from supersaturated solutions. This is a particularly attractive possibility as LLPS induction time can be measured relatively easily using this method in a high-throughput experimental set-up.

#### Raman spectroscopy

Raut *et al.*<sup>[83]</sup> utilised an *in situ* Raman probe, placed inside a dissolution set-up, to investigate the precipitation inhibition effect of vitamin E TPGS on two model compounds, probucol and indomethacin, in a self-emulsifying drug delivery systems. To achieve this, the formulations were added to a solution at pH 1.2, followed by a pH shift to pH 6.8. The Raman probe enabled the collection of time-resolved Raman spectra for both the solid precipitate and the species in solution, which were analysed for molecular interactions between the drug and excipients. For probucol, Raman peaks were observed at 540 and 1164 cm<sup>-1</sup>, corresponding to the hydroxyl groups in the molecules. However, in the presence of vitamin E TPGS, this peak dropped significantly in intensity, with 1164 cm<sup>-1</sup> disappearing completely. This was attributed to the interaction of the probucol hydroxyl groups with carbonyl groups of the PI. These interactions had a profound effect on precipitation, with no precipitation observed in the presence of vitamin E TPGS, in spite of the system being supersaturated to 100-fold of the thermodynamic solubility of probucol.<sup>[82]</sup> Similar observations were made for indomethacin. Interestingly, in the case of indomethacin, it was observed that

interactions were only evident whenever a certain ‘supersaturation threshold’ was obtained,<sup>[82]</sup> below which interactions were not observable and precipitation occurred. This is an important factor to bear in mind: although a drug and polymer may theoretically interact strongly, the formulation in question must generate a particular concentration before interactions will occur.

In addition to probing interactions in solution, Raman spectroscopy is a useful tool for investigating short-range interactions in the solid state. This can be particularly beneficial in the development of solid dispersion formulations, such as hot melt extrusion (HME) and spray-dried dispersions (SDD), where both drug–polymer miscibility and the precipitation inhibition performance of the polymer are based on these interactions. Chauhan *et al.*<sup>[91]</sup> utilised this technique, among a wide range of spectroscopic tools, to develop solid dispersions of dipyridamole. The team found that the most successful formulations consisted of drug-HPMC and drug-Eudragit E100<sup>®</sup>, which performed significantly better than all other polymers screened. Utilising solid-state Raman spectroscopy, it was revealed that interactions were present between the drug and HPMC and Eudragit E100<sup>®</sup>.<sup>[91]</sup>

Raman spectroscopy can also be applied to study the extent of drug precipitation because dissolved and solid drug generally differ in their spectra. Both types of spectra can be used in a multivariate calibration. Thus, *in-line* dispersive Raman spectroscopy has been used to monitor drug precipitation from supersaturated dipyridamole solutions using a transfer test<sup>[152]</sup>; and this spectroscopic approach has also been reported to study drug precipitation from lipid-based formulations in the course of digestion.<sup>[153]</sup>

#### Fluorescence spectroscopy

Fluorescence spectroscopy can be used to determine interaction mechanisms, changes in hydrophobicity and phase change behaviour. This is achieved by utilising fluorescence probes, such as pyrene.<sup>[48]</sup> Pyrene is a good probe for hydrophobicity, as when it preferentially partitions into hydrophobic microenvironments, a change in its fluorescence absorption bands,  $I_1$  and  $I_3$ , occurs.<sup>[48]</sup> Jackson *et al.* exploited this phenomenon in order to assess the concentration at which LLPS occurred in the presence of danazol and to determine whether a crystalline or non-crystalline phase was formed. For LLPS, it was determined that no significant change in the  $I_1/I_3$  ratio in the pyrene fluorescence spectra occurred below danazol concentrations of 13 µg/ml in the pure sample. Above this, the change in  $I_1/I_3$  aligned well with the formation of a non-crystalline LLPS, suggesting an onset of LLPS at 13 µg/ml. Additionally, it was observed that incorporation of a polymeric PI decreased the LLPS onset concentration, with HPMCAS and HPMC



having the biggest impact, decreasing LLPS onset concentration to 8 and 9 µg/ml, respectively. Observing the changes in  $I_1/I_3$  can provide information about the induction time of precipitation as, generally speaking, the  $I_1/I_3$  ratio returns to normal after recrystallisation. This is due to the disappearance of the drug-rich phase and the expulsion of pyrene from the crystal lattice and back into the aqueous phase.<sup>[154]</sup> In the study, all three polymers showed a sustained  $I_1/I_3$  ratio for at least 15 min. These data correlated with the induction times, with HPMCAS showing the longest induction time of 4 h.<sup>[48]</sup>

Creasey *et al.* utilised this technique to assess the interaction between Pluronic and Labrasol in a formulation being developed for two Johnson and Johnson compounds. Pyrene solution was added to solutions of Labrasol, Pluronic and mixtures of the two. Fluorescence spectra for pyrene were then collected to record the effect of Pluronic on the micropolarity of the Labrasol formulations.<sup>[124]</sup> In this instance, the  $I_1/I_3$  ratio in the mixture of Labrasol and Pluronic was significantly lower than for Labrasol alone, which indicates a more pronounced hydrophobic microenvironment in the sample. It was hypothesised by the researchers that this increased hydrophobicity was the key factor for inhibiting precipitation, allowing the drug to be held more tightly within the microstructures formed by the surfactant. Finally, this mechanism had a profound effect on both compounds with a 500- and 200-fold increase in concentration compared to no excipients added.<sup>[124]</sup>

#### Differential scanning calorimetry

Differential scanning calorimetry (DSC) is a thermal analysis technique that sees wide application in pharmaceutical sciences, for example in solid-state characterisation.<sup>[141]</sup> Although not as common, DSC can also be used to investigate interactions between two species. However, traditional DSC cannot achieve this and instead, modulated DSC (MDSC) must be used. MDSC differs from traditional DSC in that it operates using two simultaneous heating rates, in contrast to the single linear heating rate used in DSC. MDSC utilises both a linear heating rate and a modulated heating rate that allows simultaneous measurement of the heat capacity of the sample.

Chauhan *et al.*<sup>[91]</sup> used MDSC to investigate the mechanism by which dipyrindamole (DPD) interacts with a range of PIs. Previously, MDSC has been used to assess miscibility between a drug and polymer, based on changes in melting events. Expanding on this idea, the melting temperatures of the DPD and DPD precipitates in the presence of polymers were used to identify whether any drug-polymer interaction was taking place. For Eudragit<sup>®</sup> E100, Eudragit<sup>®</sup> S100 and HPMC, additional melting endotherms were observed in the MDSC curves. The authors of the study reasoned that

this change in the thermal behaviour occurred due to interaction of the drug with the polymers in solution, which corresponded with an increased precipitation inhibition. Indeed, out of the six polymers studied, only those polymers where a change in melting temperature of the precipitates was observed were successful PIs.<sup>[91]</sup> Moreover, the authors also cautioned that, although melting point changes were present, this was not a definitive proof of interaction as certain polymers, for example PEG, can dissolve a drug and therefore alter the melting temperature. Rather, DSC is a useful tool to determine lack of interaction, as was the case with the unsuccessful PIs, Eudragit S100, Eudragit L100 and PEG 8000. To state that an interaction is definitely present, MDSC should be used with complementary analytical techniques.

#### Synchrotron radiation

Synchrotron radiation is the electromagnetic radiation emitted from charged particles that are accelerated in a curved fashion, for example in a circular particle accelerator.<sup>[142]</sup> For diffraction studies, synchrotron radiation enhances the flux of X-ray radiation,<sup>[144]</sup> which leads to diffraction patterns with higher resolutions, obtained in a shorter period of time. The technique is a highly sophisticated analytical tool, and practical usage is limited due to the fact that the equipment is not common and is highly expensive. Therefore, synchrotron light sources exist at dedicated sites, of which there are only a few around the world (a list of dedicated sites can be found at: <http://www.lightsources.org/light-source-facility-information>).<sup>[145]</sup>

It was reported by Van Eerdenbrugh and colleagues that synchrotron radiation could be utilised to study the precipitation and crystallisation behaviour of API in a supersaturated solution.<sup>[155]</sup> This was achieved using wide-angle X-ray scattering (WAXS) with synchrotron X-ray beams. The research group concluded that the method could detect crystalline particles at a minimum *suspension* concentration of 2.6 mg/ml for all samples in their 52-sample study, including a large proportion of poorly soluble model drugs,<sup>[156]</sup> which translates to a sensitivity of around 0.26% w/w drug in aqueous suspension. This sensitivity is significantly higher than all other conventional methods for detecting crystallinity and is also in agreement with previous studies, which showed that crystals with a size of <1 nm could be detected.<sup>[155]</sup>

Further work by this group incorporated PIs into the same experimental design, to study mechanistically the effect of PIs on the crystallisation time of a range of compounds.<sup>[157]</sup> In this study, the solvent-shift method was applied to generate supersaturated solutions in the presence of a particular amount of predissolved polymer. The onset time of crystallisation was examined using several

measurements over 24 h, to determine the delay in onset of crystallisation. Combining the results with polarised light microscopy demonstrated the presence of LLPS, which was prolonged in the presence of some polymers. Similar to other reports in the literature,<sup>[73]</sup> the most hydrophobic and hydrophilic polymers were not effective PIs, supporting the hypothesis that an effective PI must interact with *both* the aqueous medium and API.<sup>[158]</sup>

Due to the high costs and low availability of the synchrotron methods and equipment, it is unlikely that this approach will ever find widespread adoption for screening of precipitation inhibitors, and certainly not in routine drug development. Additionally, although it is significantly more sensitive than standard methods, there is still a limit to how easily one can detect the early crystallisation events taking place during precipitation.

### Video microscopy

For screening of PIs, microscopy is an attractive approach as the efficiency of inhibitors can be visualised, offering insight into early crystallisation events that would not be typically observable *via* conventional methods such as detection by UV spectroscopy. However, the use of manual microscopy is not highly prevalent in the literature, probably due to the time and labour requirements. To circumvent this, various studies have combined conventional microscopy with video analysis.<sup>[114]</sup>

Recent work by Christfort *et al.* utilised such a system to investigate supersaturated solutions of tadalafil in the presence and absence of a PI, HPMC. Samples were viewed under video light microscopes, and multiparticle analysis

was carried out on the videos to assess total precipitation as a function of time.<sup>[114]</sup>

### Atomic force microscopy

Atomic force microscopy (AFM) is a type of high-resolution microscopy that can image on the nanometre scale. Due to this high resolution, AFM has been applied to study the effect of polymer surface coverage on growing crystals, and how this relates to precipitation inhibition. According to the adsorption layer model, before a solute molecule can join a growing crystal lattice, it must adsorb and interact with the surface at a site with high attraction forces. This interaction can be hindered or disrupted with the use of polymers, which can bind the solute in solution or adsorb onto the growing crystal surface. For the latter mechanism, it has been hypothesised that understanding the conformation of polymers on the surface of the growing lattice is key to inhibition of crystal growth.<sup>[75,158]</sup>

Expanding upon this idea Schram *et al.*<sup>[76]</sup> studied the effect of the pH on the adsorption of HPMCAS on felodipine crystals and the subsequent effect on precipitation inhibition, using AFM and *in situ* UV spectroscopy, respectively. It was observed during the AFM experiments that at pH 3.0 the polymer was adsorbed as small aggregates and at pH 6.8 the whole surface was covered with a monolayer. The space between two polymer aggregates at pH 3.0 ranged from 25 to 50 nm, compared to 0.9 nm at pH 6.8. Therefore, at a higher pH, there was a greater polymer surface coverage and greater inhibition of crystal growth. Indeed, the ratio of crystal growth (crystal growth rate in the absence of an inhibitor/crystal growth rate in the

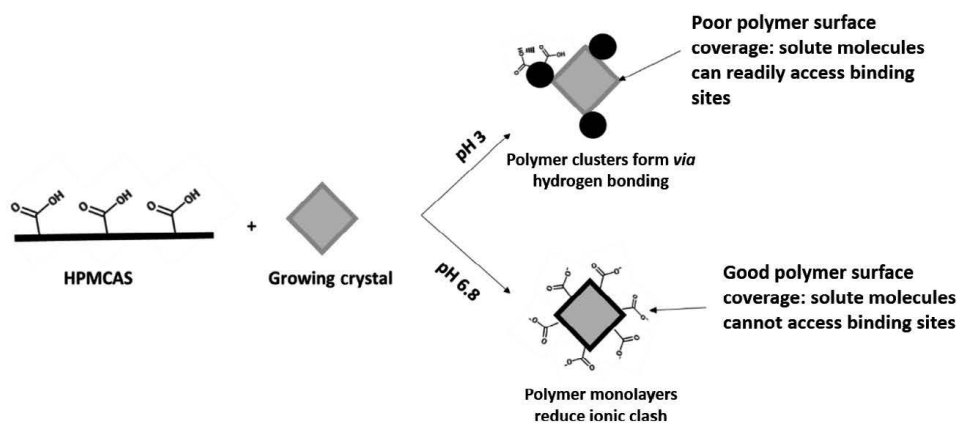


**Figure 7** Schematic diagram showing the conclusions of Schram<sup>[75]</sup>: polymer surface coverage in relevant physiological environment is a crucial factor to be considered in the selection of polymeric precipitation inhibitors.

presence of inhibitor) was 1.28 and 2.29 at pH 3 and 6.8, respectively. This was explained by the intra- and intermolecular hydrogen bonding of HPMCAS at the different pHs investigated.<sup>[75]</sup> With a pKa of 5.5, HPMCAS is unionised at pH 3. As a result, intermolecular interactions between the succinyl groups can occur, which allows the polymer to form coils and aggregates. Conversely, at pH 6.8, the polymer is ionised, and self-repulsion results in the molecules forming a monolayer on the surface with no interaction between the succinyl groups. These observations led Schram and colleagues to conclude that the conformation of a polymer, and more importantly the total surface coverage of a polymer, is crucial when considering the observed inhibitory effect (Figure 7).<sup>[75]</sup>

Additional work by Schram and colleagues was dedicated to establishing a correlation between polymer surface coverage and precipitation inhibition.<sup>[158]</sup> For this, the group again employed atomic force microscopy (AFM) to study the interaction between a range of polymers and felodipine crystals. The measurements were made in suspension, with height and phase contrast images recorded simultaneously. The phase contrast in the images is dependent on the surface characteristics of the sample, and therefore, difference between surface properties can be detected between different samples.<sup>[159]</sup> The images were then analysed using 'ImageJ', a software that can detect changes in digital images based on pixel changes,<sup>[160]</sup> and thus could be used to calculate total surface coverage of the polymer on the growing crystal. In the study, it was reported that polyacrylic acid (PAA), a hydrophilic polymer, was not adsorbed to the crystal surface, while PVP, another hydrophilic polymer, formed aggregates to decrease the surface area exposed to the crystal surface to  $8 \pm 0.8\%$  coverage. At the other end of the scale, it was observed that hydrophobic polymers like polyvinyl acetate (PVAc) also minimised their exposed surface area to the liquid by forming aggregates adsorbed on the surface of the crystal ( $14 \pm 0.7\%$  coverage).<sup>[158]</sup> By contrast, polymers with both properties (hydrophobicity and hydrophilicity), like HPMC, resulted in the best surface coverage by adsorbing to the surface of a crystal in a more monolayer-like fashion ( $54 \pm 0.8\%$  coverage).<sup>[158]</sup> A linear correlation between surface area coverage and polymer effectiveness (based on the aforementioned crystal growth ratio) was established, showing that a good surface coverage can predict good precipitation inhibition.

Atomic force microscopy is a useful tool for studying polymer surface coverage and conformation, essential parameters when considering the effectiveness of a PI in a supersaturating formulation. In combination with knowledge of the PI conformations throughout the physiological pH range, such parameters have the potential to be utilised routinely as part of a selection protocol for PIs. More work is required to bridge the gap between these proof-of-

concept studies towards a more widespread application which could operate in industrial settings. Particular emphasis should be placed on demonstrating correlations with different API-PI systems, and on the development and validation of the *in silico* models to predict polymer performance based on polymer surface coverage, which could offer a very attractive avenue in the prescreening phase of PI selection. One issue may be the accessibility and complexity of AFM, which is not often commonly used in early-stage development.

## Computational approaches

### Mathematical modelling

Mathematical modelling of physical, physicochemical and physiological processes can be a useful tool in drug development with a wide range of applications.<sup>[161-163]</sup> For precipitation inhibition, models that are related to adsorption, crystallisation and dissolution have been very valuable in a number of key studies. However, the use of mathematical models to aid in the understanding of precipitation behaviour, and the effect of inhibitors, has not yet been adopted widely.

*Adsorption modelling.* Early work in the literature utilised well-established adsorption isotherms, including the Langmuir<sup>[164]</sup> and Freundlich models,<sup>[161]</sup> to predict the adsorption of additives on crystal surfaces and consequently to estimate the crystal growth kinetics inhibition through mathematical modelling. This approach is often used in combination with crystallisation models such as the Kubota–Mullin model, which models crystal growth.<sup>[163,165,166]</sup>

The Kubota–Mullin model applies a step-growth model, which assumes that a crystal grows monolayer by monolayer. The growth inhibition depends on the PI and the distance between the adsorbed species on the surface. In the model, crystal growth is linked to fractional surface coverage,  $\theta$ , which is the ratio of the average distance between the potential adsorption sites,  $L$ , and the average distance between the adsorbed species,  $\bar{l}$ , and the free energy of the unit length (Equation 2).<sup>[163,165,166]</sup>

$$\theta = \frac{L}{\bar{l}} \quad (2)$$

Expanding on their work using AFM to probe the polymer surface coverage of a range of PIs on felodipine crystals, Schram and colleagues adapted the model to predict polymer performance from the experimentally obtained surface coverage values.<sup>[158]</sup> In this case, polymer effectiveness,  $R_p/R_0$ , is the ratio of crystal growth in the presence ( $R_p$ ) and absence of polymer ( $R_0$ ) and depends on the



fractional surface coverage,  $\theta$ ; the relative supersaturation,  $\sigma$ ; the edge free energy per unit length,  $\gamma$ ; the size of a growth unit,  $a$ ; the temperature,  $T$ ; the Boltzmann constant,  $k$ ; and the average distance between adsorbed polymers,  $l$  (Equation 3)

$$\frac{R_p}{R_0} = 1 - \frac{\gamma a}{kT\sigma(\theta l)} \theta \quad (3)$$

The average distance between polymer molecules is specific for each system and depends on the amount of polymer adsorbed to the surface. Thus,  $l$  was proportional to the experimental polymer surface coverage determined by AFM. Consequently, a correlation was established, with which  $l$  could be determined from the polymer surface coverage. This allows the calculation of the fractional surface coverage in the Kubota–Mullin model (Equation 2) and subsequently the theoretical effectiveness of crystal growth inhibitors (Equation 3). In this study, the theoretical effectiveness calculations were in good agreement with the experimental values.<sup>[158]</sup>

Alonzo *et al.*<sup>[52]</sup> also adopted the Kubota–Mullin model to study the effect of HPMC on crystal growth and nucleation of felodipine in a supersaturated solution. In combination with the Langmuir adsorption model, the research team explored the effect of HPMC on felodipine crystallisation. Based on the model, it was predicted that the effect of HPMC on the crystallisation of felodipine crystals was highly dependent on the extent of supersaturation, with greater supersaturation reducing the effect of the inhibitor. The theoretical predictions were in agreement with the experimental crystal growth rate in the presence of HPMC. It was also predicted that polymers successfully interrupting the nucleation process would be more advantageous than those that affect the crystal growth rate, which was supported experimentally.<sup>[52]</sup> Further work utilising the Kubota–Mullin model was carried out by Ilevbare *et al.*,<sup>[47]</sup> who were able to successfully estimate the crystallisation rate of the poorly soluble drug, ritonavir, in the presence and absence of a polymer.

One of the most extensive studies on the use of adsorption and crystallisation models was carried out by Patel *et al.*<sup>[69,103,151]</sup> They studied the precipitation behaviour of indomethacin in the presence of PIs. The effect of molecular weight on the inhibition potential of PVP and of N-vinylpyrrolidone on indomethacin crystallisation<sup>[69]</sup> was investigated using adsorption isotherms generated *via* the solution depletion method. Using a wide range of molecular weights, the two inhibitors were combined with indomethacin in an aqueous suspension and allowed to equilibrate for a set amount of time. The samples were then filtered and analysed using size exclusion chromatography to determine the concentration of the adsorbed polymer, which provided a value of the extent of inhibitor surface

adsorption. These values were then used to construct adsorption isotherms based on the Langmuir model. It was shown that the adsorption potential for PVP was greater than N-vinylpyrrolidone. Further, the isotherms demonstrated that the adsorption capacity for PVP was directly proportional to PVP molecular weight. These model predictions were then validated experimentally, with PVP significantly outperforming N-vinylpyrrolidone in the inhibition of indomethacin precipitation, with increasing molecular weight of PVP also correlating to a higher degree of sustained supersaturation.<sup>[103]</sup>

Further work by Patel and Anderson employed the previously developed second-derivative UV method in combination with a first-order crystal growth model to investigate the growth rates of indomethacin in the presence of various PIs.<sup>[151]</sup> HPMC and PVP significantly outperformed HP $\beta$ CD, in agreement with the inhibition models. For HP $\beta$ CD, precipitation inhibition was modelled using diffusion layer theory, based on the assumption that HP $\beta$ CD complexes with indomethacin in the diffusion layer of crystal growth. This model successfully predicted that, at high degrees of supersaturation, HP $\beta$ CD inhibition could be related to the reversible complexation between the two species at the diffusion layer.<sup>[151]</sup>

*Molecular modelling.* Many types of molecular modelling can be used in simulation of crystallisation or precipitation, from quantum mechanical approaches, to Monte Carlo methods to molecular dynamics simulations.<sup>[167]</sup> Molecular simulations of crystallisation and precipitation are of high interest as they can offer a high throughput that can be applied to a wide range of systems. Mandal *et al.*<sup>[162]</sup> developed a framework that enabled the simulation of crystallisation behaviour of a range of organic molecules in the presence of inhibitors. In this study, a coarse-grained (CG) model for crystal growth<sup>[168]</sup> based on force fields obtained from simulators was applied to a range of molecules. Coarse-graining is an approach that allows the simulation of complex systems without using extensive computation time due to the use of simplified atomistic representations. Such an approach is often used to model the interaction of proteins and small molecules.<sup>[169]</sup> There are many software packages that can carry out the CG process, such as MARTINI<sup>[168]</sup>; however, such software packages often oversimplify the molecules such that information important to understand crystallisation behaviour may be lost. To improve upon these established CG processes, Mandal and colleagues utilised a CG model based on the radial distribution functions of the molecules, which were obtained from atomic simulations carried out in the crystalline states.<sup>[162]</sup> As a result, the CG model developed was able to simulate crystal growth of the organic molecule, phenytoin, in the absence and presence of the polymer HPMCAS.<sup>[162,168]</sup>

Furthermore, the simulation was able to correctly predict that inhibition of phenytoin by HPMCAS is highly dependent on the substitution of the polymer, with an increased acetate substitution slowing crystal growth most effectively. This simulation proved to be very robust in its prediction as these observations were also demonstrated experimentally.<sup>[162]</sup>

#### Chi parameter and interaction enthalpy

A rigorous thermodynamic treatment of PI selection would have to consider the drug and PI in water as a ternary system, where both the solid–liquid equilibrium of solubility and liquid–liquid phase separation of amorphous solubility are considered.<sup>[8,40]</sup> Such a pursuit is very attractive given the high degree of information one can learn about the system. An example of such a theoretical model is the perturbed-chain statistical associating fluid theory (PC-SAFT), which bears much promise but is also demanding, due to the various parameters that are required to fully describe a system.<sup>[40]</sup> Such highly parameterised methods still have to be adopted in the area of precipitation inhibition to enable an early *in silico* screening of excipients. Moreover, a focus on equilibrium thermodynamics may not be the most descriptive way to model drug precipitation due to the importance of kinetics. Non-equilibrium thermodynamics is an even more challenging approach, and so far, attempts have only been made to consider interactions parameters of simpler thermodynamic models for empirical kinetic considerations.

To consider the kinetics of precipitation, the interaction parameter  $\chi$  of the Flory–Huggins (FH) theory<sup>[170,171]</sup> can be employed.<sup>[172,173]</sup> The Flory–Huggins solution equation (Equation 4) describes the thermodynamic behaviour of polymers in solution. The equation is an adaption of the standard Gibbs energy equation, introducing extra terms to adjust the entropy portion to account for the dissimilarity of molecular sizes. In the Flory–Huggins equation, the enthalpic portion of the Gibbs equation is represented by the chi parameter,  $\chi$ :

$$\Delta G = RT[n_1 \ln \phi_1 + n_2 \ln \phi_2 + n_1 \phi_2 \chi_{1,2}] \quad (4)$$

In the Flory–Huggins equation,  $R$  is the ideal gas constant and  $T$  is the absolute temperature.  $n_1$ ,  $n_2$  and  $\phi$  are the number of moles and volume fraction, respectively, for components 1 and 2 of the system, while  $\chi$  is the interaction enthalpy upon association between components 1 and 2.

Expanding upon the Flory–Huggins equation, one can consider mixtures of drug and polymers, whereby the enthalpic contribution becomes,  $\chi_{DP}$ . In this approach, it

is assumed that the interactions considered in  $\chi_{DP}$  are also relevant for the kinetics of sustaining drug supersaturation. This is based on the understanding that some of the mechanisms by which a polymer can inhibit precipitation are dependent on energetic interactions such as hydrophobic, polar or hydrogen bond interactions between the drug and PI.<sup>[54]</sup> The  $\chi_{DP}$  parameter can be determined experimentally by combining the Flory–Huggins equation with experimental DSC measurements.<sup>[174]</sup> This parameter has been applied to other areas of drug development, for example in the assessment of drug–polymer miscibility in the screening of candidate formulations.<sup>[175]</sup> It is possible to utilise *in silico* predictions of the  $\chi_{DP}$  parameter, which reduces the number of experiments required, thus allowing more focus on the most promising formulations. This can be achieved in a number of ways, with one key strategy combining the total solubility parameters of the drug,  $\delta_D$ , and polymer,  $\delta_P$ , in relation to the molar volume of the drug,  $V_m$ , the temperature,  $T$ , and the ideal gas constant,  $R$  (Equation 5).<sup>[176]</sup>

$$\chi_{DP} = \frac{V_m(\delta_D - \delta_P)^2}{RT} \quad (5)$$

The extended Hansen solubility parameters,  $\delta_D$ , and  $\delta_P$ , can be predicted based on chemical structure alone, using group contribution methods.<sup>[177]</sup> Indeed, this determination of  $\chi_{DP}$  via partial solubility parameters has been used to construct entire phase diagrams for solid dispersions based on the Flory–Huggins theory.<sup>[178]</sup>

In addition to group contribution methods, it has been shown that solubility parameters can be predicted based on quantitative structure–property relationships (QSPR).<sup>[179]</sup> With rising computational power, there is also the option to use molecular dynamic (MD) simulations to calculate solubility parameters and hence to determine  $\chi_{DP}$ . A first calculation option is to simulate internal energy change due to vaporisation,  $\Delta E_v$ .<sup>[182]</sup> This MD approach utilises the original definition of the solubility parameter as a cohesive energy density (CED) (Equation 6)<sup>[183]</sup>:

$$\delta = (\text{CED})^{1/2} = \left[ \frac{\Delta E_v}{V_m} \right]^{1/2} \quad (6)$$

In this instance, total energy difference for isolated molecules and for the bulk system with periodic boundary conditions provides an estimate of  $\Delta E_v$ .<sup>[183]</sup> That being said, calculation of the cohesive energy difference and conversion of the solubility parameter into  $\chi_{DP}$  are not the only way to obtain the Flory–Huggins interaction parameter by means of molecular simulations. Fan *et al.*<sup>[184]</sup> developed a molecular simulation method to derive phase diagrams of binary mixtures (Equations 7 and 8).



$$\chi_{1,2} = \frac{z\Delta w_{1,2}}{RT} \quad (7)$$

$$\Delta w_{1,2} = w_{1,2} - \frac{1}{2}(w_{1,1} + w_{2,2}) \quad (8)$$

The interaction parameter between two molecules, ( $\chi_{1,2}$ ), is obtained directly from the corresponding pairwise interactions,  $w$ , and hence the energies  $w_{1,1}$ ,  $w_{2,2}$ ,  $w_{1,2}$  (Equations 7 and 8). This can be achieved by averaging a large number of configurations using a Monte Carlo approach, taking into consideration the number of neighbouring molecules (i.e. coordination number,  $z$ ) in combination with the ideal gas constant,  $R$ , and temperature,  $T$ .

There are numerous routes to obtain the Flory-Huggins  $\chi_{DP}$ . That being said, there are only a few examples of this parameter being used to understand precipitation inhibition. Baghel *et al.*<sup>[173]</sup> studied solid dispersions of dipyrindamole (DPY) and cinnarizine (CNZ) with polyvinylpyrrolidone (PVP) and polyacrylic acid (PAA). It was found that the combinations capable of forming hydrogen bonds (DPY-PVP; DPY-PAA and CNZ-PAA) in the solution state were more effective at keeping the drug in supersaturation than those not able to hydrogen bond (CNZ-PVP). In this instance, CNZ-PVP had the highest predicted  $\chi_{DP}$  parameter, suggesting a less stable interaction, in line with the observed precipitation inhibition results. However, it was noted that, despite their significantly different supersaturation performance, the difference between the  $\chi_{DP}$  parameters of CNZ-PVP and CNZ-PAA was not great, and that other aspects such as the hydrophilicity of the polymer should also be considered.

Similar findings were also reported by Chen *et al.*<sup>[172]</sup> who compared solid dispersions of griseofulvin, felodipine and ketoconazole with PVP vinylacetate (PVP-VA) and HPMCAS. Although felodipine interacted much more effectively with PVP-VA in the solid state ( $\chi_{DP} = -1.9$ ) than with HPMCAS ( $\chi_{DP} = -0.21$ ), this behaviour was not replicated in aqueous dispersions, where the HPMCAS solid dispersion generated higher and more sustained supersaturation profiles upon dissolution. This was likely due to the hydrophilic interactions of PVP-VA with water upon exposure to an aqueous environment, which may have reduced or negated the favourable interactions with felodipine.

### Mechanistic design of precipitation inhibitors

The development and use of modern analytical techniques have provided an increased understanding of PI interactions. Utilising knowledge of potential binding modes with the drug, it has become possible to select—or even design—PIs on a drug-by-drug basis.

The first example of such an approach was published by Ting *et al.*,<sup>[68]</sup> who synthesised co-polymers inspired by HPMCAS using reversible addition–fragmentation chain transfer (RAFT) polymerisation. These novel polymers were then used in SDDs and studied for interactions with probucol, danazol and phenytoin, to determine which structural motifs were important for inhibition of precipitation. For probucol, the most efficient polymers were those with only succinyl and acetyl functionality, improving dissolution up to 180-fold. Conversely, for danazol and phenytoin, polymers that exhibited a higher prevalence of hydroxyl groups were able to better sustain supersaturation. This was supported by FTIR spectroscopy. In the FTIR spectra, –OH stretching absorptions of danazol shifted and broadened in the presence of polymers with high proportions of –OH functionality, indicating the presence of hydrogen bond interactions.<sup>[68]</sup>

Mosquera-Giraldo *et al.*<sup>[185]</sup> also utilised a mechanistic design approach to fine-tune inhibition of telaprevir precipitation by cellulosic polymers. In this approach, a large number of chemically diverse cellulosic polymers were synthesised containing different combinations of key functional group substituents such as alcohols, amides, esters, ethers, carboxylic acids and sulphides. The novel polymers were grouped into two distinct chemical groups: the  $\omega$ -carboxyalkanoates, which were cellulosic polymers with a wide variety of hydrocarbon chain lengths capped with a terminal carboxylic acid, and a second group which included the aforementioned chemically diverse functional groups. The solubility parameters for the novel polymers were calculated, and they were also screened using an *in situ* UV probe to determine the onset of precipitation in supersaturated telaprevir solutions generated with the solvent-shift approach. It was found that for the  $\omega$ -carboxyalkanoates, both the solubility parameter range and the carboxylic acid functionality were important for precipitation inhibition. Similar conclusions were reached in the second group of polymers, in which it was found that the only functional group that appeared to influence precipitation was the terminal carboxylic acid, with all other functionality showing little to no effect on precipitation inhibition. Furthermore, there was also a direct correlation with hydrocarbon chain length and ultimate PI performance. Ultimately, it was concluded that both a terminal carboxylic group and long chain length were essential for effective inhibition, with the carboxylic acid providing hydrophilicity for the drug to remain in solution, while the hydrocarbon chain was essential for hydrophobic interactions with the growing crystal surface.<sup>[185]</sup>

Expanding on the aforementioned studies, Ting *et al.*<sup>[186]</sup> were the first to demonstrate a *de novo* design of polymeric inhibitors based on molecular interactions with phenytoin. A high-throughput expedient design process that



could yield a wide range of chemically diverse polymeric fragments, referred to as 'synthons,' was applied. These synthons were selected based on the known binding interactions of phenytoin in the formation of the crystal lattice, namely the hydrogen bond interaction between carbonyl oxygen and cyclin imines. The fragments selected were N-isopropylacrylamide (NIPAm), diethyl amide (DEA) and isopropyl methacrylate (IPMA), which could insert themselves into the growing crystal lattice *via* chemical interaction with the phenytoin molecule, thereby disrupting its internal hydrogen bond interactions and thus arrest crystallisation. Hydrophilic partner fragments, dimethyl amide (DMA), amide (AM) and hydroxyethyl methacrylate (HEMA), which can interact with water, were also included in the screen. The resultant polymers thus had the ability to bind to the growing crystal, inhibit crystallisation and maintain the drug in solution.<sup>[186]</sup> Based on this chemical library of six synthons, a controlled, and high-throughput RAFT polymerisation was used to synthesise a large library of distinct novel polymers, 60 in total. These polymers were then screened for precipitation inhibition of phenytoin in a high-throughput screen utilising the solvent-shift method in combination with UV spectroscopy. Poly(NIPAm70-co-DMA30) was able to maintain phenytoin supersaturation at >1000 µg/ml for over 3 h. This was a significant improvement relative to the commercially available excipient, HPMCAS, which is able to sustain concentrations at only 100 µg/ml for 3 h.<sup>[192]</sup>

Nuclear Overhauser effect spectroscopy and DOSY spectroscopy were used to further assess the potential interaction of the drug phenytoin with the precipitation inhibitor synthons. NOESY data showed that the best performing polymer, poly(NIPAm70-co-DMA30), exhibited strong cross-peaks with the aromatic portion of phenytoin and the isopropyl portion of the polymer, coupled with complementary hydrophilic interactions offered by the DMA. Further, the DOSY data showed a significant decrease in reduced diffusion coefficients for phenytoin in the presence of the polymer. Together, the two spectroscopic techniques were able to elucidate the mechanistic interaction between poly(NIPAm70-co-DMA30) and phenytoin and explain the highly improved precipitation inhibition.<sup>[192]</sup>

Although the *de novo* design of PI to maximise interaction with API is an exciting prospect, there are some key hurdles for this technology to be widely applicable. For example, from a regulatory perspective, such an approach could be very costly and restrictive, as additional safety studies would be required to demonstrate an absence of polymer-related toxicity. Adopting a similar approach that is based on selection of polymers already approved by health authorities such as the FDA for use in pharmaceuticals might be more efficient. Such an approach would

retain some of the advantages of a bespoke PI selection process while avoiding any additional regulatory burden.

## Concluding remarks

In recent years, focus has been placed on understanding the stabilisation of the supersaturated state and the importance of PI selection. Although classical crystallisation theory has been well described and applied to *in vitro* crystallisation and precipitation inhibition, the relative importance of a wide range of PI properties including molecular weight, viscosity and number of hydrogen bond donors/acceptors is not yet entirely clear, with different studies reaching different conclusions. Ultimately, it is accepted that precipitation inhibition is not a 'one-size-fits-all' process and that each API will have different dependencies, which can make *a priori* PI selection difficult. Although a diverse set of high-throughput screening methods are available which can be used to identify suitable precipitation inhibitors, such an approach does not provide any mechanistic information about how precipitation inhibitors function. With this in mind, huge strides have been made in recent years towards elucidating the precipitation inhibition process for a wide range of drug-inhibitor systems, as covered in this review.

Spectroscopic techniques such as NMR, IR, Raman, UV-Vis and fluorescence spectroscopy can be employed to study interaction mechanisms between API and polymer as well as to gain understanding about the phase behaviour of supersaturated API solutions. Further work in this area, particularly on developing new techniques to improve sensitivity of detection, would be valuable in order to allow application to a wider range of systems. From a thermal perspective, mDSC has seen limited application in detecting subtle changes in melting points of drug-polymer mixtures, which can be indicative of molecular interaction. Additional thermal tools, such as isothermal calorimetry, could be investigated to gain insights into additive effects on nucleation and growth inhibition using various excipients. Microscopic techniques, such as atomic force microscopy, have been pivotal in building a picture of how polymers interact with the growing surface. This has been particularly important when understanding the effect of pH and polarity on polymer surface coverage, which can have a dramatic effect on PI performance. Furthermore, video microscopy has emerged recently as an interesting technique that, when coupled with image analysis, can visualise the crystallisation and nucleation behaviour of supersaturated API. This can be achieved both in the presence and absence of polymer and can allow the detection of early-stage precipitation events that may not be detectable by conventional methods. Another approach which can achieve this high sensitivity is synchrotron radiation, which has been used to study nucleation in detail. It is clear that the application of this technology is not feasible on a larger scale, so more work

should be carried out on alternative approaches that can provide increased sensitivity for detection of crystallinity. Further progress has also been made on understanding the precipitation/inhibition interplay from a theoretical perspective, using thermodynamic modelling and molecular simulations. In particular, the molecular simulation of atomistic detail in crystallisation and inhibition is a highly interesting area. Such simulations can simultaneously decrease the amount of experimental work required in the development of the formulations while increasing the amount of understanding yielded about the systems studied, which could help to lower the risk when working with the development of supersaturating formulations.

The combination of increased understanding of precipitation inhibition processes with advanced analytics has the potential to completely reshape how PIs are selected in drug development in the future. The possibility of bespoke polymer design or at least bespoke PI selection for each individual supersaturating formulation has also become possible. In this approach, it will be possible to decrease the number of experiments required and perhaps increase the absorption performance of the final formulation, which

may in turn reduce the required dose. This would have a downstream impact on the overall efficiency and cost of the development of poorly soluble drug candidates. These savings could ultimately be passed on to the patient or reinvested in innovative drug discovery and development and could lead to earlier access to breakthrough therapies for patients. Therefore, the need for increased mechanistic understanding in the selection of PIs has never been greater.

## Declarations

### Conflict of interest

The Authors declare that they have no conflict of interests to disclose.

### Funding

This project has received funding from the European Union's Horizon 2020 Research and Innovation Programme under grant agreement No. 674909.

## References

- Krishnaiah YSR. Pharmaceutical technologies for enhancing oral bioavailability of poorly soluble drugs. *J Bioequiv Bioavailab* 2010; 2: 28–36.
- Zheng W *et al.* Selection of oral bioavailability enhancing formulations during drug discovery. *Drug Dev Ind Pharm* 2012; 38: 235–247.
- Amidon GL *et al.* A theoretical basis for a biopharmaceutic drug classification: the correlation of in vitro drug product dissolution and in vivo bioavailability. *Pharm Res* 1995; 12: 413–420.
- Lipinski CA. Poor aqueous solubility – an industry-wide problem in drug discovery. *Am Pharm Rev* 2002; 5: 82–85.
- Lipinski CA. Drug-like properties and the causes of poor solubility and permeability. *J Pharmacol Toxicol Methods* 2000; 44: 235–249.
- Gardner CR *et al.* Drugs as materials: valuing physical form in drug discovery. *Nat Rev Drug Discov* 2004; 3: 926–943.
- Yu LX. An integrated model for determination of poor oral drug absorption. *Pharm Res* 1999; 16: 1883–1887.
- Taylor L, Zhang GGZ. Physical chemistry of supersaturated solutions and implications for oral absorption. *Adv Drug Deliv Rev* 2016; 101: 122–142.
- Serajuddin ATM. Salt formation to improve drug solubility. *Adv Drug Deliv Rev* 2007; 59: 603–616.
- Childs SL *et al.* Formulation of a danazol cocrystal with controlled supersaturation plays an essential role in improving bioavailability. *Mol Pharm* 2013; 10: 3112–3127.
- Kumpulainen RJ *et al.* Prodrugs: design and clinical applications. *Nat Rev Drug Discov* 2008; 7: 255–270.
- Timpe C. Strategies for formulation development of poorly water soluble candidates – a recent perspective. *Am Pharm Rev* 2007; 10: 104–109.
- Porter CJ *et al.* Lipids and lipid-based formulations: optimizing delivery of lipophilic drugs. *Nat Rev Drug Discov* 2007; 6: 231–248.
- Strickley R *et al.* Solubilizing vehicles for oral formulation development. In: Augustijns P *et al.* ed. *Solvent Systems and Their Selection in Pharmaceutics and Biopharmaceutics, Biotechnology: Pharmaceutical Aspects*, Vol. VI. New York, NY: Springer, 2007: 257–308.
- Pole DL. Physical and biological considerations in the use of nonaqueous solvents in oral bioavailability enhancement. *J Pharm Sci* 2008; 97: 1071–1088.
- Nakano M. Places of emulsions in drug delivery. *Adv Drug Deliv Rev* 2000; 45: 1–4.
- Pouton CW. Lipid formulations for oral administration of drugs: non-emulsifying, self-emulsifying and “self-microemulsifying” drug delivery systems. *Eur J Pharm Sci* 2000; 11: 93–98.
- Gursoy RN, Benita S. Self-emulsifying drug delivery systems (SEDDS) for improved oral delivery of lipophilic drugs. *Biomed Pharmacother* 2004; 58: 173–182.
- Date A *et al.* Current strategies for engineering drug nanoparticles. *Curr Opin Colloid Interface Sci* 2004; 9: 222–235.
- Brewster ME *et al.* The utility of cyclodextrins for enhancing oral bioavailability. *J Controlled Release* 2007; 123: 78–99.
- Leuner C, Dressman J. Improving drug solubility for oral delivery using solid dispersions. *Eur J Pharm Sci* 2000; 351: 209–218.

22. Chokshi RJ *et al.* Improving the dissolution rate of poorly soluble drugs by solid dispersion and solid solution: pros and cons. *Drug Deliv* 2007; 14: 33–45.
23. Laine AL *et al.* Enhanced oral delivery of celecoxib via the development of a supersaturable amorphous formulation utilising mesoporous silica and co-loaded HPMCAS. *Int J Pharm* 2016; 512: 118–125.
24. O'Shea JP *et al.* Mesoporous silica-based dosage forms improve bioavailability of poorly soluble drugs in pigs: case example fenofibrate. *J Pharm Pharmacol* 2017; 69: 1284–1292.
25. McCarthy CA. Mesoporous silica formulations strategies for drug dissolution enhancement. *Expert Opin Drug Deliv* 2016; 13: 93–108.
26. Wilson M *et al.* Hot-melt extrusion technology and pharmaceutical application. *Ther Deliv* 2012; 3: 787–797.
27. Brouwers J *et al.* Supersaturating drug delivery systems: the answer to solubility-limited oral bioavailability? *J Pharm Sci* 2009; 98: 2549–2572.
28. Gao P, Shi Y. Characterization of supersaturating formulations for improved absorption of poorly soluble drugs. *AAPS J* 2012; 5: 1–11.
29. Gao P, Morozowich W. Development of supersaturating SEDDS (S-SEDDS) formulations for improving the oral absorption of poorly soluble drugs. *Expert Opin Drug Deliv* 2005; 3: 97–110.
30. Mullin JW. *Crystallisation*. Oxford: Butterworth-Heinemann, 2001.
31. Yalkowsky SH. *Solubility and Solubilization in Aqueous Media*. New York: Oxford University Press, 1999.
32. Mer VKL. Nucleation in phase transitions. *Ind Eng Chem Res* 1952; 44: 1270–1277.
33. Xu S, Dai WG. Drug PIs in supersaturating formulations. *Int J Pharm* 2013; 453: 36–43.
34. Degen LP, Phillips SF. Variability of gastrointestinal transit in healthy women and men. *Gut* 1996; 39: 299–305.
35. Holzbach RT. Metastability behaviour of supersaturated bile. *Hepatol* 1984; 4: 155S–158S.
36. Mersmann A ed. *Crystallisation Technology Handbook*. Florida, USA: CRC Press, 2001.
37. Kashchiev D, Van Rosmalen GM. Nucleation in solutions revisited. *Cryst Res Technol* 2003; 38: 555–574.
38. Hancock BC, Parks M. What is the true solubility advantage for amorphous pharmaceuticals? *Pharm Res* 2000; 17: 397–404.
39. Murdande SB *et al.* Solubility advantage of amorphous pharmaceuticals: II. Application of quantitative thermodynamic relationships for prediction of solubility enhancement in structurally diverse insoluble pharmaceuticals. *Pharm Res* 2010; 27: 2704–2714.
40. Paus R *et al.* Predicting the solubility advantage of amorphous pharmaceuticals: a novel thermodynamic approach. *Mol Pharm* 2015; 12: 2823–2833.
41. Hoffman JD. Thermodynamic driving force in nucleation and growth processes. *J Chem Phys* 1958; 29: 1192–1193.
42. Almeida e Sousa L *et al.* Assessment of the amorphous “solubility” of a group of diverse drugs using new experimental and theoretical approaches. *Mol Pharm* 2014; 12: 484–495.
43. Mosquera-Giraldo LI, Taylor LS. Glass-liquid phase separation in highly supersaturated aqueous solutions of telaprevir. *Mol Pharm* 2015; 12: 496–503.
44. Maeda K *et al.* Novel phenomena of crystallisation and emulsification of hydrophobic solute in aqueous solution. *J Colloid Interface Sci* 2001; 234: 217–222.
45. Laffèrère L *et al.* Study of liquid-liquid demixing from drug solution. *J Cryst Growth* 2004; 269: 550–557.
46. Tung H. *Critical Issues in Crystallisation Practice. Crystallisation of Organic Compounds: An Industrial Perspective*. Hoboken, NJ: John Wiley & Sons Inc, 2008: 101–116.
47. Ilevbare GA *et al.* Liquid-liquid phase separation behaviour in highly supersaturated aqueous solutions of poorly water-soluble drugs: implications for solubility enhancing formulations. *Cryst Growth Des* 2013; 13: 1497–1509.
48. Jackson MJ *et al.* Dissolution of danazol amorphous solid dispersions: supersaturation and phase behavior as a function of drug loading and polymer type. *Mol Pharm* 2015; 13: 223–231.
49. Bonnett PE *et al.* Solution crystallisation via a submerged liquid-liquid phase boundary: oiling out. *Chem Commun* 2003; 6: 698–699.
50. Deneau E, Steele G. An in-line study of oiling out and crystallisation. *Org Process Res Dev* 2005; 9: 943–950.
51. Guzmán HR *et al.* A “spring and parachute” approach to designing solid celecoxib formulations having enhanced oral absorption. *AAPS J* 2004; 6: T2189.
52. Alonzo DE *et al.* Characterizing the impact of hydroxypropylmethyl cellulose on the growth and nucleation kinetics of felodipine from supersaturated solutions. *Cryst Growth Des* 2012; 12: 1538–1547.
53. Guzmán HR *et al.* Combined use of crystalline salt forms and precipitation inhibitors to improve oral absorption of celecoxib from solid oral formulations. *J Pharm Sci* 2007; 96: 2686–2702.
54. Warren DB *et al.* Using polymeric precipitation inhibitors to improve the absorption of poorly water-soluble drugs: a mechanistic basis for utility. *J Drug Target* 2010; 18: 704–731.
55. Lima-de-Faria J, Buerger MJ. *Historical Atlas of Crystallography*. Dordrecht, Boston: Published for International Union of Crystallography by Kluwer Academic Publishers, 1990.
56. Boistelle R, Astier JP. Crystallisation mechanisms in solution. *J Cryst Growth* 1988; 90: 14–30.
57. Kalikmanov VI. Nucleation Theory. *Lecture Notes in Physics* 860. Springer, 2013.
58. Davey RJ *et al.* Nucleation of organic crystals – a molecular perspective. *Angew Chem Int Ed* 2013; 52: 2166–2179.
59. Kashchiev D. *Nucleation: Basic Theory with Applications*. Oxford, Boston: Butterworth Heinemann, 2000.



60. Rodríguez-Hornedo N, Murphy D. Significance of controlling crystallisation mechanisms and kinetics in pharmaceutical systems. *J Pharm Sci* 1999; 88: 651–660.
61. Lindfors L *et al.* Nucleation and crystal growth in supersaturated solutions of a model drug. *J Colloids Interface Sci* 2008; 325: 404–413.
62. Dunitz JD, Bernstein J. Disappearing polymorphs. *Acc Chem Res* 1995; 28: 193–200.
63. Nyvlt J. The Ostwald rule of stages. *Cryst Res Technol* 1995; 30: 443–449.
64. Kostewicz ES *et al.* Predicting the precipitation of poorly soluble weak bases upon entry in the small intestine. *J Pharm Pharmacol* 2004; 56: 43–51.
65. Li N *et al.* A comparison of the crystallisation inhibition properties of bile salts. *Cryst Growth Des* 2016; 16: 7286–7300.
66. Loftsson T. The effect of water-soluble polymers on aqueous, solubility of drugs. *Int J Pharm* 1996; 127: 293–296.
67. Usui F *et al.* Inhibitory effects of water-soluble polymers on precipitation of RS-8359. *Int J Pharm* 1997; 154: 59–66.
68. Ting JM *et al.* Deconstructing HPMCAS: excipient design to tailor polymer-drug interactions for oral drug delivery. *ACS Biomater Sci Eng* 2015; 1: 978–990.
69. Patel DD, Anderson BD. Effect of precipitation inhibitors on indomethacin supersaturation maintenance: mechanisms and modeling. *Mol Pharm* 2014; 11: 1489–1499.
70. Chauhan H *et al.* Correlation of inhibitory effects of polymers on indomethacin precipitation in solution and amorphous solid crystallisation based on molecular interaction. *Pharm Res* 2014; 31: 500–515.
71. Somasundaran P, Krishnakumar S. Adsorption of surfactants and polymers at the solid-liquid interface. *Colloids Surf A* 1997; 123: 491–513.
72. Machefer S *et al.* Effect of polymer admixtures on the growth habit of ionic crystals. Study on crystal growth kinetics of potassium dihydrogen phosphate in water/polyol mixtures. *J Cryst Growth* 2008; 310: 5347–5356.
73. Gao P *et al.* Characterization and optimization of AMG 517 supersaturating self-emulsifying drug delivery system (S-SEDDS) for improved oral absorption. *J Pharm Sci* 2009; 98: 516–528.
74. Dinunzio JC *et al.* Amorphous compositions using concentration enhancing polymers for improved bioavailability of itraconazole. *Mol Pharm* 2008; 5: 968–980.
75. Ilevbare G *et al.* Understanding polymer properties important for crystal growth inhibition-impact of chemically diverse polymers on solution crystal growth of ritonavir. *Cryst Growth Des* 2012; 12: 3133–3143.
76. Schram CJ *et al.* Impact of polymer conformation on the crystal growth inhibition of a poorly water-soluble drug in aqueous solution. *Langmuir* 2015; 31: 171–179.
77. Pellett M *et al.* Supersaturated solutions evaluated with an in vitro stratum corneum tape stripping technique. *Int J Pharm Sci* 1997b; 151: 91–98.
78. Chavan B *et al.* Evaluation of the inhibitory potential of HPMC, PVP and PC polymers on nucleation and crystal growth. *RSC Adv* 2016; 6: 77569–77576.
79. Saal W *et al.* The quest for exceptional drug solubilization in diluted surfactant solutions and consideration of residual solid state. *Eur J Pharm Sci* 2018; 111: 96–103.
80. Dai WG *et al.* Evaluation of drug precipitation of solubility-enhancing liquid formulations using milligram quantities of a new molecular entity (NME). *J Pharm Sci* 2007; 96: 2957–2969.
81. Rosen MJ, Kunjappu JT. *Surfactants and Interfacial Phenomena*, 4th edn. Hoboken, NJ: Wiley, 2012.
82. Vogt M *et al.* Dissolution improvement of four poorly water soluble drugs by cogrinding with commonly used excipients. *Eur J Pharm Biopharm* 2008; 68: 330–337.
83. Raut Desai S. Investigating the mechanism of supersaturation and precipitation inhibition of poorly soluble drugs from self-emulsifying drug delivery systems (SEDDS). 2013 Ph.D. Thesis, Massachusetts College of Pharmacy and Health Sciences.
84. Brewster ME *et al.* Comparative interaction of 2-hydroxypropyl- $\beta$ -cyclodextrin and sulfobutylether- $\beta$ -cyclodextrin with itraconazole: phase-solubility behavior and stabilization of supersaturated drug solutions. *Eur J Pharm Sci* 2008; 32: 94–103.
85. Iervolino M *et al.* Membrane penetration enhancement of ibuprofen using supersaturation. *Int J Pharm* 2000; 198: 229–238.
86. Loftsson T *et al.* Effects of cyclodextrins on drug delivery through biological membranes. *J Pharm Sci* 2007; 96: 2532–2546.
87. Fine-Shamir N *et al.* Toward successful cyclodextrin based solubility-enabling formulations for oral delivery of lipophilic drugs: solubility-permeability trade-off, biorelevant dissolution, and the unstirred water layer. *Mol Pharm* 2017; 14: 2138–2146.
88. Westerberg G, Wiklund L.  $\beta$ -cyclodextrin reduces bioavailability of orally administered [3H]-benzo[a]pyrene in the rat. *J Pharm Sci* 2005; 94: 114–119.
89. Chen J *et al.* Bile salts as crystallization inhibitors of supersaturated solutions of poorly water-soluble compounds. *Cryst Growth Des* 2015; 15: 2593–2597.
90. Carlert S *et al.* Predicting intestinal precipitation: a case example for a basic BCS class II drug. *Pharm Res* 2010; 27: 2119–2130.
91. Chauhan H *et al.* Correlating the behaviour of polymers in solution as PI to its amorphous stabilization ability in solid dispersions. *J Pharm Sci* 2013; 102: 1924–1935.
92. Prasad D *et al.* Role of molecular interactions for synergistic precipitation inhibition of poorly soluble drug in supersaturated drug-polymer-polymer ternary solution. *Mol Pharm* 2016; 13: 756–765.
93. Li S *et al.* Enhanced bioavailability of a poorly water-soluble weakly basic compound using a combination approach of solubilization agents and PIs:

- a case study. *Mol Pharm* 2012; 9: 1100–1108.
94. Dai WG *et al.* Combination of pluronic/vitamin E TPGS as a potential inhibitor of drug precipitation. *Int J Pharm* 2008; 255: 31–37.
  95. Overhoff KA *et al.* Effect of stabilizer on the maximum degree and extent of supersaturation and oral absorption of tacrolimus made by ultra-rapid freezing. *Pharm Res* 2008; 25: 167–175.
  96. Patra C *et al.* Pharmaceutical significance of Eudragit: a review. *Future J Pharm Sci* 2017; 3: 33–45.
  97. Lee DR *et al.* A polyvinylpyrrolidone-based supersaturating self-emulsifying drug delivery system for enhanced dissolution of cyclosporine A. *Polymers* 2017; 9: 123.
  98. Wen H *et al.* Hydrogen bonding interactions between adsorbed polymer molecules and crystal surface of acetaminophen. *J Colloid Interface Sci* 2005; 290: 325–335.
  99. Martinez-Cruz N *et al.* Effect of molecular weight of polystyrene sulfonic acid sodium salt polymers on the precipitation kinetics of sodium bicarbonate. *Cryst Growth* 2004; 270: 573–581.
  100. Kawaguchi H *et al.* Crystallisation of inorganic compounds in polymer solutions. 1. Control of shape and form of calcium carbonate. *Colloid Polym Sci* 1992; 270: 1176–1181.
  101. Marsden CM *et al.* Supersaturation of zafirlukast in fasted and fed state intestinal media with and without PIs. *Eur J Pharm Sci* 2016; 25: 31–39.
  102. Vora C *et al.* Preparation and characterization of dipyrindamole solid dispersions for stabilization of supersaturation: effect of precipitation inhibitors type and molecular weight. *Pharm Dev Technol* 2016; 21: 847–855.
  103. Patel DD, Anderson BD. Adsorption of polyvinylpyrrolidone and its impact on maintenance of aqueous supersaturation of indomethacin via crystal growth inhibition. *J Pharm Sci* 2015; 104: 2923–2933.
  104. Edwards F *et al.* Using droplet-based microfluidic technology to study the precipitation of a poorly water-soluble weakly basic drug upon a pH-shift. *Analyst* 2013; 138: 339–345.
  105. Knopp MM *et al.* Effect of polymer type and drug dose on the in vitro and in vivo behavior of amorphous solid dispersions. *Eur J Pharm Biopharm* 2016; 105: 106–114.
  106. Janssens S *et al.* Characterization of ternary solid dispersions of itraconazole, PEG 6000, and HPMC 2910 E5. *J Pharm Sci* 2008; 96: 2110–2120.
  107. Vandecruys R *et al.* Use of a screening method to determine excipients which optimize the extent and stability of supersaturated drug solutions and application of this system to solid formulation design. *Int J Pharm* 2007; 342: 168–175.
  108. Lang B *et al.* Dissolution enhancement of itraconazole by hot-melt extrusion alone and the combination of hot-melt extrusion and rapid freezing – effect of formulation and processing variables. *Mol Pharm* 2014; 11: 186–196.
  109. Pereira JM *et al.* Interplay of degradation, dissolution and stabilization of clarithromycin and its amorphous solid dispersions. *Mol Pharm* 2013; 10: 4640–4653.
  110. Shan N *et al.* Improved human bioavailability of vemurafenib, a practically insoluble drug, using an amorphous polymer-stabilized solid dispersion prepared by a solvent-controlled coprecipitation process. *J Pharm Sci* 2013; 102: 967–981.
  111. Huang Y, Dai W-G. Fundamental aspects of solid dispersion technology for poorly soluble drugs. *Acta Pharm Sin B* 2014; 4: 18–25.
  112. Tajarobi F *et al.* The influence of crystallisation inhibition of HPMC and HPMCAS on model substance dissolution and release in swellable matrix tablets. *Eur J Pharm Biopharm* 2011; 78: 125–133.
  113. Curatolo W *et al.* Utility of hydroxypropyl methylcellulose acetate succinate (HPMCAS) for initiation and maintenance of drug supersaturation in the GI milieu. *Pharm Res* 2009; 26: 1419–1431.
  114. Christfort JF *et al.* Development of a video-microscopic tool to evaluate the precipitation kinetics of poorly-water soluble drugs: a case study with tadalafil and HPMC. *Mol Pharm* 2017; 14: 4154–4160.
  115. Ruff A *et al.* Evaluating the predictability of the in vitro transfer model and in vivo rat studies as a surrogate to investigate the supersaturation and precipitation behaviour of different Albendazole formulations for humans. *Eur J Pharm Sci* 2017; 105: 108–118.
  116. Pygall S *et al.* Extended release of flurbiprofen from tromethamine-buffered HPMC hydrophilic matrix tablets. *Pharm Develop Technol* 2017. <https://doi.org/10.1080/10837450.2017.1301470>. [Epub ahead of print].
  117. Kourentas A *et al.* Evaluation of the impact of excipients and an albendazole salt on albendazole concentrations in upper small intestine using an in vitro biorelevant gastrointestinal transfer (BioGIT) system. *J Pharm Sci* 2016; 105: 2898–2903.
  118. Gift AD *et al.* Influence of polymeric excipients on crystal hydrate formation kinetics in aqueous slurries. *J Pharm Sci* 2008; 97: 5198–5211.
  119. Chandy T *et al.* Inhibition of in vitro calcium phosphate precipitation in presence of polyurethane via surface modification and drug delivery. *J Appl Biomater* 1994; 5: 245–254.
  120. Dionisio M *et al.* Locust bean gum: exploring its potential for biopharmaceutical applications. *J Pharm Biotechnol* 2012; 4: 175–185.
  121. Wu Z *et al.* Absorption and tissue tolerance of ribendazole in the presence of hydroxypropyl-beta-cyclodextrin following subcutaneous injection in sheep. *Int J Pharm* 2010; 397: 96–102.
  122. Brouwers J *et al.* Early identification of availability issues for poorly water-soluble microbicide candidates in biorelevant media: a case study with saquinavir. *Antiviral Res* 2011; 91: 217–223.
  123. Peeters J *et al.* Characterization of the interaction of 2-hydroxypropyl-beta-cyclodextrin with itraconazole at pH 2, 4, and 7. *J Pharm Sci* 2002; 91: 1414–1422.

124. Creasey AA *et al.* Inhibiting the precipitation of poorly water-soluble drugs from labrasol formulations. *Pharm Technol* 2011; 23: 30–34.
125. Petrusevska M *et al.* Evaluation of a high-throughput screening method for the detection of the excipient-mediated precipitation inhibition of poorly soluble drugs. *Assay Drug Dev Technol* 2013a; 11: 117–129.
126. Yamashita T *et al.* Solvent shift method for anti-precipitant screening of poorly soluble drugs using biorelevant medium and dimethyl sulfoxide. *Int J Pharm* 2011; 419: 170–174.
127. Palmelund H *et al.* Studying the propensity of compounds to supersaturate: a practical and broadly applicable approach. *J Pharm Sci* 2016; 105: 3021–3029.
128. Madsen CM *et al.* Supersaturation of zafirlukast in fasted and fed state intestinal media with and without precipitation inhibitor. *Eur J Pharm Sci* 2016; 91: 31–39.
129. Kuentz M. Analytical technologies for real-time drug dissolution and precipitation testing on a small scale. *J Pharm Pharmacol* 2014; 67: 143–159.
130. Quan G *et al.* Supersaturable solid self-microemulsifying drug delivery system: precipitation inhibition and bioavailability enhancement. *Int J Nanomed* 2017; 12: 8801–8811.
131. Gunther H. *NMR Spectroscopy: Basic Principles, Concepts and Applications in Chemistry*, 3rd edn. Hoboken, NJ: Wiley, 2013.
132. Ohno A *et al.* Application of NMR spectroscopy in medicinal chemistry and drug discovery. *Curr Top Med Chem* 2011; 11: 68–73.
133. Garido L, Beckmann N. *New Applications of NMR in Drug Discovery and Development*, 1st edn. London, UK: Royal Society of Chemistry, 2014.
134. Kwan EE, Huang SG. Structural elucidation with NMR spectroscopy: practical strategies for organic chemists. *Eur J Organic Chem* 2008; 2018: 2671–2688.
135. Johnson CS. Diffusion ordered nuclear magnetic resonance. *Prog Nucl Magn Reson Spectrosc* 1999; 34: 203–256.
136. Higashi K *et al.* Insights into atomic-level interaction between mefenamic acid and Eudragit® EPO in a supersaturated solution by high resolution magic-angle spinning NMR spectroscopy. *Mol Pharm* 2014; 11: 351–357.
137. Gaffney JS *et al.* Fourier Transform Infrared (FTIR) spectroscopy. In: Kaufman EN, ed. *Characterization of Materials*, 2nd edn. Hoboken, NJ: Wiley, 2012: 1104–1135.
138. Watson D. *Pharmaceutical Analysis*, 4th edn. Amsterdam, the Netherlands: Elsevier, 2016.
139. Rostron P *et al.* Raman spectroscopy, review. *Int J Eng Tech Res* 2016; 6: 50–64.
140. Paudel A *et al.* Raman spectroscopy in pharmaceutical product design. *Adv Drug Deliv Rev* 2015; 89: 3–20.
141. Sheng Q. Thermal analysis of pharmaceuticals. In: Mullertz A *et al.* ed. *Analytical Techniques in the Pharmaceutical Sciences*. New York City, NY: Springer, 2016: 363–387.
142. Williams GP. A general review of synchrotron radiation, its uses and special technologies. *Vacuum* 1982; 32: 333–345.
143. Light Source. Light source facility information. <http://www.lightsources.org/light-source-facility-information>. Accessed July 21st, 2017.
144. Holmes KC *et al.* Synchrotron radiation as a source for X-ray diffraction the beginning. In: Mandelkow E, ed. *Synchrotron Radiation in Chemistry and Biology III*. Berlin, Heidelberg: Springer Berlin Heidelberg, 1989: 1–7.
145. Ueda K *et al.* Inhibitory effect of hydroxypropyl methylcellulose acetate succinate on drug recrystallization from a supersaturated solution assessed using nuclear magnetic resonance measurements. *Mol Pharm* 2013; 10: 3801–3811.
146. Li Z *et al.* Enhanced performance of blended polymer excipients in delivering a hydrophobic drug through the synergistic action of micelles and HPMCAS. *Langmuir* 2017; 33: 2837–2848.
147. Nie H *et al.* Solid-state spectroscopic investigation of molecular interactions between dofazimine and hypromellose phthalate in amorphous solid dispersions. *Mol Pharm* 2016; 13: 3964–3975.
148. Nie H *et al.* Investigating the interaction pattern and structural elements of a drug-polymer complex at the molecular level. *Mol Pharm* 2015; 12: 2459–2468.
149. Petrusevska M *et al.* Hydroxypropyl methylcellulose mediated precipitation inhibition of sirolimus: from a screening campaign to a proof-of-concept human study. *Mol Pharm* 2013b; 10: 2299–2310.
150. Mistic Z *et al.* Understanding the interactions of oleic acid with basic drugs in solid lipids on different biopharmaceutical levels. *J Excip Food Chem* 2014; 5: 113–134.
151. Patel DD *et al.* Maintenance of supersaturation I: indomethacin crystal growth kinetic modeling using an online second-derivative ultraviolet spectroscopic method. *J Pharm Sci* 2011; 100: 2623–2641.
152. Arnold YE *et al.* Advancing in-vitro drug precipitation testing: new process monitoring tools and a kinetic nucleation and growth model. *J Pharm Pharmacol* 2011; 63: 333–341.
153. Stillhart C *et al.* Insights into drug precipitation kinetics during in vitro digestion of a lipid-based drug delivery system using in-line Raman spectroscopy and mathematical modeling. *Pharm Res* 2013; 30: 3114–3130.
154. Aisha AFA *et al.* Solid dispersion of alpha-mangostin improve its aqueous solubility through self-assembly of nanomicelles. *J Pharm Sci* 2011; 101: 815–825.
155. Van Eerdenbrugh B *et al.* Classification of the crystallization behavior of amorphous active pharmaceutical ingredients in aqueous environments. *Pharm Res* 2014; 31: 969–982.
156. Dong YD *et al.* Applications of X-ray scattering in pharmaceutical science. *Int J Pharm* 2011; 417: 101–111.
157. Raina SA *et al.* Trends in the precipitation and crystallisation behavior of supersaturated aqueous solutions of poorly water-soluble drugs assessed using synchrotron radiation. *J Pharm Sci* 2015; 104: 1981–1992.



158. Schram CJ *et al.* Influence of polymers on the crystal growth rate of felodipine: correlating adsorbed polymer surface coverage to solution crystal growth inhibition. *Langmuir* 2015b; 31: 11279–11287.
159. Garcia R, Tamayo J. Deformation, contact time, and phase contrast in tapping mode scanning force microscopy. *Langmuir* 1996; 12: 4430–4435.
160. Abramoff MD *et al.* Image processing with ImageJ. *Biophoton Int* 2004; 11: 36–42.
161. Skopp J. Derivation of the Freundlich adsorption isotherm from kinetics. *J Chem Educ* 2009; 86: 1341.
162. Mandal T *et al.* A framework for multi-scale simulation of crystal growth in the presence of polymers. *Soft Matter* 2017; 13: 1904–1914.
163. Kubota N, Mullin JW. A kinetic model for crystal growth from aqueous solution in the presence of impurity. *J Cryst Growth* 1995; 152: 203–208.
164. Langmuir I. The adsorption of gases on plane surfaces of glass, mica and platinum. *J Am Chem Soc* 1918; 40: 1361–1403.
165. Kubota N *et al.* Supersaturation dependence of crystal growth in solutions in the presence of impurity. *J Cryst Growth* 1997; 182: 86–94.
166. Kubota N *et al.* The combined influence of supersaturation and impurity concentration on crystal growth. *J Cryst Growth* 2000; 212: 480–488.
167. Myerson EAS. *Molecular Modeling Applications in Crystallisation*. Cambridge: Cambridge University Press, 1999.
168. Mandal T *et al.* Coarse-grained modeling of crystal growth and polymorphism of a model pharmaceutical molecule. *Soft Matter* 2016; 12: 8246–8255.
169. Levitt M, Warshel A. Computer simulation of protein folding. *Nature* 1975; 253: 694–698.
170. Flory PJ. *Principles of Polymer Chemistry*. Ithaca, NY: Cornell University Press, 1953.
171. Flory PJ. Thermodynamics of high-polymer solutions. *J Chem Phys* 1942; 10: 51–61.
172. Chen Y *et al.* Drug-polymer-water interaction and its implication for the dissolution performance of amorphous solid dispersions. *Mol Pharm* 2014; 12: 576–589.
173. Baghel S *et al.* Theoretical and experimental investigation of drug-polymer interaction and miscibility and its impact on drug supersaturation in aqueous medium. *Eur J Pharm Biopharm* 2016; 107: 16–31.
174. Marsac PJ *et al.* Estimation of drug-polymer miscibility and solubility in amorphous solid dispersions using experimentally determined interaction parameters. *Pharm Res* 2009; 26: 139–151.
175. Qian F *et al.* Drug-polymer solubility and miscibility: stability consideration and practical challenges in amorphous solid dispersion development. *J Pharm Sci* 2010; 99: 2941–2947.
176. Rubenstein M, Colby R. *Polymer Physics*. Oxford, UK: Oxford University Press, 2003.
177. Van Krevelen DW, Te Nijenhuis K. *Properties of Polymers: Their Correlation with Chemical Structure; Their Numerical Estimation and Prediction from Additive Group Contributions*. New York, NY: Elsevier, 2009.
178. Tian B *et al.* Theoretical prediction of phase diagram for solid dispersion. *Pharm Res* 2015; 32: 840–851.
179. Gharagheizi F *et al.* Group contribution-based method for determination of solubility parameter of nonelectrolyte organic compounds. *J Ind Eng Chem Res* 2011; 50: 10344–10349.
180. Gharagheizi F. QSPR studies of solubility parameter by means of genetic algorithm-based multivariate linear regression and generalized regression neural network. *QSAR Comb Sci* 2008; 27: 165–170.
181. Tantishaiyakul V *et al.* Prediction of solubility parameters using partial least square regression. *Int J Pharm* 2006; 325: 8–14.
182. Gupta J *et al.* Prediction of solubility parameters and miscibility of pharmaceutical compounds by molecular dynamics simulations. *J Phys Chem B* 2011; 115: 2014–2023.
183. Hildebrand J, Scott R. *Solubility of Nonelectrolytes*. New York, NY: Reinhold Pub Co., 1950.
184. Fan CF *et al.* Application of molecular simulations to derive phase diagrams of binary mixtures. *Macromolecules* 1992; 25: 3667–3676.
185. Mosquera-Giraldo LI *et al.* Mechanistic design of chemically diverse polymers with applications in oral drug delivery. *Biomacromol* 2016; 17: 3659–3671.
186. Ting M *et al.* High-throughput excipient discovery enables oral delivery of poorly soluble pharmaceuticals. *ACS Cent Sci* 2016; 2: 748–755.







Contents lists available at ScienceDirect

European Journal of Pharmaceutical Sciences

journal homepage: [www.elsevier.com/locate/ejps](http://www.elsevier.com/locate/ejps)

## Calculation of drug-polymer mixing enthalpy as a new screening method of precipitation inhibitors for supersaturating pharmaceutical formulations

Daniel J. Price<sup>a,b</sup>, Anita Nair<sup>a</sup>, Martin Kuentz<sup>c</sup>, Jennifer Dressman<sup>b</sup>, Christoph Saal<sup>a,\*</sup><sup>a</sup> Merck KGaA, Darmstadt, Germany<sup>b</sup> Frankfurt Goethe University, Frankfurt, Germany<sup>c</sup> University of Applied Sciences and Arts Northwestern Switzerland, Institute of Pharma Technology, Muttenz, Switzerland

## ARTICLE INFO

## Keywords:

Precipitation inhibition  
Supersaturation  
Bioenabling formulations  
*in silico* tools  
Enthalpy  
Screening

## ABSTRACT

Supersaturating formulations are widely used to improve the oral bioavailability of poorly soluble drugs. However, supersaturated solutions are thermodynamically unstable and such formulations often must include a precipitation inhibitor (PI) to sustain the increased concentrations to ensure that sufficient absorption will take place from the gastrointestinal tract. Recent advances in understanding the importance of drug-polymer interaction for successful precipitation inhibition have been encouraging. However, there still exists a gap in how this newfound understanding can be applied to improve the efficiency of PI screening and selection, which is still largely carried out with trial and error-based approaches. The aim of this study was to demonstrate how drug-polymer mixing enthalpy, calculated with the Conductor like Screening Model for Real Solvents (COSMO-RS), can be used as a parameter to select the most efficient precipitation inhibitors, and thus realize the most successful supersaturating formulations. This approach was tested for three different Biopharmaceutical Classification System (BCS) II compounds: dipyridamole, fenofibrate and glibenclamide, formulated with the supersaturating formulation, mesoporous silica. For all three compounds, precipitation was evident in mesoporous silica formulations without a precipitation inhibitor. Of the nine precipitation inhibitors studied, there was a strong positive correlation between the drug-polymer mixing enthalpy and the overall formulation performance, as measured by the area under the concentration-time curve in *in vitro* dissolution experiments. The data suggest that a rank-order based approach using calculated drug-polymer mixing enthalpy can be reliably used to select precipitation inhibitors for a more focused screening. Such an approach improves efficiency of precipitation inhibitor selection, whilst also improving the likelihood that the most optimal formulation will be realized.

## 1. Introduction

A large proportion of active pharmaceutical ingredients (APIs) currently in development are classified as poorly soluble, with numbers quoted for the total percentage varying from 40% to 90% (Loftsson and Brewster, 2010). Given that drugs must be sufficiently solubilized in the gastrointestinal (GI) tract to be absorbed into systemic circulation, poorly soluble drugs represent a challenge for successful oral delivery (Brouwers et al., 2009). In response, a wide range of formulation techniques have been developed to enhance the apparent solubility of the API in the intestinal lumen (Zheng et al., 2012). These options can

improve absorption due to the generation of a supersaturated solution of the API in the GI tract, *i.e.* above the equilibrium solubility, which increases the driving force for absorption through the GI mucosa into the systemic circulation (Brouwers et al., 2009; Taylor and Zhang, 2016). Supersaturation is an energetically unfavorable state, and is at best metastable (Taylor and Zhang, 2016). Due to this, there is an innate tendency for the supersaturated solution to return to a lower energy state, through precipitation. Therefore, to derive maximum benefit from supersaturation of the API, such formulations often include a precipitation inhibitor to sustain the period over which the API remains in solution (Price et al., 2018). This formulation approach is often re-

\* Corresponding author at: Merck KGaA, Site-Management: Analytics Healthcare, Frankfurter Landstr. 250, 64293 Darmstadt, (Germany).  
E-mail address: [Christoph.saal@merckgroup.com](mailto:Christoph.saal@merckgroup.com) (C. Saal).

<https://doi.org/10.1016/j.ejps.2019.03.006>

Received 15 December 2018; Received in revised form 8 February 2019; Accepted 10 March 2019

Available online 12 March 2019

0928-0987/ © 2019 Elsevier B.V. All rights reserved.

ferred to as the “spring and parachute” model (Guzman et al., 2007). In this model, the ‘parachute’ is the precipitation inhibitor that inhibits or slows the precipitation of the API from the supersaturated ‘spring’ generated by the formulation.

Currently, the mechanistic details of precipitation inhibition are not fully understood, and the specific molecular properties that yield efficient precipitation inhibitors have not yet been clarified. Given this uncertainty, a variety of hypotheses for the molecular mechanisms of precipitation inhibition have been proposed (Warren et al., 2010; Price et al., 2018). Additionally, it appears that precipitation inhibition is also an API-specific process. Therefore, there may be no single mechanism that describes all cases of precipitation inhibition. For example, some studies show polymer hydrophobicity to be a critical property in precipitation inhibition (Prasad et al., 2016), some suggest that hydrogen bond interactions play a pivotal role (Warren et al., 2010), whilst yet others propose that polymer surface coverage is an important factor (Schram, 2015). In all likelihood, multiple precipitation inhibition mechanisms may contribute to the observed effect, with the balance depending on the specific properties of both the API and the precipitation inhibitor.

The current lack of clear mechanistic understanding makes selection of precipitation inhibitors rather inefficient and time consuming, due to overreliance on ‘trial and error’ based experimental approaches. Typically PI screening is carried out by generating supersaturation with a solvent-shift, in which API is dissolved in high concentrations in a favorable solvent (e.g. DMSO), which is then added to an aqueous phase to generate supersaturation. Analytical techniques such as UV spectroscopy, HPLC or nephelometry are then applied to track changes in concentration of API in solution or precipitation over time. These concentration time profiles are then used to provide a measure of PI effectiveness (Price et al., 2018). One of the recent developments in this area is the  $\mu$ DISS™ profiler, which applies *in situ* UV probes in combination with liquid handling to study supersaturation and precipitation in real time. Using this approach, Palmelund and colleagues assessed the precipitation of 6 different BCS II drugs in combination with two polymers, PVP and HPMC (Palmelund et al., 2016). But despite recent advances in this area, the experimental selection of precipitation inhibitors remains both lengthy and costly.

In addition to the time and cost resources involved, this approach is unlikely to lead to certain identification of the most effective precipitation inhibitor, but rather to “one that works”. To date, most supersaturating formulations incorporate one of a standard set of polymers, such as hydroxypropyl methyl cellulose acetate succinate (HPMCAS), polyvinylpyrrolidone (PVP) or hydroxypropyl methyl cellulose (HPMC) (Warren et al., 2010; Price et al., 2018). To overcome these drawbacks, there have recently been various attempts to establish a more mechanistic rationale for precipitation inhibitor selection, as reviewed by Price et al. (2018). One of the more recent advances is the use of experimental tools that can design new precipitation inhibitors based on a mechanistic understanding of the specific interaction between the precipitation inhibitor and the API on a structural, molecular basis (Mosquera-Giraldo et al., 2016; Ting et al., 2016). Unfortunately, such *de novo* processes often require complex syntheses that yield novel excipients, which are impractical due to the need for toxicological studies to qualify them for use in pharmaceuticals. Therefore, more work is required to establish an efficient and rational precipitation inhibitor selection process using excipients that are already approved for

pharmaceutical use.

To bridge the gap between mechanistic understanding of precipitation inhibition and the realities of selecting precipitation inhibitors during pharmaceutical development, a more practical and robust approach is required. Such an approach, that can incorporate understanding of the importance drug-polymer interactions with a quick and efficient screening process, would be very useful. For this purpose, the Conductor like Screening Model for Real Solvent (COSMO-RS), which was developed by Klamt (1995), is a highly interesting prospect. COSMO-RS combines quantum mechanical molecular calculations with fluid-phase thermodynamics. The first step is to calculate screening charge distributions of a molecule of interest in a continuum, based on density functional theory (DFT) (Kohn and Sham, 1965). The so-called ‘sigma profiles’ that are obtained from these calculations are then used in COSMO-RS, where statistical thermodynamics is applied to estimate the chemical potential and further characteristics of the system, such as solubility and partition coefficients. COSMO-RS has previously been used as a screening tool to calculate the solubility of early-development APIs in a database of excipients for pre-clinical formulations (Pozarska et al., 2013). However, further pharmaceutical applications have been limited, possibly due to the fact that the rate determining step, the quantum chemical calculations, are computationally very intensive. From a screening perspective, this is a significant drawback. A practical alternative to facilitate application of COSMO-RS theory for screening purposes is the software package COSMOquick. COSMOquick removes the need for the time-consuming quantum chemical calculations of molecular surface charges, whilst still carrying out the remaining COSMO-RS calculations to derive chemical potential. This is achieved by additively combining fragments of previously calculated sigma profiles stored in a database to compute a new sigma profile for molecules of interest (Fig. 1) (Hornig and Klamt, 2005). The COSMOquick approach has been recently applied pharmaceutically by the Kuentz group for the calculation of solubility parameters for a wide-range of molecules (Niederquell et al., 2018). Another application of the COSMOquick software is in co-crystal screening approaches, which uses the calculated excess enthalpy of interaction between API and a co-former to assess the likelihood of co-crystal formation (Loschen and Klamt, 2012).

To consider precipitation inhibition fundamentally, it is assumed that an interaction between API and polymer must be present. This interaction could take many forms (e.g. London, dipolar, hydrogen bonding and Coulombic forces) or combinations thereof. It can be hypothesized that the more efficient the interaction between the drug and polymer, the more effective the inhibition process (Price et al., 2018). However, this may be difficult to calculate, since the API and precipitation inhibitor must interact in a complex aqueous environment. We propose a simplified approach, in which the mixing (or excess) enthalpies of drug and excipient are calculated using COSMOquick. This estimated enthalpy is then used to rank potential precipitation inhibitors based on the strength of their molecular interaction with the API. It is hypothesized that this novel *in silico* protocol can be used to screen potential precipitation inhibitors allowing for a more focused selection to be carried out, thus significantly reducing the experimental burden of screening inhibitors by trial and error and ensuring the selection of an optimal inhibitor.

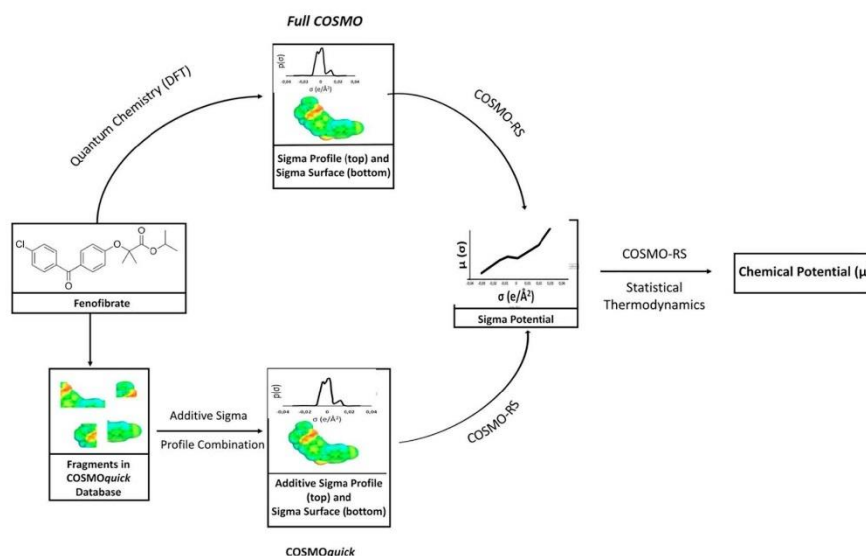


**Fig. 1.** Chemical potential, and in turn a wide-range of thermodynamic properties, can be derived from sigma profiles using COSMO-RS theory. Sigma profiles can be obtained by two ways, either through *de novo* quantum chemical calculations or through an additive combination of previously calculated molecular fragments stored in a large database. The former approach is applied in the full COSMO calculation, whilst the latter is applied in the software package COSMOquick (bottom).

## 2. Materials and methods

### 2.1. Materials

Crystalline dipyrindamole (DPD), crystalline glibenclamide (GB), crystalline fenofibrate (FF) (thermodynamic polymorphs were all purchased from MilliporeSigma (St Louis, MO), (Table 1). Poly(ethylene glycol) (PEG), poly(methyl methacrylate) (PMMA), Pluronic® (PLR), HPMC, PVP, chitosan (CH), reagent grade acetone, HPLC grade acetonitrile and HPLC grade methanol were all purchased from MilliporeSigma (St Louis, MO, USA). AQOAT (HPMCAS-MF) was purchased from ShinEtsu (Japan). Paratek® SLC was a gift sample from Merck

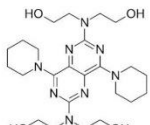
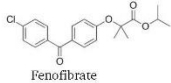
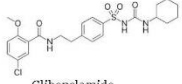
KGaA (Germany). Eudragit (Eu) RL and EPO were obtained from Evonik (Germany). Powder to make biorelevant dissolution medium, Fasted Simulated Intestinal Fluid (FaSSIF), was purchased from Biorelevant.com (UK).

### 2.2. Experimental

#### 2.2.1. Thermodynamic solubility

API (2–3 mg) was accurately weighed into a Uniprep® syringeless filter (5 mL; 0.45 μm). 2 mL of FaSSIF (Galía et al., 1998), composed of simulated intestinal fluid powder (FaSSGF, FaSSIF & FeSSIF Powder) dissolved in a pH 6.5 phosphate buffer, was added and the samples

**Table 1**  
Selected APIs and their relevant properties.

| API  | MWt [g/mol] | cLog P <sup>a</sup> | cpKa <sup>a</sup> | Number of H-bond donors | Number of H-bond acceptors |
|--|-------------|---------------------|-------------------|-------------------------|----------------------------|
| <br>Dipyrindamole | 505         | 1.5                 | 6.6 (basic)       | 4                       | 12                         |
| <br>Fenofibrate   | 361         | 5.3                 | –                 | 0                       | 5                          |
| <br>Glibenclamide | 494         | 4.7                 | 4.3(acidic)       | 3                       | 9                          |

<sup>a</sup> Calculated with ChemAxon.



agitated at 450 rpm for 24 h at 37 °C. The pH was checked at 7 h and adjusted with 0.1 N NaOH or 0.1 N HCl, if deviation greater than ± 0.05 pH units were observed. The final pH was also recorded after 24 h.

Samples were filtered after 24 h and the filtrates were diluted with acetonitrile and water (1:4) to avoid precipitation from the saturated solution. Samples were analyzed with UPLC (Thermo Dionex Ultimate 3000, Thermo Fisher, MA, USA) to determine the API concentration. API concentrations were determined by comparing the peak area to a standard calibration curve of nine standard concentrations (Eq. (1)). Three quality control samples of known concentrations were also prepared and used to check the robustness of the calibration curve. The analysis was carried out in duplicate.

$$C[\mu\text{gml}^{-1}] = \frac{a(A)F(a)}{m} \quad (1)$$

C = concentration of sample  
a(A) = peak area for analyte/mL  
m = gradient of the calibration curve  
F(A) = dilution factor for analyte.

### 2.2.2. Parteck SLC® loading procedure

All API-loaded silica samples were prepared using the solvent impregnation rotary evaporator method (Laine et al., 2016) as follows: A solution (10 mg mL<sup>-1</sup>) of API in acetone was added to Parteck SLC (1:2 w/w API/Parteck SLC®) under magnetic stirring for 15 min. The suspension was then transferred to a rotary evaporator, and solvent was removed under reduced pressure at 40 °C. After complete removal of solvent, the powder was left to dry in the rotary evaporator under reduced pressure for 2 h.

### 2.2.3. Loading content determination

To determine the % (w/w) of API in the mesoporous silica, the loaded samples were dispersed in acetone. Samples were taken after 1 h, centrifuged, and filtered before being quantified with UPLC. The percentage API content was calculated relative to the mass of loaded samples dispersed within the acetone. The study was performed in triplicate.

### 2.2.4. Combination of API loaded silica with precipitation inhibitor

API loaded silica was combined with precipitation inhibitors as a physical mixture using a mortar and pestle in the mass ratio of 1:1. This results in an API:silica:PI ratio of 1: 2: 3.

### 2.2.5. FaSSiF mini-dissolution experiment

Around 5 mg of API (or the equivalent of API-loaded silica) was weighed accurately into a glass vial. To this, 5 mL of FaSSiF was added. The vials were agitated at 37 °C for 2 h. Samples were taken at 2, 15, 60 and 120 min, filtered, diluted if appropriate, and analyzed with UPLC (Thermo Dionex Ultimate 3000, Thermo Fisher, MA, USA). Residues were collected via centrifugation and analyzed for crystallinity with powder X-ray diffraction (PXRD). This was carried out on API, API + polymer samples, API loaded silica and API loaded silica + polymers. The mini-dissolution trials were conducted in duplicate for all samples.

### 2.2.6. Powder X-ray diffraction (PXRD)

Samples were prepared between X-ray amorphous films and measured in transmission mode using Cu-Kα1 radiation and a Stoe Stadip 611 KL diffractometer equipped with Dectris Mythen1K PSD. The measurements were evaluated with the software WinXPow 3.03 by Stoe, Crystallographica Search/Match Version 3.1.0.2 and the ICDD

PDF-4+ 2014 Database and Igor Pro Version 6.34 by Wavemetrics Inc. Finger/Cox/Jephcoat. Angular range: 1–65°2θ; PSD-step width: 2°2 θ; angular resolution: 0.015°2θ; measurement time: 15 s/step, 0.25 h overall.

### 2.2.7. COSMO-RS calculations

COSMOquick (COSMOlogic, Germany, Version 1.6) was used to calculate excess enthalpy of interaction between API and polymer. APIs and PIs were entered in smiles notation. Polymer structures were approximated as trimers, since the quantum chemical calculations cannot capture the full complexity of large molecules like polymers. Furthermore, this was not deemed critical to the study as the hypothesis was related to local molecular interactions, which are assumed to be sufficiently captured by trimer forms of the polymer. Ratio of API:PI was set at 1:3 to align with the ratios used in the formulations, and the temperature was set at 37 °C.

COSMOquick calculates sigma profiles of the API and precipitation inhibitor molecules based on an additive-combination approach against a database of previously calculated quantum chemical sigma profiles (Loschen and Klamt, 2012). Once sigma profiles are generated, several equations are performed to derive the energy required to combine the sigma profile of the API and PI. First, a sigma surface segment of the PI must be removed from the surface in order to make room for a new API segment, this requires energy associated with removing pre-existing contacts between precipitation inhibitor segments,  $-\mu(\sigma')$ . Second, a new API segment must be added to the precipitation inhibitor sigma surface, this involves forming new interactions between API and PI, with related energy costs and gains associated with the two segments interacting,  $E(\sigma, \sigma')$ . This value is called the COSMO-RS interaction energy and, importantly, is calculated such that all binding modes (electrostatic, hydrogen bonding, van der Waals and combinatorial) are considered in the equation. (Appendix 3, Eqs. (1)–(3)). Once a value for the sigma potential is reached, thermodynamic calculations provide the chemical potential of mixing the API and PI (Appendix 3, Eq. (4)). From the chemical potential, a wide range of further thermodynamic properties can be calculated. In the current approach enthalpy of interaction,  $H_{\text{int}}$ , also referred to as the enthalpy change of mixing,  $\Delta H_{\text{mix}}$ , was calculated as a rank order parameter to assess the propensity of the drug to interact with excipient. As addressed in the introduction, this approach represents a substantial simplification of the more complex solid-liquid equilibrium in aqueous medium. A similar approach has been previously applied to screen co-formers in co-crystal selection and details can be inferred from the literature (Abramov et al., 2012).

In this study, the excess enthalpy of interaction between API and precipitation inhibitor is referred to as the “COSMO-Rank”. According to the working hypothesis, the more negative the calculated excess enthalpy of interaction, the higher the COSMO-Rank and thus the better the inhibition of precipitation of the API. For a full description of the calculations carried out within the software package, readers are referred to Loschen and Klamt (2012).

### 2.2.8. Spearman's rank correlation coefficient

Spearman's rank correlation coefficient is a non-parametric method that allows statistical rank correlation to be carried out between two sets of rankings. In this instance, Spearman's rank correlation coefficient analysis was applied to the COSMO-rank and the rank order of the formulation performance. For the latter, AUC<sub>0–120</sub> of the dissolution profiles, was selected as the best overall descriptor of formulation performance and was calculated using Eq. (2).

**Table 2**  
UPLC gradient and flow rates.

| Time (mins) | Flow rate (mL/min) | % (v:v) mobile phase A | % (v:v) mobile phase B |
|-------------|--------------------|------------------------|------------------------|
| 0           | 0.83               | 90                     | 10                     |
| 0.83        | 0.83               | 10                     | 90                     |
| 1.2         | 1.5                | 90                     | 10                     |
| 2           | 1.5                | 90                     | 10                     |
| 2.01        | 0.83               | 90                     | 10                     |

**Table 3**  
Thermodynamic solubilities of dipyrnidamole, glibenclamide and fenofibrate in FaSSIF, pH 6.5 at 37 °C.

| Compound      | FaSSIF thermodynamic solubility (µg/mL) |
|---------------|---|
| Dipyrnidamole | 19.6 ± 0.7                              |
| Glibenclamide | 8.1 ± 0.1                               |
| Fenofibrate   | 14.0 ± 0.3                              |

$$AUC_{0-120} = \sum \left( \frac{C_n + C_{n+1}}{2} \times (t_{n+1} - t_n) \right) \quad (2)$$

$C$  = concentration (µg/mL)

$T$  = time (minutes)

$n$  = sampling point at time,  $t$ .

Spearman's rank correlation coefficient was calculated by Rstudio (R version 2.15.12) using the code

```
corr <- cor.test(x = FILENAME$VARIABLE1, y = FILENAME$VARIABLE2, method = 'spearman')
```

### 2.2.9. UPLC method

UPLC analysis was performed using a Thermo Dionex Ultimate 3000 (Thermo Fisher, MA, USA) equipped with a diode array detector (Thermo Fisher, MA, USA). Chromatographic separation was achieved on an Acquity UPLC BEH column C8 (2.1 × 50 mm, 1.7 µm, Waters, MA, USA). The mobile phases A and B consisted of water:formic acid 99:1 (v:v) and acetonitrile:formic acid 99:1 (v:v), respectively. Gradient and flow rate is shown in Table 2. System management, data acquisition and processing were performed with the Chromeleon™ software package, version 7.2 (Thermo Fisher, MA, USA).

## 3. Results

### 3.1. Dissolution profile of crystalline API

The thermodynamic solubilities of dipyrnidamole, glibenclamide and fenofibrate are shown in Table 3. All three compounds are classified as “poorly soluble” in FaSSIF, pH 6.5 (Amidon et al., 1995).

For all three compounds, the thermodynamic solubility was approached over the duration of the FaSSIF dissolution test (Fig. 2). The rate of approach differed among the APIs, which may be related to differences in particle size and morphology. The average concentration of glibenclamide slightly exceeded the measured solubility after 2 h of dissolution, but this was not statistically significant. Furthermore, some variation in glibenclamide FaSSIF thermodynamic solubility has been recorded in the literature, with values ranging from 8 to 10 µg/mL. This is in accordance with the observed dissolution behavior (Fagerberg et al., 2010; Fagerberg et al., 2012; Wie et al., 2006).

### 3.2. Loading onto mesoporous silica

Successful loading of APIs onto mesoporous silica was confirmed

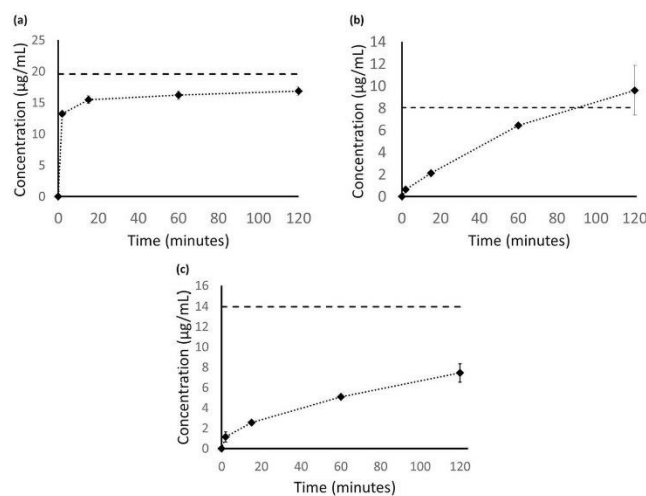


**Fig. 2.** FaSSIF dissolution profiles (2 h) of dipyrnidamole (a), glibenclamide (b) and fenofibrate (c). The thermodynamic solubility of the respective API is represented by the dashed line in each figure.

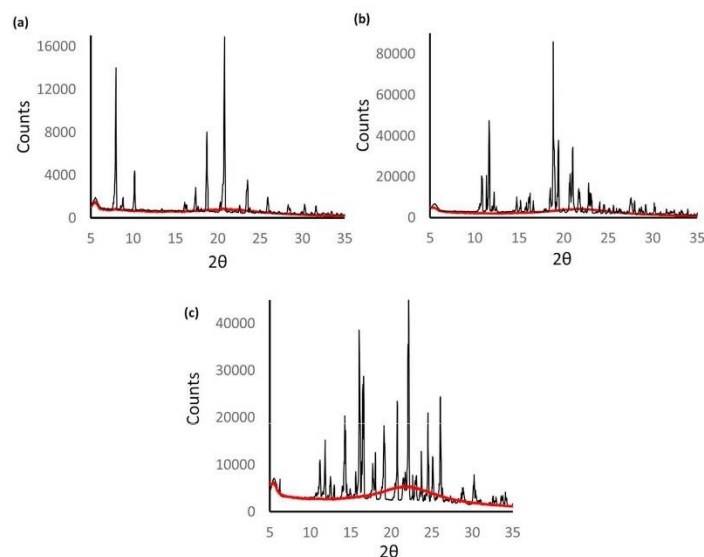


Fig. 3. PXRD diffraction patterns of the pure API (black) and API loaded onto mesoporous silica (red) for dipyrindamole (a), glibenclamide (b) and fenofibrate (c). (For interpretation of the references to color in this figure legend, the reader is referred to the web version of this article.)

**Table 4**  
API loaded silica total API content.

| API           | % loading of API onto mesoporous silica (w/w %) |
|---------------|---|
| Dipyrindamole | 30.1 ± 0.1                                      |
| Glibenclamide | 29.4 ± 0.1                                      |
| Fenofibrate   | 29.7 ± 0.3                                      |

with PXRD by showing a successful shift from the crystalline (pure API) to the amorphous solid-state form after loading onto the mesoporous silica. The absence of Bragg diffraction patterns is indicative of an amorphous material (Fig. 3).

Loading content was similar (~30% w/w) for all three compounds, as determined by UPLC (Table 4).

Delivering the API in the amorphous form significantly improved the dissolution performance in FaSSiF for all three compounds (Fig. 4). As seen in Fig. 4, dipyrindamole, glibenclamide and fenofibrate showed 4, 25 or 3-fold supersaturation relative to the thermodynamic solubility, respectively. However, all three profiles also show precipitation and a decrease in concentration towards the thermodynamic solubility within around 30 min.

### 3.3. Precipitation inhibitor screening: calculation of excess enthalpy

The COSMO-RS *in silico* screening protocol was based on calculation

of the enthalpy of interaction between each of the APIs with different potential precipitation inhibitors. Results are summarized in Fig. 5. According to the hypothesis, the more negative the calculated enthalpy of interaction, the higher the 'COSMO Rank'. A COSMO rank of 1 thus indicates the best potential for successful precipitation inhibition. By contrast, the more positive the enthalpy of interaction, the less likely the polymer is to be of use as a precipitation inhibitor. Of the inhibitors studied experimentally, Eudragit EPO, was predicted to be the best precipitation inhibitor for both dipyrindamole and glibenclamide, whereas for fenofibrate, PMMA was assigned the highest COSMO rank. For all three compounds, chitosan was assigned COSMO rank 9, reflecting its high calculated enthalpy of interaction, which was hypothesized to translate into poor precipitation inhibition performance.

### 3.4. Dissolution data for API loaded onto mesoporous silica with precipitation inhibitor added

Each of the loaded mesoporous silica samples were physically combined with a selection of polymers (HPMCAS, HPMC, PVP, PEG, Eudragit EPO, Pluronic, PMMA, Eudragit RLPO and Chitosan) such that the final ratio of API:PI was 1:3, w/w (API:PI:Silica; 1:3:2, w/w). Therefore, Table 5 shows the final % API content in the formulations after combination with the precipitation inhibitors. The final API concentrations are similar to conventional supersaturating formulations that require precipitation inhibitors.

To assess the predictive power of the COSMO calculation, dissolution in FaSSiF was carried out for each of the API-loaded mesoporous

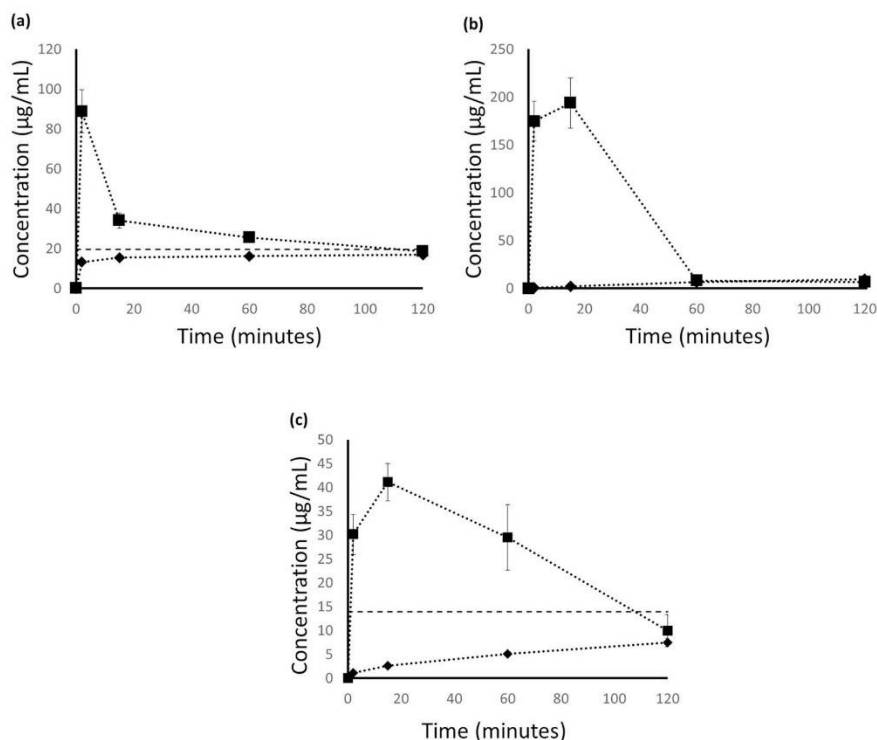


Fig. 4. Dissolution profiles of pure API (◆), and API loaded onto mesoporous silica (■) for dipyridamole (a), glibenclamide (b) and fenofibrate (c) in FaSSIF, pH 6.5 at 37 °C.

silica samples in combination with each of the selected precipitation inhibitors. (Figs. 6–8).

### 3.5. Spring-parachute plots

The performance of the precipitation inhibitor is rated in terms of its ability to sustain supersaturation. To reflect this, the data in Fig. 9 indicates the maximum concentration (“Spring”) achieved compared to the concentration at the end of the assay (“Parachute”).

### 3.6. Spearman's rank correlation analysis

The overall formulation performance was assessed by calculating the AUC of the dissolution profiles for each system (Eq. (2)). Statistical analysis was then carried out to determine the correlation between COSMO-rank and formulation performance, with a higher AUC indicating a better formulation performance (Tables 6–8).

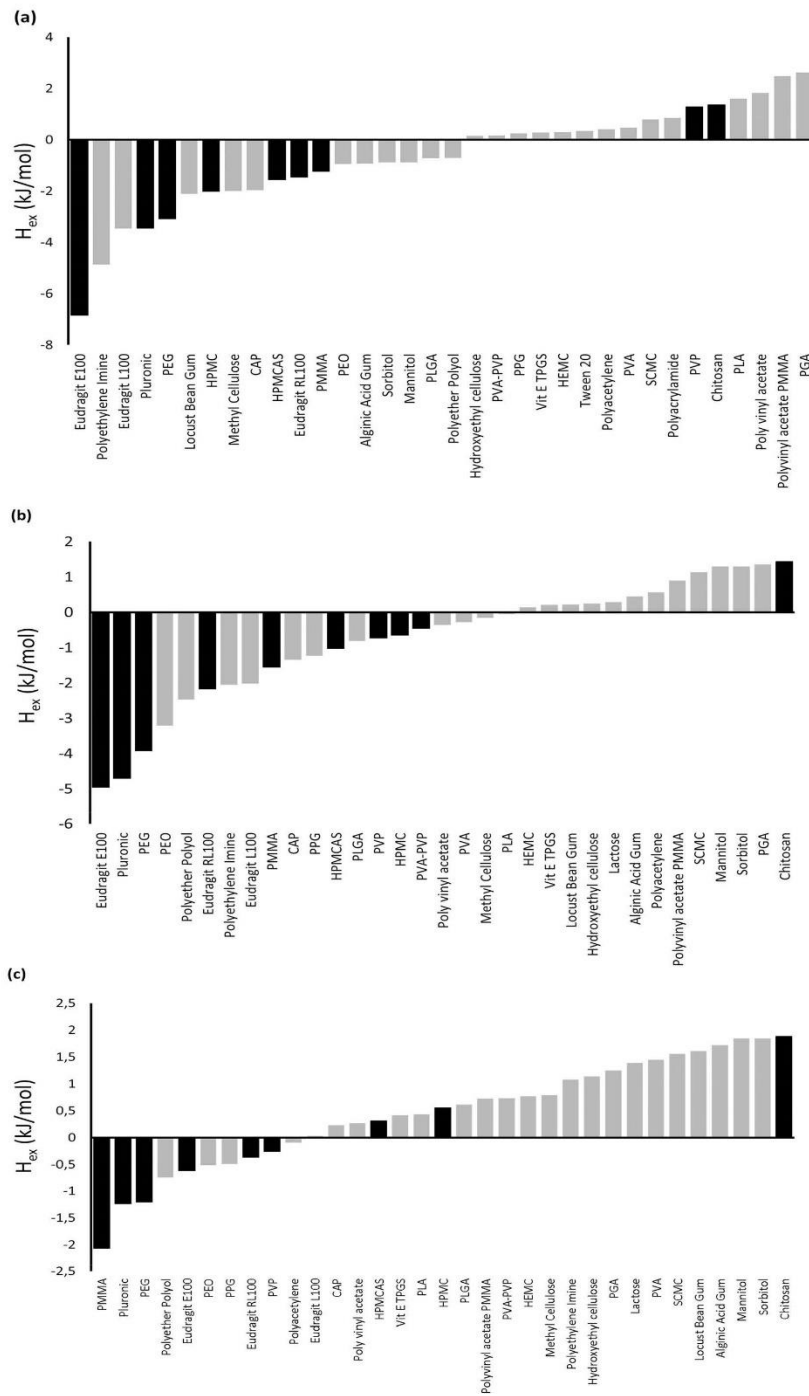
Given that dissolution performance for PEG formulations appears to consistently deviate from the correlation of COSMO rank with dissolution performance for all three APIs, the statistical analysis was re-

run without PEG. For all samples, the correlation improved, with the Spearman's rank correlation coefficients for dipyridamole and glibenclamide both increased to 0.98 (0.0004,  $p < 0.05$ ), indicating a strong positive correlation. For fenofibrate, removing PEG from the set also improved the Spearman's rank coefficient to 0.8 (0.022,  $p < 0.05$ ) and passes the significance criterion. The results suggest that PEG may behave as an outlier in the COSMO calculations.

## 4. Discussion

*In silico* tools are an attractive option for bridging the gap between our current understanding of precipitation inhibitors and practical selection of inhibitors to be used in supersaturating formulations in pharmaceutical development. In this work, we applied the COSMO-RS model as a novel *in silico* screening tool to successfully predict the formulation performance of a wide range of precipitation inhibitors in formulations of glibenclamide, fenofibrate and dipyridamole. Specifically, it was hypothesized that free enthalpy of mixing (API-polymer) could be used as a parameter for ranking inhibitors, from highest potential for successful precipitation inhibition to lowest, based





(caption on next page)



**Fig. 5.** COSMO-RS Screen: calculated excess enthalpy of interaction between dipyrindamole (a), glibenclamide (b) and fenofibrate (c) with a range of potential precipitation inhibitors. Polymers studied experimentally to test the correlation are highlighted as dark bars: Eudragit EPO, Pluronic (PLR), PEG, HPMCAS, PVP, HPMC, Eudragit RLPO, PMMA and Chitosan.

**Table 5**  
Final API content (% w/w) in the formulations after incorporation of precipitation inhibitors.

| API           | % Loading of API onto mesoporous silica (w/w %) | Final API content (%) |
|---------------|---|-----------------------|
| Dipyridamole  | 30.1 ± 0.1                                      | 15.1                  |
| Glibenclamide | 29.4 ± 0.1                                      | 14.7                  |
| Fenofibrate   | 29.7 ± 0.3                                      | 14.9                  |

on the theoretical interaction between the inhibitor and the API. For all three compounds a strong positive correlation was observed between the rank assigned based on the calculated free enthalpy of mixing and the overall formulation performance.

#### 4.1. The Importance of enabling formulations

The experimental thermodynamic solubility values for dipyrindamole, glibenclamide and fenofibrate in FaSSiF are in line with values previously reported in the literature (Table 2) (Leigh et al., 2013;

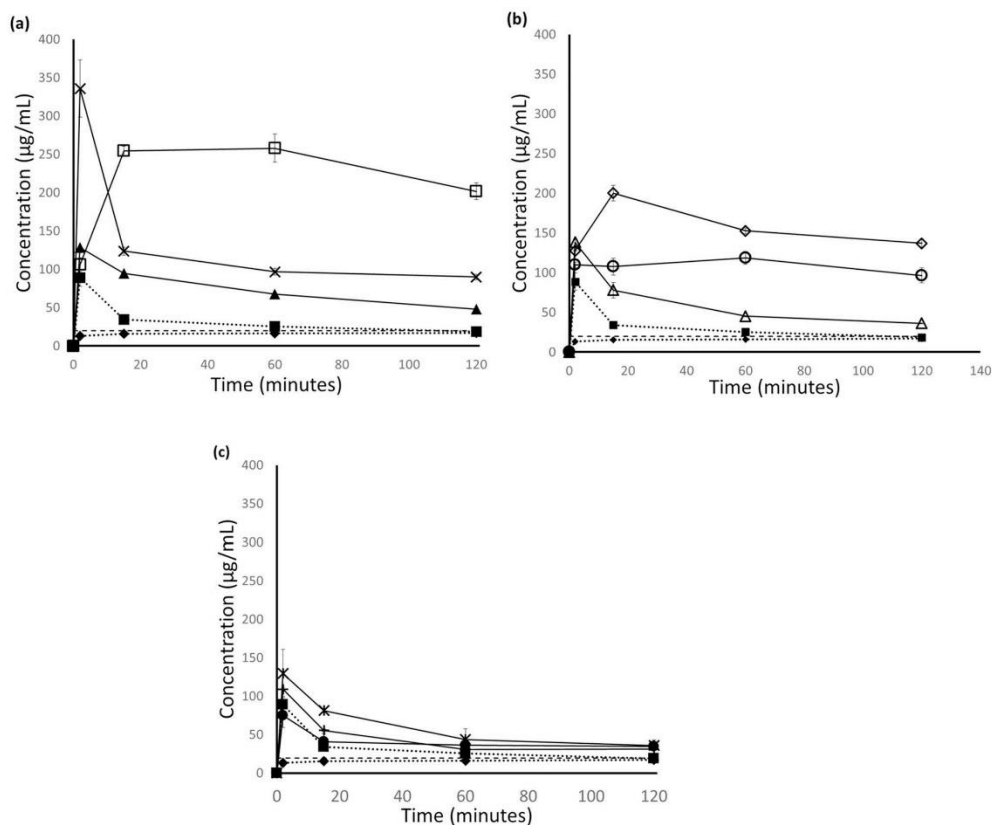


**Fig. 6.** Dissolution profiles in FaSSiF for dipyrindamole (◆), dipyrindamole loaded mesoporous silica (■) and dipyrindamole loaded mesoporous silica with precipitation inhibitors selected from the COSMO-RS screen. (a): Eudragit EPO (□), Pluronic (X), PEG (▲); (b): HPMC (○), HPMCAS (○), Eudragit RLPO (△) and (c): PMMA (.), PVP (●) and Chitosan (+). The order of the listed inhibitors corresponds to the rank order in the COSMO screen (i.e. Eudragit EPO COSMO rank #1 – Chitosan COSMO rank #9).

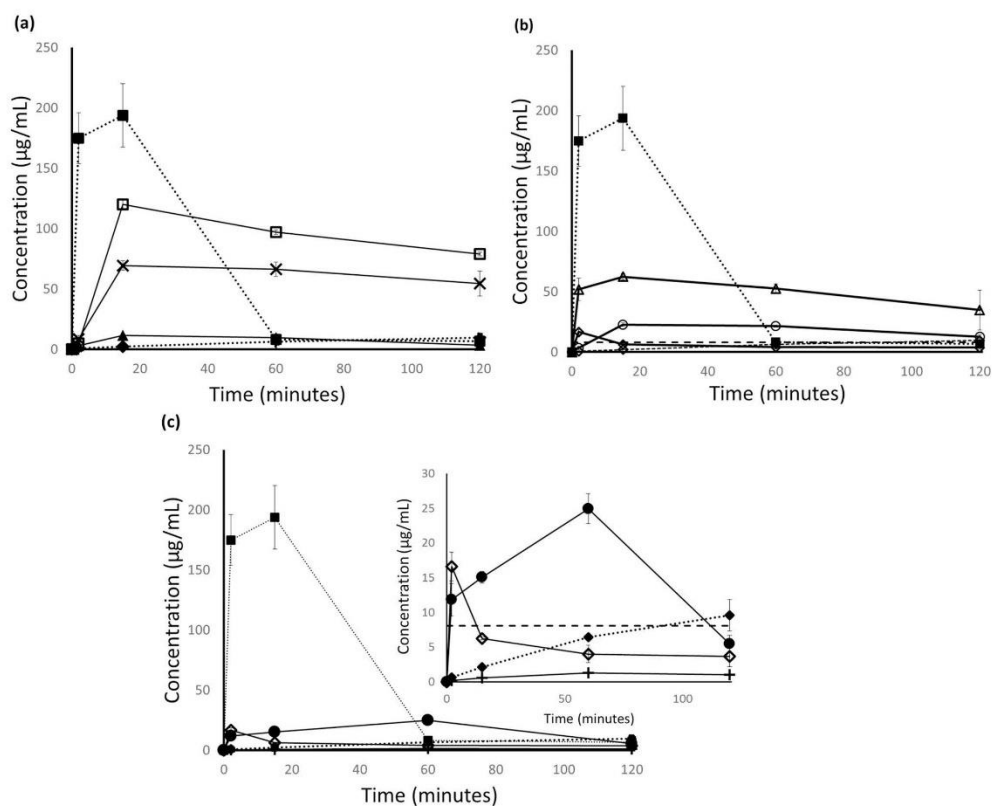


Fig. 7. Dissolution profiles in FaSSiF for glibenclamide (◆), glibenclamide loaded mesoporous silica (■) and glibenclamide loaded mesoporous silica with precipitation inhibitors selected from the COSMO-RS screen. (a): Eudragit EPO (□), Pluronic (X), PEG (▲); (b): HPMCAS (○), HPMC (◊), Eudragit RLPO (△) and (c): PMMA (◊), PVP (●) and Chitosan (+). The order of the listed inhibitors corresponds to the rank order in the COSMO screen (i.e. Eudragit EPO COSMO rank #1 – Chitosan COSMO rank #9).

Fagerberg et al., 2012 and Buch et al., 2010). All three compounds represent Biopharmaceutical Classification System (BCS) II APIs (Amidon et al., 1995). This low solubility, coupled with the incomplete dissolution of the drugs in biorelevant media (Fig. 2), signals the potential for oral absorption and bioavailability risks during development (Zheng et al., 2012). The selected APIs represent a typical range of molecular weights, charge, hydrophobicity and number of hydrogen bond donors and acceptors typical for poorly soluble drugs. Therefore, all three APIs are model candidates for absorption enhancement by formulation with enabling formulations. Indeed, there are already many examples in the literature of combining each of these APIs with enabling formulations such as lipid-based formulations, addition of surfactants to the formulation and formulations containing high-energy forms of the API such as solid dispersions (Thongnopkoo and Puttipatckachorn, 2016; Guo et al., 2011; Zecevic et al., 2018; Theil et al., 2017; Taniguchi et al., 2013).

#### 4.2. Mesoporous silica: a model supersaturating formulation

In the current approach, mesoporous silica was selected as a model supersaturating formulation. Mesoporous silica stabilizes the amorphous API via nano-encapsulation in the pores, which have an approximate mean diameter of 4 nm. Upon contact with an aqueous environment, the drug is released in a molecularly dispersed fashion and thus supersaturation is generated (Ditzinger et al., 2019). Both fenofibrate and glibenclamide have previously been formulated with mesoporous silica in the literature. Van Speybroeck and co-workers reported that, after successfully loading onto ordered mesoporous silica, glibenclamide was completely released within 30 min, compared to just 60% release at 120 min for the commercial formulation, Daonil (Van Speybroeck et al., 2011). Furthermore, the improved *in vitro* dissolution performance translated into an improved *in vivo* performance in rats, with the extent of absorption fourfold higher for glibenclamide

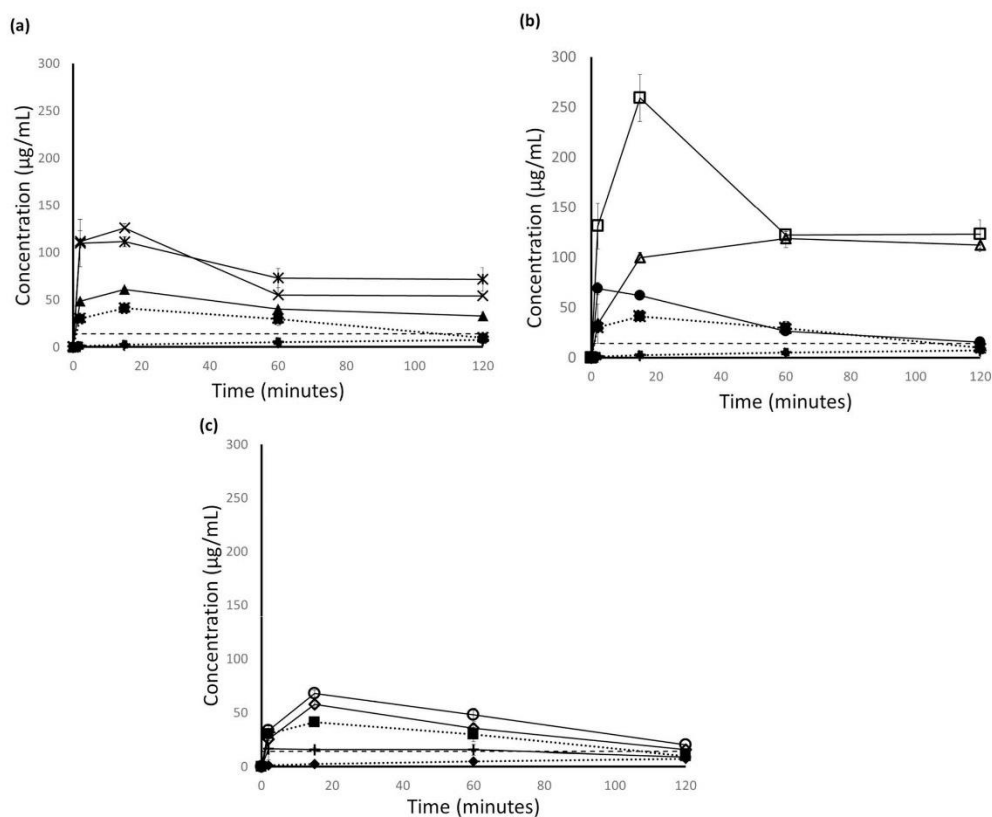


Fig. 8. Dissolution profiles in FaSSiF for fenofibrate (◆), fenofibrate loaded mesoporous silica (■) and fenofibrate loaded mesoporous silica with precipitation inhibitors selected from the COSMO-RS screen. (a): PMMA (◻), Pluronic (×), PEG (▲); (b): Eudragit EPO (□), Eudragit RLPO (△), PVP (●) and (c): HPMCAS (○), HPMC (◇) and Chitosan (+). The order of the listed inhibitors corresponds to the rank order in the COSMO screen (i.e. PMMA COSMO rank #1 – Chitosan COSMO rank #9).

loaded silica than the commercial formulation (Van Speybroeck et al., 2011).

Mesoporous silica has also been demonstrated to improve both *in vitro* and *in vivo* performance of fenofibrate versus commercially available products (Van Speybroeck et al., 2010; Ahern et al., 2013; Uejo et al., 2013; Hong et al., 2016; Bukara et al., 2016; O'Shea et al., 2017; Dressman et al., 2016). Furthermore, fenofibrate was the API chosen for the first proof of concept clinical trial of mesoporous silica in man (Bukara et al., 2016). In that study, which compared fenofibrate loaded silica with the commercially available micronized Lipanthyl® formulation, a 77% increase in  $C_{max}$ , a reduced  $t_{max}$  and a 54% increase  $AUC_{0-24h}/dose$  for fenofibrate loaded silica was observed, demonstrating that loading this API onto mesoporous silica can increase both the rate and extent of absorption.

Given this pre-established success with mesoporous silica for glibenclamide and fenofibrate, successful loading onto silica, as demonstrated by the solid-state shift from crystalline to amorphous, was expected for both compounds (Fig. 3). Furthermore, the loading efficiency

and extent of supersaturation was in line with previous examples in the literature (Table 4; Fig. 4) (O'Shea et al., 2017; Van Speybroeck et al., 2011). In contrast, for dipyrindimole, which has been formulated with other enhancing approaches such as solid dispersions, there have not yet been any published reports of formulation with mesoporous silica. For this molecule, a successful loading was also confirmed by the change in solid-state from crystalline to amorphous (Fig. 3). Additionally, supersaturation was generated, and the observed loading efficiency obtained was in line with typical loading values reported in the literature (Table 4; Fig. 4) (McCarthy et al., 2016).

For all three APIs, loading onto mesoporous silica resulted in the typical 'spring' profile in the FaSSiF dissolution curves (Fig. 4). First reported by Guzman (Guzman, 2007), the presence of short-lived supersaturation followed by precipitation is typical for delivery of the compound in the amorphous form, such as with mesoporous silica. This is related to the metastable nature of the supersaturated state, which is returned to a thermodynamically more favorable state *via* the precipitation of the supersaturated API (Taylor and Zhang, 2016). The

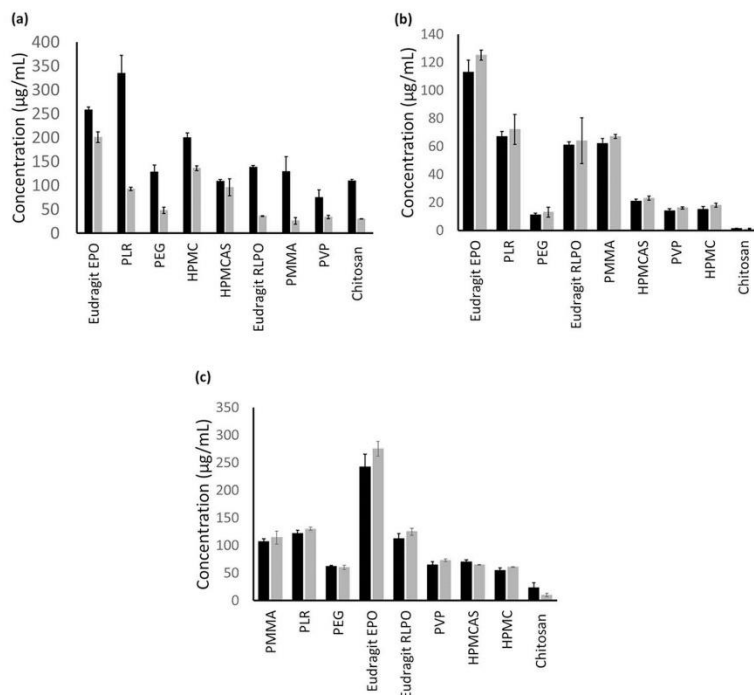


Fig. 9. Maximum concentration, ‘Spring’, (dark bars) versus the concentration at the end of the dissolution experiment at 120 min, ‘Parachute’, (light bars) for dipyr-damole (a), glibenclamide (b) and fenofibrate (c) loaded mesoporous silica in combination with a range of precipitation inhibitors during FaSSIF dissolution, with decreasing COSMO-rank for the respective API from left to right.

Table 6  
Spearman's rank correlation coefficient analysis: dipyr-damole.

| Polymer                                 | Calculated enthalpy (kJ/mol) | AUC (µgmg mL <sup>-1</sup> ) | COSMO rank | Dissolution rank |
|---|------------------------------|------------------------------|------------|------------------|
| Eudragit EPO                            | -6.84                        | 29,000                       | 1          | 1                |
| PLR                                     | -3.45                        | 14,000                       | 2          | 3                |
| PEG                                     | -3.08                        | 8600                         | 3          | 5                |
| HPMC                                    | -2.12                        | 19,000                       | 4          | 2                |
| HPMCAS                                  | -2.01                        | 13,000                       | 5          | 4                |
| Eudragit RLPO                           | -1.55                        | 6600                         | 6          | 6                |
| PMMA                                    | -1.46                        | 5800                         | 7          | 7                |
| PVP                                     | -1.23                        | 5300                         | 8          | 8                |
| Chitosan                                | 1.28                         | 5100                         | 9          | 9                |
| Spearman's rank correlation coefficient | 0.91                         | Significance                 | p < 0.001  |                  |

Table 7  
Spearman's rank correlation coefficient analysis: glibenclamide.

| Polymer                                 | Calculated enthalpy (kJ/mol) | AUC (µgmg mL <sup>-1</sup> ) | COSMO rank | Dissolution rank |
|---|------------------------------|------------------------------|------------|------------------|
| Eudragit EPO                            | -4.96                        | 11,000                       | 1          | 1                |
| PLR                                     | -4.70                        | 7200                         | 2          | 2                |
| PEG                                     | -3.92                        | 960                          | 3          | 7                |
| HPMC                                    | -2.17                        | 6000                         | 4          | 4                |
| HPMCAS                                  | -1.55                        | 6100                         | 5          | 3                |
| Eudragit RLPO                           | -1.03                        | 2100                         | 6          | 5                |
| PMMA                                    | -0.72                        | 2000                         | 7          | 6                |
| PVP                                     | -0.64                        | 600                          | 8          | 8                |
| Chitosan                                | 1.44                         | 100                          | 9          | 9                |
| Spearman's rank correlation coefficient | 0.81                         | Significance                 | p < 0.01   |                  |

dissolution profiles of the three API-loaded silica confirm the need for a precipitation inhibitor, or a ‘parachute’, to maintain the API concentration in solution over physiologically relevant time scales.

#### 4.3. Precipitation inhibitor selection with COSMO-RS

Given the current lack of understanding surrounding structure-inhibition relationships, selection of precipitation inhibitors has typically been empirical, requiring a large amount of experimental screening (Price et al., 2018). Such time-consuming experimental approaches have been reported in the literature for fenofibrate. Petrussevska et al.

employed a high-throughput screening protocol that coupled a solvent-shift approach with off-line chromatography to screen a wide-range of precipitation inhibitors for fenofibrate (Petrusevska et al., 2013). In the study, it was determined that surfactant-based inhibitors were the most optimal for fenofibrate, as opposed to the cellulosic polymers, which proved to be optimal for carbamazepine (Petrusevska et al., 2013). Interestingly, the top performing polymers highlighted in the current study were not included in the high-throughput screen, which further indicates that, in addition to the large resource costs involved in experimental screening, the most optimal inhibitors may be missed due



**Table 8**  
Spearman's rank correlation coefficient analysis: fenofibrate.

| Polymer                                 | Calculated enthalpy (kJ/mol) | AUC (µgmg mL <sup>-1</sup> ) | COSMO rank | Dissolution rank |
|---|------------------------------|------------------------------|------------|------------------|
| PMMA                                    | -2.07                        | 10,000                       | 1          | 3                |
| PLR                                     | -1.24                        | 9000                         | 2          | 4                |
| PEG                                     | -1.21                        | 5200                         | 3          | 7                |
| Eudragit EPO                            | -0.62                        | 19,000                       | 4          | 1                |
| Eudragit RLPO                           | -0.37                        | 13,000                       | 5          | 2                |
| PVP                                     | -0.26                        | 5400                         | 6          | 5                |
| HPMCAS                                  | 0.31                         | 5300                         | 7          | 6                |
| HPMC                                    | 0.55                         | 4200                         | 8          | 8                |
| Chitosan                                | 1.88                         | 1700                         | 9          | 9                |
| Spearman's rank correlation coefficient | 0.63                         | Significance                 | 0.08       | p < 0.05         |

to practical limitations on the number of inhibitors that can be screened experimentally. This problem is especially pronounced when, instead of conducting a high-throughput experimental precipitation inhibitor screen, two to three "usual suspects" are selected for experimental screening. In this approach, polymers such as PVP, HPMCAS or HPMC are often selected and individually screened in combination with the supersaturating formulation of interest, after which the most successful polymer of the three is selected. This approach introduces a large amount of uncertainty as to whether the most efficient formulation has been realized (He et al., 2010; O'Shea et al., 2017; Laine et al., 2016; Vora et al., 2016).

To reduce the resources required for precipitation inhibitor screening, it would be highly desirable to replace experimental with *in-silico* tools. Using the COSMO-RS screening protocol described herein, drug-polymer mixing enthalpy can be calculated for an API in combination with ~50 potential precipitation inhibitors in as little as two minutes. This represents a significant time-saving versus traditional experimental screening. During early pharmaceutical development, time can be the most critical factor in the success of failure of a project, so such savings are highly attractive. Furthermore, there is no limit to the number of molecules that can be included in the database. All potential inhibitors can be assessed using enthalpy of interaction as a rank-order parameter, which is designated the "COSMO Rank" (Fig. 5a–c). This is related to the hypothesis that the more negative the enthalpy, the higher the chance of successful precipitation inhibition based on interaction between API and PI. This hypothesis is links back to the principle that interactions between the API and PI are essential to efficient precipitation inhibition, which has been demonstrated in many studies (Price et al., 2018).

Even without considering the dissolution data generated in these studies, the rank order proposed by the COSMO-RS screen already points towards promising results. For example, in a study by Chauhan and co-workers, it was reported that Eudragit EPO and HPMC were able to sustain supersaturated solutions of dipyrindamole significantly longer than all other polymers studied (Eudragit S100, Eudragit RL100, PEG and PVP). Both the *in silico* prediction and the dissolution studies carried out in our studies reflect these findings. Interestingly, PVP, which is often used as a first-line candidate in precipitation inhibitor selection, did not perform well as a precipitation inhibitor in the study by Chauhan et al. (2013). The COSMO calculation for dipyrindamole (Fig. 5a) was able to identify that PVP would not be a suitable polymer ( $\Delta H = +1.28$  kJ/mol) for dipyrindamole.

#### 4.4. Correlation of COSMO-rank with dissolution performance

In addition to the general observation that the COSMO-RS calculated excess enthalpy of interaction appears to be a useful rank-order parameter for the selection of precipitation inhibitors, a statistical

analysis of the correlation between the COSMO-RS rank and the dissolution data was also conducted (Tables 4–6). Comparing these two parameters with Spearman's rank correlation coefficient analysis, the correlation between the rank order predicted by COSMO-RS and the rank order observed in the dissolution experiments was determined to be 0.91 (0.001,  $p < 0.05$ ), 0.81 (0.01,  $p < 0.05$ ) and 0.61 (0.076,  $p < 0.5$ ) for dipyrindamole, glibenclamide and fenofibrate, respectively. For dipyrindamole and glibenclamide, the very strong positive correlation between COSMO prediction and formulation performance demonstrated that the COSMO-RS screening protocol can be used to select the most optimal precipitation inhibitors whilst avoiding the costly and time-consuming experimental screening. For fenofibrate, the correlation observed between the predictions and the results was lower. Furthermore, the significance in the Spearman's rank correlation coefficient analysis was  $> 0.05$  for fenofibrate, which introduces uncertainty as to the conclusions that can be drawn based on the analysis. However, when PEG was excluded from the analysis, all correlations improved substantially and the correlation coefficient for fenofibrate (0.8) reached statistical significance ( $p < 0.05$ ). It thus seems that PEG may be an outlier in terms of the COSMO predictions, although this would have to be tested with more APIs to be sure. We note that a strong positive correlation was independently achieved for each API, which suggests that the presented approach can be applied robustly and reliably.

In addition to the area under the curve of the dissolution profile, one can also consider how well the API sustains the API in solution by addressing the differences between the peak, 'spring', concentration and the final, 'parachute', concentration. As shown in Fig. 9, there is a good correlation between how well an inhibitor sustains the initial 'spring' concentrations and the COSMO-rank. By combining both the AUC of the dissolution profiles and spring-parachute behavior of an inhibitor, a broad landscape of precipitation inhibitor performance can be seen, which aligns well with the COSMO-RS predictions.

From a mechanistic perspective, the COSMO approach is highly attractive. Specifically, to calculate the energy required to combine the quantum sigma surfaces of the API and PI, the sigma potential ( $\rho\sigma^*$ ), the energy of forming new contacts between the two must be considered, this is reflected in the COSMO-RS energy term,  $E(\alpha,\sigma^*)$ . This term significantly improves the mechanistic applicability of the approach, as all potential modes of interaction between API and PI are considered: hydrogen bond interactions, coulombic interactions and van de Waals interactions (see Appendix 3).

As recently reviewed by our group (Price et al., 2018) the majority of precipitation inhibitors sustain supersaturated API in solution *via* interactions. Although varying from system to system, the most common interactions are hydrogen bond interactions and hydrophobic interactions. For example, in accord with our findings, there have been a number of papers that show the successful precipitation inhibition of supersaturated APIs by Eudragit EPO, this is based on its ability to interact strongly *via* both hydrogen bonding and hydrophobic interactions. For example, Higashi and co-workers studied the effect of Eudragit EPO in combination with the poorly soluble drug mefenamic acid with 2D NOESY NMR (Higashi et al., 2014). The team found that the successful precipitation inhibition of Eudragit EPO was related to hydrophobic interactions between the aromatic portion of the API and the EPO polymer backbone; as well as a hydrophilic hydrogen bond interaction between the aminoalkyl groups of EPO and the carbonyl groups of the API. Such interactions are also possible with dipyrindamole, fenofibrate and glibenclamide.

Furthermore, considering the precipitation inhibitors that did not perform well, one can relate the calculation, dissolution performance and potential points of interaction from a mechanistic perspective. One of the interesting cases here is the lack of successful inhibition of dipyrindamole precipitation by PVP. As previously mentioned, PVP is one of the polymers most commonly used as a precipitation inhibitor. However, PVP has been shown to be ineffective in sustaining

dipyridamole in solution, this was also identified by the COSMO-screen and is reflected in the dissolution performance of the formulation in this study. Chauhan and colleagues demonstrated that no interaction takes place between PVP and dipyridamole in the solid state (Chauhan et al., 2013), this is in line with the results in the current study as well as the fact that the COSMO-calculated enthalpy of interaction was positive and thus unfavorable.

Ultimately, these robust mechanistic calculations increase the successful prediction of API-PI interaction and thus precipitation inhibition, as reflected in the strong positive correlations achieved between the COSMO-rank and the final formulation performance. For a full overview of the COSMO-RS equations, see Appendix 3.

#### 4.5. Assumptions and limitations of the proposed *in silico* screening protocol

Our approach, which utilized excess enthalpy calculations to screen precipitation inhibitors, does not take into consideration the impact of water on the interaction between the API and PI. It has been repeatedly suggested that for a precipitation inhibitor to successfully sustain drug in solution, it must interact with both the API and the water in the medium or GI tract (Ting et al., 2016; Schram, 2015; Price et al., 2018). To exclude consideration of water's role in mediating API interactions with the precipitation inhibitor becomes especially problematic when considering polymers that have very high hydrophobicity or hydrophilicity, as demonstrated by Schram and co-workers (Schram, 2015; Schram et al., 2016). From the data presented in this study, it is clear that the COSMO prediction for PEG did not correlate to the overall dissolution performance. Furthermore, PEG was the only clear outlier in the correlation for all three samples. This may be due to the aforementioned potential problem: PEG is very hydrophilic and is expected to bind and interact preferentially with water. This reduces the direct interaction with the API and therefore the desired precipitation inhibitor performance is not realized. The effect of removing PEG from the dataset is pronounced for all three compounds, such that when the Spearman's rank correlation coefficient analysis was repeated without PEG, the correlation between COSMO-rank and dissolution-rank significantly improved to 0.98 (0.0004,  $p < 0.05$ ) for dipyridamole and glibenclamide, and to 0.8 (0.022,  $p < 0.05$ ) for fenofibrate. Due to this, the COSMO-RS protocol should be applied with the foresight that outliers and exceptions may be possible for very hydrophobic and hydrophilic inhibitors.

Another limitation of the COSMO-RS *in-silico* approach is the focus on local molecular interactions, whereas any supramolecular effects are neglected. Although factors such as molecular weight, viscosity and diffusivity of the precipitation inhibitors play an important role in precipitation inhibition (Warren et al., 2010; Price et al., 2018), insufficient information regarding these factors is available for many of the polymers. There are two main hypotheses with respect to the importance of these parameters to precipitation inhibition. The first, and lesser reported, states that molecular weight and viscosity affect precipitation inhibition *via* changes in the diffusion kinetics of both the drug and polymer in solution (Warren et al., 2010). Such effects cannot be taken into account by the COSMO-RS approach at the moment. The second, and more widely reported hypothesis, relates to an increasing number of binding sites when molecular weight and viscosity are increased (Warren et al., 2010). Such binding sites increase when a polymer is at least to some extent swollen in aqueous medium, but such swelling and the theta condition of the polymer in aqueous medium is an aspect that was not considered in the presented *in silico* screening. It would thus be beyond the scope of this approach to determine the effect of viscosity or molecular weight with the current COSMO-RS protocol. Finally, to complement the enthalpic considerations of interaction of PI with API, there are also entropic considerations that are not easily considered using the current COSMO-RS approach, therefore, for some API-precipitation inhibitor combinations, where the interaction is entropically unfavorable, the COSMO-RS approach may fail to predict the

experimental result. Of course, it is also possible that the interaction is entropically favorable e.g. in the case of disruption of supramolecular structuring of polymers in aqueous solution, as previously reported (Schram et al., 2015a, 2015b).

## 5. Conclusions

In this work, we describe a novel *in silico* screening protocol for the selection of precipitation inhibitors for supersaturating formulations. The protocol uses the COSMO-RS model to calculate excess enthalpy of interaction between API and precipitation inhibitors, which is then used as a rank-order parameter to select potential precipitation inhibitors. Conceptually, such an approach may be applied for any enabling formulation that requires precipitation inhibitors, for example HME or SDD, but further work is required to validate this cross-formulation applicability. Despite the simplifications and assumptions in the presented COSMO-RS protocol, strong positive correlations were obtained between the rank-order prediction and formulation performance for the APIs studied. Furthermore, given the high-throughput and high-speed nature of the *in-silico* calculations, the screening protocol is very attractive as a score-card approach for the design of enabling formulations for poorly soluble APIs in the pharmaceutical industry. Ultimately, this study highlights how *in-silico* tools can be used to improve efficiency of precipitation inhibitor selection as well as the likelihood that the most optimal formulation will be realized.

## Acknowledgements

We would like to thank Axel Becker and Michael Lange (Merck KGaA, Darmstadt) for their helpful discussions and input into developing understanding of COSMO-RS and the applications currently applied.

## Funding

This work has received funding from the European Union's Horizon 2020 research and innovation programme under grant agreement No. 674909 (PEARRL).

## Appendix A. Supplementary data

Supplementary data to this article can be found online at <https://doi.org/10.1016/j.ejps.2019.03.006>.

## References

- Abramov, Y.A., et al., 2012. Rational coformer or solvent selection for pharmaceutical cocrystallization or desolvation. *J. Pharm. Sci.* 101 (10), 3687–3697. <https://doi.org/10.1002/jps.23227>.
- Ahern, J.A., et al., 2013. Comparison of fenofibrate–mesoporous silica drug-loading processes for enhanced drug delivery. *Eur. J. Pharm. Sci.* 50 (3–4), 400–409. <https://doi.org/10.1016/j.ejps.2013.08.026>.
- Amidon, G.L., et al., 1995. A theoretical basis for a biopharmaceutic drug classification: the correlation of *in vitro* drug product dissolution and *in vivo* bioavailability. *Pharm. Res.* 12 (3), 413–420.
- Brouwers, J., et al., 2009. Supersaturating drug delivery systems: the answer to solubility-limited oral bioavailability? *J. Pharm. Sci.* 98 (8), 2549–2572. <https://doi.org/10.1002/jps.21650>.
- Buch, P., et al., 2010. IVIVR in oral absorption for fenofibrate immediate release tablets using dissolution and dissolution permeation methods. *Pharmazie* 65, 723–728. <https://doi.org/10.1691/ph.2010.0114>.
- Bukara, K., et al., 2016. Ordered mesoporous silica to enhance the bioavailability of poorly water-soluble drugs: proof of concept in man. *Eur. J. Pharm. Biopharm.* 108, 220–225. <https://doi.org/10.1016/j.ejpb.2016.08.020>.
- Chauhan, H., et al., 2013. Correlating the behavior of polymers in solution as precipitation inhibitor to its amorphous stabilization ability in solid dispersions. *J. Pharm. Sci.* 102 (6), 1924–1935.
- Ditzinger, F., et al., 2019. Lipophilicity and hydrophobicity considerations in bio-enabling oral formulations approaches—a PEARRL review. *J. Pharm. Pharmacol.* 71, 464–482.
- Dressman, J.B., et al., 2016. Mesoporous silica-based dosage forms improve release characteristics of poorly soluble drugs: case example fenofibrate. *J. Pharm.*



- Pharmacol. 68 (5), 634–645. <https://doi.org/10.1111/jphp.12465>.
- Fagerberg, J.H., et al., 2010. Dissolution rate and apparent solubility of poorly soluble drugs in biorelevant dissolution media. *Mol. Pharm.* 7 (5), 1419–1430. <https://doi.org/10.1021/mp100049m>.
- Fagerberg, J.H., et al., 2012. Ethanol effects on apparent solubility of poorly soluble drugs in simulated intestinal fluid. *Mol. Pharm.* 9, 1942–1952. <https://doi.org/10.1021/mp2006467>.
- Galia, E., et al., 1998. Evaluation of various dissolution media for predicting in vivo performance of class I and II drugs. *Pharm. Res.* 15 (5), 698–705.
- Guo, F., et al., 2011. Self-microemulsifying drug delivery system for improved oral bioavailability of dipyrindamole: preparation and evaluation. *Arch. Pharm. Res.* 34 (7), 1113–1123. <https://doi.org/10.1007/s12272-011-0709-8>.
- Guzman, H.R., et al., 2007. Combined use of crystalline salt forms and precipitation inhibitors to improve oral absorption of celecoxib from solid oral formulations. *J. Pharm. Sci.* 96 (10), 2686–2702.
- He, H., et al., 2010. In vitro and in vivo evaluation of fenofibrate solid dispersion prepared by hot-melt extrusion. *Drug Dev. Ind. Pharm.* 36 (6), 681–687. <https://doi.org/10.3109/03639040903449720>.
- Higashi, K., et al., 2014. Insights into atomic-level interaction between mefenamic acid and eudragit® EPO in a supersaturated solution by high-resolution magic-angle spinning NMR spectroscopy. *Mol. Pharm.* 11 (1), 351–357.
- Hong, S., et al., 2016. High drug load, stable, manufacturable and bioavailable fenofibrate formulations in mesoporous silica: a comparison of spray drying versus solvent impregnation methods. *Drug Deliv.* 23 (1), 316–327. <https://doi.org/10.3109/10717544.2014.913323>.
- Homig, M., Klamt, A., 2005. COSMOfrag: a novel tool for high-throughput ADME property prediction and similarity screening based on quantum chemistry. *J. Chem. Inf. Model.* 45 (5), 1169–1177. <https://doi.org/10.1021/ci0501948>.
- Klamt, A., 1995. Conductor-like screening model for real solvents: a new approach to the quantitative calculation of solvation phenomena. *J. Phys. Chem.* 99 (7), 2224–2235. <https://doi.org/10.1021/j100007a062>.
- Kohn, W., Sham, L.J., 1965. Self-consistent equations including exchange and correlation effects. *Phys. Rev.* 140.
- Laine, A.L., et al., 2016. Enhanced oral delivery of celecoxib via the development of a supersaturable amorphous formulation utilising mesoporous silica and co-loaded HPMCAS. *Int. J. Pharm.* 512 (1), 118–125. <https://doi.org/10.1016/j.ijpharm.2016.08.034>.
- Leigh, M., et al., 2013. Comparison of the solubility and dissolution of drugs in fasted-state biorelevant media (FaSSiF and FaSSiF-V2). *Dissolution Tech.* <https://doi.org/10.14227/DT200313P44>.
- Lofsson, T., Brewster, M.E., 2010. Pharmaceutical applications of cyclodextrins: basic science and product development. *J. Pharm. Pharmacol.* 62, 1607–1621. <https://doi.org/10.1111/j.2042-7158.2010.01030.x>.
- Loschen, C., Klamt, A., 2012. COSMOquick: a novel interface for fast  $\sigma$ -profile composition and its application to COSMO-RS solvent screening using multiple reference solvents. *Ind. Eng. Chem. Res.* 51 (43), 14303–14308. <https://doi.org/10.1021/ie3023675>.
- McCarthy, C.A., et al., 2016. Mesoporous silica formulation strategies for drug dissolution enhancement: a review. *Exp. Opin. Drug Deliv.* 13, 93–108. <https://doi.org/10.1517/17425247.2016.1100165>.
- Mosquera-Giraldo, et al., 2016. Mechanistic design of chemically diverse polymers with applications in oral drug delivery. *Biomacromol.* 17 (11), 3659–3671. <https://doi.org/10.1021/acs.biomac.6b01156>.
- Niederquell, A., et al., 2018. New prediction methods for solubility parameters based on molecular sigma profiles using pharmaceutical materials. *Int. J. Pharm.* 546 (1–2), 137–144.
- O'Shea, J., et al., 2017. Mesoporous silica-based dosage forms improve bioavailability of poorly soluble drugs in pigs: case example fenofibrate. *J. Pharm. Pharmacol.* 69 (10), 1284–1292. <https://doi.org/10.1111/jphp.12767>.
- Palmehund, H., et al., 2016. Studying the propensity of compounds to supersaturate: a practical and broadly applicable approach. *J. Pharm. Sci.* 105, 3021–3029.
- Petusevskra, M., et al., 2013. Evaluation of a high-throughput screening method for the detection of the excipient-mediated precipitation inhibition of poorly soluble drugs. *Assay Drug Dev. Technol.* 11 (2), 117–129. <https://doi.org/10.1089/adt.2012.466>.
- Pozarska, A., et al., 2013. Application of COSMO-RS as an excipient ranking tool in early formulation development. *Eur. J. Pharm. Sci.* 49 (4), 505–511.
- Prasad, D., et al., 2016. Role of molecular interactions for synergistic precipitation inhibition of poorly soluble drug in supersaturated drug–polymer–polymer ternary solution. *Mol. Pharm.* 13 (3), 756–765. <https://doi.org/10.1021/acs.molpharmaceut.5b00655>.
- Price, D.J., et al., 2018. Approaches to increase mechanistic understanding and aid in the selection of precipitation inhibitors for supersaturating formulations - a PEARRL review. *J. Pharm. Pharmacol.* <https://doi.org/10.1111/jphp.12927>. (epub ahead of print).
- Schram, C.J., et al., 2015a. Impact of polymer conformation on the crystal growth inhibition of a poorly water-soluble drug in aqueous solution. *Langmuir* 31 (1), 171–179. <https://doi.org/10.1021/la503644m>.
- Schram, C.J., et al., 2015b. Influence of polymers on the crystal growth rate of felodipine: correlating adsorbed polymer surface coverage to solution crystal growth inhibition. *Langmuir* 31 (41), 11279–11287. <https://doi.org/10.1021/acs.langmuir.5b02486>.
- Schram, C.J., et al., 2016. Polymer inhibition of crystal growth by surface poisoning. *Crystal Growth and Design* 16 (4), 2094–2103. <https://doi.org/10.1021/acs.cgd.5b01779>.
- Taniguchi, C., et al., 2013. New dipyrindamole salt with improved dissolution and oral bioavailability under hypochlorhydric conditions. *Drug Metab. Pharmacokinet.* 28 (5), 383–390.
- Taylor, L.S., Zhang, G.G.Z., 2016. Physical chemistry of supersaturated solutions and implications for oral absorption. *Adv. Drug Deliv. Rev.* 101, 122–142. <https://doi.org/10.1016/j.addr.2016.03.006>.
- Theil, F., et al., 2017. Extraordinary long-term stability in kinetically stabilized amorphous solid dispersions of fenofibrate. *Mol. Pharm.* 14 (12), 4636–4647. <https://doi.org/10.1021/acs.molpharmaceut.7b00735>.
- Thongnopkoo, T., Pattipatitachachorn, S., 2016. New metastable form of glibenclamide prepared by redispersion from ternary solid dispersions containing polyvinylpyrrolidone-K30 and sodium lauryl sulfate. *Drug Dev. Ind. Pharm.* 42 (1), 70–79.
- Ting, M., et al., 2016. High-throughput excipient discovery enables oral delivery of poorly soluble pharmaceuticals. *ACS Central Sci* 2 (10), 748–755. <https://doi.org/10.1021/acscentsci.6b00268>.
- Uejo, F., et al., 2013. Dissolution improvement of fenofibrate by melting inclusion in mesoporous silica. *Asia J. Pharm. Sci.* 8 (6), 329–335. <https://doi.org/10.1016/j.ajps.2013.11.001>.
- Van Speybroeck, M., et al., 2011. Preventing release in the acidic environment of the stomach via occlusion in ordered mesoporous silica enhances the absorption of poorly soluble weakly acidic drugs. *J. Pharm. Sci.* 100 (11), 4864–4876. <https://doi.org/10.1002/jps.22703>.
- Van Speybroeck, M., et al., 2010. Enhanced absorption of the poorly soluble drug fenofibrate by tuning its release rate from ordered mesoporous silica. *Eur. J. Pharm. Sci.* 41 (5), 623–630. <https://doi.org/10.1016/j.ejps.2010.09.002>.
- Vora, C., et al., 2016. Preparation and characterization of dipyrindamole solid dispersions for stabilization of supersaturation: effect of precipitation inhibitors type and molecular weight. *Pharm. Dev. Technol.* 21 (7), 847–855.
- Warren, D.B., et al., 2010. Using polymeric precipitation inhibitors to improve the absorption of poorly water-soluble drugs: a mechanistic basis for utility. *J. Drug Targ.* 18 (10), 704–731. <https://doi.org/10.3109/1061186X.2010.525652>.
- Wie, H., et al., 2006. Biorelevant dissolution media as a predictive tool for glyburide a class II drug. *Eur. J. Pharm. Sci.* 29 (1), 45–52. <https://doi.org/10.1016/j.ejps.2006.05.004>.
- Zeecevic, D.E., et al., 2018. From benchtop to pilot scale-experimental study and computational assessment of a hot-melt extrusion scale-up of a solid dispersion of dipyrindamole and copovidone. *Int. J. Pharm.* 537 (1–2), 132–139. <https://doi.org/10.1016/j.ijpharm.2017.12.033>.
- Zheng, W., et al., 2012. Selection of oral bioavailability enhancing formulations during drug discovery. *Drug Dev. Ind. Pharm.* 38 (2), 235–247. <https://doi.org/10.3109/03639045.2011.602406>.





## Incorporation of HPMCAS during loading of glibenclamide onto mesoporous silica improves dissolution and inhibits precipitation



Daniel J. Price<sup>a,b</sup>, Anita Nair<sup>a</sup>, Johanna Becker-Baldus<sup>c</sup>, Clemens Glaubit<sup>c</sup>, Martin Kuentz<sup>d</sup>, Jennifer Dressman<sup>b</sup>, Christoph Saal<sup>a,\*</sup>

<sup>a</sup> Merck KGaA, Darmstadt, Germany

<sup>b</sup> Institute of Pharmaceutical Technology, Goethe University, Frankfurt, Germany

<sup>c</sup> Institute for Biophysical Chemistry & Centre for Biomolecular Magnetic Resonance, Goethe University, Frankfurt, Germany

<sup>d</sup> University of Arts and Applied Sciences Northwestern Switzerland, Basel, Switzerland

### ARTICLE INFO

#### Keywords:

Mesoporous silica  
Supersaturation  
Precipitation inhibition  
Solid dispersion  
Mechanistic

### ABSTRACT

Mesoporous silica has emerged as an enabling formulation for poorly soluble active pharmaceutical ingredients (APIs). Unlike other formulations, mesoporous silica typically does not inhibit precipitation of supersaturated API therefore, a suitable precipitation inhibitor (PI) should be added to increase absorption from the gastrointestinal (GI) tract. However, there is limited research about optimal processes for combining PIs with silica formulations. Typically, the PI is added by simply blending the API-loaded silica mechanically with the selected PI. This has the drawback of an additional blending step and may also not be optimal with regard to release of drug and PI. By contrast, loading PI simultaneously with the API onto mesoporous silica, i.e. co-incorporation, is attractive from both a performance and practical perspective. The aim of this study was to demonstrate the utility of a co-incorporation approach for combining PIs with silica formulations, and to develop a mechanistic rationale for improvement of the performance of silica formulations using the co-incorporation approach. The results indicate that co-incorporating HPMCAS with glibenclamide onto silica significantly improved the extent and duration of drug supersaturation in single-medium and transfer dissolution experiments. Extensive spectroscopic characterization of the formulation revealed that the improved performance was related to the formation of drug-polymer interactions already in the solid state; the immobilization of API-loaded silica on HPMCAS plates, which prevents premature release and precipitation of API; and drug-polymer proximity on disintegration of the formulation, allowing for rapid onset of precipitation inhibition. The data suggests that co-incorporating the PI with the API is appealing for silica formulations from both a practical and formulation performance perspective.

### 1. Introduction

Among the various administration routes for drugs, oral administration is the most commonly employed. It is cost-effective and convenient for the patient, leading to a very high patient compliance (Krishnaiah, 2010). APIs must be absorbed to become orally bioavailable, a process which relies in turn on sufficient solubility and permeability of the API (Zheng, 2012). In recent years there has been an exponential increase in drugs exhibiting poor solubility: it is reported that approximately 60% of all drugs on the market are poorly soluble (Taylor and Zhang 2016). It has been suggested that anywhere between 80 and 90% of compounds in development also demonstrate low solubility (Loftsson and Brewster, 2010). These estimates highlight the

need for effective formulation approaches to avoid low bioavailability associated with poor aqueous solubility.

To overcome these challenges, formulators have developed a series of promising formulation strategies (Ditzinger, 2018). These approaches include: (i) solvents, co-solvents and lipids; (ii) micelle systems; (iii) particle size reduction; (iv) complexation; and (v) amorphous technologies (Zheng, 2012). One of the most common approaches for improving bioavailability is *via* the generation of supersaturated solutions in the GI-tract, which can drive improved absorption (Zheng, 2012). However, these systems are metastable due to the energetic propensity of the compound to precipitate (Price, 2018). Therefore, precipitation inhibitors (PIs) are often used to sustain the supersaturated state by inhibiting or slowing down precipitation of

\* Corresponding author: Merck KGaA, Site-Management - Analytics Healthcare, Frankfurter StraÙer. 250, Darmstadt, 64293, Germany.  
E-mail addresses: [daniel-joseph.price@merckgroup.com](mailto:daniel-joseph.price@merckgroup.com) (D.J. Price), [Christoph.saal@merckgroup.com](mailto:Christoph.saal@merckgroup.com) (C. Saal).

<https://doi.org/10.1016/j.ejps.2019.105113>

Received 6 June 2019; Received in revised form 16 October 2019; Accepted 18 October 2019

Available online 23 October 2019

0928-0987/ © 2019 Elsevier B.V. All rights reserved.

drug (Warren, 2010). Successful PI systems can sustain drug supersaturation over physiologically relevant time-scales by interfering with the crystallization process (Price, 2018). Precipitation inhibitors can kinetically prevent re-crystallization via a number of mechanisms, including: viscosity, co-solvency and drug-polymer interactions, with the latter widely being reported to be especially important (Warren, 2010; Price, 2018). Recent advances in precipitation inhibition design and selection include *de novo* precipitation inhibitor design (Ting, 2017) and *in silico* calculation of drug-polymer mixing enthalpies for precipitation inhibitor selection (Price et al., 2019).

One under-utilized formulation technology to generate drug supersaturation is mesoporous silica. Mesoporous silica is a silicon dioxide excipient that has a highly porous network, consisting of mesopores between 2 and 50 nm in diameter (Ditzinger, 2018). These materials have very high specific surface areas and are used in catalysis, environmental clean-up, chromatography, and drug delivery (McCarthy, 2016). Poorly soluble APIs can become molecularly adsorbed on the surface of the silica and sterically confined such that recrystallization cannot occur (Knapik, 2016). Indeed, this is one of the most widely reported advantages of mesoporous silica, in its enhanced stabilization capabilities due to nanoconfinement in the porous network (McCarthy, 2016). Mesoporous silica-based 'spring and parachute' formulations have been widely demonstrated in the literature, from both an *in vitro* and *in vivo* perspective (Ditzinger, 2018; McCarthy, 2016). Van Speybroeck and colleagues originally described how such precipitation inhibitors, including HPMC and HPMCAS, can enhance the oral absorption of itraconazole released from mesoporous silica in rats (Van Speybroeck, 2010). This was also demonstrated in pigs, with O'Shea and colleagues using the precipitation inhibitor HPMCAS to improve the oral absorption of fenofibrate released from mesoporous silica (O'Shea, 2016). Recent work on precipitation inhibitors for mesoporous silica has also taken place, Price and co-workers developed of an *in silico* screening approach which calculates drug-polymer mixing enthalpy for the optimized selection of precipitation inhibitors for mesoporous silica formulations (Price et al., 2019). In spite of these recent advances in mesoporous silica and precipitation inhibition, the method of combining precipitation inhibitors with mesoporous silica remains relatively inefficient. Typically, PIs are mechanically blended with the API-loaded silica formulations after the drug is loaded (usually with a mortar and pestle). However, it has recently been shown that incorporating the PI into the API loading process itself can dramatically improve both *in vitro* and *in vivo* performance of a celecoxib loaded silica formulation (Laine, 2016). In light of this proof of concept, there is a need for further mechanistic research. This study aims to demonstrate the utility of a co-incorporation approach for combining PIs with silica formulations, and to develop a mechanistic rationale to explain the improvement in performance of silica formulations using the co-incorporation approach.

## 2. Experimental

### 2.1. Materials

Crystalline glibenclamide (GB), reagent grade acetone, HPLC grade acetonitrile and HPLC grade methanol were all purchased from MilliporeSigma (St Louis, MO, USA). AQQAT (HPMCAS-MF) was purchased from ShinEtsu (Japan). Parateck® SLC was a gift sample from Merck KGaA (Germany). FaSSGF/FaSSIF/FeSSIF powder to make biorelevant dissolution medium, Fasted Simulated Intestinal Fluid (FaSSIF), was obtained from Biorelevant.com (UK).

### 2.2. Methods

#### 2.2.1. Determination of thermodynamic solubility

FaSSIF was prepared by weighing 45 mg of FaSSGF/FaSSIF/FeSSIF powder into 45 mL of phosphate buffer (pH 6.5) (Galia et al., 1998).

SGF (pH 1.2) was prepared according to USP monographs. Glibenclamide (2–3 mg) was accurately weighed into a Uniprep® syringeless filter (5 mL; 0.45 µm). 2 mL of either FaSSIF (pH 6.5) or SGF (pH 1.2) was added and the samples were agitated at 450 rpm for 24 h at 37 °C. The pH was checked at 7 h and adjusted with 0.1 N NaOH or 0.1 N HCl, if a deviation greater than  $\pm 0.05$  pH units was observed. The final pH was also recorded after 24 h.

Samples were filtered with PTFE 0.45 µm Whatman filters after 24 h. Filtrates were diluted with acetonitrile and water (1:4) to avoid precipitation from the saturated solution. Samples were analyzed with ultra-high performance liquid chromatography (UPLC) (Thermo Dionex Ultimate 3000, Thermo Fisher, MA, USA) to determine the API concentration. API concentration was determined based on a standard calibration curve of nine standard concentrations (50, 30, 10, 5, 3, 1, 0.5, 0.3, 0.1 µg/mL). Three quality control samples of known concentrations (30, 3, 0.3 µg/mL) were prepared and used to check the robustness of the calibration curve. The determination was carried out in duplicate.

#### 2.2.2. UPLC method

UPLC analysis was performed using a Thermo Dionex Ultimate 3000 (Thermo Fisher, MA, USA) equipped with a diode array detector at 240 nm (Thermo Fisher, MA, USA). Chromatographic separation was achieved on an Acquity UPLC BEH column C8 (2.1 × 50 mm, 1.7 µm, Waters, MA, USA). The mobile phases A and B consisted of water: formic acid 99:1 (v:v) and acetonitrile : formic acid 99:1 (v: v), respectively. Gradient and flow rate is shown in Table 2. System management, data acquisition and processing were performed with the Chromeleon™ software package, version 7.2 (Thermo Fisher, MA, USA)

#### 2.2.3. Parateck SLC® standard loading procedure and standard PI incorporation

Glibenclamide loaded silica was prepared using the solvent impregnation rotary evaporator method (Laine, et al. 2016) as follows: A solution (10 mg/mL) of API in acetone was added to Parateck SLC (1:2 w/w API/Parateck SLC®) under magnetic stirring for 30 min. The suspension was then transferred to a rotary evaporator, and the solvent was removed under reduced pressure at 40 °C. After complete removal of the solvent, the powder was left to dry in the rotary evaporator under reduced pressure for a further 2 h. The formulation was then physically combined with HPMCAS (API: Parateck SLC®: HPMCAS 1: 2: 3 w/w) using a pestle and mortar.

#### 2.2.4. Parateck SLC® API/PI co-incorporation procedure

Glibenclamide/HPMCAS co-incorporated Silica samples were prepared using the solvent impregnation rotary evaporator method. A solution of API (1.0 mg/mL) and HPMCAS (30 mg/mL) in acetone was added to Parateck SLC (1 : 2 : 3 API: Parateck SLC®: HPMCAS) under magnetic stirring, which was continued for 30 min. The suspension was transferred to a rotary evaporator, and the solvent was removed under reduced pressure at 40 °C. After complete removal of the solvent, the powder was left to dry in the rotary evaporator under reduced pressure for a further 2 h.

#### 2.2.5. Preparation of an API-HPMCAS sample as control

A control sample consisting of only of API and HPMCAS was also prepared. A solution with the same concentrations of API (1.0 mg/mL) and HPMCAS (30 mg/mL) as described above for the API – silica – PI system in acetone was prepared under magnetic stirring for 15 min. The solution was then transferred to a rotary evaporator, and the solvent was removed under reduced pressure at 40 °C. After complete removal of the solvent, the powder was left to dry in the rotary evaporator under reduced pressure for a further 2 h. Residual solvent concentration was recorded with 2D <sup>1</sup>H NMR to ensure residual solvent was below the ICH limit of 0.5% (data not shown).



### 2.2.6. Determination of glibenclamide loading onto mesoporous silica

To determine the % (w/w) of API in the mesoporous silica, the loaded samples were dispersed and stirred in DMSO as this solvent is known to dissolve glibenclamide readily. Samples were taken after 1 h, centrifuged, filtered and diluted before being quantified by UPLC, according to the method described in 2.2.2. The API content was calculated relative to the mass of loaded samples dispersed within the DMSO. The study was performed in triplicate.

### 2.2.7. Powder X-ray diffraction (PXRD)

Samples were prepared between X-ray amorphous films and measured in transmission mode using Cu-K $\alpha$ 1-radiation and a Stoe StadiP 611 KL diffractometer equipped with Dectris Mythen1K PSD. The measurements were evaluated with the software WinXPow 3.0.3 by Stoe, Crystallographica Search/Match Version 3.1.0.2, the ICDD PDF-4+ 2014 Database and Igor Pro Version 6.34 by Wavemetrics Inc. Finger/Cox/Jephcoat. Angular range: 1–65°2 $\theta$ ; PSD-step width: 2° 2  $\theta$ ; angular resolution: 0.015°2 $\theta$  measurement time: 15 s/step, 0.25 h overall.

### 2.2.8. FaSSiF mini-dissolution experiment

Around 5 mg of API (or the equivalent of API-loaded silica) was weighed accurately into a glass vial. 5 mL of FaSSiF was added. The vials were agitated at 37 °C and 450 rpm in a shaker for 2 h. Samples were taken at 2, 15, 60 and 120 min, filtered (0.45 PTFE Whatman filters), diluted, and analyzed by UPLC. Solid residues at the end of the experiment were collected via centrifugation and analyzed for crystallinity with powder X-ray diffraction (PXRD). This was carried out on the following samples: API, API + polymer, API loaded silica and API loaded silica + PI. The mini-dissolution trials were conducted in duplicate for all samples.

### 2.2.9. Biorelevant transfer experiments

The experimental set-up for the transfer experiments is demonstrated in Fig. 1.

Around 150 mg of API or equivalent was accurately weighed in a 100 mL stoppered flask - the exact sample masses varied dependent on the formulation (see Table 1).

25 mL of simulated gastric fluid (pH 1.2) prepared according to USP monographs was added to the flask and agitated at 450 rpm and 37 °C. 50 mL of FaSSiF were added to a separate flask, which was also agitated at 450 rpm and 37 °C. After 30 min, the API suspension in SGF pH 1.2 was transferred at a zero-order rate of 0.85 mL/min using a peristaltic pump, until the complete gastric contents were transferred (~30 min) into the FaSSiF compartment. Samples were withdrawn from the intestinal compartment at regular time points using a 1 mL syringe to a sampling tube fitted with a pre-filter of 10  $\mu$ m and filtered again using a 0.45  $\mu$ m PTFE Whatman syringe filter and diluted. Samples were then

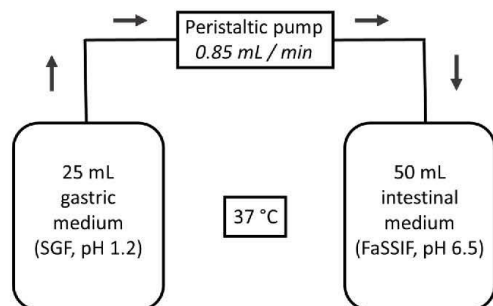


Fig. 1. Experimental diagram showing mini-transfer set-up

Table 1

Transfer dissolution sample preparation

| Formulation                          | Weighed mass (mg) | API mass (mg) |
|--------------------------------------|-------------------|---------------|
| GB loaded silica                     | 450               | 150           |
| GB loaded silica HPMCAS Blend        | 900               | 150           |
| GB and HPMCAS co-incorporated silica | 900               | 150           |

Table 2

UPLC gradient and flow rates

| Time (mins) | Flow rate (mL/min) | % (v:v) Mobile phase A | % (v:v) Mobile phase B |
|-------------|--------------------|------------------------|------------------------|
| 0           | 0.83               | 90                     | 10                     |
| 0.83        | 0.83               | 10                     | 90                     |
| 1.2         | 1.5                | 90                     | 10                     |
| 2           | 1.5                | 90                     | 10                     |
| 2.01        | 0.83               | 90                     | 10                     |

analyzed by UPLC for API content. The post-dissolution residues were then collected and analyzed for crystallinity with XRPD.

### 2.2.10. Single medium SGF dissolution assay (in tandem to transfer assay)

Around 150 mg of API or equivalent was accurately weighed into a 100 mL stoppered flask. The exact sample masses varied dependent on the formulation (see Table 1). 25 mL of SGF (pH 1.2, gastric compartment) was added to the flask and the contents agitated at 450 rpm and 37 °C. Samples were withdrawn at regular time points using a 1 mL syringe to a sampling tube fitted with a pre-filter of 10  $\mu$ m and filtered again using a 0.45  $\mu$ m PTFE Whatman syringe filter and suitably diluted. Samples were then analyzed with UPLC for API content. The post-dissolution residues were directly collected and analyzed for crystallinity with PXRD.

### 2.2.11. Scanning electron microscopy (SEM) and energy-dispersive X-ray spectroscopy (EDX)

Samples were prepared on copper tape and imaged using a Hitachi TM3000 Tabletop Microscope, W cathode, low vacuum, accelerating voltage 5 kV and 15 kV, 4-Quadrant BSE detector, magnification 15x – 30,000x. For the energy dispersive X-ray spectroscopy (EDX) data, a standard-less quantitative analysis was performed by using the ZAF correction, considering the correction for light elements standardless element coefficient factors (SEC).

### 2.2.12. Solid-state nuclear magnetic resonance (NMR) spectroscopy

Solid-state NMR experiments were performed under magic-angle-sample (MAS) spinning using a Bruker 4 mm MAS HXY probe in double resonance mode in combination with a Bruker Avance 600 MHz wide bore NMR spectrometer (Bruker). The sample spinning frequency was 10 kHz, and the readout on the probe thermocouple was set to 290 K. <sup>13</sup>C-CP experiments were performed using a contact time of 1 ms and 100 kHz high power proton decoupling following the SPINAL64 scheme was applied during acquisition. The recycle delay was 3 s. The spectra were indirectly referenced to DSS via the CH<sub>2</sub> signal of Adamantane at 40.49 ppm. Solid-state NMR measurements were repeated on multiple batches to ensure reliability of the interpretation.

## 3. Results

### 3.1. Solid-state form of glibenclamide in formulations

The glibenclamide powder used in this work is crystalline in the solid-state as shown by XRPD (Fig. 2a). Successful loading of glibenclamide onto mesoporous silica was demonstrated by the absence of distinct Bragg peaks in XRPD patterns, which indicated a shift from the

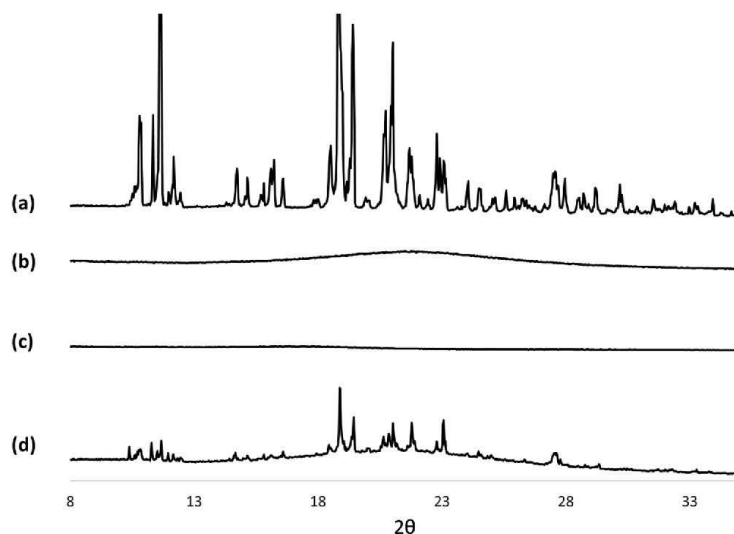


Fig. 2. XRPD pattern for crystalline glibenclamide (GB) (a), glibenclamide loaded silica (b), GB and HPMCAS co-incorporated silica (c) and GB and HPMCAS prepared by rotary evaporation (d)

crystalline to the amorphous state (Fig. 2b). The co-incorporation process did not interfere with the solid-state conversion of glibenclamide: the co-incorporated sample exhibited the same shift from crystalline to amorphous post-loading (Fig. 2c). However, the control sample, which consisted of HPMCAS/GB prepared by solvent evaporation, showed partial crystallinity, which aligned with the XRPD pattern for the unmodified crystalline glibenclamide (Fig. 2d).

### 3.2. Loading content of glibenclamide in mesoporous silica formulations

The % loading of glibenclamide determined by UPLC is shown in Table 3. The final glibenclamide content in the final mesoporous silica formulations was around 15%, irrespective of whether the drug was first loaded onto the silica and then combined with HPMCAS, or the HPMCAS was incorporated during drug loading. Drug loading levels are modest, which could be a limitation for drugs that are administered at high doses. However, they are in line with usual supersaturating drug formulations that require precipitation inhibitors (Price et al., 2019; Ditzinger, 2018).

### 3.3. Scanning electron microscopy (SEM) and electron dispersive X-ray spectroscopy (EDX)

SEM images for glibenclamide loaded silica, glibenclamide loaded silica + HPMCAS Blend and SEM and EDX images for glibenclamide and HPMCAS co-incorporated silica are shown in Fig. 3. The unloaded

silica is shown in Fig. 3a. In glibenclamide loaded silica, the characteristic silica particles are also present (Fig. 3b). This is also the case for glibenclamide loaded silica + HPMCAS physical mixture (Fig. 3c), where the particles are simply 'diluted' by the addition of the polymer, which is depicted as the dark texture in between the silica particles. However, large platelet particles were observed when HPMCAS was incorporated during the loading step onto the silica (Fig. 3d). The EDX images show that the platelet particles are carbon based and therefore likely composed of HPMCAS. The silica particles appear to be embedded in the HPMCAS plate, as when the image was zoomed to the same resolution as Fig. 3, the images looked similar to characteristic silica particles. Chlorine, used as a marker for glibenclamide, was observed within the silica particles on the HPMCAS plate, with no API observable outside of the platelets. These observations suggest that the formulation is a solid dispersion of API loaded silica in HPMCAS (Fig. 3 bottom).

Based on this potential combination of silica loading and classical solid dispersion, it was important to assess what role the silica plays in the formulations. As can be seen in Fig. 4, the particles produced in the solvent evaporation of glibenclamide and HPMCAS (control sample) are similar to the particles produced when the HPMCAS is incorporated during the drug loading step onto the silica. However, EDX analysis shows a key difference between the formulations, in that the drug marker, chlorine, is no longer confined within the polymer (plates), but is freely distributed in the control sample.

### 3.4. FaSSiF mini-dissolution

In FaSSiF mini-dissolution experiments, the concentration of the pure drug approached the thermodynamic solubility value of 8.1 µg/mL (Appendix 1) (Fig. 5a). From the glibenclamide loaded silica formulations, a significant improvement in dissolution was observed in the FaSSiF mini-dissolution experiments, reaching a 25-fold supersaturation (Fig. 5). However, due to the metastable nature of the supersaturation, these extremely high concentrations were short-lived and the concentration reverted to the thermodynamic solubility within 60 min (Fig. 5).

Table 3  
API loaded silica total API content

| Formulation                                     | Theoretical loading (%) | Actual loading (UPLC) (%) |
|---|-------------------------|---------------------------|
| Glibenclamide loaded silica (without HPMCAS)    | 30                      | 30.1 ± 0.1                |
| Glibenclamide and HPMCAS co-incorporated silica | 15                      | 15.9 ± 0.2                |
| Glibenclamide loaded silica + HPMCAS blend      | -                       | 15.1                      |

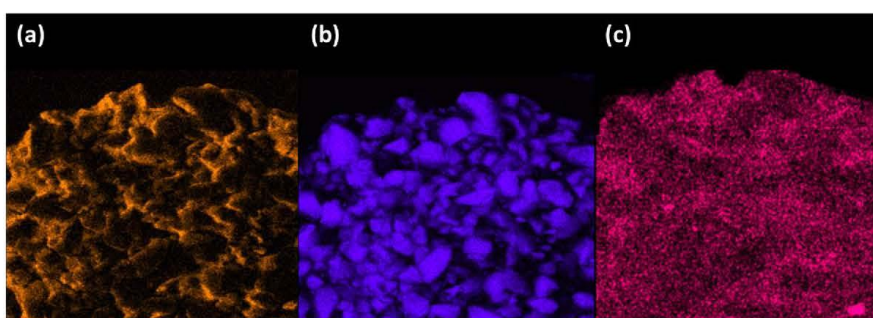
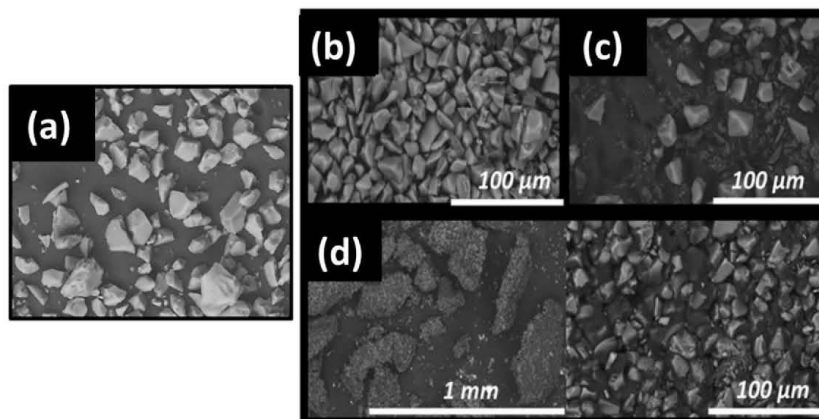


Fig. 3. Top: SEM (left) of unloaded mesoporous silica (a), glibenclamide loaded silica (b), glibenclamide loaded silica + HPMCAS physical mixture (c) and HPMCAS incorporated during loading of glibenclamide onto silica (d). Bottom: SEM EDX of HPMCAS incorporated during loading of glibenclamide onto silica. Carbon (a), silicon (b) and chlorine (c) atoms are highlighted. Chlorine is a marker for glibenclamide.

Physically blending the glibenclamide loaded silica with HPMCAS prolonged the duration of supersaturation to at least 2 h, although the degree of supersaturation was lower (about 3-fold) (Fig. 6). Co-incorporating the HPMCAS with the glibenclamide onto the silica further improved the dissolution and precipitation performance, with higher supersaturation (about 6-fold) achieved over the time course of the experiment (Fig. 6). Finally, the control sample, which used the same process as the co-incorporated in the absence of silica, showed almost

no improvement in the FaSSiF mini-dissolution relative to the crystalline API. This result is in agreement with the partial crystallinity observed in the XRPD (Fig. 6).

Post-dissolution residues were collected for each of the samples and analyzed by XRPD. Crystalline glibenclamide precipitated in all samples except the co-incorporated formulation, in which the solid residue at the end of the experiment was amorphous (Appendix 2).

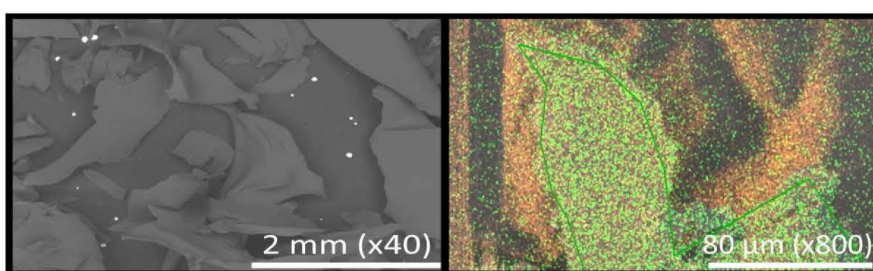


Fig. 4. SEM (left) and EDX (right) images of glibenclamide and HPMCAS prepared by solvent evaporation shows the same particle size and morphology as the co-incorporated samples. However, in this sample the drug (indicated by green) is no longer confined within the polymer plate and is freely distributed throughout the sample.



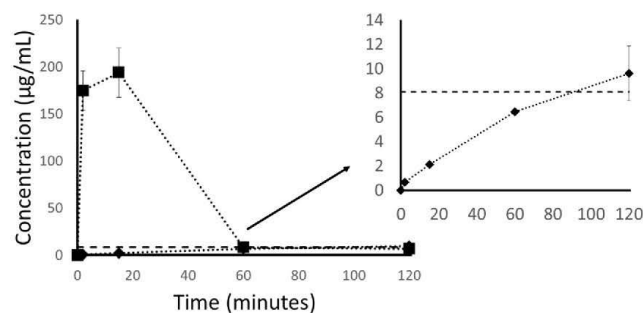


Fig. 5. Mini-dissolution profiles of glibenclamide (◆), and glibenclamide loaded silica (■) in FaSSIF, pH 6.5 at 37 °C ( $n = 2$ ). Mean Glibenclamide thermodynamic solubility in FaSSIF is represented by the dashed horizontal line. In the insert on the right, the dissolution of crystalline glibenclamide has been magnified for better comparison.

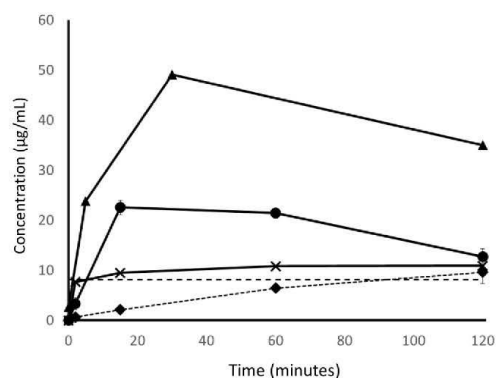


Fig. 6. Mini-dissolution profiles of glibenclamide (◆), glibenclamide loaded silica + HPMCAS blend (●) and glibenclamide and HPMCAS Co-incorporated silica (▲) and control: glibenclamide/HPMCAS prepared by solvent evaporation (X) in FaSSIF, pH 6.5 at 37 °C ( $n = 2$ ).

### 3.5. Transfer model experiments

During transfer model dissolution experiments with pure glibenclamide, no concentrations were detected in the SGF portion of the assay (Fig. 7). This is in line with the thermodynamic solubility results, which indicated that the solubility of glibenclamide was under the limit of detection of the UPLC method (Appendix 1). After transfer into the FaSSIF portion of the experiment, the concentration profile closely overlapped with the mini-dissolution profile, suggesting that the dissolution of crystalline glibenclamide was largely unaffected by pre-wetting in SGF (Fig. 7).

Comparison of results from transfer model and mini-dissolution experiments of glibenclamide loaded silica in the absence of any precipitation inhibitors suggests that single-medium dissolution may lead to different expectations of formulation performance. In the transfer model experiments with glibenclamide loaded silica (Fig. 7); the performance of the loaded silica formulation was even poorer than the unmodified, crystalline parent.

Crystallinity was observed in the post-SGF dissolution residues for glibenclamide loaded silica (Appendix 3). This suggests that, although no release was detectable in SGF, the drug did indeed release but then rapidly precipitated to the crystalline form.

Combination of glibenclamide loaded silica with HPMCAS significantly improved the transfer dissolution performance, with the formulation generating supersaturation in the intestinal phase of the assay (Fig. 7). It was also possible to detect glibenclamide in the SGF

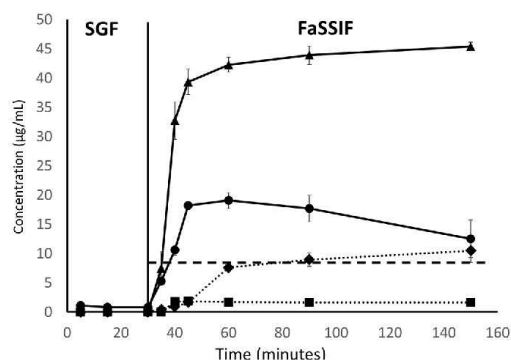


Fig. 7. Biorelevant transfer dissolution of glibenclamide loaded silica (■), crystalline glibenclamide (◆), glibenclamide Loaded Silica + HPMCAS Blend (●) and glibenclamide and HPMCAS co-incorporated silica (▲) ( $n = 2$ ). Transfer from SGF to FaSSIF occurred at 30 min. N.B. no API was detectable during the SGF dissolution for glibenclamide loaded silica and crystalline glibenclamide. FaSSIF thermodynamic solubility is shown by the dotted line.

portion of the assay, suggesting that supersaturation occurred in this medium. Similarly to the glibenclamide loaded silica, crystallinity was observed in the post-SGF residue for the sample containing a physical mixture of HPMCAS with the drug loaded silica (Appendix 3). This finding was in agreement with the XRPD patterns obtained post-FaSSIF mini-dissolution (Appendix 2).

The transfer dissolution of the sample where HPMCAS was incorporated during the drug loading step is shown in Fig. 7. Unlike the sample where HPMCAS was added post-loading, no release of glibenclamide was observed in the SGF of the portion of the assay. This is likely explained by the immobilization of the drug loaded silica onto the HPMCAS platelets, which do not disintegrate in the gastric environment. As observed in the mini-dissolution experiments, (i) the supersaturation of glibenclamide during the FaSSIF portion of the experiment was significantly greater and more sustained from the co-incorporated formulation compared to the blend. In this case (unlike the pure drug), similar concentrations were achieved in the mini-dissolution and transfer model experiments.

Visually, the transfer dissolution of the sample in which HPMCAS was incorporated during the drug loading step was also quite different from the glibenclamide loaded silica and physical mixture of glibenclamide loaded silica with HPMCAS samples. For glibenclamide loaded silica with and without post-loading addition of HPMCAS, the powder was immediately dispersed in the dissolution vessel, creating a suspension. Conversely, no such dispersion was observed within the



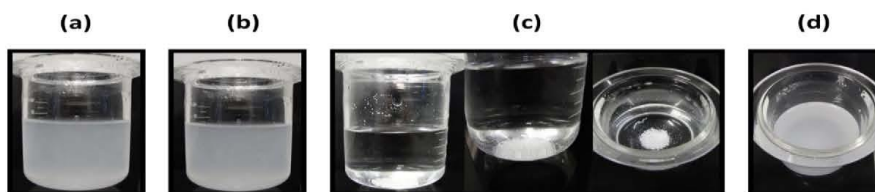


Fig. 8. Images of glibenclamide loaded silica (a) and glibenclamide loaded silica + HPMCAS (b) dispersed in SGF; and glibenclamide and HPMCAS co-incorporated silica dispersed in SGF (c) and FaSSiF (d)

sample in which HPMCAS was incorporated in the drug loading step and the dispersion remained clear (Fig. 8).

Unlike the other silica formulations, the post-SGF dissolution residue for the co-incorporated formulation remained amorphous (Appendix 3).

The control sample was not investigated during the transfer dissolution as it was fully crystalline and behaved identically to pure crystalline glibenclamide during dissolution in FaSSiF. Furthermore, given that the thermodynamic solubility of crystalline glibenclamide is < LOD it was not anticipated that any useful observations could be made from the control sample during the SGF portion of the transfer dissolution.

### 3.5.1. Post-dissolution SEM

To examine the physical behavior of the formulation with HPMCAS incorporated during the drug loading step, the post-SGF and post-FaSSiF residues were characterized with SEM. Post-SGF dissolution, the large platelets (Fig. 3) were unchanged (Fig. 9). Increasing the magnification, one can still observe the loaded silica particles immobilized within the the polymer platelets. Conversely, in post-FaSSiF dissolution, the only observable particles are of silica, suggesting the polymer platelets had dissolved, allowing the drug to be released from the silica (Fig. 9)

### 3.5.2. Solid-state NMR spectroscopy

SS-NMR spectroscopy was carried out on all samples (Fig. 10). The full spectra are provided in Appendix 4. The  $^{13}\text{C}$  peaks for the API were identical in all samples except the co-incorporated formulation. In the co-incorporated formulation, a low field shift of 0.2 – 0.3 ppm for all API peaks was observed. For example, the characteristic API peak at 53 ppm was observable in all samples except the co-incorporated formulation, in which the peak shifted to 53.5 ppm. This is indicative of an interaction taking place between the drug and the polymer in the solid-state, which can take place once the drug is immobilized in the silica

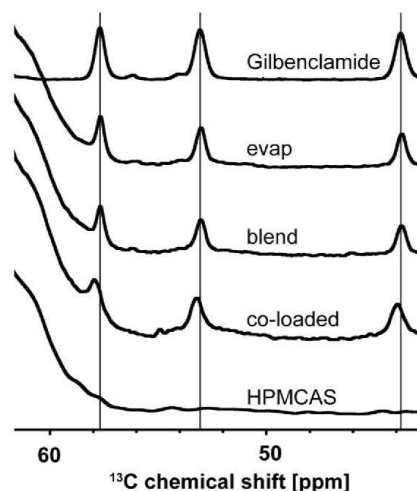


Fig. 10. A section of the  $^{13}\text{C}$  NMR spectra for all samples showing characteristic peaks for API  $^{13}\text{C}$  atoms at 43.5, 53 and 58 ppm. Analysis was carried out on multiple batches ( $n = 2$ ) of co-incorporated formulation and in all cases a 0.2–0.3 ppm peak-shift was observed for the co-incorporated formulation versus all other samples, with the co-incorporated formulation showing API  $^{13}\text{C}$  peaks at 44, 53.5 and 58.5 ppm. Given that the spectra were unchanged for different batches and repeats, only one dataset is shown. Full spectra are available in Appendix 4.

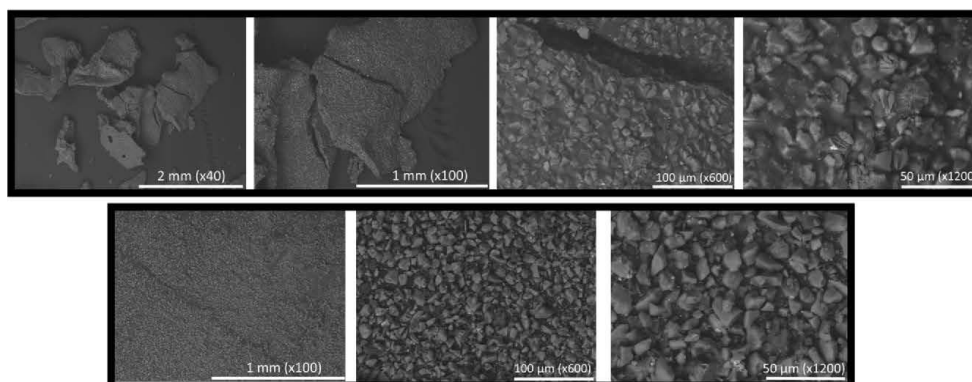


Fig. 9. SEM images of glibenclamide and HPMCAS co-incorporated silica after dissolution in SGF (top) and FaSSiF (bottom)

and subsequently in the HPMCS plate. By contrast, no peak shift was observed in the control sample, GB/HPMCAS, which was prepared by rotary evaporation. The results suggest that solid-state drug-polymer interactions and hence dissolution performance can be altered by changing the method used to manufacture the formulation.

#### 4. Discussion

Mesoporous silica is an emerging oral delivery technique to formulate low soluble drugs. Upon impregnation of the silica with a concentrated API solution, drug can be molecularly adsorbed onto the surface of the silica. Due to the size of the pores, which have an approximate mean diameter of 4 nm, the molecularly adsorbed API is locally and sterically confined, preventing recrystallization (Ditzinger, 2018; Price, 2018). More understanding is required to fully resolve the relative importance of the various considerations in the design and development of mesoporous silica formulations. Particularly critical is incorporation of precipitation inhibitors in the final formulation, since without such additives, the supersaturated state of the API is barely stabilized.

To date there has been no systematic study of how best to incorporate precipitation inhibitors in mesoporous silica formulations. Current practice for preparation on a small scale involves combining PIs in a physical mixture with the API loaded silica, either by mortar and pestle or overhead stirring. Due to the lack of a standard protocol, there is uncertainty about the reliability of this approach and how well the PI is blended with the loaded silica. In addition to the practical limitations of incorporating the PI post-loading, it represents a further step in product manufacture. By contrast, incorporation of the PI during the loading step removes these limitations while maintaining improvement in dissolution of the API. Laine and co-workers demonstrated that incorporation of HPMCAS during loading of celecoxib onto mesoporous silica substantially improved both the *in vitro* and *in vivo* performance of this poorly soluble API (Laine, 2016). In the current study, we have not only demonstrated a marked improvement in dissolution of the BCS II compound, glibenclamide, by the co-incorporation approach, but have additionally proposed a mechanistic hypothesis of how this enhanced performance is achieved.

##### 4.1. Understanding the effect of adsorption onto mesoporous silica on release in a transfer experiment

In the current study, a successful conversion of glibenclamide to the amorphous form after loading onto mesoporous silica was confirmed with XRPD. This conversion led to 25-fold supersaturation during FaSSiF mini-dissolution (Figs 2b and 5). Given the instability of the supersaturated state, the system rapidly precipitated and returned to its thermodynamic solubility, in line with previous studies with mesoporous silica (McCarthy, 2016; Laine, 2016; Price et al., 2019). Although precipitation was observed in the single-medium FaSSiF dissolution test, the full effect of precipitation on the overall performance was only realized by considering transfer dissolution data. In these experiments, no dissolution of crystalline glibenclamide (i.e. pure API) was observed in SGF, because its thermodynamic solubility is below the limit of detection at this pH. By contrast, in the transfer dissolution of the supersaturating silica formulation, API was detected in the SGF phase, suggesting that supersaturation occurred (Fig. 7). This supersaturation of API in the SGF portion of the assay allowed precipitation to commence, along with the generation of seed crystals. This resulted in significantly poorer dissolution performance of the API-silica formulation in the FaSSiF portion of the experiment, relative to the single-medium approach (Fig. 7). Therefore, one should consider the effect of transfer from the stomach to the intestine when assessing the dissolution performance of supersaturating formulations, especially mesoporous silica-based formulations.

##### 4.2. Application of HPMCAS as a precipitation inhibitor: blending vs. co-incorporation

For the current study, HPMCAS was selected as model precipitation inhibitor. HPMCAS is a well-established PI and has a track record in the literature of successfully sustaining supersaturated solutions for a range of APIs (Warren, 2010; Price, 2018; Laine, 2016; Udea, 2015).

From a practical perspective, the co-incorporation of precipitation inhibitor in the same formulation step is appealing, however, one potential concern for the co-incorporation approach is the accessibility of the pores for the API so that adsorption and nanoconfinement can still occur (Laine, 2016). Encouragingly, co-incorporating HPMCAS with glibenclamide onto mesoporous silica successfully converted the solid-state form of the API from the crystalline to the amorphous phase. This is in line with previous experience with celecoxib (Laine, 2016). Previous literature, which describes the incorporation of a polymer into the loading process as a “co-load” might infer the adsorption of the polymer inside the porous network. However, the molecular weight of the HPMCAS polymer used is approximately 18,000 Da. This is 36-times larger than the API, glibenclamide, which has a molecular weight of 484 Da. Given the very small size of the pore, 6 nm in diameter, it is highly unlikely that the polymer is actually co-loaded inside the pore. Further, the particles in samples where HPMCAS has been incorporated into the formulation appear to be larger and different in shape than API-loaded silica samples without HPMCAS (Fig. 3) data confirmed that these plate-like particles were composed of carbon and, therefore, it was concluded that the plate-like particles were comprised of HPMCAS.

The next important consideration, on the location of the API within the formulation, was addressed with EDX spectroscopy. EDX is a useful tool to envisage the distribution of a drug within a formulation. In the samples where HPMCAS was incorporated during the drug loading step, it was observed that drug was adsorbed onto the mesoporous silica particles and partly within the HPMCAS plate. Crucially, there was no API observed outside of these newly present HPMCAS plates. Therefore, it was concluded that co-incorporating the PI resulted in a solid dispersion of glibenclamide as the loaded silica. This appears to be the first example of such a solid dispersion in the literature. Given the novelty of this system, further work should be carried out to investigate the solid-state stability of the amorphous API in the system, which is an essential consideration for amorphous formulations (Ditzinger, 2018). Specifically, future work is planned to assess the amorphous stability of the API in the formulation, in line with the ICH Q1 conditions for accelerated stability.

Neither the formulation in which HPMCAS was incorporated during the loading step nor the sample where it was added post-loading was able to capture the extremely high 25-fold supersaturation generated by simply loading the drug onto the silica. However, it has often been observed that the efficiency of precipitation inhibition is not able to capture the full supersaturation potential generated by the enabling formulation alone (Price, 2018; Price et al., 2019). In spite of this, it was observed that when HPMCAS was incorporated during rather than after the drug loading step, the dissolution profile was much higher. Addition of HPMCAS post-loading improved the performance of glibenclamide loaded silica during both single-medium and transfer dissolution experiments, but there was some evidence of re-crystallization, suggesting that in a simple physical mixture HPMCAS is not able to completely inhibit precipitation. Indeed, incorporating the HPMCAS during the drug loading step demonstrated a 3-fold enhancement in dissolution performance compared to the simple physical mixture (Figs. 6 and 7). Such an improved precipitation inhibition effect could be related to the formation of drug polymer interactions already in the solid-state, which appears to be crucial for maximum precipitation inhibition (Price, 2018). This was supported by solid-state NMR data, in which a peak-shift was observed for co-incorporated formulations but not for other samples (Fig. 10). Although the peak-shift was small (0.2–0.3 ppm), it was consistently observed for different batches. Alternative



methods for obtaining information about drug-polymer interaction, for example 2D NOESY NMR, were unsuccessful because sufficiently concentrated solutions of drug-polymer could not be achieved. Another potential mechanism for enhanced precipitation inhibition in the formulation in which HPMCAS was incorporated during the drug loading step is the generation of an increased viscosity in the microenvironment surrounding the dissolving plates in FaSSiF. Such an increased viscosity would decrease the diffusion time out of the formulation and allow drug and polymer to remain in close proximity, both of which have been shown to be crucial factors in nucleation time in the presence of precipitation inhibitors (Price, 2018; Warren, 2010). However, further work would be required to fully confirm this hypothesis.

During the transfer experiment, it was observed that the HPMCAS plates do not disperse in SGF (Fig. 8). This is a significant benefit, given that the HPMCAS plates did not break down, the API-loaded silica remained immobilized and API could not be released from the silica. Therefore, the formation of seed crystals in SGF was prevented. Ultimately, this has a significant effect on the dissolution performance and provides an additional mechanism by which formulations with HPMCAS incorporated during the drug loading step can improve dissolution performance. In addition, it is interesting to observe that a change in manufacturing process - without a change in the qualitative and quantitative composition of the formulation - can introduce new properties to the product. By incorporating the HPMCAS during the loading step rather than post-loading, premature release of the drug from the formulation was circumvented without the need to add extra excipients, coating processes or special capsules, which are typically otherwise required (Qiu and Lee, 2017). This property should be especially advantageous in the delivery of poorly soluble basic compounds, whose premature release and supersaturation in the stomach (due to ionization in acidic conditions) with subsequent precipitation in the intestine could be avoided. Although Van Speybroeck and colleagues described an improved oral absorption of itraconazole loaded silica in rats, they found that silica formulations with post-loading incorporation of HPMCAS were unable to prevent the release of API in the stomach and therefore absorption was reduced (Van Speybroeck, 2010). The potential for incorporation of HPMCAS during the drug loading step on the dissolution performance of poorly soluble weak base drugs should be further explored.

#### 4.3. Co-incorporated formulations: just a solid dispersion?

Given the improvement of the formulation performance when HPMCAS was incorporated during the loading step rather than post-loading, it was important to rule out that a simple solid dispersion was formed directly, and that the silica in the formulation plays an

important role in the dissolution enhancement. EDX indicates that the drug is localized in the silica particles and on the HPMCAS plate when the polymer is incorporated during the loading step (Fig. 3, bottom panel), but is distributed freely throughout the entire sample when no silica is present (Fig. 5). The results suggest that drug is confined within the mesoporous silica particles, which are in turn were immobilized in the polymer platelets when HPMCAS is incorporated in the drug loading step. Without the nanoconfinement effects of the silica (Ditzinger, 2018), the drug can re-crystallize, as observed in the XRPD (Fig. 7). Ultimately, this resulted in the control sample showing no improvement in FaSSiF dissolution versus crystalline API (Fig. 6). Furthermore, if a portion of the sample was able to remain amorphous in the polymer platelets, the absence of drug-polymer interaction (as shown in the solid-state NMR spectra) would reduce the precipitation inhibition effect of the polymer (Fig. 10).

## 5. Conclusions

A novel co-incorporated formulation of glibenclamide and the precipitation inhibitor, HPMCAS, onto mesoporous silica is described. By co-incorporating the precipitation inhibitor, the formulation significantly outperformed the commonly applied simple physical blend, regarding improved supersaturation and dissolution in both single-medium FaSSiF and transfer dissolution assays. Furthermore, the co-incorporation approach allows the removal of a time-consuming and inefficient blending step. To provide a physical mechanistic basis for the improved performance the co-incorporated formulation, a range of spectroscopic tools were utilized. It was concluded that the improved dissolution performance is a synergistic effect related to two key factors: formation of drug-polymer interactions in the solid state, and lack of release and premature precipitation under gastric conditions due to the immobilization of API-loaded silica particles within the enteric HPMCAS plates. Crucially, both of these properties are absent in a simple HPMCAS blend. Ultimately, the co-incorporation of precipitation inhibitors with the API on mesoporous silica formulations has the potential to improve both the process and formulation efficiency in the development of poorly soluble drugs.

## Acknowledgements

The authors would like to thank Dr. Dieter Lubda, Dr Gudrun Birke and Dr. Finn Bauer for providing the Parateck SLC® and for helpful and constructive discussions and feedback.

This work has received funding from the European Union's Horizon 2020 research and innovation programme under grant agreement No. 674909 (PEARRL). [www.pearrl.eu](http://www.pearrl.eu)

## Supplementary materials

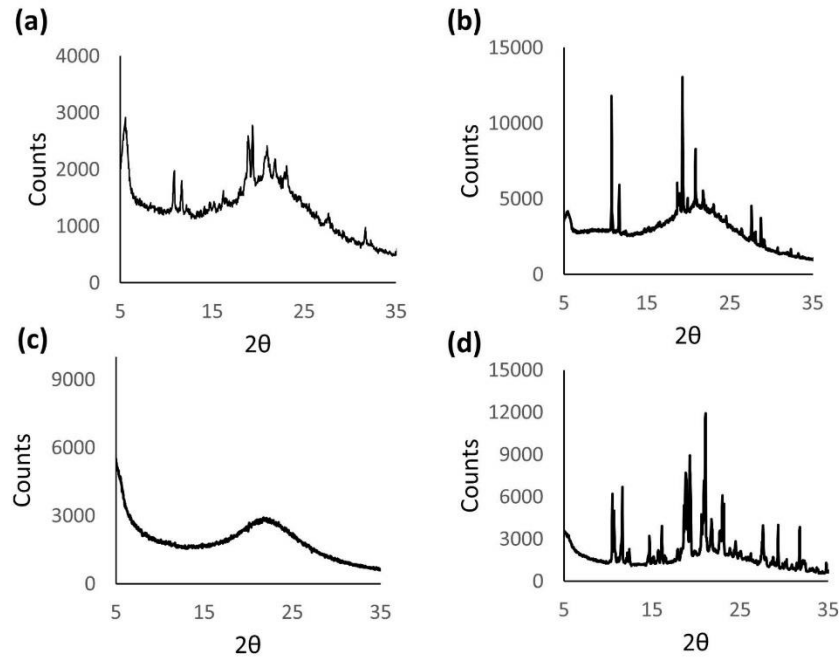
Supplementary material associated with this article can be found, in the online version, at [doi:10.1016/j.ejps.2019.105113](https://doi.org/10.1016/j.ejps.2019.105113).

## Appendix 1: thermodynamic solubility values For glibenclamide

| Appendix 1, Table 1. glibenclamide thermodynamic solubility values |                    |
|--|--------------------|
| Medium   | Solubility (µg/mL) |
| FaSSiF   | 8.1 ± 0.1          |
| SGF  | <LOD*              |

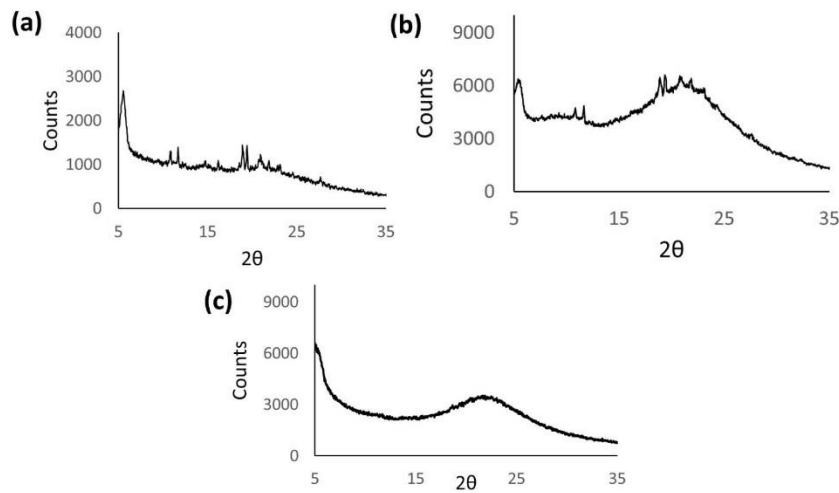
Appendix 2: Post-FaSSIF dissolution XRPD

**Appendix 2.** XRPD patterns for post-FaSSIF dissolution residues for (a) glibenclamide loaded silica, (b) glibenclamide loaded silica + HPMCAS blend, (c) glibenclamide and HPMCAS co-incorporated silica and (d) glibenclamide and HPMCAS prepared by rotary evaporation (control)

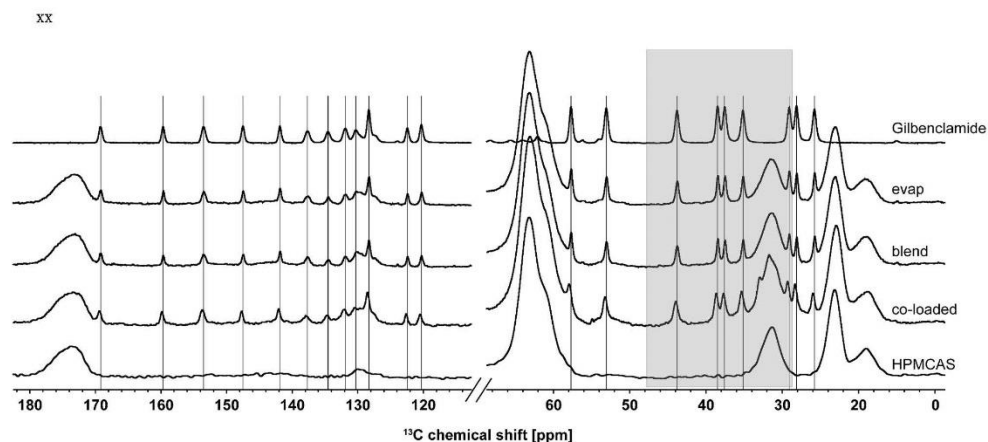


Appendix 3: Post-SGF transfer dissolution XRPD patterns

**Appendix 3.** XRPD pattern for Glibenclamide loaded silica (a), glibenclamide loaded silica + HPMCAS blend (b) and GB/HPMCAS co-incorporated silica (c) residues post-SGF transfer dissolution **Appendix 4. SS-NMR spectra**



**Appendix 4: Full solid-state NMR spectra for all samples showing peak shift in co-incorporated samples. The section highlighted corresponds to the section included in the main body of text**





## References

- Ditzinger, F., et al., 2018. Lipophilicity and hydrophobicity considerations in bio-enabling oral formulations approaches—a PEARRL review. *J. Pharm. Pharmacol* Epub ahead of print.
- Galla, E., Nicolaidis, E., Hörter, D., Löbenberg, R., Reppas, C., Dressman, J.B., 1998. Evaluation of various dissolution media for predicting in vivo performance of class I and class II drugs. *Pharm. Res.* 15, 698–705. <https://doi.org/10.1111/jphp.12465>.
- Knapik, J., 2016. Stabilization of the amorphous ezetimibe by confining its dimension. *Mol. Pharm.* 13 (4), 1308–1316.
- Krishnalakshmi, Y.S.R., 2010. Pharmaceutical technologies for enhancing oral bioavailability of poorly soluble drugs. *J. Bioequivalence Bioavailability* 2, 28–36.
- Laine, A., et al., 2016. Enhanced oral delivery of celecoxib via the development of a supersaturable amorphous formulation utilising mesoporous silica and co-loaded HPMCAS. *Int. J. Pharm.* 512 (1), 118–125. <https://doi.org/10.1016/j.ijpharm.2016.08.034>.
- Lofsson, T., Brewster, M.E., 2010. Pharmaceutical applications of cyclodextrins: basic science and product development. *J. Pharm. Pharmacol.* 62, 1607–1621. <https://doi.org/10.1111/j.2042-7158.2010.01030.x>.
- McCarthy, C.A., et al., 2016. Mesoporous silica formulation strategies for drug dissolution enhancement: a review. *Exp. Op. Drug Deliv.* 13, 93–108. <https://doi.org/10.1517/17425247.2016.1100165>.
- O'Shea, J.P., et al., 2016. Mesoporous silica-based dosage forms improve release characteristics of poorly soluble drugs: case example fenofibrate. *J. Pharm. Pharmacol.* 68 (5), 634–645.
- Price, D.J., et al., 2018. Approaches to increase mechanistic understanding and aid in the selection of precipitation inhibitors for supersaturating formulations: A PEARRL review. *J. Pharm. Pharmacol.* <https://doi.org/10.1111/jphp.12927>. Epub ahead of print.
- Price, D.J., et al., 2019. Calculation of drug-polymer mixing enthalpy as a new screening method of precipitation inhibitors for supersaturating pharmaceutical formulations. *EJPS* 142–156.
- Qiu, Y., Lee, P.I., 2017. Rational design of oral modified-release drug delivery systems. in: *Developing solid oral dosage forms*. Pharm. Theory Pract. 519–554.
- Udea, K., et al., 2015. Equilibrium state at supersaturated drug concentration achieved by hydroxypropyl methylcellulose acetate succinate: molecular characterization using <sup>1</sup>H NMR technique. *Mol. Pharm.* 12 (4), 1097–1104.
- Van Speybroeck, M., et al., 2010. Combined use of ordered mesoporous silica and precipitation inhibitors for improved oral absorption of the poorly soluble weak base itraconazole. *Eur. J. Pharm. Biopharm.* 75 (3), 354–365.
- Warren, D.B., et al., 2010. Using polymeric precipitation inhibitors to improve the absorption of poorly water-soluble drugs: A mechanistic basis for utility. *J. Drug Targ.* 18 (10), 704–731. <https://doi.org/10.3109/1061186X.2010.525652>.
- Zheng, W., et al., 2012. Selection of oral bioavailability enhancing formulations during drug discovery. *Drug Dev. Ind. Pharm.* 38 (2), 235–247.



Article

# Opportunities for Successful Stabilization of Poor Glass-Forming Drugs: A Stability-Based Comparison of Mesoporous Silica Versus Hot Melt Extrusion Technologies

Felix Ditzinger <sup>1,2,†</sup> , Daniel J. Price <sup>3,4,†</sup>, Anita Nair <sup>3</sup>, Johanna Becker-Baldus <sup>5</sup>, Clemens Glaubitz <sup>5</sup>, Jennifer B. Dressman <sup>4</sup>, Christoph Saal <sup>3</sup> and Martin Kuentz <sup>2,\*</sup> 

<sup>1</sup> Department of Pharmaceutical Sciences, University of Basel, 4056 Basel, Switzerland; felix.ditzinger@fhnw.ch

<sup>2</sup> Institute of Pharma Technology, University of Applied Sciences and Arts Northwestern Switzerland, 4132 Muttenz, Switzerland

<sup>3</sup> Merck KGaA, 64293 Darmstadt, Germany; daniel-joseph.price@merckgroup.com (D.J.P.); anita.nair@merckgroup.com (A.N.); Christoph.Saal@merckgroup.com (C.S.)

<sup>4</sup> Institute of Pharmaceutical Technology, Goethe University, 60438 Frankfurt, Germany; dressman@em.uni-frankfurt.de

<sup>5</sup> Institute for Biophysical Chemistry & Centre for Biomolecular Magnetic Resonance, Goethe University, 60438 Frankfurt, Germany; j.baldus@em.uni-frankfurt.de (J.B.-B.); Glaubitz@chemie.uni-frankfurt.de (C.G.)

\* Correspondence: martin.kuentz@fhnw.ch; Tel.: +41-61-228-56-42

† These authors contributed equally to this work.

Received: 25 September 2019; Accepted: 1 November 2019; Published: 4 November 2019



**Abstract:** Amorphous formulation technologies to improve oral absorption of poorly soluble active pharmaceutical ingredients (APIs) have become increasingly prevalent. Currently, polymer-based amorphous formulations manufactured by spray drying, hot melt extrusion (HME), or co-precipitation are most common. However, these technologies have challenges in terms of the successful stabilization of poor glass former compounds in the amorphous form. An alternative approach is mesoporous silica, which stabilizes APIs in non-crystalline form via molecular adsorption inside nano-scale pores. In line with these considerations, two poor glass formers, haloperidol and carbamazepine, were formulated as polymer-based solid dispersion via HME and with mesoporous silica, and their stability was compared under accelerated conditions. Changes were monitored over three months with respect to solid-state form and dissolution. The results were supported by solid-state nuclear magnetic resonance spectroscopy (SS-NMR) and scanning electron microscopy (SEM). It was demonstrated that mesoporous silica was more successful than HME in the stabilization of the selected poor glass formers. While both drugs remained non-crystalline during the study using mesoporous silica, polymer-based HME formulations showed recrystallization after one week. Thus, mesoporous silica represents an attractive technology to extend the formulation toolbox to poorly soluble poor glass formers.

**Keywords:** glass forming ability; hot melt extrusion; mesoporous silica; amorphous stability; supersaturation

## 1. Introduction

The increasing prevalence of poorly water-soluble drugs has driven the field of pharmaceutical technology to develop modern approaches for formulation development. A well-established technique is to formulate the drug in an amorphous form, which results in an increase in apparent solubility, dissolution performance, and subsequent oral bioavailability [1,2]. However, such an approach comes



with difficulties related to thermodynamic instability of the amorphous state, which can lead to recrystallization and thus negation of the aforementioned formulation advantages [3].

To give guidance on the recrystallization tendency of drugs, Baird et al. developed a classification system based on a molecule's "glass forming ability" (GFA). The GFA is related to recrystallization behavior from super cooled melts [4–6]. Three classes of substances were defined: class one (GFA-I) drugs recrystallize upon cooling from the molten state, class two (GFA-II) drugs recrystallize after a heating–cooling–heating cycle, and class three (GFA-III) drugs remain amorphous throughout the entire experiment. Although the classification was developed for undercooled melts, which can be directly related to hot melt extrusion (HME), it has proven to be accurate for solvent evaporation processes as well [7]. This is a particularly relevant consideration for mesoporous silica systems, given that drug loading is driven by solvent penetration into pores and subsequent evaporation [8].

GFA-I compounds, poor glass formers, are particularly prone to recrystallization in amorphous formulations [9]. One strategy to tackle this instability is to combine the drug with a polymer in an amorphous solid dispersion. A very common technique to manufacture amorphous solid dispersions is HME [10,11]. In this process, polymer and API are mixed in the molten state to form an extrusion strand, which is further processed into a solid dosage form, e.g., tablet or a capsule.

Another approach is to formulate GFA-I drugs with mesoporous silica. This is of particular interest due to the high stability of the amorphous API once it has been loaded into the porous network of the silica. This enhanced stability is related to nano-confinement in the meso-scale pores, which by definition range from 2–50 nm [12,13]. Stability is further improved with complementary pore-API interactions that lower the free energy of the system [14]. Muller and co-workers demonstrated amorphous stability at ambient and accelerated conditions for 30 different mesoporous silica formulations [15]. One key consideration for mesoporous silica formulations is the location of the API within the sample. For GFA-I compounds, it is essential that the loading process is carried out carefully, avoiding oversaturation of the silica, to ensure the drug is loaded within the pores and not on the outer surface. GFA-I compounds adsorbed on the outer surface are prone to rapid crystallization, which can be observed with techniques such as differential scanning calorimetry (DSC) and powder X-ray diffraction (PXRD). However, upon successful loading of the drug in the internal porous network, silica formulations can provide a viable alternative for drugs that fail to form a stable amorphous formulation in classical solid dispersions [16–18]. Although amorphous stability in mesoporous silica has been previously described, there has been no comparison on stability of poor glass formers in HME and mesoporous silica technology published to date.

Certainly, solid-state stability is not the only important formulation consideration for poorly soluble drugs that are also poor glass formers. It is also essential to consider stability of the supersaturation generated upon dissolution. Indeed, recent work has demonstrated that, due to their high propensity for recrystallization, poor glass formers may also have issues with rapid onset of precipitation upon release, thus limiting their therapeutic potential [19]. This is in line with the well-established "Spring and Parachute" model [20], which identifies the need for additional excipients to sustain supersaturation of APIs in solution [21]. For polymer-based solid dispersions, the polymer may be able to meet both requirements: suspending the drug in an amorphous form and inhibiting precipitation from the supersaturated state. An example of such a polymer is polyvinyl alcohol that is interesting due to its low hygroscopicity and for which a special grade has been introduced recently for HME [22]. Unlike polymer-based solid dispersions, the ability of mesoporous silica to inhibit precipitation of the supersaturated API is limited. Therefore, it is often necessary to incorporate precipitation inhibitors into mesoporous silica formulations [23].

In this study, the amorphous stability of two model poor glass formers, haloperidol and carbamazepine, formulated as HME and with mesoporous silica, was investigated in line with ICH Q1 accelerated stability conditions [24] over three months. The stability was monitored by means of PXRD and underscored with DSC measurements of the samples before and at the end of the study. To the best of our knowledge, such a comparative study has not been reported previously. This

stability comparison was complemented by non-sink release testing in biorelevant media [25,26] to monitor drug release and dissolution throughout the study [23,27]. It is important to note that non-sink dissolution was not used as a direct comparison between the two formulations, as the mesoporous formulations do not inhibit precipitation upon release. Rather, the release curves are demonstrative of the decrease in dissolution performance that can be observed upon solid-state transformation. Finally, solid-state nuclear magnetic resonance (SS-NMR) spectroscopy was applied to investigate any qualitative changes drug–polymer spectra in HME formulations over the duration of the stability study [28].

From a practical perspective, both drugs have no thermal instability, which avoids the risk of heat-induced degradation during the HME process [29,30]. The drug load selected for the technology comparison was the highest amount that enabled initial amorphous loading for both HME and mesoporous silica formulations, so that a direct comparison between techniques could be attained.

It was hypothesized that mesoporous silica formulations of haloperidol and carbamazepine would show enhanced solid-state stability over time compared to solid dispersion obtained from HME.

## 2. Materials and Methods

### 2.1. Materials

Haloperidol, carbamazepine, HPLC grade acetonitrile, and HPLC grade methanol were purchased from MilliporeSigma (Darmstadt, Germany). Parateck MXP<sup>®</sup> (PVA) and Parateck SLC<sup>®</sup> were kindly provided by Merck KGaA (Darmstadt, Germany). FaSSGF/FaSSIF/FeSSIF powder to make biorelevant dissolution medium, Fasted Simulated Intestinal Fluid (FaSSIF), was obtained from Biorelevant (Biorelevant.com, London, UK).

### 2.2. Methods

#### 2.2.1. Thermodynamic Solubility Determination

FaSSIF was prepared by weighing 45 mg of FaSSGF/FaSSIF/FeSSIF powder into 45 mL of phosphate buffer (pH 6.5) [31]. API (2–3 mg) was accurately weighed into a Uniprep<sup>®</sup> syringeless filter (5 mL; 0.45  $\mu$ m). 2 mL of FaSSIF was added and the samples were agitated at 450 rpm for 24 h at 37 °C. The pH was checked at 7 h and adjusted with 0.1 N NaOH or 0.1 N HCl, if a deviation greater than  $\pm 0.05$  pH units was observed. The final pH was also recorded after 24 h.

Samples were filtered into the inner chamber of the Uniprep through the built-in PTFE 0.45  $\mu$ m Whatman filter after 24 h. Filtrates were immediately diluted with acetonitrile and water (1:4 *v/v*) to avoid precipitation from the saturated solution. Samples were analyzed with UHPLC (Thermo Dionex Ultimate 3000, Thermo Fisher, Waltham, MA, USA) to determine the API concentration. API concentration was determined based on a standard calibration curve of nine standard concentrations (50, 30, 10, 5, 3, 1, 0.5, 0.3, 0.1  $\mu$ g/mL). Three control samples of known concentrations (30, 3, 0.3  $\mu$ g/mL) were prepared and used to check the robustness of the calibration curve. The determination was carried out in duplicate.

#### 2.2.2. Ultra-High Performance Liquid Chromatography (UHPLC)

UHPLC analysis was performed using a Thermo Dionex Ultimate 3000 (Thermo Fisher, Waltham, MA, USA) equipped with a diode array detector at 282 nm for carbamazepine and 247 nm for haloperidol (Thermo Fisher, Waltham, MA, USA). The separation was achieved on an Acquity UPLC BEH column C8 (2.1  $\times$  50 mm, 1.7  $\mu$ m, Waters, Milford, MA, USA). The mobile phases A and B consisted of water:formic acid 999:1 (*v/v*) and acetonitrile:formic acid 999:1 (*v/v*), respectively. Gradient and flow rate is shown in Table 1. System management, data acquisition and processing were based on the Chromeleon<sup>™</sup> software package, version 7.2 (Thermo Fisher, Waltham, MA, USA).

Table 1. UHPLC gradient and flow rates.

| Time (min) | Flow Rate (mL/min) | % (v/v) Mobile Phase A | % (v/v) Mobile Phase B |
|------------|--------------------|------------------------|------------------------|
| 0.00       | 0.83               | 90                     | 10                     |
| 0.83       | 0.83               | 10                     | 90                     |
| 1.20       | 1.50               | 90                     | 10                     |
| 2.00       | 1.50               | 90                     | 10                     |
| 2.01       | 0.83               | 90                     | 10                     |

### 2.2.3. Preparation of Hot Melt Extrudates

PVA was selected as an optimal polymer for hot-melt extrusion. This was based on three factors: (1) the grade of PVA was specifically designed for optimal HME due to particle size distribution and viscosity, (2) consideration of partial solubility parameters for both drugs, and PVA (3) low hygroscopicity of PVA to reduce water uptake in of the extrudates.

Binary mixtures of polyvinyl alcohol (PVA, Parateck MXP<sup>®</sup>) and drug at various drug loadings were mixed in a mortar and extruded on a ZE9 ECO twin-screw extruder by ThreeTec (Birren, Switzerland) with 9 mm diameter and 180 mm length co-rotating screws. A screw speed of 80 rpm was applied at a temperature of 190 °C through all three heating zones, which is in accordance with recommendation by the polymer manufacturer [32]. After extrusion, the extrudates were ground in a mortar, and the fraction retained between mesh sizes 150 and 425 µm was retained for use in the study. The final extruded mixtures were cooled to room temperature and stored in falcon tubes. Mixing feasibility of the selected polymer for both drugs was verified by the Hansen solubility parameters [33,34], which were calculated using the quantitative structure property relationship (QSPR) method of the COSMOquick software (COSMOlogic, Leverkusen, Germany, Version 1.6) [35,36]. For the investigation of the formulations, a 7.5% (*w/w*) drug loading of haloperidol and 20% (*w/w*) was used for carbamazepine. This was selected on the basis of the highest drug load that was initially successful for both formulation technologies, and was the result of a formulation screening.

### 2.2.4. Preparation of API-Loaded Silica Formulations

Mesoporous silica formulations were prepared using the incipient wetness method [13]. API (3 g) was dissolved in acetone (300 mL; 10 mg/mL), which was added drop-wise at a rate of 0.5 mL/min to Parateck<sup>®</sup> SLC mesoporous silica (7 g), under constant stirring and heating at 60 °C. After complete addition of the concentrated API solution, the samples were dried overnight in a vacuum oven at 60 °C to ensure complete removal of the solvent. The formulations were prepared at a drug loading of 7.5% (*w/w*) for haloperidol and 20% (*w/w*) for carbamazepine.

### 2.2.5. Storage of Samples for Stability Studies

For storage of the samples in the stability study, each of the formulations was placed in a separate glass jar with a secure lid. A separate beaker containing saturated sodium chloride solution, also placed in the beaker, ensured a constant relative humidity of 75% in the surrounding environment [37]. This enclosed system was then placed in a stability cabinet set to 40 °C to obtain storage conditions in accordance with ICH Q1.

### 2.2.6. Powder X-Ray Diffraction (PXRD)

Samples were prepared between X-ray amorphous films and measured in transmission mode using Cu-Kα1-radiation and a Stoe StadiP 611 KL diffractometer (STOE & Cie GmbH, Darmstadt, Germany) in transmission mode equipped with Dectris Mythen1K PSD (DECTRIS Ltd., Baden-Daettwil, Switzerland). The measurements were evaluated with the software WinXPow 3.03 by Stoe (STOE & Cie GmbH, Darmstadt, Germany), the ICDD PDF-4+ 2014 Database (ICDD, Newtown Square, PA,



USA), and Igor Pro Version 6.34 (Wavemetrics Inc., Lake Oswego, OR, USA) Angular range: 1–40° 2 $\theta$ ; PSD-step width: 2° 2 $\theta$ ; angular resolution: 0.015° 2 $\theta$  measurement time: 15 s/step, 0.25 h overall.

#### 2.2.7. Non-Sink-Mini-Dissolution in FaSSiF

The equivalent of 5 mg API of extrudate or API-loaded silica was weighed into a glass vial. Five milliliters of FaSSiF was added. The vials were agitated at 37 °C and 450 rpm in a shaker (IKA-Werke GmbH & CO. KG, Staufen, Germany) for 120 min. Samples of 0.3 mL were taken at 2, 15, 60, 90, and 120 min, filtered (0.45 PTFE Whatman filters), diluted with acetonitrile and water, and analyzed by UHPLC. The mini-dissolution trials were conducted in duplicate for all samples.

#### 2.2.8. Scanning Electron Microscopy (SEM)

Samples were prepared on carbon tape and imaged using a TM3000 Tabletop Scanning Electron Microscope (Hitachi, Tokyo, Japan), tungsten source, using low vacuum and accelerating voltage of 5 and 15 kV. A 4-Quadrant BSE detector was used, and imaging was at a magnification between 15 $\times$  and 30,000 $\times$ .

#### 2.2.9. Differential Scanning Calorimetry (DSC)

Samples were assessed by differential scanning calorimetry on a DSC 3 (Mettler Toledo, Greifensee, Switzerland). An amount of 5 to 9 mg sample was placed in a 40  $\mu$ L aluminum pan with a pierced lid. A heating rate of 10 °C/min from 20 to 200 °C was applied under nitrogen purging at 200 mL/min. The thermograms were analyzed with the STARe Evaluation-Software Version 16 (Mettler Toledo, Greifensee, Switzerland).

#### 2.2.10. Solid-State Nuclear Magnetic Resonance (SS-NMR) Spectroscopy

SS-NMR experiments were conducted with magic-angle-sample (MAS) spinning using a Bruker 4 mm MAS HXY probe in double resonance mode with a Bruker Avance I 600 MHz wide bore NMR spectrometer (Bruker, Rheinstetten, Germany) with a 4 mm rotor. The readout on the probe thermocouple was set to 290 K. The sample spinning frequency was set to 10 kHz. All spectra were recorded with <sup>1</sup>H-<sup>13</sup>C-cross polarization (CP) using a contact time of 1 ms. 100 kHz high power proton decoupling following the SPINAL64 scheme was applied during acquisition. The recycle delay was 3 s. The spectra were indirectly referenced to 4,4-dimethyl-4-silapentane-1-sulfonic acid (DSS) via the CH<sub>2</sub> signal of Adamantane at 40.49 ppm.

### 3. Results

#### 3.1. Macro- and Microscopic Changes

Qualitative macroscopic differences were observed between the fresh and one-week stressed samples of the hot-melt extrudates (Figure 1). Extrudates of carbamazepine and haloperidol were transparent immediately after manufacturing. This indicates the presence of molecularly dispersed API throughout the polymer in the amorphous form [11]. However, after only 7 days exposure to 40 °C and 75% RH, both extrudates became opaque, indicating phase separation in the formulations [38]. This was in contrast to mesoporous silica formulations, in which no macroscopic differences were observed between the fresh and one-week stressed samples. Indeed, the appearance of mesoporous silica formulations remained consistent over the duration of the 3 month study.

Changes in the extrudate samples over time were also observed on a microscopic level in the SEM images. In freshly prepared formulations, the extrudates showed no heterogeneity but at the end of the stability study, after 90 days, phase separation and recrystallization were observed. API-loaded silica formulations, however, did not exhibit qualitative changes under either visual inspection or by SEM (Figure 2; Figure 3).

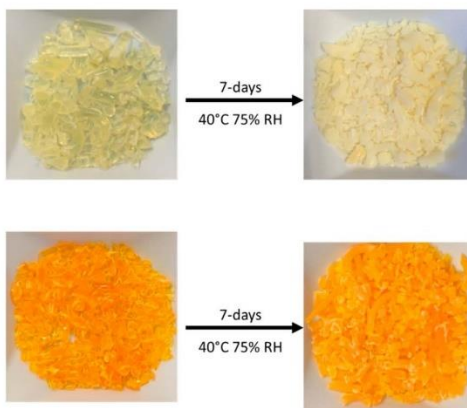


**Figure 1.** Haloperidol (top) and carbamazepine (bottom) hot melt extrusion (HME) before (left) and after (right) 7 days accelerated stability conditions as specified in the materials and methods section.

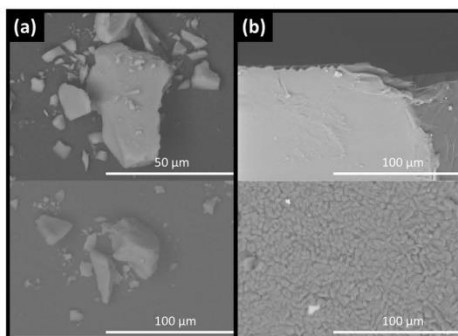


**Figure 2.** SEM images for carbamazepine loaded silica (a) and IIME (b) showing particle size and morphology at 0 days (top) and 90 days stability (bottom) as specified in the materials and methods section.

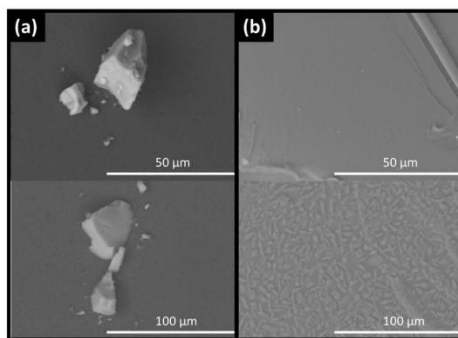


**Figure 3.** SEM images for haloperidol loaded silica (a) and IIME (b) showing particle size and morphology at 0 days (top) and 90 days stability (bottom) as specified in the materials and methods section.

### 3.2. Solid-State Stability of the Amorphous Form

Both haloperidol and carbamazepine were crystalline before formulation with either HME or mesoporous silica. The outcome of the empirical loading approach is shown in Table 2. For mesoporous silica, both APIs were successfully stabilized in the amorphous form at an initial concentration of 30% (*w/w*). However, HME was only successful in stabilizing amorphous API for carbamazepine at 20% (*w/w*) and haloperidol at 7.5% (*w/w*) (data not shown). At higher concentrations, the extrudates were crystalline upon cooling. Therefore, for the comparative accelerated stability study of the formulations a drug load of 20% (*w/w*) carbamazepine and 7.5% (*w/w*) haloperidol was selected for both the mesoporous silica and HME based solid dispersions. PXRD indicated that the initial form in both formulations was amorphous (Figure 4; Figure 5).

**Table 2.** Loading Capacities for Both Formulation Techniques.

| Formulation                 | Loading Content (%) ( <i>w/w</i> ) |             |             |           |
|-----------------------------|------------------------------------|-------------|-------------|-----------|
|                             | 30                                 | 20          | 15          | 7.5       |
| Haloperidol HME             | Crystalline                        | Crystalline | Crystalline | Amorphous |
| Haloperidol loaded silica   | Amorphous                          | Amorphous   | Amorphous   | Amorphous |
| Carbamazepine HME           | Crystalline                        | Amorphous   | Amorphous   | Amorphous |
| Carbamazepine loaded silica | Amorphous                          | Amorphous   | Amorphous   | Amorphous |

Differences between silica-based formulations and PVA extrudates were apparent after one month of storage at elevated temperatures, with both HME formulations showing development of crystallinity. The crystalline percentage increased month by month over the duration of the study (Figure 4; Figure 5).

Conversely, both API-loaded mesoporous silica formulations remained amorphous for the duration of the three-month stability study, with no evidence of crystallinity in the PXRD patterns (Figure 4; Figure 5).

These findings were underscored by the absence of melting endotherms in the DSC thermograms of the silica-based formulations after 90 days [39]. By contrast, melting peaks were observed in both samples of the extruded formulations after 90 days, indicating the presence of drug crystallinity (data not shown).

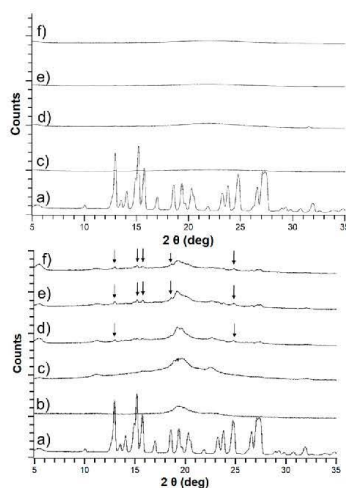


**Figure 4.** Powder X-ray (PXRD) patterns for carbamazepine loaded silica (top) and carbamazepine HME (bottom) showing crystalline carbamazepine (a), pure Parateck MXP® (PVA) (b), unstressed carbamazepine formulation (c) and stressed carbamazepine formulations at 30 (d), 60 (e), and 90 (f) days. The arrows indicate crystalline peaks in the diffractograms.



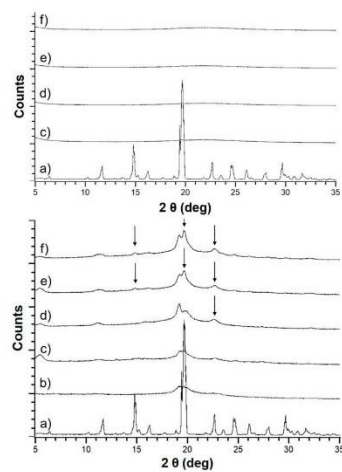


**Figure 5.** PXRD patterns for haloperidol loaded silica (top) and haloperidol HME (bottom) showing crystalline haloperidol (a), pure PVA (b), unstressed haloperidol formulation (c) and stressed haloperidol formulations at 30 (d), 60 (e), and 90 (f) days. The arrows indicate crystalline peaks in the diffractograms.

Although there were no pronounced drug–polymer interactions detectable in the SS-NMR spectroscopy for carbamazepine and haloperidol HME, it was possible to observe qualitative differences before and after storage of the samples at 45 °C/70% RH. Specifically, the freshly prepared samples had broad peaks in the spectra, related to the amorphous state of the sample. By contrast, an increased fine structure observed in the NMR-spectra at the end of the study indicated an increase in crystallinity. This was especially pronounced for haloperidol, with the stressed sample exhibiting peaks corresponding to the crystalline pure drug (Figure 6c) at 118, 153, and 200 ppm in Figure 6a.

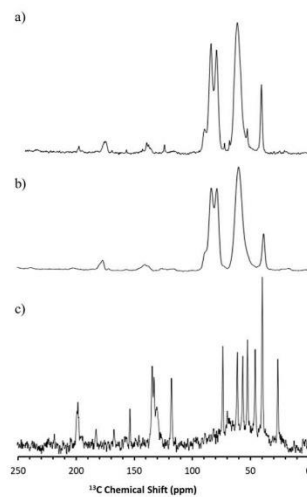


**Figure 6.**  $^{13}\text{C}$  Solid-state nuclear magnetic resonance spectroscopy (SS-NMR) spectra for crystalline haloperidol (c), HME formulation at 0 days (b) and 90 days (a).

For carbamazepine, the change was more subtle, because of overlapping peaks. However, it was obvious that the stressed sample exhibited crystalline peaks that were not observed in the freshly prepared samples e.g., at 131 ppm, as shown in Figure 7. The presence of sharper peaks in the stressed samples underscores the recrystallization in the formulations suggested by the X-ray diffraction data.

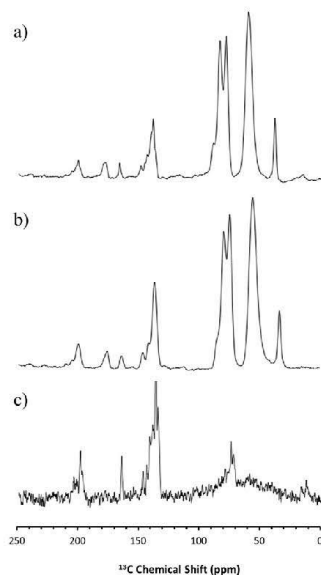


**Figure 7.**  $^{13}\text{C}$  SS-NMR spectra for crystalline carbamazepine (c) and carbamazepine HME formulation at 0 days (b) and 90 days (a).

### 3.3. Stability of the Supersaturated State in FaSSiF

The thermodynamic solubility of haloperidol and carbamazepine in FaSSiF was measured to be  $259 (\pm 1) \mu\text{g/mL}$  and  $203 (\pm 2) \mu\text{g/mL}$ . Accordingly, the crystalline APIs showed a dissolution profile approaching these values over the course of the FaSSiF dissolution experiment.

Although both drugs have some solubility in FaSSiF, the dissolution was enhanced by both the mesoporous silica and HME formulations. For carbamazepine, a maximum supersaturation of 1.8 and 1.5-fold was generated for the silica and HME formulations, respectively. For haloperidol, a maximum supersaturation of about 2.0-fold was generated for both silica and HME.

The PVA in the HME formulation was able to sustain supersaturated concentrations for both APIs by inhibiting precipitation from aqueous medium. Mesoporous silica, on the other hand, was unable to inhibit drug precipitation from the supersaturated state and therefore, precipitation was observed for both APIs, with concentrations returning to the thermodynamic solubility. For mesoporous silica formulations, further development of the formulation would include a screening and a selection of a precipitation inhibitor to include in the formulation. The precipitation inhibitor would prevent the precipitation of the supersaturated API and could subsequently enhance oral absorption. However, although important, the precipitation inhibitor in a mesoporous silica formulation is not expected to impact on the solid-state stabilization of the API in the amorphous form. This is due to the fact that precipitation inhibitors are simply blended with the drug-loaded silica when the drug is already loaded onto the porous silica and stabilized in the solid state. Therefore, as the focus of this study was on the innate stabilization potential of mesoporous silica using poor glass formers, incorporation of a precipitation inhibitor was out of scope.

For both APIs, the dissolution profiles from mesoporous silica formulations were comparable throughout the duration of the entire accelerated stability study. Particularly notable was that the degree of supersaturation, or ‘spring’, remained consistent over the whole stability study (Figure 8; Figure 9). For HME formulations, the curves showed a decrease in supersaturation in each successive month of the stability study. After 30 days, the HME formulation containing carbamazepine was still able to generate supersaturation, but the profile was no longer stable; the carbamazepine concentration returned to the thermodynamic solubility within 60 min. This difference between fresh and 30 day carbamazepine samples was indicative of the presence of seed crystals in the formulations. Such seeds foster crystallization in the formulation as well as in solution to most likely override the inhibition of precipitation by the polymer [40]. Furthermore, the release performance of carbamazepine HME declined even further at 60 and 90 days. By 90 days, no supersaturation was observed at any measured time point during the experiment, and the dissolution curve resembled that of crystalline carbamazepine more closely (Figure 8).

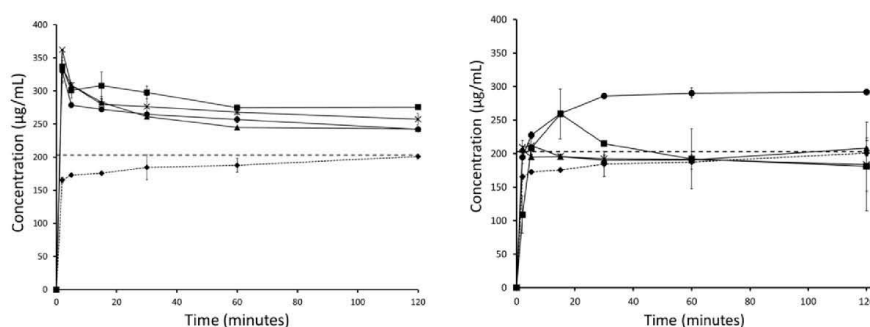


**Figure 8.** Fasted Simulated Intestinal Fluid (FaSSIF) mini-dissolution curves for carbamazepine loaded silica (left) and carbamazepine HME formulation (right) showing crystalline carbamazepine (◆), unstressed carbamazepine formulation (●), and stressed carbamazepine formulations at 30 (■), 60 (X), and 90 (▲) days.

Similar reductions in dissolution performance with storage were observed for the HME formulation of haloperidol. Although the dissolution performance of the haloperidol HME did not decline as quickly as that of the carbamazepine HME, its dissolution profile also resembled that of the crystalline API after 90 days (Figure 9).

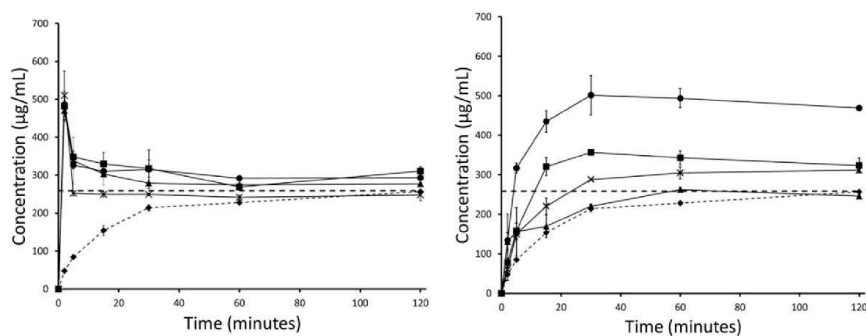


**Figure 9.** FaSSIF mini-dissolution curves for haloperidol loaded silica (left) and haloperidol HME formulation (right) showing crystalline haloperidol (◆), unstressed haloperidol formulation (●), and stressed haloperidol formulations at 30 (■), 60 (X), and 90 (▲) days.

#### 4. Discussion

Development of amorphous solid dispersions requires a thorough understanding of the factors that influence stability in the amorphous form. One such factor is the GFA. According to the classification system proposed by Baird et al. [4], GFA-I drugs are especially challenging when developing amorphous formulations, due to the high propensity for recrystallization of such compounds. It is essential to demonstrate good physical stability in amorphous formulations to ensure that recrystallization does not occur over time, as this would reduce the shelf life of the product [41]. As crystallization is based on the stochastic nucleation process, a lack of physical stability could lead to variable product quality among batches. Any initial crystallization in the batch, or differences in the rate of crystallization, could lead to out-of-specification results based on insufficient drug product performance, for example in dissolution testing. Variability among batches would thus be problematic in terms of meeting regulatory and commercial requirements. Herein, it has been demonstrated that mesoporous silica can be used to successfully stabilize compounds of poor amorphous stability that are unsuitable for formulation in standard polymer-based amorphous solid dispersions.

Initial formulation development demonstrated the potential impact that such a poor amorphous stability could have on the viability of a formulation. For both HME formulations, significantly lower percentage drug loads were attainable in the initial formulation development. This is a crucial topic for the development of amorphous formulations. Taking the example of haloperidol, it was only possible to stabilize 7.5% (*w/w*) of the API in the amorphous form in the HME. Assuming a theoretical dose of 200 mg, one would require a tablet of approximately 2.6 g in weight to incorporate the entire dose in a single dosage form. Furthermore, this represents a very conservative estimation, as the actual API content would likely be reduced further to 3.75% when one considers that 50% of the tablet may consist of fillers, binders, glidants, and disintegrants. Ultimately, a low drug loading would be a substantial risk to the viability of the formulation, and could result in failure of the project. Mesoporous silica, however, was successful in stabilizing more reasonable drug loads in non-crystalline form.

Furthermore, the successful low drug loading HME formulations developed for carbamazepine and haloperidol were observed to be unstable during the ICH Q1 stability study (Figure 4; Figure 5). Instability in polymeric amorphous solid dispersions can be linked with increasing temperature and humidity. As temperature or water content in amorphous formulations increases, mobility of the drug within the polymer dispersion increases. Mehta and co-workers demonstrated this effect on model amorphous solid dispersions (ASDs). In their study, an increase in molecular mobility of all APIs in the polymer ASDs led to a decrease in recrystallization time [41,42]. As both studies by Mehta and colleagues investigated the physical stability of good to moderate glass formers (GFA-II/III), it is likely that the effect of moisture and temperature on increasing molecular mobility and subsequent physical instability would be even greater for GFA-I compounds. The observed instability of these poor glass formers is even more remarkable when one considers that, of the available polymers for HME, PVA has a substantially low hygroscopicity. This low hygroscopicity would have a stabilizing effect on the formulation due to a reduction in the uptake of water upon storage at humid conditions. However, this beneficial characteristic of PVA was not enough to prevent the poor glass formers from recrystallizing in the extrudates [32].

For mesoporous silica, however, molecular mobility is greatly reduced regardless of moisture or temperature. Brás and colleagues demonstrated that adsorption and nano-confinement of ibuprofen onto mesoporous silica resulted in a significant reduction of all known types of molecular mobility [43]. Most interestingly, the Johari–Goldstein  $\beta$  relaxation, a type of molecular mobility associated with recrystallization, was reduced. This was a crucial observation, as it has been shown that increased Johari–Goldstein relaxation is related to physical instability of the amorphous form [42,43]. Similar to the work by Mehta and colleagues, Brás et al. focused on good glass formers (GFA-III). Additional work demonstrated that a reduction in molecular mobility leads to successful stabilization of the very poor glass former menthol (GFA-I), which has a glass transition temperature of  $-54.3\text{ }^{\circ}\text{C}$  [44]. This stabilization was related to a decrease in molecular mobility of both  $\alpha$  (free transitional mobility in space)



and the aforementioned Johari–Goldstein  $\beta$  relaxations. Furthermore, a new type of molecular mobility, the S-type, was observed. S-type refers to mobility of a hindered molecule that is nano-confined within a single pore, and is much slower than standard molecular mobility events [44]. Based on these findings as well as those of our study (Figure 4; Figure 5), mesoporous silica may be a suitable way forward to stabilizing GFA-I glass formers under accelerated conditions.

There are only a handful of known GFA-I compounds that are also BCS II compounds and which would thus benefit from the apparent solubility increase of the amorphous form. In a recent review, Kawakami provided an overview of pharmaceutical compounds according to GFA classes [45]. Of the GFA-I compounds in the database only 29% were determined to be BCS II/IV, which is far lower than the commonly reported percentage of commercial compounds that fall into the poor solubility category (60%) [8]. Hence, there appears to be a disconnect between the prevalence of compounds with poor solubility and the occurrence of poor glass formers on the market. This could be related to the difficulty in formulating such compounds, and the reduction in formulation performance related to physical instability.

For the two model BCS II drugs selected in this study, clear differences were observed in the non-sink release profiles of loaded silica and HME formulations. As expected from the literature, silica alone was not able to sustain supersaturated concentrations of API in solution resulting in precipitation [23]. Conversely, in the HME formulations, the API is sustained in solution by the polymer itself, which can function not only as a matrix polymer but also as a precipitation inhibitor during drug release. However, it was observed that dissolution of API loaded silica formulations remained consistent throughout the 3 month study (Figure 8; Figure 9), whereas the kinetic release of HME formulations tended towards crystalline drug solubility (Figure 8; Figure 9). Here, we see the effect of phase separation and recrystallization on the dissolution performance of amorphous solid dispersions, with the presence of a crystalline phase reducing the achievable supersaturation and decreasing the dissolution performance of the compound [45]. Interestingly, both HME formulations retained some supersaturation after the first month of the stability study, indicating that full conversion from amorphous to crystalline had not yet occurred (Figure 8; Figure 9). However, the supersaturated solutions generated by the carbamazepine HME were less stable than those generated by the haloperidol HME, and precipitation occurred (Figure 8). This was related to the presence of seed crystals in the formulation, which sped up the rate of nucleation and reduced the ability of the polymer to prevent precipitation. Patel and co-workers demonstrated that a small amount of crystalline indomethacin significantly increased its recrystallization from the supersaturated state, even in the presence of precipitation inhibitors [40]. The present results support the view that GFA-I compounds may not be good candidates for formulation in polymeric amorphous solid dispersions, such as hot-melt extrudates, which have been investigated here. However, this is also expected by other formulations based on polymeric amorphous dispersions, e.g., spray dried dispersions or co-precipitates. Mesoporous silica, on the other hand, is an attractive formulation option for poorly soluble glass formers, generating consistent and supersaturated dissolution profiles.

## 5. Conclusions

The increasing prevalence of poorly soluble BCS II drug candidates in pharmaceutical development remains a challenging issue. Although polymer-based stabilization of the API in an amorphous form has been a common approach to their formulation for several decades. Such an approach may not be suitable for poorly soluble compounds that also show poor GFA. These compounds, which demonstrate both poor solubility and poor amorphous stability, are challenging for formulation with typical polymer-based technologies due to possible phase separation and recrystallization. Ultimately, these compounds may have an increased risk of failure during pharmaceutical development, as they constitute a risk from both a bioavailability and amorphous stability perspective. In this study, we demonstrated that poor glass forming (GFA-I) APIs have increased risk of recrystallization in polymer-based amorphous solid dispersions. By contrast, mesoporous silica was shown to provide

optimal stabilization for such APIs. Therefore, mesoporous silica could be an attractive formulation technology to expand the formulation toolbox for APIs that are poor glass formers. More research in the future will clarify whether mesoporous silica should become a method of choice for oral delivery of poorly soluble GFA-I compounds.

**Author Contributions:** Conceptualization, F.D., D.J.P. and M.K.; Funding acquisition, J.B.D., C.S. and M.K.; Investigation, F.D., D.J.P. and J.B.-B.; Methodology, F.D., D.J.P., A.N., C.S. and M.K.; Project administration, J.B.D., C.S. and M.K.; Resources, A.N. and C.S.; Software, F.D., D.J.P. and J.B.-B.; Supervision, A.N., C.G., C.S. and M.K.; Visualization, F.D. and D.J.P.; Writing—original draft, F.D. and D.J.P.; Writing—review & editing, F.D., D.J.P., A.N., J.B.-B., C.G., J.B.D., C.S. and M.K.

**Funding:** This project has received funding from the European Union’s Horizon 2020 Research and Innovation Program under grant agreement No 674909.

**Acknowledgments:** The authors like to thank Dieter Lubda, Gudrun Birke, Finn Bauer and Thomas Kipping for providing the ParTECK<sup>®</sup> excipients, for helpful and constructive discussions and feedback.

**Conflicts of Interest:** Daniel J. Price, Anita Nair and Christoph Saal are full-time employees of Merck KGaA. Otherwise, the authors report no conflict of interest. The studies were performed under the auspices of the EU grant, including all funding, and independent of the company.

## References

- Hancock, B.C.; Parks, M. What is the True Solubility Advantage for Amorphous Pharmaceuticals? *Pharm. Res.* **2000**, *17*, 397–404. [[CrossRef](#)]
- Leuner, C.; Dressman, J. Improving drug solubility for oral delivery using solid dispersions. *Eur. J. Pharm. Biopharm.* **2000**, *50*, 47–60. [[CrossRef](#)]
- Rams-Baron, M.; Jachowicz, R.; Boldyreva, E.; Zhou, D.; Jamroz, W.; Paluch, M. Physical Instability: A Key Problem of Amorphous Drugs. In *Amorphous Drugs*; Springer International Publishing: Cham, Switzerland, 2018; pp. 107–157.
- Baird, J.A.; Van Eerdenbrugh, B.; Taylor, L.S. A Classification System to Assess the Crystallization Tendency of Organic Molecules from Undercooled Melts. *J. Pharm. Sci.* **2010**, *99*, 3787–3806. [[CrossRef](#)] [[PubMed](#)]
- Alhalaweh, A.; Alzghoul, A.; Mahlin, D.; Bergström, C.A.S. Physical stability of drugs after storage above and below the glass transition temperature: Relationship to glass-forming ability. *Int. J. Pharm.* **2015**, *495*, 312–317. [[CrossRef](#)] [[PubMed](#)]
- Wytttenbach, N.; Kirchmeyer, W.; Alsenz, J.; Kuentz, M. Theoretical Considerations of the Prigogine–Defay Ratio with Regard to the Glass-Forming Ability of Drugs from Undercooled Melts. *Mol. Pharm.* **2016**, *13*, 241–250. [[CrossRef](#)] [[PubMed](#)]
- Van Eerdenbrugh, B.; Baird, J.A.; Taylor, L.S. Crystallization Tendency of Active Pharmaceutical Ingredients Following Rapid Solvent Evaporation—Classification and Comparison with Crystallization Tendency from Under cooled Melts. *J. Pharm. Sci.* **2010**, *99*, 3826–3838. [[CrossRef](#)] [[PubMed](#)]
- Ditzinger, F.; Price, D.J.; Ilie, A.-R.; Köhl, N.J.; Jankovic, S.; Tsakiridou, G.; Aleandri, S.; Kalantzi, L.; Holm, R.; Nair, A.; et al. Lipophilicity and hydrophobicity considerations in bio-enabling oral formulations approaches—A PEARRL review. *J. Pharm. Pharmacol.* **2019**, *71*, 464–482. [[CrossRef](#)]
- Blaabjerg, L.L.; Bulduk, B.; Lindenberg, E.; Löbmann, K.; Rades, T.; Grohgan, H. Influence of glass forming ability on the physical stability of supersaturated amorphous solid dispersions. *J. Pharm. Sci.* **2019**, *108*, 2561–2569. [[CrossRef](#)]
- Wytttenbach, N.; Kuentz, M. Glass-forming ability of compounds in marketed amorphous drug products. *Eur. J. Pharm. Biopharm.* **2017**, *112*, 204–208. [[CrossRef](#)]
- Repka, M.A.; Bandari, S.; Kallakunta, V.R.; Vo, A.Q.; McFall, H.; Pimparade, M.B.; Bhagurkar, A.M. Melt extrusion with poorly soluble drugs—An integrated review. *Int. J. Pharm.* **2018**, *535*, 68–85. [[CrossRef](#)]
- Sliwinska-Bartkowiak, M.; Dudziak, G.; Gras, R.; Sikorski, R.; Radhakrishnan, R.; Gubbins, K.E. Freezing behavior in porous glasses and MCM-41. *Colloids Surfaces A Physicochem. Eng. Asp.* **2001**, *187–188*, 523–529. [[CrossRef](#)]
- McCarthy, C.A.; Ahern, R.J.; Dontireddy, R.; Ryan, K.B.; Crean, A.M. Mesoporous silica formulation strategies for drug dissolution enhancement: A review. *Expert Opin. Drug Deliv.* **2016**, *13*, 93–108. [[CrossRef](#)] [[PubMed](#)]



14. Azais, T.; Tourné-Péteilh, C.; Aussenac, F.; Baccile, N.; Coelho, C.; Devoisselle, J.-M.; Babonneau, F. Solid-State NMR Study of Ibuprofen Confined in MCM-41 Material. *Chem. Mater.* **2006**, *18*, 6382–6390. [[CrossRef](#)]
15. Müller, R.H.; Wei, Q.; Keck, C.M. CapsMorph: >4 Years Long-Term Stability of Industrially Feasible Amorphous Drug Formulations. In Proceedings of the Annual Meeting of the Controlled Release Society, Honolulu, HI, USA, 21–24 July 2013.
16. Mellaerts, R.; Houthoofd, K.; Elen, K.; Chen, H.; Van Speybroeck, M.; Van Humbeeck, J.; Augustijns, P.; Mullens, J.; Van den Mooter, G.; Martens, J.A. Aging behavior of pharmaceutical formulations of itraconazole on SBA-15 ordered mesoporous silica carrier material. *Microporous Mesoporous Mater.* **2010**, *130*, 154–161. [[CrossRef](#)]
17. Salonen, J.; Kaukonen, A.M.; Hirvonen, J.; Lehto, V.-P. Mesoporous Silicon in Drug Delivery Applications. *J. Pharm. Sci.* **2008**, *97*, 632–653. [[CrossRef](#)] [[PubMed](#)]
18. Williams, H.D.; Trevaskis, N.L.; Charman, S.A.; Shanker, R.M.; Charman, W.N.; Pouton, C.W.; Porter, C.J.H. Strategies to address low drug solubility in discovery and development. *Pharmacol. Rev.* **2013**, *65*, 315–499.
19. Knopp, M.M.; Wendelboe, J.; Holm, R.; Rades, T. Effect of amorphous phase separation and crystallization on the in vitro and in vivo performance of an amorphous solid dispersion. *Eur. J. Pharm. Biopharm.* **2018**, *130*, 290–295. [[CrossRef](#)]
20. Guzmán, H.R.; Tawa, M.; Zhang, Z.; Ratanabanangkoon, P.; Shaw, P.; Gardner, C.R.; Chen, H.; Moreau, J.; Almarsson, Ö.; Remenar, J.F. Combined Use of Crystalline Salt Forms and Precipitation Inhibitors to Improve Oral Absorption of Celecoxib from Solid Oral Formulations. *J. Pharm. Sci.* **2007**, *96*, 2686–2702. [[CrossRef](#)]
21. Price, D.J.; Ditzinger, F.; Koehl, N.J.; Jankovic, S.; Tsakiridou, G.; Nair, A.; Holm, R.; Kuentz, M.; Dressman, J.B.; Saal, C. Approaches to increase mechanistic understanding and aid in the selection of precipitation inhibitors for supersaturating formulations—A PEARRL review. *J. Pharm. Pharmacol.* **2019**, *71*, 483–509. [[CrossRef](#)]
22. Brough, C.; Miller, D.A.; Keen, J.M.; Kucera, S.A.; Lubda, D.; Williams, R.O. Use of Polyvinyl Alcohol as a Solubility-Enhancing Polymer for Poorly Water Soluble Drug Delivery (Part 1). *AAPS PharmSciTech* **2016**, *17*, 167–179. [[CrossRef](#)]
23. Price, D.J.; Nair, A.; Kuentz, M.; Dressman, J.; Saal, C. Calculation of drug-polymer mixing enthalpy as a new screening method of precipitation inhibitors for supersaturating pharmaceutical formulations. *Eur. J. Pharm. Sci.* **2019**, *132*, 142–156. [[CrossRef](#)] [[PubMed](#)]
24. ICH Expert Working Group. ICH Guideline Q1A(R2) Stability Testing of New Drug Substances and Products. International Conference on Harmonization. 2003. Available online: [https://www.ema.europa.eu/en/documents/scientific-guideline/ich-q-1-r2-stability-testing-new-drug-substances-products-step-5\\_en.pdf](https://www.ema.europa.eu/en/documents/scientific-guideline/ich-q-1-r2-stability-testing-new-drug-substances-products-step-5_en.pdf) (accessed on 25 September 2019).
25. Vertzoni, M.; Fotaki, N.; Nicolaidis, E.; Reppas, C.; Kostewicz, E.; Stippler, E.; Leuner, C.; Dressman, J. Dissolution media simulating the intraluminal composition of the small intestine: Physiological issues and practical aspects. *J. Pharm. Pharmacol.* **2004**, *56*, 453–462. [[CrossRef](#)] [[PubMed](#)]
26. Dressman, J.B.; Amidon, G.L.; Reppas, C.; Shah, V.P. Dissolution testing as a prognostic tool for oral drug absorption: Immediate release dosage forms. *Pharm. Res.* **1998**, *15*, 11–22. [[CrossRef](#)] [[PubMed](#)]
27. Edueng, K.; Mahlin, D.; Gräsjö, J.; Nylander, O.; Thakrani, M.; Bergström, C.A.S. Supersaturation Potential of Amorphous Active Pharmaceutical Ingredients after Long-Term Storage. *Molecules* **2019**, *24*, 2731. [[CrossRef](#)] [[PubMed](#)]
28. Paudel, A.; Geppi, M.; Mooter, G. Van den Structural and Dynamic Properties of Amorphous Solid Dispersions: The Role of Solid-State Nuclear Magnetic Resonance Spectroscopy and Relaxometry. *J. Pharm. Sci.* **2014**, *103*, 2635–2662. [[CrossRef](#)]
29. Lee, H.L.; Vasoya, J.M.; Cirqueira, M.D.L.; Yeh, K.L.; Lee, T.; Serajuddin, A.T.M. Continuous Preparation of 1:1 Haloperidol–Maleic Acid Salt by a Novel Solvent-Free Method Using a Twin Screw Melt Extruder. *Mol. Pharm.* **2017**, *14*, 1278–1291. [[CrossRef](#)]
30. Djuris, J.; Nikolakakis, I.; Ibric, S.; Djuris, Z.; Kachrimanis, K. Preparation of carbamazepine–Soluplus® solid dispersions by hot-melt extrusion, and prediction of drug–polymer miscibility by thermodynamic model fitting. *Eur. J. Pharm. Biopharm.* **2013**, *84*, 228–237. [[CrossRef](#)]
31. Galia, E.; Nicolaidis, E.; Hörter, D.; Löbenberg, R.; Reppas, C.; Dressman, J.B. Evaluation of various dissolution media for predicting in vivo performance of class I and II drugs. *Pharm. Res.* **1998**, *15*, 698–705. [[CrossRef](#)]

32. Zheng, M.; Bauer, F.; Birk, G.; Lubda, D. Polyvinyl Alcohol in Hot Melt Extrusion to Improve the Solubility of Drugs. Available online: [https://www.sigmaaldrich.com/content/dam/sigma-aldrich/0/content/pdf/PS-PVA-HME-Improve-Solubility-03-2017\\_EN\\_MS.pdf](https://www.sigmaaldrich.com/content/dam/sigma-aldrich/0/content/pdf/PS-PVA-HME-Improve-Solubility-03-2017_EN_MS.pdf) (accessed on 2 May 2019).
33. Forster, A.; Hempenstall, J.; Tucker, I.; Rades, T. Selection of excipients for melt extrusion with two poorly water-soluble drugs by solubility parameter calculation and thermal analysis. *Int. J. Pharm.* **2001**, *226*, 147–161. [[CrossRef](#)]
34. Laitinen, R.; Priemel, P.A.; Surwase, S.; Graeser, K.; Strachan, C.J.; Grohgan, H.; Rades, T. Theoretical Considerations in Developing Amorphous Solid Dispersions. In *Amorphous Solid Dispersions*; Springer: New York, NY, USA, 2014; pp. 35–90.
35. Niederquell, A.; Wyttenbach, N.; Kuentz, M. New prediction methods for solubility parameters based on molecular sigma profiles using pharmaceutical materials. *Int. J. Pharm.* **2018**, *546*, 137–144. [[CrossRef](#)]
36. Loschen, C.; Klamt, A. COSMO quick: A Novel Interface for Fast  $\sigma$ -Profile Composition and Its Application to COSMO-RS Solvent Screening Using Multiple Reference Solvents. *Ind. Eng. Chem. Res.* **2012**, *51*, 14303–14308. [[CrossRef](#)]
37. Greenspan, L. Humidity fixed points of binary saturated aqueous solutions. *J. Res. Natl. Bur. Stand. Sect. A Phys. Chem.* **1977**, *81A*, 89–96. [[CrossRef](#)]
38. Thiry, J.; Krier, F.; Evrard, B. A review of pharmaceutical extrusion: Critical process parameters and scaling-up. *Int. J. Pharm.* **2015**, *479*, 227–240. [[CrossRef](#)] [[PubMed](#)]
39. Kissi, E.O.; Ruggiero, M.T.; Hempel, N.-J.; Song, Z.; Grohgan, H.; Rades, T.; Löbmann, K. Characterising glass transition temperatures and glass dynamics in mesoporous silica-based amorphous drugs. *Phys. Chem. Chem. Phys.* **2019**. [[CrossRef](#)]
40. Patel, D.D.; Anderson, B.D. Effect of Precipitation Inhibitors on Indomethacin Supersaturation Maintenance: Mechanisms and Modeling. *Mol. Pharm.* **2014**, *11*, 1489–1499. [[CrossRef](#)]
41. Mehta, M.; Suryanarayanan, R. Accelerated Physical Stability Testing of Amorphous Dispersions. *Mol. Pharm.* **2016**, *13*, 2661–2666. [[CrossRef](#)]
42. Mehta, M.; Kothari, K.; Ragoonanan, V.; Suryanarayanan, R. Effect of Water on Molecular Mobility and Physical Stability of Amorphous Pharmaceuticals. *Mol. Pharm.* **2016**, *13*, 1339–1346. [[CrossRef](#)]
43. Brás, A.R.; Fonseca, I.M.; Dionísio, M.; Schönhals, A.; Affouard, F.; Correia, N.T. Influence of Nanoscale Confinement on the Molecular Mobility of Ibuprofen. *J. Phys. Chem. C* **2014**, *118*, 13857–13868. [[CrossRef](#)]
44. Cordeiro, T.; Castiñeira, C.; Mendes, D.; Danède, F.; Sotomayor, J.; Fonseca, I.M.; Gomes da Silva, M.; Paiva, A.; Barreiros, S.; Cardoso, M.M.; et al. Stabilizing Unstable Amorphous Menthol through Inclusion in Mesoporous Silica Hosts. *Mol. Pharm.* **2017**, *14*, 3164–3177. [[CrossRef](#)]
45. Kawakami, K. Crystallization Tendency of Pharmaceutical Glasses: Relevance to Compound Properties, Impact of Formulation Process, and Implications for Design of Amorphous Solid Dispersions. *Pharmaceutics* **2019**, *11*, 202. [[CrossRef](#)]



© 2019 by the authors. Licensee MDPI, Basel, Switzerland. This article is an open access article distributed under the terms and conditions of the Creative Commons Attribution (CC BY) license (<http://creativecommons.org/licenses/by/4.0/>).

## Lipophilicity and hydrophobicity considerations in bio-enabling oral formulations approaches – a PEARRL review

Felix Ditzinger<sup>a,b</sup> , Daniel J. Price<sup>c,d</sup> , Alexandra-Roxana Ilie<sup>e,f</sup>, Niklas J. Köhl<sup>e</sup>, Sandra Jankovic<sup>a,b</sup> , Georgia Tsakiridou<sup>g,h</sup>, Simone Aleandri<sup>b</sup>, Lida Kalantzi<sup>g</sup>, René Holm<sup>f</sup>, Anita Nair<sup>c</sup>, Christoph Saal<sup>c</sup>, Brendan Griffin<sup>e</sup>  and Martin Kuentz<sup>b</sup> 

<sup>a</sup>Department of Pharmaceutical Sciences, University of Basel, Basel, <sup>b</sup>Institute of Pharma Technology, University of Applied Sciences and Arts Northwestern Switzerland, Muttenz, Switzerland, <sup>c</sup>Analytics Healthcare, Merck KGaA, Darmstadt, <sup>d</sup>Goethe University, Frankfurt, Germany, <sup>e</sup>School of Pharmacy, University College Cork, Cork, Ireland, <sup>f</sup>Drug Product Development, Janssen Research and Development, Johnson and Johnson, Beerse, Belgium, <sup>g</sup>Product Design & Evaluation, Pharmathen SA, Athens and <sup>h</sup>Faculty of Pharmacy, National and Kapodistrian University of Athens, Athens, Greece

### Keywords

crystal lattice energy; hydrophobicity; lipophilicity; modern formulation approaches; poorly water-soluble drug

### Correspondence

Martin Kuentz, Institute of Pharma Technology, University of Applied Sciences and Arts Northwestern Switzerland, Gründenstrasse 40, 4132 Muttenz, Switzerland.  
E-mail: Martin.Kuentz@fhnw.ch

Received March 8, 2018  
Accepted June 27, 2018

doi: 10.1111/jpp.12984

### Abstract

**Objectives** This review highlights aspects of drug hydrophobicity and lipophilicity as determinants of different oral formulation approaches with specific focus on enabling formulation technologies. An overview is provided on appropriate formulation selection by focussing on the physicochemical properties of the drug. **Key findings** Crystal lattice energy and the octanol–water partitioning behaviour of a poorly soluble drug are conventionally viewed as characteristics of hydrophobicity and lipophilicity, which matter particularly for any dissolution process during manufacturing and regarding drug release in the gastrointestinal tract. Different oral formulation strategies are discussed in the present review, including lipid-based delivery, amorphous solid dispersions, mesoporous silica, nanosuspensions and cyclodextrin formulations.

**Summary** Current literature suggests that selection of formulation approaches in pharmaceuticals is still highly dependent on the availability of technological expertise in a company or research group. Encouraging is that, recent advancements point to more structured and scientifically based development approaches. More research is still needed to better link physicochemical drug properties to pharmaceutical formulation design.

### Introduction

The use of modern drug discovery approaches, such as combinatorial chemistry and high-throughput screening as well as structural understanding of drug–target binding by X-ray diffraction and molecular modelling, has resulted in an increasing percentage of highly potent lead compounds. However, these compounds present increasing issues for formulation development as they often have high-melting points ( $T_m$ ) and high octanol–water partition coefficients ( $\log P$ ).<sup>[1–4]</sup> While  $T_m$  is a characteristic of crystal lattice energy,  $\log P$ , as a partition coefficient, denotes a solvation tendency or a lack of the same. These properties are in the chemical space of poorly soluble drugs often associated with hydrophobicity and lipophilicity, respectively.<sup>[5]</sup> Most

importantly, high values of  $T_m$  and  $\log P$  limit aqueous solubility and as a consequence thereof often bioavailability when administered orally in conventional dosage forms.<sup>[3,4,6]</sup> These limiting factors of drug solubility can be assigned to separate idealised dissolution processes. A molecule first has to overcome crystal lattice energy to interact with solvent molecules in the consecutive process of solvation. Figure 1a depicts the crystal structure of a model compound (cinnarizine), which is used to highlight molecular interactions in the solid state. Figure 1b shows a molecule dissolved in water that requires interactions for the solvation step; hence, the ease of this hydration depends on the solute affinity to water.

The general chemical meaning of the word hydrophobicity is the physical characteristic of a molecule that it is



repelled by water. Such a rather broad definition of hydrophobicity includes different reasons that cause a molecule to behave in this way. This umbrella use of hydrophobicity leads to some overlap with lipophilicity. A more specific use of hydrophobicity focuses on pharmaceutical compounds that exhibit limited aqueous solubility due to high crystal lattice energy.<sup>[5]</sup>

This has become a widespread convention in pharmaceutical sciences when poorly soluble drugs are considered. Hydrophobicity in this context has to be clearly differentiated from lipophilicity. Thus, lipophilicity as a scale is conventionally viewed as relative in the given chemical space. For example, values of  $\log P < 2$  mark a low range of lipophilicity for poorly soluble drugs, whereas a high regimen of lipophilicity starts in this chemical space beyond about  $\log P > 6$ . Such ranges are tentatively assigned and can be subject to change.

In line with these considerations,  $T_m$  and  $\log P$  are generally seen as two important properties of biopharmaceutical drug profiling.<sup>[7]</sup> Such profiling is required to predict biopharmaceutical issues early on and to propose adequate formulation strategies. The design, development and characterisation of bio-enabling formulations are among the

core objectives of PEARRL (Pharmaceutical Education And Research with Regulatory Links), a European Network, focused on pharmaceutical education and research for faster patient access to breakthrough therapies. This study addresses the need to review oral bio-enabling formulation approaches from a specific viewpoint of compound lipophilicity and hydrophobicity characteristics.

### Theoretical Aspects of Lipophilicity and Hydrophobicity

The molar solubility of a compound  $x_{\text{eq}}$  can be obtained as a function of temperature,  $T$ , by considering the solid-liquid equilibrium, which can be expressed as follows:<sup>[8,9]</sup>

$$\ln x_{\text{eq}} = \frac{\Delta H_f}{R} \left( \frac{1}{T_m} - \frac{1}{T} \right) - \frac{1}{RT} \int_{T_m}^T \Delta C_p dT + \frac{1}{R} \int_{T_m}^T \frac{\Delta C_p}{T} dT - \ln \gamma_{\text{eq}} \quad (1)$$

where  $\Delta H_f$  is a compound's enthalpy of fusion,  $R$  is the gas constant and  $\Delta C_p$  represents the heat capacity difference between the supercooled melt and the solid. The activity coefficient of the solute in the saturated solution is given by  $\gamma_{\text{eq}}$  and estimation of this property is a central task of various thermodynamic theories. A classical and rather simple approach is the regular solution theory of Scatchard-Hildebrand,<sup>[10]</sup> which has been used by Jain and Yalkowsky<sup>[11]</sup> to describe drug solubility in octanol,  $S_o$ . Such solubility estimation of an organic molecule in an organic solvent, such as octanol, appears to be simpler than a direct estimation of a drug's water solubility,  $S_w$ . The two properties are linked via the partition coefficient  $\log P$  as approximated by:

$$\log S_w = \log S_o - \log P. \quad (2)$$

Use of the regular solution theory was complemented with further simplifications (for example Walden's assumption of a constant entropy change upon fusion,  $\Delta S_f$ ) to obtain the general solution equation (GSE) for non-electrolytes.<sup>[11]</sup>

$$\log S_w = 0.5 - 0.01 (T_m - 25) - \log P. \quad (3)$$

The above GSE has particular importance for the present review because  $\log S_w$  is a function of a compound's crystal lattice energy and lipophilicity as expressed by  $T_m$  in K and  $\log P$ , respectively. This GSE approach (Equation 3) allows an estimation of how a drug's lattice energy (conventionally seen as hydrophobicity for poorly soluble drugs) and lipophilicity determine solubility. Compounds with high  $T_m$  values and moderate or low  $\log P$  values are often called

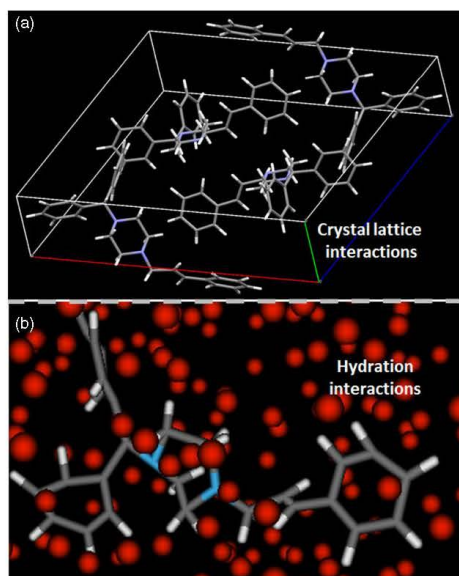


**Figure 1** (a) Model poorly soluble compound (cinnarizine) is shown as the unit cell of the crystal lattice and upon (b) aqueous solvation (water molecules are shown without hydrogens for clarity of presentation).

'brick-dust', whereas low  $T_m$  and high  $\log P$  values often give molecules the properties of so-called grease balls. While the brick-dust compounds exhibit a solid-state limited solubility with breakdown of the crystal lattice as most difficult step, the grease balls have the solvation step in water as the main hurdle for drug dissolution.<sup>[5,6]</sup> The GSE can provide initial estimates of aqueous drug solubility, but for more precise values, it has been suggested to assume a non-constant entropy change between the solid and a supercooled melt.<sup>[12]</sup>

Hydrophobicity and lipophilicity are not only important characteristics for the different approaches to predict solubility<sup>[13]</sup> but they are also interesting regarding further pharmaceutical aspects. Accordingly, one field of interest is about which molecular features or moieties lead to brick-dust or grease ball characteristics. It has, for example, been observed that structural features related to rigidity or aromaticity were correlated with restricted solubility due to stable crystal structures and thus hydrophobicity.<sup>[14]</sup> Regarding solvation-limited solubility, it makes sense to consider the molecular features that lead to high partitioning into an apolar phase, for example as inferred from the Abraham solvation predictors.<sup>[15,16]</sup> This approach has recently been used to obtain a better understanding of the molecular drug characteristics that drive solubilisation in biorelevant media.<sup>[17]</sup> It is clear that an improved molecular understanding of solubility limitations would be of great help in the drug discovery phase when designing and selecting drug candidates. General developability criteria, such as Lipinski's rule of 5,<sup>[18]</sup> could be further refined so there is clearly more research to be performed in this field. However, the current review approaches hydrophobicity and lipophilicity primarily from a formulator's perspective and provides guidance regarding the selection of excipients and bio-enabling formulation approaches.

## Lipophilicity and Hydrophobicity Regarding Different Formulation Approaches

### Lipid-based formulations

The utility of lipid-based formulations (LBF) as a bio-enabling formulation approach for poorly water-soluble drugs is well recognised and has fostered the development of several marketed drug products.<sup>[4]</sup> Oral LBFs are defined as delivery systems, which present the drug in a mixture of excipients consisting of triglyceride oils, partial glycerides, surfactants or cosurfactants and cosolvents.<sup>[19]</sup> The key advantage of most marketed LBFs as a bio-enabling strategy is the ability to enhance drug solubilisation *in vivo* as the drug is generally dissolved in lipids.<sup>[4]</sup> Following oral administration, the drug is ideally maintained in the

solubilised/supersaturated state in the course of lipid dispersion and digestion. There is a risk of drug precipitation from LBFs, which is especially pronounced with formulations containing high percentages of cosolvents.

The thermodynamic factors governing drug solubility in lipids are illustrated in Figure 2. A drug sublimation helps to emphasise the crystal lattice hurdle and this idealised step comes with the Gibbs free energy change of  $\Delta G_{\text{crystal-gas phase}}^0$ . This is followed by a second idealised step of drug solvation in the lipid vehicle with the free energy change of  $\Delta G_{\text{gas phase-lipid}}^0$ .<sup>[20]</sup>

In terms of predicting which classes of drugs will be soluble in lipids, grease ball molecules are considered advantageous for LBFs because of their dominant lipophilic characteristics and relatively weak crystal lattice energy, which both favour solubilisation in lipids. In the case of brick-dust molecules, drug solubility in lipids will be limited by a high crystal lattice energy. However, compounds with medium hydrophobicity and lipophilicity are not categorisable as clear brick-dust or grease balls, as there is often a mixture of solid-state and solvation-limited solubility. Within the chemical space of compounds emerging from drug discovery, there is a need of better understanding how lipophilic and/or hydrophobic properties predict drug solubility in LBFs.

Regarding crystal lattice energy, it has been reported that compounds with  $T_m$  values below 423.15 K mostly show a reasonable solubility in glycerides.<sup>[21,22]</sup> These studies further showed a clear trend towards reduced solubility in lipid excipients with increased  $T_m$  values of the drug. However,  $T_m$  is only one characteristic of the crystal lattice and equals to the ratio of changes in  $\Delta H_f$  and entropy of fusion ( $\Delta S_f$ ). More refined consideration of the solid state can therefore be advantageous.

Accordingly, Persson *et al.*<sup>[21]</sup> reported that the accuracy of solubility predictions in lipids slightly increased, when

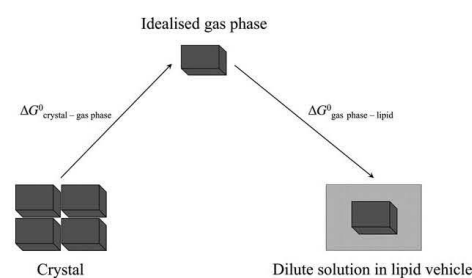


**Figure 2** Factors that drive drug solubility in lipids as idealised steps of sublimation from crystal lattice and solvation in lipid vehicle. Further details and definitions of variables are given in the text. Adapted from Rane and Anderson.<sup>[20]</sup>

$T_m$  and  $\Delta S_f$  were both considered. More recently, Gautschi *et al.*<sup>[23]</sup> similarly found that  $T_m$  alone could not reliably predict drug solubility in C-8 and C-10 triglycerides (TGs). Consequently, solubility estimations for lipids solely based on  $T_m$  appear to describe only a part of data variability and may only be valid for a rather narrow chemical space. Interestingly, as illustrated in Figure 3, there is a large variability in  $T_m$  of drugs approved as LBFs by the FDA, ranging from approximately 330.15 to 623.15 K. However,  $T_m$  values should still be considered as an important descriptor in solubility models and a guiding predictor for decisions in formulation design. Therefore, a thorough solid-state characterisation is important to understand the factors that govern drug suitability in LBFs. For example, a compound with a high  $T_m$  combined with a low  $\Delta S_f$  is less favourable to dissolve in pure TGs and therefore unlikely to be suitable for a LBF.<sup>[22]</sup> However, it is also worth noting that there are further limitations reported on the use of  $T_m$  in models to estimate the solubility in ethoxylated excipients, which are commonly used excipients in LBFs.<sup>[21,22]</sup> Additional work seems to be required to clarify such effects of individual excipient classes.

Apart from overcoming the crystal lattice energy, a favourable solvation process is crucial for the solubility in any solvent.<sup>[7]</sup> In the case of drug solubility in LBFs, this is generally associated with a high  $\log P$  value. It has been suggested that a  $\log P$  of  $>4$  would be desirable to achieve adequate solubility in pure TGs, while an intermediate  $\log P$ , between 2 and 4, may still show suitable solubility in LBF mixtures containing TGs, surfactants and cosolvents.<sup>[19]</sup> These considerations of lipophilicity can provide initial formulation guidance but aspects of crystal lattice energy as well as dose strength must be also taken into account. Recently, an analysis of 36 LBFs (26 different drugs) approved by the FDA showed that the range of  $\log P$  was 0.8–7.5 with a median of 4.9.<sup>[19]</sup> The distribution of  $\log P$  for the 26 drugs is illustrated in Figure 3. Moreover,

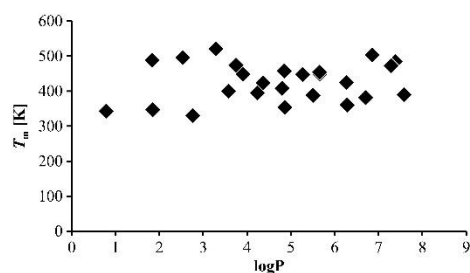


**Figure 3**  $T_m$  vs  $\log P$  of drugs in FDA approved LBFs. Only three compounds have a  $\log P$  below 2, however, a high variability for  $\log P$  as well as  $T_m$  can be observed. LBFs, lipid-based formulations.

Figure 4 highlights the distribution of molecular weight (MW),  $\log P$  and  $T_m$  of the FDA approved LBFs. The majority of drugs have a  $\log P$  above 2 which underpins the above-mentioned lipophilicity considerations.

Delving further into exploring the relationship between  $\log P$  and lipid solubility, Figures 5 and 6 present the lipid solubility as a function of  $\log P$  for a range of poorly water-soluble drugs from Alskär *et al.*<sup>[22]</sup> (halofantrine omitted). Among the 34 model drugs included, there was a subtle trend of increased solubility in both medium chain (Captex 355) and long chain TGs (Soybean oil) between a  $\log P$  of 2–5. However, the situation is more complex for  $\log P$  values larger than 5, where solubility appears to decrease (Figures 5 and 6). A larger data set is probably needed to draw final conclusions on the relationship between  $\log P$  and lipid solubility.

In the framework of this solubility analysis in lipids, it should be noted that poor aqueous solubility is only one rationale for LBFs. Also practical aspects such as, for example, high potency, hygroscopicity or instability can be reasons to select this formulation strategy. When a biopharmaceutical rationale is given, solubility in a LBF is only one aspect to consider, while it is also important how a drug solubilises upon dispersion/digestion as well as how the absorption step is influenced.  $\log P$  has also been used to predict further biopharmaceutical properties of drugs including the propensity for lymphatic transport, intestinal permeability, potential presystemic clearance, susceptibility to efflux pumps or further drug disposition.<sup>[24,25]</sup> However, such a broad scope was not intended for the current review, but this should be kept in mind to avoid any dogmatic rules of formulation selection that are based solely on drug solubility in LBF.

Besides the drug characteristics, also the choice of excipients merits further discussion. In general, it was shown in two studies that the solubility of a data set of 10 and 35 structurally diverse compounds followed a general solubility ranking of long-chain TG < medium-chain TG < surfactant.<sup>[22,26]</sup> LBFs can be classified depending on the oil, surfactant and cosolvent content,<sup>[19,27]</sup> with four proposed classification types. Type I contains solely oils as TGs, diglycerides (DG), monoglycerides (MG) or a mixture thereof, whereas Type IV formulations do not contain lipids but are mixtures of surfactants and cosolvents. Type II, IIIA and IIIB contain different kinds of lipids, surfactants and cosolvents.<sup>[27]</sup> The more lipophilic a drug molecule is, the more likely it will dissolve in Type I, II and IIIA formulations. On the other hand, hydrophobic drug molecules would be more suited for Type IIIB or IV formulation given the more polar characteristics.<sup>[27]</sup>

Furthermore, several excipient properties can be used to predict and guide the choice of lipids, surfactants and cosolvents.<sup>[28]</sup> It was shown that the polarity expressed as the relative permittivity, hydrophilic and lipophilic balance



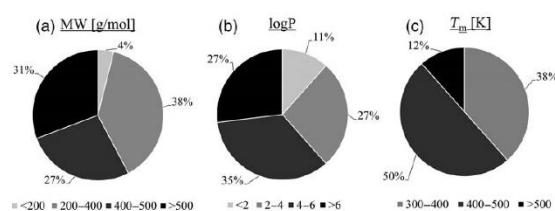


**Figure 4** Physicochemical drug properties of drugs in FDA approved LBFs. The different panels are explained in the text. LBFs, lipid-based formulations.

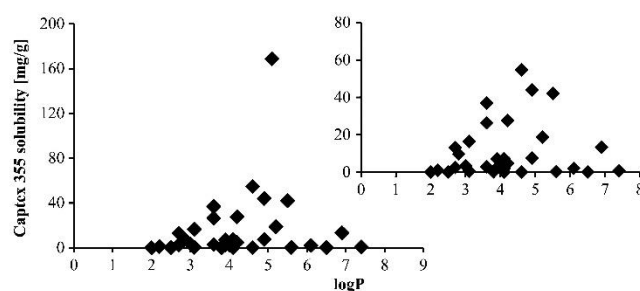


**Figure 5** Solubility in Captopex 355 plotted against the  $\log P$ . Dataset from Alskär *et al.*<sup>[22]</sup> Insert: Close up with fenofibrate omitted. The  $T_m$  values of all used drugs were below 423.15 K.

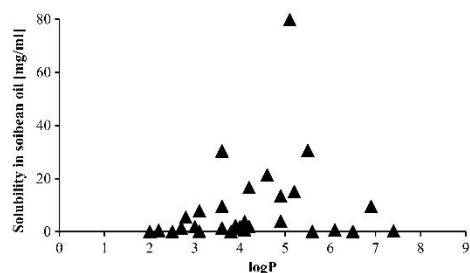


**Figure 6** Solubility in soybean oil (SBO) plotted against the  $\log P$ . Dataset from Alskär *et al.*<sup>[22]</sup> The  $T_m$  values of all used drugs were below 423.15 K.

(HLB), ester concentration (in TGs), solubility parameter, surface tension,  $\log P$ , chain length, MW and molecular volume can be helpful to guide excipient selection.<sup>[28,29]</sup> The polarity describes the capability of a drug or excipient to interact through dipole interactions and possibly also through hydrogen bonding. These molecular interactions are different from the dispersive interactions of the more apolar parts of molecules. In formulation design, it is critical for the excipient selection to know if the compound of interest needs to form polar and/or non-polar interactions

with a given excipient. Such interactions of a drug molecule and an excipient can be visualised in molecular dynamics simulations to improve the understanding of where a drug molecule resides in a LBF and in the complex mixture after aqueous dispersion/digestion.<sup>[23,30]</sup> As an example, these studies can be used to explain why high solubility in LBFs may not entail high solubility after dispersion or digestion in the intestinal media. It was, for example, observed for medium chain TGs that a C8 chain length resulted in the best LBF solubilisation for several drugs, whereas the corresponding digestion phases yielded best solubilisation in favour of the C10 chain length TGs.<sup>[23]</sup> These observations were similar to a previous study exploring lipid chain length and drug solubilisation.<sup>[31]</sup> More data is needed to draw final conclusions on drug solubility effects in lipids while keeping in mind that lipid solubility is only one factor of adequate formulation design.

In an effort to overcome inherent solubility limitations for challenging drug candidates, a number of advanced LBF technologies have been investigated. Widespread is the concept of self-nanoemulsifying drug delivery systems (SNEDDS), which relies on the combination of drug, surfactant, oil and a coemulsifier resulting in the formation of a nanoemulsion upon aqueous dispersion. More recently, this approach has been advanced to so-called super-SNEDDS that are supersaturated LBFs.<sup>[32]</sup> This type of

formulation is suitable for highly hydrophobic drugs and offers an option to solubilise more active pharmaceutical ingredient (API) than conventional LBF. Formulation of a super-SNEDDS involves heating of the drug–lipid mixture, to overcome the drug’s crystal lattice energy. After cooling, the drug is maintained in a supersaturated state within the lipid vehicle and such formulations have been found to be kinetically stable, for drugs such as simvastatin or fenofibrate.<sup>[33,34]</sup> Further studies are required to assess whether the kinetic stability is maintained throughout the commercial shelf life of super-SNEDDS formulations.

A recent approach proposed to use lipophilic counter ions to form a more lipophilic salt.<sup>[35]</sup> This approach increases drug lipophilicity and due to the nature of the specific counter ion, the salt formation could reduce crystal lattice energy and  $T_m$  of the free drug. Furthermore, the higher lipophilicity promotes the solute–solvent interaction. For example, the solubility of the lipid salt of atazanavir in an unoptimised LBF vehicle increased several fold compared with the free base.<sup>[35]</sup> Therefore, formation of ionic liquids (as defined by  $T_m < 373.15$  K for the resulting salt) has the potential to increase drug solubility of hydrophobic compounds in LBFs.<sup>[36]</sup> Ionic liquids were synthesised using bulky and highly lipophilic counter ions. In the case of itraconazole, a 72-fold solubility increase with a dioctyl sulfosuccinate salt in a long-chain LBF was observed.<sup>[36]</sup> In addition to the improved solubility in the formulation, the lipophilic salt can also promote drug absorption in the gastrointestinal tract. These approaches therefore broaden the applicability of LBFs, but for future market formulations, the toxicological and regulatory acceptability of the used counter ions must be assured.<sup>[37]</sup>

An alternative strategy is to employ lipophilic prodrugs to improve lipophilicity. While the use of lipophilic prodrug strategies is more commonly employed to improve biopharmaceutical properties such as increased intestinal permeability and lymphatic transport, the increased lipophilicity is often favourable regarding solubility in LBF.<sup>[3]</sup> A study with a range of prodrugs for an anticancer drug (SN38) showed a significant increase in solubility in Soybean oil of 11 - 444-fold.<sup>[38]</sup> However, increasing lipophilicity via a prodrug approach also introduces risks to altered stability and pharmacokinetics, which must be adequately assessed. For example, while a TG ester prodrug of mycophenolic acid showed significant improvement in lymphatic transport and drug concentrations in lymphocytes, an alkyl ester prodrug showed poor metabolic stability and low permeability.<sup>[39]</sup>

While much focus to date has been on the use of lipid solutions as a bio-enabling strategy for challenging drugs, it has been reported that lipid suspensions may confer similar advantages in terms of improved biopharmaceutical

performance.<sup>[40,41]</sup> Thomas *et al.*<sup>[34]</sup> reported, for example, that a lipid suspension of fenofibrate displayed similar oral bioavailability to a comparable lipid solution. However, the number of studies employing lipid suspension is relatively few and further studies are needed to assess reliability and reproducibility of this formulation approach.

In summary, lattice energy and lipophilicity considerations are important for the choice of the lipid delivery approach and for the selection of excipients. While  $T_m$  has proven useful in predicting lipid solubility of drugs,  $\log P$  does not generally represent a reliable quantitative predictor of solubility. Therefore, the hydrophobic, or solid-state properties of a drug, appear to be crucial relative to their lipophilicity. The presented analysis of drugs marketed as LBFs suggests that poor hydrophobicity alone may not limit commercial development. There are a number of emerging formulation approaches such as ionic liquids, lipophilic prodrugs or lipid suspensions that may offer promise in addressing unfavourable hydrophobicity characteristics. Future work may provide more complex structural and physicochemical factors for guiding the design and development of LBFs.

### Amorphous solid dispersions

The formulation approach of amorphous solid dispersion (ASD) was introduced by Chiou and Riegelmann in 1969<sup>[42]</sup> because of an increasing number of poorly water-soluble compounds that required a new formulation perspective. Since then, this approach has been common practise for solubility enhancement of hydrophobic or lipophilic drugs.<sup>[43]</sup>

From a thermodynamic viewpoint, an amorphous state has generally a higher Gibbs free energy than a crystal. Therefore, an amorphous state is either labile or metastable with a considerable risk of crystallisation in non-stabilised ASDs.

Figure 7 emphasises the differences in Gibbs Energy between amorphous and crystalline material.<sup>[44]</sup> Moreover, it shows the changes in this energy compared with increasing temperature, going from an amorphous state to the final transition in the liquid molten state, respectively. The two temperatures in Figure 7 mark the transition of an amorphous to the crystalline state. The glass transition temperature ( $T_g$ ) represents the alteration between an amorphous state and a supercooled liquid. The other change in the solid state can be observed at  $T_m$ , when the crystals melt and become liquid.

Furthermore, the difference in Gibbs free energy shown in Figure 7 also results in an enhanced apparent solubility compared to the crystalline form.<sup>[45]</sup> This so-called amorphous solubility advantage was coined by Hancock and Parks, who associated the difference in free energy with the

difference in apparent solubility according to Equation 4.<sup>[46]</sup>

$$\Delta G_T^{a,c} = -RT \ln \left( \frac{\sigma_T^a}{\sigma_T^c} \right) \quad (4)$$

The different solubilities of the amorphous and the crystalline state at a fixed temperature are represented by  $\sigma_T^a$  and  $\sigma_T^c$ , respectively. Consequently,  $\Delta G_T^{a,c}$  is the difference in free energy at a given temperature. A higher difference in free energy can be associated with a larger solubility advantage of the amorphous form over the crystalline form. Such increased apparent solubility has to be balanced with the general drawback of potential physical instability of an amorphous state. A possible crystallisation to the original crystal form or any other polymorph has to be monitored by adequate solid-state analysis.

Due to the high relevance of identification and quantification of amorphous drug in a solid dispersion, there are several methods commonly applied. A widely used technique is X-ray powder diffraction (XRPD), where an amorphous form shows a halo and absence of any Bragg peaks.<sup>[47]</sup> This result underlines the lack of long-range order in the solid state.<sup>[48]</sup> Another common method is differential scanning calorimetry (DSC), where the absence of a melting endotherm and the presence of a  $T_g$  indicate an amorphous state. The spectrum of further characterisation methods is very broad including also spectroscopic methods such as Raman or infrared spectroscopy as well as solid-state nuclear magnetic resonance spectroscopy. However, XRPD and DSC are still the most common methods,

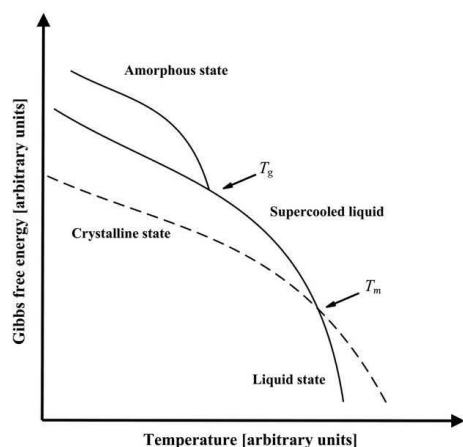


**Figure 7** Gibbs Free Energy of amorphous and crystalline material. Adapted from Hancock and Shamblin.<sup>[44]</sup>

because of their rather simple handling and good reproducibility.

Solid dispersions can be categorised according to the physical state of the given phases.<sup>[49]</sup> The first dispersions were often eutectic mixtures, which were miscible in the molten state. A disadvantage of the eutectic systems is that recrystallisation occurs at the characteristic eutectic temperature, which typically takes place during the cooling process. Pioneer solid dispersions were prepared with a water-soluble carrier such as citric acid, and a poorly water-soluble drug (e.g. griseofulvin).<sup>[42]</sup> Depending on the individual composition, it is possible to obtain an amorphous solid solution, where a compound is dispersed molecularly in the amorphous carrier.<sup>[50]</sup> Leuner and Dressman pointed out that solid solutions can be continuous vs discontinuous or substitutional vs interstitial. Systems with an amorphous carrier are generally called glasses where glass solutions can be differentiated from glass suspensions depending on the physical state of the drug and whether one or two phases are present in the system.<sup>[50]</sup>

As ASDs have a long tradition, different generations of formulation types have been in use. Those different generations were described in detail by Vo *et al.*<sup>[51]</sup> Main differences are given in the types of excipients selected during the pharmaceutical development of solid dispersions (Figure 8).

In the first generation of solid dispersions, crystalline carriers (i.e. mostly small molecular additives) were used for dispersing the drug homogeneously in the solid state, which had the disadvantage that a rather fast drug precipitation upon aqueous dispersion was often observed. Therefore, a second generation of improved formulations was proposed that were based on polymeric carriers, which were advantageous regarding the biopharmaceutical fate of the drug. Such ASDs typically showed a dissolution rate that was widely controlled by the hydration and dissolution of the polymeric matrix.<sup>[52]</sup> The third-generation solid dispersions consisted mainly of polymeric carriers combined either with each other or with surfactants to improve the aqueous dispersion following oral administration. Interesting is here a combined functionality such as, for example, the BASF polymer Soluplus, which represents a polymer (polyvinyl caprolactam-polyvinyl acetate-polyethylene glycol graft copolymer) with significant amphiphilic characteristics of a surfactant.

The production of the formulations mentioned above can be mainly divided into melt-based and solvent-based methods.<sup>[45]</sup> This is critical as the preparation has a substantial effect on the physicochemical characteristics, stability and therefore performance of ASDs.<sup>[53]</sup> Considering the marketed solid dispersions, it is interesting to see that a rather limited number of polymeric carriers and



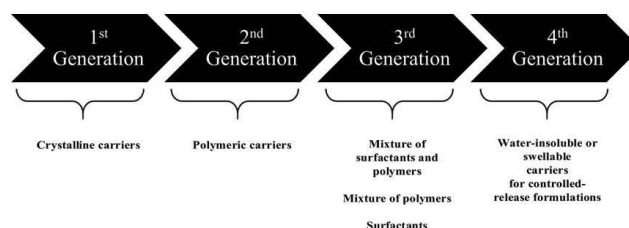


**Figure 8** Different generations of solid dispersions. Adapted from Vo *et al.*<sup>[51]</sup>

production techniques have been used.<sup>[54]</sup> While the choice of the formulation components is generally based on physical and chemical considerations and long series of experiments during development, the production methods are often more arbitrarily selected depending on available technological knowledge and equipment.<sup>[55]</sup> Selection of the manufacturing method based upon the physicochemical drug properties is therefore desirable. Such an approach also may accelerate process development and should finally result in a robust manufacturing of drug product.

Different melt and fusion techniques represent the classical methods to prepare ASDs.<sup>[55,56]</sup> For the melting of the API and a carrier, temperatures should be above the  $T_m$  of the API.<sup>[57]</sup> Raising the temperature above the  $T_g$  of the mixture creates adequate molecular mobility for the API to be incorporated in the carrier.<sup>[55]</sup> Although a variety of method modifications have been introduced throughout the years, ASDs with APIs presenting high  $T_m$  values (e.g. quercetin) typically encounter issues of lacking temperature stability of the carrier. These high-melting APIs therefore only have a limited range of available polymers that can be used at the needed process temperatures. Moreover, high shear forces in a process of hot melt extrusion may facilitate, besides the vigorous mixing and the desirable dispersion of the API in the carrier, the removal of oxygen and moisture.<sup>[51,58]</sup> This enables the incorporation and usage of APIs that are sensitive to oxidation. However, high shear forces may also compromise the stability of thermo-sensitive APIs, due to possible local high temperatures.<sup>[58]</sup>

An alternative to any melt method is to prepare a solution of drug and carrier in a solvent. The fate of the solution may vary, from solvent evaporation to amorphous precipitation. The solvent evaporation method includes first the dissolution of API and carrier in a common organic solvent (or solvent mixture) and the subsequent removal of the solvent by heating, spray drying or freeze-drying.<sup>[59]</sup> The choice of a common solvent for the API-carrier systems may prove to be limiting, as it is challenging to identify a solvent for combinations that vary significantly in polarity.<sup>[59]</sup> Generally, thermal degradation is not a

common limitation in the solvent evaporation methods, as temperatures are kept low. Specifically for thermo-labile compounds, a freeze-drying method is of interest, where the API-carrier solution is frozen and the solvent or solvent mixture is sublimated at temperatures below the  $T_g$  of the mixture.<sup>[55]</sup> A sublimation above this critical temperature comes with increased molecular mobility that can facilitate recrystallisation. Consequently, APIs with extremely low  $T_g$ 's may not be suitable for this method. In addition, during the removal of the solvent by heating, molecular mobility is critical, as elevated temperatures (above  $T_g$ ) may facilitate API diffusion from the carrier, thereby creating a phase separation and subsequent crystallisation. This suggests that this method may be less suitable for APIs with a  $T_g$  below the boiling point of common organic solvents (e.g. methanol, ethanol, acetone ~60–70 °C).

It seems that API lipophilicity has barely been investigated for its effect on different ASD manufacturing methods. Due to the fact that solubility is governed either by lipophilicity ( $\log P$ ) or by the crystal lattice energy (hydrophobicity),<sup>[14]</sup> it is expected that these molecular properties are relevant for selection and manufacturing of solid dispersions. Finally, the ratio of  $T_m/T_g$  merits consideration because it is an indicator of glass-forming ability that can again be related to molar volume and  $\Delta S_f$ .<sup>[60]</sup> The latter entropy change can be estimated from chemical structure. Such *in silico* estimations of glass-forming ability are of high interest, not only for drug discovery, but also in development because  $T_g$  is not easy to measure with fast crystallizing compounds.<sup>[60]</sup>

In line with these considerations of solid dispersion developability, Friesen *et al.* introduced the classification of several drugs according to the ratio of  $T_m$  and  $T_g$  plotted against  $\log P$ . Different groups of active substances were introduced.<sup>[61]</sup> For drugs with  $T_m/T_g$  ratio of maximum 1.25 (group 1), it was considered possible to form an amorphous state. Group 2 with  $T_m/T_g$  ratios of 1.25–1.40 was estimated to have a limited drug load of 35–50% (w/w) due to lower amorphous stability. Most challenging compounds in terms of stability exhibit a  $T_m/T_g$  range of higher

than 1.4 and consequently, a drug load of maximum 35% (w/w) was proposed. These drugs with a  $\log P$  smaller than 6 were assigned to group 3, whereas all other lipophilic drugs with  $\log P$  higher than 6 were viewed as generally problematic regarding dissolution and assigned into group 4 regardless of their  $T_m/T_g$  ratios.

For this review, the described categorisation approach was applied to drugs for which formation of a stable ASD was reported in the literature.<sup>[60,62,63]</sup> The distribution of the MW, the  $\log P$  and  $T_m$  values of these drugs are displayed in Figure 9.

Figure 9a suggests that most substances successfully formulated in an amorphous state have a MW between 200 and 400 g/mol. This is in accordance with the publications of Edueng *et al.*<sup>[5]</sup> and Mahlin *et al.*,<sup>[64]</sup> who also found a limited occurrence of very small molecules, as MWs above 300 g/mol are more optimal for good glass-forming ability. The pie chart (Figure 9b) of the  $\log P$  value reveals a broad distribution with a lowest fraction of highly lipophilic drugs. Furthermore,  $T_m$  (Figure 9c) is mostly between 400 and 500 K. These distributions of physicochemical properties cannot only be explained by ASD rationales as they are likely biased by the natural occurrence of MW,  $\log P$  and  $T_m$  among available drugs.

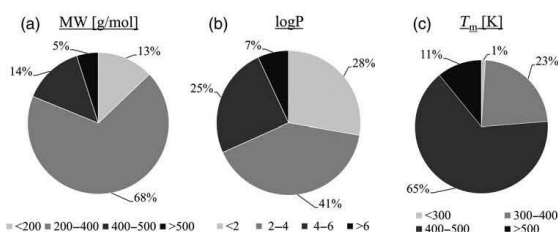
A novelty compared to the data gathered by Friesen *et al.*<sup>[61]</sup> is the inclusion of melt-based amorphisation techniques. If only the subset of marketed drugs in amorphous products is considered, which are not included in Figure 10, a challenging  $T_m/T_g > 1.4$  was only observed with etravirine and vemurafenib.<sup>[65]</sup> This can be compared to glass-forming ability, which can be determined by means of a DSC method.<sup>[62]</sup> Vemurafenib was verified as a fast crystallizing compound, while this is hard to demonstrate for etravirine due to thermal decomposition.<sup>[54]</sup> Interestingly, etravirine as well as vemurafenib are manufactured in their market products by a solvent-based method. Apart from these drugs, other market compounds are in group 4 due to their high  $\log P > 6$ , which is the case for itraconazole and everolimus. While Figure 10 shows the compounds found in scientific publications, it emphasises that

more melt-based manufacturing methods have been reported in group 4. However, there are also reports on drugs for which melt-based as well as solvent-based techniques were used. Also in group 3, where the majority of the compounds is located, there is not a clear dominance of either the melt or solvent-based method, so clear trends of a preferred method are missing. There is also currently no established molecular rationale for the selection of a manufacturing method and this choice is greatly influenced by the available expertise of individual formulation scientists.

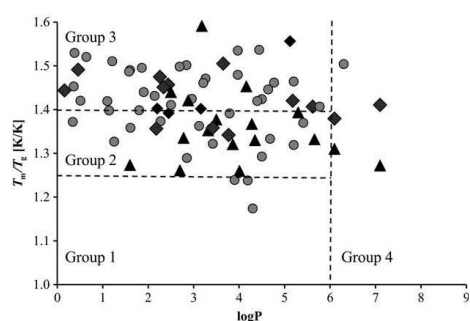
For a better evaluation of hydrophobicity and lipophilicity influences, the graph was modified to show  $T_m$  vs  $\log P$  (Figure 11). Furthermore, the graph represents the drugs differentiated by their amorphisation method in accordance with Figure 10.

Figure 11 indicates that melt-based methods were primarily used in research for compounds with  $\log P > 2$ . Moreover, there are not many substances that have a  $T_m > 500$  K and substances of  $\log P > 6$ . The distribution of data points shows an accumulation between  $\log P$  values of 2 and about 5, which may not be specific for the selection of solid dispersion technology, but also reflects the natural distribution of drug lipophilicity for the compounds studied.

In summary, Figure 11 as a plot of lipophilic and hydrophobic drugs does not reveal pronounced tendencies with respect to the process technique. It seems that melt-based methods are limited regarding high  $T_m$ , because of possible degradation issues of drug and excipients. However, also a solvation step can be clearly limited by excessive hydrophobicity. A more recently introduced solvent-based method is the microprecipitated bulk powder, where amorphous coprecipitation occurs with a polymer, which is based on ionisable groups to facilitate drug-excipient interactions.<sup>[66]</sup> This broadens the applicability of ASDs for APIs with high  $T_m$  values. Currently, there is only one drug (i.e. vemurafenib) formulated in this way on the market, but this can change in the future. At least for ionisable compounds, the possibilities for



**Figure 9** Properties of APIs formulated as ASD. The different panels are explained in the text. API, active pharmaceutical ingredient; ASD, amorphous solid dispersion.



**Figure 10** APIs gathered from the literature,<sup>[60,62,63]</sup> for which solid dispersions were successfully formulated, labelled by their amorphisation method. Diamonds represent melt-based amorphisation. Dots stand for solvent-based amorphisation and triangles are drugs that were formulated by both approaches. The lines indicate the different groups according to Friesen *et al.*<sup>[61]</sup> API, active pharmaceutical ingredient.

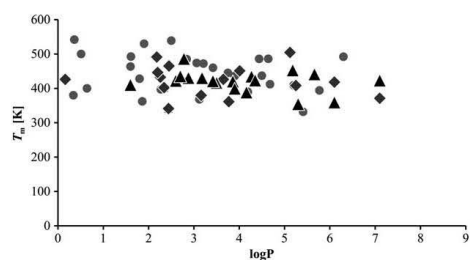


**Figure 11** Scatter plot of drug melting temperature vs the  $\log P$  values for further evaluation of hydrophobicity (data taken from the literature<sup>[60,62,63]</sup>). The colours and makers are analogues to Figure 10.

solvent-based approaches can be broadened for compounds with very high  $T_m$  values.

This section approached amorphous systems from the viewpoint of hydrophobicity and lipophilicity, but further molecular aspects are relevant for the different quality attributes of amorphous systems. This has become a developing field of research and more information on molecular descriptors applicable to ASD attributes can be inferred from recent publications.<sup>[5,67]</sup>

### Mesoporous silica formulations

Mesoporous silica refers to any number of a variety of materials synthesised to produce a  $\text{SiO}_2$  mesoporous structure.<sup>[68]</sup> Mesoporous silica can be ordered or non-ordered.<sup>[69,70]</sup> The former include structures such as SBA-

15 and MCM-41,<sup>[71]</sup> whilst the latter include novel, proprietary excipients manufactured by drug delivery specialists, such as the excipients Parreck SLC (Merck Millipore)<sup>[72,73]</sup> and Neusilin (Fuji Chemical).<sup>[74]</sup> Such systems have a wide range of applications, including: tissue engineering,<sup>[75]</sup> catalysis,<sup>[76]</sup> chromatography,<sup>[77]</sup> adsorbents in environmental modelling<sup>[78]</sup> and drug delivery systems for poorly soluble APIs.<sup>[79]</sup> For the latter, it has been widely reported that mesoporous silica can act as a solubility enhancer by ‘trapping’ API in non-crystalline form within the mesoporous network.<sup>[72,73,80–83]</sup>

For this purpose, there are various methods of loading crystalline API onto mesoporous silica, which can be grouped into three broad categories: solvent-based,<sup>[72]</sup> mechanical activation<sup>[84]</sup> and vapour-mediated.<sup>[85]</sup> A thorough overview of these loading methods of poorly soluble API onto mesoporous silica is beyond the scope of this review, but the interested reader is referred to a number of publications that provide more details on the different routes to API-loaded silica.<sup>[68,84,86–88]</sup>

Although a rather broad variety of methods is present in the literature; the solvent-based approach is most commonly employed. This can be attributed to the poor loading efficiencies and time-consuming processes involved in the solvent-free loading methods such as melt and supercritical fluid-based processes.<sup>[84]</sup> The solvent approaches can be grouped into two main categories: solvent impregnation and incipient wetness. During the solvent impregnation loading approach, API is dissolved in organic solvent and added to mesoporous silica. Adsorption of API onto the silica is then initiated through mechanical agitation or sonication of the slurry. Finally, the solvent is removed, which can be achieved using a number of methods including vacuum drying, spray drying, lyophilisation or rotary evaporation.<sup>[68,72,89,90]</sup> The second approach, incipient wetness, involves the steady addition of small volumes of concentrated API solution onto the silica, so the full amount of solvent is adsorbed into the network and then rapidly evaporated, which leaves the API within the pores.<sup>[73,82]</sup> Both methods result in an API-loaded silica, in which the previously crystalline API is now amorphous or molecularly dispersed. This can be confirmed with analytical methods such as DSC or XRPD.

In general, the theoretical maximum drug content that can be loaded onto mesoporous silica is dependent on the surface area,<sup>[91]</sup> pore volume<sup>[92]</sup> and pore geometry of the silica<sup>[93]</sup> with values as high as 75% reported in the literature.<sup>[89]</sup> However, such very high loads are experimentally barely achievable and residual crystallinity is often observed in drug-loads exceeding 50% (w/w).<sup>[89]</sup> Most cases of API-loaded silica in the literature do not exceed 40% loading.

The loading process can be considered from an energetic perspective of drug adsorption onto the carrier, but there is



currently insufficient information available. Some hypotheses include the following: hydrogen bond interactions,<sup>[94,95]</sup> hydrophobic interactions,<sup>[83]</sup> capillary action<sup>[89]</sup> and ionic interactions,<sup>[96,97]</sup> although the latter depends on the silanol groups on the surface of the silica to be deprotonated and negative.

One of the potential benefits of mesoporous silica relative to alternative amorphous formulations is the high stability that is achievable. This is due to the very small environment of the mesoporous network (so-called nanoconfinement)<sup>[98]</sup> and complimentary interactions (yet to be fully resolved) with the silica surfaces, which lower the free energy of the system further.<sup>[99]</sup> API-loaded silica can often be stored in open containers and at elevated temperatures and pressures, although this can be API-dependent as well. For example, Muller and coworkers demonstrated stability of an amorphous form at ambient and accelerated conditions for 30 different formulations of API-loaded silica, exceeding the requirements for regulatory stability studies.<sup>[100]</sup> This could be particularly used for compounds that have high tendency to recrystallise, e.g. low  $T_g$ , where otherwise classical solid dispersions may fail to provide stable formulations.<sup>[51,71,101]</sup>

Following dispersion in an aqueous medium, such as in the gastrointestinal tract, the API is displaced from the mesoporous network and has the potential to generate supersaturation. The release mechanism can be considered using diffusion kinetics. However, due to the complexity of the porous network and multiple phases, a more refined view will likely emerge in the future when more research has focused on the topic. Simplified, upon administration to an aqueous environment, there is a diffusion of water into the porous network *via* capillary action. This in turn solubilises the loaded API, which generates a concentration gradient between the inside of the silica and the outside medium. This gradient drives the release of API *via* diffusion along a concentration gradient, generating supersaturation and potentially increased absorption.<sup>[83]</sup>

Such a release behaviour can be approximated by classical matrix diffusion (Equation 5), which was proposed by Higuchi in 1961<sup>[102]</sup> to describe API release from thin ointment films:

$$M_t = A\sqrt{2c_{ini}Dc_s t}, \quad (5)$$

where  $M_t$  is the amount of drug released from the inorganic carrier;  $A$  is the surface area available for release;  $c_{ini}$  is initial drug concentration in the carrier;  $D$  the diffusion coefficient of drug in the insoluble carrier and  $c_s$  is the maximum (saturation) concentration of the drug in the carrier.

The approach can also be expanded to describe the release of any API adsorbed or entrapped within an

inorganic and insoluble matrix into an external medium via diffusion.<sup>[103]</sup>

When one considers the above Higuchi equation, the release of API from mesoporous carriers can be described as a diffusion-driven process. Similarly, to loading efficiency, drug release is further dependent on pore surface area, pore volume and pore morphology. However, there have been a number of examples in the literature, where Higuchi diffusion kinetics successfully modelled release of, for example, ibuprofen from mesoporous materials.<sup>[104–106]</sup>

There is surely more research needed to more specifically model release from mesoporous materials and to better understand molecular interactions of the loaded API with the porous carrier.

After the compound is released, a high energy state of drug supersaturation is typically obtained. Therefore, mesoporous formulations are often coupled with so-called precipitation inhibitors such as polymers such as poly(vinylpyrrolidone), which should inhibit a potential crystallisation. This maintenance of initial drug supersaturation forms the basis of the parachute in the spring and parachute model first proposed by Guzman,<sup>[107]</sup> and is more generally used in formulations that generate supersaturation.

Mesoporous silica is a relatively novel formulation option for poorly soluble drugs, with no examples of commercially available formulations so far, and limited proof of concept studies in man that are available in public domain.<sup>[108]</sup> However, there has been a dramatic increase in the interest for mesoporous silica-based formulations in the past decade. A summary of drug properties reported in mesoporous silica formulations is shown in Figure 12.

For MW, there might exist a ‘sweet spot’. For very small molecules, there is efficient and deep penetration within the porous network, but microcrystalline domains can rise (extra space for critical nuclei formation),<sup>[98]</sup> while release can often occur too quickly (high risk of precipitation).<sup>[80]</sup> On the other hand, molecules that are too large and bulky may have problems accessing the pores efficiently, with only impractically low loading efficiencies being obtainable. Another factor of loading efficiency using larger molecules is the pore geometry of the porous network, with open 3D pore structures such as Parateck SLC likely being more accessible than the classical ordered 2D mesoporous silica such as MCM-41. Therefore, in the case of MW, it makes sense that the majority of compounds investigated are in the ‘middle ground’ of 300–500 Da. Further investigation into very small (<200 Da) and very large (>500 Da) molecules would offer interesting insights based on future work. Such additional work may study different quality attributes of amorphous systems. A previous study highlighted, for example, the importance of MW and  $T_m$  for the amorphous solubility advantage, which could be further investigated specifically for mesoporous systems.<sup>[109]</sup>

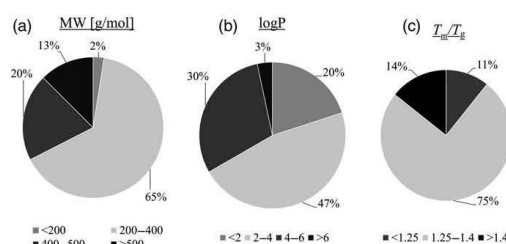


**Figure 12** Properties of APIs formulated with mesoporous silica in the literature. The different panels are explained in the text. API, active pharmaceutical ingredient.

For  $\log P$ , and the hydrophobicity of the molecule, the retrospective analysis of reported mesoporous formulations is less clear. It is likely that the hydrophobicity of a molecule is of great importance in terms of with how it interacts with the surface of the mesoporous silica, and in turn how it is loaded and released. For example, not only polar but also dispersive interactions between API and the silica are expected to play an important role. However, in line with previous considerations of solid dispersions, a very high  $\log P$  value is problematic with respect to drug dissolution. The  $\log P$  data of mesoporous formulations show that most of the formulated poorly water-soluble compounds fall in the  $\log P$  range of 3–5. Thus, in line with the previous comment surrounding MW, future studies on very lipophilic and hydrophobic molecules can only add to the growing understanding of mesoporous silica, and will significantly help towards creating a more rational selection criteria of the most ‘suitable’ candidates for this purpose.

Another parameter that can be considered is again the ratio  $T_m/T_g$ . A higher  $T_m/T_g$  ratio indicates decreased glass-forming ability and decreased stability, which comes with higher propensity for recrystallisation.<sup>[61]</sup>

Previously, it was highlighted that mesoporous silica can enhance shelf life stability via nano-confinement in combination with complementary API-pore interactions, making them suitable even for fast crystallisers as critical compounds in class 3 and 4 of the Friesen plot mentioned above. However, it seems based on  $T_m/T_g$  values that not many more of these difficult drugs have been formulated using mesoporous silica as compared to other solid dispersions. Thus, current literature trials with mesoporous silica have been carried out with the so-called ‘usual suspects’, that being the compounds that are known to work well with other amorphous formulations, such as those obtained by spray drying. This represents a gap in the literature. More work should be carried out to identify a chemical space, where mesoporous silica has particular advantages compared to existing technologies, such as spray-dried dispersions and hot melt extrudates. It is possible that

mesoporous silica could be an especially attractive formulation option for critical compounds with  $T_m/T_g > 1.4$ . Further studies with such compounds would be helpful to map which technical option is the most promising to obtain an optimal amorphous system for a given drug linked to its physicochemical properties.

In line with the previous consideration of hydrophobicity (in terms of  $T_m$ ), Figure 14 highlights the observation that the commonly used APIs are interestingly confined to within a rather limited chemical space.

This leads to the initial impression from Figures 13 and 14 that, there is currently no pronounced difference to the other solid dispersion approaches even though mesoporous silica is an exciting prospect to add to the formulator’s toolbox when considering poorly soluble API. As it stands, more work is required in key areas to better understand: the loading process, the interaction between API and porous surfaces and the release process. More research in this area will allow a more rational selection of mesoporous silica as a viable formulation option, based on a thorough understanding of the chemical drug space that is optimal for this formulation approach. This would avoid some unnecessary formulation screening and lead to a more focused drug development process. It is only when this understanding is established that there will be a shift away from the one-size-fits-all approach in terms of solid dispersions towards more tailored formulation techniques.

### Nanosuspensions

The previous sections outlined the different strategies of how to solubilise poorly water-soluble drugs in the dosage form or how to convert their crystalline solid form, into an amorphous state. An alternative approach is to formulate such challenging drugs as nanosuspensions.<sup>[110]</sup> This formulation technique is of particular interest when high crystal lattice energy is limiting the alternative solubilisation in, for example, LBF. This high lattice energy can be so pronounced that drug candidates might be neither soluble in

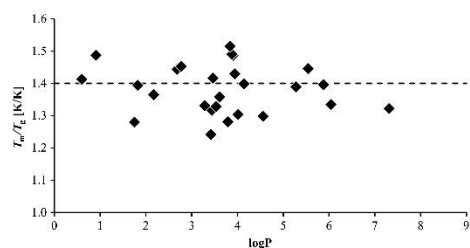


**Figure 13**  $T_m/T_g$  vs  $\log P$  for APIs formulated with mesoporous silica. The dotted line indicates the fragile boundary, above with stability issues can be expected with the amorphous form. API, active pharmaceutical ingredient.

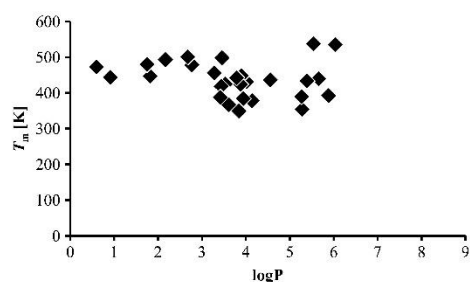


**Figure 14**  $\log P$  as a function of  $T_m$  of compounds in formulations containing mesoporous silica.

polar nor apolar solvents or excipients.<sup>[111]</sup> Nanosuspensions can be formed by breaking larger micron-sized particles down (i.e. top-down approach) and stabilised by a mixture of polymer/surfactant, as in a wet milling technique.<sup>[112]</sup> Several examples such as Rapamune (Wyeth), Emcend (Merck), TriCor (Abbott Laboratories) and Triglide (Skye Pharma) are already on the market.<sup>[113]</sup> In earlier phases of drug development, nanosuspensions are often used to formulate poorly soluble compounds because high doses are administered in toxicological studies. It is here an advantage that wet milling is a rather versatile method to enable nanosuspension production with the majority of compounds. However, many of them do not achieve sufficient physical stability and therefore fail with their critical quality attributes of the nanosuspension. According to current literature, poorly soluble drugs with high MW, high  $T_m$  values, and with a surface energy comparable to that of a given stabiliser, are able to form stable nanosuspensions.<sup>[114]</sup> Specific interactions between the functional groups of stabilisers and drug particle surfaces in the stabilisation process have been demonstrated.<sup>[115]</sup> However, despite extensive efforts, most formulation scientists still

evaluate their suspensions in a trial and error screening of stabilisers, even though some notable guidance has been reported by George *et al.*<sup>[116]</sup> The main goal of their study was to correlate the characteristics of the drugs ( $\log P$  and  $\Delta H_f$ ) with feasibility of forming a stable nanosuspension. According to the data presented, the best candidates were drugs with a high  $\Delta H_f$  (or  $T_m$  so high lattice energy) and high lipophilicity ( $\log P$ ), which can be stabilised either electrostatically or sterically. Thus, a wide range of stabilizing surfactants may result in stable nanosuspensions. On the other hand, drugs with comparatively low  $\Delta H_f$  (or  $T_m$ ) and rather low lipophilicity are poor candidates, irrespective of the stabiliser used. High  $\Delta H_f$  drugs with rather low  $\log P$  values may require an ionic surfactant as stabiliser. Drugs with lower lattice energies, which were more lipophilic (high  $\log P$ ), were proposed to be stabilised by an ionic surfactant with rather high IILB value like sodium lauryl sulphate. This formulation guidance can provide some initial help but more research is needed to rationally design pharmaceutical nanosuspensions. Future research should address mechanisms of stabilisation. Until a more educated approach is available, it seems that the presented considerations of lipophilicity and lattice energy offer at least a starting point for nanosuspension development.

#### Cyclodextrin formulations

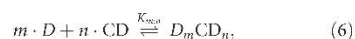
Enzymes belonging to the group cyclodextrin cycloglycosyltransferases (GCRase, EC 2.4.1.19) convert starch into cyclic oligosaccharides, known as cyclodextrins (CDs). These structures are composed of  $\alpha$ -(1,4) linked glucopyranose subunits. The  $\alpha$ ,  $\beta$ , or  $\gamma$ CDs, consisting of six, seven, or eight glucose units, respectively, are the most investigated CDs.<sup>[117,118]</sup> The CD molecule has the shape of a torus due to the chair conformation of the glucopyranose units. Furthermore, the CD molecule has a spatial distribution of polar hydroxyl groups on the outer rim and apolar (relative to water) glucoside oxygens and hydrogens in the cavity. This is why the CD molecule has a hydrophilic outside and a hydrophobic cavity. As a consequence of this structure, CDs have the ability to form inclusion complexes through molecular encapsulation with a wide range of organic compounds.<sup>[117,118]</sup> This special characteristic makes CDs valuable in a number of disciplines, including pharmaceuticals, where the increased solubility of complexes can be used to increase the apparent solubility of poorly soluble drugs.<sup>[119–132]</sup>

While natural  $\alpha$ - and  $\gamma$ CD have good aqueous solubility, natural  $\beta$ CD only has an aqueous solubility of 18.5 g/l, which is believed to be a reflection of the very rigid structure formed through H-bonding of the C2-hydroxyl of one glucopyranose unit with the C-3 hydroxyl of an adjacent unit.<sup>[133]</sup> In the  $\beta$ CD molecule, a complete set of seven



intramolecular H-bonds can be formed, effectively lowering the thermodynamic driving force for interaction with the solvent.<sup>[134]</sup> Moreover, CDs can be chemically modified by e.g. hydroxylation, alkylation or sulfoalkylation, thereby breaking this belt of H-bonds around the CD ring, which for  $\beta$ CD increases the solubility significantly. Different chemically modified CDs with improved physical-chemical properties have been prepared and commercialised, including, 2-hydroxypropyl  $\beta$ -cyclodextrin (HP $\beta$ CD), 2-hydroxypropyl  $\gamma$ -cyclodextrin, methyl  $\beta$ CD (m $\beta$ CD), and sulfobutylether  $\beta$ -cyclodextrin. Due to the low toxicity of the CDs, they can be used for all administration routes (with the exception of parenteral applications of natural  $\beta$ CD). Kurkov and Loftsson recently made a comparative analysis of the more than 30 known CD containing commercial formulations across these administration routes and reported that the most frequently used CD was natural  $\beta$ CD followed by HP $\beta$ CD.<sup>[130]</sup> In total, natural and modified  $\beta$ CDs were included in 83.4% of the formulations.

Cyclodextrins inclusion complexes are molecular complexes, which are formed by a reversible complexation that can be described by the following equilibrium:



where  $m$  is the number of drug ( $D$ ) molecules associated with  $n$  molecules of CDs to form a complex with the stoichiometry of  $m : n$  and  $K_{m:n}$  is the stability constant. As the stoichiometry of the complex is often a 1 : 1 the stability constant can normally be written as;

$$K = \frac{[D \cdot CD]}{[D] \cdot [CD]} \quad (7)$$

The total solubility in the presence of a CD is therefore the intrinsic solubility plus the drug fraction complexed with the CD. Across different routes of administration, the compounds included in commercial formulations containing CDs displayed an average MW of  $369 \pm 130$  g/mol. The distribution in MW was not associated with the type of CD used in the formulation, i.e. the lower MW molecules were not

predominantly formulated with  $\alpha$ CD and the larger compounds with  $\gamma$ CD. The  $\log P$  of the molecules were  $3.2 \pm 1.8$  with a distribution from  $-0.4$  to  $7.8$ , see Figure 15b, with most of the compounds having a  $\log P$  of 2–4. This places the compounds used with CDs in the mid-range of the  $\log P$  field, i.e. there is not a trend that this solubilising approach is used for the real grease balls among drug substances.

The compounds formulated with CDs had an average  $T_m$  of  $436 \pm 82$  K distributed from 194 K for nicotine to higher than 633 K for mitomycin, with most of the compounds having a  $T_m$  in the range of 473–573 K.

When investigating  $\log P$  as a function of  $T_m$  (Figure 16), it is clear that the compounds formulated with CDs tend to have a  $\log P$  from 2–4.5 and a  $T_m$  between 473 and 573 K. Based upon these data, compounds in the mid-range of the spectrum of these limits seem to provide most successful formulations with CDs.

The discriminating power between  $\log P$  and the  $T_m$  revealed some value as a predictor for the useful application of CDs in a formulation. Important for the excipient functionality is the stability constant of inclusion complexation.<sup>[130]</sup> The observed values for stability constants are usually reported to be between 50 to 2000  $M^{-1}$ . Therefore, an important element is also to define how the molecular usage of the CDs can be optimised, that is as high a

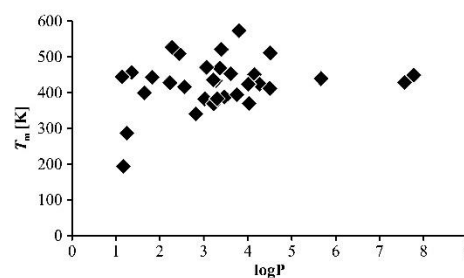


Figure 16  $\log P$  as a function of  $T_m$  of compounds included in commercial formulations containing cyclodextrins.

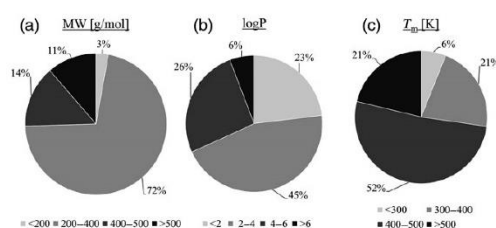


Figure 15 Properties of compounds included in commercial formulations containing cyclodextrins. The different panels are explained in the text.

complexation efficacy as possible.<sup>[132]</sup> As the complexation efficacy is defined as a function of the stability constant multiplied with the intrinsic aqueous solubility, different influences on these factors (e.g. ionisation of the drug, addition of cosolvents, addition of polymers, etc.) could be used to affect the complexation efficacy.<sup>[130]</sup> When investigating the Yalkowsky equation presented in the theoretical section (Equation 3), it is clear that both  $\log P$  and the  $T_m$  are part of the equation controlling the aqueous solubility.<sup>[11]</sup> Consequently, molecules with a relatively low values of  $\log P$  and  $T_m$  would naturally seem to be good candidates to obtain a high complexation efficacy in CDs. However, Chari *et al.*<sup>[135]</sup> concluded with a training set of 258 ligands that the most important molecular descriptor to describe the interaction with CDs was primarily  $\log P$ . Li *et al.*<sup>[136]</sup> reported the parameters of VAMP polarisation YY and VAMP dipole Y component, representing a semi-empirical molecular orbital package in the TSAR software,  $\log P$ , Balaban topological index, and cosmic electrostatic energy, as the five most important structural parameters influencing the binding constant between drugs and  $\beta$ CD. Hence, there seems to be a general agreement that  $\log P$  is a fair descriptor of potential interaction between drug molecules and CDs. Interestingly,  $T_m$  has not been mentioned in any of the studies focusing on molecular descriptors. It therefore seems that rather solvation-limited solubility than a high crystal energy of drug candidates would favour the choice of CD formulations. Moreover, geometric molecular fit requirements must be given drugs to achieve successful complexation with CDs.<sup>[137]</sup>

## Conclusions

As lipophilicity is conventionally understood as a relative scale for given compounds, it should be clearly distinguished from hydrophobicity as a solubility limitation for poorly water-soluble drugs. The properties  $T_m$  (or  $\Delta H_f$ ) and  $\log P$  have to be considered for the selection of a promising bio-enabling oral formulation. It is for example

reasonable to assume that very high  $T_m$  values can lead to issues of solubility in any solvent-based process and any LBF. While this can indeed give a first orientation about the formulation strategy, one should refrain from any absolute statements. Recent developments in LBF were discussed that may cope with quite hydrophobic drug bases. Also in the field of solid dispersions and mesoporous silica, a consideration of  $T_m$  or  $T_m/T_g$  is important to guide initial experiments and to assess the stability of an amorphous state, but such simple approaches have their limits. It seems particularly difficult to obtain clear guidance on the selection of the manufacturing method based on available literature data. Novel approaches such as the mesoporous formulations or coprecipitated amorphous formulations are likely to become more important in the future. More work is also expected with respect to molecular modelling that can highlight effects of molecular size and specific interactions for example in cyclodextrin formulations or regarding stability in nanosuspensions. It can be expected that considerations of hydrophobicity and lipophilicity will also be of importance in the future but only for a rough assessment of the formulation strategy because more refined considerations require additional molecular properties for a rationale and structured development of bio-enabling formulations.

## Declarations

### Conflict of interest

The authors declare that they have no conflict of interest to disclose.

### Funding

This project has received funding from the European Union's Horizon 2020 Research and Innovation Programme under grant agreement No 674909.

## References

- Porter CJH *et al.* Lipids and lipid-based formulations: optimizing the oral delivery of lipophilic drugs. *Nat Rev Drug Discov* 2007; 6: 231–248.
- Mu H *et al.* Lipid-based formulations for oral administration of poorly water-soluble drugs. *Int J Pharm* 2013; 453: 215–224.
- Feeney OM *et al.* 50 years of oral lipid-based formulations: provenance, progress and future perspectives. *Adv Drug Deliv Rev* 2016; 101: 167–194.
- Savla R *et al.* Review and analysis of FDA approved drugs using lipid-based formulations. *Drug Dev Ind Pharm* 2017; 43: 1–16. <https://doi.org/10.1080/03639045.2017.1342654>.
- Edueng K *et al.* The need for restructuring the disordered science of amorphous drug formulations. *Pharm Res* 2017; 34: 1754–1772.
- Bergström CAS *et al.* Poorly soluble marketed drugs display solvation limited solubility. *J Med Chem* 2007; 50: 5858–5862.
- Bergström CAS *et al.* Computational prediction of formulation strategies for beyond-rule-of-5 compounds. *Adv Drug Deliv Rev* 2016; 101: 6–21.
- Nordström FL, Rasmuson ÅC. Determination of the activity of a molecular solute in saturated solution. *J Chem Thermodyn* 2008; 40: 1684–1692.



9. Nordström FL, Rasmuson ÅC. Prediction of solubility curves and melting properties of organic and pharmaceutical compounds. *Eur J Pharm Sci* 2009; 36: 330–344.
10. Hildebrand J, Scott R. *The Solubility of Nonelectrolytes*. New York, NY: Reinhold, 1950.
11. Jain N, Yalkowsky SH. Estimation of the aqueous solubility I: application to organic nonelectrolytes. *J Pharm Sci* 2001; 90: 234–252.
12. Wassvik CM *et al.* Contribution of solid-state properties to the aqueous solubility of drugs. *Eur J Pharm Sci* 2006; 29(3–4 SPEC. ISS.): 294–305.
13. Elder D, Holm R. Aqueous solubility: simple predictive methods (in silico, in vitro and bio-relevant approaches). *Int J Pharm* 2013; 453: 3–11.
14. Wassvik CM *et al.* Molecular characteristics for solid-state limited solubility. *J Med Chem* 2008; 51: 3035–3039.
15. Abraham MH *et al.* Determination of olive oil-gas and hexadecane-gas partition coefficients, and calculation of the corresponding olive oil-water and hexadecane-water partition coefficients. *J Chem Soc Perkin Trans* 1987; 11. <http://pubs.rsc.org/-/content/articlepdf/1987/p2/p29870000797> (accessed 10 July 2017).
16. Abraham MH, Le J. The correlation and prediction of the solubility of compounds in water using an amended solvation energy relationship. *J Pharm Sci* 1999; 88: 868–880.
17. Niederquell A, Kuentz M. Biorelevant drug solubility enhancement modeled by a linear solvation energy relationship. *J Pharm Sci* 2017; 107: 503–506.
18. Lipinski CA *et al.* Experimental and computational approaches to estimate solubility and permeability in drug discovery and development. *Adv Drug Deliv Rev* 2001; 46: 3–26.
19. Pouton CW. Lipid formulations for oral administration of drugs: non-emulsifying, self-emulsifying and “self-microemulsifying” drug delivery systems. *Eur J Pharm Sci* 2000; 11 (Suppl 2): S93–S98.
20. Rane SS, Anderson BD. What determines drug solubility in lipid vehicles: is it predictable? *Adv Drug Deliv Rev* 2008; 60: 638–656.
21. Persson LC *et al.* Computational prediction of drug solubility in lipid based formulation excipients. *Pharm Res* 2013; 30: 3225–3237.
22. Alskär LC *et al.* Tools for early prediction of drug loading in lipid-based formulations. *Mol Pharm* 2016; 13: 251–261.
23. Gautschi N *et al.* Rapid determination of drug solubilization versus supersaturation in natural and digested lipids. *Int J Pharm* 2016; 513: 164–174.
24. Constantinides PP, Wasan KM. Lipid formulation strategies for enhancing intestinal transport and absorption of P-glycoprotein (P-gp) substrate drugs: in vitro/in vivo case studies. *J Pharm Sci* 2007; 96: 235–248.
25. Caliph SM *et al.* Effect of short-, medium-, and long-chain fatty acid-based vehicles on the absolute oral bioavailability and intestinal lymphatic transport of halofantrine and assessment of mass balance in lymph-cannulated and non-cannulated rats. *J Pharm Sci* 2000; 89: 1073–1084.
26. Thi TD *et al.* Formulate-ability of ten compounds with different physicochemical profiles in SMEDDS. *Eur J Pharm Sci* 2009; 38: 479–488.
27. Pouton CW. Formulation of poorly water-soluble drugs for oral administration: physicochemical and physiological issues and the lipid formulation classification system. *Eur J Pharm Sci* 2006; 29: 278–287.
28. Dumanli I. Mechanistic studies to elucidate the role of lipid vehicles on solubility, formulation and bioavailability of poorly soluble compounds. *Open Access Diss* 2002 (Paper 171). [http://digitalcommons.uri.edu/oa\\_diss/171](http://digitalcommons.uri.edu/oa_diss/171).
29. Hauss D. *Oral Lipid-Based Formulations: Enhancing the Bioavailability of Poorly Water-Soluble Drugs (Drugs and the Pharmaceutical Sciences)*. Boca Raton: CRC Press, 2007.
30. Birru WA *et al.* Computational models of the gastrointestinal environment. 1. The effect of digestion on the phase behavior of intestinal fluids. *Mol Pharm* 2017; 14: 566–579.
31. Williams HD *et al.* Strategies to address low drug solubility in discovery and development. *Pharmacol Rev* 2013; 65: 315–499.
32. Thomas N *et al.* In vitro and in vivo performance of novel supersaturated self-nanoemulsifying drug delivery systems (super-SNEDDS). *J Control Release* 2012; 160: 25–32.
33. Thomas N *et al.* Supersaturated self-nanoemulsifying drug delivery systems (Super-SNEDDS) enhance the bioavailability of the poorly water-soluble drug simvastatin in dogs. *AAPS J* 2013; 15: 219–227.
34. Thomas N *et al.* In vitro lipolysis data does not adequately predict the in vivo performance of lipid-based drug delivery systems containing fenofibrate. *AAPS J* 2014; 16: 539–549.
35. Morgen M *et al.* Lipophilic salts of poorly soluble compounds to enable high-dose lipidic SEDDS formulations in drug discovery. *Eur J Pharm Biopharm* 2017; 117: 212–223.
36. Sahbaz Y *et al.* Transformation of poorly water-soluble drugs into lipophilic ionic liquids enhances oral drug exposure from lipid based formulations. *Mol Pharm* 2015; 12: 1980–1991.
37. Williams HD *et al.* Transformation of biopharmaceutical classification system class I and III drugs into ionic liquids and lipophilic salts for enhanced developability using lipid formulations. *J Pharm Sci* 2017; 107: 203–216. <https://doi.org/10.1016/j.xphs.2017.05.019>.
38. Bala V *et al.* Lipophilic prodrugs of SN38: synthesis and in vitro characterization toward oral chemotherapy. *Mol Pharm* 2016; 13: 287–294.
39. Han S *et al.* Targeted delivery of a model immunomodulator to the lymphatic system: comparison of alkyl ester versus triglyceride mimetic lipid prodrug strategies. *J Control Release* 2014; 177: 1–10.

40. Larsen A *et al.* Lipid-based formulations for danazol containing a digestible surfactant, Labrafil M2125CS: in vivo bioavailability and dynamic in vitro lipolysis. *Pharm Res* 2008; 25: 2769–2777.
41. Dahan A, Hoffman A. The effect of different lipid based formulations on the oral absorption of lipophilic drugs: the ability of in vitro lipolysis and consecutive ex vivo intestinal permeability data to predict in vivo bioavailability in rats. *Eur J Pharm Biopharm* 2007; 67: 96–105.
42. Chiou WL, Riegelman S. Preparation and dissolution characteristics of several fast-release solid dispersions of griseofulvin. *J Pharm Sci* 1969; 58: 1505–1510.
43. Goldberg AH *et al.* Increasing dissolution rates and gastrointestinal absorption of drugs via solid solutions and eutectic mixtures II. *J Pharm Sci* 1966; 55: 482–487.
44. Hancock BC, Shamblin SL. Molecular mobility of amorphous pharmaceuticals determined using differential scanning calorimetry. *Thermochim Acta* 2001; 380: 95–107.
45. Gupta P *et al.* Physical stability and solubility advantage from amorphous celecoxib: the role of thermodynamic quantities and molecular mobility. *Mol Pharm* 2004; 1: 406–413.
46. Hancock BC, Parks M. What is the true solubility advantage for amorphous pharmaceuticals? *Pharm Res* 2000; 17: 397–404.
47. Bragg WL. Diffraction of short electromagnetic waves by a crystal. *Proc Camb Philos Soc* 1913; 17: 43–57.
48. Klug HP, Alexander LE. *X-Ray Diffraction Procedures for Polycrystalline and Amorphous Materials*. Hoboken: John Wiley & Sons, 1974.
49. Chiou WL, Riegelman S. Pharmaceutical applications of solid dispersion systems. *J Pharm Sci* 1971; 60: 1281–1302.
50. Leuner C, Dressman J. Improving drug solubility for oral delivery using solid dispersions. *Eur J Pharm Biopharm* 2000; 50: 47–60.
51. Vo CL-N *et al.* Current trends and future perspectives of solid dispersions containing poorly water-soluble drugs. *Eur J Pharm Biopharm* 2013; 85: 799–813.
52. Chen Y *et al.* Initial drug dissolution from amorphous solid dispersions controlled by polymer dissolution and drug-polymer interaction. *Pharm Res* 2016; 33: 2445–2458.
53. Patterson JE *et al.* Preparation of glass solutions of three poorly water soluble drugs by spray drying, melt extrusion and ball milling. *Int J Pharm* 2007; 336: 22–34.
54. Wyttenbach N, Kuentz M. Glass-forming ability of compounds in marketed amorphous drug products. *Eur J Pharm Biopharm* 2017; 112: 204–208.
55. Meng F *et al.* Classification of solid dispersions: correlation to (i) stability and solubility (ii) preparation and characterization techniques. *Drug Dev Ind Pharm* 2015; 41: 1401–1415.
56. Gurunath S *et al.* Amorphous solid dispersion method for improving oral bioavailability of poorly water-soluble drugs. *J Pharm Res* 2013; 6: 476–480.
57. Sekiguchi K, Obi N. Studies on absorption of eutectic mixture. I. A comparison of the behavior of eutectic mixture of sulfathiazole and that of ordinary sulfathiazole in man. *Chem Pharm Bull (Tokyo)* 1961; 9: 866–872.
58. Repka MA *et al.* Melt extrusion with poorly soluble drugs – an integrated review. *Int J Pharm* 2018; 535: 68–85.
59. Paudel A *et al.* Manufacturing of solid dispersions of poorly water soluble drugs by spray drying: formulation and process considerations. *Int J Pharm* 2013; 453: 253–284.
60. Wyttenbach N *et al.* Theoretical considerations of the prigogine-defay ratio with regard to the glass-forming ability of drugs from undercooled melts. *Mol Pharm* 2016; 13: 241–250.
61. Friesen DT *et al.* Hydroxypropyl methylcellulose acetate succinate-based spray-dried dispersions: an overview. *Mol Pharm* 2008; 5: 1003–1019.
62. Baird JA *et al.* A classification system to assess the crystallization tendency of organic molecules from undercooled melts. *J Pharm Sci* 2010; 99: 3787–3806.
63. Alhalaweh A *et al.* Physical stability of drugs after storage above and below the glass transition temperature: relationship to glass-forming ability. *Int J Pharm* 2015; 495: 312–317.
64. Mahlin D, Bergström CAS. Early drug development predictions of glass-forming ability and physical stability of drugs. *Eur J Pharm Sci* 2013; 49: 323–332.
65. Page S *et al.* Structured development approach for amorphous systems. In: Williams RO III *et al.*, eds. *Formulating Poorly Water Soluble Drugs*, Vol. 22. Basel: Springer International Publishing, 2016: 329–382.
66. Shah N *et al.* Development of novel microprecipitated bulk powder (MBP) technology for manufacturing stable amorphous formulations of poorly soluble drugs. *Int J Pharm* 2012; 438: 53–60.
67. DeBoyace K, Wildfong PLD. The application of modeling and prediction to the formation and stability of amorphous solid dispersions. *J Pharm Sci* 2018; 107: 57–74.
68. Linnell T *et al.* Drug delivery formulations of ordered and nonordered mesoporous silica: comparison of three drug loading methods. *J Pharm Sci* 2011; 100: 3294–3306.
69. Barbé C *et al.* Silica particles: a novel drug-delivery system. *Adv Mater* 2004; 16: 1959–1966.
70. Kresge CT *et al.* Ordered mesoporous molecular sieves synthesized by a liquid-crystal template mechanism. *Nature* 1992; 359: 710–712.
71. Mellaerts R *et al.* Aging behavior of pharmaceutical formulations of itraconazole on SBA-15 ordered mesoporous silica carrier material. *Microporous Mesoporous Mater* 2010; 130: 154–161.
72. Lainé A-L *et al.* Enhanced oral delivery of celecoxib via the development of a supersaturable amorphous formulation utilising mesoporous silica and co-loaded HPMCAS. *Int J Pharm* 2016; 512: 118–125.

73. O'Shea JP *et al.* Mesoporous silica-based dosage forms improve bioavailability of poorly soluble drugs in pigs: case example fenofibrate. *J Pharm Pharmacol* 2017; 69: 1284–1292.
74. Khanfar M, Al-Nimry S. Stabilization and amorphization of lovastatin using different types of silica. *AAPS PharmSciTech* 2017; 18: 2358–2367.
75. Vallet-Regí M. Ordered mesoporous materials in the context of drug delivery systems and bone tissue engineering. *Chemistry* 2006; 12: 5934–5943.
76. Saad A *et al.* Triazole/triazine-functionalized mesoporous silica as a hybrid material support for palladium nanocatalyst. *Langmuir* 2017; 33: 7137–7146.
77. Majors RE. High-performance liquid chromatography on small particle silica gel. *Anal Chem* 1972; 44: 1722–1726.
78. Bhatnagar A, Sillanpää M. Utilization of agro-industrial and municipal waste materials as potential adsorbents for water treatment – a review. *Chem Eng J* 2010; 157: 277–296.
79. Wang S. Ordered mesoporous materials for drug delivery. *Microporous Mesoporous Mater* 2009; 117: 1–9.
80. Van Speybroeck M *et al.* Enhanced absorption of the poorly soluble drug fenofibrate by tuning its release rate from ordered mesoporous silica. *Eur J Pharm Sci* 2010; 41: 623–630.
81. Vialpando M *et al.* Potential of ordered mesoporous silica for oral delivery of poorly soluble drugs. *Ther Deliv* 2011; 2: 1079–1091.
82. Dressman JB *et al.* Mesoporous silica-based dosage forms improve release characteristics of poorly soluble drugs: case example fenofibrate. *J Pharm Pharmacol* 2016; 68: 634–645.
83. Xu W *et al.* Mesoporous systems for poorly soluble drugs. *Int J Pharm* 2013; 453: 181–197.
84. Qian KK, Bogner RH. Spontaneous crystalline-to-amorphous phase transformation of organic or medicinal compounds in the presence of porous media, part 1: thermodynamics of spontaneous amorphization. *J Pharm Sci* 2011; 100: 2801–2815.
85. Zhang Z *et al.* Loading amorphous Asarone in mesoporous silica SBA-15 through supercritical carbon dioxide technology to enhance dissolution and bioavailability. *Eur J Pharm Biopharm* 2015; 92: 28–31.
86. McCarthy CA *et al.* Mesoporous silica formulation strategies for drug dissolution enhancement: a review. *Expert Opin Drug Deliv* 2016; 13: 93–108.
87. Watanabe T *et al.* Solid state radical recombination and charge transfer across the boundary between indomethacin and silica under mechanical stress. *J Solid State Chem* 2002; 164: 27–33.
88. Hillerström A *et al.* Solvent strategies for loading and release in mesoporous silica. *Colloid Interface Sci Commun* 2014; 3: 5–8.
89. Wei Q *et al.* Oral hesperidin—amorphization and improved dissolution properties by controlled loading onto porous silica. *Int J Pharm* 2017; 518: 253–263.
90. Meer T *et al.* Solubility modulation of bicalutamide using porous silica. *J Pharm Investig* 2013; 43: 279–285.
91. Vallet-Regí M *et al.* Drug confinement and delivery in ceramic implants. *Drug Metab Lett* 2007; 1: 37–40.
92. Yang Z *et al.* Microstructure of an immiscible polymer blend and its stabilization effect on amorphous solid dispersions. *Mol Pharm* 2013; 10: 2767–2780.
93. Heikkilä T *et al.* Evaluation of mesoporous TCPSi, MCM-41, SBA-15, and TUD-1 materials as API carriers for oral drug delivery. *Drug Deliv* 2007; 14: 337–347.
94. Wang F *et al.* Oxidized mesoporous silicon microparticles for improved oral delivery of poorly soluble drugs. *Mol Pharm* 2010; 7: 227–236.
95. Kinnari P *et al.* Comparison of mesoporous silicon and non-ordered mesoporous silica materials as drug carriers for itraconazole. *Int J Pharm* 2011; 414: 148–156.
96. Atkin R *et al.* Mechanism of cationic surfactant adsorption at the solid–aqueous interface. *Adv Colloid Interface Sci* 2003; 103: 219–304.
97. Turku I *et al.* Thermodynamics of tetracycline adsorption on silica. *Environ Chem Lett* 2007; 5: 225–228.
98. Sliwinska-Bartkowiak M *et al.* Freezing behavior in porous glasses and MCM-41. *Colloids Surf A Physicochem Eng Asp* 2001; 187–188: 523–529.
99. Azais T *et al.* Solid-state NMR study of ibuprofen confined in MCM-41 material. *Chem Mater* 2006; 18: 6382–6390.
100. Müller RH *et al.* CapsMorph: >4 years long-term stability of industrially feasible amorphous drug formulations. In: *Int. Symp. Control. Rel. Bioact. Mater.* 40. Honolulu/Hawaii, 2013.
101. Salonen J *et al.* Mesoporous silicon in drug delivery applications. *J Pharm Sci* 2008; 97: 632–653.
102. Higuchi T. Rate of release of medications from ointment bases containing drugs in suspension. *J Pharm Sci* 1961; 50: 874–875.
103. Siepmann J, Peppas NA. Higuchi equation: derivation, applications, use and misuse. *Int J Pharm* 2011; 418: 6–12.
104. Andersson J *et al.* Influences of material characteristics on ibuprofen drug loading and release profiles from ordered micro- and mesoporous silica matrices. *Chem Mater* 2004; 16: 4160–4167.
105. Horcajada P *et al.* Influence of pore size of MCM-41 matrices on drug delivery rate. *Microporous Mesoporous Mater* 2004; 68: 105–109.
106. Zhao W *et al.* Uniform rattle-type hollow magnetic mesoporous spheres as drug delivery carriers and their sustained-release property. *Adv Funct Mater* 2008; 18: 2780–2788.
107. Guzmán HR *et al.* Combined use of crystalline salt forms and precipitation inhibitors to improve oral absorption of celecoxib from solid oral formulations. *J Pharm Sci* 2007; 96: 2686–2702.



## X. Thesis Publications

Felix Ditzinger *et al.*

Lipophilicity and hydrophobicity considerations

108. Bukara K *et al.* Ordered mesoporous silica to enhance the bioavailability of poorly water-soluble drugs: proof of concept in man. *Eur J Pharm Biopharm* 2016; 108: 220–225.
109. Kuentz M, Imanidis G. In silico prediction of the solubility advantage for amorphous drugs – are there property-based rules for drug discovery and early pharmaceutical development? *Eur J Pharm Sci* 2013; 48: 554–562.
110. Chen H *et al.* Nanonization strategies for poorly water-soluble drugs. *Drug Discov Today* 2011; 16: 354–360.
111. Rabinow BE. Nanosuspensions in drug delivery. *Nat Rev Drug Discov* 2004; 3: 785–796.
112. Van Eerdenbrugh B *et al.* Top-down production of drug nanocrystals: nanosuspension stabilization, miniaturization and transformation into solid products. *Int J Pharm* 2008; 364: 64–75.
113. Merisko-Liversidge E, Liversidge GG. Nanosizing for oral and parenteral drug delivery: a perspective on formulating poorly-water soluble compounds using wet media milling technology. *Adv Drug Deliv Rev* 2011; 63: 427–440.
114. Lee J *et al.* Characteristics of polymers enabling nano-comminution of water-insoluble drugs. *Int J Pharm* 2008; 355: 328–336.
115. Lee MK *et al.* Hydrophilic and hydrophobic amino acid copolymers for nano-comminution of poorly soluble drugs. *Int J Pharm* 2010; 384: 173–180.
116. George M, Ghosh I. Identifying the correlation between drug/stabilizer properties and critical quality attributes (CQAs) of nanosuspension formulation prepared by wet media milling technology. *Eur J Pharm Sci* 2013; 48: 142–152.
117. Szejtli J. *Cyclodextrin Technology*. Dordrecht: Springer Netherlands, 1988. <https://doi.org/10.1007/978-94-015-7797-7>.
118. Szejtli J. Chemistry, physical and biological properties of cyclodextrins. In: Szejtli J, Osa T, eds. *Cyclodextrines*. Amsterdam: Elsevier Science Ltd., 1996: 189–204.
119. Carrier RL *et al.* The utility of cyclodextrins for enhancing oral bioavailability. *J Control Release* 2007; 123: 78–99.
120. Davis ME, Brewster ME. Cyclodextrin-based pharmaceuticals: past, present and future. *Nat Rev Drug Discov* 2004; 3: 1023–1035.
121. Brewster ME, Loftsson T. Cyclodextrins as pharmaceutical solubilizers. *Adv Drug Deliv Rev* 2007; 59: 645–666.
122. Loftsson T *et al.* Role of cyclodextrins in improving oral drug delivery. *Am J Drug Deliv* 2004; 2: 261–275.
123. Szejtli J. Medicinal applications of cyclodextrins. *Med Res Rev* 1994; 14: 353–386.
124. Rajewski RA, Stella VJ. Pharmaceutical applications of cyclodextrins. 2. In vivo drug delivery. *J Pharm Sci* 1996; 85: 1142–1169.
125. Uekama K, Otagiri M. Cyclodextrins in drug carrier systems. *Crit Rev Ther Drug Carrier Syst* 1987; 3: 1–40.
126. Challa R *et al.* Cyclodextrins in drug delivery: an updated review. *AAPS PharmSciTech* 2005; 6: E329–E357.
127. Arima H *et al.* Recent aspects of cyclodextrin-based pharmaceutical formulations. *Recent Res Dev Chem Pharm Sci* 2002; 2: 155–193.
128. Thompson DO. Cyclodextrins – enabling excipients: their present and future use in pharmaceuticals. *Crit Rev Ther Drug Carrier Syst* 1997; 14: 1–104.
129. Uekama K. Design and evaluation of cyclodextrin-based drug formulation. *Chem Pharm Bull (Tokyo)* 2004; 52: 900–915.
130. Kurkov SV, Loftsson T. Cyclodextrins. *Int J Pharm* 2013; 453: 167–180.
131. Loftsson T, Brewster ME. Cyclodextrins as functional excipients: methods to enhance complexation efficiency. *J Pharm Sci* 2012; 101: 3019–3032.
132. Jambhekar SS, Breen P. Cyclodextrins in pharmaceutical formulations II: solubilization, binding constant, and complexation efficiency. *Drug Discov Today* 2016; 21: 363–368.
133. Saenger W *et al.* Flip-flop hydrogen bonds in  $\beta$ -cyclodextrin – a generally valid principle in polysaccharides? *Angew Chem Int Ed Engl* 1983; 22: 883–884.
134. Naidoo KJ *et al.* Molecular properties related to the anomalous solubility of  $\beta$ -cyclodextrin. *J Phys Chem B* 2004; 108: 4236–4238.
135. Chari R *et al.* Development of improved empirical models for estimating the binding constant of a beta-cyclodextrin inclusion complex. *Pharm Res* 2009; 26: 161–171.
136. Li H *et al.* Structure-based in silico model profiles the binding constant of poorly soluble drugs with  $\beta$ -cyclodextrin. *Eur J Pharm Sci* 2011; 42: 55–64.
137. Hazai E *et al.* Cyclodextrin KnowledgeBase a web-based service managing CD-ligand complexation data. *J Comput Aided Mol Des* 2010; 24: 713–717.

## Application of the solubility parameter concept to assist with oral delivery of poorly water-soluble drugs – a PEARRL review

Sandra Jankovic<sup>a,b</sup> , Georgia Tsakiridou<sup>c,d</sup>, Felix Ditzinger<sup>a,b</sup> , Niklas J. Koehl<sup>e</sup>, Daniel J. Price<sup>f,g</sup> , Alexandra-Roxana Ilie<sup>e,h</sup>, Lida Kalantzi<sup>c</sup>, Kristof Kimpe<sup>i</sup>, René Holm<sup>h</sup>, Anita Nair<sup>f</sup>, Brendan Griffin<sup>e</sup> , Christoph Saal<sup>f</sup> and Martin Kuentz<sup>b</sup> 

<sup>a</sup>Department of Pharmaceutical Sciences, University of Basel, Basel, <sup>b</sup>Institute of Pharma Technology, University of Applied Sciences and Arts Northwestern Switzerland, Muttenz, Switzerland, <sup>c</sup>Pharmathen SA, Product Design & Evaluation, <sup>d</sup>Faculty of Pharmacy, National and Kapodistrian University of Athens, Athens, Greece, <sup>e</sup>School of Pharmacy, University College Cork, Cork, Ireland, <sup>f</sup>Merck Group, Molecule Characterisation, Darmstadt, <sup>g</sup>Goethe University, Frankfurt, Germany, <sup>h</sup>Drug Product Development and <sup>i</sup>Pharmaceutical Sciences, Janssen Research and Development, Johnson & Johnson, Beerse, Belgium

### Keywords

enabling formulation; *in silico* prediction; poorly water-soluble drug; solubility parameter

### Correspondence

Martin Kuentz, Institute of Pharma Technology, University of Applied Sciences and Arts Northwestern Switzerland, Gründenstrasse 40, 4132 Muttenz, Switzerland.  
E-mail: Martin.Kuentz@fhnw.ch

Received February 21, 2018  
Accepted May 28, 2018

doi: 10.1111/jphp.12948

### Abstract

**Objectives** Solubility parameters have been used for decades in various scientific fields including pharmaceuticals. It is, however, still a field of active research both on a conceptual and experimental level. This work addresses the need to review solubility parameter applications in pharmaceuticals of poorly water-soluble drugs.

**Key findings** An overview of the different experimental and calculation methods to determine solubility parameters is provided, which covers from classical to modern approaches. In the pharmaceutical field, solubility parameters are primarily used to guide organic solvent selection, cocrystals and salt screening, lipid-based delivery, solid dispersions and nano- or microparticulate drug delivery systems. Solubility parameters have been applied for a quantitative assessment of mixtures, or they are simply used to rank excipients for a given drug.

**Summary** In particular, partial solubility parameters hold great promise for aiding the development of poorly soluble drug delivery systems. This is particularly true in early-stage development, where compound availability and resources are limited. The experimental determination of solubility parameters has its merits despite being rather labour-intensive because further data can be used to continuously improve *in silico* predictions. Such improvements will ensure that solubility parameters will also in future guide scientists in finding suitable drug formulations.

### Introduction

Solubility parameters have received much attention and numerous applications have been reported in diverse scientific fields.<sup>[1]</sup> Pharmaceuticals has been a prime discipline for applying solubility parameters to formulation design. Previous studies have, for example, reported the use of solubility parameters to predict suitable solvents for solutes, select polymer blends, and to describe surface and adhesion phenomena.<sup>[1]</sup> It would be interesting to have an overview of such pharmaceutical applications with a particular emphasis on the development of poorly soluble drug formulations.

Development of new formulations requires the use of different tools to predict and analyse the physicochemical properties and interactions of dosage form components.<sup>[2,3]</sup> For prediction of material properties and their interactions, for example, solubility parameters are routinely used with high levels of success.<sup>[2]</sup> Historically, this strategy has been employed in drug development for the selection of solvents for coating. Since then, further applications, as well as more robust thermodynamic methods for solubility parameter calculations, have also been reported. Specifically, such thermodynamic methods can be used for study and



prediction of the physical and chemical properties of compounds together with their effects on mixtures and dosage forms.<sup>[2]</sup>

The definition of solubility parameter was first coined by Hildebrand and Scott in 1950.<sup>[1]</sup> An important theoretical development was then proposed later in 1967 with introduction of the so-called Hansen solubility parameter (HSP).<sup>[1]</sup> This concept divides the total solubility parameter ( $\delta_t$ ) into three different contributions: polar, nonpolar and hydrogen bonding, and it is therefore more versatile than the original one-dimensional solubility parameter defined by Hildebrand, which does not account for these specific contributions.<sup>[2]</sup>

Solubility parameters can be derived experimentally from heat of vaporisation, internal pressures, surface tensions and other material characteristics as outlined by Hildebrand and Scott.<sup>[4]</sup> Since then, a number of researchers have reported new methods to more accurately predict solubility parameter values, considering, for example, purely acidic or basic compounds<sup>[5]</sup> for a specific process technique.<sup>[6]</sup> More recent predictions of solubility parameters rely on molecular dynamics simulations or on the conductor-like screening model (COSMO), and these computational methods have been compared by Diaz *et al.*<sup>[7]</sup> Important in this context is the research of Panayiotou and coworkers who contributed to the theoretical concept of solubility parameter and proposed a modern quantitative structure–property relationship.<sup>[8]</sup> Furthermore the recent article by Louwerse *et al.* broadly summarised limitations of the solubility parameter concept and proposed theoretical improvements.<sup>[9]</sup>

Previously, various authors<sup>[2,10,11]</sup> have shown the practical importance of solubility parameters, but a general overview of their applications in the pharmaceutical field is missing. This article addresses the particular need to review the use of solubility parameters in pharmaceuticals with respect to formulation of poorly soluble drugs. The latter oral delivery systems are central to the PEARL research consortium that is deals with the design of such formulations and new tools for their biopharmaceutical assessment.

## Theory and experimental aspects of the solubility parameter concept

### Introduction to the solubility parameter concept

The principle of ‘like dissolves like’ is a well-known term within chemical and pharmaceutical sciences, which can be more generally described as ‘like seeks like’. The usefulness of such approaches depends of course on the ability to assign a numerical value to molecular similarity or dissimilarity. Such a quantitative number is provided by the

solubility parameter, which is a rather simple but very powerful approach.

For a better understanding of the solubility parameter concept, it is helpful to discuss its historical origins that are linked to the theory of nonideal solutions. For such solutions, the activity of a solute,  $\alpha_2$ , is the product of the concentration  $X_2$  (mole fraction) and the activity coefficient,  $\gamma_2$  (Equation 1):

$$\alpha_2 = X_2\gamma_2 \quad (1)$$

It is a central task of thermodynamic theories to predict  $\gamma_2$  and a classical approach is that by Scatchard<sup>[12]</sup> and by Hildebrand and Wood.<sup>[13]</sup>

$$\ln(\gamma_2) = (w_{22} + w_{11} - 2w_{12}) \frac{V_2\phi_1^2}{RT} \quad (2)$$

where  $V_2$  is the volume of the solute and  $\phi_1$  is the volume fraction of the solvent and  $R$  and  $T$  are the gas constant and temperature, respectively (Equation 2). The term  $w_{11}$  denotes the energy needed to remove solute molecules from the bulk, while  $w_{22}$  equals to the idealised removal of solvent molecules to generate a cavity in the solvent for the molecule to dissolve. Such an idealised transfer of the molecule would lead to gained insertion energy in the solvent or release of solvation energy of  $-2w_{12}$ . It was an important idea to approximate the interaction term  $w_{12}$  by the square root of the product of  $w_{11}$  and  $w_{22}$  so that the following equation is obtained:

$$\ln(\gamma_2) = [(w_{11})^{0.5} - (w_{22})^{0.5}]^2 \frac{V_2\phi_1^2}{RT} \quad (3)$$

The advantage of having only pure component properties of the solvent and solute in Equation 3 is that they can be listed for the different chemicals without the need to additionally determine a specific interaction parameter like  $w_{12}$ . Hildebrand and Scott<sup>[4]</sup> coined the notion of the solubility parameter  $\delta_x$  that is here given for the solute as follows (Equation 4):

$$\delta_2 = (w_{22})^{0.5} \quad (4)$$

The solubility parameter is the square root of energy per volume, and it is often named as square root of cohesive energy density. Units can also be expressed in MPa<sup>0.5</sup> and hence can also be viewed as an internal pressure.

Equations (3) and (4) show that in the absence of differences in the solubility parameters, the activity coefficient  $\gamma_2$  becomes unity so that ideal solubility is reached and activity and concentration are equal. Regular solution theory does not consider more complex nonideal solutions that may lead to an activity coefficient of smaller than unity. Even though regular solution theory is limited in scope, it marked the birth of the solubility parameter concept that is more broadly applicable.

The solubility parameter, for example, can be applied to any mixing process. According to Hildebrand and Scott, the enthalpy of a mixing process is proportional to the square difference in solubility parameters for the mixture components,  $\delta_1$  and  $\delta_2$  (Equation 5)<sup>[4]</sup>:

$$\Delta H_M = \varphi_1 \varphi_2 V_M (\delta_1 - \delta_2)^2 \quad (5)$$

where  $\varphi_1$  and  $\varphi_2$  are the volume fractions of the mixing components that can be, for example, a drug and polymer.

Apart from mixing enthalpy, a solubility parameter can be linked to any thermal property or to any other molecular interaction parameter. A latter example is the well-known Flory chi parameter  $\chi_{12}$  that can be expressed in terms of Equation 6 for mixtures that involve a polymer<sup>[1,14]</sup>:

$$\chi_{12} = \frac{V(\delta_1 - \delta_2)^2}{RT} + \beta \quad (6)$$

where  $\beta$  is an entropy correction term and  $V$  is the molar volume of a solvent or drug in mixture with a polymer. It seems that  $\beta$  may not be required for essentially nonpolar systems, but in other cases, such an empirical correction of  $\beta$  may be needed to avoid under prediction of  $\chi_{12}$ .<sup>[1,14]</sup> These examples show that particular care is needed when the solubility parameter is used for quantitative conversion to other physicochemical properties or parameters.

The solubility parameter approach is comparatively simple but the art lies in correct application for each given system. The total solubility parameter is, for example, primarily useful to describe apolar components, whereas Hansen introduced the more versatile concept of partial solubility parameters.<sup>[1,15]</sup> As previously mentioned, the basic idea in this approach is to split the total cohesion energy ( $E_{tot}$ ) into different parts that originate from separate molecular interactions. The dispersive energy ( $E_d$ ) stems from atomic nonpolar forces, i.e. dispersive Van der Waals interactions, whereas forces between molecules of permanent dipoles constitute a polar energy contribution ( $E_p$ ). Due to the specific nature of hydrogen bonding, this energy contribution is considered separately ( $E_h$ ). These partial cohesion energies  $E_d$ ,  $E_p$  and  $E_h$  are divided by molar volume to result in the corresponding total and partial solubility parameters according to Equations (7) and (8)<sup>[1]</sup>:

$$\frac{E_{tot}}{V} = \frac{E_d}{V} + \frac{E_p}{V} + \frac{E_h}{V} \quad (7)$$

$$\delta_t^2 = \delta_d^2 + \delta_p^2 + \delta_h^2 \quad (8)$$

Equation 8 shows that a three dimensional (3-D) version of the solubility parameter is obtained by consideration of the different partial contributions to cohesive energy density. Figure 1 depicts a series of solvents in this space of dispersive, polar and hydrogen bonding contribution to the

HSP. The invention of partial solubility parameters has certainly advanced the original cohesive energy density approach and opened the field to diverse potential applications wherever molecular interactions of the type 'like seeks like' play a critical role. We will in the following part first describe the different ways to obtain total or partial solubility parameters and will then discuss the different applications in the pharmaceutical field. Finally, gaps and current trends will be discussed.

## Experimental and *in silico* determination of solubility parameters

### Introduction to solubility parameter determination

Solubility parameters can be evaluated directly by vaporisation of solvents (or sublimation of solids) as described in the original definition. This, however, is only feasible for materials that can be either vaporised or sublimated (in case of solids), which is often not possible. Many pharmaceutically relevant materials, such as coating polymers, polymers for amorphous solid dispersions, drug compounds or surfactants, require other methods. Therefore, indirect methods have been widely used in the literature for determination of solubility parameters, which are based upon relationships between diverse physicochemical properties and cohesion energy. Solubility parameters can be deduced from measurements of other substance properties than vaporisation. Some of the different methods to obtain a solubility parameter are schematically depicted in Figure 2, and for further reference, see the comprehensive review on this topic by Barton.<sup>[16]</sup> Values for solubility parameters determined using these various methods may vary based upon method set-up and/or material. This section describes the methods that have or could be used to characterise pharmaceutical compounds.

### Classical determination of solubility parameter

*Classical approach via latent heat of evaporation.* As mentioned earlier, the (total) solubility parameter, was introduced by Hildebrand and Scott, and was defined as the root of the cohesive energy density (CED). The cohesive energy density was in turn defined as the energy needed to break all attractive interactions in one mole of a solvent divided by the molar volume according to Equation 9:

$$\delta_t = (CED)^{\frac{1}{2}} = \left( \frac{\Delta E_v}{V_m} \right)^{1/2} \quad (9)$$

where  $\Delta E_v$  is the latent energy of evaporation and  $V_m$  is the molar volume of the solvent. This molar cohesive energy can be further expressed as follows:

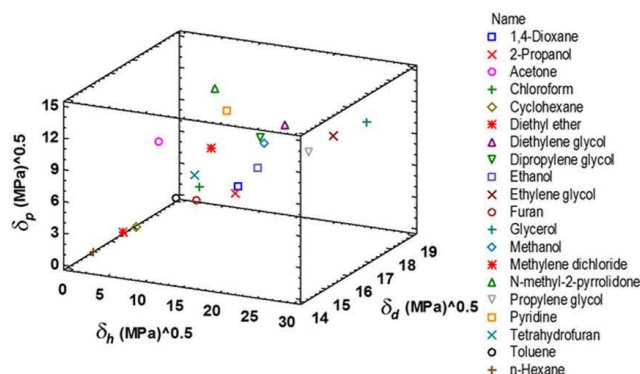


**Figure 1** Common solvents are displayed according to their Hansen solubility parameter (HSP) with dispersive ( $\delta_d$ ), polar ( $\delta_p$ ) and hydrogen bonding ( $\delta_h$ ) contribution. Other excipients or also drugs can be represented in this Hansen space and a close proximity of substances suggests their miscibility (for colour codes please refer to the online version of the article).

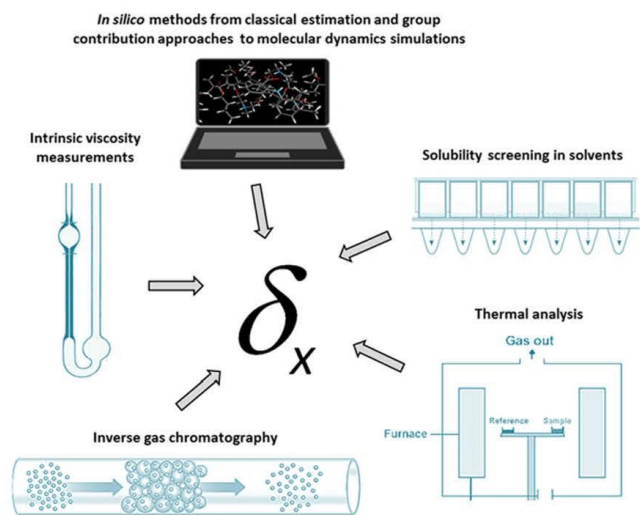


**Figure 2** Different methods to obtain one or three dimensional solubility parameter ( $\delta_x$ ).

$$\Delta E_v = \Delta H_v - RT \quad (10)$$

Equation 10 can be expressed in terms of latent heat of vaporisation  $\Delta H_v$  (in case of solvents) the universal gas constant  $R$  and the absolute temperature  $T$ .  $\Delta H_v$  can be obtained from calorimetric or vapour-pressure data to finally determine  $\delta_v$ .

Hansen expanded the total solubility parameter into three components,  $\delta_{db}$ ,  $\delta_p$  and  $\delta_h$ , as discussed for

Equation 8. This means for nonpolar molecules that  $\delta_p$  and  $\delta_h$  are zero, and hence,  $\delta_v$  equals  $\delta_d$ . For polar molecules, the situation is more difficult and calculation methods were developed to assess the partial solubility parameters based on accessible physical properties.

*Calculation of the nonpolar dispersion solubility parameter.* The energy of evaporation can be divided into a polar and nonpolar part using the homomorph approach.<sup>[17 19]</sup>



The homomorph of a polar molecule is a nonpolar molecule with nearly the same size and shape as that of the polar molecule of interest. The dispersion energy part of evaporation of a polar molecule is therefore approached by the energy of evaporation of the homomorph at the same reduced temperature,  $T_r$ . The reduced temperature  $T_r$  is defined as follows:

$$T_r = \frac{T}{T_c} \quad (11)$$

Equation 11 includes the absolute temperature  $T$  and the critical temperature  $T_c$  which can be estimated based upon the Lydersen group contributions.<sup>[1]</sup> Corrections to this approach are required for molecules containing atoms which are significantly greater than carbon, e.g. chlorine, bromine, sulfur, but not for oxygen and nitrogen.<sup>[1]</sup> For instance, when the evaporation energy of the nonpolar carbon tetrachloride is compared with the nonpolar homomorph 2,2 dimethyl propane, a difference of 1580 cal/mol (6610 J/mol) is found. This difference is divided by four to obtain a correction factor for a chlorine atom in a molecule.<sup>[20]</sup> Dividing by the molar volume and then taking the square root (see Equation 9) gives the dispersion solubility parameter.<sup>[1]</sup>

**Calculation of the polar solubility parameter.** The polar parameter of a polar molecule was originally calculated by Hansen and Skaarup<sup>[20]</sup> using the Böttcher equation and expressed in cal/cm<sup>3</sup> (Equation 12):

$$\delta_p^2 = \frac{12108}{V_m^2} \frac{\epsilon - 1}{2\epsilon + n_D^2} (n_D^2 + 2) \mu^2 \quad (12)$$

where  $\mu$  is the dipole moment, in Debye,  $V_m$  the molar volume in cm<sup>3</sup>/mole,  $n_D$  the refractive index using the sodium  $D$  line and  $\epsilon$  the dielectric constant. Later a more simplified equation was used by Hansen and Beerbower<sup>[21]</sup> according to Equation 13 in (MPa)<sup>1/2</sup>:

$$\delta_p = \frac{37.4\mu}{V_m^{1/2}} \quad (13)$$

**Calculation of the hydrogen bond solubility parameter.** Hansen and Skaarup<sup>[20]</sup> used data from infrared spectroscopy to assign an energy of evaporation of 5000 cal/mol for the OH–O hydrogen bond; hence, for a solvent containing hydroxyl groups, the hydrogen solubility parameter can be calculated utilising Equation 14:

$$\delta_h = \sqrt{\frac{5000N}{V_m}} \quad (14)$$

where  $N$  is the number of alcohol groups in the solvent molecule. More often,  $\delta_h$  is calculated by subtracting the dispersion and polar contributions from the total solubility parameter according to Equation 15<sup>[1,22]</sup>:

$$(\delta_h)^2 = (\delta_t)^2 - (\delta_p)^2 - (\delta_d)^2 \quad (15)$$

As hydrogen bonding has a profound effect on solubility, attempts have been undertaken to further expand the hydrogen bond solubility parameter. A hydrogen bond comprises a hydrogen bond donor and a hydrogen bond acceptor, and molecules can therefore be classified as<sup>[16]</sup> (1) proton donor, e.g. trichloromethane; (2) proton acceptor, e.g. ketones, aldehydes, esters, ethers, tertiary amines, aromatic hydrocarbons, alkenes; (3) proton donor/acceptor, e.g. alcohols, carboxylic acids, water, primary and secondary amines; and (4) proton nondonor/nonacceptor, e.g. alkanes, carbon disulfide and tetrachloromethane. From a qualitative point of view, miscibility can be predicted if hydrogen bonds are formed upon mixing, while demixing occurs when hydrogen bonds are destroyed (e.g. water mixed with alkanes).

An extension of the hydrogen bond solubility parameter to account for hydrogen bond donor and acceptor properties has been suggested by Small<sup>[23]</sup> and others (Sorenson *et al.*<sup>[24]</sup>), using Equation 16:

$$\delta_h^2 = 2\delta_a\delta_b \quad (16)$$

where  $\delta_a$  is the acidic solubility parameter (the donor proton of the hydrogen bond, which is the electron acceptor in the Lewis acid framework) and  $\delta_b$  is the basic solubility parameter (Lewis base, electron donor). Beerbower and Martin<sup>[21]</sup> developed the concept to estimate the solubility of naphthalene, benzoic acid, *p*-hydroxybenzoic acid and methyl *p*-hydroxybenzoate in different solvents.<sup>[25]</sup> However, improvement in accurate miscibility prediction was limited (e.g. benzoic acid: 63% acceptable – i.e. less than 30% error vs observed – predictions using four parameters vs 60% acceptable predictions with the three Hansen solubility parameters).

#### Determination of partial solubility parameters using solvent solubility data

Determination of solubility parameters for drug substances and polymers typically cannot be accomplished through the measurement of the energy of evaporation (because of their nonvolatility and due to the fact that evaporation frequently is accompanied by degradation) and therefore only indirect methods can be used. Solubility determination of a solid in a series of selected solvents, which cover the solubility design space in terms of  $\delta_d$ ,  $\delta_p$  and  $\delta_h$ , is a frequently used technique to achieve this goal.<sup>[1,26–32]</sup>

Typically, 10–40 solvents are used for the solubility measurements, which can be conducted as, e.g. a classical shake-flask approach where the thermodynamic solubility

**Table 1** Overview of experimentally determined HSP for pharmaceutical polymers

| Polymer   | $\delta_d$ (MPa) <sup>1/2</sup> | $\delta_p$ (MPa) <sup>1/2</sup> | $\delta_h$ (MPa) <sup>1/2</sup> | References                | Remarks   |
|---|---------------------------------|---------------------------------|---------------------------------|---------------------------|---|
| HPMC 2906, F4M  | 18.2                            | 16.5                            | 15.5                            | [34]                      | 34 solvents   |
| HPMC 2208, K4M  | 18.0                            | 15.3                            | 19.4                            | [34]                      | 34 solvents   |
| HPMC 2910 E4M   | 17.4                            | 14.9                            | 19.3                            | [34]                      | 34 solvents   |
| HPMC 2910 E15   | 18.8                            | 9.4                             | 11.8                            | [194]                     | 29 solvents, calculation using HSPiP software <sup>[67]</sup>                               |
| HPMC 2910 E5  | 18.7                            | 9.8                             | 11.6                            | [194]                     | 29 solvents, calculation using HSPiP software <sup>[67]</sup>                               |
| Methylcellulose A4M                                       | 18.0                            | 15.3                            | 19.4                            | [34]                      | 17 solvents   |
| HPC, Klucel H Dow data                                    | 17.2                            | 9.8                             | 13.5                            | [34]                      |   |
| HPC, Klucel H, Solubility data from Exxon Dow calculation | 17.6                            | 10.2                            | 15.4                            | [34]                      |   |
| HPMCAS 716 (L grade)                                      | 17.7                            | 11.87                           | 10.19                           | Dow technical information | Not mentioned   |
| HPMCAS 912 (M-grade)                                      | 16.73                           | 12.37                           | 10.33                           | Dow technical information | Not mentioned   |
| HPMCAS 126 (H grade)                                      | 18.09                           | 12.76                           | 9.67                            | Dow technical information | Not mentioned   |
| HPMCAS MG/Aquat MG  | 16.2                            | 10.9                            | 9.0                             | [40]                      | Jansen analysis using HSPiP software of the solubility data of 110 solvents <sup>[67]</sup> |
| HPMCAS L grade  | 18.9                            | 12.4                            | 9.0                             | [194]                     | 29 solvents, calculation using HSPiP software <sup>[67]</sup>                               |
| HPMC phthalate HP 50                                      | 20.4                            | 10.2                            | 11.7                            | [194]                     |   |
| PVP K30   | 18.3                            | 12.9                            | 11.4                            | [194]                     |   |

is determined or only kinetic solubility values are estimated by continuously adding small drug amounts to solvents with optical detection of residual drug. Generally, the solvents are selected such that the compound of interest has good solubility in at least half of the solvents screened. The solubility parameters can then be calculated with multiple regression analysis based on mole fractions solubilised in the various solvents<sup>[27,28]</sup> or with more modern computer software that uses an iterative method for improving drug solubility parameter estimates in a Cartesian coordinate system (Figure 1) of  $\delta_d$ ,  $\delta_p$ ,  $\delta_h$ . The distances between the sample reference point to point representations are calculated for solvents. Then the iterative method adjusts the partial solubility parameters such that the distance between compatible and incompatible solvents are minimised and maximised, respectively. This iterative minimisation/maximisation process can then determine a more reliable solubility parameter as recently done by Howell and coworkers.<sup>[33]</sup>

Drug substances as well as polymers can be used as samples. For example, HPMC and HPMCAS are frequently used polymers in stabilised amorphous solid dispersions and with the 'like dissolves like' approach the solubility parameter seems as a feasible way to provide a first guess on the active pharmaceutical ingredient (API) miscibility in these systems. An overview of experimentally determined HSP using the solvent method is provided in Table 1. For HPMCAS, the values were consistent between three independent determinations (see references given in Table 1). For HPMC, a difference was noted for the polarity and hydrogen bonding parameters between Janssen and

Archer.<sup>[34]</sup> This may be attributed both to (1) substantial difference in molecular weight, (2) the usage of a limited number of solvents, e.g. 10 and (3) the usage of water as solvent by Archer,<sup>[34]</sup> which is generally not recommended due to the complexity of the solvent.<sup>[1]</sup>

Solubility parameters obtained *via* the solvent approach have also been reported for characterisation of drug molecules and solid excipients such as, preservatives.<sup>[25, 27,32,35,36]</sup> These studies use about 10–25 different solvents to obtain an accurate determination of the partial solubility parameters, which seems to be reasonable given the number of unknowns in the regression analysis. Verheyen and coworkers<sup>[27]</sup> investigated five chemically related molecules and reported that the method was sufficient enough to capture the differences between molecules. Barra *et al.*<sup>[26]</sup> reported a similar finding by investigating a number of free acids and their associated sodium salts and finally, as well as those results published by Kitak and coworkers<sup>[32]</sup> could find differences between two ibuprofen salts and the free acid. The method is therefore generally perceived as sufficiently precise to determine accurate partial solubility parameters by solubility screening in a number of organic solvents or mixtures of these.

#### Determination of partial solubility parameters using intrinsic viscosity measurements

The use of viscosity measurements is a frequently used technique to determine the solubility parameter for



polymers.<sup>[1,37-46]</sup> In this approach, the intrinsic viscosity of the polymer of interest is determined in a number of solvents.<sup>[1,37,39]</sup> Intrinsic viscosity,  $[\eta]$ , is given by:

$$[\eta] = \lim_{c \rightarrow 0} \left( \frac{\eta_s - \eta_0}{\eta_0 c} \right) \quad (17)$$

Equation 17 can be expressed in terms of the solution viscosity ( $\eta_s$ ) or the solvent viscosity ( $\eta_0$ ) where  $c$  is the solution concentration. The conformation of a polymer in solution is dependent on its interactions with the solvent. In so-called good solvents with many interactions, the polymers can swell to some extent, which increases of solutions viscosity. By contrast, in solvents with limited interactions (i.e. a 'poor solvent') the polymer will reduce the contact area to the solvent by shrinking. An interesting approach is to normalise intrinsic viscosities for a polymer in a solvent that provides the highest viscosity value. These normalised data can be used to determine the HSP according to the Equations below 18–20<sup>[39]</sup>:

$$\delta_{D2} = \sum (\delta_{Di} \times [\eta]_i) / \sum [\eta]_i \quad (18)$$

$$\delta_{F2} = \sum (\delta_{Fi} \times [\eta]_i) / \sum [\eta]_i \quad (19)$$

$$\delta_{H2} = \sum (\delta_{Hi} \times [\eta]_i) / \sum [\eta]_i \quad (20)$$

where the subscript 2 indicates the polymer and 'i' the solvents. The intrinsic viscosity of the  $i$ -th solvent is described by the parameter  $[\eta]_i$ . The solvents that are most compatible have the highest intrinsic viscosities and are closest to the geometric centre of a sphere in the Hansen space that encloses good solvents.<sup>[1]</sup> The separating distance from the centre of the sphere to a last still compatible solvent provides the interaction sphere radius  $R_0$  and is defined according to Equation 21:

$$R_0^2 = 4(\delta_{di} - \delta_{dp})^2 + (\delta_{pi} - \delta_{pp})^2 + (\delta_{hi} - \delta_{hp})^2 \quad (21)$$

where  $\delta_{dp}$ ,  $\delta_{pi}$  and  $\delta_{hi}$  are partial solubility parameters of the last still compatible solvent, whereas  $\delta_{dp}$ ,  $\delta_{pp}$  and  $\delta_{hp}$  denote the partial solubility parameters of the sample polymer. Analogous to Equation 21, is possible to calculate the distance between the sample polymer and any solvent, which is called 'solubility parameter distance',  $R_a$ . This distance parameter is of more general use and is not restricted to viscosimetry to determine solubility parameters.

An alternative method to determine the partial solubility parameters *via* intrinsic viscosity was developed by Mieczkowski.<sup>[47,48]</sup> In this method, the values of the volume fraction of a solvent ( $\varphi_s$ ) were determined for three mixtures of solvents at which the maximum intrinsic viscosity was found. These fractions were then inserted into to Equation 22:

$$\sum_{i=1}^3 p_i (a_i - b_i) - \left[ \varphi_s \sum_{i=1}^3 (a_i - b_i)^2 + \sum_{i=1}^3 b_i (a_i - b_i) \right] = 0 \quad (22)$$

where  $p_i$  is the component of the solubility parameter of the polymer,  $a_i$  is the component of the first solvent and  $b_i$  is the component of the second solvent. Using this method, the HSPs for PEO (polyethylene oxide) 2000 were determined as  $\delta_d$ :  $17.3 \pm 2 \text{ MPa}^{1/2}$ ,  $\delta_p$ :  $3.0 \pm 1 \text{ MPa}^{1/2}$  and  $\delta_h$ :  $9.4 \pm 0.5 \text{ MPa}^{1/2}$ .

Furthermore, Bustamante *et al.*<sup>[43]</sup> also employed viscosity to determine the partial solubility parameter of HPMC with 28–30% methoxy and 7–12% hydroxypropyl content and an approximate molecular weight of 86 kDa (equivalent to Dow E4M). The experimental results were fitted according to following regression model (Equation 23):

$$\ln[\eta] = C_0 + C_1 \delta_{1d} + C_2 \delta_{1d}^2 + C_3 \delta_{1p} + C_4 \delta_{1p}^2 + C_5 \delta_{1h} + C_6 \delta_{1h}^2 \quad (23)$$

whereas the subscript 1 refers to solvent and the subscript 2 in the following Equations 24–26 to the polymer:

$$\delta_{2d} = - \left( \frac{C_1}{2C_2} \right) \quad (24)$$

$$\delta_{2p} = - \left( \frac{C_3}{2C_4} \right) \quad (25)$$

$$\delta_{2h} = - \left( \frac{C_5}{2C_6} \right) \quad (26)$$

An extended regression model was used to allow the determination of the Lewis acid ( $\delta_a$ ) and base ( $\delta_b$ ) solubility parameters according to Equation 27:

$$\ln[\eta] = C_0 + C_1 \delta_{1d} + C_2 \delta_{1d}^2 + C_3 \delta_{1p} + C_4 \delta_{1p}^2 + C_5 \delta_{1a} + C_6 \delta_{1b} + C_7 \delta_{1a} \delta_{1b} \quad (27)$$

Solubility parameters of HPMC for dispersion, polarity and hydrogen bonding were reported to be 14, 16.8 and  $31 \text{ MPa}^{1/2}$ , respectively. As can be seen in Table 1, the data obtained by Bustamante<sup>[43]</sup> for  $\delta_d$  and  $\delta_p$  were in line with the values obtain by Archer<sup>[34]</sup> while there was a substantial difference for the  $\delta_h$  solubility parameter. This difference may be attributed to the use of different Hansen solubility parameters for water. Bustamante used 15.5, 15.95 and  $42.34 \text{ MPa}^{1/2}$ , while Archer used 19.5, 17.8 and  $17.6 \text{ MPa}^{1/2}$  for dispersion, polar and hydrogen bonding respectively. Additionally, Madsen and coworkers<sup>[44]</sup> employed viscosity to determine the solubility parameter for the pharmaceutical

polymers, PLGA and polycaprolactone (PCL). The authors demonstrated that the solubility parameter could be correlated with protein release from the two polymer systems. This example underpins again, how broadly the solubility parameter approach can be applied.

#### Determination of partial solubility parameters of liquids using inverse gas chromatography

The HSP for pharmaceutical liquids are difficult to determine experimentally using 'solubility' methods. Additionally, many pharmaceutical substances including, for example, polymers, polysorbates, ethoxylated oils and vitamin E TPGS are complex mixtures without defined chemical structure and hence are difficult to approach theoretically. In such cases, the determination of the HSP by inverse gas chromatography, is a valuable option. Inverse gas chromatography has been applied to investigate the solubility parameters of polymers,<sup>[40,49–52]</sup> surfactants,<sup>[53,54]</sup> epoxidised soybean oil,<sup>[55]</sup> triglycerides<sup>[56]</sup> and liquid crystal systems.<sup>[57–59]</sup> For measurement of solids, it is recommended for the samples to contain some amorphous fraction, so that the probe gases can enter the bulk. Otherwise, only surface interactions could skew the results for estimated solubility parameters.

Using the inverse gas chromatography method, the material of interest is the stationary phase and is placed into a column. It is then characterised using diverse volatile probes (i.e. volatile solvents with known HSPs). The HSP of the material can then be calculated based on the retention data of the solvent probes.<sup>[54]</sup> First, the retention times of the solvent probes are converted to specific retention volumes ( $V_g$ ). These are then used to calculate the Flory–Huggins interaction parameter between the solvent and the sample using the following equation (Equation 28)<sup>[60–62]</sup>:

$$\chi_{1,2}^{\infty} = \ln \left( \frac{273.15}{M_1 V_g^2 P_1^2} \cdot R \right) - \frac{P_1^{\circ}}{R \cdot T} (B_{11} - V_1^{\circ}) + \ln \left( \frac{\rho_1}{\rho_2} \right) - \left( 1 - \frac{V_1^{\circ}}{V_2^{\circ}} \right) \quad (28)$$

where  $\chi_{1,2}^{\infty}$  is the Flory–Huggins interaction parameter between the material of interest and the solvent probe,  $M_1$  is the molecular mass,  $P_1^{\circ}$  is the vapour pressure of the solvent probe at the measurement temperature calculated using the Antoine equation,  $V_1^{\circ}$  is the molar volume of the probe,  $V_2^{\circ}$  is the molar volume of the examined material,  $B_{11}$  is the second virial coefficient of the solvent probe calculated according to Voelkel and Fall,<sup>[63]</sup>  $\rho_1$  and  $\rho_2$  are the densities of the solvent probe and material, respectively. The total solubility parameter is then

calculated using Equation 29<sup>[50,53,64,65]</sup>:

$$\frac{\delta_1^2}{RT} - \frac{\chi_{1,2}^{\infty}}{V_i} = \frac{2\delta_2}{RT} \delta_1 - \left( \frac{\delta_2^2}{RT} + \frac{\chi_S^{\infty}}{V_i} \right) \quad (29)$$

where  $\delta_1$  is the total solubility parameter of the consecutive test solutes and  $\delta_2$  the total solubility parameter of the material of interest,  $\chi_S^{\infty}$  is the entropic part of the Flory–Huggins interaction constant and is usually estimated in the range 0.2–0.4 or 0.6.<sup>[52]</sup> By plotting the left hand side of the equation vs  $\delta_1$ , a straight line is obtained of which the slope and intercept are used to calculate  $\delta_2$ .

Voelkel and Janas<sup>[66]</sup> extended this original concept, introduced by Price and Shillcock<sup>[57]</sup> to obtain partial solubility parameters from the linear relationships for solvent groups ( $n$ -alkanes for  $\delta_{2d}$ , polar solvents for  $\delta_{2p}$  and hydrogen bonding solvents for  $\delta_{2h}$ , while  $S$  is indicated as the value for the slope) according to Equations 30–32:

$$\delta_{2d} = \frac{S_{n\text{-alkanes}}}{2} RT \quad (30)$$

$$\delta_{2p} = \frac{(S_{\text{polar}} - S_{n\text{-alkanes}})}{2} RT \quad (31)$$

$$\delta_{2h} = \frac{(S_{h\text{-bonds}} - S_{n\text{-alkanes}})}{2} RT \quad (32)$$

Using this approach Adamska and Voelkel<sup>[52]</sup> determined the HSPs of di- $n$ -butyladipat (Cetiol), caprylocaproyl macrogol-8 glycerides (Labrasol, Gattefosse) and polysorbate 80 (Tween 80) using inverse gas chromatography. Packing of columns with semi-solids and liquid compounds often require special preparation and here, the excipients were dissolved in a suitable solvent to coat on a solid support by slow solvent evaporation. By comparison, an alternative method with fewer assumptions has been used for some of the same excipients investigated by Adamska and Voelkel<sup>[54]</sup> as described in Table 2. The method used has some parallels with the solubility approach described above. In this method the three partial parameters were iteratively and systematically changed to give the best fit between predicted and experimental values for the interaction parameter,  $\chi_{1,2}^{\infty}$ , for all the solvent probes tested; hence, no solvent probe families were needed. The predicted interaction constant was calculated according to Equation 33:

$$\chi_{1,2}^{\infty} = C_1 + V_m \cdot C_2 \cdot \left[ 4(\delta_{1d} - \delta_{2d})^2 + (\delta_{1p} - \delta_{2p})^2 + (\delta_{1h} - \delta_{2h})^2 \right] \quad (33)$$

where  $C_1$  and  $C_2$  are constants and  $V_m$  is the molar volume of the solvent probe. This approach is adopted in the software package 'Hansen Solubility Parameters in

**Table 2** Hansen solubility parameters obtained for materials using inverse gas chromatography compared using different data treatment

| Material           | $\delta_d$ (MPa) <sup>1/2</sup> | $\delta_p$ (MPa) <sup>1/2</sup> | $\delta_h$ (MPa) <sup>1/2</sup> | Remark                     | References            |
|--------------------|---------------------------------|---------------------------------|---------------------------------|----------------------------|-----------------------|
| Cetiol             | 16.5                            | 1.4                             | 4.8                             | Inverse gas chromatography | [54]                  |
| Labrasol           | 18.0                            | 0.8                             | 3.2                             |                            |                       |
| Tween 80           | 19.3                            | 0.9                             | 2.8                             |                            |                       |
| PEG 2000 (at 85°C) | 19.4                            | 1.6                             | 1.2                             |                            | [52]                  |
| Labrasol           | 18.3                            | 5.8                             | 7.2                             | Inverse gas chromatography | Internal Janssen data |
| PEG 400            | 19.7                            | 8.3                             | 8.8                             | followed by iterative      |                       |
| Tween 80           | 19                              | 5.3                             | 5.6                             | calculation using HSPiP    |                       |
| Olive oil          | 16.9                            | 0.6                             | 4.2                             |                            |                       |

Practice', HSPiP.<sup>[67]</sup> This software is helpful as it provides tools for many processes such as determining HSP from solubility data and, estimating HSP from the chemical structure as well as databases, which include HSP values for many polymers and excipients. The values obtained for polysorbate 80 and caprylocaproyl macrogol-8 glycerides (Labrasol, Gattefosse) were somewhat different than the ones obtained by Adamska and Voelkel.<sup>[54]</sup> This is possibly due to the use of different sample preparation methods and column packing material, which influences the retention volume determination. However, it should be also noted that it may be problematic to determine a solubility parameter for surfactants and other amphiphilic substances (e.g. some copolymers) by the use of only a single set of partial solubility parameters. Superstructures such as liquid-crystalline phases are typically formed and probe gas molecules can interact with different microdomains, which is an issue of sample heterogeneity.

Klar and Urbanetz<sup>[40]</sup> investigated the solubility parameter for hypromellose acetate succinate (granular type M HPMCAS) by turbidimetric titration, inverse gas chromatography and seven different calculation methods. The total solubility parameter determined by turbidity was  $24.7 \pm 3.2$  MPa<sup>1/2</sup> for moderately hydrogen bonded solvents and  $24.4 \pm 0.3$  MPa<sup>1/2</sup> when determined by inverse gas chromatography. Furthermore, the partial HSPs that were determined by inverse gas chromatography and obtained data (17.69, 12.06 and 11.7 MPa<sup>1/2</sup> for dispersion, polar and hydrogen bonding respectively) showed good accordance with the value generated by the calculation methods, especially those calculated *via* the Hoy and Te Nijenhuis method, using experimentally determined molecular volumes,<sup>[40]</sup> as well as the Janssen and Dow values determined from solubility data, see Table 1.

In summary, even though the practice and the theory to determine solubility parameters by inverse gas chromatography has a long tradition, there are new theoretical and practical developments.<sup>[56,68]</sup> For future applications, it is interesting to evaluate different calculation methods for inverse gas chromatography. The use of the Flory–Huggins

interaction parameters is quite abundant but the theory was developed initially for polymers so that small molecules may be better described by, for example, the Bragg–Williams interaction parameters.<sup>[53]</sup>

#### Other experimental methods to determine solubility parameter

Besides the typical methods described in the section above, a number of other analytical techniques used to determine the solubility parameter have been reported. These include swelling,<sup>[69–74]</sup> turbidity,<sup>[40,74–77]</sup> ultraviolet spectroscopy, and differential scanning calorimetry (DSC) as well as differential scanning microcalorimetry ( $\mu$ DSC).<sup>[78]</sup>

Geer described<sup>[79]</sup> the swelling of rubber in various liquids to derive its solubility parameter, an approach which has also been applied in more recent studies. For example, Eroğlu *et al.*<sup>[73]</sup> and Çavuş *et al.*<sup>[69]</sup> measured the weight of a polymer before and after addition of different solvent systems with known solubility parameters by gravimetry and then defined the solubility at the point where optimal swelling was observed. Furthermore, Çavuş *et al.*<sup>[69]</sup> also investigated the swelling of PVC and found good correlations to the theoretical calculation of the solubility parameter based upon the van Krevelen–Hoftyzer and Hoy methods.<sup>[69]</sup> The simplicity of the method is highly attractive but the swelling must be of course detectable.

For turbidimetric titration, a polymer (or another relevant excipient) is dissolved in an appropriate solvent. A second solvent that is miscible with the first solvent but acts as anti-solvent for the polymer is then added until precipitation occurs. Shu and coworkers<sup>[75,76]</sup> developed a method whereby the solubility parameter could be determined from these data. As described above Klar and Urbanetz<sup>[40]</sup> showed good correlation between the solubility parameter for HPMCAS determined by inverse gas chromatography and turbidity titration. In addition, Schenderlein *et al.*<sup>[74]</sup> reported the turbidity titration to be more precise relative to the swelling approach when investigating different proportions of lactide to glycolide for poly(D,L-lactide-co-glycolide) (PLGA).



Carvalho *et al.*<sup>[78]</sup> used several methods to determine the solubility parameter for naphthalene, phenanthrene and pyrene and reported UV-vis as the most suited method for a wider molar mass range. For compounds with a low molar mass determination of the vapour enthalpy by DSC was argued to be better based on the similar results and a lower quantity of compound consumption, whereas the  $\mu$ DSC method still required some optimisation. Mieczkowski<sup>[46]</sup> used refractive index in several solvents to determine the partial solubility parameter for polystyrene and compared these experimental results together with calculations according to the Van Krevelen approach. Ravindra *et al.*<sup>[38]</sup> derived the solubility parameter of chitosan from intrinsic viscosity, surface tension and the dielectric constant for data comparison including different group contribution calculations. The average of the calculation methods yielded 43.1 MPa<sup>1/2</sup> for chitosan, while the experimental data provided 41.5, 39.8 and 37.0 MPa<sup>1/2</sup> when determined by viscosity, surface tension and dielectric constant, respectively. This demonstrates the variation that might be seen across methods. All of the mentioned approaches have their specific assumptions and limitations both with experimental design and data evaluation.

#### Group contribution methods to calculate partial solubility parameters

The partial solubility parameters describe the ability of a molecule to interact with another molecule *via* intermolecular forces. Given that molecules contain several structural fragments/groups that can contribute to such molecular forces and volume, group contribution methods are meaningful to estimate solubility parameters based only on the chemical structure. The most frequently applied methods are the approaches described by Hoy,<sup>[80]</sup> Fedors,<sup>[81]</sup> and Van Krevelen and Hoftyzer,<sup>[82]</sup> however newer approaches have also been reported, e.g. by Stefanis and Panayiotou.<sup>[5,83]</sup> An example of solubility parameter calculation is given for lacidipine according to Hoftyzer/Van Krevelen (Table 3). Group contribution calculations are attractive as they require pure *in silico* approach, which demands less computation time compared to, for example, molecular dynamics simulations.

A solubility parameter from calculations or modelling is typically a bulk property of a liquid or of a supercooled melt. For that reason, it is essential to know whether a compound or polymer is completely amorphous or contains crystalline parts, which may affect precision of the calculation. Computational concepts assume values for atomic or group contributions to the total cohesive energy. Most of the computational methods are related to the molar volume  $V_m$  of a substance, thus  $V_m$  has to be either known or calculated. Therefore, some researchers published values of

**Table 3** Example of the parameters required for solubility parameter calculation for lacidipine according to Hoftyzer and Van Krevelen (modified from Forster<sup>[85]</sup>). Whereas  $z$  indicates the functional group,  $F_{di}$  is the group dispersion component giving  $\delta_d$ ,  $F_{pi}^2$  is the group polar component,  $E_{hi}$  is the hydrogen bonding component, and  $V$  is the molar volume

| Group <sub>z</sub>  | $F_{di}$ | $F_{pi}^2$ | $E_{hi}$ | $\Sigma^{\infty}V/\text{cm}^3 \text{ mol}^{-1}$ |
|---------------------|----------|------------|----------|---|
| (7) CH <sub>3</sub> | 2940     | 0          | 0        | 234.5   |
| (2) CH <sub>2</sub> | 540      | 0          | 0        | 32.2  |
| (1) NH              | 160      | 210        | 3100     | 4.5   |
| (1) C               | -70      | 0          | 0        | -19.2   |
| (1) CH              | 80       | 0          | 0        | -1.0  |
| (4) C=              | 280      | 0          | 0        | -22   |
| (1) Phenylene       | 1270     | 110        | 0        | 52.4  |
| (2) HC=             | 400      | 0          | 0        | 27  |
| (3) COO             | 1170     | 1470       | 21 000   | 54  |
| (1) Ring (6)        | 190      |            |          | 16  |
| $\Sigma$            | 6960     | 1790       | 24 100   | 378.4   |

group contributions to  $V_m$ , as in some cases, reliable values of solubility parameters can be calculated best, when using two complementary methods. Whereas, other concepts, e.g. the concept by Hoy, are suited to be combined  $V_m$  ascertained by experimental techniques.<sup>[80]</sup> Especially for high molecular materials as polymers, experimentally determined  $V_m$  can provide more precise values for solubility parameters, although an experimentally determined  $V_m$  is not recommended in all cases. For example, the method proposed by Fedors can only yield concise results when using the correlated calculation concept for  $V_m$ , as  $V_m$  of Fedors' method is often different to other calculations or experimentally determined  $V_m$ . Based on such differences it would be a pragmatic approach to use different *in silico* methods to work with the mean of these predictions.<sup>[52,38]</sup>

Based on these group contribution components the partial solubility parameters can be calculated;

$$\delta_d = \frac{\sum F_{di}}{V} = \frac{6960}{378.4} = 18.4 \text{ MPa}^{1/2} \quad (34)$$

$$\delta_p = \frac{\sqrt{\sum F_{pi}^2}}{V} = \frac{\sqrt{1790}}{378.4} = 0.11 \text{ MPa}^{1/2} \quad (35)$$

$$\delta_h = \frac{\sqrt{\sum E_{hi}}}{V} = \frac{\sqrt{24100}}{378.4} = 7.98 \text{ MPa}^{1/2} \quad (36)$$

From which the total solubility parameter can be calculated:

$$\begin{aligned} \delta_t &= \sqrt{\delta_d^2 + \delta_p^2 + \delta_h^2} = \sqrt{18.4^2 + 0.11^2 + 7.98^2} \\ &= 20.1 \text{ MPa}^{1/2} \end{aligned} \quad (37)$$

The ease of the calculations has seen group contribution approaches being widely adopted, e.g. Shah and Agrawal<sup>[84]</sup> used the Van Krevelen and Hoftyzer method to estimate

the partial solubility parameters for a number of lipid excipients, including Dynasan 114, Capmul MCM, Migloyol 812N and others. This approach has also been used for the calculation of solubility parameters for drug substances,<sup>[26,27,32,35,85]</sup> which are often compared to experimentally obtained data. Besides the classical group contribution methods it is in principle also possible to employ, for example, the COSMO-RS<sup>[86]</sup> approach, molecular dynamics simulations,<sup>[87]</sup> or quantitative structure–property relationships. Future research may compare such a modern approach to classical group contribution methods for pharmaceutical dataset.

## Applications of solubility parameters in pharmaceuticals

### Organic solvent selection

Knowledge of solubility in pure solvents and solvent mixtures is crucial for designing the crystallisation process of drug substances. The first step in finding the optimal crystallisation conditions is usually a solvent screening. To minimise time and resource investment, it would be desirable to conduct *in silico* screenings using solubility parameters or other modelling approaches to reach an educated first guess.<sup>[88]</sup> For this purpose, the use of solubility parameters is simpler than more advanced and complex theoretical models such as COSMO-RS (conductor-like screening model for real solvents), which is computation intensive, and PC-SAFT (perturbed-chain statistical associating fluid theory), which requires extensive parameter determination.<sup>[88,89]</sup> Thus, *in silico* solubility parameter determination is not the only way to rank solvents for further experiments, however it is significantly more straightforward, especially when considering group contribution methods.

Furthermore, solvent selection can be essential when considering these processes. For example, Rogers and Marangoni<sup>[90]</sup> reported that changes in solvent chemistry affected nucleation and crystal growth events and therefore defined the physical properties of obtained crystals. In addition, solvent selection can change, solvent–gelator compatibility, affecting the degree of undercooling, chemical potential, kinetics of gelation and crystal morphology. These parameters are all interrelated and can be correlated to partial solubility parameters. Liu *et al.*,<sup>[59]</sup> studied crystallisation behaviour of two anhydrous as well as the monohydrate form of piroxicam. Interestingly, additives with a similar hydrogen bonding pattern to piroxicam facilitated crystallisation of anhydrous form I. It was argued that such additives would affect the formation of the different molecular clusters in the supersaturated solution. As a consequence, these additives had a higher ability to influence the

nucleation of the different polymorphs. These data suggested that the HSP could indeed be used for preliminary screening of additives for the solid form control of piroxicam during the crystallisation processes.<sup>[59]</sup> Zhu *et al.*<sup>[91]</sup> used the partial solubility parameters to select the optimum solvent system for aerogels, which are open-porous predominantly mesoporous solids with a wide range of applications, including oil-spill clean-up and CO<sub>2</sub> capture. A HSP based search method was used to target a specific gel system and because the solvent in this case had a functional influence, its selection was of crucial importance.<sup>[91]</sup> Solubility parameters can also be used for defining extraction processes, as described by Masurel *et al.*<sup>[92]</sup> for the removal of tar from flue gas, but also other publication focus on the use of solubility parameters for liquid extraction,<sup>[93–96]</sup> even though the applications are not necessarily pharmaceutical. In particular, the partial solubility parameters seem to have several applications within the space of organic solvent selection for either crystallisation or extraction. These processes are especially important for the final steps of drug substance manufacture and even though a solubility parameter approach, however more can be done to harness the power of the HSP in the area of pharmaceutical solvent selection.

### Cocrystal and salt screening

Solubility as well as dissolution rate can be significantly influenced by the selection of a suitable solid-state form. Generally high solubility and fast dissolution rate is realised by usage of an amorphous solid-state form.<sup>[97]</sup> However, a direct use of the amorphous form, e.g. in a capsule or tablet, bears the risk of uncontrolled conversion to the crystalline solid-state form, which has inferior solubility and dissolution behaviour. Therefore, amorphous APIs are not normally used directly but stabilised by suitable formulation techniques,<sup>[98]</sup> which will not be discussed in this section. Instead, we focus on optimisation of solubility and dissolution by choosing advantageous crystalline solid-state forms. Generally, these comprise pharmaceutical salts, polymorphs – including pseudopolymorphs such as hydrates and solvates – and cocrystals. Optimisation of aforementioned properties by polymorph selection comes with the same risks as discussed for the amorphous form. Selection of metastable polymorphs increases solubility, but bears the risk of uncontrolled conversion to the thermodynamically stable form. Therefore, a thermodynamically stable polymorph is typically chosen for clinical development, and only in rare cases or when there is limited knowledge of the APIs polymorph landscape, is the metastable form selected. Examples of cases where metastable polymorphs have been used in clinical development can be found in the literature.<sup>[99–101]</sup> Additionally, compared to



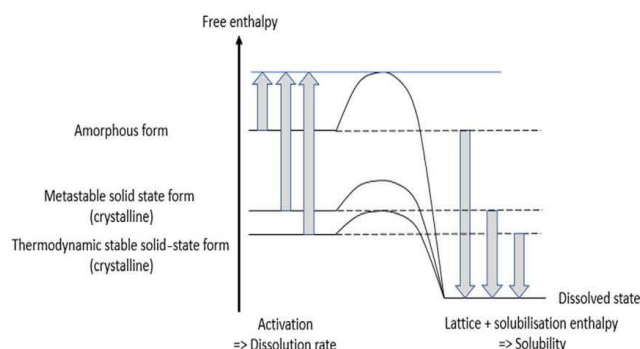


**Figure 3** Enthalpic processes involved in the dissolution process.

the amorphous state, metastable polymorphs provide a much lower increase in solubility, which is why they are less attractive to develop. A schematic summary of the enthalpic processes involved in the dissolution process is given in Figure 3.

For this reason, optimisation of solubility, dissolution rate and consequently bioavailability can be best realised by selecting an appropriate pharmaceutical salt or cocrystal. Even though salt selection is well established in the pharmaceutical industry, cocrystals have also emerged during recent years as part of more educated solid form engineering.

A comprehensive summary of salt selection is given by Stahl<sup>[102]</sup> as well as Neau.<sup>[103]</sup> Historically, there have also been a few publications which summarise the use of pharmaceutical salts.<sup>[104–108]</sup> From such analysis, it is clear that hydrochlorides historically represented the most frequently used pharmaceutical salts for basic APIs and the same was true for sodium if acidic APIs were used. However, in recent decades, it has been clearly recognised that these ‘one-fits-all’ counterions did not always lead to the desired properties intended by the salt formation. This is in line with the observation that new drug candidates entering clinical development, in addition to newly approved drugs, exhibit significantly lower solubility (BCS class II and IV) and require more individualised solutions to optimise their physicochemical behaviour. This does not only include above-mentioned solubility and dissolution aspects, but also further parameters such as hygroscopicity, melting point, chemical and physical stability as well as crystal habit. Several examples of optimising such properties can be found in the literature.<sup>[109–112]</sup> In many cases, sulfonate salts such as mesylates, tosylates, napsylates and edisilates showed far better performance with regards to increased solubility and dissolution rate<sup>[113]</sup> compared to other salt forms. Lower dissolution rate of the parent (either free base or free acid) compared to pharmaceutical salts can be easily

explained by the presence of ions in the crystal lattice of a pharmaceutical salt, leading to stronger interactions between the crystal lattice and water as the dissolution medium. However, a similar explanation as to why, for example, sulfonate salts generally show excellent dissolution rate so far is not available. This phenomenon remains unexplained at least by simple chemical reasoning.

However, there are other more systematic approaches to improve solubility by usage of pharmaceutical salts, which are based on mechanistic understanding: as solubility depends on crystal lattice energy, and high lattice energy will generally result in low solubility, reducing the lattice energy represents a means to improve solubility. For pharmaceutical salts, Coulomb interactions contribute with a major part to the lattice energy. Use of large, ‘noncoordinating’ counterions with low charges (one positive charge or one negative charge) are useful in designing such pharmaceutical salts with improved solubility.<sup>[114]</sup> In the extreme case, such pharmaceutical salts do not even represent solid APIs anymore, but become liquids.<sup>[115–118]</sup> As stability can be more challenging for such ionic liquids compared to solids due to increased mobility, this certainly has to be assessed critically. Moreover, toxicological assessment and regulatory acceptance represent the major hurdles for the use of such noncoordinating ions in humans, as none of these salt formers are currently used in human beings or ‘generally regarded as safe’ (GRAS) by the FDA.<sup>[119]</sup> Therefore, this promising conceptual work on noncoordinating ions has not yet led to approved drugs on the market nor in clinical development.

From a more practical standpoint, several aspects must be considered for selection of pharmaceutical salts or cocrystals. The process steps include salt- or cofomer screening and physicochemical characterisation with a typical focus on solubility and dissolution rate but also regarding chemical and physical stability while considering

toxicological aspects of the selected salts or coformers. This screening stage represents the starting points for the selection of a salt or cocrystal, respectively. Earlier, such screening was carried out as a typical synthesis process in lower gram-scale. Today salt or coformer screening is conducted on the lower mg-scale which saves API and allows conductance of such screens earlier during the research process. For this purpose, different screening approaches exist in the pharmaceutical industry. A salt or cocrystal screening might be carried out in an automated way using robotic systems that employ different solvents and solvent mixtures according to a fixed protocol. Alternatively, salt or cocrystal screens can be based on a rationale, nonautomated process where small-scale crystallisation trials are performed and crystallisation is closely observed. This allows information to be obtained sequentially from one experiment to another. Even though for a single trial, larger amounts of API are required compared to the automated approach a repetition of unsuccessful experiments is avoided. A useful comparison of different screening approaches can be found in the literature for salt selection.<sup>[120]</sup>

Following initial screening of possible salt and cocrystal formation, characterisation of solid-state properties, including melting point, hygroscopicity and stability is important; as well as analysis of solubility, dissolution and supersaturation. The aforementioned steps to salt and cocrystal formation offer different opportunities to use solubility parameters. One application is certainly the selection of organic solvents or antisolvents for solid form screening, which is in line with the previous section. Other applications of partial solubility parameters are selection of ionic liquids even though they are still currently quite toxic or not sufficiently characterised leading to regulatory hurdles in pharmaceutical development. More important therefore are applications to the field of cocrystals where it has been attempted to predict formation based on HSP.<sup>[121]</sup> A recent study conducted cocrystal search of itraconazole during which the HSP was used to rank different amino acids as potentially suitable coformers.<sup>[122]</sup> In spite of such reports, there are also typical limitations of solubility parameters because they cannot account for specific aspects of the crystal lattice. There are currently methods in structural informatics that can use the Cambridge Structural Database to assist *in silico* screening of the energy landscape of possible crystals. These approaches together with other computational methods used in pharmaceutical solid-state chemistry have been recently reviewed in an excellent book.<sup>[123]</sup> Therefore, partial solubility parameters can be applied successfully in the field of salt and cocrystal screening, however in cases where details of a crystal lattice energy landscape should be considered, alternative methods of solid-state modelling are recommended.

### Solubility parameter concept in lipid-based formulations

Lipid-based formulations have been an important part of the toolbox to formulate low water-soluble compounds for over 50 years. Additionally, an increased prevalence of such poorly soluble drug candidates in the last two decades has also intensified the interest in lipid-based drug delivery systems (LBDDS). The biopharmaceutical advantages of LBDDS include the potential to enhance bioavailability, decrease pharmacokinetic variability as well as food effects, promote lymphatic absorption and support controlled drug release.<sup>[124]</sup>

A key element of LBDDS is that the drug substance is dissolved within the lipid excipients before administration, hereby presenting the drug in a presolubilised state in the gastrointestinal tract. The level of solubility in the LBDDS is, hence, important to achieve the above-mentioned biopharmaceutical advantages. Therefore, options to predict and rank drug solubility in lipid excipient mixtures are of high interest to guide LBDDS formulation development. Generally, the solubility in lipid excipients is determined experimentally; however, these experiments are costly, time-consuming, resource-intensive and the experimental protocols vary substantially between different research groups.<sup>[125]</sup> Also, LBDDS are often mixtures of different excipients, e.g. lipids, surfactant and cosolvents, so the number of typical solubility studies required can be very extensive.<sup>[125,126]</sup> Recently, the utility of empirical models to predict drug solubility in lipids has been explored, using multivariate data analysis with several molecular descriptors.<sup>[125-127]</sup> A disadvantage of any such multivariate approach is that the size and quality of the calibration dataset highly influences the accuracy of the prediction. Thus, an alternative to complex computational models, is the HSP approach that has been proposed to guide lipid-excipient selection. Dumanli *et al.*<sup>[128]</sup> used the HSP to rank compound solubility and miscibility in/with lipids. The required solubility parameters can be obtained either from experiments or from calculations as previously outlined in Section 2. For lipid-based excipients, vapour pressure and boiling point determinations, miscibility of reference liquids (with known cohesive energy), inverse gas chromatography and calculations using group contribution methods are of particular interest to determine HSP.<sup>[129]</sup> Solubility parameters have been commonly employed for this purpose, especially for characterisation and release of raw materials for cosmetics<sup>[130-132]</sup> and in the oil and textile industry.<sup>[133]</sup> However, there are not many applications of solubility parameters for lipid-based systems in the pharmaceutical field. Most studies determine the solubility parameter using theoretical group contribution approaches



and often only consider simple mixtures, i.e. compound A in oil B.<sup>[84,134]</sup>

De La Peña-Gil and coworkers<sup>[135]</sup> investigated methods to predict and calculate HSP of complex lipidic mixtures (i.e. vegetable oils) using the HSPiP software.<sup>[67]</sup> Two approaches were used to determine HSPs. In one approach it was assumed that each functional group (fatty acids, fatty acids + glycerol and fatty acid methyl esters) present in triglycerides, had an additive contribution to the dispersion, dipole-dipole and hydrogen bonding interactions. Therefore, the composition of triglycerides was divided into different functional groups and each component of the total HSP ( $\delta_T$ ) was calculated (i.e.  $\delta_d$ ,  $\delta_p$  and  $\delta_h$ ). The second approach assumed that vegetable oils are mixtures of simple triacylglycerols in the same mass fractions as the fatty acids.<sup>[135]</sup>

Two studies by Shah and Agrawal<sup>[84,136]</sup> investigated the utility of HSP as a predictor for optimal carrier and solvent system selection:<sup>[136]</sup> firstly to describe the solubility behaviour of a drug (ciprofloxacin HCl) and lipid excipients and secondly, for the design of solid lipid nanoparticles (SLNs).<sup>[84]</sup> Both studies used the Van Krevelen/Hoflyzer group contribution approach to calculate the HSP for different solvents, polymers and lipids using the Molecular Modeling Pro software. Calculation of the solubility parameter was based on at single repeating polymeric unit for the polymers whilst, for lipids consisting of mixture of glycerides the calculation was carried out based on an average predominant ratio.<sup>[136]</sup> With the Van Krevelen approach, the molar attraction constant ( $F$ ) was calculated and all the extended HSPs determined. The calculated values of the total HSP were matched between different lipids, organic solvents and drug compounds and when similar values were observed then the systems were considered miscible. Shah and Agrawal<sup>[84]</sup> validated the mathematical model used by experimental testing of drug solubility in the selected excipients and solvents. Both studies<sup>[84,136]</sup> succeeded in qualitatively predicting the solubility of ciprofloxacin HCl in different lipids and subsequently the solubility of lipids in various organic solvents using the HSP determination/calculation. This approach resulted in identifying the most promising lipid candidates for maximum drug loading in SLN formulation consisting of glyceryl monocaprylate and glycerol monostearate 40–55. These studies demonstrate the possibility of using the HSP for optimal selection of excipients in designing SLNs and qualitative prediction of excipient–drug compatibility.

Another application of the HSP was suggested by Li *et al.*<sup>[137]</sup> to estimate the compatibility between materials to facilitate the design of polymer–lipid hybrid nanoparticles (PLN). Specifically, the enthalpies of mixing for a drug–polymer complex (i.e. verapamil in dextran-sulfate-sodium) and 15 different lipids including triglycerides, fatty

acids, glycerol esters and mixtures of glycerol esters were predicted by accounting for the volume fractions of components in the mixture. The study also used the Van Krevelen/Hoflyzer group contribution approach to calculate HSP and showed the suitability of the HSP theory in the screening of lipid carriers for PLN design of verapamil.<sup>[137]</sup>

While useful to determine how a lipid or lipid mixtures may behave as solvent(s) and the possibility to predict how some compounds solubilise in lipids, the HSP concept has also some limitations. Firstly, the concept only considers the energies derived from direct contact of components and does not account for the entropy effects and the free volume of, for example, amorphous solids.<sup>[84]</sup> The free volume is defined as an empty space in a solid or liquid that is not occupied by the molecules. Generally, amorphous solids are inefficiently packed and present a considerable amount of free volume compared to ordered materials. Additionally, it was mentioned before as a disadvantage that a given crystalline solid-state form is not accounted for. By contrast, experimental HSP determinations are generally conducted with the most stable polymorph. Studies have suggested that HSP calculations based on group contribution methods provide accurate predictions if materials with similar structures are compared, as the calculation does not account for the dependencies on conformation, concentration and specific intermolecular interactions that might occur in binary mixtures.<sup>[134]</sup> Finally, another limitation of the theoretical model is that it disregards specific self-association of molecules, which is also the case with further thermodynamic approaches other than SAFT (statistical associating fluids theory) calculations.

The HSP approach within LBDDS has only been investigated to a limited extent, potentially due to the variability and complexity of the lipid excipient composition and the multitude of drug–excipient interactions. However, there are further pharmaceutical applications that are to some extent linked to lipids in general such as intestinal drug absorption,<sup>[138]</sup> skin penetration of topically applied drugs,<sup>[139]</sup> and prediction of drug–nail interactions.<sup>[140]</sup> The available studies suggest that partial solubility parameters have the potential to be a useful tool in early development of LBDDS.

## Solid dispersions

### Amorphous solid dispersions

Modification of the solid drug form to increase solubility and dissolution rate has been mentioned before (Cocrystal and salt screening section). In this endeavour, the high energy that the amorphous state can provide is especially interesting.<sup>[2,141–143]</sup> However, the amorphous state is thermodynamically unstable and tends to revert to a crystalline

polymorph. The amorphous drug state can be stabilised by solid dispersion,<sup>[144,145]</sup> complexation with large (e.g. cyclodextrins)<sup>[146]</sup> or small molecules,<sup>[147]</sup> and spatial confinement (e.g. absorption on silica).<sup>[148,149]</sup>

Solid dispersions involving the immobilisation of amorphous API in polymer have been studied extensively in the literature<sup>[145,150–152]</sup> and are one of the most widely employed approaches to formulate an amorphous drug form. Amorphous solid dispersions (ASD) is an umbrella term for different types, which can be glass solution, glass suspension and solid solutions of drug in the carrier.<sup>[145,153]</sup> Drug–polymer miscibility is a key parameter to consider when formulating solid dispersions<sup>[154,155]</sup> and to obtain a single phase system, both the API and the carrier have to be miscible. Such miscibility can be calculated using advanced thermodynamic models, such as the previously mentioned PC-SAFT and COSMO-RS theories or the simpler Flory–Huggins model may be applied.<sup>[156]</sup> The advantages of suitable prediction accuracy of advanced thermodynamic approaches have to be balanced against drawbacks like either extensive computation time or the need for parameters that have to be based on extensive experimentation. This makes the simpler solubility parameter approach very attractive and either the total Hildebrand solubility parameter can be considered or partial solubility parameters. Thus, HSP has been extensively used to identify drug–excipient miscibility with a general rule of thumb that molecules with similar  $\delta$  values are assumed to be miscible.<sup>[32,121,155,157]</sup> This method considers the dispersion and polar interactions of a system as well as the hydrogen bond contributions of the test molecules. We emphasise again that HSP hereby addresses the main limitation of the conventional Hildebrand solubility parameter, which does not discriminate the different partial contributions to cohesive energy density.<sup>[1]</sup>

However, ASD formulation miscibility has been investigated with both the Hildebrand<sup>[158]</sup> as well as the Hansen<sup>[85,159–161]</sup> approach. It was proposed by Greenhalgh and coworkers<sup>[155]</sup> that systems with a difference in solubility parameters from 1.6 to 7.0 MPa<sup>0.5</sup> present no miscibility problems. However, substances with a difference of 10.8 to 18.0 MPa<sup>0.5</sup> were considered immiscible. Further practical measurements showed that systems with a difference of 1.6 to 7.5 MPa<sup>0.5</sup> could be considered miscible in the molten stage. Systems with a difference of 7.4 to 15 MPa<sup>0.5</sup> were slightly immiscible in the liquid state. Total immiscibility was observed in systems with differences greater than 15 MPa<sup>0.5</sup>.<sup>[155]</sup>

With the Hansen approach similar observations were made when testing the miscibility of 2 drugs in 11 excipients.<sup>[65]</sup> Systems that were predicted to be miscible using the Greenhalgh values formed glass solution *via* hot melt extrusion while those combinations that were predicted to

be immiscible formed solid dispersions in which the amorphous drugs was dispersed in crystalline carriers. On the other hand, when the Hildebrand approach was utilised in combination with  $\log P$ ,  $pK_a$  and  $T_g$  considerations, amorphous miscibility between additives and polymers failed to be predicted for systems in which acid–base interactions took place.<sup>[158]</sup> Systems which were predicted to be immiscible, but showed acid–base interactions, still resulted in ASD formulations. Contrastingly, this approach accurately predicted miscibility and ASD formation for systems produced *via* a solvent evaporation method without acid–base interactions. This underlines again that the Hildebrand concept with a single value for total solubility parameter cannot adequately account for specific or hydrogen bonding interactions.

As mentioned previously, the HSP concept offers a 3-D solubility parameter concept that can be visualised in the Hansen space (Figure 1). A way to project a 3-D solubility parameter in a two-dimensional plane was proposed by Bagley *et al.*<sup>[162]</sup> It was argued that the thermodynamic contribution to the solubility parameter of the polar and dispersion interactions are often similar, and therefore, a combined solubility parameter ( $\delta_v^2$ ) can be derived from Equation 8 to yield the following Equation<sup>[162]</sup>:

$$\delta_d^2 + \delta_p^2 = \delta_v^2 \quad (38)$$

The plot of  $\delta_v$  vs  $\delta_b$  simplifies the 3-D Hansen space into the 2-D plane, which is referred to as a Bagley plot. Analogues to the previously discussed Hansen space, it is assumed that molecules in vicinity of each other are more likely to be miscible.<sup>[32,154]</sup> The Bagley plot has been utilised to evaluate and predict miscibility between molecules using the  $R_a(v)$  parameter, which gives an idea of the ‘area of miscibility’ around a molecule, and should be  $\leq 5.6 \text{ MPa}^{1/2}$  for miscibility. This parameter is analogous to the  $R_a$  in Equation 21 but uses the simplification of Equation 39 to a drug–polymer system:

$$R_a(v)^2 = [4(\delta_{v2} - \delta_{v1})^2 + (\delta_{h2} - \delta_{h1})^2] \quad (39)$$

Bagley plots are highly versatile and have been used to investigate the miscibility of polymers in solvents,<sup>[82]</sup> drugs in excipients<sup>[32,154,157]</sup> and polymers in polymers.<sup>[163]</sup> It is important to consider the selected method when calculating solubility parameters, as different methods can give rise to different Bagley plots, which was highlighted by Meaurio and colleagues.<sup>[163]</sup>

These theoretical considerations were applied to ASD formations by different authors.<sup>[154,157]</sup> One study tested 84 drug molecules for their miscibility in PEG and demonstrated a good correlation between the group of drugs forming ASDs with PEG with the plot region around PEG derived from theoretical solubility parameter calculation.<sup>[154]</sup>



Alhalaweh *et al.*<sup>[157]</sup> compared experimentally derived miscibility data of indomethacin and excipients with predicted miscibility data. The Bagley plots of these data sets were almost identical and the predicted data showed a good correlation to the ASD formation.

Another prerequisite for the formation and stability of successful ASDs is that the change in the free energy of the system upon mixing should be negative. Because ideal mixing increases the entropy of the system, the entropy contribution should facilitate mixing. Consequently, it is the enthalpy contribution that may prevent free mixing energy  $\Delta G_m$  to be negative. In drug–polymer systems the Flory–Huggins equation has been adapted to align with the lattice-based Equation (40) used for the dissolution of polymers in solvents<sup>[164–167]</sup> as previously described in Equation 5.

$$\Delta H_m = V_{dp}\phi_d\phi_p(\delta_d - \delta_p)^2 \quad (40)$$

where subscript *d* and *p* describe drug and polymer respectively, while  $\Delta H_m$  can, also, be given by the van Laar expression according to Equation 42:

$$\Delta H_m = \chi_{dp}\phi_d\phi_pRT \quad (41)$$

From Equation 42 it can be seen that the value of the drug–polymer interaction parameter,  $\chi_{dp}$ , could be a surrogate for the enthalpy of the system, for given conditions. By combining Equations (40) and (41), the drug–polymer interaction parameter can be given by Equation 42 (neglecting  $\beta$ ) which is in line with the previously discussed Equation 6:

$$\chi_{dp} = \frac{V_{dp}(\delta_d - \delta_p)^2}{RT} \quad (42)$$

where  $V_{dp}$  is volume of mixture,  $\phi_d$  and  $\phi_p$  are volume fractions of drug and polymer, and  $\delta_d$  and  $\delta_p$  are solubility parameters of drug and polymer.

Similar to the total (or Hildebrand) solubility parameter, the HSP has also been linked to the drug–polymer interaction parameter ( $\chi_{dp}$ ) by consideration of partial contributions to cohesive energy density.<sup>[82]</sup>

The drug–polymer interaction parameter has been used widely for the investigation of binary mixtures especially, miscibility based on a negative  $\Delta G_m$ . Although this parameter can be determined by melting point depression,<sup>[165,167–169]</sup> there are also some studies that use the 3-D solubility parameter approach<sup>[154,167,169]</sup> to investigate drug–excipient miscibility in a more quantitative way. Such construction of phase diagrams show the differentiation of single and two phase system at equilibrium (binodal line) and kinetic decomposition of metastable mixtures (spinodal line) can be estimated.<sup>[170,171]</sup> It is attractive to construct entire phase diagrams but this objective is more

ambitious than use of the solubility parameters to simply rank excipient selection based on rules of thumb, such as based on the proximity of drug and excipient representations in the Hansen space or Bagley plot. A key strength of the solubility parameter is that such approaches are in general rather simple. A more ambitious quantitative calculation of entire phase diagrams can suffer from the simplifications of the thermodynamic approach as well as from lacking prediction of solubility parameter estimates. Phase diagrams constructed *via* solubility parameters might therefore be better considered as a first approximation only.

### Mesoporous silica

Recent developments suggests mesoporous silica as a new and promising material to formulate poorly water-soluble drugs with the intent to increase dissolution rate and solubility.<sup>[149,172–176]</sup>

Loaded mesoporous silica is prepared *via* adsorption of API from a concentrated organic solution followed by evaporating the solvent. This adsorption into the porous network stabilises the API in the amorphous state, due to steric effects. Upon administration, the amorphous API is then released and the dissolution is increased.<sup>[173]</sup>

Utilisation of the solubility parameter in the development of amorphous mesoporous silica is still largely unemployed without commercial formulations that are globally on the market. This represents a key gap in the literature, as solubility parameters can guide the selection of suitable solvent to maximise the penetration efficiency of API into mesoporous silica, which was demonstrated by Hideo Hata and coworkers.<sup>[177]</sup> They showed that, of six different solvents used to incorporate taxol onto mesoporous silica, only two resulted in effective loading of the API. They concluded that solubility parameter was a key factor in this observation; where solvents that interacted strongly with taxol resulted in the most effective loading, whereas those with weak interaction showed poor loading efficiency. Such interaction can be determined using solubility parameter approach.<sup>[177]</sup> However, the range of solvents suitable for use with formulation development is limited. Those solvents that show the strongest solubilisation power are often seen as ‘no-go’ solvents based on ICH guidelines.<sup>[178]</sup> Therefore, most instances of mesoporous silica use in the literature are carried out with either ethanol, acetone or dichloromethane, with even the latter being less utilised due to toxicity considerations.<sup>[149]</sup> The ICH list certainly limits solvent selection but not to the extent as it is currently reflected in the literature on mesoporous silica so there is a potential to access a wider range of solvents by employing a rank-order-based protocol based on *in silico* solubility parameter calculation.



Amorphous solid dispersions systems have proved to be a useful formulation tools in battling the solubility issues of pharmaceutical molecules. However, because of their limitations in stability, miscibility of the system is of crucial importance for a successful formulation. This makes the identification of tools to evaluate miscibility in the development phase, not only useful, but imperative. Herein the application of solubility parameter concepts to assess miscibility has been reviewed and discussed in the previous section. It should be emphasised again that a consideration of partial solubility parameters is preferred to a simple comparison of total (i.e. Hildebrand) solubility parameters. Moreover, the need of a complete database for partial solubility parameter either for drug and polymer was highlighted when using HSP. A limited number of data is not only available with respect to experimentally determined values but also for group contributions as used for *in silico* prediction of solubility parameters. The latter limitation can be especially troublesome in case of HSP estimation for more complex drug molecules. Application of the modified solubility parameter approach was applied by Piccinni<sup>[179]</sup> and even though the usefulness for early excipient ranking was recognised, it was also emphasised that physical screening tests should not be replaced by the *in silico* method until more robust prediction methods are available. This supports what was discussed in the previous sections that solubility parameters can be calculated *in silico* to rank excipients for a subsequent experimental screening. Such a screening phase can therefore be designed in a more focused and cost-effective way rather than be entirely replaced.

#### Application of solubility parameters in the formulation of nano- and microparticulate systems

One of the most used methods for dissolution improvement of poorly water-soluble drugs is particle size reduction. The decrease in size increases the surface to volume ratio, which accelerates dissolution kinetics. Especially interesting here are sizes well below 1  $\mu\text{m}$ , which have the highest potential increase the kinetic drug solubility<sup>[180,181]</sup> in addition to the dissolution rate enhancement. Thus, by bringing particle size to the nanoscale, solvation pressure increases and facilitates the disruption of the intrasolute bonds thus promoting solubilisation.<sup>[182]</sup>

Micronisation and nanosizing methods can be grouped into two categories: the top-down methods that entails size reduction of bigger particles by the use of shear forces and the bottom-up methods that involve the isolation of drug particles after recrystallisation from a highly supersaturated drug solution.<sup>[181]</sup> Although traditional micronisation techniques, such as dry-milling, are still being used, bottom-up

approaches are becoming increasingly sophisticated, gaining merit as techniques that can circumvent typical process limitations.<sup>[183]</sup> These limitations may involve unwanted amorphisation, disruption of the crystal lattice and unpredictable particle size distributions.<sup>[184]</sup> However, bottom-up approaches also face their individual limitations. Due to the fact that they rely on the controlled precipitation of particles from supersaturated solutions, miscibility and solubility considerations should be taken into account for the optimal choice of formulation combinations.

Moreover, technical developments in both top-down (e.g. 'pearl' milling and high-pressure homogenisation) and bottom-up techniques (e.g. new-generation spray dryers, supercritical fluid technology and freeze drying) have broadened the availability of nanosizing approaches. As nanoparticles exhibit high surface cohesive energies, they are especially prone to aggregation,<sup>[185,186]</sup> making their stabilisation indispensable. The use of various stabilisers, often surfactants and/or polymers, has been reported. It is proposed that they work by sterically or ionically stabilising the surface of nanoparticles, to limit aggregation.<sup>[187]</sup> The choice of appropriate stabilisers seems to greatly depend on the physical characteristics of the surface of drug molecules.<sup>[188]</sup> Consequently, the need for reliable tools to estimate possible candidates for nanoparticle formulations is evident.

Several attempts for nano- and micronised formulations have been reported in literature using a variety of materials including proteins, lipids and polymers.<sup>[189]</sup> We considered here not only the classical top-down and bottom-up approaches but more broadly reviewed also micro- and nanoparticle formation. Calculated solubility parameters are used eventually here as an early evaluation of miscibility of solvent-solute combinations as well as miscibility between molecules. However, evidence of using solubility parameters later during formulation development is very limited. To the best of our knowledge, only few relevant literature references exist, i.e. where a solubility parameter approach has been used for choosing the appropriate lipids in drug-polymer-lipid nanoparticles,<sup>[137]</sup> for choosing the drug-polymer combinations for the construction of polymeric micelles and for predicting drug loading.<sup>[190,191]</sup> Furthermore, Mahmud *et al.*<sup>[191]</sup> and Dwan'Isa *et al.*<sup>[190]</sup> used the HSP to calculate the Flory-Huggins interaction parameter of drug-polymer combinations ( $\chi_{dp}$ ) and considered it as a measure of miscibility.<sup>[192]</sup> Dwan'Isa *et al.* tested 19 drugs for their interactions with a diblock copolymer (MePEG-*b*-(PCL-*co*-TMC)), while Mahmud *et al.* studied the interactions of one anticancer drug (curcubitin I) against a variety of core-forming polymers. In both studies, the calculation of the  $\chi_{dp}$  parameter was able to reveal the optimal drug-polymer combinations, as well as to predict the drug loading capacity of the polymer micelle formulations. Even though the calculation of the interaction parameter provided a reasonably accurate

method for the qualitative prediction of drug solubilisation in the polymeric micelles, a definite rank order of combination miscibility among the variations tested could not be achieved, which may be attributed to the limitations of the Flory–Huggins theory as well as lacking accuracy of estimating the interaction parameter. Simplifications included the disregard of polymer molecular weight and polymer solvent interactions.<sup>[192]</sup> Nevertheless, the calculations of the HSP and the Flory–Huggins interaction parameter have been proven to be adequate tools for the primary selection of potentially miscible nano- and microparticulate systems, which helps in reducing the number of early screening experiments.

### Conclusions

Solubility parameters have proven to be useful in diverse scientific fields, and this review has outlined the different applications concerning oral delivery of poorly water-soluble compounds. These compounds typically require bioenabling formulation for successful development and solubility parameters can help, for example with ranking of solvents and excipients to achieve a more focused formulation development. Herein, predictions based on chemical structure are particularly interesting as only limited compound is available in early development. Despite the usefulness of applying solubility parameters in pharmaceuticals, there are also some gaps. In particular, drugs in a solid crystalline state or also rather complex molecules in general

may result in erratic predictions of solubility parameters. However, it is promising that new theoretical developments have been reported that present conceptual improvements. Moreover, experimental methods such as high-throughput solubility testing or greater availability of inverse gas chromatography will help in generating more data. Important is to obtain more comparative data of experimental and computational methods to better learn about variability of results. This can in turn help to further improve *in silico* predictions of solubility parameters, and a just accepted article has been following this research direction.<sup>[193]</sup> Therefore, it can be expected that solubility parameters will also in the future rank among the mostly used thermodynamic approaches in pharmaceuticals.

### Declarations

#### Conflict of interest

The Authors declare that they have no conflict of interests to disclose.

#### Funding

This project has received funding from the European Union's Horizon 2020 Research and Innovation Programme under Grant Agreement No 674909 (PEARRL).

### References

- Hansen CM. *Hansen Solubility Parameter a User's Handbook*, 2nd edn. Boca Raton, FL: CRC Press, 2007.
- Hancock B *et al.* The use of solubility parameters in pharmaceutical dosage form design. *Int J Pharm* 1997; 148: 1–21.
- Kuentz M *et al.* Methodology of oral formulation selection in the pharmaceutical industry. *Eur J Pharm Sci* 2016; 87: 136–163.
- Hildebrand JH, Scott RL. *Solubility of Nonelectrolytes*, 3rd edn. New York, NY: Dover, 1964.
- Stefanis E, Panayiotou C. Prediction of hansen solubility parameters with a new group-contribution method. *Int J Thermophys* 2008; 29: 568–585.
- Just S *et al.* Improved group contribution parameter set for the application of solubility parameters to melt extrusion. *Eur J Pharm Biopharm* 2013; 85(3 Part B): 1191–1199.
- Díaz I *et al.* Comparison between three predictive methods for the calculation of polymer solubility parameters. *Fluid Phase Equilib* 2013; 337: 6–10.
- Panayiotou C *et al.* Redefining solubility parameters: bulk and surface properties from unified molecular descriptors. *J Chem Thermodyn* 2017; 111: 207–220.
- Louwerse MJ *et al.* Revisiting Hansen solubility parameters by including thermodynamics. *ChemPhysChem* 2017; 18: 2999–3006.
- Bustamante P *et al.* The modified extended Hansen method to determine partial solubility parameters of drugs containing a single hydrogen bonding group and their sodium derivatives: benzoic acid/Na and ibuprofen/Na. *Int J Pharm* 2000; 194: 117–124.
- Bashimam M. Hansen solubility parameters: a quick review in pharmaceutical aspect. *J Chem Pharm Res* 2015; 7: 597–599.
- Scatchard G. Equilibria in non-electrolyte solutions in relation to the vapor pressures and densities of the components. *Chem Rev* 1931; 8: 321–333.
- Hildebrand JH, Wood SE. The derivation of equations for regular solutions. *J Chem Phys* 1933; 1: 817.
- Biroa J *et al.* Prediction of the  $\chi$  parameter by the solubility parameter and corresponding states theories. *Macromolecules* 1971; 4: 30–35.
- Hansen CM. *The Three Dimensional Solubility Parameter and Solvent Diffusion Coefficient. Their Importance in Surface Coating Formulation*. Danish Technical Press, 1967. Available at: <https://hansen-solubility.com/contents/HSP1967-OCR.pdf>.
- Barton A. *Handbook of Solubility Parameters and Other Cohesion Parameters*, 2nd edn. Boca Raton, FL: CRC Press, 1991.
- Brown HC, Grayson M. Homomorphs of 2,6-dimethyl-t-butylbenzene. *J Am Chem Soc* 1953; 75: 20–24.

18. Brown HC *et al.* Strained homomorphs. <sup>1</sup> 14. General summary. *J Am Chem Soc* 1953; 75: 1–6.
19. Blanks RF, Prausnitz JM. Thermodynamics of polymer solubility in polar and nonpolar systems. *Ind Eng Chem Fundam* 1964; 3: 1–8.
20. Hansen CM, Skaarup K. Independent calculation of the parameter components. *J Paint Technol* 1967; 37: 511–515.
21. Hansen CM, Beerbower CH. Solubility parameters. *Kirk-Othmer Encycl Chem Technol* 1971; 75: 889–910.
22. Hansen CM. 50 Years with solubility parameters—past and future. *Prog Org Coat* 2004; 51: 77–84.
23. Small PA. Some factors affecting the solubility of polymers. *J Chem Technol Biotechnol* 1953; 3: 71–80.
24. Sorenson P. Application of the acid/base concept describing the interaction between pigments, binders, and solvents. *J Paint Technol* 1975; 47: 31.
25. Beerbower A *et al.* Expanded solubility parameter approach I: naphthalene and benzoic acid in individual solvents. *J Pharm Sci* 1984; 73: 179–188.
26. Barra J *et al.* Proposition of group molar constants for sodium to calculate the partial solubility parameters of sodium salts using the van Krevelen group contribution method. *Eur J Pharm Sci* 2000; 10: 153–161.
27. Verheyen S *et al.* Determination of partial solubility parameters of five benzodiazepines in individual solvents. *Int J Pharm* 2001; 228: 199–207.
28. Bustamante P *et al.* A modification of the extended Hildebrand approach to predict the solubility of structurally related drugs in solvent mixtures. *J Pharm Pharmacol* 1993; 45: 253–257.
29. Jouyban A, Acree WE. Comments on “Prediction of Drug Solubility in Lipid Mixtures from the Individual Ingredients”. *AAPS PharmSciTech* 2014; 15: 83–85.
30. Vay K *et al.* Application of Hansen solubility parameters for understanding and prediction of drug distribution in microspheres. *Int J Pharm* 2011; 416: 202–209.
31. Muela S *et al.* Influence of temperature on the solubilization of thiabendazole by combined action of solid dispersions and co-solvents. *Int J Pharm* 2010; 384: 93–99.
32. Kitak T *et al.* Determination of solubility parameters of ibuprofen and ibuprofen lysinate. *Molecules* 2015; 20: 21549–21568.
33. Howell J *et al.* A functional approach to solubility parameter computations. *J Phys Chem B* 2017; 121: 4191–4201.
34. Archer WL. Determination of Hansen solubility parameters for selected cellulose ether derivatives. *Ind Eng Chem Res* 1991; 30: 2292–2298.
35. Bustamante P *et al.* Partial solubility parameters of piroxicam and niflumic acid. *Int J Pharm* 1998; 174: 141–150.
36. Martin A *et al.* Extended Hansen solubility approach: naphthalene in individual solvents. *J Pharm Sci* 1981; 70: 1260–1264.
37. Van Dyk JW *et al.* Solubility, solvency, and solubility parameters. *Ind Eng Chem Prod Res Dev* 1985; 24: 473–478.
38. Ravindra R *et al.* Solubility parameter of chitin and chitosan. *Carbohydr Polym* 1998; 36: 121–127.
39. Segarceanu O, Leca M. Improved method to calculate Hansen solubility parameters of a polymer. *Prog Org Coat* 1997; 31: 307–310.
40. Klar F, Urbanetz NA. Solubility parameters of hypromellose acetate succinate and plasticization in dry coating procedures. *Drug Dev Ind Pharm* 2016; 42: 1621–1635.
41. Kent DJ, Rowe RC. Solubility studies on ethyl cellulose used in film coating. *J Pharm Pharmacol* 1978; 30: 808–810.
42. Han KH *et al.* Prediction of solubility parameter from intrinsic viscosity. *J Ind Eng Chem* 2013; 19: 1130–1136.
43. Bustamante P *et al.* A new method to determine the partial solubility parameters of polymers from intrinsic viscosity. *Eur J Pharm Sci* 2005; 24: 229–237.
44. Madsen CG *et al.* Simple measurements for prediction of drug release from polymer matrices – solubility parameters and intrinsic viscosity. *Eur J Pharm Biopharm* 2015; 92: 1–7.
45. Weerachanchai P *et al.* Determination of solubility parameters of ionic liquids and ionic liquid/solvent mixtures from intrinsic viscosity. *ChemPhysChem* 2014; 15: 3580–3591.
46. Mieczkowski R. The determination of the solubility parameter components of polystyrene by partial specific volume measurements. *Eur Polym J* 1988; 24: 1185–1189.
47. Mieczkowski R. The determination of the solubility parameter components of polystyrene. *Eur Polym J* 1989; 25: 1057–1057.
48. Mieczkowski R. Solubility parameter components of some polyols. *Eur Polym J* 1991; 27: 377–379.
49. Huang J-C. Methods to determine solubility parameters of polymers at high temperature using inverse gas chromatography. *J Appl Polym Sci* 2004; 94: 1547–1555.
50. DiPaola-Baranyi G, Guillet JE. Estimation of polymer solubility parameters by gas chromatography. *Macromolecules* 1978; 11: 228–235.
51. Ito K, Guillet JE. Estimation of solubility parameters for some olefin polymers and copolymers by inverse gas chromatography. *Macromolecules* 1979; 12: 1163–1167.
52. Adamska K, Voelkel A. Hansen solubility parameters for polyethylene glycols by inverse gas chromatography. *J Chromatogr A* 2006; 1132: 260–267.
53. Choi P *et al.* Measurement of three-dimensional solubility parameters of nonyl phenol ethoxylates using inverse gas chromatography. *J Colloid Interface Sci* 1996; 180: 1–8.
54. Adamska K, Voelkel A. Inverse gas chromatographic determination of solubility parameters of excipients. *Int J Pharm* 2005; 304: 11–17.
55. Wang Q *et al.* Determination of the solubility parameter of epoxidized soybean oil by inverse gas chromatography. *J Macromol Sci Part B* 2013; 52: 1405–1413.
56. Adamska K *et al.* New procedure for the determination of Hansen solubility parameters by means of inverse gas chromatography. *J Chromatogr A* 2008; 1195: 146–149.



57. Price GJ, Shillcock IM. Inverse gas chromatographic measurement of solubility parameters in liquid crystalline systems. *J Chromatogr A* 2002; 964: 199–204.
58. Cakar F et al. Physicochemical characterization of 5-decyloxy-2-[[[4-hexyloxyphenyl] imino] methyl] phenol liquid crystal by inverse gas chromatography. *Optoelectron Adv Mater Commun* 2008; 2: 871–875.
59. Liu G et al. Crystallization of piroxicam solid forms and the effects of additives. *Chem Eng Technol* 2014; 37: 1297–1304.
60. Langer SH et al. Gas-chromatographic study of the solution thermodynamics of hydroxylic derivatives and related compounds. *J Phys Chem* 1982; 86: 4605–4618.
61. Coca J et al. Thermodynamic properties of some organic compounds with tetrachloroterephthaloyl oligomers by gas chromatography. *J Chem Eng Data* 1989; 34: 280–284.
62. Voelkel A et al. Characterization of the interactions in polymer/silica systems by inverse gas chromatography. *Macromol Symp* 2001; 169: 45–55.
63. Voelkel A, Fall J. Influence of prediction method of the second virial coefficient on inverse gas chromatographic parameters. *J Chromatogr A* 1996; 721: 139–145.
64. Price GJ et al. Measurement of solubility parameters by gas-liquid chromatography. *J Chromatogr A* 1986; 369: 273–280.
65. Voelkel A, Grzeskowiak T. Properties of zirconate modified silica gel as examined by inverse gas chromatography. *Macromol Symp* 2001; 169: 35–44.
66. Voelkel A, Janas J. Solubility parameters of broad and narrow distributed oxyethylates of fatty alcohols. *J Chromatogr A* 1993; 645: 141–151.
67. Abbott S et al. *Hansen Solubility Parameters in Practice, HSPiP, a package of software, datasets and eBook*. 2017. Available at: <http://www.hansen-solubility.com/HSPiP>, accessed 05-June-2017.
68. Panayiotou CG. Inverse gas chromatography and partial solvation parameters. *J Chromatogr A* 2012; 1251: 194–207.
69. Çavus S et al. Solvent dependent swelling behaviour of poly(*N*-vinylcaprolactam) and poly(*N*-vinylcaprolactam-co-itaconic acid) gels and determination of solubility parameters. *Chem Pap* 2015; 69: 1367–1377.
70. Bristow GM, Watson WF. Cohesive energy densities of polymers. Part 1.—Cohesive energy densities of rubbers by swelling measurements. *Trans Faraday Soc* 1958; 54: 1731–1741.
71. Bristow GM, Watson WF. Cohesive energy densities of polymers. Part 2.—Cohesive energy densities from viscosity measurements. *Trans Faraday Soc* 1958; 54: 1742–1747.
72. Aharoni SM. The solubility parameters of aromatic polyamides. *J Appl Polym Sci* 1992; 45: 813–817.
73. Eroglu MS et al. Determination of solubility parameters of poly(epichlorohydrin) and poly(glycidyl azide) networks. *Polymer (Guildf)* 1997; 38: 1945–1947.
74. Schenderlein S et al. Partial solubility parameters of poly(*d,l*-lactide-co-glycolide). *Int J Pharm* 2004; 286: 19–26.
75. Suh KW, Corbett JM. Solubility parameters of polymers from turbidimetric titrations. *J Appl Polym Sci* 1968; 12: 2359–2370.
76. Suh KW, Clarke DH. Cohesive energy densities of polymers from turbidimetric titrations. *J Polym Sci Part A-1 Polym Chem* 1967; 5: 1671–1681.
77. Lin X et al. Hansen solubility parameters of coal tar-derived typical PAHs using turbidimetric titration and an extended Hansen approach. *J Chem Eng Data* 2017; 62: 954–960.
78. Carvalho SP et al. Determining Hildebrand solubility parameter by ultraviolet spectroscopy and microcalorimetry. *J Braz Chem Soc* 2013; 24: 1998–2007.
79. Gee G. The interaction between rubber and liquids. III. The swelling of vulcanized rubber in various liquids. *Rubber Chem Technol* 1943; 16: 263–267.
80. Hoy KL. New values of the solubility parameters from vapor pressure data. *J Paint Technol* 1970; 42: 76–118.
81. Fedors RF. A method for estimating both the solubility parameters and molar volumes of liquids. *Polym Eng Sci* 1974; 14: 147–154.
82. van Krevelen DW. *Properties of Polymers: Their Correlation with Chemical Structure; Their Numerical Estimation and Prediction from Additive Group Contributions*, 4th edn. Amsterdam, The Netherlands: Elsevier, 2009.
83. Stefanis E, Panayiotou C. A new expanded solubility parameter approach. *Int J Pharm* 2012; 426: 29–43.
84. Shah M, Agrawal Y. High throughput screening: an *in silico* solubility parameter approach for lipids and solvents in SLN preparations. *Pharm Dev Technol* 2013; 18: 582–590.
85. Forster A et al. Selection of excipients for melt extrusion with two poorly water-soluble drugs by solubility parameter calculation and thermal analysis. *Int J Pharm* 2001; 226: 147–161.
86. Klamt A. *COSMO-RS: From Quantum Chemistry to Fluid Phase Thermodynamics and Drug Design*, 1st edn. Amsterdam, The Netherlands: Elsevier, 2005.
87. Gupta J et al. Prediction of solubility parameters and miscibility of pharmaceutical compounds by molecular dynamics simulations. *J Phys Chem B* 2011; 115: 2014–2023.
88. Ruether F, Sadowski G. Modeling the solubility of pharmaceuticals in pure solvents and solvent mixtures for drug process design. *J Pharm Sci* 2009; 98: 4205–4215.
89. Jouyban A et al. Comment on “Measurement and Correlation of Solubilities of (Z)-2-(2-Aminothiazol-4-yl)-2-methoxyiminoacetic Acid in Different Pure Solvents and Binary Mixtures of Water + (Ethanol, Methanol, or Glycol)”. *J Chem Eng Data* 2012; 57: 1344–1346.
90. Rogers MA, Marangoni AG. Kinetics of 12-hydroxyoctadecanoic acid SAFIN crystallization rationalized using hansen solubility parameters. *Langmuir* 2016; 32: 12833–12841.
91. Zhu Z et al. Superinsulating polyisocyanate based aerogels: a targeted search for the optimum solvent system. *ACS Appl Mater Interfaces* 2017; 9: 18222–18230.

## X. Thesis Publications

Sandra Jankovic *et al.*

Solubility parameter in pharmaceuticals

92. Masurel E *et al.* Screening method for solvent selection used in tar removal by the absorption process. *Environ Technol* 2015; 36: 2556–2567.
93. Cascant MM *et al.* A green analytical chemistry approach for lipid extraction: computation methods in the selection of green solvents as alternative to hexane. *Anal Bioanal Chem* 2017; 409: 3527–3539.
94. Laboukhi-Khorsī S *et al.* Efficient solvent selection approach for high solubility of active phytochemicals: application for the extraction of an antimalarial compound from medicinal plants. *ACS Sustain Chem Eng* 2017; 5: 4332–4339.
95. Sánchez-Camargo AP *et al.* Application of Hansen solubility approach for the subcritical and supercritical selective extraction of phlorotannins from *Cystoseira abies-marina*. *RSC Adv* 2016; 6: 94884–94895.
96. Fardī T *et al.* Artwork conservation materials and Hansen solubility parameters: a novel methodology towards critical solvent selection. *J Cult Herit* 2014; 15: 583–594.
97. Pudīpeddī M, Serajuddīn ATM. Trends in solubility of polymorphs. *J Pharm Sci* 2005; 94: 929–939.
98. Liu R. *Water-Insoluble Drug Formulation*, 2nd edn. Bosa Roca, USA: Taylor & Francis Inc., 2008.
99. Bauer J *et al.* Ritonavir: an extraordinary case of conformational polymorphism. *Pharm Res* 2001; 18: 859–866.
100. Dinnebier RE *et al.* Structural characterization of three crystalline modifications of telmisartan by single crystal and high-resolution X-ray powder diffraction. *J Pharm Sci* 2000; 89: 1465–1479.
101. Cimarosti Z *et al.* Development of drug substances as mixture of polymorphs: studies to control form 3 in casopitant mesylate. *Org Process Res Dev* 2010; 14: 1337–1346.
102. Stahl P, Wermuth CG. *Handbook of Pharmaceutical Salts*, 2nd edn. Zurich: Wiley-VCH, 2011.
103. Neau SH. Pharmaceutical salts. In: Liu R, ed. *Water-Insoluble Drug Formulation*, 2nd edn. Bosa Roca, USA: Taylor & Francis Inc., 2008.
104. Gould PL. Salt selection for basic drugs. *Int J Pharm* 1986; 33: 201–217.
105. Paulekuhn GS *et al.* Trends in active pharmaceutical ingredient salt selection based on analysis of the orange book database. *J Med Chem* 2007; 50: 6665–6672.
106. Saal C, Becker A. Pharmaceutical salts: a summary on doses of salt formers from the Orange Book. *Eur J Pharm Sci* 2013; 49: 614–623.
107. Berge SM *et al.* Pharmaceutical salts. *J Pharm Sci* 1977; 66: 1–19.
108. Haynes DA *et al.* Occurrence of pharmaceutically acceptable anions and cations in the Cambridge structural database. *J Pharm Sci* 2005; 94: 2111–2120.
109. Paulekuhn GS *et al.* Salt screening and characterization for poorly soluble, weak basic compounds: case study albendazole. *Pharmazie* 2013; 68: 555–564.
110. Nechipadappu SK, Trivedī DR. Pharmaceutical salts of ethionamide with GRAS counter ion donors to enhance the solubility. *Eur J Pharm Sci* 2017; 96: 578–589.
111. Fini A *et al.* Diclofenac salts, Part 7: are the pharmaceutical salts with aliphatic amines stable? *J Pharm Sci* 2012; 101: 3157–3168.
112. Surov AO *et al.* New solid forms of the antiviral drug arbidol: crystal structures, thermodynamic stability, and solubility. *Mol Pharm* 2015; 12: 4154–4165.
113. Elder DP *et al.* The utility of sulfonate salts in drug development. *J Pharm Sci* 2010; 99: 2948–2961.
114. Saal C, Weber K-DF. Compositions of anions and cations with pharmacological activity. 2016.
115. Balk A *et al.* Ionic liquid versus pro-drug strategy to address formulation challenges. *Pharm Res* 2015; 32: 2154–2167.
116. Frizzo CP *et al.* Pharmaceutical salts: solids to liquids by using ionic liquid design. In: Kadokawa J, ed. *Ionic Liquids: New Aspects for the Future*. Rijeka: InTech, 2013: Ch. 21.
117. Kumar V, Malhotra SV. Ionic liquids as pharmaceutical salts: a historical perspective. In: ACS Symposium series American chemical Society, ed. *Ionic Liquid Applications: Pharmaceuticals, Therapeutics, and Biotechnology*, 2010: 1–12.
118. Hough WL *et al.* The third evolution of ionic liquids: active pharmaceutical ingredients. *New J Chem* 2007; 31: 1429–1436.
119. FDA. *List of Generally Regarded as Safe Ingredients*. Available at: <http://www.fda.gov/Food/IngredientsPackagingLabeling/GRAS/>. Accessed November 21, 2017.
120. Fernández Casares A *et al.* An evaluation of salt screening methodologies. *J Pharm Pharmacol* 2015; 67: 812–822.
121. Mohammad MA *et al.* Hansen solubility parameter as a tool to predict cocrystal formation. *Int J Pharm* 2011; 407: 63–71.
122. Shetea A *et al.* Cocrystals of itraconazole with amino acids: screening, synthesis, solid state characterization, *in vitro* drug release and antifungal activity. *J Drug Deliv Sci Technol* 2015; 28: 46–55.
123. Abramov YA. *Computational Pharmaceutical Solid State Chemistry*, 1st edn. Hoboken, NJ: Wiley Online Library, 2016.
124. Rane SS, Anderson BD. What determines drug solubility in lipid vehicles: Is it predictable? *Adv Drug Deliv Rev* 2008; 60: 638–656.
125. Persson LC *et al.* Computational prediction of drug solubility in lipid based formulation excipients. *Pharm Res* 2013; 30: 3225–3237.
126. Patel SV, Patel S. Prediction of the solubility in lipidic solvent mixture: investigation of the modeling approach and thermodynamic analysis of solubility. *Eur J Pharm Sci* 2015; 77: 161–169.
127. Alskär LCC *et al.* Tools for early prediction of drug loading in lipid-based formulations. *Mol Pharm* 2016; 13: 251–261.
128. Dumanli I. Mechanistic studies to elucidate the role of lipid vehicles on solubility, formulation and bioavailability of poorly soluble compounds. 2002.
129. Shah NH *et al.* *Oral Lipid-Based Formulations – Enhancing the*



- Bioavailability of Poorly Water-Soluble Drugs* (Hauss DJ, ed.). London, UK: Informa Healthcare, 2007.
130. Vaughan CD. Solubility parameters for characterizing new raw materials. *Cosmet Toilet* 1993; 108: 57–64.
  131. Van Loon . Van Loon Chemical Innovations Brochure. Van Loon Chem Innov Brochure. Available at: [http://www.in-cosmetics.com/\\_novadocuments/326978?v=636220595266800000](http://www.in-cosmetics.com/_novadocuments/326978?v=636220595266800000). Accessed November 21, 2017.
  132. Yamamoto DH. *Hansen Solubility Parameter (HSP) and Allergens for Cosmetics*. Hansen Solubility Param Allergens Cosmet. Available at: <https://www.pirika.com/NewHP/PirikaE/Allergens.html>. Accessed November 21, 2017.
  133. Vaughan CD. Using solubility parameters in cosmetics formulation. *J Soc Cosmet Chem* 1985; 36: 19–333.
  134. Huynh L *et al.* Computational approaches to the rational design of nanoemulsions, polymeric micelles, and dendrimers for drug delivery. *Nanomedicine* 2012; 8: 20–36.
  135. De La Peña-Gil A *et al.* Simplifying Hansen solubility parameters for complex edible fats and oils. *Food Biophys* 2016; 11: 283–291.
  136. Shah M, Agrawal Y. Ciprofloxacin hydrochloride-loaded glyceryl monostearate nanoparticle: factorial design of Lutrol F68 and Phospholipon 90G. *J Microencapsul* 2012; 29: 331–343.
  137. Li Y *et al.* Screening of lipid carriers and characterization of drug-polymer-lipid interactions for the rational design of polymer-lipid hybrid nanoparticles (PLN). *Pharm Res* 2006; 23: 1877–1887.
  138. Breitzkreutz J. Prediction of intestinal drug absorption properties by three-dimensional solubility parameters. *Pharm Res* 1998; 15: 1370–1375.
  139. Abd E. *Targeted Skin Delivery of Topically Applied Drugs by Optimised Formulation Design*. 2015.
  140. Hossin B *et al.* Application of Hansen solubility parameters to predict drug–nail interactions, which can assist the design of nail medicines. *Eur J Pharm Biopharm* 2016; 102: 32–40.
  141. Kawabata Y *et al.* Formulation design for poorly water-soluble drugs based on biopharmaceutics classification system: basic approaches and practical applications. *Int J Pharm* 2011; 420: 1–10.
  142. Einfalt T *et al.* Methods of amorphization and investigation of the amorphous state. *Acta Pharm* 2013; 63: 305–334.
  143. Leuner C. Improving drug solubility for oral delivery using solid dispersions. *Eur J Pharm Biopharm* 2000; 50: 47–60.
  144. Serajuddin ATM. Solid dispersion of poorly water-soluble drugs: early promises, subsequent problems, and recent breakthroughs. *J Pharm Sci* 1999; 88: 1058–1066.
  145. Chiou WL, Riegelman S. Pharmaceutical applications of solid dispersion systems. *J Pharm Sci* 1971; 60: 1281–1302.
  146. Zhang J, Ma PX. Cyclodextrin-based supramolecular systems for drug delivery: recent progress and future perspective. *Adv Drug Deliv Rev* 2013; 65: 1215–1233.
  147. Hoppu P *et al.* Characterisation of blends of paracetamol and citric acid. *J Pharm Pharmacol* 2007; 59: 373–381.
  148. Simovic S *et al.* Silica materials in drug delivery applications. *Curr Drug Discov Technol* 2011; 8: 250–268.
  149. Xu W *et al.* Mesoporous systems for poorly soluble drugs. *Int J Pharm* 2013; 453: 181–197.
  150. Huang Y, Dai W-G. Fundamental aspects of solid dispersion technology for poorly soluble drugs. *Acta Pharm Sin B* 2014; 4: 18–25.
  151. Karavas E *et al.* Investigation of the release mechanism of a sparingly water-soluble drug from solid dispersions in hydrophilic carriers based on physical state of drug, particle size distribution and drug–polymer interactions. *Eur J Pharm Biopharm* 2007; 66: 334–347.
  152. Baghel S *et al.* Polymeric amorphous solid dispersions: a review of amorphization, crystallization, stabilization, solid-state characterization, and aqueous solubilization of biopharmaceutical classification system class II drugs. *J Pharm Sci* 2016; 105: 2527–2544.
  153. Sekiguchi K, Obi N. Studies on absorption of eutectic mixture. I. A comparison of the behavior of eutectic mixture of sulfathiazole and that of ordinary sulfathiazole in man. *Chem Pharm Bull* 1961; 9: 866–872.
  154. Thakral S, Thakral NK. Prediction of drug-polymer miscibility through the use of solubility parameter based flory-huggins interaction parameter and the experimental validation: PEG as model polymer. *J Pharm Sci* 2013; 102: 2254–2263.
  155. Greenhalgh DJ *et al.* Solubility parameters as predictors of miscibility in solid dispersions. *J Pharm Sci* 1999; 88: 1182–1190.
  156. DeBoyace K, Wildfong PLD. The application of modeling and prediction to the formation and stability of amorphous solid dispersions. *J Pharm Sci* 2017; 107: 57–74.
  157. Alhalaweh A *et al.* Data mining of solubility parameters for computational prediction of drug–excipient miscibility. *Drug Dev Ind Pharm* 2014; 40: 904–909.
  158. Yoo S *et al.* Miscibility/stability considerations in binary solid dispersion systems composed of functional excipients towards the design of multi-component amorphous systems. *J Pharm Sci* 2009; 98: 4711–4723.
  159. Djuris J *et al.* Preparation of carbamazepine–Soluplus® solid dispersions by hot-melt extrusion, and prediction of drug–polymer miscibility by thermodynamic model fitting. *Eur J Pharm Biopharm* 2013; 84: 228–237.
  160. Sarode AL *et al.* Hot melt extrusion (HME) for amorphous solid dispersions: predictive tools for processing and impact of drug–polymer interactions on supersaturation. *Eur J Pharm Sci* 2013; 48: 371–384.
  161. Meng F *et al.* Investigation and correlation of drug polymer miscibility and molecular interactions by various approaches for the preparation of amorphous solid dispersions. *Eur J Pharm Sci* 2015; 71: 12–24.
  162. Bagley EB *et al.* Three-dimensional solubility parameters and their

- relationship to internal pressure measurements in polar and hydrogen bonding solvents. *J Paint Technol* 1971; 43: 35–42.
163. Meaurio E *et al.* Predicting miscibility in polymer blends using the Bagley plot: blends with poly(ethylene oxide). *Polymer (Guildf)* 2017; 113: 295–309.
164. Arrighi V *et al.* Miscibility. In: *Encyclopedia of Polymer Science and Technology*, 3rd edn. Hoboken, NJ: John Wiley & Sons, Inc., 2002.
165. Paudel A *et al.* Theoretical and experimental investigation on the solid solubility and miscibility of naproxen in poly(vinylpyrrolidone). *Mol Pharm* 2010; 7: 1133–1148.
166. Qian F *et al.* Solution behavior of PVP-VA and HPMC-AS-based amorphous solid dispersions and their bioavailability implications. *Pharm Res* 2012; 29: 2766–2776.
167. Tian Y *et al.* Construction of drug-polymer thermodynamic phase diagrams using Flory-Huggins interaction theory: identifying the relevance of temperature and drug weight fraction to phase separation within solid dispersions. *Mol Pharm* 2013; 10: 236–248.
168. Marsac PJ *et al.* Theoretical and practical approaches for prediction of drug-polymer miscibility and solubility. *Pharm Res* 2006; 23: 2417–2426.
169. Zhao Y *et al.* Prediction of the thermal phase diagram of amorphous solid dispersions by Flory-Huggins theory. *J Pharm Sci* 2011; 100: 3196–3207.
170. Koningsveld R *et al.* *Polymer Phase Diagrams: A Textbook*. Oxford, USA: Oxford University Press, 2001.
171. Friesen DT *et al.* Hydroxypropyl methylcellulose acetate succinate-based spray-dried dispersions: an overview. *Mol Pharm* 2008; 5: 1003–1019.
172. O'Shea JP *et al.* Mesoporous silica-based dosage forms improve bioavailability of poorly soluble drugs in pigs: case example fenofibrate. *J Pharm Pharmacol* 2017; 69: 1284–1292.
173. Lainé A-L *et al.* Enhanced oral delivery of celecoxib via the development of a supersaturable amorphous formulation utilising mesoporous silica and co-loaded HPMCAS. *Int J Pharm* 2016; 512: 118–125.
174. Van Speybroeck M *et al.* Enhanced absorption of the poorly soluble drug fenofibrate by tuning its release rate from ordered mesoporous silica. *Eur J Pharm Sci* 2010; 41: 623–630.
175. Dressman JB *et al.* Mesoporous silica-based dosage forms improve release characteristics of poorly soluble drugs: case example fenofibrate. *J Pharm Pharmacol* 2016; 68: 634–645.
176. McCarthy CA *et al.* Mesoporous silica formulation strategies for drug dissolution enhancement: a review. *Expert Opin Drug Deliv* 2016; 13: 93–108.
177. Hata H *et al.* Adsorption of taxol into ordered mesoporous silicas with various pore diameters. *Chem Mater* 1999; 11: 1110–1119.
178. ICH Expert Working Group. *Impurities: Guideline for Residual Solvents*. 2016. Available at: [https://www.ich.org/fileadmin/Public\\_Web\\_Site/ICH\\_Products/Guidelines/Quality/Q3C/Q3C\\_R6\\_Step\\_4.pdf](https://www.ich.org/fileadmin/Public_Web_Site/ICH_Products/Guidelines/Quality/Q3C/Q3C_R6_Step_4.pdf). Accessed July 31, 2017.
179. Piccinni P *et al.* Solubility parameter-based screening methods for early-stage formulation development of itraconazole amorphous solid dispersions. *J Pharm Pharmacol* 2016; 68: 705–720.
180. Sun J *et al.* Effect of particle size on solubility, dissolution rate, and oral bioavailability: evaluation using coenzyme Q<sub>10</sub> as naked nanocrystals. *Int J Nanomed* 2012; 7: 5733–5744.
181. Williams HD *et al.* Strategies to address low drug solubility in discovery and development. *Pharmacol Rev* 2013; 65: 315–499.
182. Junghanns J-UAH, Müller RH. Nanocrystal technology, drug delivery and clinical applications. *Int J Nanomed* 2008; 3: 295–309.
183. Khacka P *et al.* Pharmaceutical particle technologies: an approach to improve drug solubility, dissolution and bioavailability. *Asian J Pharm Sci* 2014; 9: 304–316.
184. Rasenack N, Müller BW. Micron-size drug particles: common and novel micronization techniques. *Pharm Dev Technol* 2004; 9: 1–13.
185. Kundu S. *Silk Biomaterials for Tissue Engineering and Regenerative Medicine*, 1st edn. Amsterdam, Boston: Woodhead Publishing, 2014.
186. Singh AK. *Engineered Nanoparticles: Structure, Properties and Mechanisms of Toxicity*. Cambridge, MA: Academic Press, 2015.
187. Merisko-Liversidge EM, Liversidge GG. Drug nanoparticles: formulating poorly water-soluble compounds. *Toxicol Pathol* 2008; 36: 43–48.
188. Date AA, Patravale VB. Current strategies for engineering drug nanoparticles. *Curr Opin Colloid Interface Sci* 2004; 9: 222–235.
189. Wu L *et al.* Physical and chemical stability of drug nanoparticles. *Adv Drug Deliv Rev* 2011; 63: 456–469.
190. Latere Dwan'Isa JP *et al.* Prediction of drug solubility in amphiphilic diblock copolymer micelles: The role of polymer-drug compatibility. *Pharmazie* 2007; 62: 499–504.
191. Mahmud A *et al.* Self-associating poly(ethylene oxide)-*b*-poly( $\alpha$ -cholesteryl carboxylate- $\epsilon$ -caprolactone) block copolymer for the solubilization of STAT-3 inhibitor curcubitacin I. *Biomacromol* 2009; 10: 471–478.
192. Flory PJ. *Principles of Polymer Chemistry*, 3rd edn. Ithaca, NY: Cornell University Press, 1953.
193. Niederquell A *et al.* New prediction methods for solubility parameters based on molecular sigma profiles using pharmaceutical materials. *Int J Pharm* 2018; 546: 137–144.
194. Jansen. *Development of a semi-automated system for the determination of the Hansen solubility parameters of pharmaceutical excipients*. Unpublished data 2015. <https://doi.org/10.1111/jphhp.12948>.



Contents lists available at ScienceDirect

International Journal of Pharmaceutics

journal homepage: [www.elsevier.com/locate/ijpharm](http://www.elsevier.com/locate/ijpharm)

## Enhanced oral delivery of celecoxib via the development of a supersaturable amorphous formulation utilising mesoporous silica and co-loaded HPMCAS



A.-L. Lainé<sup>a,\*</sup>, D. Price<sup>a</sup>, J. Davis<sup>a</sup>, D. Roberts<sup>a</sup>, R. Hudson<sup>a</sup>, K. Back<sup>b</sup>, P. Bungay<sup>a</sup>, N. Flanagan<sup>a</sup>

<sup>a</sup> Pfizer—Neuroscience and Pain Research Unit, Granta Park, Cambridge CB21 6GS, United Kingdom

<sup>b</sup> Pfizer, Discovery Park, Ramsgate Rd, Sandwich CT13 9ND, United Kingdom

### ARTICLE INFO

#### Article history:

Received 27 May 2016

Received in revised form 10 August 2016

Accepted 15 August 2016

Available online 16 August 2016

#### Keywords:

Amorphous formulation

Pharmacokinetic study

Mesoporous material

*In vitro* pH shift assay

### ABSTRACT

Stabilization of amorphous formulations via mesoporous silica has gained considerable attention for oral delivery of poorly soluble drugs. The release of the drug from the silica is expected to generate supersaturation which is often associated with subsequent precipitation. The aim of the study was hence to develop a novel supersaturable amorphous formulation through the co-loading of a BCS class II drug Celecoxib (CXB) with a precipitation inhibitor hydroxypropyl methylcellulose acetate succinate (HPMCAS) onto the silica. The addition of HPMCAS did not hamper the adsorption but on the contrary promoted the complete solid state conversion of the drug as proved by DSC analysis. In an *in vitro* pH shift assay, the CXB-HPMCAS co-loaded silica achieved a 5-fold solubility increase over the crystalline CXB and over the CXB-loaded silica blended with HPMCAS which did not show any enhancement. The drug co-loaded silica was then suspended in an aqueous vehicle facilitating the dosing to animals. The CXB-HPMCAS co-loaded silica suspension achieved 15-fold solubility increase *in vitro* over the crystalline counterpart which translated in 1.35-fold C<sub>max</sub> increase *in vivo* after oral dosing in rats. This approach represents a novel formulation strategy to maximize *in vivo* exposure of poorly soluble drugs critical for discovery studies.

© 2016 Elsevier B.V. All rights reserved.

### 1. Introduction

Oral delivery of poorly soluble drugs remains one of the greatest challenges that formulation scientists face during drug discovery process. With the emergence of combinatorial chemistry and high throughput screening, new chemical entities often show suboptimal physicochemical properties such as high lipophilicity and low aqueous solubility leading to poor bioavailability (Lipinski et al., 2001). The identification of a suitable drug delivery system is therefore critical to achieve sufficient *in vivo* exposure. Several strategies (Kalepu and Nekkanti, 2015; Leucuta, 2014; Williams et al., 2013) have been developed in that regard such as particles size reduction (Dizaj et al., 2015), salt formation (Serajuddin, 2007), nanoparticles (Merisko-Liversidge and Liversidge, 2008), self-emulsifying drug delivery systems (SEDDS) (Pouton, 2000),

lipid formulation (Pouton and Porter, 2008; Hauss, 2007) and cocrystal (Elder et al., 2013). More recently, amorphous materials (Van den Mooter, 2012; Newman et al., 2015) have gained considerable attention for solubility enhancement as they can generate several-fold higher solution concentration (called supersaturation) compared to the corresponding crystalline form due to the lack of long range order and high free energy. However, a disadvantage of the high energy state of amorphous solids is the inherent metastability driving recrystallization under storage. Additionally, when the glassy solid is introduced into an aqueous medium, it often rapidly generates a transient supersaturated state immediately followed by a steep concentration decrease due to precipitation triggered by thermodynamic force. This dissolution profile, known as the spring effect (Guzman et al., 2007), creates a limited supersaturation window that may not offer a bioavailability increase after *in vivo* dosing. Accordingly, to benefit from the amorphous form and design a suitable drug product, the stability of the glassy form needs to be addressed (Grohganz et al., 2014; Laitinen et al., 2013). The most common way to stabilize the amorphous drug is by formulating it within an inert polymeric

\* Corresponding author at: Medimmune—AstraZeneca, Aaron Klug Building, Granta Park, Cambridge, CB21 6GH, United Kingdom.

E-mail address: [lainea@medimmune.com](mailto:lainea@medimmune.com) (A.-L. Lainé).



matrix, referred to as a solid dispersions (Newman et al., 2015). Besides its function of amorphous stabilizer, the polymer also plays the role of precipitation inhibitor (PI) helping to maintain supersaturation state after dissolution (spring and parachute effect). The most common manufacturing processes include hot melt extrusion (Lakshman et al., 2008; Wilson et al., 2012) and spray-drying (Paudel et al., 2013) which require specific equipment and are not always appropriate for low volume laboratory scale production. Alternatively, in the past decade, mesoporous silica (Shen et al., 2013; Vialpando et al., 2011; Xu et al., 2013) has shown appealing characteristics as an amorphous drug stabilizer and carrier due to high pore volume and surface area contributing to high drug loading capacity. The adsorption in the confined and restricted space of the pores prevents the compound from crystallizing. Additionally, silica is widely used in tablet manufacture and is generally regarded as orally biocompatible (Rowe et al., 2006). Whereas numerous *in vitro* studies have demonstrated the ability of drug loaded silica to increase the solubility of poorly soluble drugs, only a few have shown *in vivo* absorption improvement as recently highlighted by Van Speybroeck (Van Speybroeck et al., 2010). The probable cause for the lack of correlation is that unlike solid dispersion, the silica cannot act as precipitation inhibitor once the compound is released from its pores. Consequently, the addition of a polymer is required to maintain the supersaturated solubility which is critical for enhanced *in vivo* oral delivery. Van Speybroeck et al. (2010) were then the first to combine Itraconazole loaded silica with a PI and showed successful *in vivo* translation of the *in vitro* solubility increase. Based on this result, the aim of the present study was to develop a novel supersaturable amorphous formulation through the co-loading of a precipitation inhibitor and the drug onto the silica. Celecoxib (CXB), a nonsteroidal anti-inflammatory drug (Frampton and Keating, 2007) widely prescribed for treatment of osteoarthritis, rheumatoid arthritis and acute pain, was used as an example of poorly soluble compound. Belonging to the BCS class II substance, CXB is highly lipophilic and poorly water soluble with a good permeability. The absorption of CXB has been reported to be limited by its dissolution (Paulson et al., 2001). As a consequence, the clinical dosage form, marketed under the trade name Celebrex<sup>®</sup>, was designed to enhance the oral absorption of CXB through particle size reduction (D90 below 25 µm) and the addition of a wetting agent (sodium lauryl sulfate) (Gao et al., 2000). Due to its dissolution limited absorption characteristic, Celecoxib has been the subject of many solubility enhancing formulation attempts including, salt formation (Guzman et al., 2007), nanoparticles (Morgen et al., 2012), complexation with cyclodextrins (Rawat and Jain, 2004) and supersaturating SEDDS (Song et al., 2014). As the mechanism of adsorption onto the silica is mainly governed by hydrogen-bond interaction, CXB is a good model drug for this approach since it contains both hydrogen bond donor and acceptors. The mesoporous material utilised in the present work was a non-ordered silica named Parateck SLC<sup>®</sup> (developed by Merck Millipore) and hydroxypropyl methylcellulose acetate succinate (HPMCAS) was evaluated as PI. The performance of the resulting CXB-HPMCAS co-loaded silica was assessed firstly in an *in vitro* transfer dissolution assay aiming to simulate physiological pH change conditions and, then *in vivo* in a rat pharmacokinetic (PK) study. Its behavior was compared with that of CXB loaded silica blended with HPMCAS

## 2. Materials and methods

### 2.1. Materials

Ethanol, DMSO and acetonitrile were purchased from Sigma Aldrich (Sigma-Aldrich, St. Louis, MO, USA). Celecoxib, Celebrex

200 mg capsules (composition: lactose monohydrate, Sodium Lauryl Sulfate (SLS), povidone, croscarmellose sodium, magnesium stearate) and HPMCAS-HF were supplied through Pfizer central stores (Pfizer, Groton, CT, USA). Parateck SLC<sup>®</sup> (non ordered silica with mesopores size ranging from 2 to 7 nm) was kindly provided by Merck Millipore<sup>®</sup> (Merck Millipore, Darmstadt, Germany). Simulated Intestinal Fluid (SIF) was purchased from Biorelevant (Biorelevant, Surrey, UK). Methocel A4M (methylcellulose) and Tromethamine was provided by Dow chemical company (Midland, USA) and Sigma-Aldrich (St Louis, USA), respectively. All water used was purified using the Millipore Milli-Q Integral water purification system (Merck Millipore, Darmstadt, Germany).

### 2.2. Thermodynamic solubility

The thermodynamic solubility of CXB was determined in three media: 0.01 M HCl (pH 2), phosphate buffer (pH 6.5) and FaSSIF (pH 6.5). Approximately 1 mg of CXB was accurately weighed into an Eppendorf tube and 400 µL of medium pre-heated to 37 °C was added. The tubes were shaken for 18 h at 37 °C. The resultant dispersions were then double centrifuged at 37 °C for 15 and 30 min. The supernatant was then diluted in acetonitrile/water, 20/80, v/v and quantified for API concentration via HPLC against a standard calibration curve.

### 2.3. HPLC analysis

Two stock solutions of CXB, referred to as a standard stock solution and a quality control (QC) stock solution, were prepared in DMSO at 1 mg/mL. A calibration curve ranging from 0.1 to 50 µg/mL was obtained using serial dilutions in Acetonitrile/Water (20/80; v/v) from the standard stock. Serial dilutions were also done from the QC stock solution to prepared QC samples (0.3, 3 and 30 µg/mL).

HPLC analysis was performed using an Agilent 1200 series (Agilent technologies, Santa Clara, USA) system equipped with a UV detector (detection wavelength: 220 nm). Chromatographic separation was achieved on a Luna C18 column (50 × 4.6 mm, 3 µm particle size, 100 Å Phenomenex, California, USA). The mobile phases consisted of 90:10 water: ACN and 0.1% trifluoroacetic acid (TFA) for mobile phase A and 100% ACN + 0.1% TFA for mobile phase B and a linear gradient method was applied from 95% of mobile phase A to 95% of mobile phase B at a flow rate of 1 mL/min. System management and data acquisition and processing were performed via the Empower<sup>®</sup> software package (Waters, Milford MA).

### 2.4. Loading procedure

#### 2.4.1. Single drug loading procedure

CXB-Loaded Silica was prepared using the solvent impregnation rotary evaporator method developed in-house. Briefly, a solution (10 mg/mL) of CXB in ethanol was added to Parateck SLC (1:2 API/Parateck SLC<sup>®</sup>) under magnetic stirring for 15 min. The suspension was then transferred to a rotary evaporator in order to remove the solvent under reduced pressure at 45 °C. After observing the complete removal of solvent, the powder was left to dry under reduced pressure for 2 h.

#### 2.4.2. CXB- HPMCAS co-loading procedure

In order to co-load the hydroxypropyl methylcellulose acetate succinate (HPMCAS) and the CXB onto the silica (CXB: silica 1:2), the polymer was firstly homogenized using an ultraturax mixer in the concentrated API solution prior to addition of Parateck SLC<sup>®</sup>. The subsequent steps were identical to the single loading method. The resulting powder was ground with a mortar and pestle to break into



finer particles. The targeted ratio CXB/HPMCAS was 10/3 w/w and the theoretical loading of CXB was 30%  $W_{\text{CXB}}/W_{\text{silica+HPMCAS+CXB}}$ .

#### 2.4.3. Physical blend CXB co-loaded silica and HPMCAS

For the preparation of the physical blend, the two components of CXB loaded silica and HPMCAS were combined using a pestle and mortar to achieve an overall ratio of 10:3 CXB: HPMCAS.

### 2.5. Preparation of the buffers and CXB formulations

#### 2.5.1. Preparation of silica suspension

The drug loaded silica was suspended in an aqueous vehicle composed of 0.5% w/v Methocel (MC) A4M and 0.5% w/v HPMCAS in Tris Buffered water. The stock solution of the aqueous vehicle was firstly prepared and stored at 4 °C. Briefly, 0.24% w/v tromethamine and 0.5% w/v HPMCAS-HF were added in purified water and stirred until fully dissolved. The solution was then heated to 70 °C and 0.5% Methocel A4M was added gradually under vigorous stirring. Once the addition of Methocel completed, the heating was stopped and the solution was kept under magnetic stirring until cooling down to room temperature. The pH was subsequently adjusted to 7.4.

The CXB-HPMCAS co-loaded silica suspension was then prepared at 1.6 mg/mL in the (0.5% w/v Methocel (MC) A4M/ 0.5% w/v HPMCAS in Tris buffered water) vehicle by homogenization with a pestle in a mortar.

In order to assess and monitor the release kinetic and solid state conversion rate of the silica suspension over time, the formulation was kept at room temperature over 2 days and samples were taken regularly (0, 1 h, 4 h, 55 h post preparation), over the course of the assay. Each sample was centrifuged twice. The residue was assessed via XRPD and PLM for solid state evaluation and the supernatant was quantified via HPLC for free CXB concentration.

#### 2.5.2. Preparation of the CXB solution

A CXB solution was prepared in 40% v/v PEG400/60% v/v (20% w/v SBE-cyclodextrin in water) at 1.6 mg/mL. Briefly, CXB was firstly dissolved in PEG 400 to which (20% w/v SBE-cyclodextrin in water) component was added and mixed.

#### 2.5.3. Preparation of concentrated FaSSIF

Concentrated Fasted state simulated intestinal fluid (FaSSIF) pH 7.0 was prepared based on Biorelevant.com guidance but with a 3.4 factor applied to all the excipient contents. The concentration factor was due to the subsequent 3.4 dilution factor in the transfer dissolution assay. Briefly, NaOH (29.6 mM),  $\text{NaH}_2\text{PO}_4$  (96.6 mM) and NaCl (360.1 mM) were dissolved in 90% of purified water. The pH was then adjusted to 7.0 with 0.1 M HCl prior to making to final volume with purified water. To prepare the concentrated FaSSIF, 0.76% w/v of SIF-v1 powder (3.4-fold higher than recommended by biorelevant) was added to the concentrated phosphate buffer pH 7.0 and stirred. The final composition of the concentrated FaSSIF was 10.2 mM of sodium taurocholate and 2.55 mM of lecithin.

### 2.6. Characterization

#### 2.6.1. Crystallinity assessment: X-ray powder diffraction (XRPD)

2–4 mg of powder was placed on a XRPD disc and transferred to the D2 Phaser (Bruker, Billerica) with Cu-K $\alpha$  radiation ( $\lambda = 1.54 \text{ \AA}$ ) at 30 kV and 10 mA. Data were collected over 10 min from 3 to 55° 2 $\theta$ .

#### 2.6.2. Differential scanning calorimetry (DSC) analysis

Approximately 1–3 mg of powder was accurately weighed into an aluminium Tzero pan. This was sealed with a Tzero lid and crimped shut. The sample was run on a TA Instruments Discovery differential scanning calorimeter against an empty

reference pan of the same type, using a method that heated the sample from 25 °C to 200 °C at 10 °C/minute, with a nitrogen purge gas.

#### 2.6.3. Loading quantification

Approximately 10 mg of loaded silica were accurately weighed in triplicate to which 5 mL of DMSO were added and the samples were vortex mixed. 3 × 1 mL were then taken, double centrifuged, and the supernatant diluted (1:50) with 20:80 acetonitrile (ACN): water and analysed for CXB content against known standards using HPLC. Percentage loading was then calculated.

#### 2.6.4. Non-sink transfer dissolution

The transfer dissolution assays were performed firstly on dry powder samples (simulating a readily disintegrating tablet administration) and then on samples suspended in an aqueous vehicle (0.5% w/v MC/0.5% w/v HPMCAS in tris buffered water). For the powder samples, crystalline CXB, CXB loading silica, CXB-HPMCAS-co-loading silica or CXB loaded silica blended with HPMCAS weighings were made in order to obtain 4 mg of CXB active drug. 2.5 mL of water was added to this. For the suspensions 4 mg CXB in 2.5 mL of 0.5% w/v MC/0.5% w/v HPMCAS in tris buffered water vehicle was used. Samples were then transferred to a water bath at 37 °C and kept under magnetic stirring. 300  $\mu\text{L}$  of 37 °C pre-heated 0.1 M HCl was then added. 200  $\mu\text{L}$  samples were taken (15 and 30 min), double centrifuged and 50  $\mu\text{L}$  of supernatant diluted in ACN/H $_2$ O for HPLC analysis. At 30 min, 1 mL of concentrated FaSSIF solution was added to the vial to give a final pH of 6.8. The remaining samples were then taken at a cumulative time of 42, 55, 70, 90, 120 and 180 min. The samples were analysed by HPLC against a calibration curve. The temperature was maintained at 37 °C throughout and the pH checked at various time points.

After the end of the dissolution, a sample was taken from the dissolution vials and centrifuged. The solid residue was transferred to the D2 XRPD and analysed as previously described.

### 2.7. In vivo pharmacokinetic study

All experimental procedures were conducted in accordance with UK Animals (Scientific Procedures) Act 1986 and followed the guidelines under the International Association for the Study of Pain.

Male CD rats (Charles River Sprague Dawley) were allowed to acclimatize for at least one week prior to the study. Water and food were available ad libitum throughout the experiment. The animals ( $n = 3$  per group) were dosed by oral gavage with 5.8 mg/kg CXB at 3.6 mL/kg as either crystalline suspension, amorphous CXB-HPMCAS co-loaded silica suspension or in solution in 40% v/v PEG400/60% v/v (20% w/v SBE-cyclodextrin in water). Blood samples (20  $\mu\text{L}$ ) were taken from the tail vein at 0.5 h, 1 h, 2 h, 4 h, 8 h and 24 h post-dose and collected onto dry blood spot (DBS) cards.

DBS samples, together with the calibration and QC samples, were cut using a 3 mm punch into a 96 well plate. 10  $\mu\text{L}$  tolbutamide (375 ng/mL) in 25% acetonitrile were added as an internal standard (except for control blank). Samples were extracted by the addition of 300  $\mu\text{L}$  methanol for approximately 10 min on a plate shaker. All samples (excluding paper spots) were then transferred to a clean 96 well plate and evaporated under liquid nitrogen at 40 °C. Following evaporation, samples were reconstituted in 200  $\mu\text{L}$  25: 75 acetonitrile: water and injected (80  $\mu\text{L}$ ) into an HPLC-MS/MS system with resolution on a Kinetex XB-C18 50 × 3 mm 2.6  $\mu\text{m}$  column. For MS/MS,  $m/z$  Q1/Q3 transitions were 382.1/206.7 for celecoxib and 271.2/172.1 for tolbutamide (internal standard). Quantitation was performed by



reference to peak area ratio of celecoxib: internal standard over a calibration range of 5–2000 ng/mL.

### 2.8. Statistical analysis

The statistical comparison of the rate and extent of CXB absorption (AUC and C<sub>max</sub>) obtained with the various formulations was performed on the log-transformed data using a one way analysis of variance (ANOVA) with the InVivoStat software (version 3.0). The significance level was set a P values of <0.05.

## 3. Result and discussion

### 3.1. Celecoxib thermodynamic solubility

The thermodynamic solubility of celecoxib was generated at pH 2 in 0.01 M HCl (stomach pH simulating medium), in phosphate buffer (PBS) pH 6.5 and in FaSSiF (Fasted state simulating intestinal fluid pH6.5) (Table 1).

As CXB is a neutral molecule, the solubility at pH 2 and pH 6.5 (PBS) appeared similar as expected and very low (3.7 and 2.4 µg/mL respectively). A 20-fold increase solubility was observed in FaSSiF in comparison to PBS which was attributed to solubilisation within the micelles formed by the phospholipids and bile salts present in the medium.

### 3.2. CXB loaded silica characterization

The preparation method involved impregnation of silica with a concentrated drug solution in ethanol followed by evaporation of the solvent leading to drug entrapment within the pores. The entire process was relatively rapid taking 3 h in total to obtain a dry powder. The DSC thermograms of crystalline CXB, CXB loaded silica and CXB-HPMCAS-co-loaded silica are shown in Fig. 1. The melting point of crystalline CXB appears at 162 °C. Whereas XRPD turned out not to be sensitive enough to detect any signs of crystallinity in the two silica batches, DSC revealed an endothermic event in the single CXB loaded silica thermogram at 164 °C corresponding to the CXB melting point. This suggests that a small portion of drug remained in the crystalline form. Interestingly, the co-loading with HPMCAS seemed to promote the complete conversion of CXB in an amorphous state. It is worth mentioning that according to the literature, HPMCAS is one of the most effective polymers at preventing drug crystallization and hence maintaining supersaturation (Curatolo et al., 2009; Ueda et al., 2013). Finally, the HPLC analysis confirmed a CXB loading of 31.1% w/w demonstrating that the co-loading by solvent impregnation rotary evaporator method developed in-house was successful.

### 3.3. In vitro transfer dissolution assay

The dissolution performance of CXB-HPMCAS co-loaded silica was evaluated through an *in vitro* non sink transfer dissolution (TD) model. This assay was designed to simulate the journey of a drug from the stomach environment to the intestine compartment and hence try and predict the behavior of the formulation performance *in vivo*. As such, all volumes used were scaled down from physiological estimates resulting in a non-sink dissolution

experiment. Whereas most of the pH shift dissolution assay in the literature are carried out under sink conditions, non-sink conditions utilized here are critical to capture any potential precipitation event.

The various CXB formulations (crystalline CXB, Celebrex<sup>®</sup>, CXB-loaded silica, CXB-loaded silica blended with HPMCAS and CXB-HPMCAS co-loaded silica) were initially introduced in the TD assay as powder simulating a tablet (Fig. 2). As expected the crystalline CXB solubility profile closely correlated to the aforementioned thermodynamic solubility for each medium with an increase in solubility in FaSSiF. In comparison to the bulk CXB, the marketed formulation Celebrex reached a higher solubility plateau in FaSSiF, most likely due to the presence of the SLS surfactant and confirming the hypothesis that CXB is influenced by micellar solubilisation. The loading of CXB onto the silica did not improve its dissolution profile but conversely generated a lower solubility in FaSSiF medium. This unexpected effect could be due to re-adsorption of the CXB onto the silica did not improve its dissolution profile but conversely generated a lower solubility in FaSSiF medium. This unexpected effect could be due to re-adsorption of the CXB onto the silica did not improve its dissolution profile but conversely generated a lower solubility in FaSSiF medium.

When CXB loaded silica was blended with HPMCAS, the presence of the polymer seemed to reduce the re-adsorption of CXB onto the silica once released. The co-loading of HPMCAS with CXB onto the silica led to a slower release in FaSSiF resulting in a 4-fold solubility increase over the crystalline CXB which was sustained over 1.5 h. These data suggest that the addition of HPMCAS through co-loading proved to be more efficient to generate and maintain supersaturation than introduction via physical blending.

The post transfer dissolution residue was assessed via PXRD and PLM for the various formulations (Supplementary information). All samples showed crystalline residue at the end of the assay demonstrating that the amorphous formulation partly converted back to crystalline CXB parent.

It was also noteworthy that for all the loaded silica, no major release was observed in the acidic medium over 30 min as indicated by the concentrations measured at 15 and 30 min (Table 2). The increase in solubility appeared only upon addition of FaSSiF. It is commonly hypothesized that the drug is released upon exposure with an aqueous media due to competition for the hydrophilic silica surface with water molecules displacing the drug from its confinement. However, this present finding seems to suggest that the drug desorption is most likely to happen in a medium promoting solubilisation such as the micelle containing FaSSiF medium. This observation is in accordance with previous data published in the literature where a non-release in acid medium was also shown for Indomethacin and glibenclamide (van Speybroeck et al., 2011).

Interestingly, this new understanding of the release mechanism offers alternative use of the silica. While the drug loaded silica is commonly dosed to animals via capsules to avoid release before dosing, the possibility of dosing the silica as a suspension can be considered and was evaluated in this work. Thus, CXB-HPMCAS co-loaded silica was suspended in an aqueous vehicle (0.5% HPMCAS/0.5% MC in TRIS buffer pH 7.4) at 1.6 mg/mL and aimed to be dosed *in vivo*. This vehicle corresponds to the vehicle used to prepare extemporaneous suspension in a typical first-in human clinical trial and was chosen to reinforce the parachute effect via the presence of HPMCAS. A stability study was performed on the suspension in order to assess and monitor the release kinetic and solid state conversion rate. The suspension was maintained at room temperature over 2 days and samples were taken regularly over the course of the assay (Table 3.; X-ray diffractograms in Supplementary information). The fraction solubilized reached up to 20% of the formulation concentration (1.6 mg/mL) in 2 h and maintained that level for 2 days. Additionally no conversion to crystalline parent was observed as determined via polarized light

**Table 1**  
Thermodynamic solubility of Celecoxib.

| Medium    | 0.01 M HCl pH 2<br>(µg/mL) | Phosphate Buffer pH 6.5<br>(µg/mL) | FaSSiF pH 6.5<br>(µg/mL) |
|-----------|----------------------------|------------------------------------|--------------------------|
| Celecoxib | 3.7 ± 0.1                  | 2.4 ± 0.4                          | 43.3 ± 0.7               |

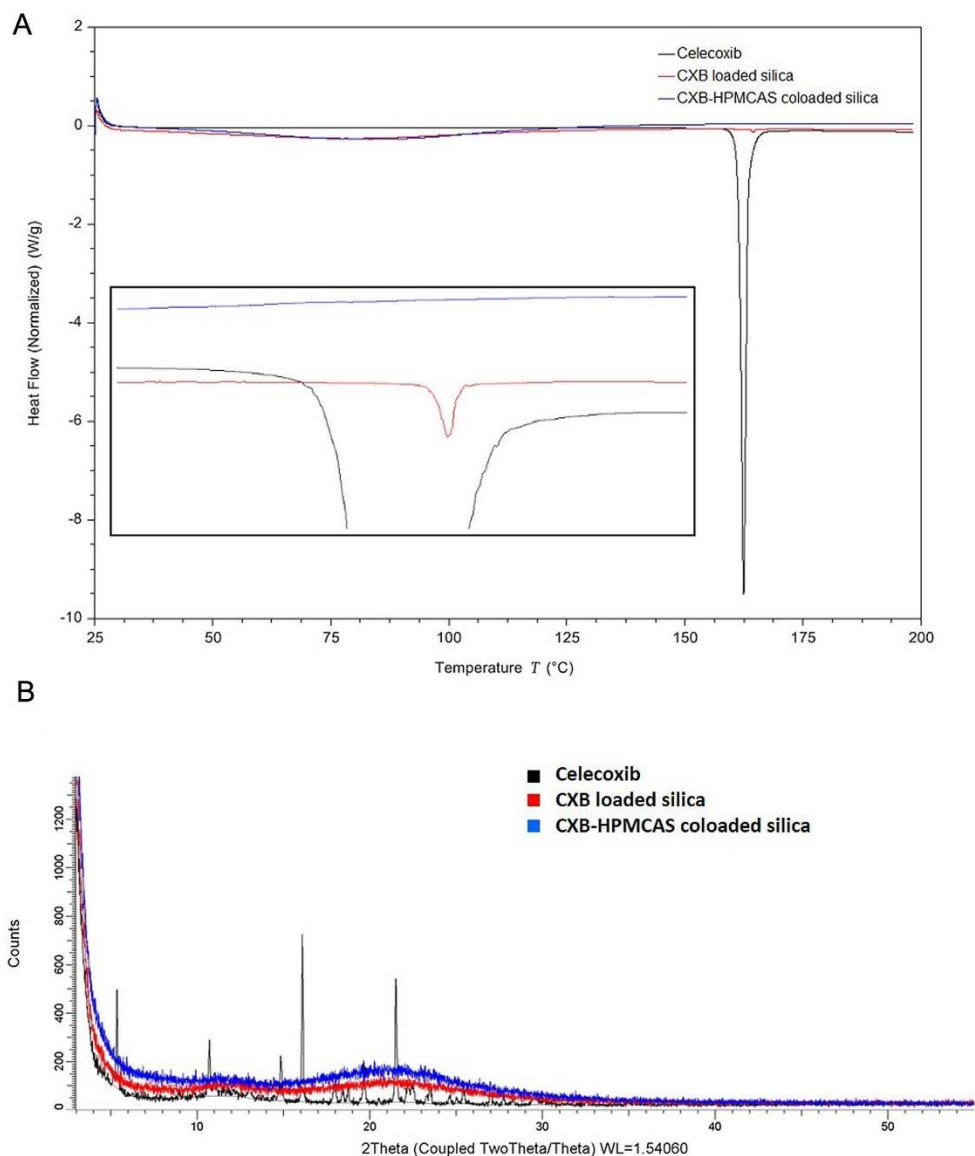


**Fig. 1.** Solid state characterization of CXB, CXB loaded silica and CXB-HPMCAS co-loaded silica via DSC (A) and XRPD (B). For the CXB trace on the DSC curve (A), there is a single endotherm with an onset of 161 °C. For the CXB loaded silica, there is a single endotherm with an onset of 163.9 °C. The inset box shows a higher magnification view of the endotherm in the CXB loaded silica.

microscopy (PLM). Despite the release, CXB seemed to stay in solution likely due to the high HPMCAS content.

Collectively, these data suggested that dosing the CXB-HPMCAS loaded silica as a suspension was a viable option. In conjunction with the TD data demonstrating the most promising dissolution performance enhancement, only the co-loaded formulation was selected for a pharmacokinetic study. Before running the *in vivo*

experiment, *in vitro* transfer dissolution assay was carried out with the CXB-HPMCAS co-loaded silica suspension in comparison to a crystalline CXB suspension to predict its performance. The amorphous CXB suspension achieved 15-fold solubility increase compared to the crystalline CXB suspension (Fig. 3) and a 3-fold increase over that seen previously with the powder in Fig. 2. This significant increase is most likely due to the presence of HPMCAS in



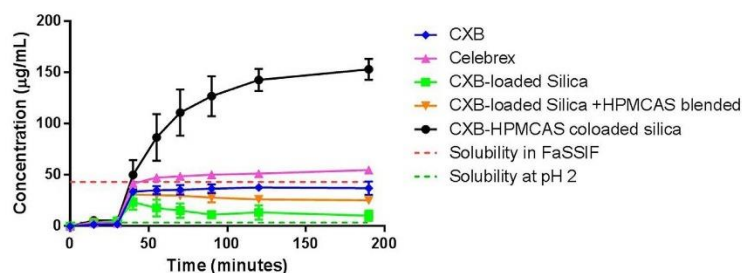


Fig. 2. Concentration vs time profile of crystalline CXB, Celebrex, CXB loaded silica, CXB loaded silica blended with HPMCAS, CXB-HPMCAS co-loaded silica obtained through the *in vitro* transfer dissolution assay (n=4).

Table 2  
Concentrations of the various CXB formulations at 15 min and 30 min in the acidic medium during the transfer dissolution assay.

|          | CXB<br>(µg/mL) | Celebrex<br>(µg/mL) | CXB loaded silica<br>(µg/mL) | CXB loaded silica + HPMCAS Blend<br>(µg/mL) | CXB-HPMCAS co-loaded silica<br>(µg/mL) |
|----------|----------------|---------------------|------------------------------|---|--|
| T 15 min | 1.9            | 3.2                 | 3.8                          | 4.1   | 5.8                                    |
| T 30 min | 1.8            | 3.1                 | 4.0                          | 3.9   | 5.6                                    |

Table 3  
Physical stability of CXB-HPMCAS co-loaded silica suspension (PLM: polarized light microscopy).

| Time point | XRPD/PLM                 | Solubilised fraction (µg/mL) |
|------------|--------------------------|------------------------------|
| T0         | Absence of crystallinity | 157                          |
| 1 h        | Absence of crystallinity | 283                          |
| 4 h        | Absence of crystallinity | 305                          |
| 55 h       | Absence of crystallinity | 316                          |

the vehicle which is crucial to prevent precipitation and maintain supersaturation as confirmed by the amorphous residue obtained post assay (Supplementary information).

### 3.4. *In vivo* pharmacokinetic comparison

The CXB-HPMCAS co-loaded silica suspension was then assessed through a PK study in rats in comparison to the crystalline CXB suspension. The dose and dose volume were selected to correspond to clinical practice. As the limiting factor for CXB absorption is the dissolution rate, a CXB solution was dosed as a positive control to overcome this parameter. To ensure a reliable positive control, the CXB solution performance was assessed in the *in vitro* transfer dissolution aiming to predict any precipitation upon dosing. The profile of the solution maintained at 100%

solubility over the whole course of the assay including stomach and intestine compartment indicating a low risk of precipitation *in vivo* (data not shown). The three formulations were subsequently dosed and the resulting systemic exposure compared altogether (Fig. 4, Table 4).

In this study, crystalline CXB suspension displayed a reasonable oral absorption profile in spite of its low solubility. It is worth pointing out that the experiment was carried out on fed animals with food available *ad libitum*, so that CXB exposure may have been promoted by a food effect, as previously demonstrated in dogs (Paulson et al., 2001). Nevertheless, despite a similar bioavailability between the formulations (represented by AUC), the plasma concentration vs. time profile of the crystalline suspension was distinct, with a slower rate of absorption than the solution and the CXB-HPMCAS co-loaded silica suspensions groups. Significantly higher  $C_{max}$  were indeed observed for the amorphous suspension and the solution compared to the crystalline suspension (1.35 and 1.44-fold increase respectively,  $p < 0.005$ ). The data demonstrate that CXB co-loaded silica suspension effectively produced the same profile of a solution dosed in rat at 5.8 mg/kg proving that the silica technology can overcome poor dissolution rate. Additionally, the possibility of dosing the silica in a suspension rather than in capsules as conventionally administered renders the technology more suitable and accessible for preclinical studies.

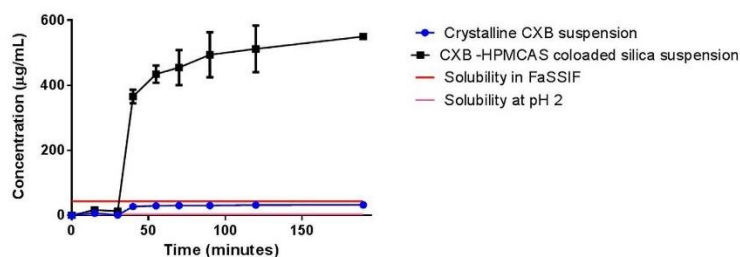


Fig. 3. *In vitro* transfer dissolution profile of crystalline CXB suspension (n=2) and CXB-HPMCAS co-loaded silica suspension (n=4).

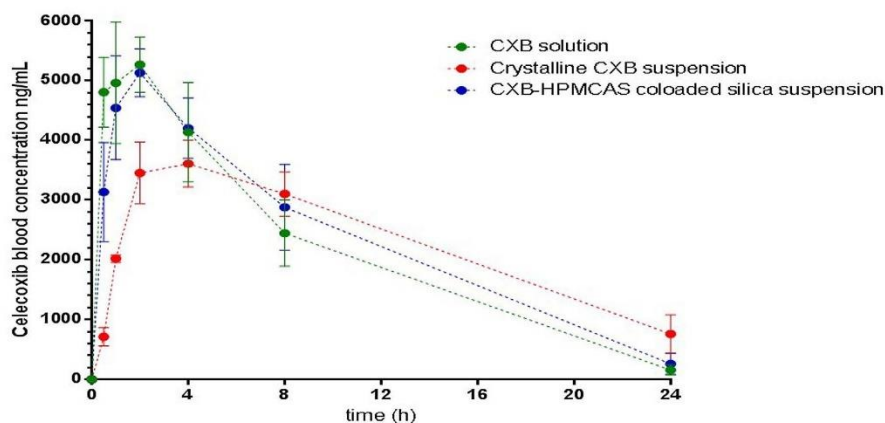


Fig. 4. Plasma concentration vs time profile of crystalline CXB suspension, CXB solution and CXB-HPMCAS co-loaded silica suspension after oral dosing in rats + table with pk parameters.

Table 4  
Pharmacokinetic parameters after oral absorption of various CXB formulations.

|                           | Solution |      | Crystalline CXB suspension |      | CXB-HPMCAS co-loaded silica suspension |       |
|---------------------------|----------|------|----------------------------|------|--|-------|
|                           | mean     | sd   | mean                       | Sd   | mean                                   | sd    |
| AUC ng h mL <sup>-1</sup> | 50977    | 6689 | 54790                      | 6891 | 55383                                  | 11493 |
| Cmax ng/mL                | 5507     | 438  | 3817                       | 276  | 5133                                   | 402   |

#### 4. Conclusion

A supersaturable amorphous suspension was developed through a quick one-step process based on the co-loading of a precipitation inhibitor (HPMCAS) and the drug (Celecoxib) onto the mesoporous silica. A simple *in vitro* transfer dissolution test was effective in showing the enhanced performance of different formulations for selection in subsequent *in vivo* studies. The co-loaded formulation has demonstrated a sustained supersaturation *in vitro* and enhanced *in vivo* absorption rate of the poorly soluble CXB after oral delivery. Whereas further work is required to better understand the release mechanism, this technology represents a novel easy preclinical formulation approach to maximize *in vivo* exposure critical for discovery studies.

#### Acknowledgement

The authors would like to thank Merck Millipore for providing the Parreck® SLC and for their technical support.

#### Appendix A. Supplementary data

Supplementary data associated with this article can be found, in the online version, at <http://dx.doi.org/10.1016/j.ijpharm.2016.08.034>.

#### References

- Curatolo, W., Nightingale, J.A., Herbig, S.M., 2009. Utility of hydroxypropylmethylcellulose acetate succinate (HPMCAS) for initiation and maintenance of drug supersaturation in the GI milieu. *Pharm. Res.* 26 (6), 1419–1431.
- Dizaj, S.M., Vazifehasl, Z., Salatin, S., Adibkia, K., Javadzadeh, Y., 2015. Nanosizing of drugs: effect on dissolution rate. *Res. Pharm. Sci.* 10 (2), 95–108.
- Elder, D.P., Holm, R., Diego, H.L., 2013. Use of pharmaceutical salts and cocrystals to address the issue of poor solubility. *Int. J. Pharm.* 453 (1), 88–100.
- Frampton, J.E., Keating, G.M., 2007. Celecoxib: a review of its use in the management of arthritis and acute pain. *Drugs* 67 (16), 2433–2472.
- Gao, D., Hlinak, A.J., Mazhary, A.M., Truelove, J.E., Vaughn, M.B.W., 2000. Celecoxib compositions. Google Patents.
- Grohgan, H., Priemel, P.A., Lobmann, K., Nielsen, L.H., Laitinen, R., Mullertz, A., et al., 2014. Refining stability and dissolution rate of amorphous drug formulations. *Expert Opin. Drug Deliv.* 11 (6), 977–989.
- Guzman, H.R., Tawa, M., Zhang, Z., Ratanabanangkoon, P., Shaw, P., Gardner, C.R., et al., 2007. Combined use of crystalline salt forms and precipitation inhibitors to improve oral absorption of celecoxib from solid oral formulations. *J. Pharm. Sci.* 96 (10), 2686–2702.
- Haus, D.J., 2007. Oral lipid-based formulations. *Adv. Drug Deliv. Rev.* 59 (7), 667–676.
- Kalepu, S., Nekkanti, V., 2015. Insoluble drug delivery strategies: review of recent advances and business prospects. *Acta Pharm. Sin.* 36 (5), 442–453.
- Laitinen, R., Lobmann, K., Strachan, C.J., Grohgan, H., Rades, T., 2013. Emerging trends in the stabilization of amorphous drugs. *Int. J. Pharm.* 453 (1), 65–79.
- Lakshman, J.P., Cao, Y., Kowalski, J., Serajuddin, A.T., 2008. Application of melt extrusion in the development of a physically and chemically stable high-energy amorphous solid dispersion of a poorly water-soluble drug. *Mol. Pharm.* 5 (6), 994–1002.
- Leucuta, S.E., 2014. Selecting oral bioavailability enhancing formulations during drug discovery and development. *Expert Opin. Drug Discov.* 9 (2), 139–150.
- Lipinski, C.A., Lombardo, F., Dominy, B.W., Feeney, P.J., 2001. Experimental and computational approaches to estimate solubility and permeability in drug discovery and development settings. *Adv. Drug Deliv. Rev.* 46 (1–3), 3–26.
- Merisko-Liversidge, E.M., Liversidge, G.G., 2008. Drug nanoparticles: formulating poorly water-soluble compounds. *Toxicol. Pathol.* 36 (1), 43–48.
- Morgen, M., Bloom, C., Beyersack, R., Bello, A., Song, W., Wilkinson, K., et al., 2012. Polymeric nanoparticles for increased oral bioavailability and rapid absorption using celecoxib as a model of a low-solubility, high-permeability drug. *Pharm. Res.* 29 (2), 427–440.
- Newman, A., Nagapudi, K., Wenslow, R., 2015. Amorphous solid dispersions: a robust platform to address bioavailability challenges. *Ther. Deliv.* 6 (2), 247–261.
- Paudel, A., Worku, Z.A., Meeus, J., Guns, S., Van den Mooter, G., 2013. Manufacturing of solid dispersions of poorly water soluble drugs by spray drying: formulation and process considerations. *Int. J. Pharm.* 453 (1), 253–284.
- Paulson, S.K., Vaughn, M.B., Jessen, S.M., Lawal, Y., Gresk, C.J., Yan, B., et al., 2001. Pharmacokinetics of celecoxib after oral administration in dogs and humans: effect of food and site of absorption. *J. Pharmacol. Exp. Ther.* 297 (2), 638–645.

- Pouton, C.W., Porter, C.J., 2008. Formulation of lipid-based delivery systems for oral administration: materials, methods and strategies. *Adv. Drug Deliv. Rev.* 60 (6), 625–637.
- Pouton, C.W., 2000. Lipid formulations for oral administration of drugs: non-emulsifying, self-emulsifying and 'self-microemulsifying' drug delivery systems. *Eur. J. Pharm. Sci.* 11 (Suppl. 2), S93–S98.
- Rawat, S., Jain, S.K., 2004. Solubility enhancement of celecoxib using  $\beta$ -cyclodextrin inclusion complexes. *Eur. J. Pharm. Biopharm.* 57 (2), 263–267.
- Rowe, R.C., Sheskey, P.J., Owen, S.C., American Pharmacists Association, 2006. *Handbook of Pharmaceutical Excipients*. Pharmaceutical Press.
- Serajuddin, A.T., 2007. Salt formation to improve drug solubility. *Adv. Drug Deliv. Rev.* 59 (7), 603–616.
- Shen, S.C., Ng, W.K., Chia, L.S., Dong, Y.C., Tan, R.B., 2013. Applications of mesoporous materials as excipients for innovative drug delivery and formulation. *Curr. Pharm. Des.* 19 (35), 6270–6289.
- Song, W.H., Yeom, D.W., Lee, D.H., Lee, K.M., Yoo, H.J., Chae, B.R., et al., 2014. In situ intestinal permeability and in vivo oral bioavailability of celecoxib in supersaturating self-emulsifying drug delivery system. *Arch. Pharm. Res.* 37 (5), 626–635.
- Ueda, K., Higashi, K., Yamamoto, K., Moribe, K., 2013. Inhibitory effect of hydroxypropyl methylcellulose acetate succinate on drug recrystallization from a supersaturated solution assessed using nuclear magnetic resonance measurements. *Mol. Pharm.* 10 (10), 3801–3811.
- Van Speybroeck, M., Mols, R., Mellaerts, R., Thi, T.D., Martens, J.A., Van Humbeeck, J., et al., 2010. Combined use of ordered mesoporous silica and precipitation inhibitors for improved oral absorption of the poorly soluble weak base itraconazole. *Eur. J. Pharm. Biopharm.* 75 (3), 354–365.
- Van den Mooter, G., 2012. The use of amorphous solid dispersions: a formulation strategy to overcome poor solubility and dissolution rate. *Drug Discov. Today Technol.* 9 (2), e71–e174.
- van Speybroeck, M., Mellaerts, R., Thi, T.D., Martens, J.A., Van Humbeeck, J., Annaert, P., et al., 2011. Preventing release in the acidic environment of the stomach via occlusion in ordered mesoporous silica enhances the absorption of poorly soluble weakly acidic drugs. *J. Pharm. Sci.* 100 (11), 4864–4876.
- Vialpando, M., Martens, J.A., Van den Mooter, G., 2011. Potential of ordered mesoporous silica for oral delivery of poorly soluble drugs. *Ther. Deliv.* 2 (8), 1079–1091.
- Williams, H.D., Trevaskis, N.L., Charman, S.A., Shanker, R.M., Charman, W.N., Pouton, C.W., et al., 2013. Strategies to address low drug solubility in discovery and development. *Pharmacol. Rev.* 65 (1), 315–499.
- Wilson, M., Williams, M.A., Jones, D.S., Andrews, G.P., 2012. Hot-melt extrusion technology and pharmaceutical application. *Ther. Deliv.* 3 (6), 787–797.
- Xu, W., Riikonen, J., Lehto, V.P., 2013. Mesoporous systems for poorly soluble drugs. *Int. J. Pharm.* 453 (1), 181–197.



1            *In silico, in vitro* and *in vivo* evaluation of  
2            precipitation inhibitors in supersaturated lipid-  
3            based formulations of venetoclax

4    *Niklas J. Koehl<sup>1</sup>, Laura J. Henze<sup>1</sup>, Harriet Bennett-Lenane<sup>1</sup>, Daniel J. Price<sup>2,3</sup>*  
5    *René Holm<sup>4,5</sup>, Martin Kuentz<sup>6</sup>, Brendan T. Griffin<sup>1\*</sup>*

6

7    <sup>1</sup> School of Pharmacy, University College Cork; College Road, Cork, T12 YN60 Ireland

8    <sup>2</sup> Merck KGaA, Darmstadt, Germany

9    <sup>3</sup> Goethe University Frankfurt, Frankfurt am Main, Germany

10   <sup>4</sup> Drug Product Development, Janssen Research and Development, Johnson & Johnson,  
11   Turnhoutseweg 30, 2340 Beerse, Belgium

12   <sup>5</sup> Department of Science and Environment, Roskilde University, 4000 Roskilde, Denmark

13   <sup>6</sup> University of Applied Sciences and Arts Northwestern Switzerland, Institute of Pharma  
14   Technology, Muttenz, Switzerland

15

16   \*Corresponding author:

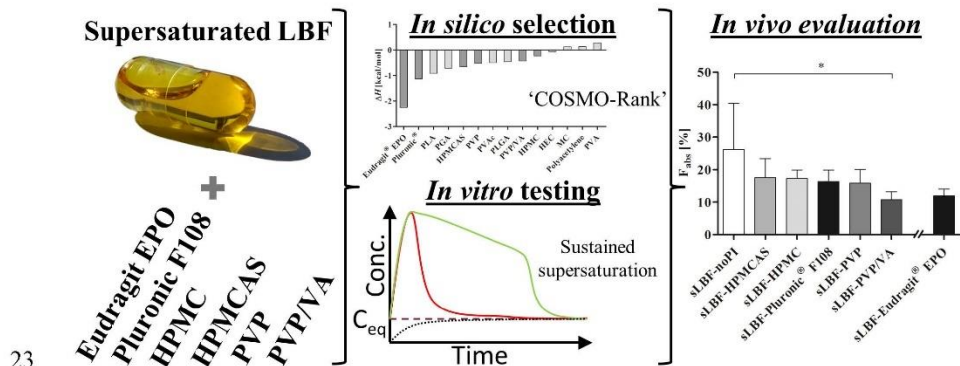
17   Brendan Griffin, University College Cork, School of Pharmacy, Cavanagh Building, College  
18   Road, Cork, Ireland

19   Phone: +353 (0) 21 490 1657, Fax: +353 (0) 21 490 1656, e-mail: [Brendan.Griffin@ucc.ie](mailto:Brendan.Griffin@ucc.ie)

20

21

22 TABLE OF CONTENT



23

24

25 ABSTRACT

26 The concept of using precipitation inhibitors (PIs) to sustain supersaturation is well established  
 27 for amorphous formulations, but less in the case of lipid-based formulations (LBF). This study  
 28 applied a systematic *in silico-in vitro-in vivo* approach to assess the merits of incorporating PIs  
 29 in supersaturated LBFs (sLBF) using the model drug venetoclax. sLBFs containing HPMC,  
 30 HPMCAS, PVP, PVP/VA, Pluronic® F108 and Eudragit® EPO were assessed *in silico*  
 31 calculating a drug-excipient mixing enthalpy, *in vitro* using a PI solvent shift test and finally  
 32 bioavailability was assessed *in vivo* in landrace pigs. The estimation of pure interaction  
 33 enthalpies of drug and excipient were deemed useful in determining the most promising PIs for  
 34 venetoclax. The sLBF alone (i.e. no PI present) displayed high initial concentration in the  
 35 aqueous phase during *in vitro* screening. sLBF with Pluronic® F108 displayed the highest  
 36 venetoclax concentration in the aqueous phase and sLBF with Eudragit® EPO the lowest. *In*  
 37 *vivo*, the sLBF alone showed the highest bioavailability of 26.3 ± 14.2%. Interestingly, a trend  
 38 towards a decreasing bioavailability was observed for sLBF containing PIs, with PVP/VA  
 39 being significantly lower compared to sLBF alone. In conclusion, the ability of a sLBF to

## X. Thesis Publications

40 generate supersaturated concentrations of venetoclax *in vitro* was translated to increased  
41 absorption *in vivo*. While *in silico* and *in vitro* PI screening suggested benefits in terms of  
42 prolonged supersaturation, addition of a PI did not increase *in vivo* bioavailability. The findings  
43 of this study are of particular relevance to pre-clinical drug development, where the high *in vivo*  
44 exposure of venetoclax was achieved using a sLBF approach and despite a perceived risk of  
45 drug precipitation from a sLBF, including of a PI may not be merited in all cases.

46

47

48 KEYWORDS:

49 Precipitation inhibitor, Lipid based formulation, Venetoclax, SEDDS, SNEDDS, SMEDDS,

50 Lipid suspension, Polymers, Super-SNEDDS, supersaturation, Super-SMEDDS,

51 Supersaturating Drug Delivery Systems

52

53 ABBREVIATIONS

54 COSMO, COnductor like Screening Model; LBF, lipid-based formulation; PI, precipitation

55 inhibitor; sLBF, supersaturated lipid-based formulation; sLBF-PI, supersaturated lipid-based

56 formulation with incorporated precipitation inhibitor; sLBF-aqPI, supersaturated lipid-based

57 formulation with pre-dissolved precipitation inhibitor in the dispersion media

58

### 59 INTRODUCTION

60 Favourable solubility in the gastrointestinal fluids and intestinal permeability is a prerequisite  
61 for a high oral bioavailability of any drug. However, drug discovery approaches such as high  
62 throughput screenings, modifications during lead optimization as well as the noticeable  
63 therapeutic target shift towards intracellular targets deliver more drugs displaying low aqueous  
64 solubility and beyond Rule-of-Five properties.<sup>1-3</sup> These drug candidates display sub-optimal  
65 biopharmaceutical properties and create a need for bio-enabling formulation approaches. The  
66 design of such formulations includes strategies to generate and maintain high concentrations or  
67 supersaturation in intraluminal fluids. Prominent examples of such supersaturating  
68 formulations are amorphous solid dispersions and the use of lipid-based formulations (LBF).<sup>4</sup>  
69 <sup>5</sup> In particular, drugs with a low aqueous solubility, a high lipophilicity and/or bioavailability  
70 that is increased by co-ingestion of fatty meals, LBFs can offer particular formulation  
71 advantages.<sup>4-6</sup> The most convenient and conventional LBFs are lipid solutions, where the drug  
72 is dissolved in the lipid vehicle, and hence most widely applicable for drugs that show high  
73 lipid solubility. As the drug is dissolved in the LBF solution, this circumvents the dissolution  
74 process and provides an enhanced intestinal solubilisation for lipophilic drugs in the  
75 gastrointestinal environment.<sup>7</sup> Upon digestion of the lipid excipient, the changing nature of the  
76 intraluminal colloids potentially generates supersaturated drug concentrations in the  
77 gastrointestinal fluids effectively promoting absorption.<sup>7</sup> Alternatively, for drugs which display  
78 low solubility in lipid vehicles, strategies to increase dose loading in the lipid vehicles may be  
79 required such as lipid suspensions,<sup>8-10</sup> supersaturated LBFs (sLBF),<sup>11-14</sup> lipophilic salts,<sup>15-17</sup>  
80 or lipid-hybrid systems.<sup>18-20</sup>

81

82 sLBFs can be beneficial in delivering drug candidates of this type and interest in their  
83 application has increased over the past number of years. The most common method to generate

Page 4

## X. Thesis Publications

84 drug supersaturation in lipids is by heating excess drug in the lipids, followed by cooling,<sup>13</sup>  
85 whereupon the amount of dissolved drug in the lipid excipients may exceed the thermodynamic  
86 solubility (at lower temperatures) and the LBF becomes supersaturated. A supersaturated  
87 formulation is considered kinetically stable, and sLBFs have successfully been applied to  
88 improve oral bioavailability of a number of poorly water-soluble drugs such as cinnarizine,  
89 simvastatin and halofantrine.<sup>11, 12, 21-23</sup> An sLBF formulation approach offers a number of  
90 advantages particularly in early stages of development. These advantages include the ease of  
91 preparation, suitability for ease of dosing in pre-clinical models and the ability to prepare  
92 prototype formulations on a small scale while keeping the development costs low at times  
93 where the attrition rate is usually high. Thomas *et al.* developed a sLBF of simvastatin at 150%  
94 of the saturation solubility and assessed bioavailability in dogs.<sup>11</sup> Oral bioavailability of the  
95 sLBF was 1.8-fold higher when compared to the same dose of a LBF solution at 75% of the  
96 saturation solubility.<sup>11</sup> Recently, our group has reported that a sLBF of venetoclax (containing  
97 venetoclax at 350% of the apparent saturation solubility) increased oral bioavailability 2.1-fold  
98 when compared to a control LBF (i.e. lipid suspension) and 3.8-fold when compared to the  
99 crude drug powder.<sup>14</sup> Additionally, the venetoclax study demonstrated during *in vitro* lipolysis  
100 testing of the sLBF that the drug concentration of venetoclax in the aqueous digest phase were  
101 in the range of the reported amorphous solubility in fasted state simulated intestinal fluid  
102 (FaSSIF).<sup>14</sup> With such elevated aqueous phase concentrations reached by a sLBF, the risk of  
103 precipitation is deemed high and hence it was hypothesized that incorporation of a precipitation  
104 inhibitor (PI) may be beneficial.

105

106 While the incorporation of PIs in a supersaturated drug delivery system has been widely  
107 explored for solid solutions, to the best of our knowledge, to date no study has reported the  
108 incorporation of PIs in sLBFs testing *in vivo*. A limited number of studies have explored the

Page 5



## X. Thesis Publications

109 use of PIs to reduce the risk of drug precipitation upon dispersion and digestion of classical  
110 LBFs. <sup>24-27</sup> Gao and co-workers developed an undersaturated self-emulsifying LBF for  
111 paclitaxel with hydroxypropyl methylcellulose (HPMC) as PI. <sup>26</sup> The HPMC concentration was  
112 50 mg/mL and a 10-fold higher oral bioavailability was observed by incorporating HPMC  
113 compared to a HPMC-free formulation in rats. <sup>26</sup> Gao and colleagues described such  
114 formulations as ‘supersaturable’ referring primarily to the ability of many LBFs to generate  
115 supersaturated drug concentrations on dispersion/digestion in intestinal fluids. However, it is  
116 worth noting that supersaturable LBFs explored by Gao *et al.* contain drug below saturation  
117 solubility and are distinct from sLBFs even though this nomenclature is not consistently used  
118 throughout the literature. A subsequent study examined the effect of incorporating HPMC in  
119 LBFs for the investigational drug PNU-91325. The study confirmed that the use of HPMC as a  
120 PI resulted in a higher aqueous phase concentration *in vitro* as well as the increases in  
121 bioavailability in dogs. <sup>25</sup> The LBFs explored in these studies contained 70 – 100% (w/w) co-  
122 solvents and surfactants (i.e. type IV of the lipid formulation classification system (LFCS) <sup>28,</sup>  
123 <sup>29</sup>), which in general present a greater risk of drug precipitation on dispersion. Similarly, Suys  
124 *et al.* recently reported that the utility of PIs to prolong supersaturation was more evident for a  
125 type IV (50% co-solvent) and type IIIB (25% co-solvent and 25% surfactants) formulation,  
126 whereas for a type IIIA formulation (no co-solvent, 35% surfactant), the PIs studied had no  
127 impact on prolonging supersaturation during *in vitro* digestion. <sup>27</sup> Collectively, these studies  
128 demonstrate the merits of incorporating PIs in a LBF where there is a perceived high risk of  
129 precipitation on dispersion/digestion due to for example a rapid co-solvent depletion. However,  
130 to date no study has explored the utility of PIs to maintain supersaturation in sLBFs, which the  
131 present study aimed to investigate.  
132

## X. Thesis Publications

133 Venetoclax is a highly lipophilic drug ( $\log P$  of 5.5<sup>30</sup>) with a high molecular mass of 868.44  
134 g/mol<sup>30</sup> and a melting point of 139 °C (Table S 1) represents a recently licenced drug with  
135 properties in the beyond Rule-of-Five space . The drug is classified as a BCS class IV drug  
136 based on low aqueous solubility and permeability. The commercial formulation Venclyxto®  
137 displays a pronounced food dependent oral bioavailability with a 3.4-fold increase in oral  
138 bioavailability after a low-fat meal and a 5-fold increase after a high fat meal compared to the  
139 fasted state.<sup>30</sup>

140

141 This study explored the merits of PIs on the oral bioavailability of an oil-based sLBF of  
142 venetoclax. A range of promising PIs have been identified based on calculated excess enthalpy  
143 of mixing (COSMOquick software), which served to estimate molecular excipient interaction  
144 in the more complex aqueous dispersions. The ability of the selected PIs to maintain  
145 supersaturation of venetoclax in biorelevant media was tested *in vitro* and the impact of  
146 incorporating PIs into the sLBF in comparison to the separate addition (pre-dissolved) of the  
147 PIs in the simulated intestinal fluids was evaluated. A subsequent *in vivo* study examined the  
148 impact of incorporated PIs in sLBFs on the oral bioavailability of venetoclax in landrace pigs.

149

### 150 MATERIALS AND METHODS

#### 151 *Chemicals and materials*

152 Venetoclax was purchased from Kemprotec Ltd. (UK) (Batch # 1810004). Olive oil, highly  
153 refined and low acidity, taurodeoxycholic acid (NaTDC) and pancreatic lipase (8 x USP) were  
154 ordered from Sigma-Aldrich (Ireland). Lipoid® E PC S was obtained from Lipoid GmbH  
155 (Germany) and Eudragit® EPO was obtained from Evonik (Germany). Hydroxypropyl  
156 methylcellulose acetate succinate (HPMCAS) (AQQAT (HPMCAS-MF)) was purchased from  
157 ShinEtsu (Japan) and Pluronic® F108, hydroxypropyl methylcellulose (HPMC),

Page 7

## X. Thesis Publications

158 Polyvinylpyrrolidone (PVP) were purchased from MilliporeSigma (St Louis, MO, USA).  
159 Kollidon<sup>®</sup> VA 64 (PVP/VA) was kindly donated by BASF (Germany). Capmul MCM<sup>®</sup> and  
160 Captex<sup>®</sup> 1000 were kindly donated by Abitec corporation. A sample of Peceol<sup>®</sup> was kindly  
161 donated by Gattefossé (France) and SIF powder Version 1 was kindly donated by  
162 biorelevant.com (UK). Water was purified by a MilliQ<sup>®</sup> water system. All other chemicals and  
163 solvents were of analytical or high-performance liquid chromatography (HPLC) grade and were  
164 purchased from Sigma-Aldrich (Ireland) and used as received.

165

### 166 *Apparent solubility*

167 Apparent solubility was determined in olive oil, Captex<sup>®</sup> 1000, Peceol<sup>®</sup> and Capmul MCM<sup>®</sup>.  
168 In brief, an excess of venetoclax was added to 2 mL of the excipients and stirred at 200 rpm  
169 (25% power) (Mixdrive 15, 2MAG, Germany) at 37 °C. Solid excipients were melted at 50 °C  
170 and cooled to 37 °C prior to venetoclax addition. Samples were taken after 24 h, 48 h, 72 h and  
171 centrifuged at 21,380g and 37 °C for 15 min (Mikro 200 R, Andreas Hettich GmbH & Co. KG,  
172 Germany). The supernatant was transferred to a new sample tube and centrifuged again using  
173 identical conditions. To solubilise the oily excipient, the supernatant was diluted in  
174 acetonitrile:ethyl acetate (1:3 v/v). Followed by further 1:10 (v/v) dilution with  
175 acetonitrile:ethyl acetate (3:1 v/v). The obtained samples were diluted appropriately with  
176 mobile phase before analysis by reverse phase HPLC as described below. All samples were run  
177 in triplicates.

178

### 179 *Biorelevant solubility*

180 FaSSIF and fed state simulated intestinal fluids (FeSSIF) were prepared according to the  
181 instructions by biorelevant.com. FeSSIF was used directly, whereas FaSSIF was left at room  
182 temperature for 2 h prior to usage. Excess venetoclax was added to 2 mL of biorelevant media

Page 8

## X. Thesis Publications

183 and placed in a water bath shaker at 200 shakes/min (GLS400, Grant Instruments, UK) and  
184 37 °C. Samples were taken after 3 h, 6 h and 24 h and centrifuged at 21,380g and 37 °C for 15  
185 min (Mikro 200 R, Andreas Hettich GmbH & Co. KG, Germany). The supernatant was  
186 transferred to a new sample tube and centrifuged again under identical conditions. Subsequently,  
187 the supernatant was diluted with a mobile phase before analysis by HPLC.

188

189 The samples were analysed using an Agilent 1200 series HPLC system (Agilent Technology  
190 Inc., US) that comprised a binary pump, degasser, autosampler and variable wavelength  
191 detector. Data were analysed using the software EZChrom Elite® version 3.2. Venetoclax was  
192 separated from the sample matrix with a Zorbax® Eclipse Plus-C18 column (5 µm, 4.6 mm x  
193 150 mm) including a Zorbax® Eclipse Plus-C18 guard column (5 µm, 4.6 mm x 12.5 mm) at  
194 40 °C. The mobile phase consisted of (a) acetonitrile with 0.5% trifluoroacetic acid (TFA) and  
195 (b) water with 0.5% TFA at a ratio of 53:47 (a:b v/v) and was used at a flow rate of 1 mL/min.  
196 The injection volume was 20 µL and the detection wavelength was set to 316 nm. The limit of  
197 detection (LOD) was 20 ng/mL and the limit of quantification (LOQ) 65 ng/mL determined  
198 using the standard error of y-intercept according to International Council for Harmonisation  
199 (ICH) Q2 guideline.<sup>31</sup>

200

201 *Formulations for in vivo and in vitro studies*

202 In the *in vivo* study and *in vitro* PI screen, the supersaturated lipid solution (sLBF) was prepared  
203 as previously reported with a lower temperature to reduce the thermal impact on the drug and  
204 excipient.<sup>14</sup> In brief, 300 mg venetoclax were added to 6 mL Peceol® and dispersed at 600 rpm  
205 (Stuart CD162 heat-stir, Cole-Parmer, UK) and sealed with parafilm. A continuous nitrogen  
206 stream into the vial removed oxygen throughout the preparation. After suspending the drug  
207 particles, the obtained suspension was slowly heated to 55 °C (Stuart CD 162 heat-stir, Cole-

Page 9

## X. Thesis Publications

208 Parmer, UK). The mixture was kept at 55 °C for 10 min and cooled to 25 °C while continuously  
209 stirring at 600 rpm. Subsequently, the mixture was heated a second time under the same  
210 conditions as stated above and cooled to room temperature to obtain the final sLBF. The  
211 absence of crystals was confirmed using cross-polarized light microscopy. For the *in vivo* study,  
212 sLBF was administered in hard gelatine capsules size 00EL (Licaps<sup>®</sup>, Capsugel, Lonza Group  
213 Ltd.) with 1 mL/capsule.

214

215 For the preparation of the sLBF with PI, HPMC, HPMCAS, Pluronic<sup>®</sup> F108, Eudragit<sup>®</sup> EPO,  
216 PVP and PVP/VA were added to the sLBF at a drug:PI ratio of 1:1 (w/w). At the given PI  
217 concentration (50 mg/mL) Pluronic<sup>®</sup> F108, Eudragit<sup>®</sup> EPO, PVP and PVP/VA were soluble in  
218 Peceol<sup>®</sup> at 37 °C, while HPMC and HPMCAS resulted in a suspension. In the case of the soluble  
219 PIs, the Peceol<sup>®</sup>-PI-solution was used to prepare the PI containing sLBF using the method  
220 described above. In the case of HPMC and HPMCAS, the sLBF was prepared as described  
221 above and HPMC and HPMCAS were added and dispersed *ad hoc* into the sLBF before *in vitro*  
222 and *in vivo* experiments. The amount of PI in the lipid vehicle (50 mg/mL) was based on  
223 previous work by Gao *et al.*<sup>24,25</sup>

224

225 *Cross-polarised light microscopy*

226 The absence of crystalline material in the supersaturated solutions was confirmed by means of  
227 cross-polarised light microscopy using an Olympus BX51 with an Olympus SC100 camera  
228 operated by Olympus Stream<sup>®</sup> essentials 2.3.3. The light was polarized using the polarizer U-  
229 POT and analysed with the analyser U-ANT. The absence of crystals was assumed, if no  
230 birefringence was observed.

231



## X. Thesis Publications

232 *In vitro* evaluation: drug solubilization during formulation dispersion and digestion  
233 *In vitro* lipolysis was performed using a pH-stat apparatus (Metrohm AG, Herisau, Switzerland)  
234 comprising a Titrand® 907 stirrer, 804 Ti-stand, a pH electrode (Metrohm AG, Herisau,  
235 Switzerland) and two 800 Dosino® dosing units coupled to a 20 mL autoburette. The system  
236 was operated by the Tiamo® 2.2 software. The *in vitro* protocol was used as previously reported.  
237 <sup>32</sup> In brief, the buffer contained 2 mM TRIS maleate, 150 mM NaCl, 1.4 mM CaCl<sub>2</sub> · 2H<sub>2</sub>O,  
238 adjusted to pH 6.5. For the digestion experiments the buffer was supplemented with 3 mM  
239 NaTDC and 0.75 mM PC (digestion buffer) and stirred for 12 h before further usage. The  
240 pancreatin extract was prepared freshly by adding 5 mL of 5 °C digestion buffer to 1 g of  
241 porcine pancreatic enzymes (8x USP), which was vortexed thoroughly. The mixture was  
242 centrifuged for 15 min at 5 °C, 2800g (Rotina 380 R, Andreas Hettich GmbH & Co. KG,  
243 Germany) and 4 mL of supernatant was recovered and stored at 2 – 8 °C before further usage.  
244 The pancreatic extract had a pancreatic lipase activity of ~10 000 TBU/mL (to provide  
245 approximately 1000 TBU per mL of digest), where 1 TBU represents the amount of enzyme  
246 that liberates 1 µmol of FA from tributyrin per min. <sup>33</sup>  
247  
248 For the *in vitro* lipolysis experiment 1.075 g of lipid formulation was dispersed into 39 mL of  
249 digestion buffer for 10 min. Three 1 mL samples were taken at 2.5, 5 and 10 min from the  
250 middle of the vessel. pH of the media was adjusted and maintained at 6.5 using 0.2 M NaOH.  
251 To the remaining 36 mL (1.0 g lipid formulation) dispersion 4 mL of pancreatin extract was  
252 added to initialize digestion. After 60 min the released non-ionized free fatty acids were  
253 determined by a pH increase of the buffer to pH 9. The stirring speed throughout dispersion and  
254 digestion was set at 450 rpm.  
255

## X. Thesis Publications

256 Samples of 1.0 mL were taken at 5, 10, 15, 30, 45 and 60 min during the digestion experiment  
257 from the middle of the vessel. In each sample and after 60 min the enzymes were inhibited by  
258 the addition of 1 M 4- bromophenylboronic acid in methanol (5  $\mu$ L per mL sample).  
259 Additionally, to each 1 mL sample during digestion a 100  $\mu$ L sample was taken and added to  
260 900  $\mu$ L of acetonitrile and mixed. This sample was used to quantify the total drug recovery,  
261 which allowed adjustment of inhomogeneous samples. All samples were centrifuged at 37 °C  
262 and 21,000g for 30 min using a benchtop centrifuge of the type Hettich Micro 200 R (Andreas  
263 Hettich GmbH & Co. KG, Germany).

264

265 *In silico precipitation inhibitor screening: COSMO-RS calculations*

266 The excess enthalpy of mixing between venetoclax and the polymeric PI was calculated using  
267 the COSMOquick software (COSMOlogic, Germany, Version 1.6). The software is based on  
268 the Conductor like Screening Model for Real Solvents<sup>34, 35</sup> that combined quantum chemical  
269 surface charge calculations with statistical thermodynamics. The COSMOquick approach in  
270 particular allows for a fast estimation of these surface charge densities for further calculations.  
271 <sup>36</sup> Venetoclax and the polymers were entered in smiles notation. As the quantum chemical  
272 calculations cannot capture the full complexity of the polymers, the polymer structures were in  
273 this study approximated as trimers. The drug:PI ratio was set at a stoichiometric ratio of 1:1 to  
274 represent the formulations used *in vitro* and *in vivo* and the temperature was set to 37 °C. In line  
275 with previous applications of COSMOquick for co-former screening in co-crystal selection,<sup>37</sup>  
276 drug solubility estimations in glycerides<sup>38</sup> and polymer screening for supersaturated  
277 formulations,<sup>39</sup> a more negative value of calculated excess enthalpy ranks the strength of  
278 molecular drug-excipient interaction. This is just an approximation, as the presence of an  
279 aqueous phase is not considered in the calculations nor the complexity of any biorelevant  
280 medium. Therefore, the results should be understood as a first *in silico* estimation of relative

Page 12

## X. Thesis Publications

281 excipient comparison. This has previously been referred to as a higher or lower ‘COSMO-  
282 Rank’.<sup>39</sup>

283

284 *In vitro precipitation inhibitor testing*

285 The *in vitro* PI testing for venetoclax was done by means of a solvent shift. The effect of a fully  
286 hydrated PI (dissolved in FaSSIF) was compared against the PI in the formulation. Thus, the  
287 employed PIs HPMC, HPMCAS, Eudragit® EPO, PVP, PVP/VA and Pluronic® F108 were  
288 dissolved in either FaSSIF or either suspended or dissolved in the supersaturated lipid solution.  
289 For the hydrated PI test, 5 mg PI was dissolved in 5 mL FaSSIF (prepared according to  
290 biorelevant.com) and 5 mg of venetoclax dissolved in either DMSO (100 mg/mL) or Peceol®  
291 (sLBF 50 mg/mL) was added. For the evaluation of the PI in the lipid formulation, 100 µL of  
292 the sLBF (50 mg/mL venetoclax and 50 mg/mL PI) was added to 5 mL FaSSIF. The vials were  
293 sealed and placed in a water bath shaker at 200 shakes/min and 37 °C (GLS400, Grant  
294 Instruments, UK). After 2, 5, 10, 15, 30, 60, 120, 180 min 250 µL samples were taken. The  
295 samples were filtered with a 0.2 µm syringe filter (Whatman® Spartan 13/0.2) and samples that  
296 contained lipids were additionally centrifuged for 30 min at 21,380g and 37 °C (Mikro 200 R,  
297 Hettich GmbH, Germany). The aqueous phase was collected, and one part was diluted 1:10  
298 (v/v) with acetonitrile (including 0.5% (v/v) TFA). A pure (non-diluted) and diluted sample  
299 was analysed by HPLC as described above.

300

301 Additionally, the solubility of venetoclax was determined in FaSSIF with dissolved PI. Excess  
302 venetoclax was added to 5 mL FaSSIF with 5 mg PI. 250 µL samples were taken at 3 h, 6 h,  
303 24 h and filtered through a 0.2 µm syringe filter (Whatman® Spartan 13/0.2), diluted with  
304 acetonitrile (containing 0.5% (v/v) TFA) and analysed by HPLC as described above.

305

Page 13

## X. Thesis Publications

306 *In vivo study*

307 All experiments were approved and conducted with licences issued by the Health Product  
308 Regulatory Authority, Ireland (project licence AE19130/P058) as directed by the EU Statutory  
309 instruments of the EU directive 2010/63/EU (Protection of Animals used for Scientific  
310 Purposes). Local ethical approval was granted by University College Cork Animal  
311 Experimentation Ethics Committee (AEEC). In order to test all PIs two bioavailability studies  
312 had to be conducted. The first study was with 5 pigs and a 6-way crossover and the second  
313 study with 3 pigs and a 4-way crossover. Both studies were randomised and conducted in male  
314 landrace pigs (15 – 17 kg) and each pig received a single dose of 100 mg venetoclax. Pigs were  
315 fed approximately 175 g of standard weanling pig pellet feed twice daily. In the fasted study  
316 legs the final feed of 175 g was given 24 h prior to dosing. As part of the study design any  
317 remaining food was removed 16 h before dosing, however, no food remained at this point in  
318 any of the groups. On day 1, an indwelling intravenous catheter was inserted from the ear vein  
319 into the jugular vein under general anaesthesia, which was used for repeated blood sampling  
320 throughout the study. In the first study, on day 3, following an overnight fast of 16 h, pigs were  
321 administered either sLBF or sLBF with PI, respectively. The tested PIs included HPMC,  
322 HPMCAS, PVP, PVP/VA, Pluronic® F108. In the second study, on day 3, following an  
323 overnight fast of 16 h, pigs were administered either a reference capsule with venetoclax  
324 powder, a venetoclax Peceol® suspension, a sLBF or a sLBF including Eudragit® EPO,  
325 respectively. The results of the venetoclax powder, Peceol® suspension and sLBF have  
326 previously been reported<sup>14</sup> and are not further described in the current study. In both studies  
327 all formulations were administered with the aid of a dosing gun followed by 50 mL of water  
328 via a syringe. In order to control the water intake with the dosage forms, the water availability  
329 was restricted for 3 h post dosing. At all other times water was available *ad libitum*. To facilitate  
330 handling during the oral administration, an intramuscular dose of ketamine (5mg/kg) and

Page 14

## X. Thesis Publications

331 xylazine (1mg/kg) was administered in both studies. Blood samples were collected after 0.5, 1,  
332 1.5, 2, 3, 4, 5, 6, 7, 8, 9, 10, 12, 24 h in heparinised tubes. Upon collection, blood samples were  
333 immediately centrifuged at 3000g, 4 °C for 5.5 min (Eppendorf 5702 R, Rotor A-4-38,  
334 Eppendorf Ltd., UK). The supernatant plasma was harvested and stored at -20 °C until further  
335 analysis. A 6-day washout period was maintained between the study legs.

336

### 337 *Bioanalysis*

338 The plasma concentrations of venetoclax were determined by reversed phase HPLC. The  
339 Agilent 1260 series HPLC system (Agilent Technology Inc., US) comprised a binary pump,  
340 degasser, temperature controlled autosampler, column oven and diode array detector. The  
341 system was operated, and the data analysed with EZChrom Elite® version 3.3.2. A Zorbax®  
342 Eclipse Plus-C18 column (5 µm, 4.6 mm x 150 mm) with a Zorbax® Eclipse Plus-C18 guard  
343 column (5 µm, 4.6 mm x 12.5 mm) was used for the separation of venetoclax. The mobile phase  
344 consisted of water and acetonitrile with 0.5% (v/v) TFA at a ratio of 47:53 (v/v) and was used  
345 at a flow rate of 1.0 mL/min. The sample and column temperature were set at 5 °C and 40 °C,  
346 respectively, and the detection wavelength was set to 250, 290 and 316 nm. Venetoclax was  
347 extracted from the plasma samples by liquid-liquid extraction as reported previously.<sup>14</sup> In brief,  
348 venetoclax was extracted from 500 µL plasma using acetonitrile and ethyl acetate. Vemurafenib  
349 was used as internal standard. The extraction solvents were dried under a nitrogen stream at  
350 60 °C and the residues were reconstituted in 100 µL mobile phase (excluding TFA) followed  
351 by centrifugation at 25 °C, 11,500g for 5 min (Mikro 200 R, Andreas Hettich GmbH & Co. KG,  
352 Germany). The injection volume used for HPLC analysis of the supernatant was 50 µL.

353



## X. Thesis Publications

### 354 *Data Analysis*

355 Prior to statistical analysis the Bartlett's test was used to check for equal variances. A one-way  
356 analysis of variance (one-way ANOVA) was performed for the lipolysis data using a Tukey  
357 post-hoc test to compare the different formulation performances. While the concentration time  
358 profiles of the *in vitro* PI test were analysed using a two-way ANOVA with the Bonferroni  
359 post-test, the area under the curve (AUC) was analysed using a one-way ANOVA with a Tukey  
360 post-hoc test. The pharmacokinetic parameters were calculated using Microsoft® Excel® by  
361 means of the trapezoidal rule. The plasma concentration profiles were analysed by non-  
362 compartmental analysis. The statistical analysis for the *in vivo* parameters of the formulations  
363 within the same crossover study was performed using a one-way ANOVA after using the  
364 Bartlett's test to check for equal variances. The pairwise comparison of the groups was done  
365 using Tukey's multiple comparison test. All statistical analyses were carried out using  
366 GraphPad Prism® 5.

367

### 368 RESULTS

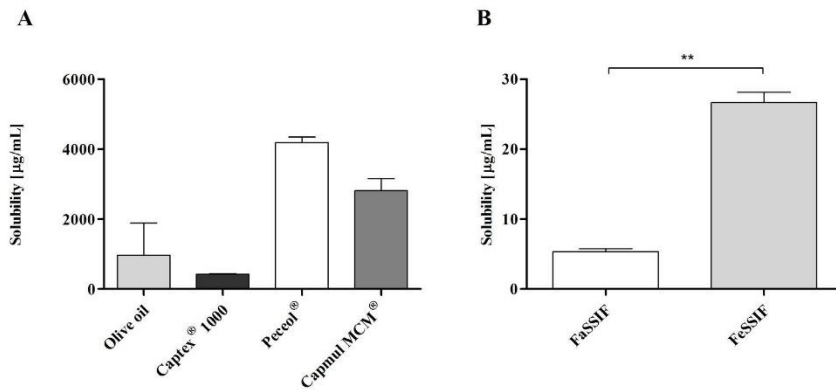
#### 369 *Apparent solubility of venetoclax in lipid excipients*

370 Solubility screening in pure lipid excipient indicated that venetoclax showed a higher apparent  
371 solubility in long chain than medium chain based excipients (Figure 1 A). Within the long chain  
372 and medium chain excipients, a higher apparent solubility was observed for the monoglycerides  
373 compared to the triglycerides. Subsequently, biorelevant solubility of venetoclax was  
374 determined (Figure 1 B). Solubility in FaSSIF was  $6.8 \pm 1.8$  µg/mL translating to only 1.7% of  
375 a 100 mg dose venetoclax in 250 mL of gastrointestinal fluid. In the fed state the solubility  
376 increased 3.9-fold to 6.7% of the 100 mg venetoclax dose, which in general is in agreement  
377 with the observation in increased bioavailability for venetoclax reported from clinical studies.

378 <sup>30</sup>

Page 16

379



380

381 **Figure 1.** A: Solubility in the lipid excipients at 37 °C (n = 3, mean  $\pm$  SD), B: Solubility in  
 382 fasted state simulating intestinal fluids (FaSSIF) and fed state simulating intestinal fluids  
 383 (FeSSIF) at 37 °C (n = 3, mean  $\pm$  SD).

384

385 *sLBF* achieves high aqueous drug concentration during in vitro dispersion and digestion.

386 Previous studies by our group developed a venetoclax sLBF using a preparation method at 70  
 387 °C.<sup>14</sup> Process optimisation in this study focused on improving the thermally-induced  
 388 supersaturation process by lowering the overall energy input while maintaining the desired level  
 389 of supersaturation. sLBFs were prepared at the target dose load of 50 mg/mL by heating a LBF  
 390 suspension (50 mg/mL) to 55 °C. The (s)LBF was kept at 55 °C for 10 min to dissolve  
 391 venetoclax before cooling the solution to room temperature. In this study, the obtained sLBF  
 392 had a 11.9-fold (1193.7%) higher drug load compared to the apparent saturation solubility. The  
 393 venetoclax concentrations in the aqueous phase during dispersion and digestion are shown in  
 394 Table 1 and Figure S 1.

395

396 **Table 1.** Venetoclax concentration in the *in vitro* lipolysis experiment after 10 min of dispersion  
 397 and after 5 min and 60 min of digestion. Venetoclax was formulated as sLBF (50 mg/mL),  
 398 Peceol<sup>®</sup> suspension (50 mg/mL) and aqueous suspension (50 mg/mL). All experiments were  
 399 run with n = 3 and results are shown as mean ± SD.

| Formulation                      | Venetoclax concentration (µg/mL) in aqueous phase (AP) during<br>LBF dispersion and digestion |                                    |                                     |
|----------------------------------|---|------------------------------------|-------------------------------------|
|                                  | AP <sub>Dispersion</sub><br>(10 min)  | AP <sub>Digestion</sub><br>(5 min) | AP <sub>Digestion</sub><br>(60 min) |
| sLBF <sup>a)</sup>               | 18.7 ± 0.0  | 37.5 ± 3.2                         | 73.8 ± 6.4                          |
| LBF suspension <sup>b,c)</sup>   | 1.0 ± 0.1   | 1.7 ± 0.3                          | 2.9 ± 0.5                           |
| aqueous suspension <sup>c)</sup> | 3.0 ± 0.1   | 9.1 ± 0.2                          | 9.4 ± 0.3                           |

400 <sup>a)</sup> sLBF drug loading was 1194% of determined apparent solubility

401 <sup>b)</sup> LBF drug loading was 100% solubilised + 158% suspended of determined apparent solubility

402 <sup>c)</sup> Data as previously reported. <sup>14</sup>

403

404 As the drug needs to be dissolved prior to absorption by the body, the solubilised drug in the  
 405 aqueous phase of the *in vitro* lipolysis test is often used as a guide to formulation performance  
 406 *in vivo*. The sLBF displayed relatively high concentrations in the aqueous phase throughout *in*  
 407 *vitro* lipolysis, with an average venetoclax concentration of 18.6 ± 1.3 µg/mL during dispersion  
 408 and 73.8 ± 6.4 µg/mL after 60 min of digestion. Interestingly, the final concentration at the end  
 409 of the digestion, was equivalent to 6.4 ± 0.5% of the venetoclax dose used in the experiment  
 410 and was 2.8-fold higher when compared to the apparent solubility of venetoclax in FeSSIF.  
 411 Additionally, the measured concentration was higher than the reported amorphous solubility in  
 412 FeSSIF of 26.4 – 54.6 µg/mL. <sup>40</sup> Most of venetoclax was recovered in the lipid phase with an  
 413 average of 98.5 ± 2.8% of the venetoclax dose during dispersion and 88.6 ± 0.2% after 60 min  
 414 of digestion (Figure S 1). The lipid phase can act as a reservoir for the drug, which gradually

Page 18

## X. Thesis Publications

415 diffuses into the aqueous phase during the transit through the gastrointestinal tract. Additionally,  
416 the lipid phase is digested during the transit releasing venetoclax. In the case of the sLBF the  
417 lowest amount of venetoclax was recovered in the solid phase. sLBF showed no precipitation  
418 during dispersion and after 60 min of digestion only  $6.2 \pm 0.6\%$  of the venetoclax dose was  
419 precipitated. These results are in line with previous studies showing a superior performance  
420 (high aqueous phase concentration, low solid phase concentration) of the sLBF *in vitro* relative  
421 to a lipid-based suspension and aqueous suspension.<sup>14</sup> The optimised processing method,  
422 therefore, yielded comparable formulation performance.

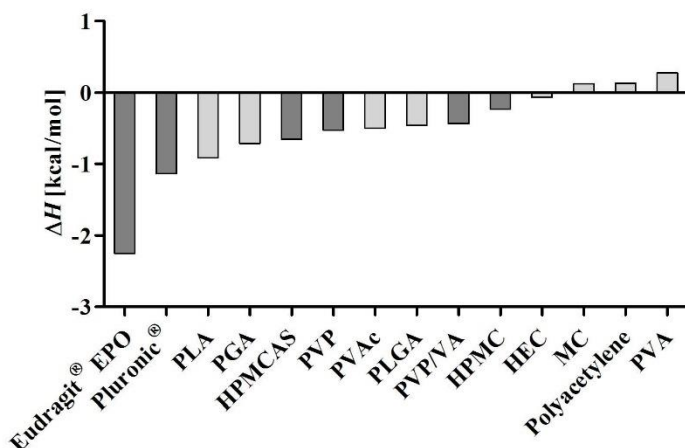
423

424 *COSMO-RS as a preliminary in silico screening tool for PI selection*

425 To identify the most promising PIs, reduce the extent of *in vitro* testing and to evaluate the  
426 utility of this computational tool in the formulation design of sLBFs, the interactions between  
427 venetoclax and various PIs were evaluated *in silico*. Based on the COSMO-RS theory<sup>34,41</sup> that  
428 combines quantum chemistry and statistical thermodynamics, the COSMOquick software was  
429 utilized to predict the PI-drug interactions similarly to previous reports where this screening  
430 technique of PI selection was utilised for silica formulations.<sup>39</sup> The COSMOquick software  
431 predicts the interactions of two molecules based on equilibrium thermodynamics and the  
432 predicted chemical potential in liquids. The stronger the interaction between venetoclax and the  
433 PI, the more negative the calculated excess enthalpy of interaction. A simplified view assigns  
434 to a PI that has a more negative excess enthalpy, a higher 'COMSO-Rank' with respect to its  
435 suitability as PI. While this tool may be beneficial to reduce *in vitro* testing by identifying the  
436 most promising PI-drug interactions as shown for other formulation approaches,<sup>39</sup> it must be  
437 acknowledged that the *in silico* calculations did not consider the presence of water nor other  
438 formulation excipients, potentially limiting the applicability of this tool for the more complex  
439 bio-enabling formulation approach of LBFs. In the present study, the excess enthalpy of mixing

Page 19

440 for a variety of PIs was calculated, and PIs with varying negative enthalpy of mixing were  
 441 selected. The chosen PIs had the following ‘COSMO-Rank’: Eudragit<sup>®</sup> EPO > Pluronic<sup>®</sup> >  
 442 HPMCAS ≥ PVP ≥ PVP/VA > HPMC as shown in Figure 2.  
 443



444  
 445 **Figure 2.** COSMOquick screen. Calculated excess enthalpy of interaction between venetoclax  
 446 and the PIs. The dark grey PIs were selected for further *in vitro* and *in vivo* evaluation. The  
 447 calculation was based on a 1:1 ratio of drug to PI. PLA: Polylactic acid, PGA: Polyglycolic  
 448 acid, HPMCAS: Hydroxypropyl methylcellulose acetate succinate, PVP: Polyvinylpyrrolidone,  
 449 PVAc: Polyvenyl acetate, PLGA: Poly lactic-co-glycolic acid, PVP/VA: Polyvinylpyrrolidone-  
 450 co-vinyl acetate, HPMC: Hydroxypropyl methylcellulose, HEC: Hydroxypropyl cellulose, MC:  
 451 Methylcellulose, PVA: Polyvinyl alcohol

452  
 453 *In vitro testing for PIs for prolonging supersaturation*

454 The selected PIs from the *in silico* screening were further evaluated experimentally *in vitro* to  
 455 assess the PI performance (aqueous phase concentration) under simulated conditions and with



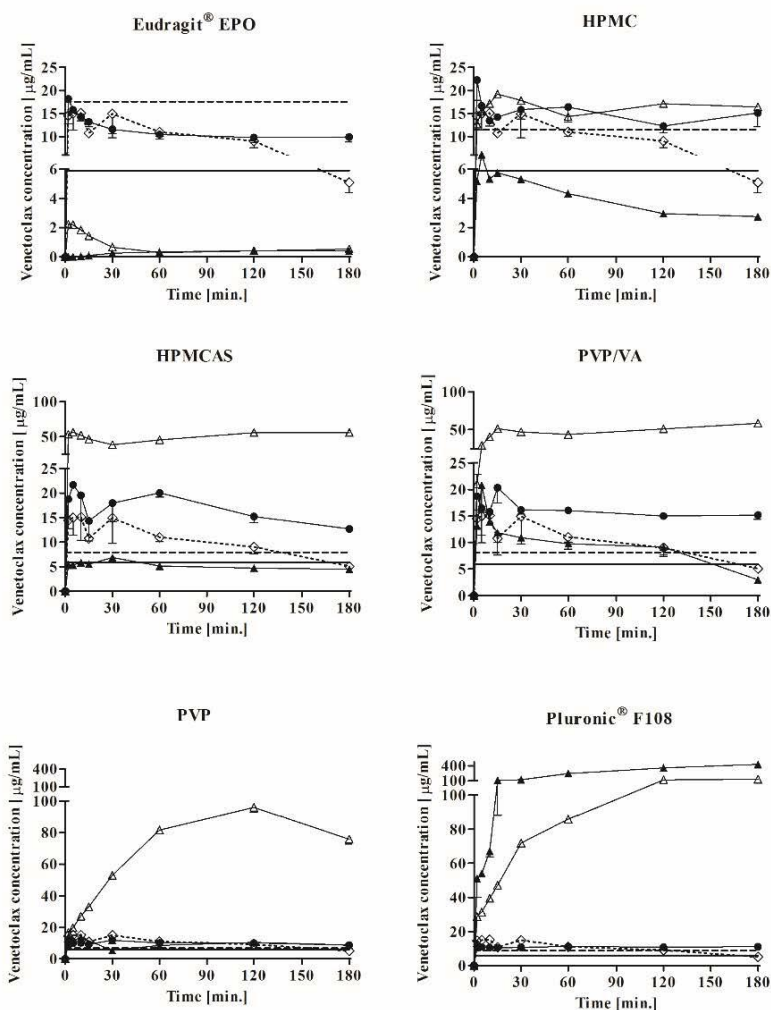
## X. Thesis Publications

456 LBFs. The *in vitro* PI test was performed by means of solvent shift by dispersing the  
457 formulation in (i) FaSSIF or (ii) FaSSIF with pre-dissolved PI (FaSSIF-PI). In FaSSIF-PI was  
458 dispersed (a) venetoclax dissolved in DMSO (100 mg/mL), as a positive control and (b) sLBF  
459 (sLBF-aqPI). In FaSSIF was dispersed (c) sLBF without PI (sLBF-noPI) and (d) sLBF with  
460 incorporated PI (sLBF-PI). Polymers that were soluble at the tested concentration of 50 mg/mL  
461 were dissolved in sLBF (PVP, PVP/VA, Pluronic® F108, Eudragit® EPO) and those that were  
462 not soluble in the sLBF were therefore *ad hoc* suspended in the sLBF (HPMC, HPMCAS).  
463 Additionally, the solubility of venetoclax in FaSSIF-PI was measured. The results of the PI  
464 testing are shown in Figure 3 and Table 2.

465

466 In all cases, the venetoclax solubility in FaSSIF-PI was higher compared to the solubility in  
467 FaSSIF with an increase in solubility from 1.3-fold to 3.4-fold. In order of decreasing solubility  
468 in FaSSIF-PI the ranking was Eudragit® EPO, HPMC, Pluronic® F108, PVP/VA, HPMCAS  
469 and PVP. In general, upon dispersion of the DMSO solution in FaSSIF-PI HPMC, Pluronic®  
470 F108, PVP/VA, HPMCAS and PVP venetoclax concentrations reached FaSSIF-PI solubility,  
471 which was maintained throughout the experiment. In the case of Eudragit® EPO a decrease  
472 below the FaSSIF-PI solubility was observed.

473



474

475 **Figure 3.** *In vitro* evaluation of venetoclax concentration profile during dispersion of sLBFs in  
 476 FaSSiF (mean  $\pm$  SD with n = 3). The dashed line represents the apparent venetoclax solubility  
 477 in FaSSiF with pre-dissolved PI (FaSSiF-PI) and the solid line represents FaSSiF solubility.  
 478 The dotted line ( $\diamond$ ) represents the sLBF alone dispersed in FaSSiF (sLBF-noPI). Venetoclax  
 479 dissolved in DMSO dispersed in FaSSiF-PI ( $\bullet$ ), sLBF dispersed in FaSSiF-PI (sLBF-aqPI)  
 480 ( $\blacktriangle$ ), sLBF with PI (sLBF-PI) dispersed in FaSSiF ( $\Delta$ ).

## X. Thesis Publications

481 **Table 2.** Area under the curve (AUC) of the *in vitro* PI testing for sLBF dispersed in FaSSiF-PI (sLBF-aqPI), sLBF with PI incorporated in the  
 482 formulation (sLBF-PI) and dispersed in FaSSiF, venetoclax dissolved in DMSO dispersed in FaSSiF-PI (DMSO) and sLBF alone dispersed in FaSSiF  
 483 (sLBF-noPI), % solubilised venetoclax and apparent supersaturation ratio for sLBF-aqPI and sLBF-PI as well as FaSSiF-PI solubility (mean  $\pm$  SD,  
 484 n = 3).

| PI             | AUC [mg*min/mL] |                 |                | Apparent FaSSiF-PI solubility [ $\mu$ g/mL] | solubilised venetoclax [%] <sup>a)</sup> |                | apparent supersaturation ratio <sup>b)</sup> |                |
|----------------|-----------------|-----------------|----------------|---|--|----------------|--|----------------|
|                | DMSO            | sLBF-aqPI       | sLBF-PI        |   | sLBF-aqPI                                | sLBF-PI        | sLBF-aqPI                                    | sLBF-PI        |
| Eudragit® EPO  | 1.9 $\pm$ 0.3   | 0.1 $\pm$ 0.004 | 0.1 $\pm$ 0.02 | 17.6 $\pm$ 0.8                              | 0.03 $\pm$ 0.002                         | 0.1 $\pm$ 0.01 | < LOQ  | 0.3 $\pm$ 0.03 |
| HPMC           | 2.6 $\pm$ 0.5   | 0.7 $\pm$ 0.1   | 2.9 $\pm$ 0.3  | 11.5 $\pm$ 2.4                              | 0.4 $\pm$ 0.04                           | 1.6 $\pm$ 0.2  | 0.9 $\pm$ 0.2                                | 2.3 $\pm$ 0.2  |
| HPMCAS         | 3.0 $\pm$ 0.3   | 0.9 $\pm$ 0.03  | 9.1 $\pm$ 0.4  | 7.9 $\pm$ 1.6                               | 0.5 $\pm$ 0.02                           | 5.1 $\pm$ 0.2  | 0.8 $\pm$ 0.1                                | 8.3 $\pm$ 0.3  |
| PVP            | 1.8 $\pm$ 0.3   | 1.5 $\pm$ 0.2   | 13.5 $\pm$ 0.1 | 6.7 $\pm$ 0.2                               | 0.9 $\pm$ 0.1                            | 7.5 $\pm$ 0.04 | 1.7 $\pm$ 0.2                                | 2.9 $\pm$ 0.4  |
| PVP/VA         | 2.8 $\pm$ 0.2   | 1.6 $\pm$ 0.2   | 8.8 $\pm$ 0.3  | 8.1 $\pm$ 1.4                               | 0.9 $\pm$ 0.1                            | 4.9 $\pm$ 0.2  | 3.0 $\pm$ 1.6                                | 4.3 $\pm$ 0.3  |
| Pluronic® F108 | 2.0 $\pm$ 0.4   | 50.4 $\pm$ 2.4  | 17.5 $\pm$ 0.6 | 8.9 $\pm$ 0.2                               | 28.1 $\pm$ 1.3                           | 9.8 $\pm$ 0.3  | 7.9 $\pm$ 0.2                                | 4.6 $\pm$ 0.2  |
| sLBF-noPI      |                 | 1.8 $\pm$ 0.3   |                |   |  | 1.0 $\pm$ 0.2  |  | 2.2 $\pm$ 0.5  |

Page 23

485 <sup>a)</sup> % solubilised was calculated by dividing the AUC of the concentration versus time profiles by the maximum AUC, i.e. representing 100% solubilised,  
 486 over the same period of time.

487 <sup>b)</sup> Apparent supersaturation ratio of venetoclax after 5 min dispersion (determined venetoclax concentration relative to FaSSiF solubility)

488

Page 24

## X. Thesis Publications

489 In the case of the sLBF-noPI, a high initial concentration was observed ( $14.5 \pm 1.7 \mu\text{g/mL}$ ),  
490 which was above the FaSSIF solubility ( $5.2 \pm 0.4 \mu\text{g/mL}$ ). In addition, the initial venetoclax  
491 concentrations of sLBF-noPI was above FaSSIF-PI in the case of HPMC, PVP/VA, HPMCAS,  
492 PVP and Pluronic® F108 indicating that the investigated PI-free sLBF-noPI was able to  
493 generate supersaturation, i.e. a spring effect upon dispersion. The observed initial venetoclax  
494 concentrations, i.e. spring effect, of the sLBF-noPI were also similar to all the initial aqueous  
495 phase concentrations of the positive control with DMSO, which had the PIs pre-dissolved in  
496 the media. Relative to the FaSSIF solubility, an apparent supersaturation ratio of  $2.2 \pm 0.5$  after  
497 5 min of dispersion was observed for the sLBF-noPI (Table 2). The degree of supersaturation  
498 from the sLBF-noPI gradually decreased to  $1.3 \pm 0.2$  after 2 h, whereas at 3 h the drug  
499 concentration had dropped to FaSSIF solubility. However, while the sLBF-noPI was not able  
500 to maintain supersaturated concentrations throughout the experiment, the use of PIs in the  
501 positive control maintained supersaturation ratios  $> 1$  for up to 3 h. As the function of the PIs  
502 was intended as a ‘parachute’ to prolong supersaturation, the results indicated a beneficial  
503 precipitation inhibitory effect of PIs on the formulation performance.

504

505 Interestingly, the combination of PIs in sLBF (sLBF-PI) yielded a higher spring concentration  
506 in the case of HPMCAS, PVP, PVP/VA and Pluronic® F108 when compared to sLBF-noPI and  
507 the positive control with DMSO. While the sLBF-PI with HPMC showed an initial venetoclax  
508 concentration similar to sLBF-noPI, sLBF-PI with Eudragit® EPO resulted in a statistically  
509 significant lower venetoclax concentration in the media when compared to sLBF-noPI and  
510 DMSO ( $p < 0.05$ ). In fact, the venetoclax concentration was below FaSSIF and FaSSIF-PI  
511 solubility when Eudragit® EPO and lipid were present simultaneously. In the case of dispersing  
512 sLBF into FaSSIF-PI (sLBF-aqPI), an increased initial venetoclax concentration was only

## X. Thesis Publications

513 evident for Pluronic® F108 when compared to sLBF-noPI. All other PIs resulted in a similar or  
514 decreased initial concentration.

515

516 The impact of polymer-sLBF combinations on the ability to solubilise venetoclax and prolong  
517 supersaturation across six different PIs is summarised in Table 2 and Figure 3. In the case of  
518 HPMC, HPMCAS and Eudragit® EPO, the sLBF-aqPI resulted in a lower amount of solubilised  
519 venetoclax throughout the experiment compared to sLBF-noPI. Similarly, in comparison to  
520 DMSO controls the sLBF-aqPI resulted in a lower AUC in the case of Eudragit® EPO, HPMC,  
521 HPMCAS and PVP/VA. As an example, the amount of the solubilised venetoclax dose was  
522  $0.033 \pm 0.002\%$  for Eudragit® EPO in the case of sLBF-aqPI. In addition, sLBF-aqPI resulted  
523 in the case of Eudragit® EPO, HPMC, HPMCAS, PVP and PVP/VA in a similar or lower  
524 apparent supersaturation ratio compared to sLBF-noPI and the respective DMSO controls. In  
525 the case of Pluronic® F108, the amount of venetoclax solubilised and the apparent  
526 supersaturation ratio was increased compared to the sLBF-noPI and DMSO control.  
527 Nevertheless, overall the results of the sLBF-aqPI suggested that a pre-dissolved PI in FaSSiF  
528 was less effective at prolonging venetoclax supersaturation, indicating that concomitant  
529 administration (i.e. chase dosing) a PI with a sLBF would not potentially offer benefits in terms  
530 of sustained high concentrations for absorption *in vivo*.

531

532 In the case of incorporating HPMC, HPMCAS, PVP, PVP/VA and Pluronic® F108 within the  
533 sLBF higher amount of venetoclax was solubilised compared to sLBF-noPI. Furthermore, the  
534 sLBF-PIs resulted in a higher amount of solubilised venetoclax in comparison to the sLBF-  
535 aqPI. In addition, higher apparent supersaturation ratios (after 5 min of dispersion) were  
536 observed for sLBF-PI relative to sLBF-noPI. In the case of HPMC, HPMCAS, PVP and  
537 PVP/VA the apparent supersaturation ratios were higher compared to the sLBF-aqPI indicating

Page 26



## X. Thesis Publications

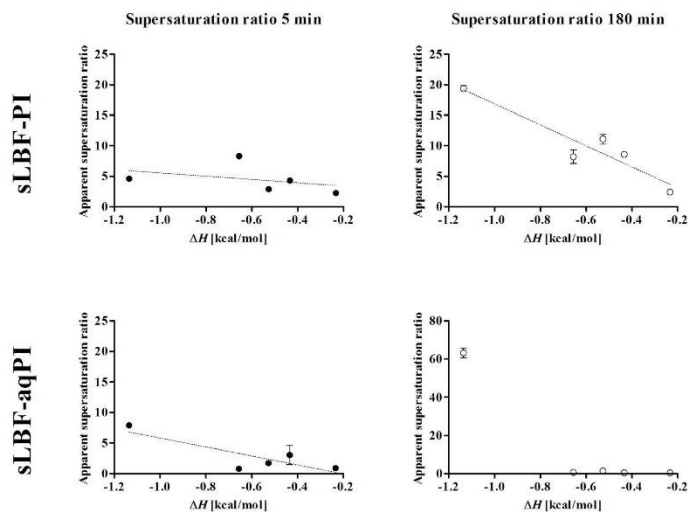
538 that these sLBF-PI combinations achieved a balance between generating and maintaining  
539 supersaturated concentrations. However, Pluronic<sup>®</sup> F108 and Eudragit<sup>®</sup> EPO did not follow this  
540 trend. Pluronic<sup>®</sup> F108 showed a higher supersaturation ratio and % solubilised venetoclax for  
541 the sLBF with pre-dissolved Pluronic<sup>®</sup> F108 (sLBF-aqPI), compared to the incorporation into  
542 the sLBF (sLBF-PI). Such high venetoclax concentrations and supersaturation ratios in the  
543 presence of Pluronic<sup>®</sup> F108 may be attributed to the surfactant nature of the polymer, which  
544 can increase the solubilisation capacity of the test media, especially when pre-dissolved. In the  
545 case of Eudragit<sup>®</sup> EPO, a significantly decreased amount of solubilised venetoclax and  
546 supersaturation ratios < 1 in all cases of lipid excipient-PI combinations were observed.

547

548 Based on the amount of venetoclax solubilised in the *in vitro* PI test, the general performance  
549 ranking was Pluronic<sup>®</sup> F108 > PVP > HPMCAS ≥ PVP/VA > HPMC > Eudragit<sup>®</sup> EPO in the  
550 case of sLBF-PI and Pluronic<sup>®</sup> F108 > PVP/VA ≥ PVP ≥ HPMCAS ≥ HPMC > Eudragit<sup>®</sup> EPO  
551 in the case of sLBF-aqPI. While this performance ranking was not in line with the *in silico*  
552 calculated COSMO-Rank, it should be acknowledged that Eudragit<sup>®</sup> EPO was not able to  
553 generate supersaturated venetoclax concentrations in the presence of the lipid excipient.  
554 Therefore, this particular PI, may not be suitable to enhance the sLBF performance.  
555 Subsequently, the relationship between the *in vitro* determined solubilised venetoclax and the  
556 *in silico* calculated COSMO-Rank was reassessed without Eudragit<sup>®</sup> EPO. The results for  
557 sLBF-PI and sLBF-aqPI are summarised in Figure 4. It was evident that there is a trend that a  
558 higher COSMO-Rank, i.e. higher interaction between venetoclax and the PIs resulted in a  
559 higher supersaturation ratio in the aqueous phase of the *in vitro* test in the case of sLBF-PI.  
560 From the *in silico* screen and *in vitro* experiments a relationship between COSMO-Rank and  
561 venetoclax solubilisation and supersaturation was less evident for sLBF-aqPI (no relationship  
562 was observed after 180 min). The results of both approaches (*in silico* and *in vitro*) indicated

Page 27

563 that for lipid systems an overly strong interaction between the drug and the PI may be less  
 564 favourable and in the case of Eudragit® EPO resulted in a depletion of aqueous venetoclax  
 565 concentrations.  
 566



567  
 568 **Figure 4.** Relationship between excess enthalpy of mixing calculating *in silico* using  
 569 COSMOquick and the *in vitro* determined apparent supersaturation ratio after 5 min and 180  
 570 min, respectively for sLBF with incorporated PI added to FaSSiF (sLBF-PI) and sLBF that was  
 571 added to FaSSiF-PI (sLBF-aqPI). Eudragit® EPO was excluded from the dataset due to the  
 572 inability to generate supersaturation. Data is presented as mean ± SD, n = 3.

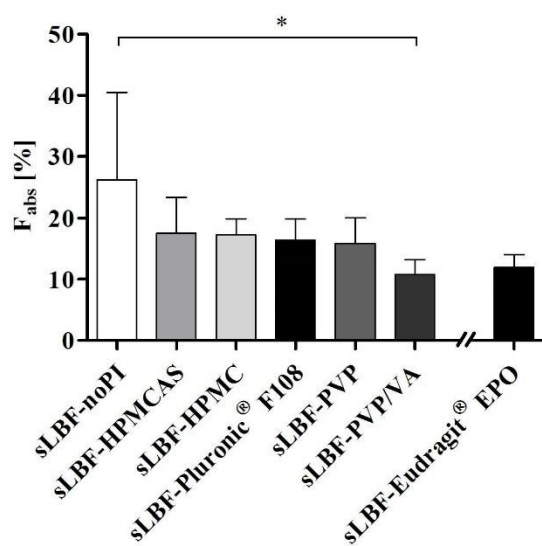
573

574 *Impact of PIs on in vivo bioavailability of venetoclax from sLBFs*

575 The aim of the *in vivo* study was to explore whether the *in vitro* observations would translate  
 576 to *in vivo* using sLBF-PI across six different PIs. Venetoclax formulations (50 mg/mL) were  
 577 prepared as a supersaturated Peceol® solution alone (sLBF-noPI) or in combination with HPMC,

## X. Thesis Publications

578 HPMCAS, PVP, PVP/VA, Pluronic® F108, Eudragit® EPO at a ratio of 1:1, respectively. PVP,  
579 PVP/VA, Pluronic® F108 and Eudragit® EPO were readily soluble in the sLBF, whereas HPMC  
580 and HPMCAS were not soluble in the sLBF and were therefore mixed in the sLBF prior to oral  
581 administration. An oral dose of 100 mg venetoclax was used. Absolute bioavailability was  
582 determined with reference to intravenous data that has been previously reported for landrace  
583 pigs. The absolute bioavailability as a function of each formulation is shown in Figure 5 and  
584 the associated pharmacokinetic parameters presented in Table 3. Individual plasma profiles for  
585 all tested formulations are shown in Figure S 2 and Figure S 3 in the supporting information.  
586 While it was only feasible to conduct a full six by six way cross-over study in this experiment  
587 facility, a seventh study leg using Eudragit® EPO was performed in a separate group of three  
588 pigs. In this case only mean comparisons were possible, whereas for all other groups  
589 formulation differences within each pig were performed.  
590



591

## X. Thesis Publications

592 **Figure 5.** Absolute bioavailability ( $F_{abs}$ ) in landrace pigs for 100 mg venetoclax as a 6-way  
593 crossover with sLBF-noPI, sLBF-HPMC, sLBF-HPMCAS, sLBF-PVP, sLBF-PVP/VA, sLBF-  
594 Pluronic® F108 and an additional study including sLBF-Eudragit® EPO. All data is presented  
595 as mean  $\pm$  SD, where n = 5 (except sLBF- Eudragit® EPO, where n = 3).

596

597 The sLBF-noPI showed the highest mean bioavailability ( $26.3 \pm 14.2\%$ ) compared to all other  
598 tested lipid formulations. An increased bioavailability was not observed by incorporation of PIs  
599 but rather a trend towards a decreased oral bioavailability, albeit only the sLBF-PVP/VA  
600 formulation displayed statistically significant lower bioavailability relative to the sLBF-noPI  
601 ( $p < 0.05$ ). The rank order of the oral bioavailability was sLBF-noPI  $\geq$  sLBF-HPMCAS  $\geq$  sLBF-  
602 HPMC  $\geq$  sLBF-Pluronic® F108  $\geq$  sLBF-PVP  $\geq$  sLBF-Eudragit® EPO  $\geq$  sLBF-PVP/VA. The  
603 observed bioavailability for sLBF-noPI is in agreement with previously reported venetoclax  
604 bioavailability in fasted pigs ( $17.3 \pm 5.5\%$ ). The time to reach the maximum plasma  
605 concentrations ( $t_{max}$ ), the mean residence time (MRT) and mean absorption time (MAT) tended  
606 to increase with lower oral bioavailability, however, this observation is not statistically  
607 significant. Overall the results showed that the use of PIs did not enhance the sLBF formulation  
608 performance *in vivo*.

## X. Thesis Publications

609 **Table 3.** Pharmacokinetic parameters of the follow up study of venetoclax. Oral administration of 100 mg/pig to male landrace pigs. Venetoclax was  
 610 administered in a 6-way crossover as a supersaturated Peceol® solution (sLBF-noPI) and as sLBF with HPMC (sLBF-HPMC), HPMCAS (sLBF-  
 611 HPMCAS), PVP (sLBF-PVP), PVP/VA (sLBF-PVP/VA), Pluronic® F108 (sLBF- Pluronic® F108) and in a 2-way crossover including Eudragit®  
 612 EPO (sLBF- Eudragit® EPO), respectively.  $t_{max}$ , MAT and MRT are given as median (range), all other parameters as mean  $\pm$  SD (n = 5, except sLBF-  
 613 Eudragit® EPO, where n = 3).

| Pharmacokinetic parameters                                 |                     |                      |                      |                      |                      |                        |                                     |
|--|---------------------|----------------------|----------------------|----------------------|----------------------|------------------------|-------------------------------------|
|  | sLBF-noPI           | sLBF-HPMC            | sLBF-HPMCAS          | sLBF-PVP             | sLBF-PVP/VA          | sLBF-Pluronic®<br>F108 | sLBF-Eudragit®<br>EPO <sup>b)</sup> |
| $c_{max}$ [ $\mu\text{g}/\text{mL}$ ]                      | 1.38 $\pm$ 0.84     | 0.92 $\pm$ 0.24      | 0.83 $\pm$ 0.20      | 0.81 $\pm$ 0.19      | 0.48 $\pm$ 0.67      | 0.80 $\pm$ 0.20        | 0.51 $\pm$ 0.28                     |
| $t_{max}$ [h] (range)                                      | 6 (2–10)            | 6 (6-8)              | 8 (7-10)             | 8 (6-8)              | 9 (8-10)             | 9 (6-10)               | 10 (7-10)                           |
| AUC 0 h – inf.<br>[ $\mu\text{g}\cdot\text{h}/\text{mL}$ ] | 11.40 $\pm$ 6.15    | 7.39 $\pm$ 1.40      | 7.69 $\pm$ 2.53      | 6.90 $\pm$ 1.83      | 4.73 $\pm$ 1.08      | 7.19 $\pm$ 1.50        | 5.23 $\pm$ 1.60                     |
| MRT [h] (range)  | 8.64 (7.41 – 14.20) | 10.17 (9.43 – 15.23) | 10.96 (9.69 – 12.03) | 10.44 (9.49 – 11.71) | 11.48 (8.67 – 11.73) | 10.62 (8.54 – 12.58)   | 13.67 (10.82 – 15.62)               |
| MAT [h] (range)  | 4.76 (3.53 – 10.32) | 6.29 (5.55 – 11.35)  | 7.08 (5.81 – 8.15)   | 6.56 (5.62 – 7.83)   | 7.61 (4.79 – 7.86)   | 6.74 (4.66 – 8.70)     | 9.79 (6.94 – 11.74)                 |
| $F_{rel}$ [%] <sup>a)</sup>                                | 100                 | 76.62 $\pm$ 32.34    | 78.86 $\pm$ 37.81    | 72.22 $\pm$ 30.56    | 52.95 $\pm$ 29.23    | 80.24 $\pm$ 42.16      | 68.87 $\pm$ 21.01 <sup>c)</sup>     |
| $F_{abs}$ [%]  | 26.28 $\pm$ 14.20   | 17.25 $\pm$ 2.63     | 17.57 $\pm$ 5.80     | 15.84 $\pm$ 4.18     | 10.76 $\pm$ 2.44     | 16.39 $\pm$ 3.47       | 11.95 $\pm$ 3.64                    |

Page 31

614 <sup>a)</sup> Relative to sLBF

615 <sup>b)</sup> sLBF-Eudragit® EPO originated from a second *in vivo* study. sLBF for the second *in vivo* study has previously been published.<sup>14</sup>

616 <sup>c)</sup> Relative to a previously published sLBF<sup>14</sup>

Page 32



### 617 DISCUSSION

618 Bio-enabling formulations that enhance the extent of oral drug absorption are increasingly  
619 required to meet the challenge of poor water-soluble properties of drugs emerging from  
620 discovery pipelines. Drug candidates which fail to meet Lipinski's Rule-of-Five criteria are a  
621 common target for such bio-enabling formulation strategies <sup>2</sup> due to poor biopharmaceutical  
622 properties, resulting from low aqueous solubility and/or poor permeability. Ideally, a  
623 formulation design that rapidly generates elevated drug concentrations in the gastrointestinal  
624 fluids, i.e. that generates the so-called 'spring effect' to increase concentration above the  
625 saturation solubility in gastrointestinal fluids and therein promote absorption. In order to  
626 maintain such high drug concentrations, PIs have been used to delay the onset of precipitation,  
627 i.e. the so-called parachute. <sup>42, 43</sup> This fundamental advantage of prolonged supersaturated drug  
628 concentrations in the intraluminal environment is assumed to be beneficial for absorption *in*  
629 *vivo*. <sup>42, 44, 45</sup> However, the choice of suitable PIs can be complicated <sup>24</sup> as the inhibitory effect  
630 is reported to be drug specific and there are gaps in our understanding which PIs are suited for  
631 a particular drug type. <sup>27, 42</sup> While various *in vitro* screening tests have been reported, to date  
632 the PI selection is mostly empirical and there is a lack of comprehensive studies comparing  
633 across all the various PI types. <sup>42</sup> Attempts have been made to increase the mechanistic  
634 understanding to aid with the selection of PIs to streamline formulation development, <sup>42</sup>  
635 however, it is often not known how effective an *in vitro* tool is in estimating the impact on *in*  
636 *vivo* absorption, especially for rather complex bio-enabling formulations. In addition, given the  
637 complexity of polymer-drug interactions, there is also a need for more computational tools to  
638 guide excipient selection.

639

640 In recent years, LBF approaches have been mechanistically described as 'supersaturable' drug  
641 delivery systems, on the basis of generating supersaturation following dispersion/digestion in

## X. Thesis Publications

642 the intraluminal environment. Indeed, it is widely recognised that dispersion/digestion can  
643 present a key risk to prolonged supersaturation, where there is a lower solubilisation capacity  
644 of the post digestive milieu. In particular, LBFs that contain high % of co-solvents (such as  
645 LFCS type IV systems) are considered to be at greatest risk of drug precipitation in the  
646 gastrointestinal tract. It has been shown for such type IIIB/IV LBF systems that the addition of  
647 an excipient to prolong supersaturation can lead to enhanced bioavailability.<sup>24-27</sup> The present  
648 study, therefore, aimed to explore the utility of PIs to enhance performance for supersaturated  
649 lipid solutions (sLBFs). Such systems are being explored particularly for poorly water-soluble  
650 drugs when a high drug load and exposure is needed for example in pre-clinical development  
651 studies. Our group and others have previously shown that sLBFs enhance oral bioavailability  
652 of poorly water-soluble drugs, albeit there is a perceived risk of drug precipitation due to the  
653 systems being considered merely kinetically stable. To address this, in the current study, the  
654 utility of several PIs to enhance formulation performance of a sLBF of venetoclax has been  
655 evaluated *in vitro* and *in vivo*. We further calculated the excess enthalpy of mixing of the drug  
656 and various polymers to approximate the interaction between venetoclax and the PIs in a more  
657 complex aqueous environment. This approach facilitated a rationalisation of *in vitro* testing,  
658 which was based on a solvent shift to assess the precipitation inhibitory effect.

659

660 The *in vitro* lipolysis confirmed the ability of sLBF to generate supersaturated aqueous phase  
661 concentrations of venetoclax during dispersion and digestion, which exceeded the  
662 experimentally determined apparent solubility in FaSSIF (Figure 1) and the reported values for  
663 the experimentally determined amorphous solubility in FaSSIF ( $20.7 \pm 0.5 \mu\text{g/mL}$ , pH 5.3;  
664  $33.7 \pm 13.5 \mu\text{g/mL}$ , pH 6.9) and FeSSIF ( $26.4 \pm 0.2 \mu\text{g/mL}$ , pH 5.3;  $54.6 \pm 2.0 \mu\text{g/mL}$ , pH 6.9).

665 <sup>40</sup> Such elevated concentrations were not observed for an aqueous and lipid based suspension  
666 and therefore confirm the ability of sLBF to generate supersaturated drug concentrations on

Page 34

## X. Thesis Publications

667 dispersion/digestion in intestinal fluids. Additionally, as a class III glass former<sup>14</sup> and due to  
668 the high molecular weight, venetoclax tends to crystallise more slowly. Moreover, venetoclax  
669 has been reported to undergo liquid-liquid-phase separation at concentrations above the  
670 amorphous solubility and it was assumed that supersaturation is maintained for a duration that  
671 is physiologically promising (24 h).<sup>40</sup> While in the case of the sLBF the physical state of the  
672 drug in such a separated drug-rich phase is unknown it can potentially serve as a reservoir of  
673 absorbable drug.<sup>40</sup> The co-existence of a drug rich phase and an aqueous phase at amorphous  
674 solubility (which were not separated) may explain the amount of venetoclax measured above  
675 the amorphous solubility in this test setup.

676

677 The *in vitro* PI screening method revealed that the incorporation of the PI into the sLBF resulted  
678 in higher venetoclax concentration in the aqueous phase compared to the addition of sLBF to  
679 the media containing pre-dissolved PI. Interestingly, the sLBF formulation demonstrated an  
680 initial supersaturated venetoclax concentration, which was maintained for up to 2 h even in the  
681 absence of a PI (i.e. sLBF-noPI). These findings are in line with the observations during *in vitro*  
682 lipolysis and confirm the ability of sLBF approaches to generate supersaturation, i.e. to act as  
683 a spring. The incorporation into the sLBF (sLBF-PI) of PIs: PVP/VA, HPMCAS, PVP,  
684 Pluronic<sup>®</sup> F108 and HPMC proved beneficial for venetoclax resulting in prolonged  
685 supersaturation *in vitro* (apparent supersaturation ratio > 2.4 for all polymers after 180 min of  
686 dispersion). However, the incorporation of Eudragit<sup>®</sup> EPO resulted in a decrease in venetoclax  
687 concentration in the aqueous phase, to below FaSSIF solubility (0.08-fold reduction relative to  
688 FaSSIF solubility). It was also noticeable that the sLBF-Eudragit<sup>®</sup> EPO was poorly dispersible  
689 in FaSSIF, forming a two-phase system with drug rich agglomerates dispersed in buffer (Figure  
690 S 4). In contrast, all the sLBF-noPI and sLBFs containing PIs dispersed consistently in FaSSIF  
691 to form a homogenous dispersion on mixing. One possible explanation for the significant lower

Page 35

## X. Thesis Publications

692 venetoclax concentrations observed for the sLBF-Eudragit® EPO system may reflect the poor  
693 dispersion in FaSSIF. This observation suggested that venetoclax may have remained within  
694 the lipid-rich agglomerates and was not released from the formulation into the aqueous phase.  
695 Additionally, Eudragit® EPO (in the unionised form) and venetoclax are relatively lipophilic  
696 and interact strongly with each other, as indicated by the calculated negative excess enthalpy  
697 of interaction with the *in silico* tool, which may have further promoted the drug retention in the  
698 lipid phase. Another aspect is that the unionised Eudragit® EPO was not expected to swell in  
699 aqueous medium and such a swelling of a more hydrophilic polymer is likely to contribute to  
700 the performance of a PI. This complexity in aqueous medium was not captured by the simple  
701 mixing enthalpy calculations of binary drug-polymer systems.

702

703 The *in vivo* study demonstrated that the highest oral bioavailability was obtained with the sLBF-  
704 noPI. The sLBF-PI formulations showed a trend towards a decreased oral bioavailability, when  
705 compared to sLBF-noPI. While the overall bioavailability of  $26.3 \pm 14.2\%$  is in line with  
706 previous reports of venetoclax bioavailability in large animal models.<sup>14,46</sup> However, the results  
707 of the present study were unexpected since previously published studies exploring the inclusion  
708 of PIs with LBF resulted in an increased bioavailability.<sup>24-26</sup> However, in the previous reported  
709 studies LFCS type IIIB/IV LBFs systems were used, which contained high amounts of co-  
710 solvents and exhibit a high risk of precipitation due to the dilution effect upon dispersion.<sup>27</sup>  
711 Therefore, this confirmed that the ability of an oil-only sLBF to generate supersaturated  
712 concentrations of venetoclax *in vitro* was translated to increased absorption *in vivo* and that the  
713 duration of supersaturation for the sLBF was sufficient to obviate the inclusion of a PI. This  
714 observation that a PI was not required may be specific for venetoclax, given that the drug as a  
715 class III glass former has a low tendency to crystallise.<sup>40</sup> Hence, for other drugs such as poor  
716 glass formers as well as sLBF containing higher proportions of co-solvents further studies are

Page 36

## X. Thesis Publications

717 required to assess whether sLBF approaches with PIs are needed to maximise absorption and  
718 mitigate a perceived risk of precipitation *in vivo*.

719

720 The median MAT for the sLBF-PI formulations was higher among all PI containing  
721 formulations relative to sLBF-noPI (Table 3). Overall, given the variability in absorption rate  
722 of venetoclax in each group, no statistically significant differences were observed. However, it  
723 would appear that the inclusion of a PI may present a risk of a delayed absorption that may  
724 reflect a delay of drug release from the formulation. An explanation for this observation might  
725 be a combined effect of the extent of drug-polymer interaction and a reduced polymer swelling.  
726 The incorporation of the PI into the sLBF may have reduced polymer swelling (which normally  
727 happened in the aqueous media) and caused trapping of the drug. In addition, the interaction  
728 between the PIs and the drug reduces diffusion of both PI and drug and hence the partitioning  
729 of venetoclax and PIs from the sLBF to the aqueous phase. The partitioning may be further  
730 reduced due to an increased viscosity of the sLBF-PI formulations, which further decreases  
731 diffusion, but also dispersibility and subsequently digestibility. A less dispersed LBF exhibits  
732 a lower surface area, which potentially leads to less drug released from the sLBF. However,  
733 further studies are needed to explore the effect of viscosity on sLBF performance *in vivo*.

734

735 From the *in vivo* data it appears that the solubility of the polymer in the sLBF may have  
736 impacted the bioavailability. In the cases of PIs being soluble in the sLBF, i.e. Pluronic® F108,  
737 PVP, PVP/VA and Eudragit® EPO dissolved completely in the sLBF, a lower bioavailability  
738 was observed when compared to the PIs that showed a lower solubility in the sLBF, i.e. HPMC  
739 and HPMCAS formed suspensions in the sLBF. One explanation for this observation may be  
740 that a PI that is soluble in the lipid vehicle can, in combination with a high drug affinity of the  
741 PI, lead to a drug retention in the vehicle instead of showing a more favourable PI functionality

Page 37



## X. Thesis Publications

742 of reducing precipitation once the sLBF has dispersed in the intraluminal fluids. On the other  
743 hand, a more hydrophilic polymer that is suspended in the sLBF may lead to polymer swelling  
744 upon aqueous dispersion to allow for drug release and the intended PI functionality. Further  
745 studies exploring polymer solubility in sLBF and its effect on drug release may therefore be  
746 merited to fully predict the impact of PIs on *in vivo* performance.

747

748 Overall, a relationship between the *in silico* calculated excess enthalpy of mixing and the *in*  
749 *vitro* determined supersaturation ratios and amounts of venetoclax solubilised was established  
750 in the case of PIs that generated supersaturated concentrations. This study showed that with  
751 increasing ‘COSMO-Rank’ (i.e. lower excess enthalpy of mixing), higher apparent  
752 supersaturation ratios and higher amounts of solubilised venetoclax were obtained. Since  
753 Eudragit® EPO resulted in undersaturated aqueous solutions (venetoclax concentration below  
754 FaSSIF saturation solubility) due to a lower release from the formulation, the PI was not  
755 considered in the analysis of the relationship between *in silico* and *in vitro*. However, the result  
756 of Eudragit® EPO showed a simple consideration of high negative excess enthalpy for a more  
757 lipophilic polymer in sLBF should be interpreted with care regarding PI performance.

758

759 The deviation of the *in vivo* results from the *in silico* calculations by the COSMOquick software  
760 may reflect an oversimplification of calculated parameters. The calculations considered the  
761 interactions between the drug and the PI, but the interaction between the drug or the PI with  
762 formulation excipients, water or the components of gastrointestinal fluids such as bile salts and  
763 phospholipids were not taken into account. While this might have not been crucial for an *in*  
764 *vitro* dispersion experiment, the digestion of the lipid excipients *in vivo* further increased the  
765 complexity of the gastrointestinal fluids, by releasing fatty acids and other digestion products  
766 in the gastrointestinal environment. It is, hence, unclear whether a drastic simplification to

Page 38

## X. Thesis Publications

767 solely the drug and PI by the selected COSMOquick approach is applicable for LBFs to define  
768 PIs. Nevertheless, the current *in silico* approach may be useful for type IV LBFs/sLBFs that  
769 contain less digestible excipients, i.e. co-solvents, and may be a quick screening tool to reduce  
770 the initial PI choice to a reasonable number, which subsequently can be tested *in vitro* and *in*  
771 *vivo*. Furthermore, the complementing *in vitro* and *in silico* techniques used in the present study  
772 may be helpful in understanding the formulation behaviour of sLBFs *in vivo*.

773

774 A lack of PI impact on increasing bioavailability may also reflect that the *in vitro* model was  
775 poorly predictive of the *in vivo* situation. The reasons for the *in vitro* test not being predictive  
776 of a reduce overall drug absorption in the presence of PIs can be manifold such as (a) more  
777 complex intestinal conditions *in vivo*,<sup>47</sup> (b) a lack of absorptive sink *in vitro*<sup>48</sup> or (c) a  
778 venetoclax specific effect. The employed *in vitro* test exhibited a high drug and lipid load as  
779 well as higher hydrodynamics compared to *in vivo*. In addition, a solvent shift may meet the  
780 industry need for a fast screening tool, however, in the case of LBFs it is not physiologically  
781 relevant. A combined dispersion-digestion setup<sup>27</sup> or a dispersion-digestion setup with  
782 absorptive sink<sup>49-51</sup> may provide more mechanistic, albeit lower throughput, results. A further  
783 limitation of the study may have been the incorporation of the PI into the sLBF. While this  
784 decision was guided by *in vitro* data, in light of the *in vivo* results it is unclear whether  
785 separating the PI and sLBF may have conferred advantages *in vivo*.

786

### 787 CONCLUSION

788 The formulation approach of using PIs to prolong supersaturation is well recognised for  
789 amorphous formulations, but less well explored for sLBFs. The present study, applied *in silico*,  
790 *in vitro* and *in vivo* models to extend the concept of PIs in an oil-only sLBF. An *in silico* tool  
791 was successfully used for an initial PI selection and aided in explaining the low free venetoclax

## X. Thesis Publications

792 concentration *in vitro* in case of the sLBF with Eudragit® EPO. It was found that the strong  
793 predicted interaction between the drug and the polymer may have led to an overall reduction in  
794 drug release from the formulation. In addition, the *in vitro* PI screening tool showed that the  
795 incorporation of the PI into the sLBF yielded higher free drug concentrations compared to the  
796 separate addition of the PI. While the *in vitro* screening showed prolonged supersaturated  
797 concentrations in the presence of PIs in five out of six cases, *in vivo* a trend towards a lower  
798 overall bioavailability was observed for PI containing formulations, indicating that  
799 incorporating a PI into the sLBF was not necessary. The oral bioavailability of venetoclax was  
800 highest for the PI free sLBF-noPI, which suggests that reduced oral absorption due to  
801 precipitation from an oil-only sLBF was low.

802

### 803 ACKNOWLEDGEMENTS

804 N.J. Koehl, L.J. Henze, D.J. Price, B.T. Griffin, R. Holm and M. Kuentz are part of the  
805 PEARRL European Training network, which has received funding from the Horizon 2020  
806 Marie Skłodowska-Curie Innovative Training Networks programme under grant agreement No.  
807 674909.

808

809 REFERENCES

- 810 1. Bergstrom, C. A.; Charman, W. N.; Porter, C. J. Computational prediction of  
811 formulation strategies for beyond-rule-of-5 compounds. *Adv Drug Deliv Rev* **2016**, *101*, 6-21.
- 812 2. DeGoey, D. A.; Chen, H. J.; Cox, P. B.; Wendt, M. D. Beyond the Rule of 5: Lessons  
813 Learned from AbbVie's Drugs and Compound Collection. *J Med Chem* **2018**, *61*, (7), 2636-  
814 2651.
- 815 3. Di, L.; Fish, P. V.; Mano, T. Bridging solubility between drug discovery and  
816 development. *Drug Discov Today* **2012**, *17*, (9-10), 486-95.
- 817 4. Porter, C. J. H.; Pouton, C. W.; Cuine, J. F.; Charman, W. N. Enhancing intestinal drug  
818 solubilisation using lipid-based delivery systems. *Adv Drug Deliver Rev* **2008**, *60*, (6), 673-691.
- 819 5. Porter, C. J. H.; Trevaskis, N. L.; Charman, W. N. Lipids and lipid-based formulations:  
820 optimizing the oral delivery of lipophilic drugs. *Nat Rev Drug Discov* **2007**, *6*, (3), 231-248.
- 821 6. Kuentz, M. Lipid-based formulations for oral delivery of lipophilic drugs. *Drug Discov*  
822 *Today Technol* **2012**, *9*, (2), e71-e174.
- 823 7. Feeney, O. M.; Crum, M. F.; McEvoy, C. L.; Trevaskis, N. L.; Williams, H. D.; Pouton,  
824 C. W.; Charman, W. N.; Bergstrom, C. A.; Porter, C. J. 50years of oral lipid-based formulations:  
825 Provenance, progress and future perspectives. *Adv Drug Deliv Rev* **2016**, *101*, 167-94.
- 826 8. Koehl, N. J.; Holm, R.; Kuentz, M.; Griffin, B. T. New Insights into Using Lipid Based  
827 Suspensions for "Brick Dust" Molecules: Case Study of Nilotinib. *Pharm Res-Dordr* **2019**, *36*,  
828 (4).
- 829 9. Dahan, A.; Hoffman, A. The effect of different lipid based formulations on the oral  
830 absorption of lipophilic drugs: the ability of in vitro lipolysis and consecutive ex vivo intestinal  
831 permeability data to predict in vivo bioavailability in rats. *Eur J Pharm Biopharm* **2007**, *67*, (1),  
832 96-105.

## X. Thesis Publications

- 833 10. Koehl, N. J.; Holm, R.; Kuentz, M.; Griffin, B. T. Chase dosing of lipid formulations  
834 to enhance oral bioavailability of nilotinib in rats. *Pharm Res* **2020**, *accepted*.
- 835 11. Thomas, N.; Holm, R.; Garmer, M.; Karlsson, J. J.; Mullertz, A.; Rades, T.  
836 Supersaturated self-nanoemulsifying drug delivery systems (Super-SNEDDS) enhance the  
837 bioavailability of the poorly water-soluble drug simvastatin in dogs. *Aaps J* **2013**, *15*, (1), 219-  
838 27.
- 839 12. Thomas, N.; Holm, R.; Mullertz, A.; Rades, T. In vitro and in vivo performance of  
840 novel supersaturated self-nanoemulsifying drug delivery systems (super-SNEDDS). *J Control*  
841 *Release* **2012**, *160*, (1), 25-32.
- 842 13. Ilie, A. R.; Griffin, B. T.; Kolakovic, R.; Vertzoni, M.; Kuentz, M.; Holm, R.  
843 Supersaturated lipid-based drug delivery systems - exploring impact of lipid composition type  
844 and drug properties on supersaturability and physical stability. *Drug Dev Ind Pharm* **2020**, 1-9.
- 845 14. Koehl, N. J.; Henze, L. J.; Kuentz, M.; Holm, R.; Griffin, B. T. Supersaturated lipid-  
846 based formulations to enhance oral bioavailability of venetoclax *Pharmaceutics* **2020**, (under  
847 review).
- 848 15. Morgen, M.; Saxena, A.; Chen, X. Q.; Miller, W.; Nkansah, R.; Goodwin, A.; Cape, J.;  
849 Haskell, R.; Su, C.; Gudmundsson, O.; Hageman, M.; Kumar, A.; Chowan, G. S.; Rao, A.;  
850 Holenarsipur, V. K. Lipophilic salts of poorly soluble compounds to enable high-dose lipidic  
851 SEDDS formulations in drug discovery. *Eur J Pharm Biopharm* **2017**, *117*, 212-223.
- 852 16. Williams, H. D.; Ford, L.; Han, S.; Tangso, K. J.; Lim, S.; Shackelford, D. M.; Vodak,  
853 D. T.; Benameur, H.; Pouton, C. W.; Scammells, P. J.; Porter, C. J. H. Enhancing the Oral  
854 Absorption of Kinase Inhibitors Using Lipophilic Salts and Lipid-Based Formulations. *Mol*  
855 *Pharm* **2018**.
- 856 17. Williams, H. D.; Ford, L.; Lim, S.; Han, S.; Baumann, J.; Sullivan, H.; Vodak, D.;  
857 Igonin, A.; Benameur, H.; Pouton, C. W.; Scammells, P. J.; Porter, C. J. H. Transformation of



## X. Thesis Publications

- 858 Biopharmaceutical Classification System Class I and III Drugs Into Ionic Liquids and  
859 Lipophilic Salts for Enhanced Developability Using Lipid Formulations. *J Pharm Sci* **2018**,  
860 *107*, (1), 203-216.
- 861 18. Maghrebi, S.; Prestidge, C. A.; Joyce, P. An update on polymer-lipid hybrid systems  
862 for improving oral drug delivery. *Expert Opin Drug Deliv* **2019**, *16*, (5), 507-524.
- 863 19. Simovic, S.; Heard, P.; Hui, H.; Song, Y.; Peddie, F.; Davey, A. K.; Lewis, A.; Rades,  
864 T.; Prestidge, C. A. Dry hybrid lipid-silica microcapsules engineered from submicron lipid  
865 droplets and nanoparticles as a novel delivery system for poorly soluble drugs. *Mol Pharm* **2009**,  
866 *6*, (3), 861-72.
- 867 20. Tan, A.; Simovic, S.; Davey, A. K.; Rades, T.; Prestidge, C. A. Silica-lipid hybrid (SLH)  
868 microcapsules: a novel oral delivery system for poorly soluble drugs. *J Control Release* **2009**,  
869 *134*, (1), 62-70.
- 870 21. Thomas, N.; Richter, K.; Pedersen, T. B.; Holm, R.; Mullertz, A.; Rades, T. In vitro  
871 lipolysis data does not adequately predict the in vivo performance of lipid-based drug delivery  
872 systems containing fenofibrate. *Aaps J* **2014**, *16*, (3), 539-49.
- 873 22. Siqueira Jorgensen, S. D.; Al Sawaf, M.; Graeser, K.; Mu, H.; Mullertz, A.; Rades, T.  
874 The ability of two in vitro lipolysis models reflecting the human and rat gastro-intestinal  
875 conditions to predict the in vivo performance of SNEDDS dosing regimens. *Eur J Pharm*  
876 *Biopharm* **2018**, *124*, 116-124.
- 877 23. Siqueira, S. D.; Mullertz, A.; Graeser, K.; Kasten, G.; Mu, H.; Rades, T. Influence of  
878 drug load and physical form of cinnarizine in new SNEDDS dosing regimens: in vivo and in  
879 vitro evaluations. *Aaps J* **2017**, *19*, (2), 587-594.
- 880 24. Gao, P.; Akrami, A.; Alvarez, F.; Hu, J.; Li, L.; Ma, C.; Surapaneni, S. Characterization  
881 and Optimization of AMG 517 Supersaturable Self-Emulsifying Drug Delivery System (S-  
882 SEDDS) for Improved Oral Absorption. *J Pharm Sci-US* **2009**, *98*, (2), 516-528.

## X. Thesis Publications

- 883 25. Gao, P.; Guyton, M. E.; Huang, T.; Bauer, J. M.; Stefanski, K. J.; Lu, Q. Enhanced oral  
884 bioavailability of a poorly water soluble drug PNU-91325 by supersaturatable formulations.  
885 *Drug Dev Ind Pharm* **2004**, *30*, (2), 221-9.
- 886 26. Gao, P.; Rush, B. D.; Pfund, W. P.; Huang, T.; Bauer, J. M.; Morozowich, W.; Kuo, M.  
887 S.; Hageman, M. J. Development of a supersaturable SEDDS (S-SEDDS) formulation of  
888 paclitaxel with improved oral bioavailability. *J Pharm Sci* **2003**, *92*, (12), 2386-98.
- 889 27. Suys, E. J. A.; Chalmers, D. K.; Pouton, C. W.; Porter, C. J. H. Polymeric Precipitation  
890 Inhibitors Promote Fenofibrate Supersaturation and Enhance Drug Absorption from a Type IV  
891 Lipid-Based Formulation. *Mol Pharm* **2018**, *15*, (6), 2355-2371.
- 892 28. Pouton, C. W. Formulation of poorly water-soluble drugs for oral administration:  
893 physicochemical and physiological issues and the lipid formulation classification system. *Eur*  
894 *J Pharm Sci* **2006**, *29*, (3-4), 278-87.
- 895 29. Pouton, C. W. Lipid formulations for oral administration of drugs: non-emulsifying,  
896 self-emulsifying and 'self-microemulsifying' drug delivery systems. *Eur J Pharm Sci* **2000**, *11*,  
897 (Suppl 2), 93-8.
- 898 30. FDA Venclexta (Venetoclax) Clinical pharmacology and biopharmaceutics review(s)  
899 application number: 208573Orig1s000.  
900 [https://www.accessdata.fda.gov/drugsatfda\\_docs/nda/2016/208573Orig1s000ClinPharmR.pdf](https://www.accessdata.fda.gov/drugsatfda_docs/nda/2016/208573Orig1s000ClinPharmR.pdf)  
901 (January 23rd ),
- 902 31. ICH, G. u. i. d. e. l. i. n. e. In *Validation of analytical procedures: text and methodology*  
903 *Q2 (R1)*, International conference on harmonization, Geneva, Switzerland, 2005; ICH  
904 harmonised tripartite guideline.
- 905 32. Koehl, N. J.; Holm, R.; Kuentz, M.; Jannin, V.; Griffin, B. T. Exploring impact of  
906 surfactant type and digestion: Highly digestible surfactants improve oral bioavailability of  
907 nilotinib. *Mol Pharmaceut* **2020**, under review.

## X. Thesis Publications

- 908 33. Sek, L.; Porter, C. J.; Charman, W. N. Characterisation and quantification of medium  
909 chain and long chain triglycerides and their in vitro digestion products, by HPTLC coupled with  
910 in situ densitometric analysis. *J Pharm Biomed Anal* **2001**, *25*, (3-4), 651-61.
- 911 34. Klamt, A.; Eckert, F. COSMO-RS: a novel and efficient method for the a priori  
912 prediction of thermophysical data of liquids. *Fluid Phase Equilibria* **2000**, *172*, (1), 43-72.
- 913 35. Hornig, M.; Klamt, A. COSMOfrag: a novel tool for high-throughput ADME property  
914 prediction and similarity screening based on quantum chemistry. *J Chem Inf Model* **2005**, *45*,  
915 (5), 1169-77.
- 916 36. Loschen, C.; Klamt, A. COSMOquick: A Novel Interface for Fast sigma-Profile  
917 Composition and Its Application to COSMO-RS Solvent Screening Using Multiple Reference  
918 Solvents. *Ind Eng Chem Res* **2012**, *51*, (43), 14303-14308.
- 919 37. Abramov, Y. A.; Loschen, C.; Klamt, A. Rational coformer or solvent selection for  
920 pharmaceutical cocrystallization or desolvation. *J Pharm Sci* **2012**, *101*, (10), 3687-97.
- 921 38. Alsenz, J.; Kuentz, M. From Quantum Chemistry to Prediction of Drug Solubility in  
922 Glycerides. *Mol Pharm* **2019**, *16*, (11), 4661-4669.
- 923 39. Price, D. J.; Nair, A.; Kuentz, M.; Dressman, J.; Saal, C. Calculation of drug-polymer  
924 mixing enthalpy as a new screening method of precipitation inhibitors for supersaturating  
925 pharmaceutical formulations. *Eur J Pharm Sci* **2019**, *132*, 142-156.
- 926 40. Emami Riedmaier, A.; Lindley, D. J.; Hall, J. A.; Castleberry, S.; Slade, R. T.; Stuart,  
927 P.; Carr, R. A.; Borchardt, T. B.; Bow, D. A. J.; Nijsen, M. Mechanistic Physiologically Based  
928 Pharmacokinetic Modeling of the Dissolution and Food Effect of a Biopharmaceutics  
929 Classification System IV Compound-The Venetoclax Story. *J Pharm Sci* **2018**, *107*, (1), 495-  
930 502.
- 931 41. Klamt, A. The COSMO and COSMO-RS solvation models. *WIREs Computational*  
932 *Molecular Science* **2011**, *1*, (5), 699-709.

## X. Thesis Publications

- 933 42. Price, D. J.; Ditzinger, F.; Koehl, N. J.; Jankovic, S.; Tsakiridou, G.; Nair, A.; Holm, R.;  
934 Kuentz, M.; Dressman, J. B.; Saal, C. Approaches to increase mechanistic understanding and  
935 aid in the selection of precipitation inhibitors for supersaturating formulations - a PEARRL  
936 review. *J Pharm Pharmacol* **2019**, *71*, (4), 483-509.
- 937 43. Xu, S.; Dai, W. G. Drug precipitation inhibitors in supersaturable formulations. *Int J*  
938 *Pharm* **2013**, *453*, (1), 36-43.
- 939 44. Gao, P.; Shi, Y. Characterization of supersaturable formulations for improved  
940 absorption of poorly soluble drugs. *Aaps J* **2012**, *14*, (4), 703-13.
- 941 45. Brouwers, J.; Brewster, M. E.; Augustijns, P. Supersaturating drug delivery systems:  
942 the answer to solubility-limited oral bioavailability? *J Pharm Sci* **2009**, *98*, (8), 2549-72.
- 943 46. Choo, E. F.; Boggs, J.; Zhu, C.; Lubach, J. W.; Catron, N. D.; Jenkins, G.; Souers, A.  
944 J.; Voorman, R. The role of lymphatic transport on the systemic bioavailability of the Bel-2  
945 protein family inhibitors navitoclax (ABT-263) and ABT-199. *Drug Metab Dispos* **2014**, *42*,  
946 (2), 207-12.
- 947 47. Griffin, B. T.; Kuentz, M.; Vertzoni, M.; Kostewicz, E. S.; Fei, Y.; Faisal, W.; Stillhart,  
948 C.; O'Driscoll, C. M.; Reppas, C.; Dressman, J. B. Comparison of in vitro tests at various levels  
949 of complexity for the prediction of in vivo performance of lipid-based formulations: Case  
950 studies with fenofibrate. *Eur J Pharm Biopharm* **2014**, *86*, (3), 427-437.
- 951 48. Stillhart, C.; Imanidis, G.; Griffin, B. T.; Kuentz, M. Biopharmaceutical Modeling of  
952 Drug Supersaturation During Lipid-Based Formulation Digestion Considering an Absorption  
953 Sink. *Pharm Res-Dordr* **2014**, *31*, (12), 3426-3444.
- 954 49. Keemink, J.; Martensson, E.; Bergstrom, C. A. S. Lipolysis-Permeation Setup for  
955 Simultaneous Study of Digestion and Absorption in Vitro. *Mol Pharm* **2019**, *16*, (3), 921-930.

## X. Thesis Publications

- 956 50. Alvebratt, C.; Keemink, J.; Edueng, K.; Cheung, O.; Stromme, M.; Bergstrom, C. A. S.  
957 An in vitro dissolution-digestion-permeation assay for the study of advanced drug delivery  
958 systems. *Eur J Pharm Biopharm* **2020**, *149*, 21-29.
- 959 51. O'Dwyer, P.; Box, K.; Koehl, N. J.; Bennett-Lenane, H.; Reppas, C.; Holm, R.; Kuentz,  
960 M.; Griffin, B. T. A Novel Biphasic Lipolysis Method to Predict In Vivo Performance of Lipid  
961 Based Formulations. *Mol Pharmaceut* **2020**, *under review*.
- 962
- 963



964 **Supporting information**

965 *In silico, in vitro* and *in vivo* evaluation of  
 966 precipitation inhibitors in supersaturated lipid-  
 967 based formulations of venetoclax

968 Niklas J. Koehl<sup>1</sup>, Laura J. Henze<sup>1</sup>, Harriet Bennett-Lenane<sup>1</sup>, Daniel J. Price<sup>2,3</sup>,  
 969 René Holm<sup>4,5</sup>, Martin Kuentz<sup>6</sup>, Brendan T. Griffin<sup>1\*</sup>

970

971 <sup>1</sup> School of Pharmacy, University College Cork; College Road, Cork, T12 YN60 Ireland

972 <sup>2</sup> Merck KGaA, Darmstadt, Germany

973 <sup>3</sup> Goethe University Frankfurt, Frankfurt am Main, Germany

974 <sup>4</sup> Drug Product Development, Janssen Research and Development, Johnson & Johnson,  
 975 Turnhoutseweg 30, 2340 Beerse, Belgium

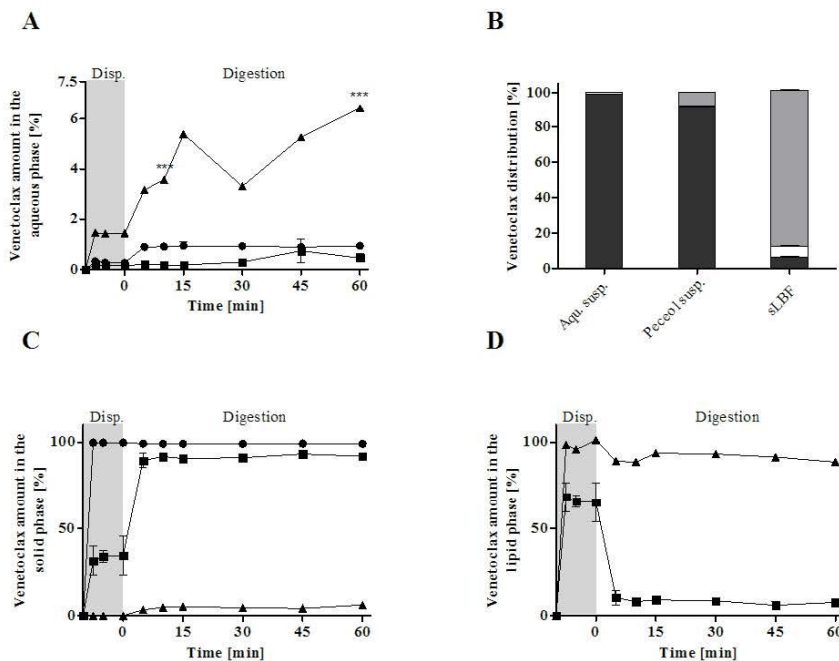
976 <sup>5</sup> Department of Science and Environment, Roskilde University, 4000 Roskilde, Denmark

977 <sup>6</sup> University of Applied Sciences and Arts Northwestern Switzerland, Institute of Pharma  
 978 Technology, Muttenz, Switzerland

979

| Content   | Page |
|---|------|
| <i>In vitro</i> lipolysis: Venetoclax concentrations in the different phases (Figure S 1) | 2    |
| Individual plasma concentration time profiles, study 1 (Figure S 2)                       | 3    |
| Individual plasma concentration time profiles, study 2 (Figure S 3)                       | 3    |
| PI test samples of sLBF-PI with HPMC, Eudragit® EPO and HPMCAS (Figure S 4)               | 4    |
| Thermal properties of venetoclax (Table S 1)  | 4    |

980



981

982 **Figure S 1.** *In vitro* lipolysis of venetoclax formulated as supersaturated Peceol<sup>®</sup> solution

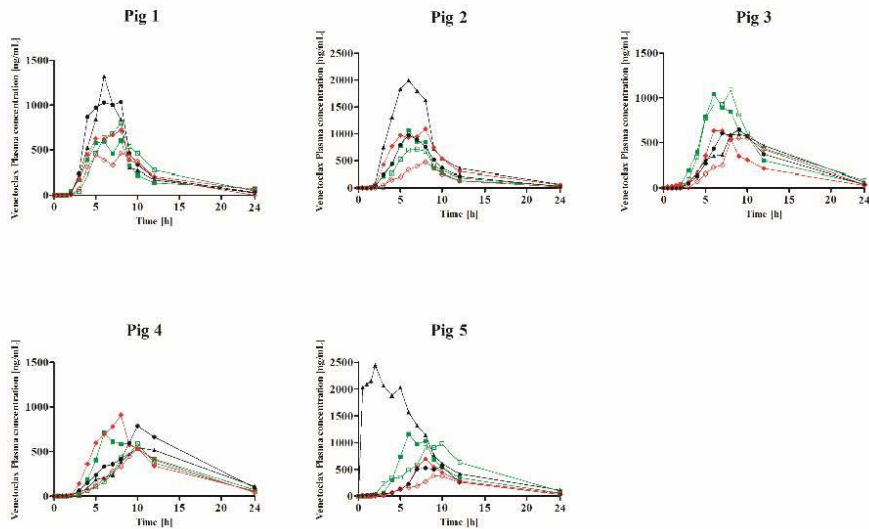
983 (sLBF) (▲), as well as previously reported aqueous suspension (●), Peceol<sup>®</sup> suspension (■).<sup>14</sup>

984 A: % of venetoclax in the aqueous phase, B: Distribution of venetoclax into the different phases

985 after 60 min of lipolysis, C: % of venetoclax in the solid phase, D: % of the venetoclax in the

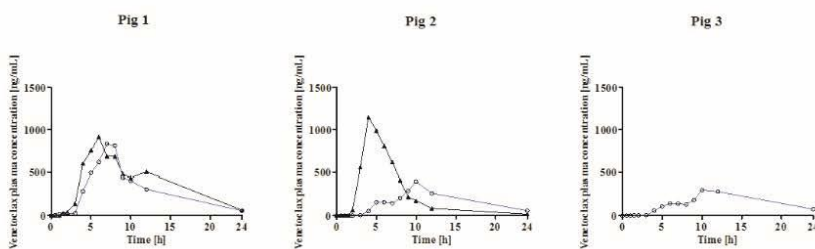
986 lipid phase. All experiments were run with n = 3 and results are shown as mean ± SD.

987



988

989 **Figure S 2.** Individual plasma concentration profile from 0 – 24 h of 100 mg venetoclax in  
 990 landrace pigs for the tested formulations. sLBF-noPI (▲), sLBF-HPMC (■ - green), sLBF-  
 991 HPMCAS (□ - green), sLBF-PVP (◆ - red), sLBF-PVP/VA (◇ - red), sLBF-Pluronic® F108 (●).

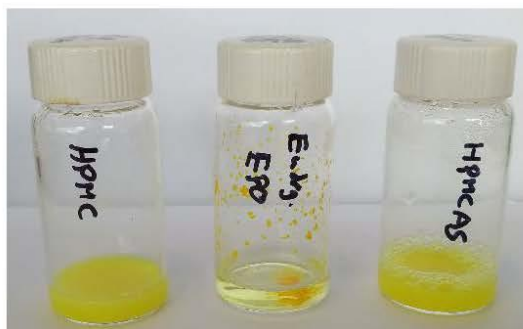


992

993 **Figure S 3.** Individual plasma concentration time profiles from 0 - 24 h of 100 mg venetoclax  
 994 in landrace pigs for the tested formulations. sLBF-noPI (▲), sLBF-Eudragit® EPO (○ - blue).  
 995 Due to an administration error, the sLBF-noPI of pig 3 was not obtained. sLBF-noPI has  
 996 previously been reported.<sup>14</sup>

997

998



999

1000 **Figure S 4.** PI test samples of sLBF-PI with HPMC, Eudragit® EPO and HPMCAS after 180  
 1001 min in FaSSiF. Agglomeration of Eudragit® EPO can be observed.

1002

1003 **Table S 1.** Thermal properties of venetoclax. Melting point ( $T_m$ ), Enthalpy of fusion ( $\Delta H_{fus}$ ),  
 1004 Entropy of fusion ( $\Delta S_{fus}$ ).

|                             | $T_m$ [°C]       | $\Delta H_{fus}$ [kJ/mol] | $\Delta S_{fus} \times 10^{-2}$<br>[kJ/mol/K] |
|-----------------------------|------------------|---------------------------|---|
| Venetoclax batch<br>1810004 | $139.1 \pm 0.03$ | $19.2 \pm 0.03$           | $4.7 \pm 0.01$                                |

1005